Springer Series on Atomic, Optical and Plasma Physics 74

Mario Capitelli
Domenico Bruno
Annarita Laricchiuta

Fundamental Aspects of Plasma Chemical Physics

Transport

Springer

Springer Series on

ATOMIC, OPTICAL, AND PLASMA PHYSICS 74

Springer Series on

ATOMIC, OPTICAL, AND PLASMA PHYSICS

The Springer Series on Atomic, Optical, and Plasma Physics covers in a comprehensive manner theory and experiment in the entire field of atoms and molecules and their interaction with electromagnetic radiation. Books in the series provide a rich source of new ideas and techniques with wide applications in fields such as chemistry, materials science, astrophysics, surface science, plasma technology, advanced optics, aeronomy, and engineering. Laser physics is a particular connecting theme that has provided much of the continuing impetus for new developments in the field. The purpose of the series is to cover the gap between standard undergraduate textbooks and the research literature with emphasis on the fundamental ideas, methods, techniques, and results in the field.

For further volumes:
http://www.springer.com/series/411

Mario Capitelli • Domenico Bruno
Annarita Laricchiuta

Fundamental Aspects of Plasma Chemical Physics

Transport

Springer

Mario Capitelli
Dipartimento di Chimica
Università di Bari
Via Orabona 4
70126 Bari
Italy
mario.capitelli@ba.imip.cnr.it

Domenico Bruno
Istituto di Metodologie Inorganiche e Plasmi
Consiglio Nazionale delle Ricerche (CNR)
Via Amendola 122/D
70126 Bari
Italy
domenico.bruno@ba.imip.cnr.it

Annarita Laricchiuta
Istituto di Metodologie Inorganiche e Plasmi
Consiglio Nazionale delle Ricerche (CNR)
Via Amendola 122/D
70126 Bari
Italy
annarita.laricchiuta@ba.imip.cnr.it

ISSN 1615-5653
ISBN 978-1-4419-8171-4 ISBN 978-1-4419-8172-1 (eBook)
DOI 10.1007/978-1-4419-8172-1
Springer New York Heidelberg Dordrecht London

Library of Congress Control Number: 2013931850

The non-equilibrium statistical mechanics is of more recent development and is one of the frontier fields of research today. The special case of dilute gases was investigated about a century ago by Maxwell, Boltzmann, and others, using somewhat special methods. With these latter techniques is customarily associated the name "kinetic theory".

J. O. Hirschfelder, C. F. Curtiss, R. Byron Bird
from Chap. 2 of Molecular Theory of Gases and Liquids

Preface

In this book we develop basic and advanced concepts of plasma transport for LTE (local thermodynamic equilibrium) plasmas starting from the famous monograph of Hirschfelder, Curtiss and Bird (HCB).[1] The HCB monograph, while being essential in developing the Chapman–Enskog method for the solution of the Boltzmann transport equation as well as the basic quantum mechanical approaches for deriving interaction potentials, presents problems when applied to ionized gases.

In a thermal plasma a lot of collisions involving molecule–molecule, atom–molecule, atom–atom, atom–ion, electron–atom, electron–electron, electron–ion and ion–ion do coexist so that refined formulations of interaction potentials need to get the input data, i.e. the collision integrals, in the transport equations. In addition in these last years it has been shown that the collision integrals of electronically excited states can play an important role in affecting the transport properties of thermal plasmas, due to their dramatic dependence on the principal quantum number. In this case charge- and excitation-exchange cross sections need to be calculated implying the knowledge of a huge number of potential curves, today still a prohibitive task despite the enormous progress of quantum chemistry. This problem can be solved by using the asymptotic theory that allows a reliable estimation of the *gerade–ungerade* potential pair differences avoiding the exact quantum mechanical calculation. This problem will be widely discussed in this book by presenting different examples of diffusion-type collision integrals involving (1) excited hydrogen atoms colliding with protons and (2) excited helium atoms colliding with He^+. This theory is also extended to the calculation of diffusion-type collision integrals for *low-* and *high-lying* electronically excited states for atoms and ions relevant to air plasmas. A similar problem is considered for the viscosity-type collision integrals, not affected by charge-exchange cross sections, derived in the frame of a phenomenological approach, avoid-

[1] Refers to 2nd edition in Structure and Matter Series of Hirschfelder et al. (1966) of Chap. 1.

ing the computationally expensive multi-potential quantum approach. Two chapters of this book are dedicated to these topics. On the other hand other important topics are discussed, in particular dealing with (1) the failure of the Eucken approximation in the presence of non-Boltzmann vibrational distributions under shock wave and expanding flow situations, (2) the analysis of the numerous approaches developed in the literature for two-temperature plasmas, emphasizing the role of *non-uniqueness* of two-temperature Saha equations in affecting the corresponding transport coefficients, and (3) the role of the magnetic field in transforming the corresponding transport equations in tensorial form.

The different applications, all discussed by means of several examples, are preceded by theoretical chapters illustrating the Chapman–Enskog method in his modern formulation as well as the quantum and classical approaches for calculating the transport cross sections. Finally the last chapter presents accurate tables of transport coefficients for high-temperature planetary (Earth, Jupiter, Mars) atmospheres, which can be directly used in fluid dynamics applications.

Some overlaps occur in the different chapters to keep part of them self-consistent, allowing undergraduate and Ph.D. students as well researchers to construct a *personal road* in the understanding of the relevant topics. It is worth noting that the structure of the book can be considered complementary to our book on thermodynamics (Capitelli et al., 2011 of Chap. 3). recently published, so that appropriate selections of chapters from both books can be used for courses on thermodynamics and transport of plasmas addressed to undergraduate and Ph.D. students in physics, chemistry, and engineering.

Introduction

Transport properties (thermal conductivity, diffusion coefficients, viscosity and electrical conductivity) of ionized gases are important topics of plasma technology because these quantities determine the heat flux from plasma to different samples of materials which can be heated during the plasma-material interaction. The experimental determination of transport properties of ionized gases is very difficult to be achieved so that one demands to the theory the availability of these quantities.

Transport properties can be obtained once known the velocity distribution functions (*vdf*) of the different species, which in turn can be obtained by the solution of coupled Boltzmann transport equations. In this book we consider plasmas in which the deviation of *vdf* from the Maxwell behavior is small so that the Chapman–Enskog solution of the Boltzmann equation can be considered adequate for solving the problem.

The corresponding equations have been worked out many years ago by different authors and are being used in many applications of thermal plasmas including plasma treatment of materials, plasma waste destruction, aerospace reentry problems, including meteorite impact with the atmosphere, inductive coupled plasma (ICP) and laser induced plasma spectroscopy (LIBS) analytical techniques.

Nowadays a renewed interest in the transport properties of thermal plasmas is appearing in the literature so that one can use the well-established theory for discussing many problems, which still require further studies. We refer in particular to a better description of transport cross sections as well as to the influence of electronically and vibrationally excited states on the different transport coefficients. Multi-temperature plasma transport properties, being a topic largely discussed by the thermal plasma community, still need a more basic approach for their complete understanding.

The first two chapters give the possibility to the reader to understand the theories at the basis of the development of transport coefficients mixing very sophisticated statistical mechanics approaches and simplified intuitive methods. Chapter 1 introduces the transport phenomenology and illustrates the

kinetic theory formalism adopted in its study, with emphasis on the coefficients of internal and reactive thermal conductivities. In Chapter 2 explicit expressions are derived for the transport coefficients and they are shown to reduce to the popular Hirschfelder and Devoto formulas under suitable approximations. Then follow three chapters dealing with accurate calculations of transport cross-sections (collision integrals) involving in particular open-shell atoms and ions. Chapter 3 introduces the reader to the calculation of collision integrals of the different interactions acting in a plasma either by using the multi-potential approach or by using phenomenological approaches for reducing the multi-potential approach to a single potential. Chapter 4 is devoted to the resonant charge-exchange cross sections, a process playing an important direct and indirect role in affecting the transport properties of the plasma. The rigorous quantum mechanical approach is developed to this end, while large use is made of the asymptotic theory developed in the last 50 years by the Russian school to get accurate values of the relevant cross sections. Two case studies are discussed involving the charge transfer cross sections of $N–N^+$ and $O–O^+$ collisions; particular attention is devoted to the quantum mechanical description of the *gerade–ungerade* potential pairs arising in the interaction. The good agreement of the charge-exchange cross sections based on the quantum mechanical *gerade–ungerade* pairs and the corresponding values from the asymptotic theory is a clear indication of the possibility of using the last theory for very complicated systems.

Chapter 5 reports the transport cross sections of electronically excited states taking into account also the resonant charge- and excitation-exchange processes. Particular emphasis is given to the dependence of diffusion-type collision integrals on the principal quantum number for the interactions of the so-called *high-lying* excited states (i.e. states with principal quantum number different from the ground state) as well as to the corresponding values for the *low-lying* excited states i.e. electronic states arising from the ground state electronic configuration by rearrangement of valence electrons.

The next four chapters discuss in detail the transport properties of equilibrium and non-equilibrium systems. In particular Chap. 6 discusses the role of non-equilibrium vibrational distributions of diatomic species in affecting the transport of the vibrational energy under shock waves and expansion flows. In this case the difference with the Eucken approximation derives from the non-Boltzmann vibrational distributions of the diatom rather than from the dependence of collision integrals on the vibrational quantum number.

Chapter 7 presents in detail the influence of electronically excited states on the transport coefficients of an LTE hydrogen plasma. Different approaches are presented either by using an appropriate Brokaw equation or by using a more compact model. The partial equivalence of the two methods is also discussed. In the same chapter a new model is presented to study the role of electronically excited states in a nitrogen plasma.

Chapter 8 reports the transport coefficients of two-temperature plasmas discussing the theories and the non-uniqueness of the two-temperature Saha

equation and their role in affecting the input data in the relevant transport equations. Numerous numerical examples are reported to shed light on this topic.

Chapter 9 treats the influence of the magnetic field on the transport coefficients of LTE plasmas emphasizing the tensorial character of the different transport coefficients in the presence of magnetic field.

Chapter 10, that can be regarded as a bridge between formal theory and applications, discusses several problems including the convergence of the Chapman–Enskog method and the selection of existing collision integral databases. It also includes a new discussion on inelastic and quantum effect in affecting transport cross sections ending with the comparison between theory and experiments.

Finally in Chap. 11 the collision integral database for interactions relevant to high-temperature planetary atmosphere (Earth, Mars, Jupiter) mixtures is reported together with corresponding transport coefficients, in tabular format, in a wide range of temperature and pressure.

Bari, Italy

Mario Capitelli
Domenico Bruno
Annarita Laricchiuta

Acknowledgements

This book contains many results published by the authors in collaboration with friends and colleagues including Claudine Gorse, Domenico Giordano and Fernando Pirani, as well as many other co-workers in the references. Many thanks to Gianpiero Colonna and Antonio D'Angola for their invaluable aid in preparing Chap. 11 as well as for many other topics. Thanks also to Boris M. Smirnov, Alexander Eletskii and Alexander Kosarim for the collaboration on the calculation of resonant charge-transfer cross section for excited species interactions in the frame of the asymptotic approach. DB would like to acknowledge Vincent Giovangigli as the author of the modern and elegant formulation of the Chapman–Enskog method for molecular and partially ionized gases adopted here. A special thanks to Ettore Molinari, who initiated one of the authors (MC) to the jungle of transport cross sections by introducing him to the Ramsauer effect in electron–atom collisions.

Mario Capitelli dedicates this book to Giuliana, Paolo, Francesco, Cinzia, Alberto and Stefano; Domenico Bruno to Foteini, Matilda and Massimo; Annarita Laricchiuta to Antonietta, Giacinto and Roberta.

Contents

Chapter 1
Transport Processes in Dilute Polyatomic Gases

In this chapter, the general theoretical framework needed to describe the transport properties of a reactive gas mixture will be introduced.

Starting from a semiclassical transport kinetic equation, kinetic theory tools are applied for the determination of the transport coefficients. This formal derivation is required, in particular, for an in-depth discussion of the role of internal degrees of freedom and of chemical energy in affecting the thermal conductivity of a reactive medium.

First, however, a rough estimation of the transport coefficients is given, based on a simplified picture. This serves the purpose of introducing the transport phenomenology and the underlying physics.

1.1 Mean Free Path Theory of Transport

In this section, formulas are derived for the transport coefficients based on a simple physical model (Hirschfelder et al. 1966). The idea is that molecules transport physical properties (mass, momentum, energy, electric charge, etc.) and release them in a different point in space when a collision occurs. As we shall see in the following, this simple picture allows to estimate at the same time the main transport properties (*diffusion*, *viscosity* and *thermal conductivity*) of low-pressure gases. More subtle effects (e.g. *thermal diffusion*, *bulk viscosity*, *relaxation pressure*) need a rigorous kinetic theory derivation.

Consider, therefore, a gas of hard spheres of diameter σ and of mass m. The macroscopic state of the gas is described by the number density, n, the average velocity, $\boldsymbol{v}$, and temperature, T. The macroscopic properties may have spatial variations. We shall assume the following simplifications:

- All molecules have the same speed with respect to the average velocity: $C \equiv \|\boldsymbol{c} - \boldsymbol{v}\| = \sqrt{\frac{8k_{\mathrm{B}}T}{\pi m}}$.
- Macroscopic gradients are considered only in one spatial direction, call it z.

M. Capitelli et al., *Fundamental Aspects of Plasma Chemical Physics*,
Springer Series on Atomic, Optical, and Plasma Physics 74,
DOI 10.1007/978-1-4419-8172-1_1, © Springer Science+Business Media, LLC 2013

- Only the y-component of the fluid average velocity, v_y is nonuniform.
- The number density, n, is uniform.

The collision frequency per particle is readily evaluated:

$$\nu = n\pi\sigma^2 C = n\pi\sigma^2\sqrt{\frac{8k_{\mathrm{B}}T}{\pi m}} \tag{1.1}$$

The mean free path, l_{c}, i.e. the average distance between two successive collisions, is obtained as the ratio of the distance travelled in the time Δt (i.e. $C\Delta t$) to the number of collisions undergone in the same time (i.e. $\nu\Delta t$)

$$l_{\mathrm{c}} = \frac{C\Delta t}{\nu\Delta t} = \frac{1}{n\pi\sigma^2} \tag{1.2}$$

In addition, in order to deal with the diffusion phenomenon, we shall tag a fraction of all particles with subscript i. When moving, particles transport physical quantities like mass, momentum and energy. For each, we can define a property density and a corresponding flux. In turn, the flux will be shown to be proportional to the gradient of some macroscopic quantity, the transport coefficient being the proportionality constant (Table 1.1).

Table 1.1 Definition of physical properties and related densities, fluxes and transport properties

Property	Density	Flux	Gradient	Coefficient
m_i	ρ_i	J_{iz}	ρ_i	D
mC_y	ρv_y	P_{yz}	v_y	η
$\frac{1}{2}mC^2$	$nc_{\mathrm{v}}T$	q_z	T	λ

where $c_{\mathrm{v}} = \frac{3}{2}k_{\mathrm{B}}$ is the (translational) constant volume specific heat.

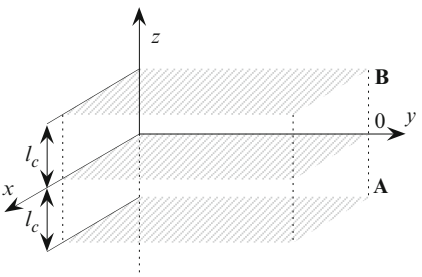

Fig. 1.1 Pictorial view of the net flux of the property in the z-direction through the plane 0, after last collision at distance l_c from the 0 plane

With reference to Fig. 1.1, we are assuming that particles crossing the $z = 0$ plane had their last collision a distance l_{c} away where they acquired

the molecular velocity $\boldsymbol{c}$. For each property density P, we can then write

$$P_A = P_0 - l_c \frac{\mathrm{d}P}{\mathrm{d}z} \tag{1.3}$$

$$P_B = P_0 + l_c \frac{\mathrm{d}P}{\mathrm{d}z} \tag{1.4}$$

Since the gas is assumed to be locally isotropic, $\frac{1}{6}$ of all particles will travel in each direction. The net flux of the property, Φ_P, across $z = 0$ is therefore

$$\Phi_P = \tfrac{1}{6} C (P_A - P_B) = -\tfrac{1}{3} C l_c \frac{\mathrm{d}P}{\mathrm{d}z} \tag{1.5}$$

For each physical property we then get

$$J_{iz} = -\tfrac{1}{3} C l_c \frac{\mathrm{d}\rho_i}{\mathrm{d}z} = -D \frac{\mathrm{d}\rho_i}{\mathrm{d}z} \tag{1.6}$$

$$P_{yz} = -\tfrac{1}{3} C l_c \frac{\mathrm{d}\rho v_y}{\mathrm{d}z} = -\tfrac{1}{3} C l_c \rho \frac{\mathrm{d}v_y}{\mathrm{d}z} = -\eta \frac{\mathrm{d}v_y}{\mathrm{d}z} \tag{1.7}$$

$$q_z = -\tfrac{1}{3} C l_c \frac{\mathrm{d}n c_v T}{\mathrm{d}z} = -\tfrac{1}{3} C l_c n c_v \frac{\mathrm{d}T}{\mathrm{d}z} = -\lambda \frac{\mathrm{d}T}{\mathrm{d}z} \tag{1.8}$$

The transport coefficients are then given by

$$\text{Diffusion:} \quad D = \tfrac{1}{3} C l_c = \frac{\sqrt{\pi m k_B T}}{\pi \sigma^2} \frac{1}{\rho} \tag{1.9}$$

$$\text{Viscosity:} \quad \eta = \tfrac{1}{3} C l_c \rho = \frac{\sqrt{\pi m k_B T}}{\pi \sigma^2} \tag{1.10}$$

$$\text{Thermal conductivity:} \quad \lambda = \tfrac{1}{3} C l_c n c_v = \frac{\sqrt{\pi m k_B T}}{\pi \sigma^2} \frac{c_v}{m} \tag{1.11}$$

The transport coefficients thus obtained are not all independent and obey instead:

$$D = \frac{\lambda m}{\rho c_v} \tag{1.12}$$

$$\eta = \rho D \tag{1.13}$$

$$\lambda = \frac{\eta c_v}{m} \tag{1.14}$$

This simple theory ignores the distribution of particle velocities and is limited to the simplest hard sphere model for the description of the collision process; inclusion of these effects requires a rigorous theory of transport that will be presented in Sect. 1.2. Also, the model is not able to provide an expla-

nation to more subtle transport phenomena like thermal diffusion and bulk viscosity.

Nonetheless the model captures correctly the dependence of the transport coefficients on gas density: the diffusion coefficient is inversely proportional to gas density whereas viscosity and thermal conductivity do not depend on it. Additionally, it gives indications on the dependence on temperature, collision cross sections and particle properties like mass and specific heat.

Before turning to the exposition of the kinetic theory of transport, we briefly introduce the concepts of internal degrees of freedom and the associated transport phenomena that are very important in the description of the transport properties of molecular gases.

1.1.1 Transport of the Energy of Internal Degrees of Freedom

The mean free path model approach can be used to estimate the transport of the energy stored in the internal degrees of freedom of the gas particles (Hirschfelder et al. 1966). Let $\mathcal{E}_{\text{int}}$ be the energy density of the internal degrees of freedom of the gas. We assume that this energy relaxes to its equilibrium value, $\mathcal{E}^*_{\text{int}}$, according to a linear law:

$$\frac{\mathrm{d}\mathcal{E}_{\text{int}}}{\mathrm{d}t} = \frac{\mathcal{E}^*_{\text{int}} - \mathcal{E}_{\text{int}}}{\tau_{\text{c}} Z_{\text{int}}} \tag{1.15}$$

where τ_{c} is the mean collision time and Z_{int} is the average number of collisions needed for the relaxation of the internal energy of a particle to its equilibrium value. Three different cases arise, according to the value of Z_{int}.

(a) $Z_{\text{int}} = 1$

In this case, one collision is sufficient, on average, to relax the internal energy of the particle to the equilibrium value, i.e. the mean free path for energy exchange l_{int} is equal to the collision mean free path l_{c}.

The derivation proceeds as in Sect. 1.1. The density of internal energy to be transported in the temperature gradient is

$$P = nc^{\text{int}}T \tag{1.16}$$

where $c^{\text{int}} = \frac{\partial}{\partial T}\left(\frac{\mathcal{E}_{\text{int}}}{n}\right)$ is the internal specific heat (assumed constant).

As in Eqs. (1.3) and (1.4), we now have

$$P_A = P_0 - l_{\text{c}}\frac{\mathrm{d}T}{\mathrm{d}z} \tag{1.17}$$

$$P_B = P_0 + l_{\text{c}}\frac{\mathrm{d}T}{\mathrm{d}z} \tag{1.18}$$

The relevant flux is given by

$$q_{\text{int}} = \tfrac{1}{6}C(P_A - P_B) = -\tfrac{1}{3}Cl_{\text{c}}nc^{\text{int}}\frac{\mathrm{d}T}{\mathrm{d}z} \tag{1.19}$$

We then define the internal thermal conductivity:

$$\lambda_{\text{int}} = \tfrac{1}{3}Cl_{\text{c}}nc^{\text{int}} = \rho\mathcal{D}\frac{c^{\text{int}}}{m} = \eta\frac{c^{\text{int}}}{m} \tag{1.20}$$

This result is very similar to Eq. (1.11), describing the transport of translational energy, the only difference being in the nature of the specific heat. Equation (1.20) can describe qualitatively the transport of rotational energy of nonpolar molecules.

(b) $Z_{\text{int}} \gg 1$
In this case, many collisions are necessary to exchange a quantum of internal energy, i.e. the mean free path for energy exchange l_{int} is much larger than the collision mean free path l_{c}. At the same time, the average velocity to be used in Eq. (1.5), C', decreases. It can be shown that

$$l_{\text{int}} = \sqrt{Z_{\text{int}}}l_{\text{c}} \tag{1.21}$$

$$C' = \frac{C}{\sqrt{Z_{\text{int}}}} \tag{1.22}$$

so that, again,

$$\lambda_{\text{int}} = \eta\frac{c^{\text{int}}}{m} \tag{1.23}$$

(c) $Z_{\text{int}} < 1$
Less than one collision is necessary to exchange an internal quantum, i.e. the mean free path for energy exchange l_{int} is smaller than the collision mean free path l_{c}, whereas the average velocity does not change:

$$l_{\text{int}} = Z_{\text{int}}l_{\text{c}} \tag{1.24}$$

$$C' = C \tag{1.25}$$

In this case we obtain, after some algebraic manipulations,

$$\lambda_{\text{int}} = Z_{\text{int}}\eta\frac{c^{\text{int}}}{m} \tag{1.26}$$

The internal thermal conductivity decreases by a factor Z_{int} as compared to the previous cases. The transport of rotational energy of polar molecules follows this result.

1.2 Kinetic Theory of Transport Processes in Dilute Polyatomic Gases

Kinetic theory of transport processes in dilute polyatomic gases has been discussed in several fundamental monographs (Chapman and Cowling 1970; Hirschfelder et al. 1966; Ferziger and Kaper 1972; McCourt et al. 1990). More recently, a number of studies have given an exposition of the theoretical framework while addressing more in detail thermal non-equilibrium (Nagnibeda and Kustova 2009) or the mathematical properties of the transport linear systems and the derivation of efficient computational algorithms (Ern and Giovangigli 1994). Complementary to these works, the book by Zhdanov (2002) discusses transport phenomena in multicomponent plasmas in the framework of the Grad method (Grad 1949).

Here, we consider a semiclassical framework in which the translational motion is treated classically and the internal motion quantum mechanically (Chang and Uhlenbeck 1970).

In the derivation, a symmetry condition on the quantum cross sections arises, analogous to the classical assumption of the existence of inverse collisions, which is satisfied by the use of degeneracy-averaged cross sections (Waldmann 1958; Mason and Monchick 1962).

The same results can be obtained from the quantum mechanical Waldmann–Snider (Waldmann 1957; Snider 1960) equation by pre-averaging the cross sections over all magnetic quantum numbers (McCourt and Snider 1964; Millat et al. 1988). This isotropic approximation is valid in the absence of polarisation effects (McCourt and Snider 1964; Viehland et al. 1978; Millat et al. 1988); therefore, it cannot describe the effects of magnetization or electrical polarization of the gas medium on transport properties.

The extension of the semiclassical theory to dilute polyatomic gas mixtures was given by Waldmann and Trübenbacher (1962) and by Monchick et al. (1963). Both formulations yield identical transport coefficients, the difference being in the structure of the linear systems. The former treatment yields constrained singular symmetric forms that are inverted at lower computational cost and lend themselves to simpler analytic approximations (Ern and Giovangigli 1994).

The original equation is generalized to reactive mixtures with the introduction of chemical source terms (Ludwig and Heil 1960; Grunfeld 1993; Alexeev et al. 1994; Ern and Giovangigli 1998).

As we will see in Chap. 9, this approach can be extended to treat ionized mixtures as long as the electromagnetic fields are not strong enough to perturb the collision dynamics.

For a reactive gas mixture composed of n^s chemical species having internal degrees of freedom, the state of the system is described in terms of single-particle distribution functions $f_i(t, \boldsymbol{r}, \boldsymbol{c}, I)$ where i is the index of the species, t the time, $\boldsymbol{r}$ the spatial coordinate, $\boldsymbol{c}$ the velocity and I is a set of quantum numbers describing the internal energy state.

The form of the Boltzmann equation is

$$\mathscr{D}_i(f) = \mathscr{S}_i(f) + \mathscr{C}_i(f), \quad i = 1, \dots n^s \tag{1.27}$$

$\mathscr{D}_i$ is the streaming operator describing the advection of particles under the action of the external fields:

$$\mathscr{D}_i(f) = \partial_t f_i + \boldsymbol{c}_i \cdot \partial_{\boldsymbol{r}} f_i + \boldsymbol{b}_i \cdot \partial_{\boldsymbol{c}} f_i \tag{1.28}$$

where $\boldsymbol{b}_i$ is any volume force acting on species i.

The nonreactive collision integral $\mathscr{S}_i$ takes the form (Giovangigli and Graille 2003):

$$\mathscr{S}_i(f) = \sum_j \sum_{I'JJ'} \int \left(f_i' f_j' \frac{\alpha_{iI}\alpha_{jJ}}{\alpha_{iI'}\alpha_{jJ'}} - f_i f_j \right) W_{ij}^{IJI'J'} \mathrm{d}\boldsymbol{c}_j \mathrm{d}\boldsymbol{c}_i' \mathrm{d}\boldsymbol{c}_j' \tag{1.29}$$

where α_{iI} is the degeneracy of the quantum state identified by the set I of quantum numbers and $W_{ij}^{IJI'J'}$ the transition probability. The following reciprocity relations hold for transition probabilities:

$$\alpha_{iI}\alpha_{jJ} W_{ij}^{IJI'J'} = \alpha_{iI'}\alpha_{jJ'} W_{ij}^{I'J'IJ} \tag{1.30}$$

Transition probabilities can be expressed in terms of cross sections via:

$$g\sigma^{IJI'J'} \mathrm{d}\boldsymbol{e}' = W^{I'J'IJ} \mathrm{d}\boldsymbol{c}_i' \mathrm{d}\boldsymbol{c}_j' \tag{1.31}$$

where g is the relative speed of the particles before collision and $\boldsymbol{e}'$ the direction of the relative velocity after the collision.

The reactive source term $\mathscr{C}_i(f)$ results from chemical reactions between species in the mixture. We consider an arbitrary reaction mechanism, including, in particular, bimolecular and trimolecular chemical reactions. Explicit expressions for the collision integrals are reported in Giovangigli and Graille (2003) and Nagnibeda and Kustova (2009).

1.2.1 Conservation Equations

Given the set of species indices $S = \{1, \dots, n^s\}$ and two families of functions $\xi = (\xi_i)_{i \in S}$ and $\zeta = (\zeta_i)_{i \in S}$, we follow Giovangigli and Graille (2009) and define the scalar product:

$$\langle\!\langle \xi, \zeta \rangle\!\rangle = \sum_{i,I} \int \xi_i : \bar{\zeta}_i \mathrm{d}\boldsymbol{c}_i \tag{1.32}$$

where $\xi_i : \bar{\zeta}_i$ denotes the maximum contracted product between the tensor ξ_i and the complex conjugate of tensor ζ_i.

Let ϕ be an arbitrary function of the molecular properties. The average value is defined as

$$\bar{\phi} = \langle\langle f, \phi \rangle\rangle \tag{1.33}$$

The flux of the quantity is defined by

$$\boldsymbol{\Phi} = \langle\langle f, \phi \boldsymbol{C} \rangle\rangle \tag{1.34}$$

where $\boldsymbol{C} = \boldsymbol{c} - \boldsymbol{v}$ is the *peculiar* velocity, i.e. the molecular velocity relative to the hydrodynamic velocity.

Taking the scalar product of the Boltzmann equation (1.27) with respect to ϕ provides an equation for the rate of change of $\bar{\phi}$.

Of particular importance is the rate of change for properties that do not change during collision (collisional invariants).

The scalar collisional invariants of the nonreactive collision operator form a linear space spanned by $\psi^l, l \in \{1, \ldots, n^s + 4\}$ with

$$\psi^l = \begin{cases} (\delta_{il})_{i \in S} & l \in S \\ (m_i c_{iv})_{i \in S} & l = n^s + v, v \in \{1, 2, 3\} \\ (\frac{1}{2} m_i c_i^2 + E_{iI})_{i \in S} & l = n^s + 4, \end{cases} \tag{1.35}$$

where c_{iv} is the component of $\boldsymbol{c}_i$ in the vth spatial coordinate and E_{iI} is the energy of the internal state of species i with quantum numbers I. On the other hand, the collisional invariants of the complete collision operator are constituted by the momentum and energy invariants together with the element invariants. These latter invariants are associated with the conservation of elements in chemical reactions (Ern and Giovangigli 1998).

The macroscopic properties, in particular, are written as

$$\langle\langle f, \psi^l \rangle\rangle = \begin{cases} n_l & l \in S \\ \rho v_v & l = n^s + v, v \in \{1, 2, 3\} \\ \frac{1}{2} \rho v^2 + \rho u & l = n^s + 4 \end{cases} \tag{1.36}$$

where n_i is the number density of the ith species, ρ the mixture mass density, $\boldsymbol{v}$ the mixture velocity and ρu the internal energy per unit volume.

For the collisional invariants, the contribution to the rate of change due to the collision operator vanishes and the equations turn into conservation equations for mass, momentum and energy, respectively:

$$\partial_t \rho_i + \partial_{\boldsymbol{r}} \cdot \rho_i \boldsymbol{v} + \partial_{\boldsymbol{r}} \cdot \rho_i \boldsymbol{V}_i = m_i \omega_i, \quad i \in S \tag{1.37a}$$

$$\partial_t \rho + \partial_{\boldsymbol{r}} \cdot \rho \boldsymbol{v} = 0 \tag{1.37b}$$

$$\partial_t (\rho \boldsymbol{v}) + \partial_{\boldsymbol{r}} \cdot (\mathbb{P} + \rho \boldsymbol{v}\boldsymbol{v}) = \sum_{i \in S} \rho_i \boldsymbol{b}_i \tag{1.37c}$$

$$\partial_t (\rho u + \tfrac{1}{2}\rho v^2) + \partial_{\boldsymbol{r}} \cdot \left[\boldsymbol{q} + (\rho u + \tfrac{1}{2}\rho v^2)\boldsymbol{v} + \mathbb{P} : \boldsymbol{v} \right] = \sum_{i \in S} \rho_i \boldsymbol{b}_i \cdot (\boldsymbol{v} + \boldsymbol{V}_i) \tag{1.37d}$$

where $\boldsymbol{V}_i, \mathbb{P}$ and $\boldsymbol{q}$ are the fluxes of chemical species, total momentum and total internal energy, respectively, and $m_i \omega_i$ is the macroscopic mass production rate for species i.

Note that the set of conservation Eqs. (1.37) is not closed until explicit expressions are provided for the fluxes.

Additional collisional invariants may be allowed by the particular choice of the collision integrals for each specific system of interest. This point will be discussed at length in the context of the treatment of systems out of thermal equilibrium (Chap. 8).

1.2.2 The Chapman–Enskog Method of Solution

A solution to the Boltzmann equation (1.27) is obtained by the perturbative Chapman–Enskog method (Ferziger and Kaper 1972).

The foundation of the method is the assumption that a hydrodynamic description is possible, i.e. that the equations governing the dynamics of the macroscopic variables depend explicitly on the macroscopic variables themselves and their spatial derivatives. In particular, they do not depend explicitly on time and on higher moments of the distribution function. This is equivalent to assuming that the characteristic timescale of the flow is much larger than the molecular timescale. It is therefore possible to introduce the ratio of the two as a small parameter, ϵ. Since the collisional invariants do not change in collision, the collisions do not affect the macroscopic variables directly and we can formally rewrite Eq. (1.27) as:

$$\mathscr{D}_i(f) = \frac{1}{\epsilon}\mathscr{S}_i(f) + \mathscr{C}_i(f) \quad i \in S \tag{1.38}$$

Solutions are then sought in the form

$$f_i = f_i^0(1 + \epsilon\phi_i + \mathcal{O}(\epsilon^2)) \quad i \in S \tag{1.39}$$

The perturbation analysis of Eq. (1.38) assumes the characteristic chemical times are larger than the mean free times of the molecules. In this scenario, called the *tempered reaction regime*, a frozen local equilibrium is achieved at the zeroth order and the chemical reactions act as a first-order perturbation:

the pressure tensor is modified with a relaxation pressure effect and the chemistry source terms in the species conservation equations are modified by first-order corrections. First discussed in Prigogine and Xhrouet (1949) these corrections have been worked out in detail in Kustova and Giordano (2011).

Different regimes can also be tackled by weighting differently different contributions in the transport kinetic Eqs. (1.27) (Alexeev et al. 1994; Ern and Giovangigli 1998; Nagnibeda and Kustova 2009).

1.2.3 Zero Order

Substituting the expansion (1.39) in the kinetic equations (1.38) we get to the lowest order in ϵ:

$$\mathscr{S}_i(f^0) = 0 \quad i \in S \tag{1.40}$$

It can be shown that the solution of this equation must be in the form

$$\log\left(\beta_{iI} f_i^0\right) = \alpha_i - \beta \cdot m_i \boldsymbol{c}_i - \gamma(\tfrac{1}{2} m_i c_i^2 + E_{iI}) \tag{1.41}$$

where $\beta_{iI} = \frac{{h_\mathrm{P}}^3}{\alpha_{iI} m_i^3}$ and h_P is the Planck constant. The parameters in Eq. (1.41) are arbitrary functions of space and time. They are defined by requiring that f^0 yields the local macroscopic properties:

$$\langle\!\langle f^0, \psi^l \rangle\!\rangle = \langle\!\langle f, \psi^l \rangle\!\rangle \quad l \in \{1, \ldots, n^s + 4\} \tag{1.42}$$

As a result,

$$f_i^0 = \frac{n_i}{\beta_{iI} Q_i} \exp\left(-\frac{m_i}{2k_\mathrm{B}T} C_i^2 - \frac{E_{iI}}{k_\mathrm{B}T}\right) \tag{1.43}$$

where T is the temperature and Q_i the full partition function per unit volume of the ith species:

$$Q_i = Q_i^{\mathrm{int}} Q_i^{\mathrm{tr}} \tag{1.44}$$

$$Q_i^{\mathrm{tr}} = \left(\frac{2\pi m_i k_\mathrm{B} T}{{h_\mathrm{P}}^2}\right)^{3/2} \tag{1.45}$$

$$Q_i^{\mathrm{int}} = \sum_I \alpha_{iI} \exp\left(-\frac{E_{iI}}{k_\mathrm{B}T}\right) \tag{1.46}$$

Using this solution, the fluxes of mass, momentum and energy can be evaluated to give

$$\boldsymbol{V}_i = 0, \quad i \in S \tag{1.47}$$
$$\boldsymbol{q} = 0 \tag{1.48}$$
$$\mathbb{P} = p\mathbb{I}, \quad p = nk_{\mathrm{B}}T \tag{1.49}$$

and the corresponding conservation equations are the inviscid Euler equations:

$$\partial_t \rho_i + \partial_{\boldsymbol{r}} \cdot \rho_i \boldsymbol{v} = m_i \omega_i^0, \quad i \in S \tag{1.50a}$$
$$\partial_t \rho + \partial_{\boldsymbol{r}} \cdot \rho \boldsymbol{v} = 0 \tag{1.50b}$$
$$\partial_t (\rho \boldsymbol{v}) + \partial_{\boldsymbol{r}} \cdot (p\mathbb{I} + \rho \boldsymbol{v}\boldsymbol{v}) = \sum_i \rho_i \boldsymbol{b}_i \tag{1.50c}$$
$$\partial_t (\rho u + \tfrac{1}{2}\rho v^2) + \partial_{\boldsymbol{r}} \cdot \left[(\rho u + \tfrac{1}{2}\rho v^2 + p)\boldsymbol{v}\right] = \sum_i \rho_i \boldsymbol{b}_i \cdot \boldsymbol{v} \tag{1.50d}$$

The zeroth-order chemistry production terms are given by

$$\omega_i^0 = \langle\!\langle \psi^i, \mathscr{C}(f^0) \rangle\!\rangle = \sum_I \int \mathscr{C}_i(f^0) \mathrm{d}\boldsymbol{c}_i, \quad i \in S \tag{1.51}$$

and they are compatible with the law of mass action and classical thermochemistry.

1.2.4 First Order

The first-order kinetic equations for the unknowns $\phi = (\phi_i)_{i \in S}$ are:

$$\mathscr{F}_i^{\mathscr{S}}(\phi) = -\mathscr{D}_i(\log f_i^0) + \frac{\mathscr{C}_i(f^0)}{f_i^0} \equiv \Psi_i \quad i \in S \tag{1.52}$$

where the linearized Boltzmann operator is defined as:

$$\mathscr{F}_i^{\mathscr{S}}(\phi) = \sum_{j \in S} \sum_{I'JJ'} \int f_j^0 (\phi_i + \phi_j - \phi_i' - \phi_j') W_{ij}^{IJI'J'} \mathrm{d}\boldsymbol{c}_j \mathrm{d}\boldsymbol{c}_i' \mathrm{d}\boldsymbol{c}_j' \quad i \in S \tag{1.53}$$

This operator has the important property of being rotationally invariant (isotropic), i.e. it converts a tensor constructed from $(\boldsymbol{c}_i)_{i \in S}$ into another tensor of the same type.

The RHS of the equation is evaluated from the zero-order conservation equations (1.50).

Explicit evaluation gives

$$\Psi_i = \Psi_i^f + \Psi_i^r \tag{1.54}$$

The first term is a frozen, i.e. nonreactive, term:

$$\Psi_i^f = -\Psi_i^\eta : \nabla \boldsymbol{v} - \tfrac{1}{3}\Psi_i^\kappa \nabla \cdot \boldsymbol{v} - p\sum_{j\in S}\Psi_i^{D_j}\cdot \boldsymbol{d}_j - \Psi_i^{\lambda'}\nabla\frac{1}{k_{\mathrm{B}}T} \tag{1.55}$$

where

$$\Psi_i^\eta = 2(\boldsymbol{w}_i\boldsymbol{w}_i - \tfrac{1}{3}w_i^2\mathbb{I}) \tag{1.56}$$

$$\Psi_i^\kappa = 2\frac{c_i^{\mathrm{int}}}{c_{\mathrm{V}}}(\boldsymbol{w}_i\cdot\boldsymbol{w}_i - \tfrac{3}{2}) + 2\frac{c^{\mathrm{tr}}}{c_{\mathrm{V}}}(\bar{\epsilon}_i - \epsilon_{iI}) \tag{1.57}$$

$$\Psi^{D_i} = \frac{1}{p_i}(\delta_{il} - y_i)\boldsymbol{C}_i \tag{1.58}$$

$$\Psi_i^{\lambda'} = k_{\mathrm{B}}T(\tfrac{5}{2} - w_i^2 + \bar{\epsilon}_i - \epsilon_{iI})\boldsymbol{C}_i \tag{1.59}$$

and we have used the following definitions:

$$\boldsymbol{d}_i = \nabla\left(\frac{n_i}{n}\right) + \left(\frac{n_i}{n} - \frac{\rho_i}{\rho}\right)\nabla\log p + \frac{\rho}{p}\sum_{j\in S} y_i y_j(\boldsymbol{b}_j - \boldsymbol{b}_i) \tag{1.60}$$

$$y_i = \frac{\rho_i}{\rho} \tag{1.61}$$

$$\boldsymbol{w}_i = \sqrt{\frac{m_i}{2k_{\mathrm{B}}T}}\boldsymbol{C}_i \tag{1.62}$$

$$\epsilon_{iI} = \frac{E_{iI}}{k_{\mathrm{B}}T} \tag{1.63}$$

$$\bar{\epsilon}_i = \frac{\sum_I \alpha_{iI}\epsilon_{iI}e^{-\epsilon_{iI}}}{Q_i^{\mathrm{int}}} \tag{1.64}$$

and the specific heats are as follows:

$$c^{\mathrm{tr}} = \tfrac{3}{2}k_{\mathrm{B}} \tag{1.65}$$

$$c_i^{\mathrm{int}} = \frac{\partial \bar{E}_i}{\partial T} \tag{1.66}$$

$$c^{\mathrm{int}} = \sum_{i\in S}\frac{n_i}{n}c_i^{\mathrm{int}} \tag{1.67}$$

$$c_{\mathrm{V}} = c^{\mathrm{tr}} + c^{\mathrm{int}} \tag{1.68}$$

Ψ_i^r is due to chemical reactions:

$$\Psi_i^r = \frac{\mathscr{C}_i(f^0)}{f_i^0} - \frac{\omega_i^0}{n_i} - \frac{\sum_{j\in S}(\frac{3}{2} + \bar{\epsilon}_j + h_{fj})\omega_j^0}{nc_{\mathrm{V}}/k_{\mathrm{B}}}(\tfrac{3}{2} - w_i^2 + \bar{\epsilon}_i - \epsilon_{iI}) \tag{1.69}$$

where $h_{fi} = \frac{H_{fi}}{k_{\mathrm{B}}T}$ is the reduced formation energy of species i.

Equation (1.52) is then a inhomogeneous Fredholm integral equation of the second kind. Its solubility is guaranteed by the requirement that the Eqs. (1.50) be satisfied and the solutions are determined uniquely from the constraints:

$$\langle\!\langle f^0\phi, \psi^l \rangle\!\rangle = 0 \quad l \in \{1, \ldots, n^s + 4\} \tag{1.70}$$

From Eqs. (1.50)–(1.52) with the constraints Eq. (1.70), making use of the linearity and isotropy properties of the linear Boltzmann operator, it follows ϕ_i can be cast in the form

$$\phi_i = \phi_i^f - \phi_i^r \tag{1.71}$$

$$\phi_i^f = -\phi_i^\eta : \partial_{\boldsymbol{r}} \boldsymbol{v} - \tfrac{1}{3}\phi_i^\kappa \partial_{\boldsymbol{r}} \cdot \boldsymbol{v} - p \sum_{j \in S} \phi_i^{D_j} \cdot \boldsymbol{d}_j - \phi_i^{\lambda'} \cdot \partial_{\boldsymbol{r}} \left(\frac{1}{k_\mathrm{B} T} \right) \tag{1.72}$$

Equation (1.52) therefore splits into separate equations for the different ϕ_i^μ:

$$\mathscr{F}_i^{\mathscr{S}}(\phi^\mu) = \Psi_i^\mu \tag{1.73}$$

with the constraints

$$\langle\!\langle f^0 \phi^\mu, \psi^l \rangle\!\rangle = 0 \tag{1.74}$$

With the expressions (1.71) and (1.72), we can formally evaluate the fluxes:

$$\boldsymbol{V}_i = -\sum_{j \in S} D_i^j \boldsymbol{d}_j - D_i^T \nabla \log T, \quad i \in S \tag{1.75}$$

$$\mathbb{P} = (p - \kappa \partial_{\boldsymbol{r}} \cdot \boldsymbol{v} - p^{\mathrm{rel}})\mathbb{I} - 2\eta \mathbb{S} \tag{1.76}$$

where $\mathbb{S} = \frac{1}{2}(\partial_{\boldsymbol{r}} \boldsymbol{v} + \widetilde{\partial_{\boldsymbol{r}} \boldsymbol{v}}) - \frac{1}{3}\partial_{\boldsymbol{r}} \cdot \boldsymbol{v}$ and $\tilde{\mathbb{A}}$ is the transpose of matrix $\mathbb{A}$.

$$\boldsymbol{q} = -\lambda' \nabla T - p \sum_{i \in S} D_i^T \boldsymbol{d}_i + \sum_{i \in S} n_i H_i \boldsymbol{V}_i \tag{1.77}$$

with $H_i = \frac{5}{2} k_\mathrm{B} T + \bar{E}_i + H_{fi}$ and where the transport coefficients are given by[1]

$$D_i^j = \tfrac{1}{3} p k_\mathrm{B} T [\![\phi^{D_i}, \phi^{D_j}]\!] \tag{1.78a}$$

$$D_i^T = -\tfrac{1}{3} [\![\phi^{D_i}, \phi^{\lambda'}]\!] \tag{1.78b}$$

[1] Note that different symbols are found in literature for multicomponent and thermal diffusion coefficients, i.e. $D_{ij} \equiv D_i^j$ and $D_{Ti} \equiv D_i^T$.

$$\lambda' = \tfrac{1}{3}\frac{1}{k_B T^2}[\![\phi^{\lambda'}, \phi^{\lambda'}]\!] \tag{1.78c}$$

$$\eta = \tfrac{1}{10} k_B T [\![\phi^{\eta}, \phi^{\eta}]\!] \tag{1.78d}$$

$$\kappa = \tfrac{1}{9} k_B T [\![\phi^{\kappa}, \phi^{\kappa}]\!] \tag{1.78e}$$

$$p^{\mathrm{rel}} = \tfrac{1}{3} k_B T [\![\phi^{\kappa}, \phi^{r}]\!] \tag{1.78f}$$

where the bracket operator is defined by

$$[\![a, b]\!] = \langle\!\langle f^0 a, \mathscr{F}^{\mathscr{S}}(b) \rangle\!\rangle \tag{1.79}$$

where $a = (a_i)_{i\in S}$ and $b = (b_i)_{i\in S}$. The bracket operator is hermitian, positive semi-definite and its kernel is spanned by the collisional invariants, i.e. $[\![a, a]\!] = 0$ implies a is a collisional invariant.

Note also that the perturbed distribution function ϕ^r that depends on the reactive source term $\mathscr{C}_i$ only enters the calculation of the relaxation pressure, Eq. (1.78f) and the chemical production rates, ω_i, in Eq. (1.37a).

1.2.5 True Thermal Conductivity

Rewrite here Eq. (1.77) for the heat flux:

$$\boldsymbol{q} = -\lambda' \nabla T - p \sum_{i\in S} D_i^T \boldsymbol{d}_i + \sum_{i\in S} n_i H_i \boldsymbol{V}_i \tag{1.80}$$

Performing a direct experimental measurement of λ' in a gas mixture is impossible since a temperature gradient induces thermal diffusion and thus concentration gradients. The coefficient is therefore termed *partial* thermal conductivity.

It is useful to define the thermal diffusion ratios, $k^T = (k_i^T)_{i\in S}$,

$$\sum_{j\in S} D_i^j k_j^T = D_i^T, \quad i \in S \tag{1.81}$$

$$\sum_{i\in S} k_i^T = 0 \tag{1.82}$$

and the *true* thermal conductivity

$$\lambda = \lambda' - \frac{p}{T} \sum_{i\in S} D_i^T k_i^T \tag{1.83}$$

so that the heat flux and the diffusion velocities can be rewritten as

$$\boldsymbol{V}_i = -\sum_{j\in S} D_i^j \left(\boldsymbol{d}_j + k_j^T \nabla \log T\right), \quad i \in S \tag{1.84}$$

$$\boldsymbol{q} = -\lambda \nabla T + \sum_{i\in S} \left(pk_i^T + n_i H_i\right) \boldsymbol{V}_i \tag{1.85}$$

λ is now directly measurable in a heat conduction experiment at steady state, where all diffusion velocities vanish. Also, note that $\lambda = \lambda'$ for a pure gas.

It is, however, desirable to have a means to directly evaluate λ and the thermal diffusion ratios without the intermediate calculation of D_i^j, λ' and D_i^T. Defining

$$\phi^\lambda = \phi^{\lambda'} + pk_\mathrm{B} T \sum_{i\in S} k_i^T \phi^{D_i} \tag{1.86}$$

$$\Psi^\lambda = \Psi^{\lambda'} + pk_\mathrm{B} T \sum_{i\in S} k_i^T \Psi^{D_i} \tag{1.87}$$

it is easy to show, by linearity, that

$$\mathscr{F}_i^{\mathscr{S}}(\phi^\lambda) = \Psi_i^\lambda \tag{1.88}$$

$$\langle\!\langle f^0 \phi^\lambda, \psi^l \rangle\!\rangle = 0 \tag{1.89}$$

that, using Eqs. (1.78), yields

$$\lambda = \frac{1}{3k_\mathrm{B} T^2} [\phi^\lambda, \phi^\lambda] \tag{1.90}$$

$$k_i^T = \frac{m_i}{3pk_\mathrm{B} T} [\varphi^i, \phi^\lambda], \quad i \in S \tag{1.91}$$

where $\varphi^i \equiv (\boldsymbol{C}_i \delta_{ij})_{j\in S}$.

The difference between λ and λ' is accounted for by thermal diffusion effects. These are usually very small except for the case of electrons. Figure 1.2 shows the λ and λ' thermal conductivities of equilibrium air at atmospheric pressure. Differences between the two coefficients appear only when the electron contribution becomes substantial.

1.2.6 Electric Current

Define the electric charge density

$$\rho_e = \sum_{i\in S} n_i e_i \tag{1.92}$$

where $(e_i)_{i\in S}$ are the species electric charges, and the electric current density

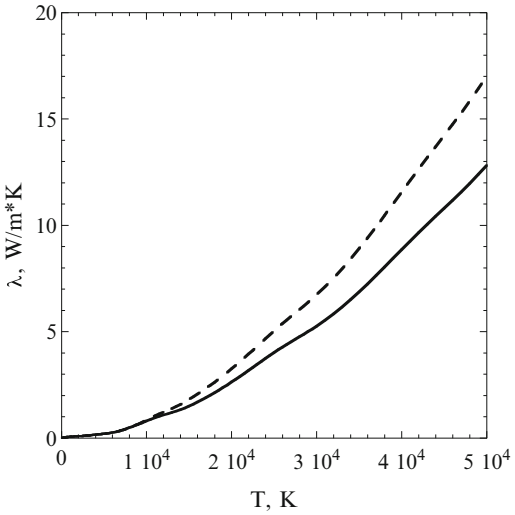

Fig. 1.2 Translational thermal conductivities of equilibrium air plasma at p=1 atm. *Solid line*: λ; *dashed line*: λ'

$$\boldsymbol{j}_e = \sum_{i \in S} n_i e_i \boldsymbol{V}_i \tag{1.93}$$

Assuming that there are only electromagnetic forces,

$$\boldsymbol{b}_i = \frac{e_i}{m_i} \boldsymbol{E}' \tag{1.94}$$

where $\boldsymbol{E}' = \boldsymbol{E} + \boldsymbol{v} \times \boldsymbol{B}$ is the electric field in the frame moving with the gas. Substituting from Eq. (1.75)

$$\boldsymbol{j}_e = -\sum_{i,j \in S} \sigma_i^j \boldsymbol{d}'_j - \sum_{i \in S} \varphi_i^T \nabla T \tag{1.95}$$

where

$$\begin{aligned} \boldsymbol{d}'_i &\equiv \frac{p}{\rho_i} \left[\frac{e_i}{m_i} - \frac{\rho_e}{\rho} \right]^{-1} \boldsymbol{d}_i \\ &= \frac{p}{\rho_i} \left[\frac{e_i}{m_i} - \frac{\rho_e}{\rho} \right]^{-1} \left[\nabla \left(\frac{n_i}{n} \right) + \left(\frac{n_i}{n} - \frac{\rho_i}{\rho} \right) \nabla \log p \right] - \boldsymbol{E}', \quad i \in S \end{aligned} \tag{1.96}$$

and the electrical conductivities and electrothermal coefficients are, respectively,

$$\sigma_i^j = \frac{n_i e_i}{p} D_i^j \rho_j \left(\frac{e_j}{m_j} - \frac{\rho_e}{\rho} \right) \tag{1.97}$$

$$\varphi_i^T = \frac{n_i e_i}{T} D_i^T \tag{1.98}$$

For the particular case of a *quasineutral* plasma in *equilibrium* (i.e. without macroscopic gradients) we have

$$\rho_e = 0 \tag{1.99}$$
$$\boldsymbol{d}_i' = -\boldsymbol{E}', \quad i \in S \tag{1.100}$$

and the electric current density is given by

$$\boldsymbol{j}_e = \sigma_e \boldsymbol{E}' \tag{1.101}$$

with

$$\sigma_e = \sum_{i,j \in S} \sigma_i^j = \frac{1}{p} \sum_{i,j \in S} n_i e_i D_i^j n_j e_j \tag{1.102}$$

1.2.7 Transport Linear Systems

The linearized Boltzmann equation (1.73) is solved approximately with a variational procedure using polynomial expansions.

The transport coefficients are then generally obtained as

$$\mu = \langle\!\langle f^0 \phi^\mu, \Psi^\mu \rangle\!\rangle \tag{1.103}$$

Given the basis set (ξ^{rk}), the distribution functions ϕ^μ are expanded in the form

$$\phi^\mu = \sum \alpha_{rk}^\mu \xi^{rk} \tag{1.104}$$

The variational procedure applied to the integral Eq. (1.73) then yields the system

$$[\![\xi^{rk}, \phi^\mu]\!] = \langle\!\langle \xi^{rk}, \Psi^\mu \rangle\!\rangle \tag{1.105}$$

which must be solved under the constraints (1.74). The relations (1.105) yield a linear system:

$$\sum_{sl} G_{kl}^{rs} \alpha_{sl}^\mu = \beta_{rk}^\mu \tag{1.106}$$

where

$$G_{kl}^{rs} = [\![\xi^{rk}, \xi^{sl}]\!] \tag{1.107}$$

$$\beta_{rk}^{\mu} = \langle\!\langle f^0 \xi^{rk}, \Psi^{\mu} \rangle\!\rangle \tag{1.108}$$

The $n + 4$ tensorial constraints (1.74) yield scalar constraints.

The basis functions ξ^{rk} are generally chosen as linear combinations of the functions ϕ^{a0cdk}:

$$\phi^{a0cdi}(\boldsymbol{c}_i, I) = S^c_{a+\frac{1}{2}}(w_i^2) W_i^d(\epsilon_{iI}) \mathbb{T}^a \tag{1.109}$$

where a, c and d are integers, $S^c_{a+\frac{1}{2}}$ the Sonine polynomial (Whittaker and Watson 1990) of order c with parameter $a + \frac{1}{2}$; W_i^d the Waldmann–Trübenbacher polynomials (Waldmann and Trübenbacher 1962) of order d for the ith species, and $\mathbb{T}^a$ is a tensor of rank a:

$$\mathbb{T}^0 = 1 \tag{1.110}$$

$$\mathbb{T}^1 = \boldsymbol{w}_i \tag{1.111}$$

$$\mathbb{T}^2 = \boldsymbol{w}_i \boldsymbol{w}_i - \tfrac{1}{3} w_i^2 \mathbb{I} \tag{1.112}$$

Therefore, in the notation ϕ^{a0cdi}, a refers to the rank order, $b = 0$ refers to the absence of polarization effects, c is the order of the Sonine polynomial, d is the order of the Waldmann–Trübenbacher polynomials and i is the species.

The polynomials used for expanding ϕ^{μ} are the Sonine polynomials (Whittaker and Watson 1990) for the dependence on the molecular velocity and the Waldmann–Trübenbacher polynomials (Waldmann and Trübenbacher 1962) for the dependence on the internal energies. The former are chosen since, for the particular case of Maxwell molecules, they are eigenvectors of the linearized (nonreactive) collision operator (Burnett 1935a,b). A detailed discussion of the merits of this particular choice has been done in Kumar (1966).

The transport linear systems are derived from a variational procedure used to solve constrained systems of linearized Boltzmann integral equations. They have a general mathematical structure inherited from the properties of Boltzmann linearized collision operators and the properties of usual variational approximation spaces associated with the transport linear systems. These features have been analysed in detail in Ern and Giovangigli (1994) where it has been shown that:

- The transport linear systems are well posed (i.e. admit a unique solution).
- The transport coefficients can be expanded as convergent series which yield approximate expressions by truncation.
- The real symmetric constrained singular semi-definite systems arising from multicomponent transport can be inverted very efficiently via iterative, conjugate gradient-type methods.

The results of this study have also been extended to the study of the anisotropic transport properties of magnetized plasmas (Giovangigli 2010).

The transport coefficients of dilute polyatomic gas mixtures have thus been expressed in terms of the solution of appropriate linear systems. These linear systems relate the transport coefficients to a series of collision cross sections describing the dynamical interaction between polyatomic molecules. However, solving these linear systems by direct methods (such as Gaussian elimination) presents two serious drawbacks. First, it does not provide expressions for the transport coefficients that can be written explicitly in a tractable manner for an arbitrary number of species in the mixture. Second, this approach is extremely expensive in computational models of multicomponent flows since the size of the linear systems can be relatively large and since transport properties have to be evaluated at each computational cell in space and time. Numerical algorithms devoted to solve the nonlinear discretized equations governing these flows may also proceed by iteration, such as Newton method, and this even increases the number of transport property evaluations. In this context, iterative methods offer an interesting alternative since they provide a rigorous way to define approximate transport coefficients by truncating convergent series. A general theory of iterative methods for evaluating transport coefficients in dilute polyatomic gas mixtures has been developed in Ern and Giovangigli (1994). Convergence theorems were presented in a rigorous mathematical framework that was extracted from the Boltzmann equation and from the variational procedure used to expand the species perturbed distribution functions. For a detailed discussion of the mathematical foundations and of the implementation of iterative methods for the determination of transport coefficients in reactive gas mixtures the reader is referred to the original work (Ern and Giovangigli 1994). These algorithms have also been extended to the case of plasmas with anisotropy effects caused by external magnetic fields (Giovangigli 2010).

1.2.8 Direct Evaluation of Heat and Mass Diffusion Fluxes

According to Eqs. (1.75) and (1.77), the evaluation of diffusion velocities and heat flux entails the calculation of the partial thermal conductivity, λ', the thermal diffusion coefficients, $\left(D_i^T\right)_{i\in S}$, and of the multicomponent diffusion coefficients, $\left(D_i^j\right)_{i,j\in S}$.

When the goal is the calculation of the fluxes, e.g. in a fluid dynamic simulation, and the explicit evaluation of the transport coefficients is of no interest, the algorithm developed by Kolesnikov (2002) can be applied successfully.

The first-order perturbation responsible for diffusion and thermal conduction is expanded:

$$\phi_i^\theta = -p \sum_{j \in S} \phi_i^{D_j} \cdot \boldsymbol{d}_j - \phi_i^{\lambda'} \cdot \partial_{\boldsymbol{r}} \left(\frac{1}{k_\mathrm{B} T} \right) = \sum_c \boldsymbol{\alpha}_{ci}^\theta \phi^{10c0i} \tag{1.113}$$

Substituting this expansion in the definition of the diffusion velocities

$$\begin{aligned} \boldsymbol{V}_i =& \langle\!\langle f, (\delta_{ij})_{j \in S} \boldsymbol{C} \rangle\!\rangle = \int \phi_i^\theta \boldsymbol{C}_i \mathrm{d}\boldsymbol{c}_i \\ =& \sum_c \boldsymbol{\alpha}_{ci}^\theta \int S_{\frac{3}{2}}^c (w_i^2) \boldsymbol{C}_i \mathrm{d}\boldsymbol{c}_i = \tfrac{1}{2} \sqrt{\frac{2k_\mathrm{B} T}{m_i}} \boldsymbol{\alpha}_{0i}^\theta \end{aligned} \tag{1.114}$$

where the properties of the Sonine polynomials have been used. Analogously, the translational heat flux vector due to the ith species is

$$\int \phi_i^\theta \left(\frac{m_i C_i^2}{2} \right) \boldsymbol{C}_i \mathrm{d}\boldsymbol{c}_i = \tfrac{5}{2} n_i k_\mathrm{B} T \cdot \left(\boldsymbol{V}_i - \tfrac{1}{2} \sqrt{\frac{2k_\mathrm{B} T}{m_i}} \boldsymbol{\alpha}_{1i}^\theta \right) \tag{1.115}$$

The integral equation for ϕ^θ is

$$\mathscr{F}_i^{\mathscr{S}}(\phi^\theta) = \Psi_i^\theta \quad i \in S \tag{1.116}$$

where

$$\Psi_i^\theta = -p \sum_{j \in S} \Psi_i^{D_j} \cdot \boldsymbol{d}_j - \Psi_i^{\lambda'} \nabla \frac{1}{k_\mathrm{B} T} \quad i \in S \tag{1.117}$$

Applying the methods of Sect. 1.2.7, the coefficients $\boldsymbol{\alpha}_{ci}^\theta$, and therefore the diffusion velocities and the translational heat flux, are obtained from the solution of a single linear system:

$$\sum_{dj} G_{ij}^{cd} \boldsymbol{\xi}_{dj}^\theta = \boldsymbol{\beta}_{ci}^\theta \tag{1.118}$$

where

$$G_{ij}^{cd} = \tfrac{25}{4} n k_\mathrm{B} \frac{2\sqrt{m_i m_j}}{3p} [\![\phi^{10c0i}, \phi^{10d0j}]\!] \tag{1.119}$$

$$\boldsymbol{\beta}_{ci}^\theta = -\delta_{c0} \boldsymbol{d}_i + \delta_{c1} \tfrac{5}{2} \frac{n_i}{n} \frac{\nabla T}{T} \tag{1.120}$$

$$\boldsymbol{\xi}_{ci}^\theta = \tfrac{1}{2} \sqrt{\frac{2k_\mathrm{B} T}{m_i}} \boldsymbol{\alpha}_{ci}^\theta \tag{1.121}$$

1.2.9 Onsager Reciprocal Relations and Alternative Formulations of the Transport Linear Systems

The Onsager relations are symmetry constraints which must hold between the transport coefficients. In the case of gases, these symmetry properties can directly be deduced from the kinetic theory of gases (de Groot and Mazur 1984). For an isotropic system, i.e. a gas mixture without magnetization, the Onsager reciprocal relations reduce to

$$D_i^j = D_j^i \tag{1.122}$$

Note, however, that the vectors $\phi_i^{D_j}$ are not uniquely determined by Eqs. (1.73) and (1.74). For $\mu = D_j$ we get, from Eq. (1.73) multiplied by $\frac{\rho_j}{\rho}$ and summed over j,

$$\sum_j \frac{\rho_j}{\rho} \mathscr{F}_i^{\mathscr{S}}(\phi^{D_j}) = \sum_j \frac{\rho_j}{\rho} \Psi_i^{D_j} = 0 \tag{1.123}$$

This implies that $\sum_j (\frac{\rho_j}{\rho}) \phi_i^{D_j}$ is a summational invariant and there is freedom to set a linear combination of the $\phi_i^{D_j}, \quad j \in S$ to a constant value. Waldmann and Trübenbacher (1962) chose to set

$$\sum_j \left(\frac{\rho_j}{\rho} \right) \phi_i^{D_j} = 0, \quad i \in S \tag{1.124}$$

This choice leads to symmetric diffusion coefficients that are formally compatible with Onsager reciprocal relations, Eq. (1.122):

$$D_i^j = D_j^i \tag{1.125}$$

$$D_i^i > 0 \tag{1.126}$$

This, together with Eq. (1.124), implies the diffusion coefficients and thermal diffusion coefficients are not linearly independent:

$$\sum_i \frac{\rho_i}{\rho} D_i^j = 0 \tag{1.127}$$

$$\sum_i \frac{\rho_i}{\rho} D_i^T = 0 \tag{1.128}$$

Symmetric diffusion coefficients have also been considered by Waldmann (1958), Chapman and Cowling (1970), Ferziger and Kaper (1972), and Curtiss (1968).

Some authors, however, opted for a different definition that destroys the natural symmetry of the diffusion coefficients. Among others, Monchick et al. (1963), Curtiss and Hirschfelder (1949), and Hirschfelder et al. (1966) have set

$$\phi_i^{D_i} = 0, \quad i \in S \tag{1.129}$$

that leads to

$$D_i^i = 0 \tag{1.130}$$

The symmetric formalism is to be preferred on grounds of theoretical consistency (Van de Ree 1967), critical for the treatment of reactive and polyatomic gas mixtures, and computational efficiency (Ern and Giovangigli 1994). The alternative formalism has been, however, very popular among users, therefore, it is worth pointing out that it gives completely equal results for the transport coefficients. In Chap. 2 we provide the necessary expressions that allow to link the two descriptions. Both formulations have been shown to yield completely equal results for the transport coefficients (Ern and Giovangigli 1994).

1.3 Internal Thermal Conductivity

In this section we discuss the contribution of the internal degrees of freedom to the thermal conductivity. We start by introducing the Eucken approximation before proceeding to a formal derivation from kinetic theory.

1.3.1 The Eucken Approach

For molecules possessing no internal degrees of freedom, viscosity and thermal conductivity are related by

$$\lambda = \tfrac{5}{2}\frac{c_{\mathrm{v}}}{m}\eta \tag{1.131}$$

Eucken (1913) suggested to extend the above expression to polyatomic gases as

$$\lambda = \left(\tfrac{5}{2}\frac{c^{\mathrm{tr}}}{m} + \frac{c^{\mathrm{int}}}{m}\right)\eta \tag{1.132}$$

In the framework of the Chapman–Enskog method, the Eucken formula, Eq. (1.132), can be justified and further improved. A simple polyatomic gas is considered as a mixture of molecules in different internal quantum states,

whereas the interaction between molecules is assumed to be independent of their internal state. Since the thermal diffusion term of a mixture of components with same mass and same intermolecular forces is zero, the heat flux vector $\boldsymbol{q}$ for such a mixture is

$$\boldsymbol{q} = -\lambda^{tr}\partial_{\boldsymbol{r}}T + \sum_i n_i H_i \boldsymbol{V}_i \tag{1.133}$$

where the sum on i runs on the internal states of the molecule, n_i, H_i and $\boldsymbol{V}_i$ are number density, enthalpy and diffusion velocity, respectively, of the ith internal state. The thermal conductivity coefficient, $\lambda' = \lambda$, has been given the superscript tr to emphasize that it describes the transport of kinetic energy exchanged in (elastic) collisions.

The enthalpy per particle can be written as

$$H_i = \tfrac{5}{2}k_{\mathrm{B}}T + E_i \tag{1.134}$$

i.e. the sum of translational and internal energy.

The diffusive term can be split in two parts:

$$\sum_i n_i H_i \boldsymbol{V}_i = \tfrac{5}{2}k_{\mathrm{B}}T\sum_i n_i \boldsymbol{V}_i + \sum_i n_i E_i \boldsymbol{V}_i \tag{1.135}$$

The first term for a mixture of quantum states of the same species (same mass and same intermolecular forces) is zero:

$$\begin{aligned}\sum_i n_i \boldsymbol{V}_i &= \sum_i n_i(\boldsymbol{v}_i - \boldsymbol{v}) \\ &= \sum_i n_i \boldsymbol{v}_i - n\boldsymbol{v} \\ &= \sum_i n_i \boldsymbol{v}_i - \frac{n}{\rho}\sum_j n_j m_j \boldsymbol{v}_j \\ &= \sum_i n_i \boldsymbol{v}_i - \frac{nm}{\rho}\sum_j n_j \boldsymbol{v}_j = 0\end{aligned}$$

The diffusion velocities can be obtained from the general expression, Eq. (1.75), using the relation, Eq. (1.127), among diffusion coefficients:

$$\boldsymbol{V}_i = -\left(\frac{n}{n_i}\right)\mathcal{D}\nabla\left(\frac{n_i}{n}\right) \tag{1.136}$$

$\mathcal{D} = \frac{n_i}{n}D_i^i$ being the self-diffusion coefficient. The main Eucken approximation is to consider the internal levels at equilibrium at the local temperature.

$$\boldsymbol{V}_i = -\left(\frac{n}{n_i}\right)\mathcal{D}\frac{\partial}{\partial T}\left(\frac{n_i}{n}\right)\partial_{\boldsymbol{r}}T \tag{1.137}$$

so that

$$\sum_i n_i H_i \boldsymbol{V}_i = -\sum_i n_i E_i \left(\frac{n}{n_i}\right) \mathcal{D} \frac{\partial}{\partial T} \left(\frac{n_i}{n}\right) \partial_{\boldsymbol{r}} T$$
$$= -n\mathcal{D} \sum_i E_i \frac{\partial}{\partial T} \left(\frac{n_i}{n}\right) \partial_{\boldsymbol{r}} T$$

Noting that the specific heat for internal energy is

$$c^{\mathrm{int}} = \frac{\partial \bar{E}_i}{\partial T} = \sum_i E_i \frac{\partial}{\partial T} \left(\frac{n_i}{n}\right) \tag{1.138}$$

we arrive at

$$\sum_i n_i H_i \boldsymbol{V}_i = -n\mathcal{D} c^{\mathrm{int}} \partial_{\boldsymbol{r}} T \tag{1.139}$$

The total heat flux can be therefore written as

$$\boldsymbol{q} = -\lambda \partial_{\boldsymbol{r}} T \tag{1.140}$$

with

$$\lambda = \lambda^{tr} + \lambda^{int} = \tfrac{5}{2} \frac{c^{\mathrm{tr}}}{m} \eta + \rho \mathcal{D} \frac{c^{\mathrm{int}}}{m} \tag{1.141}$$

so that Eq. (1.132) is generalized as

$$\lambda = \left(\tfrac{5}{2} \frac{c^{\mathrm{tr}}}{m} + \frac{\rho \mathcal{D}}{\eta} \frac{c^{\mathrm{int}}}{m} \right) \eta \tag{1.142}$$

The improvement comes from considering the Chapman–Enskog value for $\frac{\rho \mathcal{D}}{\eta}$ instead of the mean free path value of unity.

To summarize, the result (1.142) has been obtained under the following assumptions:

- The internal states are in thermal equilibrium at the local temperature.
- All molecules interact via the same force law, irrespective of their internal state.
- Inelastic collisions have been completely neglected.

The first assumption can be relaxed by providing a kinetic theory of gases in thermal non-equilibrium: this will be done in Chap. 8; the second assumption is reasonable for molecules with rotational or vibrational excitation so that the Eucken approach still gives satisfactory results for vibrational and rotational degrees of freedom. It does not work for the electronic degree of freedom since electronically excited states have transport cross sections dramatically increasing with the principal quantum number (see Chap. 7 and

Capitelli and Lamanna 1974); finally, in order to discuss the role of inelastic collisions on transport we have to resort to a full semiclassical kinetic theory to which we turn in the next section. This will also allow us to obtain a general expression of the internal thermal conductivity for gas mixtures.

1.3.2 Kinetic Theory Approach

The equations that determine the transport coefficients in the general case are Eq. (1.73) supplemented by the constraint, Eq. (1.74), that we rewrite here, specialized for $\mu = \lambda'$:

$$\mathscr{F}_i^{\mathscr{S}}(\phi^{\lambda'}) = \Psi_i^{\lambda'}, \quad i \in S \tag{1.143}$$

$$\langle\!\langle f^0 \phi^{\lambda'}, \psi^l \rangle\!\rangle = 0 \tag{1.144}$$

with

$$\begin{aligned} \Psi_i^{\lambda'} &= \left(\tfrac{5}{2} k_{\mathrm{B}} T - \tfrac{1}{2} m_i C_i^2 + \bar{\epsilon}_i - \epsilon_{iI}\right) \boldsymbol{C}_i \\ &= \sqrt{\frac{2(k_{\mathrm{B}}T)^3}{m_i}} (\phi^{1010i} + \phi^{1001i}) \end{aligned} \tag{1.145}$$

And the partial thermal conductivity is given by

$$\begin{aligned} \lambda' &= \frac{1}{3k_{\mathrm{B}}T^2} [\![\phi^{\lambda'}, \phi^{\lambda'}]\!] \\ &= \frac{1}{3k_{\mathrm{B}}T^2} \langle\!\langle f^0 \phi^{\lambda'}, \mathscr{F}^{\mathscr{S}}(\phi^{\lambda'}) \rangle\!\rangle \\ &= \frac{1}{3k_{\mathrm{B}}T^2} \langle\!\langle f^0 \phi^{\lambda'}, \Psi^{\lambda'} \rangle\!\rangle \end{aligned}$$

Applying the variational procedure described above, Sect. 1.2.7, the unknown function $\phi^{\lambda'}$ is expanded as

$$\phi_i^{\lambda'} = \sqrt{2 m_i k_{\mathrm{B}} T} \sum_{pq} \alpha_{pqi}^{\lambda'} \phi^{10pqi} \quad i \in S \tag{1.146}$$

and the coefficients $\alpha_{pqk}^{\lambda'}$ are determined from

$$\sum_j \sum_{rs} G_{ij}^{pq,rs} \alpha_{rsj}^{\lambda'} = \beta_{pqi}^{\lambda'} \tag{1.147}$$

where

$$G_{ij}^{pq,rs} = \frac{2\sqrt{m_i m_j}}{3p}[\![\phi^{10pqi}, \phi^{10rsj}]\!] \tag{1.148}$$

$$\begin{aligned}\beta_{pqi}^{\lambda'} &= \frac{\sqrt{2m_i}}{3p\sqrt{k_\mathrm{B}T}}\langle\!\langle f^0\phi^{10pqi}, \Psi^{\lambda'}\rangle\!\rangle \\ &= \frac{n_i}{n}\frac{c_\mathrm{p}^{\mathrm{tr}}}{k_\mathrm{B}}\delta_{10}^{pq} + \frac{n_i}{n}\frac{c_\mathrm{i}^{\mathrm{int}}}{k_\mathrm{B}}\delta_{01}^{pq}\end{aligned} \tag{1.149}$$

The constraint, Eq. (1.144) now reads

$$\sum_i \frac{\rho_i}{\rho}\alpha_{00i}^{\lambda'} = 0 \tag{1.150}$$

and, finally,

$$\begin{aligned}\lambda' &= \frac{p}{T}\left\langle \alpha^{\lambda'}, \beta^{\lambda'}\right\rangle \\ &= \frac{p}{T}\left(\left\langle \alpha_{10}^{\lambda'}, \beta_{10}^{\lambda'}\right\rangle + \left\langle \alpha_{01}^{\lambda'}, \beta_{01}^{\lambda'}\right\rangle\right) \\ &= \sum_{i\in S} n_i(c_\mathrm{p}^{\mathrm{tr}}\alpha_{10i}^{\lambda'} + c_\mathrm{i}^{\mathrm{int}}\alpha_{01i}^{\lambda'})\end{aligned} \tag{1.151}$$

In order to compare with the results of the previous section, Eq. (1.142), we perform an explicit evaluation to lowest order in the polynomials for a pure polyatomic gas:

$$\phi^{\lambda'} = \sqrt{2mk_\mathrm{B}T}[\alpha_{00}^{\lambda'}\phi^{1000} + \alpha_{10}^{\lambda'}\phi^{1010} + \alpha_{01}^{\lambda'}\phi^{1001}] \tag{1.152}$$

which is easily solved:

$$\alpha_{00}^{\lambda'} = 0 \tag{1.153}$$

$$\alpha_{10i}^{\lambda'} = \frac{\frac{c_\mathrm{p}^{\mathrm{tr}}}{k_\mathrm{B}}G^{01,01} - \frac{c_\mathrm{i}^{\mathrm{int}}}{k_\mathrm{B}}G^{10,01}}{G^{10,10}G^{01,01} - G^{10,01}G^{01,10}} \tag{1.154}$$

$$\alpha_{01i}^{\lambda'} = \frac{\frac{c_\mathrm{i}^{\mathrm{int}}}{k_\mathrm{B}}G^{10,10} - \frac{c_\mathrm{p}^{\mathrm{tr}}}{k_\mathrm{B}}G^{01,10}}{G^{10,10}G^{01,01} - G^{10,01}G^{01,10}} \tag{1.155}$$

In order to determine the thermal conductivity, the following collision integrals have to be evaluated:

$$G^{10,10} = \frac{2m}{3p}[\![\phi^{1010}, \phi^{1010}]\!] \tag{1.156}$$

$$G^{01,01} = \frac{2m}{3p}[\![\phi^{1001}, \phi^{1001}]\!] \tag{1.157}$$

$$G^{10,01} = G^{01,10} = \frac{2m}{3p}[\![\phi^{1010}, \phi^{1001}]\!] \tag{1.158}$$

Explicitly, each of these *bracket integrals* is a multiple integral:

$$[\![\xi,\zeta]\!] = \sum_{I,I',J,J'} \int f^0(\boldsymbol{c}_i) f^0(\boldsymbol{c}_j)(\xi_i + \xi_j - \xi_i' - \xi_j') : (\zeta_i + \zeta_j - \zeta_i' - \zeta_j') \sigma_{ij}^{IJI'J'} g d\Omega \mathrm{d}\boldsymbol{c}_i \mathrm{d}\boldsymbol{c}_j \quad (1.159)$$

where the sum runs over all possible transitions. With the standard reduction methods, explained, for example, in Chapter 7 of Ferziger and Kaper (1972), these integrals are expressed as

$$G^{10,10} = \frac{1}{2\mathcal{D}} \left(4A + \frac{25}{12} \frac{\lfloor (\Delta\epsilon)^2 \rfloor}{\Omega^{(1,1)}} \right) \quad (1.160)$$

$$G^{01,01} = \left(\frac{c^{\mathrm{int}}}{k_{\mathrm{B}} \mathcal{D}_{\mathrm{int}}} + \frac{3}{8} \frac{\lfloor (\Delta\epsilon)^2 \rfloor}{\Omega^{(1,1)} \mathcal{D}} \right) \quad (1.161)$$

$$G^{10,01} = G^{01,10} = -\frac{5}{8} \frac{\lfloor (\Delta\epsilon)^2 \rfloor}{\Omega^{(1,1)} \mathcal{D}} \quad (1.162)$$

where

$$\mathcal{D} = \frac{3 k_{\mathrm{B}} T}{8 n m \Omega^{(1,1)}} \quad (1.163)$$

$$\mathcal{D}_{\mathrm{int}} = \frac{3 k_{\mathrm{B}} T}{8 n m \Omega_{\mathrm{int}}^{(1,1)}} \quad (1.164)$$

$$A = \frac{\Omega^{(2,2)}}{2\Omega^{(1,1)}} \quad (1.165)$$

$$\Omega^{(1,1)} = \lfloor \gamma^2 - \gamma\gamma' \cos\chi \rfloor \quad (1.166)$$

$$\frac{c^{\mathrm{int}}}{k_{\mathrm{B}}} \Omega_{\mathrm{int}}^{(1,1)} = \lfloor \epsilon_I^0 ((\epsilon_I^0 - \epsilon_J^0)\gamma^2 - (\epsilon_{I'}^0 - \epsilon_{J'}^0)\gamma\gamma' \cos\chi) \rfloor \quad (1.167)$$

$$\epsilon_I^0 = \epsilon_I - \bar{\epsilon}_I \quad (1.168)$$

$$\Delta\epsilon = \epsilon_{I'} - \epsilon_I + \epsilon_{J'} - \epsilon_J \quad (1.169)$$

where the averaging operator $\lfloor . \rfloor$ is defined by

$$\lfloor a \rfloor = \sqrt{\frac{k_{\mathrm{B}} T}{\pi m}} \sum_{I,I',J,J'} \frac{\alpha_I \alpha_J}{Q^2} \int a \gamma^3 e^{-(\gamma^2 + \epsilon_I + \epsilon_J)} \sigma^{IJI'J'} d\Omega d\gamma \quad (1.170)$$

$$\gamma = g \sqrt{\frac{m}{4 k_{\mathrm{B}} T}} \quad (1.171)$$

Explicit expressions can only be obtained from the knowledge of the cross sections for the relevant inelastic collisions. For illustration purposes, we

assume that $\Delta\epsilon$ is a small quantity and derive the first two approximations. Assuming $\Delta\epsilon = 0$,

$$G^{10,10} = \frac{2A}{\mathcal{D}} \tag{1.172}$$

$$G^{01,01} = \frac{c^{\text{int}}}{k_{\text{B}}\mathcal{D}} \tag{1.173}$$

$$G^{10,01} = G^{01,10} = 0 \tag{1.174}$$

so that

$$\lambda' = \tfrac{75}{32}\frac{{k_{\text{B}}}^2 T}{m\Omega^{(2,2)}} + \tfrac{3}{8}\frac{k_{\text{B}}T}{m\Omega^{(1,1)}}c^{\text{int}} \tag{1.175}$$

This result is exactly equivalent to Eq. (1.142). A better approximation, due to Mason and Monchick (1962), assumes a hard sphere scattering for inelastic collisions:

$$(\Delta\epsilon)^2 \sin^2\chi = \tfrac{2}{3}(\Delta\epsilon)^2 \tag{1.176a}$$

$$g(\epsilon_I - \epsilon_J) = g'(\epsilon_{I'} - \epsilon_{J'}) \tag{1.176b}$$

so that

$$G^{10,10} = \frac{2\rho}{3k_{\text{B}}T}\left(4\Omega^{(2,2)} + \tfrac{25}{12}\frac{c^{\text{int}}}{k_{\text{B}}}\frac{1}{n\tau}\right) \tag{1.177}$$

$$G^{01,01} = \frac{2\rho}{3k_{\text{B}}T}\left(4\Omega^{(1,1)}\frac{c^{\text{int}}}{k_{\text{B}}} + \tfrac{25}{12}\frac{c^{\text{int}}}{k_{\text{B}}}\frac{1}{n\tau}\right) \tag{1.178}$$

$$G^{10,01} = G^{01,10} = -\frac{2\rho}{3k_{\text{B}}T}\tfrac{5}{4}\frac{c^{\text{int}}}{k_{\text{B}}}\frac{1}{n\tau} \tag{1.179}$$

where the relaxation time, τ, is defined as

$$\frac{1}{n\tau} = k_{\text{B}}\frac{c^{\text{tr}} + c^{\text{int}}}{c^{\text{tr}}c^{\text{int}}}\lfloor(\Delta\epsilon)^2\rfloor \tag{1.180}$$

and, finally, Eq. (1.142) is generalized:

$$\lambda' = \lambda'_{tr} + \lambda'_{\text{int}} \tag{1.181}$$

$$\lambda'_{tr} = \tfrac{5}{2}\frac{c^{\text{tr}}}{m}\eta\left(1 - \frac{c^{\text{int}}}{c^{\text{tr}}}\frac{\frac{5}{2}\eta - \rho\mathcal{D}}{2p\tau}\right) \tag{1.182}$$

$$\lambda'_{int} = \rho\mathcal{D}\frac{c^{\text{int}}}{m}\left(1 + \frac{\frac{5}{2}\eta - \rho\mathcal{D}}{2p\tau}\right) \tag{1.183}$$

The new terms in the brackets account for the contribution of inelastic collisions. They have been evaluated, for example, in Bruno and Giovangigli (2011) for a simple model gas.

Figure 1.3 shows the value of the second term in the bracket in Eq. (1.183). This is to be compared to unity. Note that this term does not depend on gas density. It can be a substantial contribution to the thermal conductivities, increasing as $p\tau$ decreases. It is also apparent that the approximations, Eqs. (1.176), break down when the inelastic collisions are fast enough. In order to put this results in context, Fig. 1.4 reports the value of $p\tau$ corresponding to the different values of the transition probability, p_0: most vibrational transitions lay above the $p_0 = 0.01$ curve, whereas most rotational transitions lay above the $p_0 = 0.1$ and only very fast transitions have smaller values for $p\tau$.

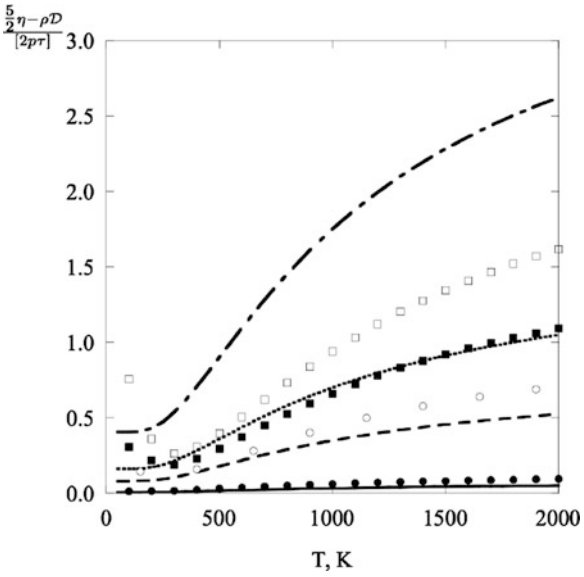

Fig. 1.3 Inelastic collision contribution to the internal thermal conductivity in Eq. (1.183). For the details of the physical model, refer to the original work (Bruno and Giovangigli 2011). The different curves refer to different values for the transition probability of inelastic collisions: p_0=0.01, 0.1, 0.2, 0.5, in increasing order. The symbols refer to the same conditions, but the collision integrals have been evaluated exactly

The transport of internal energy is a topic of current interest. Nowadays from the macroscopic point of view, one tends to abandon the local equilibrium distribution hypothesis by calculating the spatial gradients of the quantum states (see Chap. 6 and Nagnibeda and Kustova 2009). From the microscopic point of view a large effort is dedicated to understand the role of inelastic collisions in affecting the distribution function and therefore the transport coefficients. This calls for an estimation of the inelastic collision

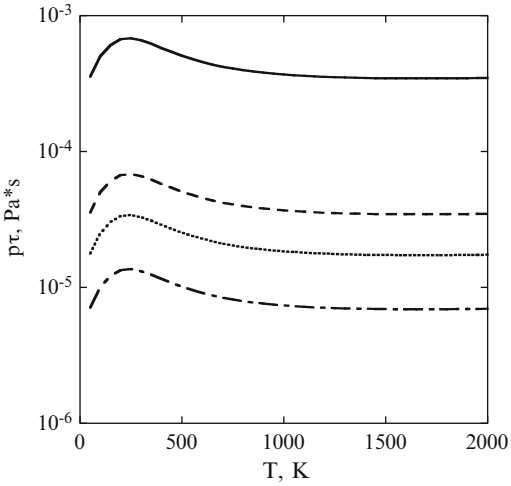

Fig. 1.4 $p\tau$ values corresponding to different values for the transition probability of inelastic collisions: p_0=0.01, 0.1, 0.2, 0.5. Increasing p_0 corresponds to smaller $p\tau$

integrals, Eqs. (1.160), (1.161), and (1.162). The Mason and Monchick hypothesis, Eqs. (1.176), amounts to assuming that the particles' trajectory in inelastic collisions is the same as for elastic encounters. While this is a reasonable assumption for rotationally inelastic transitions, the same cannot be said for vibrationally inelastic collisions. These cross sections are however much smaller than the elastic cross sections so that their effect should be not essential (Billing and Wang 1992).

1.4 Reactive Thermal Conductivity

In mixtures of gases in chemical equilibrium the thermal conductivity may be considerably higher than in "frozen" (nonreacting) mixtures. The mechanism responsible for the increased conductivity of reacting mixtures is as follows. In a pure gas, heat is conducted principally by molecular collisions, and the heat flux vector is directly proportional to the negative gradient of the temperature field: $\boldsymbol{q} = -A\nabla T$. The proportionality constant A is the thermal conductivity of the gas. In a mixture of gases which do not react, heat is also transferred by thermal diffusion; however, the quantity of heat transferred in this fashion rarely exceeds a few percent of that carried by molecular collisions. In practical cases it is usually neglected. When the components of a gas mixture react with one another, however, additional heat is transported as chemical enthalpy of molecules which diffuse in as much as concentration gradients exist in the mixture. These concentration gradients arise since the

equilibrium gas composition varies with temperature. For example, in a gas which absorbs heat by dissociating as the temperature is raised, heat is transferred when a molecule dissociates in the high-temperature region and diffuses towards the low-temperature region (since there is a lower concentration of dissociated molecules at low temperature). In the low-temperature region the gas recombines, releasing the heat absorbed from the high-temperature dissociation. This phenomenon was perhaps first recognized by Nernst (1904) who suggested that the high thermal conductivity of nitrogen dioxide be ascribed to this effect. Nernst further derived an expression for the thermal conductivity of a dissociating gas.

1.4.1 The Butler–Brokaw Theory

In order to estimate the reactive thermal conductivity we follow Butler and Brokaw (1957) and make the following assumptions:

1. The gas mixture is in thermal and chemical equilibrium.
2. Total pressure is uniform.
3. Thermal diffusion is negligible.
4. There are no external forces.
5. Diffusion is described by binary diffusion coefficients.

While the first two assumptions reflect the actual experimental conditions, the remaining are valid to a good extent for neutral gases only and will have to be improved.

The derivation proceeds as follows. Assume a mixture of n^s components $(X_i)_{i\in S}$. The convective heat flux describing the transport of enthalpy due to diffusion is defined by:

$$\boldsymbol{q}_{conv} = \sum_{i\in S} n_i H_i \boldsymbol{V}_i \tag{1.184}$$

where H_i is the enthalpy carried by i-type particles and $\boldsymbol{V}_i$ is the diffusion velocity. For each component, the enthalpy is the sum of translational energy, internal energy and formation enthalpy:

$$H_i = \tfrac{5}{2} k_{\mathrm{B}} T + \bar{E}_i + H_{fi} \tag{1.185}$$

Among the reactions taking place in the gas, we now select a linearly independent set and order the components $(X_i)_{i\in S}$ such that the first n^e appear in a single reaction. We can then write the reactions as

$$X_k = \sum_{i=n^e+1}^{n^s} b_k^i X_i, \quad k = 1, \ldots, n^e \tag{1.186}$$

From the equilibrium assumption, we also derive that the net flux of each component must vanish:

$$n_i \boldsymbol{V}_i + \sum_{k=1}^{n^e} b_k^i n_k \boldsymbol{V}_k = 0, \quad i = n^e + 1, \ldots, n^s \tag{1.187}$$

Making use of this relation, we now rewrite the convective heat flux:

$$\begin{aligned} \boldsymbol{q}_{conv} &= \sum_{i \in S} n_i H_i \boldsymbol{V}_i \\ &= \sum_{i=1}^{n^e} n_i H_i \boldsymbol{V}_i + \sum_{i=n^e+1}^{n^s} n_i H_i \boldsymbol{V}_i \\ &= \sum_{i=1}^{n^e} n_i \boldsymbol{V}_i \left(H_i - \sum_{k=n^e+1}^{n^s} H_k b_i^k \right) = -\sum_{i=1}^{n^e} n_i \boldsymbol{V}_i \Delta H_i \end{aligned} \tag{1.188}$$

where ΔH_i is the heat of the ith reaction, Eq. (1.186).

Next step is to evaluate the diffusion velocities. They are related to the spatial gradient of the concentrations:

$$\nabla x_i = \sum_{j \neq i} \frac{x_i x_j}{\mathcal{D}_i^j} \left(\boldsymbol{V}_j - \boldsymbol{V}_i \right), \quad i = 1, \ldots, n^s \tag{1.189}$$

where $x_i = \frac{n_i}{n}$ and $\mathcal{D}_i^j = \frac{3 k_\mathrm{B} T}{16 n m_{ij} \Omega_{ij}^{(1,1)}}$ are the binary diffusion coefficients and m_{ij} is the reduced mass for the (i, j) pair.

The gradients of the species concentrations are in turn expressed in terms of the equilibrium constant for each of the reactions (1.186) via van't Hoff isochore:

$$\frac{\mathrm{d} \log K_{pk}}{\mathrm{d}T} = \frac{\Delta H_k}{k_\mathrm{B} T^2} \tag{1.190}$$

so that

$$\sum_{i=n^e+1}^{n^s} b_k^i \frac{1}{x_i} \nabla x_i - \frac{1}{x_k} \nabla x_k = \frac{\Delta H_k}{k_\mathrm{B} T^2} \nabla T, \quad k = 1, \ldots, n^e \tag{1.191}$$

Using Eqs. (1.187) and (1.189) the last equation reads:

$$\frac{\Delta H_k}{k_B T^2}\nabla T = \sum_{p=1}^{n^e} x_p \boldsymbol{V}_p \left[\sum_{i=n^e+1}^{n^s}\left(\frac{b_k^i}{\mathcal{D}_i^p} + \frac{b_p^i}{\mathcal{D}_k^i} + b_k^i\frac{b_p^i}{x_i}\sum_{j=1}^{n^s}\frac{x_j}{\mathcal{D}_i^j} - b_k^i\sum_{j=n^e+1}^{n^s}\frac{b_p^j}{\mathcal{D}_i^j}\right) - \frac{1}{\mathcal{D}_k^p}\right] + \boldsymbol{V}_k\left[\sum_{j=1}^{n^s}\frac{x_j}{\mathcal{D}_k^j}\right], \quad k = 1,\ldots,n^e \tag{1.192}$$

which can be put in the form:

$$\sum_{p=1}^{n^e} A_k^p n_p \boldsymbol{V}_p = \frac{\Delta H_k}{k_B T^2}\nabla T, \quad k = 1,\ldots,n^e \tag{1.193}$$

Inverting this system, we obtain $(\boldsymbol{V}_p)_{p=1,\ldots,n^e}$ that are then substituted in Eq. (1.188) to give

$$\boldsymbol{q}_{conv} = -\lambda_r \nabla T \tag{1.194}$$

with

$$\lambda_r = -\frac{1}{k_B T^2}\frac{\begin{vmatrix} 0 & \Delta H_1 & \ldots & \Delta H_{n^e} \\ \Delta H_1 & A_1^1 & \ldots & A_{n^e}^1 \\ \ldots & \ldots & \ldots & \ldots \\ \Delta H_{n^e} & A_1^{n^e} & \ldots & A_{n^e}^{n^e} \end{vmatrix}}{|A|} \tag{1.195}$$

The A_j^i have complicated expressions (Butler and Brokaw 1957). The formalism presented here is the starting point for the discussion of reactive thermal conductivity in thermal non-equilibrium conditions (see Chap. 8 and Bonnefoi et al. 1985).

For LTE plasmas, the formulas can be simplified rewriting the independent chemical reactions as (Brokaw 1960)

$$\sum_{i\in S} n_k^i X_i = 0 \qquad k = 1,\ldots,n^e \tag{1.196}$$

The corresponding equations are reported in Chap. 7.

1.4.2 Extension to Ionized Mixtures

The above derivation has some important limitations if it is to be applied to ionized mixtures. In this case, strong volume forces manifest in the form

of ambipolar electric fields and, as we shall see in Chap. 9, the binary diffusion coefficient is not a good approximation for the multicomponent diffusion coefficients when electrons are present.

We therefore consider the case that (Meador, Jr. and Staton 1965):

1. The gas mixture is in thermal and chemical equilibrium.
2. Total pressure is uniform.
3. Thermal diffusion is negligible.
4. *There are only electromagnetic forces acting on the plasma.*
5. *The plasma is quasineutral.*
6. *The total current density equals zero (i.e. the ambipolar diffusion regime has been established, as in all actual experiments).*

The derivation proceeds as before by selecting a set of linearly independent chemical reactions so that Eq. (1.188) still holds, but now the diffusion velocities are

$$\boldsymbol{V}_i = -\sum_j D_i^j \boldsymbol{d}_j, \quad i = 1, \ldots, n^s \tag{1.197}$$

where

$$\boldsymbol{d}_i = \nabla x_i - x_i \frac{e_i \boldsymbol{E}'}{k_\mathrm{B} T}, \quad i = 1, \ldots, n^s \tag{1.198}$$

and $\boldsymbol{E}'$ is the ambipolar electric field.

Again, the concentration gradients can be related to the equilibrium constant:

$$\sum_{i=n^e+1}^{n^s} b_k^i \frac{\boldsymbol{d}_i}{x_i} - \frac{\boldsymbol{d}_k}{x_k} = \frac{\Delta H_k}{k_\mathrm{B} T^2} \nabla T, \quad k = 1, \ldots, n^e \tag{1.199}$$

In the above derivation we have used the property of electric charge conservation in chemical reactions. Recall that the diffusion driving forces are related to the diffusion velocities by (see Sect. 1.2.8)

$$\boldsymbol{V}_i = \boldsymbol{\beta}_i^0, \quad i = 1, \ldots, n^s \tag{1.200a}$$

$$\frac{\boldsymbol{d}_i}{x_i} = -\tfrac{25}{4} n k_\mathrm{B} \sum_{j=1}^{n^s} \sum_{q=0}^{n_a} A_{ij}^{0q} \boldsymbol{\beta}_j^q, \quad i = 1, \ldots, n^s \tag{1.200b}$$

$$\tfrac{5}{2} \delta_{p1} \frac{\nabla T}{T} = \tfrac{25}{4} n k_\mathrm{B} \sum_{j=1}^{n^s} \sum_{q=0}^{n_a} A_{ij}^{pq} \boldsymbol{\beta}_j^q, \quad \begin{matrix} i = 1, \ldots, n^s \\ p = 1, \ldots, n_a \end{matrix} \tag{1.200c}$$

where $\boldsymbol{\beta}_j^q = \frac{1}{2}\sqrt{\frac{2k_\mathrm{B}T}{m_j}}\boldsymbol{\alpha}_j^q$ and $A_{ij}^{pq} = \frac{1}{x_i} \Lambda_{ij}^{pq}$. Using these relations, Eq. (1.199), can be recast as

$$\tfrac{25}{4} n k_{\mathrm{B}} \sum_{j=1}^{n^s} \sum_{q=0}^{n_a} \left[A_{kj}^{0q} - \sum_{i=n^e+1}^{n^s} b_k^i A_{ij}^{0q} \right] \boldsymbol{\beta}_j^q = \frac{\Delta H_k}{k_{\mathrm{B}} T^2} \nabla T, \quad k = 1, \ldots, n^e \tag{1.201}$$

whereas the condition, Eq. (1.187) can be written as

$$x_i \boldsymbol{\beta}_i^0 + \sum_{k=1}^{n^e} b_k^i x_k \boldsymbol{\beta}_k^0 = 0, \quad i = n^e + 1, \ldots, n^s \tag{1.202}$$

Finally, the ambipolar diffusion assumption reads

$$\boldsymbol{j}_e \equiv \sum_{i=1}^{n^s} e_i n_i \boldsymbol{V}_i = 0 \tag{1.203}$$

Equations (1.202), (1.201), (1.200c), and (1.203) form a linear system of $n^s(n_a + 1) + 1$ equations required to solve for the diffusion velocities and the ambipolar electric field in terms of ∇T.

1.4.3 Transport of Dissociation Energy

In this section we apply the formalism developed in Sect. 1.4.1 above to the case of a dissociating gas. We then have $n^s = 2$ and a single chemical reaction

$$\mathrm{A}_2 = 2\mathrm{A} \tag{1.204}$$

whose heat of reaction is $\Delta H = 2H_{\mathrm{A}} - H_{\mathrm{A}_2}$. The stationary condition, Eq. (1.187), then reads

$$n_{\mathrm{A}} \boldsymbol{V}_{\mathrm{A}} + 2 n_{\mathrm{A}_2} \boldsymbol{V}_{\mathrm{A}_2} = 0 \tag{1.205}$$

and the convective heat flux is

$$\boldsymbol{q}_{conv} = -\Delta H n_{\mathrm{A}_2} \boldsymbol{V}_{\mathrm{A}_2} \tag{1.206}$$

We also have $m_{\mathrm{A}_2} = 2m_{\mathrm{A}}$ so that

$$\boldsymbol{V}_{\mathrm{A}} = -2 \frac{n_{\mathrm{A}_2}}{n_{\mathrm{A}}} \boldsymbol{V}_{\mathrm{A}_2} \tag{1.207}$$

The diffusion velocity of the molecular species is therefore

$$\boldsymbol{V}_{\mathrm{A}_2} = \frac{n^2}{n_{\mathrm{A}_2}(n + n_{\mathrm{A}_2})} \mathcal{D}_{\mathrm{A}}^{\mathrm{A}_2} \nabla x_{\mathrm{A}} \tag{1.208}$$

The gradients of the species concentrations are related to the heat of reaction as in Eq. (1.191):

$$\nabla x_{\mathrm{A}_2} = -\nabla x_{\mathrm{A}} \tag{1.209}$$

$$2\frac{\nabla x_{\mathrm{A}}}{x_{\mathrm{A}}} - \frac{\nabla x_{\mathrm{A}_2}}{x_{\mathrm{A}_2}} = \frac{\Delta H}{k_{\mathrm{B}}T^2}\nabla T \tag{1.210}$$

Using Eqs. (1.206), (1.208) and (1.209) we then have

$$\boldsymbol{q}_{conv} = -\lambda_{diss}\nabla T \tag{1.211}$$

with

$$\lambda_{diss} = \frac{x_{\mathrm{A}}(1-x_{\mathrm{A}})}{(2-x_{\mathrm{A}})^2}\left(\frac{\Delta H}{k_{\mathrm{B}}T}\right)^2 \frac{p}{T}\mathcal{D}_{\mathrm{A}}^{\mathrm{A}_2} \tag{1.212}$$

The reactive thermal conductivity depends not only on the thermodynamic and transport properties of the system but also on the composition. The term $Z = \frac{x_{\mathrm{A}}(1-x_{\mathrm{A}})}{(2-x_{\mathrm{A}})^2}$ modulates the reactive thermal conductivity so that it is interesting to study its behaviour. Figure 1.5 shows Z as a function of the molar fraction of the atomic species.

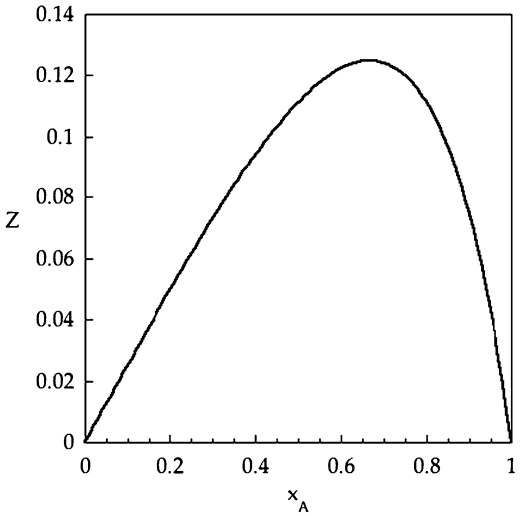

Fig. 1.5 The factor $Z = \frac{x_{\mathrm{A}}(1-x_{\mathrm{A}})}{(2-x_{\mathrm{A}})^2}$ as a function of the atom concentration, x_{A}

1.4.4 Transport of Ionization Energy

In this case the gas mixture is composed of the species A, A^+ and e^-. They are connected via the ionization reaction

$$A = A^+ + e^- \tag{1.213}$$

and the heat of the reaction can be written:

$$\Delta H = H_i + H_e - H_a \approx I \tag{1.214}$$

where I is the ionization potential and translational and internal contributions to the species' enthalpies have been neglected as they are usually much smaller; also, we use subscripts i, e and a to indicate the ion, the electron and the atom, respectively.

Equation (1.188) now reads

$$\boldsymbol{q}_{conv} = -n_a \boldsymbol{V}_a I \tag{1.215}$$

In order to estimate the diffusion velocity, however, we cannot use the binary diffusion approximation, Eq. (1.189). The conditions of quasineutrality and ambipolar regime read

$$n_e = n_i \tag{1.216}$$

$$\boldsymbol{V}_e = \boldsymbol{V}_i \tag{1.217}$$

Together with Eqs. (1.197) and (1.198), these relations imply

$$\frac{e\boldsymbol{E}'}{k_B T} = \frac{(2D_a^i - D_i^i) - (2D_a^e - D_e^e)}{2D_i^e - D_e^e - D_i^i} \frac{\nabla x_e}{x_e} \tag{1.218}$$

On the other hand, Eq. (1.191) leads to

$$\nabla x_e = \frac{x_e(1-2x_e)}{2(1-x_e)} \frac{\Delta H}{k_B T^2} \nabla T \tag{1.219}$$

Putting all together,

$$\lambda_{ion} = \frac{x_e(1-2x_e)^2}{2(1-x_e)} \left(\frac{I}{k_B T}\right)^2 \frac{p}{T} \zeta_D \tag{1.220}$$

where

$$\zeta_D \equiv \left[(2D_a^a - D_a^i - D_a^e) + (D_a^e - D_a^i) \frac{(2D_a^e - D_e^e) - (2D_a^i - D_i^i)}{2D_i^e - D_e^e - D_i^i} \right] \tag{1.221}$$

The above formula can be simplified by noting that D_a^i, depending on the large charge-exchange cross section, is much smaller than D_a^e:

$$\frac{(2D_a^e - D_e^e) - (2D_a^i - D_i^i)}{2D_i^e - D_e^e - D_i^i} \approx 1 \tag{1.222}$$

$$\frac{D_a^e - D_a^i + D_e^a - D_i^a}{D_i^e + D_e^i} \approx 1 \tag{1.223}$$

$$\begin{aligned}
&\frac{(2D_a^e - D_e^e) - (2D_a^i - D_i^i)}{2D_i^e - D_e^e - D_i^i} \\
&= \frac{(D_e^e - D_e^a) - (D_i^i - D_i^a) + (D_a^a - D_a^e) - (D_a^a - D_a^i)}{(D_e^e - D_e^i) + (D_i^i - D_i^e)} \\
&\approx \frac{(D_e^e - D_e^a) + (D_a^a - D_a^e)}{(D_e^e - D_e^i) + (D_i^i - D_i^e)} \approx 1
\end{aligned} \tag{1.224}$$

so that

$$\zeta_D \approx 2(D_a^a - D_a^i) = 2D_{ai}^H \frac{m_i n^2}{n_a \rho} \tag{1.225}$$

and, finally ($m_i \approx m_a$),

$$\lambda_{ion} = \frac{x_e x_a}{(x_a + x_e)^2} \left(\frac{I}{k_\mathrm{B} T}\right)^2 \frac{p}{T} D_{ai}^H \tag{1.226}$$

1.4.5 Transport of Rearrangement Energy

Consider the reaction:

$$\mathrm{A} = \mathrm{B} \tag{1.227}$$

The heat of reaction is

$$\Delta H = H_\mathrm{B} - H_\mathrm{A} \tag{1.228}$$

and the diffusion velocities are related by

$$n_\mathrm{A} \boldsymbol{V}_\mathrm{A} + n_\mathrm{B} \boldsymbol{V}_\mathrm{B} = 0 \tag{1.229}$$

The convective heat flux is

$$\boldsymbol{q}_{conv} = -\Delta H n_\mathrm{A} \boldsymbol{V}_\mathrm{A} \tag{1.230}$$

The diffusion velocity is

$$\boldsymbol{V}_{\mathrm{A}} = (D_{\mathrm{A}}^{\mathrm{B}} - D_{\mathrm{A}}^{\mathrm{A}})\nabla x_{\mathrm{A}} = \frac{D_{\mathrm{A}}^{\mathrm{B}}}{x_{\mathrm{A}}}\nabla x_{\mathrm{A}} = -\frac{\mathcal{D}_{\mathrm{A}}^{\mathrm{B}}}{x_{\mathrm{A}}}\nabla x_{\mathrm{A}} \tag{1.231}$$

and

$$\frac{\nabla x_{\mathrm{B}}}{x_{\mathrm{B}}} - \frac{\nabla x_{\mathrm{A}}}{x_{\mathrm{A}}} = \frac{\Delta H}{k_{\mathrm{B}}T^2}\nabla T \tag{1.232}$$

or

$$\nabla x_{\mathrm{A}} = -x_{\mathrm{A}}x_{\mathrm{B}}\frac{\Delta H}{k_{\mathrm{B}}T^2}\nabla T \tag{1.233}$$

and, finally,

$$\lambda_r = x_{\mathrm{A}}x_{\mathrm{B}}\left(\frac{\Delta H}{k_{\mathrm{B}}T}\right)^2 \frac{p}{T} n k_{\mathrm{B}} \mathcal{D}_{\mathrm{A}}^{\mathrm{B}} \tag{1.234}$$

Appendix A: Simple Derivation of the Boltzmann Equation

In this Appendix, we present a simple derivation of the Boltzmann transport equation for a pure gas of unstructured particles. The particles' motion is described in terms of their mass, m, velocity, $\boldsymbol{c}$ and specific volume force, $\boldsymbol{b}$. The gas is described in terms of the particle distribution function, $f = f(\boldsymbol{r}, \boldsymbol{c}, t)$. The transport equation is a balance equation for f.

Neglecting collisions, the changes in f during a small time step, $\mathrm{d}t$, are due to particles' motion only:

$$f(\boldsymbol{r} + \boldsymbol{c}\mathrm{d}t, \boldsymbol{c} + \boldsymbol{b}\mathrm{d}t, t + \mathrm{d}t) = f(\boldsymbol{r}, \boldsymbol{c}, t) \tag{1.235}$$

so that

$$\mathrm{d}t\,(\boldsymbol{c}\cdot\partial_{\boldsymbol{r}} f + \boldsymbol{b}\cdot\partial_{\boldsymbol{c}} f + \partial_t f) = 0 \tag{1.236}$$

It is customary to define the streaming operator

$$\mathscr{D} = \partial_t + \boldsymbol{c}\cdot\partial_{\boldsymbol{r}} + \boldsymbol{b}\cdot\partial_{\boldsymbol{c}} \tag{1.237}$$

so that Eq. (1.236) can be rewritten:

$$\mathscr{D}(f) = 0 \tag{1.238}$$

The distribution function, however, can change also as a consequence of particles' collisions. The following assumptions are required:

1. The collision event is point-like in space and time.
2. Only binary collision events are considered.
3. Particles are uncorrelated before each collision.

The first assumption means the resulting equation cannot deal with angular momentum exchanging collisions or nonideal gases. Lifting this requirement entails the derivation of the full quantum Waldmann–Snider transport equation (Waldmann 1957; Snider 1960) whose transport theory has been developed in McCourt et al. (1990). The second assumption restricts the applicability to dilute gases. The third assumption, also known as the *molecular chaos* or *Stosszahlansatz* assumption, brings in the kinetic equation the time asymmetry needed for it to satisfy the second principle of thermodynamics. The meaning of this assumption and its generalizations in the derivation of a quantum Boltzmann equation from the BBGKY hierarchy are discussed in the work of Snider (Snider et al. 1995).

When two particles, i and j, collide, the particles' velocities change:

$$\boldsymbol{c}_i + \boldsymbol{c}_j \to \boldsymbol{c}_i' + \boldsymbol{c}_j' \tag{1.239}$$

The collision dynamics is specified by the relative speed before collision, $g \equiv |\boldsymbol{c}_i - \boldsymbol{c}_j|$, the impact parameter, b, and the scattering solid angle, Ω. Let us also define

$$f_i \equiv f\left(\boldsymbol{r}, \boldsymbol{c}_i, t\right) \tag{1.240}$$

From the molecular chaos assumption, we derive that the number of collisions involving particle pairs with velocities $\boldsymbol{c}_i$ and $\boldsymbol{c}_j$ colliding per unit time according to Eq. (1.239) is

$$f_i f_j g b \mathrm{d}b \mathrm{d}\Omega \tag{1.241}$$

Integrating this expression over all collisions (i.e. impact parameter and scattering angle) and over all collision partners (i.e. $\boldsymbol{c}_j$) yields the loss term of the collisional contribution to the distribution function balance equation.

The gain term is given by collisions in which the *final* velocity of particle i is $\boldsymbol{c}_i$:

$$\boldsymbol{c}_i' + \boldsymbol{c}_j' \to \boldsymbol{c}_i + \boldsymbol{c}_j \tag{1.242}$$

The collision in Eq. (1.242) is called the *inverse collision* of that in Eq. (1.239). The number of inverse collisions is thus

$$f_i' f_j' g' b' \mathrm{d}b' \mathrm{d}\Omega' \tag{1.243}$$

where $f_i' \equiv f\left(\boldsymbol{r}, \boldsymbol{c}_i', t\right)$.

From the kinematics of elastic collisions, it follows that direct and inverse collisions are related by

$$g' = g \tag{1.244}$$

$$b'\mathrm{d}b'\mathrm{d}\Omega'\mathrm{d}\boldsymbol{c}'_j = b\mathrm{d}b\mathrm{d}\Omega\mathrm{d}\boldsymbol{c}_j \tag{1.245}$$

Putting all together we can write the balance equation for the particle distribution function as

$$\mathscr{D}(f) = \mathscr{S}(f) \tag{1.246}$$

where the collision integral, $\mathscr{S}$, has the form

$$\mathscr{S}(f) = \int \left(f'_i f'_j - f_i f_j\right) g b\mathrm{d}b\mathrm{d}\Omega\mathrm{d}\boldsymbol{c}_j \tag{1.247}$$

Equation (1.246) is the Boltzmann transport equation (Boltzmann 1872).

References

Alexeev BV, Chikhaoui A, Grushin IT (1994) Application of the generalized Chapman-Enskog method to the transport coeffcients calculation in a reacting gas mixture. Phys Rev E 49:2809–2825

Billing GD, Wang L (1992) Semiclassical calculations of transport coefficients and rotational relaxation of nitrogen at high temperatures. J Phys Chem 96(6):2572–2575

Boltzmann L (1872) Weitere Studien über das Wärmegleichgewicht unter Gasmolekülen. Wiener Berichte 66:275–370

Bonnefoi C, Aubreton J, Mexmain JM (1985) New approach taking into account elastic and inelastic processes for transport properties of two temperature plasmas. Zeitschrift für Naturforschung A (Astrophysik, Physik und Physikalische Chemie) 40a:885–891

Brokaw RS (1960) Thermal conductivity of gas mixtures in chemical equilibrium. II. J Chem Phys 32(4):1005–1006

Bruno D, Giovangigli V (2011) Relaxation of internal temperature and volume viscosity. Phys Fluids 23(9):093104

Burnett D (1935a) The distribution of molecular velocities and the mean motion in a non-uniform gas. Proc Lond Math Soc 40:382–435

Burnett D (1935b) The distribution of velocities in a slightly non-uniform gas. Proc Lond Math Soc 39:385–430

Butler JN, Brokaw RS (1957) Thermal conductivity of gas mixtures in chemical equilibrium. J Chem Phys 26(6):1636–1643

Capitelli M, Lamanna U (1974) Collision integrals of electronically excited states and transport coefficients of thermal plasmas. J Plasma Phys 12: 71–79

Chang CSW, Uhlenbeck GE (1970) The kinetic theory of gases. Studies in statistical mechanics, vol 5. North-Holland, Amsterdam, pp 1–75

Chapman S, Cowling TG (1970) The mathematical theory of non-uniform gases. Cambridge University Press, Cambridge

Curtiss CF (1968) Symmetric gaseous diffusion coefficients. J Chem Phys 49:2917–2919

Curtiss CF, Hirschfelder JO (1949) Transport properties of multicomponent gas mixtures. J Chem Phys 17:550–555

Ern A, Giovangigli V (1994) Multicomponent transport algorithms. In: Lecture notes in physics, vol 24. Springer, Berlin

Ern A, Giovangigli V (1998) The kinetic chemical equilibrium regime. Phys Stat Mech Appl 260:49–72

Eucken A (1913) Ueber das Wärmeleitvermoegen, die spezifische Wärme und die innere Reibung der Gase. Zeitschrift für Naturforschung A (Astrophysik, Physik und Physikalische Chemie) 14:324–332

Ferziger JH, Kaper HG (1972) Mathematical theory of transport processes in gases. North-Holland, Amsterdam

Giovangigli V (2010) Multicomponent transport algorithms for partially ionized mixtures. J Comput Phys 229(11):4117–4142

Giovangigli V, Graille B (2003) Kinetic theory of partially ionized reactive gas mixtures. Phys Stat Mech Appl 327:313–348

Giovangigli V, Graille B (2009) The kinetic theory of partially ionized reactive gas mixtures II. J Phys Math Theor 42:025503

Grad H (1949) On the kinetic theory of rarefied gases. Commun Pure Appl Math 2(4):331–407

de Groot SR, Mazur P (1984) Non-equilibrium thermodynamics. Dover books on physics. Dover, New York

Grunfeld C (1993) On a class of kinetic equations for reacting gas mixtures. Comptes Rendus de l'Académie des Sciences 316:953–958

Hirschfelder JO, Curtiss CF, Bird RB (1966) Molecular theory of gases and liquids. Wiley, New York

Kolesnikov AF (2002) General formulation of the multicomponent plasma transport equations. In: Fletcher D, Magin T, Charbonnier JM, Sarma GSR (eds) Physico-chemical models for high enthalpy and plasma flows. von Karman Institute for Fluid Dynamics, vol VKI. Rhode Saint-Genese, Belgium

Kumar K (1966) Polynomial expansions in kinetic theory of gases. Ann Phys 37(1):113–141

Kustova E, Giordano D (2011) Cross-coupling effects in chemically non-equilibrium viscous compressible flows. Chem Phys 379(1–3):83–91

Ludwig G, Heil M (1960) Boundary layer theory with dissociation and ionization. Adv Appl Mech, vol 6. Academic, New York, pp 39–118

Mason EA, Monchick L (1962) Heat conductivity of polyatomic and polar gases. J Chem Phys 36(6):1622–1639
McCourt RF, Snider RF (1964) Thermal conductivity of a gas with rotational states. J Chem Phys 41(10):3185
McCourt RF, Beenakker JJM, Köhler WE, Kuscer I (1990) Non equilibrium phenomena in polyatomic gases. Clarendon, Oxford
Meador WE Jr, Staton LD (1965) Electrical and thermal properties of plasmas. Phys Fluids 8(9):1694–1703
Millat J, Vesovic V, Wakeham W (1988) On the validity of the simplified expression for the thermal conductivity of Thijsse et al. Phys Stat Mech Appl 148(1–2):153–164
Monchick L, Yun KS, Mason EA (1963) Formal kinetic theory of transport phenomena in polyatomic gas mixtures. J Chem Phys 39(3):654–669
Nagnibeda E, Kustova E (2009) Non-equilibrium reacting gas flows: kinetic theory of transport and relaxation processes. Springer series heat and mass transfer. Springer, Berlin
Nernst W (1904) Boltzmann festschrift. verlag von J. A. Barth, Leipzig, pp 904–915
Prigogine I, Xhrouet E (1949) On the perturbation of Maxwell distribution function by chemical reactions in gases. Physica 15:913–932
Snider RF (1960) Quantum-mechanical modified Boltzmann equation for degenerate internal states. J Chem Phys 32(4):1051–1060
Snider RF, Mullin WJ, Laloë F (1995) Analysis of certain binary collision approximation closures of the BBGKY hierarchy. Phys Stat Mech Appl 218:155–182
Van de Ree J (1967) On the definition of the diffusion coefficients in reacting gases. Physica 36:118–126
Viehland LA, Mason EA, Sandler SI (1978) Effect of spin polarization on the thermal conductivity of polyatomic gases. J Chem Phys 68(11):5277
Waldmann L (1957) Die Boltzmann-Gleichung für Gase mit Rotierenden Molekülen. Zeitschrift für Naturforschung A (Astrophysik, Physik und Physikalische Chemie) 12a:660–662
Waldmann L (1958) Transporterscheinungen in gasen von Mittlerem druck. Handbuch der Physik, vol 12. Springer, Berlin, pp 295–514
Waldmann L, Trübenbacher E (1962) Formale Kinetische Theorie yon Gasgemischen aus Anregbaren Molekfilen. Zeitschrift für Naturforschung A (Astrophysik, Physik und Physikalische Chemie) 17a:363–376
Whittaker ET, Watson GNC (1990) A course in modern analysis, 4th edn. Cambridge University Press, Cambridge, Chap. 16, p 352
Zhdanov VM (2002) Transport processes in multicomponent plasma. Taylor and Francis, London

Chapter 2
Transport Coefficient Evaluation

In this chapter, we summarize the expressions for the linear systems that need to be solved for the explicit calculation of the transport coefficients. These expressions are used in many chapters of this book together with the corresponding expressions derived by Devoto (1967a), extending the formulation of Hirschfelder et al. (1966). The two approaches are equivalent as it will be shown in this chapter.

2.1 Thermal Conductivity and Thermal Diffusion

The integral equation for $\phi^{\lambda'}$ is

$$\mathscr{F}_i^{\mathscr{S}}(\phi^{\lambda'}) = \Psi_i^{\lambda'}, \quad i \in S \tag{2.1}$$

with

$$\Psi_i^{\lambda'} = \sqrt{\frac{2(k_B T)^3}{m_i}}(\phi^{1010i} + \phi^{1001i}) \tag{2.2}$$

The unknown function is expanded as

$$\phi_i^{\lambda'} = \sqrt{2m_i k_B T}\sum_{pq} \alpha_{pqi}^{\lambda'} \phi^{10pqi} \quad i \in S \tag{2.3}$$

so that the elements of the linear system, Eq. (1.106), read

$$G_{ij}^{pq,rs} = \frac{2\sqrt{m_i m_j}}{3p}[\![\phi^{10pqi}, \phi^{10rsj}]\!] \tag{2.4}$$

$$\begin{aligned}\beta_{pqi}^{\lambda'} &= \frac{\sqrt{2m_i}}{3p\sqrt{k_B T}}\langle\!\langle f^0 \phi^{10pqi}, \Psi^{\lambda'}\rangle\!\rangle \\ &= \frac{n_i}{n}\left(\frac{c_p^{\mathrm{tr}}}{k_B}\delta_{p1}\delta_{q0} + \frac{c_i^{\mathrm{int}}}{k_B}\delta_{p0}\delta_{q1}\right)\end{aligned} \tag{2.5}$$

M. Capitelli et al., *Fundamental Aspects of Plasma Chemical Physics*, Springer Series on Atomic, Optical, and Plasma Physics 74,
DOI 10.1007/978-1-4419-8172-1_2, © Springer Science+Business Media, LLC 2013

The calculation of the *bracket integrals*, $[\![\phi^{10pqi}, \phi^{10rsj}]\!]$, is detailed in the Appendix A. The system is to be solved under the constraints Eq. (1.74) that in this case amount to

$$\sum_{i \in S} y_i \alpha_{00i}^{\lambda'} = 0 \tag{2.6}$$

The partial thermal conductivity coefficient is given by

$$\begin{aligned} \lambda' &= \frac{p}{T} \left\langle \alpha^{\lambda'}, \beta^{\lambda'} \right\rangle \\ &= \frac{p}{T} \left(\left\langle \alpha_{10}^{\lambda'}, \beta_{10}^{\lambda'} \right\rangle + \left\langle \alpha_{01}^{\lambda'}, \beta_{01}^{\lambda'} \right\rangle \right) \\ &= \frac{p}{k_{\mathrm{B}} T} \sum_{i \in S} \frac{n_i}{n} (\hat{c}_{\mathrm{p}}^{\mathrm{tr}} \alpha_{10i}^{\lambda'} + \hat{c}_i^{\mathrm{int}} \alpha_{01i}^{\lambda'}) \end{aligned} \tag{2.7}$$

and the thermal diffusion vector is given by

$$\begin{aligned} D_k^T &= - \left\langle \alpha^{\lambda'}, \beta^{D_k} \right\rangle \\ &= - \left\langle \alpha_{00}^{\lambda'}, \beta_{00}^{D_k} \right\rangle \\ &= -\alpha_{00k}^{\lambda'}, \quad k \in S \end{aligned} \tag{2.8}$$

For practical calculations, the infinite expansion, Eq. (2.3), must be truncated. The ζth Chapman–Enskog approximation is obtained retaining the first ζ terms. Also, note that the linear system of Eqs. (2.4) and (2.5) becomes singular in the limit of vanishing molar fraction of any of the constituents of the mixture. This problem can be circumvented noting that both $G_{ij}^{pq,rs}$ and $\beta_{pqi}^{\lambda'}$ depend linearly on $\frac{n_i}{n}$ so that the same results are obtained with a new system defined by

$$G_{ij}^{\prime pq,rs} = \frac{n}{n_i} G_{ij}^{pq,rs} \tag{2.9}$$

$$\beta_{pqi}^{\prime \lambda'} = \frac{n}{n_i} \beta_{pqi}^{\lambda'} \tag{2.10}$$

$$\alpha_{pqi}^{\prime \lambda'} = \alpha_{pqi}^{\lambda'} \tag{2.11}$$

2.2 Diffusion

The integral equation for $\phi^{D_k}, \quad k \in S$ is

$$\mathscr{F}_i^{\mathscr{S}}(\phi^{D_k}) = \Psi_i^{D_k}, \quad i \in S \tag{2.12}$$

with

$$\Psi_i^{D_k} = \sqrt{\frac{2}{m_i k_\mathrm{B} T}} \frac{1}{n_i} (\delta_{ik} - y_i) \phi^{1000i} \tag{2.13}$$

The unknown function is expanded as

$$\phi_i^{D_k} = \frac{\sqrt{2m_i}}{p\sqrt{k_\mathrm{B} T}} \sum_{pq} \alpha_{pqi}^{D_k} \phi^{10pqi} \tag{2.14}$$

so that the elements of the linear system, Eq. (1.106), read

$$G_{ij}^{pq,rs} = \frac{2\sqrt{m_i m_j}}{3p} [\![\phi^{10pqi}, \phi^{10rsj}]\!] \tag{2.15}$$

$$\begin{aligned} \beta_{pqi}^{D_k} &= \frac{\sqrt{2m_i k_\mathrm{B} T}}{3} \langle\!\langle f^0 \phi^{10pqi}, \Psi^{D_k} \rangle\!\rangle \\ &= (\delta_{ik} - y_i)\, \delta_{p0} \delta_{q0} \end{aligned} \tag{2.16}$$

The constraints read

$$\sum_{i \in S} y_i \alpha_{00i}^{D_k} = 0, \quad k \in S \tag{2.17}$$

The diffusion coefficients are given by

$$\begin{aligned} D_i^k &= \left\langle \alpha^{D_i}, \beta^{D_k} \right\rangle \\ &= \left\langle \alpha_{00}^{D_i}, \beta_{00}^{D_k} \right\rangle \\ &= \alpha_{00k}^{D_i} = \alpha_{00i}^{D_k} \end{aligned} \tag{2.18}$$

A linear system valid for vanishing molar fractions is obtained, in this case, by setting

$$G_{ij}^{\prime pq,rs} = \frac{n}{n_j} G_{ij}^{pq,rs} \tag{2.19}$$

$$\beta_{pqi}^{\prime D_k} = \beta_{pqi}^{D_k} \tag{2.20}$$

$$\alpha_{pqi}^{\prime D_k} = \frac{n_i}{n} \alpha_{pqi}^{D_k} \tag{2.21}$$

2.3 Shear Viscosity

The integral equation for ϕ^η is

$$\mathscr{F}_i^{\mathscr{S}}(\phi^\eta) = \Psi_i^\eta, \quad i \in S \tag{2.22}$$

with

$$\Psi_i^\eta = 2\phi^{2000i} \tag{2.23}$$

The unknown function is expanded as

$$\phi_i^\eta = \frac{2}{p}\sum_{pq}\alpha_{pqi}^\eta \phi^{20pqi} \tag{2.24}$$

so that the elements of the linear system, Eq. (1.106), read

$$G_{ij}^{pq,rs} = \frac{2}{5np}[\![\phi^{20pqi}, \phi^{20rsj}]\!] \tag{2.25}$$

$$\begin{aligned}\beta_{pqi}^\eta &= \frac{1}{5n}\langle\!\langle f^0\phi^{20pqi}, \Psi^\eta\rangle\!\rangle \\ &= \frac{n_i}{n}\delta_{p0}\delta_{q0}\end{aligned} \tag{2.26}$$

The constraints are automatically satisfied and the shear viscosity coefficient is

$$\begin{aligned}\eta &= \langle\alpha^\eta, \beta^\eta\rangle \\ &= \langle\alpha_{00}^\eta, \beta_{00}^\eta\rangle \\ &= \sum_{i\in S}\frac{n_i}{n}\alpha_{00i}^\eta\end{aligned} \tag{2.27}$$

A linear system valid for vanishing molar fractions is obtained by setting

$$G_{ij}^{\prime pq,rs} = \frac{n}{n_i}G_{ij}^{pq,rs} \tag{2.28}$$

$$\beta_{pqi}^{\prime\eta} = \frac{n}{n_i}\beta_{pqi}^\eta \tag{2.29}$$

$$\alpha_{pqi}^{\prime\eta} = \alpha_{pqi}^\eta \tag{2.30}$$

2.4 Bulk Viscosity

The integral equation for ϕ^κ is

$$\mathscr{F}_i^{\mathscr{S}}(\phi^\kappa) = \Psi_i^\kappa, \quad i \in S \tag{2.31}$$

with

$$\Psi_i^\kappa = -2\frac{\mathcal{C}_{\mathrm{V}}^{\mathrm{int}}}{c_{\mathrm{V}}}\phi^{0010i} + 2\frac{\mathcal{C}_{\mathrm{V}}^{\mathrm{tr}}}{c_{\mathrm{V}}}\phi^{0001i} \tag{2.32}$$

The unknown function is expanded as

$$\phi_i^\kappa = -\frac{3}{p}\sum_{pq}\alpha_{pqi}^\kappa \phi^{00pqi} \tag{2.33}$$

so that the elements of the linear system, Eq. (1.106), read

$$G_{ij}^{pq,rs} = \frac{1}{np}[\![\phi^{00pqi}, \phi^{00rsj}]\!] \tag{2.34}$$

$$\begin{aligned}\beta_{pqi}^{\kappa} &= -\frac{1}{3n}\langle\!\langle f^0\phi^{00pqi}, \Psi^{\kappa}\rangle\!\rangle \\ &= \frac{n_i}{n}\left(\frac{c^{\text{int}}}{c_{\text{v}}}\delta_{p1}\delta_{q0} - \frac{c_i^{\text{int}}}{c_{\text{v}}}\delta_{p0}\delta_{q1}\right)\end{aligned} \tag{2.35}$$

The constraints read

$$\sum_{i\in S}\frac{n_i}{n}(c^{\text{tr}}\alpha_{10i}^{\kappa} + c_i^{\text{int}}\alpha_{01i}^{\kappa}) = 0 \tag{2.36}$$

The bulk viscosity coefficient is then

$$\begin{aligned}\kappa &= \langle\alpha^{\kappa}, \beta^{\kappa}\rangle \\ &= \langle\alpha_{10}^{\kappa}, \beta_{10}^{\kappa}\rangle + \langle\alpha_{01}^{\kappa}, \beta_{01}^{\kappa}\rangle \\ &= \sum_{i\in S}\frac{n_i}{n}\alpha_{10i}^{\kappa}\end{aligned} \tag{2.37}$$

As before, a linear system valid for vanishing molar fractions is obtained by setting

$$G_{ij}^{\prime pq,rs} = \frac{n}{n_i}G_{ij}^{pq,rs} \tag{2.38}$$

$$\beta_{pqi}^{\prime\kappa} = \frac{n}{n_i}\beta_{pqi}^{\kappa} \tag{2.39}$$

$$\alpha_{pqi}^{\prime\kappa} = \alpha_{pqi}^{\kappa} \tag{2.40}$$

2.5 Chemistry Source Terms

The integral equations for ϕ^r is

$$\mathscr{F}_i^{\mathscr{S}}(\phi^r) = \Psi_i^r, \quad i \in S \tag{2.41}$$

$$\langle\!\langle f^0\phi^r, \psi^l\rangle\!\rangle = 0 \tag{2.42}$$

Ψ_i^r is given in Eq. (1.69). Note that, unlike previous cases, this expression contains also the collision integral of chemical reaction processes, $\mathscr{C}_i(f^0)$. Explicit expressions for the matrix elements of the linear systems will therefore not be given here (Nagnibeda and Kustova, 2009).

The unknown function is expanded as

$$\phi_i^r = \frac{1}{n}\sum_{pq}\alpha_{pqi}^r\phi^{00pqi} \tag{2.43}$$

The constraints read

$$\sum_{i\in S}\frac{n_i}{n}(\overset{\text{tr}}{c}{}^{r}\alpha^{r}_{10i}+\overset{\text{int}}{c}{}^{r}_{i}\alpha^{r}_{01i})=0 \tag{2.44}$$

The relaxation pressure is obtained from

$$p^{\text{rel}}=k_{\text{B}}T\sum_{i\in S}\frac{n_i}{n}\alpha^{r}_{10i} \tag{2.45}$$

The macroscopic chemical production rates appearing in Eq. (1.37a) can be written as

$$\omega_i=\omega_i^0+\omega_i^1 \tag{2.46}$$

The zero-order terms are given in Eq. (1.51). In order to evaluate the first-order terms we first decompose the production terms as a sum over all reactions (Ern and Giovangigli, 1994; Nagnibeda and Kustova, 2009). Writing the reactions as

$$\sum_{i\in S}\nu^{i}_{r,f}X_i=\sum_{i\in S}\nu^{i}_{r,b}X_i,\quad r\in R \tag{2.47}$$

we have

$$\omega_i=\sum_{r\in R}K^{r}_{f}\tau_r \tag{2.48}$$

where τ_r acts as a driving force and is given by

$$\tau_r=\prod_{i\in S}n_i^{\nu^{i}_{r,f}}-\frac{1}{K_{r,\text{eq}}}\prod_{i\in S}n_i^{\nu^{i}_{r,b}} \tag{2.49}$$

and $K_{r,\text{eq}}$ is the equilibrium constant for the reaction.

The chemical reaction rates K^{r}_{f} can, in turn, be expressed as

$$K^{r}_{f}=K^{r(0)}_{f}+K^{r(1)}_{f}\nabla\cdot\boldsymbol{v}+K^{r(2)}_{f} \tag{2.50}$$

$K^{r(1)}_{f}$ and $K^{r(2)}_{f}$ are evaluated from the knowledge of ϕ^{κ} and ϕ^{r}, respectively.

The relaxation pressure and the first-order chemical production rates are believed to be small under many circumstances and they will not be discussed further.

Explicit calculations of first-order chemical reaction rates are reported in Kustova and Giordano (2011) whereas a discussion of the extent to which chemical reactions can perturb the distribution function is contained in Bruno et al. (2003) where a Monte Carlo method is used to solve the full Boltzmann equation for a gas mixture undergoing fast chemical reactions.

As an example, we report model calculations for the dissociation of trace H_2 in Xe (Bruno et al., 1998). Figure 2.1a shows that the chemical reaction is

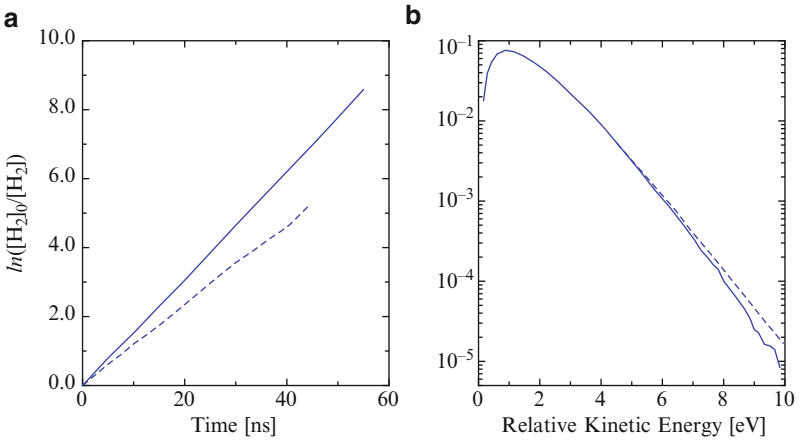

Fig. 2.1 (**a**) Temporal evolution of H_2 concentration. (**b**) Relative kinetic energy distribution for the pair Xe+H_2. (*Full lines*) DSMC, (*dashed line*) thermal behaviour

slower than that predicted by a thermal equilibrium model. This is a consequence of the depletion of the tail of the velocity distribution function, shown in Fig. 2.1b caused by the (fast) chemical reaction that is not compensated by elastic collisions.

In addition a Test Particle Monte Carlo (TPMC) method, derived from the collision kernel of the transport equation, has been recently used for calculating the transport of one component in a thermal bath of the second one, including anisotropic scattering effects (Panarese et al. 2011).

2.6 Alternative Formulations of the Transport Linear Systems

Alternative formulations of the transport linear systems exist, which give completely equivalent results for the transport coefficients. In particular, the approach due to Hirschfelder and co-authors (Hirschfelder et al. 1966) has known widespread use in the literature.

This approach has some important drawbacks:

- The transport linear systems are modified in order to explicitly account for the constraints, thus breaking the symmetry of the system. This has implications on the mathematical properties of the linear systems that eventually prevent the application of fast iterative solution algorithms (Ern and Giovangigli 1994).
- As discussed in Sect. 1.2.9, the formulation of the multicomponent diffusion coefficients fails to satisfy Onsager reciprocal relations and is therefore unsatisfactory from a conceptual point of view.

It is, however, useful to derive relationships among the coefficients discussed in this book and those derived in Hirschfelder et al. (1966) (here denoted with the superscript H).

In this approach, the structure of the linear systems is modified in order to explicitly account for the constraints, thus breaking the symmetry of the system, and the transport coefficients are expressed as ratios of determinants by applying Cramer rule to the lowest order linear systems. For simplicity, we restrict the discussion to mixtures of ν species not possessing internal degrees of freedom.

These formulas are for the first non-vanishing approximation. Higher approximations are required in the case of partially ionized gas mixtures and have been derived by Devoto (1966, 1967a,b) and Devoto and Li (1968) in a series of papers where working equations can be found (see also Bonnefoi 1975). Some of these expressions are reported in the chapters of this book.

2.6.1 Multicomponent Diffusion Coefficients

$$D_{ij}^H = \frac{\sum_{k=1}^{\nu} x_k m_k}{m_j} \frac{K^{ji} - K^{ii}}{|K|} \tag{2.51}$$

where:

$$K_{ij} = \frac{2}{3p} \left(\frac{m_j}{x_i} [\![\phi^{1000i}, \phi^{1000i}]\!] - \frac{\sqrt{m_i m_j}}{x_j} [\![\phi^{1000i}, \phi^{1000j}]\!] \right) \tag{2.52}$$

and K^{ji} are the minors obtained from K excluding the jth row and the ith column.

2.6.2 Thermal Diffusion and Partial Thermal Conductivity Coefficients

$$(D_i^T)^H = -\frac{8}{5} \frac{m_i}{k_B} \frac{\begin{vmatrix} L_{11}^{00} & \dots & L_{1\nu}^{00} & L_{11}^{01} & \dots & L_{1\nu}^{01} & 0 \\ \dots & \dots & \dots & \dots & \dots & \dots & \dots \\ L_{\nu 1}^{00} & \dots & L_{\nu\nu}^{00} & L_{\nu 1}^{01} & \dots & L_{\nu\nu}^{01} & 0 \\ L_{11}^{10} & \dots & L_{1\nu}^{10} & L_{11}^{11} & \dots & L_{1\nu}^{11} & x_1 \\ \dots & \dots & \dots & \dots & \dots & \dots & \dots \\ L_{\nu 1}^{10} & \dots & L_{\nu\nu}^{10} & L_{\nu 1}^{11} & \dots & L_{\nu\nu}^{11} & x_\nu \\ x_1\delta_{1i} & \dots & x_\nu\delta_{\nu i} & 0 & \dots & 0 & 0 \end{vmatrix}}{|L|} \tag{2.53}$$

$$(\lambda')^{\mathrm{H}} = \frac{\begin{vmatrix} L_{11}^{00} \ldots L_{1\nu}^{00} & L_{11}^{01} \ldots L_{1\nu}^{01} & 0 \\ \ldots\ldots\ldots\ldots\ldots\ldots\ldots\ldots \\ L_{\nu 1}^{00} \ldots L_{\nu\nu}^{00} & L_{\nu 1}^{01} \ldots L_{\nu\nu}^{01} & 0 \\ L_{11}^{10} \ldots L_{1\nu}^{10} & L_{11}^{11} \ldots L_{1\nu}^{11} & x_1 \\ \ldots\ldots\ldots\ldots\ldots\ldots\ldots\ldots \\ L_{\nu 1}^{10} \ldots L_{\nu\nu}^{10} & L_{\nu 1}^{11} \ldots L_{\nu\nu}^{11} & x_\nu \\ 0 \quad \ldots \quad 0 & x_1 \quad \ldots \quad x_\nu & 0 \end{vmatrix}}{|L|} \tag{2.54}$$

where

$$L_{ij}^{pq} = \frac{1}{n^2}[\![\phi^{10p0i}, \phi^{10q0j}]\!] \tag{2.55}$$

2.6.3 Viscosity Coefficient

$$\eta^H = -\frac{\begin{vmatrix} H_{11} & H_{12} \ldots H_{1\nu} & x_1 \\ H_{21} & H_{22} \ldots H_{2\nu} & x_2 \\ \ldots\ldots\ldots\ldots\ldots\ldots \\ H_{\nu 1} & H_{\nu 2} \ldots H_{\nu\nu} & x_\nu \\ x_1 & x_2 \quad \ldots \quad x_\nu & 0 \end{vmatrix}}{|H|} \tag{2.56}$$

with

$$H_{ij} = \frac{1}{n^2}[\![\phi^{2000i}, \phi^{2000j}]\!] \tag{2.57}$$

The transport coefficients so defined are related to those used in this book by

$$D_{ij}^H = \frac{n_i}{m_j}\frac{\rho}{n^2}(D_i^i - D_i^j) \tag{2.58}$$

$$(D_i^T)^H = \rho_i D_i^T \tag{2.59}$$

$$(\lambda')^{\mathrm{H}} = \lambda' \tag{2.60}$$

$$\eta^H = \eta \tag{2.61}$$

Appendix A: Evaluation of the Bracket Integrals

The matrix elements needed for the calculation of the transport coefficients are

$$[\![\phi^{abpqi}, \phi^{abrsj}]\!] = \delta_{ij}\sum_{k\in S} n_i n_k [\![\phi^{abpqi}, \phi^{abrsi}]\!]'_{ik} + n_i n_j [\![\phi^{abpqi}, \phi^{abrsj}]\!]''_{ij} \tag{2.62}$$

where

$$[\![F,G]\!]'_{jk} = \frac{1}{2n_j n_k}\int f_j^{(0)} f_k^{(0)}(G_j - G'_j)(F_j - F'_j) g\sigma \mathrm{d}\Omega \mathrm{d}\boldsymbol{c}_j \mathrm{d}\boldsymbol{c}_k$$

$$[\![F,G]\!]''_{jk} = \frac{1}{2n_j n_k}\int f_j^{(0)} f_k^{(0)}(G_j - G'_j)(F_k - F'_k) g\sigma \mathrm{d}\Omega \mathrm{d}\boldsymbol{c}_j \mathrm{d}\boldsymbol{c}_k \quad (2.63)$$

These eightfold integrals can be reduced by a standard procedure to linear combinations of elastic collision integrals as follows:

$$[\![S_{3/2}^{(p)}(w^2)\boldsymbol{w}, S_{3/2}^{(q)}(w^2)\boldsymbol{w}]\!]'_{jk} = 8\sum_{\ell,r=0}^{\infty} A'_{pq\ell r}\Omega_{jk}^{(\ell,r)} \quad (2.64)$$

$$[\![S_{3/2}^{(p)}(w^2)\boldsymbol{w}, S_{3/2}^{(q)}(w^2)\boldsymbol{w}]\!]''_{jk} = 8\nu_k^{p+1/2}\nu_j^{q+1/2}\sum_{\ell,r=0}^{\infty} A_{pq\ell r}\Omega_{jk}^{(\ell,r)} \quad (2.65)$$

$$[\![S_{5/2}^{(p)}(w^2)(\boldsymbol{w}\boldsymbol{w} - \frac{1}{3}w^2\mathbb{I}), S_{5/2}^{(q)}(w^2)(\boldsymbol{w}\boldsymbol{w} - \frac{1}{3}w^2\mathbb{I})]\!]'_{jk} = \frac{16}{3}\sum_{\ell,r=0}^{\infty} B'_{pq\ell r}\Omega_{jk}^{(\ell,r)} \quad (2.66)$$

$$[\![S_{5/2}^{(p)}(w^2)(\boldsymbol{w}\boldsymbol{w} - \frac{1}{3}w^2\mathbb{I}), S_{5/2}^{(q)}(w^2)(\boldsymbol{w}\boldsymbol{w} - \frac{1}{3}w^2\mathbb{I})]\!]''_{jk} = \frac{16}{3}\nu_k^{p+1/2}\nu_j^{q+1/2}\sum_{\ell,r=0}^{\infty} B_{pq\ell r}\Omega_{jk}^{(\ell,r)} \quad (2.67)$$

where the elastic collision integrals are defined as

$$\Omega_{jk}^{(\ell,r)} = \sqrt{\frac{k_\mathrm{B}T}{2\pi m_{jk}}}\int_0^{\infty} \exp(-\gamma^2)\gamma^{2r+3} Q_{jk}^{(\ell)} \mathrm{d}\gamma \quad (2.68)$$

$$Q_{jk}^{(\ell)} = 2\pi\int_0^{\infty}(1 - \cos^{\ell}\chi_{jk}) b \mathrm{d}b \quad (2.69)$$

and

$$m_{jk}^{-1} = m_j^{-1} + m_k^{-1} \quad (2.70)$$

$$\gamma = \sqrt{\frac{m_{jk}}{2k_\mathrm{B}T}} g; \quad \boldsymbol{g} = \boldsymbol{c}_j - \boldsymbol{c}_k \quad (2.71)$$

$$\nu_j = \frac{m_j}{m_j + m_k} \quad (2.72)$$

The coefficients $A_{pq\ell r}$ and $B_{pq\ell r}$ are universal constants, whereas $A'_{pq\ell r}$ and $B'_{pq\ell r}$ are linear combinations of ν_j, ν_k with universal coefficients. The equations needed for the actual calculations can be obtained by following Chapman and Cowling (1970).

Appendix B: Approximations in Chapman–Enskog Theory

Table 2.1 Correspondence between approximation orders for transport coefficients in Chapman–Enskog theory and in Devoto formulation

	Chapman–Enskog	Devoto
Viscosity	First *non-vanishing*	First
Diffusion	First *non-vanishing*	First
Thermal diffusion	First *non-vanishing*	Second
Electrical conductivity	First *non-vanishing*	First
Partial thermal conductivity	–	First
	First *non-vanishing*	Second
	Second *non-vanishing*	Third
True thermal conductivity	–	First
	First *non-vanishing*	Second
	Second *non-vanishing*	Third

Possible lack in congruence could depend on the assumption in Devoto formulation $[\lambda']_1=[\lambda]_1=[\lambda]_2$ (Table 2.1).

References

Bonnefoi C (1975) Contribution au calcul théorique des coefficients de transport d'un plasma d'azote per la méthode de Chapman–Enskog à l'approximation quatre de Sonine (in french). 3eme cycle these, University of Limoges, France

Bruno D, Capitelli M, Longo S (1998) DSMC modelling of vibrational and chemical kinetics for a reacting gas mixture. Chem Phys Lett 289:141

Bruno D, Capitelli M, Longo S (2003) Effect of translational kinetics on chemical rates in a direct simulation Monte Carlo model gas phase detonation. Chem Phys Lett 380:383–390

Chapman S, Cowling TG (1970) The mathematical theory of non-uniform gases. Cambridge University Press, Cambridge

Devoto RS (1966) Transport properties of ionized monatomic gases. Phys Fluids 9(6):1230–1240

Devoto RS (1967a) Simplified expressions for the transport properties of ionized monatomic gases. Phys Fluids 10(10):2105–2112

Devoto RS (1967b) Transport coefficients of partially ionized argon. Phys Fluids 10(2):354–364

Devoto RS, Li CP (1968) Transport coefficients of partially ionized helium. J Plasma Phys 2(1):17–32

Ern A, Giovangigli V (1994) Multicomponent transport algorithms. In: Lecture notes in physics, vol 24. Springer, Heidelberg

Hirschfelder JO, Curtiss CF, Bird RB (1966) Molecular theory of gases and liquids. Wiley, New York

Kustova E, Giordano D (2011) Cross-coupling effects in chemically non-equilibrium viscous compressible flows. Chem Phys 379(1–3):83–91

Nagnibeda E, Kustova E (2009) Non-equilibrium reacting gas flows: kinetic theory of transport and relaxation processes. In: Springer Series Heat and Mass Transfer. Springer, Berlin

Panarese A, Bruno D, Colonna G, Diomede P, Laricchiuta A, Longo S, Capitelli M (2011) A Monte Carlo model for determination of binary diffusion coefficients in gases. J Comput Phys 230(14):5716–5721

Chapter 3
Transport Cross Sections: Classical and Quantum Approaches

3.1 Transport Cross Sections and Collision Integrals: The Classical Approach

The heart of the Chapman–Enskog theory lies on some assumptions on the nature of elementary collisions, which are postulated to be *binary*, *elastic*, *characterized by isotropic interparticle force field, and adequately described through classical mechanics.* The collisional dynamics enters the transport equations through the so-called *collision integrals*, $\Omega_{ij}^{(\ell,s)}$, associated to the (i,j) interaction pair, characterized by the order (ℓ,s)[1] and depending on the temperature. The calculation of collision integrals usually is performed in the frame of the classical mechanics of elastic collisions. The dynamics of the two colliding particles i and j, without internal structure, moving under the action of the interaction potential $\varphi(r)$, only depending on the interparticle distance, can be straightforwardly reduced to the deflection of a particle of reduced mass $\mu = m_i m_j/(m_i + m_j)$, confined in a plane of polar coordinates (r,θ), under the action of an *effective* potential field

$$\varphi_{\text{eff}} = \varphi(r) + \frac{L^2}{2\mu r^2} \tag{3.1}$$

the second term being the *centrifugal potential* and representing the repulsive contribution to the interaction, with L the angular momentum. Simple geometrical considerations in Fig. 3.1 lead to the definition of the deflection angle

$$\vartheta = \pi - 2\theta_c \tag{3.2}$$

[1] Traditionally the orders (1,1) and (2,2) are defined as *diffusion-type* and *viscosity-type* collision integrals, respectively, due to a direct dependence of binary diffusion and viscosity coefficients from the $\Omega^{(1,1)}$ and $\Omega^{(2,2)}$ values, when calculated in the first Chapman–Enskog approximation.

M. Capitelli et al., *Fundamental Aspects of Plasma Chemical Physics*,
Springer Series on Atomic, Optical, and Plasma Physics 74,
DOI 10.1007/978-1-4419-8172-1_3,

the angle θ_c being the value of the angular coordinate at the distance of closest approach r_c. Recalling that the total energy E and the angular momentum L are invariant along the trajectory

$$\begin{cases} E = \frac{1}{2}\mu\left[(\frac{\mathrm{d}r}{\mathrm{d}t})^2 + r^2(\frac{\mathrm{d}\theta}{\mathrm{d}t})^2\right] + \varphi(r) = \frac{1}{2}\mu(\frac{\mathrm{d}r}{\mathrm{d}t})^2 + \varphi_{\mathrm{eff}} \\ L = \mu r^2 \frac{\mathrm{d}\vartheta}{\mathrm{d}t} \end{cases} \tag{3.3}$$

the time variation of r and θ can be easily derived as well as the equation of the trajectory

$$\frac{\mathrm{d}\theta}{\mathrm{d}r} = \frac{\mathrm{d}\theta}{\mathrm{d}t}\frac{\mathrm{d}t}{\mathrm{d}r} = \pm\frac{L}{r^2\left[2\mu(E-\varphi_{\mathrm{eff}})\right]^{1/2}} \tag{3.4}$$

where the negative sign corresponds to the *inward* part of the trajectory (r decreasing, θ increasing), while the positive to the *outward*, being the trajectory symmetric. It is convenient to introduce the impact parameter b through the relation with the value of the angular momentum, evaluated with respect to the initial value of the velocity v_i, this last related to the total energy ($E = \frac{1}{2}\mu v_i^2$)

$$L(t \to -\infty) = \mu r v_i \sin\vartheta = \mu v_i b = b\sqrt{2\mu E} \tag{3.5}$$

The integration of the trajectory equation leads to the expression for the deflection angle (Hirschfelder et al. 1966):

$$\vartheta(b,E) = \pi - 2b\int_{r_c}^{\infty}\left[1 - \frac{b^2}{r^2} - \frac{\varphi(r)}{E}\right]^{-1/2}\frac{\mathrm{d}r}{r^2} \tag{3.6}$$

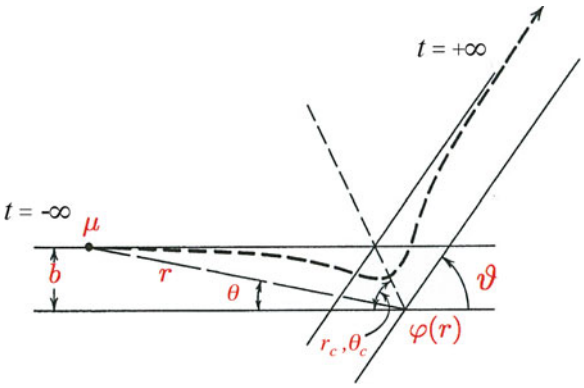

Fig. 3.1 Pictorial view of the classical trajectory in the central-field problem

Some limiting cases should be considered for a qualitative analysis. b=0 corresponds to $\vartheta = \pi$, the so-called *head-on* collision, while as the b value approaches the infinity the deflection angle tends to zero, corresponding to a weak interaction not deflecting the atom trajectories. In the most common case the interaction potential possesses a short-range repulsive region, an attractive long-range part and a more or less deep "well" characterized by position and depth (r_e,φ_0) and by the parameter σ corresponding to the distance where attractive and repulsive forces balance (see Fig. 3.2). High-energy (E_3) collisions are dominated by the repulsive interaction and increasing the impact parameter b from zero to ∞ the deflection angle monotonically decreases from π to zero, typical trajectories being shown in Fig. 3.2. At medium values of the collision energy both repulsive and attractive parts play a role, governing the dynamics at low- and high-impact parameter values, respectively, as it can be appreciated in Fig. 3.2 for E_2. The deflection angle profile decreases, assuming also negative values for trajectories dominated by the attractive forces. Some special features appear corresponding to:

- ϑ=0, the *glory angle*
- $\frac{\mathrm{d}\vartheta}{\mathrm{d}b}$=0, the rainbow angle
- ϑ approaching to $-\infty$, the orbiting angle

The *orbiting* occurs at low collision energies (E_1) and corresponds to the formation of a quasi-bound state entrapped in the centrifugal potential barrier; thus, the trajectory spends a long time near the deflection point and then departs with negative deflection angle.

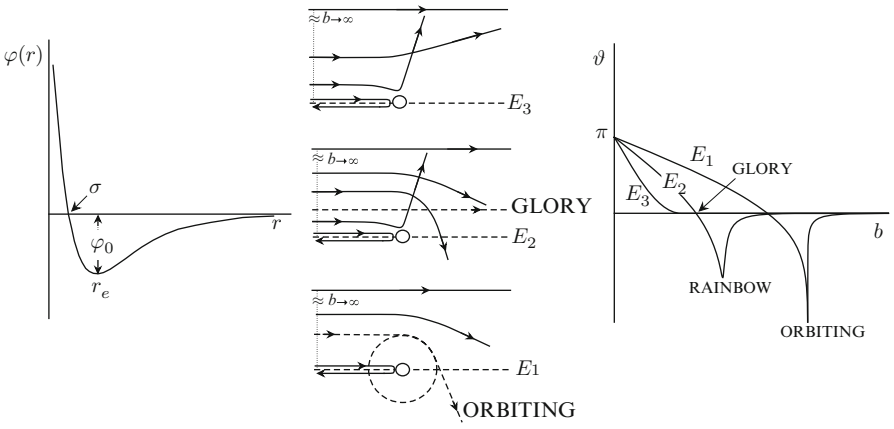

Fig. 3.2 Typical trajectories for an interaction potential with attractive and repulsive regions for different values of the collision energy $E_1 < E_2 < E_3$ and corresponding dependence of the deflection angle on the impact parameter. Special features are also emphasized

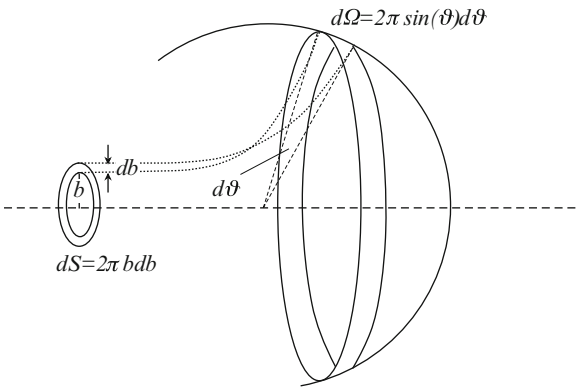

Fig. 3.3 Parameters for the cross section in a central-field problem

The differential cross section is defined as the ratio of the flux of particles deflected in the solid angle $\mathrm{d}\Omega = 2\pi \sin\vartheta \mathrm{d}\vartheta$ to the incident flux crossing the cylindrical section $\mathrm{d}S = 2\pi\ b\mathrm{d}b$ (Fig. 3.3). In the case of elastic scattering the fluxes are equal:

$$\frac{\mathrm{d}\sigma}{\mathrm{d}\Omega}(\vartheta) = \frac{\mathrm{flux_{out}}}{\mathrm{d}\Omega}\frac{\mathrm{d}S}{\mathrm{flux_{in}}} = \left|\frac{b}{\sin\vartheta\frac{\mathrm{d}\vartheta}{\mathrm{d}b}}\right| \tag{3.7}$$

It should be noted that the glory and rainbow angles represent singularities in the differential cross section, associated with angle-specific deflected beam of high intensity experimentally detected.

The total elastic cross section results from the angular integration

$$\sigma = 2\pi\int_0^\pi \frac{\mathrm{d}\sigma}{\mathrm{d}\Omega}(\vartheta)\sin\vartheta\mathrm{d}\vartheta = 2\pi\int_0^\infty b\mathrm{d}b \tag{3.8}$$

Actually the quantity relevant to transport is the so-called *momentum transfer cross section*

$$\sigma = 2\pi\int_0^\infty (1-\cos\vartheta)b\mathrm{d}b \tag{3.9}$$

the term $(1-\cos\vartheta)$ modulates the angular integration, cancelling the contribution to integral elastic cross section due to non-deflected trajectories. The general definition of transport cross section $Q^{(\ell)}$ corresponds to the ℓth moment

$$Q^{(\ell)}(E) = 2\pi\int_0^\infty \mathrm{d}b\ b(1-\cos^\ell\vartheta) \tag{3.10}$$

Finally the collision integral $\Omega^{(\ell,s)}$ is defined as an integral on the reduced energy $\gamma^2 = E/k_\mathrm{B}T$ (Hirschfelder et al. 1966) giving a thermal averaged cross section depending on the temperature

$$\Omega^{(\ell,s)}(T) = \sqrt{\frac{k_\mathrm{B}T}{2\pi\mu}} \int_0^\infty \mathrm{d}\gamma\ \gamma^{2s+3} Q^{(\ell)} e^{-\gamma^2} \tag{3.11}$$

It is worth to note that the energetic distribution of particle becomes broad as the temperature increases; therefore, usually the low-energy behaviour of transport cross section affects the low-temperature values of $\Omega^{(\ell,s)}$, while high temperatures are dominated by high-energy collisions.

3.1.1 Rigid Sphere Model

The rigid sphere model, despite its roughness in the description of elementary collision processes, is very instructive and allows the introduction of *reduced transport quantities*.

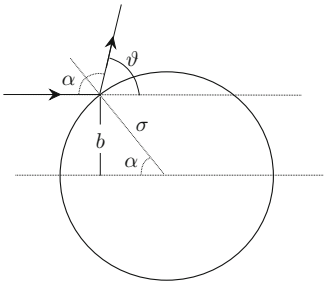

Fig. 3.4 Pictorial view of rigid sphere model, i.e. interaction potential has the form $\varphi(r)$=0 for $r > \sigma$ and $\varphi(r)$=∞ for $r \leq \sigma$

The collision geometry, depicted in Fig. 3.4, leads to the following relations:

$$\begin{aligned} &\vartheta = \pi - 2\alpha = \pi - \chi \\ &b = \sigma \sin\alpha \Rightarrow \mathrm{d}b = \sigma \cos\alpha\ \mathrm{d}\alpha \\ &b\ \mathrm{d}b = \sigma^2 \sin\alpha\ \cos\alpha\ \mathrm{d}\alpha = \tfrac{\sigma^2}{4} \sin\chi\ \mathrm{d}\chi \end{aligned}$$

$$Q^{(\ell)}_{\mathrm{RS}} = 2\pi \int_0^\infty \mathrm{d}b\ b(1 - \cos^\ell\vartheta) = \tfrac{\pi\sigma^2}{2} \int_0^\pi (1 - \cos^\ell\vartheta) \sin\chi\ \mathrm{d}\chi \tag{3.12}$$

Keeping in mind that the integral

$$\int_0^{\pi}(1-\cos^{\ell}\vartheta)\sin\chi\,\mathrm{d}\chi \overset{\cos\vartheta=x}{=} \int_{-1}^{+1}(1-x^{\ell})\mathrm{d}x = \left(x-\tfrac{x^{\ell+1}}{\ell+1}\right)\Big|_{-1}^{+1} = \left[2-\tfrac{1+(-1)^{\ell}}{1+\ell}\right]$$

$$Q_{\mathrm{RS}}^{(\ell)}(E) = \tfrac{\pi\sigma^2}{2}\left[2-\tfrac{1+(-1)^{\ell}}{1+\ell}\right] \tag{3.13}$$

By introducing the cross section in Eq. (3.11) we get the rigid sphere collision integral

$$\Omega_{\mathrm{RS}}^{(\ell,s)} = \sqrt{\tfrac{k_{\mathrm{B}}T}{2\pi\mu}}Q_{\mathrm{RS}}^{(\ell)}\int_0^{\infty}\mathrm{d}\gamma\;\gamma^{2s+3}e^{-\gamma^2} = \sqrt{\tfrac{k_{\mathrm{B}}T}{2\pi\mu}}\tfrac{(s+1)!}{2}Q_{\mathrm{RS}}^{(\ell)} \tag{3.14}$$

Recalling that the integral, it results

$$\int_0^{\infty}\mathrm{d}\gamma\;\gamma^{2s+3}e^{-\gamma^2} \overset{x=\gamma^2}{=} \tfrac{1}{2}\int_0^{\infty}\mathrm{d}x\;x^{(s+2)-1}e^{-x} = \tfrac{1}{2}\Gamma(s+2) = \tfrac{(s+1)!}{2}$$

In literature *reduced* transport quantities have been introduced, representing the dimensionless deviation of the actual values of the transport cross section and of the collision integral from the rigid sphere model

$$\begin{aligned} Q^{(\ell)\star} &= \tfrac{Q^{(\ell)}}{Q_{\mathrm{RS}}^{(\ell)}} = \tfrac{4}{\sigma^2}\left[2-\tfrac{1+(-1)^{\ell}}{1+\ell}\right]^{-1}\int_0^{\infty}\mathrm{d}b\;b(1-\cos^{\ell}\vartheta) \\ \Omega^{(\ell,s)\star} &= \tfrac{\Omega^{(\ell,s)}}{\Omega_{\mathrm{RS}}^{(\ell,s)}} = \tfrac{4(\ell+1)}{(s+1)!\,[2\ell+1-(-1)^{\ell}]\pi\sigma^2}\int_0^{\infty}\mathrm{d}\gamma\;\gamma^{2s+3}Q^{(\ell)}e^{-\gamma^2} \end{aligned}$$

Three combinations of reduced collision integrals frequently occur in the transport coefficient expressions for low approximation and are here introduced with special symbols

$$A^{\star} = \frac{\Omega^{(2,2)\star}}{\Omega^{(1,1)\star}} \qquad B^{\star} = \frac{[5\Omega^{(1,2)\star}-4\Omega^{(1,3)\star}]}{\Omega^{(1,1)\star}} \qquad C^{\star} = \frac{\Omega^{(1,2)\star}}{\Omega^{(1,1)\star}} \tag{3.15}$$

Increasing the order of the Chapman–Enskog approximation requires higher-order collision integrals. The calculation of higher-ℓ orders entails the integration in Eq. (3.10), while $(s+1)$-order collision integrals can be obtained also through the recurrence relation

$$\Omega^{(\ell,s+1)\star} = \Omega^{(\ell,s)\star} + \frac{T}{s+2}\frac{\partial\Omega(\ell,s)\star}{\partial T} \tag{3.16}$$

Throughout the book, reduced collision integrals in the form $\sigma^2 \Omega^{(\ell,s)\star}$ will be considered, thus having the dimensions of a squared length.

3.2 The Quantum Approach

The treatment of the central-field scattering in the quantum frame entails the solution of the Schrödinger equation

$$\left[-\frac{\hbar^2}{2\mu}\nabla^2(\mathbf{r}) + \varphi(r)\right]\psi(\mathbf{r}) = E\psi(\mathbf{r}) \tag{3.17}$$

assuming the physically sound boundary condition

$$\psi(\mathbf{r}) \overset{r\to\infty}{\longrightarrow} e^{\imath\kappa z} + f(\vartheta)\frac{e^{\imath\kappa r}}{r} \tag{3.18}$$

where the first term represents the incident plane wave propagating in the direction of the z axis, with wavenumber $\kappa^2 = (2\mu/\hbar^2)E$, and the second is the spherical wave resulting from the scattering process, whose anisotropic angular pattern is described by the so-called *scattering amplitude*, $f(\vartheta)$.

In the frame of the *partial wave analysis* in scattering problems (Geltman 1969) the wavefunction can be expanded in spherical harmonics

$$\psi(\mathbf{r}) = \frac{1}{r}\sum_{n=0}^{\infty} A_n \psi_n(r) P_n(\cos\vartheta) \tag{3.19}$$

$\psi_n(r)$ is the radial function associated with the n partial wave, solution of the radial second-order differential equation

$$\left[\frac{d^2}{\mathrm{d}r^2} + \kappa^2 - \frac{n(n+1)}{r^2} - \frac{2\mu\varphi(r)}{\hbar^2}\right]\psi_n(\mathbf{r}) = 0 \tag{3.20}$$

In the asymptotic region, where the interaction potential can be neglected, the general solution assumes the form

$$\psi_n = A\sin(\kappa r + \eta_n) \tag{3.21}$$

where η_n is a *phase* depending on κ, n and on the interaction potential. The *phase shift* is thus defined as the shift produced, in the asymptotic region, by the interaction with the potential, the sign of the shift being related to the attractive or repulsive nature of the potential (see Fig. 3.5).

The partial wave expansion allows to express the scattering amplitude as

$$f(\vartheta) = \frac{1}{2\imath\kappa}\sum_{n=0}(2n+1)\left(e^{2\imath\eta_n} - 1\right)P_n(\cos\vartheta) \tag{3.22}$$

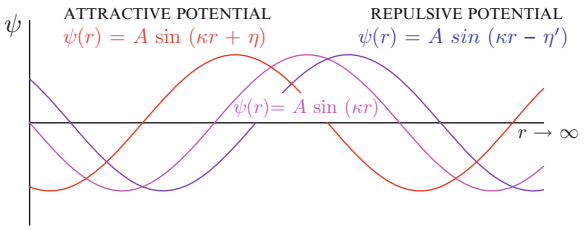

Fig. 3.5 Pictorial view of wavefunction phase shift in the asymptotic region due to the action of a repulsive (*negative phase shift*) or attractive (*positive phase shift*) potential

and recalling the general definition of differential cross section, given in the classical approach, it can be derived a quantum equivalent that leads to

$$\frac{\mathrm{d}\sigma}{\mathrm{d}\Omega}(E,\vartheta) = |f(\vartheta)|^2 = \frac{1}{4\kappa^2}\sum_{n,n'}(2n+1)(2n'+1) \left(e^{\imath(\eta_n - \eta_{n'})}\right) P_n(\cos\vartheta)P_{n'}(\cos\vartheta) \tag{3.23}$$

It is worth to note that in this quantum expression the cross section includes terms due to the interference between partial waves n and n', connected to the abandon of a classical view in the scattering. The second main consequence is that due to the uncertainty principle every value of the impact parameter should contribute to scattering at all angles, thus resulting in a loss of definiteness for the classical angles associated to singularities and orbiting resonances.

Equation (3.10) is rewritten as

$$Q^{(\ell)}(E) = 2\pi\int_0^\pi \mathrm{d}\vartheta\ \sin(\vartheta)\frac{\mathrm{d}\sigma}{\mathrm{d}\Omega}(E,\vartheta)(1-\cos^\ell\vartheta) = \frac{\pi}{2\kappa^2}\sum_{n,n'}(2n+1)(2n'+1) \left(e^{\imath(\eta_n-\eta_{n'})}\right)\int_0^\pi \mathrm{d}\vartheta\ \sin(\vartheta)(1-\cos^\ell\vartheta)P_n(\cos\vartheta)P_{n'}(\cos\vartheta) \tag{3.24}$$

Considering the relations of integrals of Legendre polynomials the low-order transport cross sections are defined in terms of phase shifts

$$Q^{(1)}(E) = \frac{4\pi}{\kappa^2}\sum_n (n+1)\sin^2(\eta_n - \eta_{n+1}) \tag{3.25}$$

$$Q^{(2)}(E) = \frac{4\pi}{\kappa^2}\sum_n \frac{(n+1)(n+2)}{2n+3}\sin^2(\eta_n - \eta_{n+2}) \tag{3.26}$$

$$Q^{(3)}(E) = \frac{4\pi}{\kappa^2}\sum_n \frac{n+1}{2n+5}\left[\frac{(n+3)(n+2)}{2n+3}\sin^2(\eta_n - \eta_{n+3}) + \frac{2(n^2+2n-1)}{2n-1}\sin^2(\eta_n - \eta_{n+1})\right] \tag{3.27}$$

and in general (Meeks et al. 1967)

$$Q^{\ell} = \frac{4\pi}{\kappa^2} \sum_{n,n'} \sum_{j,k=0}^{\xi(\ell)} \frac{(2n+1)(2n'+1)}{2^{n+n'}} \frac{(-1)^{j+k}(2n-2j)!(2n'-2k)!}{j!k!(n-2j)!(n-j)!(n'-2k)!(n'-k)!}$$
$$\cdot \left[\frac{1-(-1)^{n+n'+1}}{n+n'+1-2j-2k} - \frac{1-(-1)^{n+n'+1+\ell}}{n+n'+\ell+1-2j-2k} \right] e^{\imath(\eta_n - \eta_{n'})} \sin\eta_n \sin\eta_{n'}$$

$$\begin{aligned} \xi(\ell) &= \tfrac{\ell}{2} \quad \text{for } \ell = 0, 2, 4, \ldots \\ \xi(\ell) &= \tfrac{\ell-1}{2} \quad \text{for } \ell = 1, 3, 5, \ldots \end{aligned} \tag{3.28}$$

The WKB approximation allows the estimation of phase shifts in the effective potential energy (Mott and Massey 1965)

$$\eta_n^{\mathrm{WKB}} = \lim_{r_{\max}\to\infty} \left[\int_{r_c}^{r_{\max}} \sqrt{2\mu E - \frac{(n+\frac{1}{2})^2}{r^2} - 2\mu\varphi(r)}\, \mathrm{d}r - \int_{r_{c'}}^{r_{\max}} \sqrt{2\mu E - \frac{(n+\frac{1}{2})^2}{r^2}}\, \mathrm{d}r \right] \tag{3.29}$$

Convergency is ensured by the inclusion of a large number of partial waves.

The quantum approach to elastic collisions imposes the further consideration of symmetry effects in colliding systems with identical particles, thus limiting the series in Eqs. (3.25) and (3.26) to even or odd partial waves, respectively, depending on the appropriate statistics (*Bose–Einstein*, BE, or *Fermi–Dirac*, FD)

Bose–Einstein

$$\begin{aligned} Q_{BE}^{(1)}(E) &= 2\tfrac{4\pi}{\kappa^2} \sum_{n=0,2,4}^{\infty} (2n+1)\sin^2(\eta_n) \\ Q_{BE}^{(2)}(E) &= 2\tfrac{4\pi}{\kappa^2} \sum_{n=0,2,4}^{\infty} \tfrac{(n+1)(n+2)}{(2n+3)} \sin^2(\eta_{n+2} - \eta_n) \end{aligned} \tag{3.30}$$

Fermi–Dirac

$$\begin{aligned} Q_{FD}^{(1)}(E) &= 2\tfrac{4\pi}{\kappa^2} \sum_{n=1,3,5}^{\infty} (2n+1)\sin^2(\eta_n) \\ Q_{FD}^{(2)}(E) &= 2\tfrac{4\pi}{\kappa^2} \sum_{n=1,3,5}^{\infty} \tfrac{(n+1)(n+2)}{(2n+3)} \sin^2(\eta_{n+2} - \eta_n) \end{aligned} \tag{3.31}$$

These expressions are valid for particles with zero spin. For particles with s different from zero the cross sections are given by

$$\begin{aligned}\left[Q_{BE}^{(n)}\right]^{(s)} &= \tfrac{s+1}{2s+1}Q_{BE}^{(n)} + \tfrac{s}{2s+1}Q_{FD}^{(n)} \\ \left[Q_{FD}^{(n)}\right]^{(s)} &= \tfrac{s+1}{2s+1}Q_{FD}^{(n)} + \tfrac{s}{2s+1}Q_{BE}^{(n)}\end{aligned} \tag{3.32}$$

The $Q_{BE}^{(n)}$ and $Q_{FD}^{(n)}$ without superscript s are those calculated by Eqs. (3.30) and (3.31).

3.3 Interaction Potentials

The calculation of collision integrals is fundamentally connected to the nature of the forces governing the interaction between chemical species, i.e. interaction potential φ.

The interaction potential curves, or surfaces, result in principle from accurate ab initio electronic structure calculations; however in the past, when the required computational effort was prohibitive, different *model potentials* were considered, whose parameters were determined either by theoretical considerations or by spectroscopy. These potentials were thought to reproduce the general features of electronic states, bound states characterized by a potential well with a short-range repulsive region or purely repulsive states, monotonically increasing as the internuclear coordinate approaches to zero. The great advantage of these potential forms lies in the "full-range" character, ensuring the physically correct behaviour in the asymptotic regions and allowing the potential integration to transport cross sections in a wide energy range.

The analytical forms, referenced in Sect. 3.3.1, are constructed including exponentially decaying or inverse power terms for the repulsive interactions, while the attractive long-range asymptotic region can be expressed in the form a multipole expansion

$$\varphi(r) = \sum_{j=2} \frac{C_{2j}}{r^{2j}}$$

The terms in the expansion are reciprocal of the internuclear distance with powers that depends on the nature of the interacting particles, r^{-4} corresponding to the electrostatic point-charge-induced-dipole interaction the so-called *polarization interactions*, r^{-6} representing the interaction of a permanent dipole with induced dipole (*induction*) or mutually induced dipoles (*dispersion*) and higher even powers r^{-8}, r^{-10} accounting for the higher-order induction or dispersion forces due to quadrupole and multipole terms (*van der Waals interactions*).

3.3.1 Model Potentials

In the following a list of the most widely used model potentials is reported. The integration of these potentials in a quantum, semiclassical or classical frame results in transport cross section evaluation:

- Inverse power (Kihara et al. 1960)

$$\varphi(r) = \frac{d}{r^{\delta}} \quad \begin{cases} d > 0 \text{ repulsive} \\ d < 0 \text{ attractive} \end{cases} \tag{3.33}$$

A special case of the general inverse power potential is the attractive *polarization potential*

$$\varphi(r) = -\frac{ze^2\alpha_{\text{pol}}}{8\pi\varepsilon_0 r^4} \tag{3.34}$$

being z the ion charge and α_{pol} the polarizability of neutral collider, with δ=4 and $d = -\frac{ze^2\alpha_{\text{pol}}}{8\pi\varepsilon_0}$. In this case collision integrals assume a closed form (Kihara et al. 1960)

$$\sigma^2\Omega^{(\ell,s)\star} = \frac{4(\ell+1)}{(s+1)![2\ell+1-(-1)^{\ell}]} A^{(\ell)}(\delta) \sqrt{\frac{\mathrm{d}\delta}{k_{\text{B}}T}} \Gamma\left(s+2-\frac{2}{\delta}\right) \tag{3.35}$$

where Γ is the Gamma function and $A^{(\ell)}$ is a temperature-free coefficient correlated to the transport cross section.
The $A^{\ell}(4)$ values have been estimated by Smith (1967) for ℓ=1, 2 and 3 in the attractive case ($A^1(4)$=0.5523, $A^2(4)$=0.3846, $A^3(4)$=0.6377), leading to simple relations

$$\begin{aligned}
&\sigma^2\Omega^{(1,1)\star} = 424.443z\sqrt{\frac{\alpha_{\text{pol}}}{T}} \\
&\sigma^2\Omega^{(1,2)\star} = 0.833\ \sigma^2\Omega^{(1,1)\star} \qquad \sigma^2\Omega^{(2,2)\star} = 0.870\ \sigma^2\Omega^{(1,1)\star} \\
&\sigma^2\Omega^{(1,3)\star} = 0.729\ \sigma^2\Omega^{(1,1)\star} \qquad \sigma^2\Omega^{(2,3)\star} = 0.761\ \sigma^2\Omega^{(1,1)\star} \\
&\sigma^2\Omega^{(1,4)\star} = 0.656\ \sigma^2\Omega^{(1,1)\star} \qquad \sigma^2\Omega^{(2,4)\star} = 0.685\ \sigma^2\Omega^{(1,1)\star} \\
&\sigma^2\Omega^{(1,5)\star} = 0.602\ \sigma^2\Omega^{(1,1)\star} \qquad \sigma^2\Omega^{(3,3)\star} = 0.842\ \sigma^2\Omega^{(1,1)\star}
\end{aligned} \tag{3.36}$$

- Exponential repulsive (Monchick, 1959; Kalinin and Dubrovitskii 2000)

$$\varphi(r) = Ae^{-\rho r} \tag{3.37}$$

- Morse (Smith and Munn 1964)

$$\varphi(r) = \varphi_0 \left[\exp\left(-\frac{2C}{\sigma}(r-r_{\text{e}})\right) - 2\exp\left(-\frac{C}{\sigma}(r-r_{\text{e}})\right)\right] \tag{3.38}$$

where the potential parameters fulfill the relation

$$\sigma = \frac{C r_e}{C + \ln 2} \tag{3.39}$$

- Lennard-Jones (Neufeld et al. 1972)

$$\varphi(r) = 4\varphi_0 \left[\left(\frac{\sigma}{r} \right)^{12} - \left(\frac{\sigma}{r} \right)^{6} \right] \tag{3.40}$$

- Modified Buckingham (Mason 1954)

$$\varphi(r) = \frac{\varphi_0}{1 - 6/\alpha} \left[\frac{6}{\alpha} e^{\alpha(1 - r/r_e)} - \left(\frac{r_e}{r} \right)^{6} \right] \tag{3.41}$$

- Hulburt–Hirschfelder (Rainwater et al. 1982)

$$\begin{aligned} \varphi(r) = \varphi_0 \Bigg\{ & \exp\left[-2\alpha_{HH} \left(\frac{r}{r_e} - 1 \right) \right] - 2 \exp\left[-\alpha_{HH} \left(\frac{r}{r_e} - 1 \right) \right] \\ & + \beta_{HH} \left(\frac{r}{r_e} - 1 \right)^3 \left[1 + \gamma_{HH} \left(\frac{r}{r_e} - 1 \right) \right] \exp\left[-2\alpha_{HH} \left(\frac{r}{r_e} - 1 \right) \right] \Bigg\} \end{aligned} \tag{3.42}$$

This model is nowadays widely employed due to its flexibility in accommodating different features like the presence of a long-range minimum or short-range shoulder in the potential energy curve.

Also more complex functions should be mentioned, characterized by a large number of parameters and allowing the accurate description of realistic interaction potentials.

- Tang and Toennies (2003)

$$\varphi(r) = A \exp(-br) - \sum_{j=3}^{J} f_{2j}(br) \frac{C_{2j}}{r^{2j}} \tag{3.43}$$

being C_{2j} the dispersion coefficients and

$$f_{2j}(x) = 1 - e^{-x} \sum_{k=0}^{2j} \frac{x^k}{k!} = 1 - \frac{\Gamma(2j+1, x)}{(2j)!} \tag{3.44}$$

- Aziz and Slaman (1990)

$$\varphi(r) = \varphi_0 A \exp\left[-\alpha \left(\frac{r}{r_e} \right) + \beta \left(\frac{r}{r_e} \right)^2 - F(r/r_e) \sum_{j=0}^{2} \frac{c_{2j+6}}{(r/r_e)^{2j+6}} \right] \tag{3.45}$$

with

$$F(x) = \begin{cases} \exp\left[-(D/x - 1)^2 \right] & x < D \\ 1 & x > D \end{cases} \tag{3.46}$$

In principle it is possible to use suitable combination of the above-referenced potential forms to construct a function with a full-range character, guided by the experimental information on the interaction, considering that in different experimental conditions, different regions of the interparticle potential are actually probed (Hirschfelder and Eliason 1957).

Tabulations of *reduced* collision integrals, as a function of the *reduced temperature* $T^\star = \frac{k_B T}{\varphi_0}$, do exist in literature for the listed potentials, expressed in a *reduced form*, $\varphi^\star(r^\star) = \frac{\varphi}{\varphi_0}$, with $r^\star = \frac{r}{\sigma}$. $\varphi^\star(r^\star)$ represents the most general form of the potential function, depending only on potential parameters, varied in a parametric way and in a suitable range. Once the potential parameters for the actual systems are known, both the physical parameters (σ,r_e,φ_0) and those associated with the selected representation of the interaction and derived through a best-fitting procedure, $\sigma^2 \Omega^{(\ell,s)\star}$ values could be straightforwardly estimated.

However, it should be pointed out that nowadays several numerical codes are available, based on the quantum phase shift or the classical trajectory approaches, for the direct integration of the interaction potential. The new algorithms, overcoming the limits of past codes (O'Hara and Smith 1971), can deal with potentials regardless the number of extrema and the complexity of the adopted analytical form (Rainwater et al. 1982; Colonna and Laricchiuta 2008), also considering the anisotropy of the interaction potential involving linear molecules treated as rigid rotors (Heck and Dickinson 1996).

3.3.1.1 Screened Coulomb Potential for Charged-Particle Interactions

Particular attention has to be devoted to the screened Coulomb potential, being the model for interactions involving charged particles, dominating the high-temperature region due to the onset of ionization equilibria. The potential has the form

$$\varphi(r) = \frac{Z_i Z_j e^2}{r} e^{-r/\lambda_D} = \frac{\varphi_0}{r/\lambda_D} e^{-r/\lambda_D} \tag{3.47}$$

with Z_i and Z_j the charges of the ions i and j and λ_D the Debye length, defined as

$$\lambda_D = \sqrt{\frac{k_B T}{4\pi e^2 (n_e + \sum_i n_i Z_i^2)}} \tag{3.48}$$

i.e. including both electron, n_e, and ion, n_i, densities. This model corresponds to the one recently adopted in André et al. (2007), where the Debye length has been calculated accounting of the screening effect of ions. However, a different choice has been proposed in literature (Mason et al. 1967; Devoto

1968; Hahn et al. 1971; Murphy 2000) accounting only for the screening due to electrons. The choice can have no-negligible effects at very high temperature, when multi-charged ions become the predominant species (see Chap. 10).

Closed forms for collision integrals were derived by Liboff (Liboff 1959; Devoto 1967) having a general form

$$\sigma^2 \Omega^{(\ell,s)\star} = f(\ell,s) b_0^2 \left[\ln \tfrac{2\lambda_D}{b_0} - \mathcal{O}(1)\right]$$

$\mathcal{O}(1)$ representing higher-order correction terms.

Expressions for $\ell \leq 4$ are reported in the following:

$$\begin{aligned}
\sigma^2 \Omega^{(1,s)\star} &= \left[\tfrac{4}{s(s+1)}\right] b_0^2 \left[\ln \tfrac{2\lambda_D}{b_0} - \frac{1}{2} - 2\overline{\gamma} + \psi(s)\right] \\
\sigma^2 \Omega^{(2,s)\star} &= \left[\tfrac{12}{s(s+1)}\right] b_0^2 \left[\ln \tfrac{2\lambda_D}{b_0} - 1 - 2\overline{\gamma} + \psi(s)\right] \\
\sigma^2 \Omega^{(3,s)\star} &= \left[\tfrac{12}{s(s+1)}\right] b_0^2 \left[\ln \tfrac{2\lambda_D}{b_0} - \frac{7}{6} - 2\overline{\gamma} + \psi(s)\right] \\
\sigma^2 \Omega^{(4,s)\star} &= \left[\tfrac{16}{s(s+1)}\right] b_0^2 \left[\ln \tfrac{2\lambda_D}{b_0} - \frac{4}{3} - 2\overline{\gamma} + \psi(s)\right]
\end{aligned} \tag{3.49}$$

where $b_0 = \frac{Z_i Z_j e^2}{2k_B T}$, $\overline{\gamma}$ the Euler constant and $\psi(s) = \sum_1^{s-1}(1/n)$, $[\psi(1) = 0]$. Results by Hahn et al. (Hahn et al. 1971) have been interpolated with the formula

$$(T^\star)^2 \Omega^{(\ell,s)\star} = \frac{\ell N_\ell}{s(s+1)} \ln\left[\left(\frac{4T^\star}{\gamma^2}\right) \exp\left(A_s - C_\ell\right) + 1\right] \tag{3.50}$$

$$\begin{aligned}
C_\ell &= \left(1 + \tfrac{1}{3} + \tfrac{1}{5} + \ldots + \tfrac{1}{\ell}\right) - \tfrac{1}{2\ell} \quad \ell \text{ odd} \\
C_\ell &= 1 + \tfrac{1}{3} + \tfrac{1}{5} + \ldots + \tfrac{1}{\ell-1} \qquad \ell \text{ even}
\end{aligned} \tag{3.51}$$

$$A_1 = 0, \quad A_s = 1 + \tfrac{1}{2} + \tfrac{1}{3} + \ldots + \tfrac{1}{s-1} \tag{3.52}$$

This interpolation neglects the difference between repulsive and attractive potentials and any quantum correlation effect and it is practically equivalent to the Kihara results (Kihara and Aono 1963) except that it behaves better at low temperatures.

Recently accurate collision integrals by Mason (Mason et al. 1967; Hahn et al. 1971) have been fitted by the following equation (D'Angola et al. 2008):

$$\ln\left(\Omega^\star\right) = \sum_{j=0}^{6} c_j \ln^j T^\star \tag{3.53}$$

with c_j coefficients reported in Table 3.1 for attractive an repulsive interactions.

Table 3.1 Coefficients c_j entering Eq. (3.53) for reduced Coulomb collision integrals in (a) attractive and (r) repulsive interactions

(a)	c_6	c_5	c_4	c_3	c_2	c_1	c_0
(1,1)	−6.8907164(−7)	3.9962681(−5)	−9.1726603(−4)	1.1119743(−2)	−8.6680553(−2)	−1.4201786	−0.7920630
(1,2)	−5.7227070(−7)	3.2934374(−5)	−7.4777692(−4)	8.9360011(−3)	−6.8914896(−2)	−1.5259733	−1.4388180
(1,3)	−4.3210796(−7)	2.5069749(−5)	−5.7744446(−4)	7.0875826(−3)	−5.7252758(−2)	−1.5798792	−1.9240126
(2,2)	−7.3601073(−7)	4.6128777(−5)	−1.1591771(−3)	1.5291388(−2)	−1.2062283(−1)	−1.3061990	−0.8119872
(2,3)	−9.9732643(−7)	5.8539823(−5)	−1.3501321(−3)	1.5966952(−2)	−1.1181856(−1)	−1.3939960	−1.2004374
(r)	c_6	c_5	c_4	c_3	c_2	c_1	c_0
(1,1)	4.5117138(−7)	−1.8071172(−5)	1.0779533(−4)	4.6897082(−3)	−9.5164062(−2)	−1.1924897	−1.3985613
(1,2)	1.8550098(−7)	−2.9457724(−6)	−2.0524258(−4)	7.2736296(−3)	−9.6108844(−2)	−1.3028643	−1.8990738
(1,3)	−4.9754626(−8)	9.4148622(−6)	−4.3259106(−4)	8.7680260(−3)	−9.3477251(−2)	−1.3767661	−2.2877081
(2,2)	3.7088651(−7)	−1.2368963(−5)	−4.3287839(−5)	6.4520586(−3)	−1.0180688(−1)	−1.2242632	−1.1096929
(2,3)	1.3746615(−7)	4.8295307(−8)	−2.7706436(−4)	8.0837639(−3)	−1.0007200(−1)	−1.2999675	−1.4700797

Corrections to shielded Coulomb transport cross sections from accurate ion–ion interaction potentials have been estimated in Stallcop et al. (1992) for N^+–N^+, N^+–O^+ and O^+–O^+ relevant to high-temperature and high-pressure plasmas.

3.3.2 Potentials from Experiments

3.3.2.1 Molecular Beam Experiments

The treatment shown above provides the theoretical tools for the evaluation of differential and integral cross section given the interaction potential; however from the experimental point of view, the investigation of elastic scattering represents the mean to gain fundamental information on the nature of the intermolecular forces and on the features of the interaction potential. This is the *inversion problem*, having a more general character in physics, and in this case it should be pointed out that though offering an insight in the collisional dynamics, actually it is quite difficult to determine the potential from measurements unless some assumptions are made about the analytical form of the potential, allowing the estimation of potential parameter.

Centrepiece of this investigation is the development of the molecular beam techniques. The scheme of an experimental apparatus is reported in Fig. 3.6. The attenuation of the velocity-selected beam I^o by a target species, confined in a scattering chamber, is measured, analysing the angular pattern of the emerging beam I by a suitable detector.

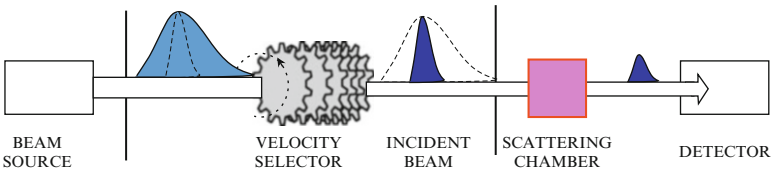

Fig. 3.6 Schematic view of components in the apparatus a molecular beam experiment

The intensity of the scattered beam is related to the incident beam through the Lambert–Beer-type relation

$$I = I^o e^{-n\sigma d} \tag{3.54}$$

where n represents the density of particles in the scattering chamber, d the chamber linear dimension and σ accounts for the attenuation power and is fundamentally connected to the scattering cross section and depends on the velocity of particles in the incident beam. A crossed beam configuration is used for differential cross section measurements, with a rotating detector

able to capture the particles scattered in any elementary solid angle $d\Omega = d\phi \sin\vartheta d\vartheta$.

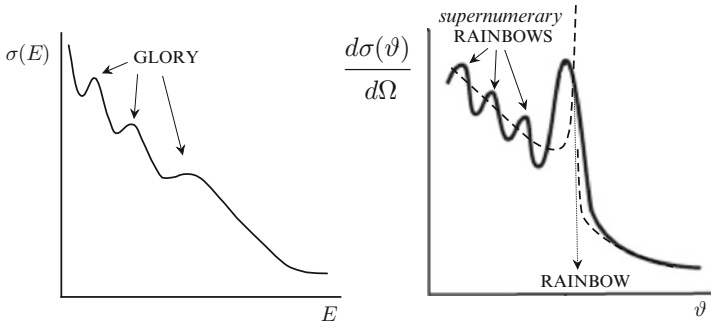

Fig. 3.7 Pictorial view of structures in measured integral and differential elastic cross sections, also classical differential cross sections, with the singularity at the rainbow angle, is reported (*dashed line*)

Structures appear in the profile of integral and differential cross sections (see Fig. 3.7) determined by the quantum nature of scattering. Glory oscillation arises in the energy profile of σ due to the interference of different waves in the forward scattering (ϑ=0), i.e. in the classical view those trajectories characterized either by high-impact parameters or by low-impact parameters but not deflected due to the balance of repulsive and attractive forces at *glory angles*. The differential profile exhibits oscillations associated to the *rainbow singularity*, originating a maximum where the classical approach predicts a discontinuity, as depicted in Fig. 3.7, and additional maxima are observed, called *supernumerary rainbows* due to quantum interference. The rainbow structure gives information about the depth of potential well; in fact as shown by Mason (1957) the rainbow angle is mainly correlated to the ratio of collision energy to φ_0.

Measurements of absolute total scattering cross sections, in the thermal energy range, have been considered in a *multiproperty* analysis, together with other experimental data such as molecular vibrational energy spacing and virial coefficients, yielding a very accurate estimation of the van der Waals interaction potentials for a number of neutral colliding pairs (Brunetti et al. 1978, 1981, 1983; Beneventi et al. 1991). Using a highly flexible spherically symmetric potential model, i.e. exponential-spline–Morse-spline–van der Waals (ESMSV), an analysis on O_2–O_2, O_2–N_2, O–N_2 systems has been performed (Brunetti et al. 1981), deriving position and depth of the attractive minimum and dispersion coefficients in the long-range potential expansion (3.3) through best-fitting procedure of glory structure and of the absolute value of the elastic cross section (see Table 3.2).

The repulsive part of the potential characterized by high-energy collisions, determining the high-temperature transport properties, is less

Table 3.2 ESMSV parameters for the different interactions (Brunetti et al. 1981)

Parameters	O_2–O_2	O_2–N_2	O–N_2
φ_0 [$\times 10^{-15}$ erg]	18.3	17.0	14.7
r_e [Å]	3.94	3.69	3.41
C_6 [$\times 10^{-12}$ erg Å^6]	74.7	70.5	40.4
C_8 [$\times 10^{-12}$ erg Å^8]	418.3	394.6	209.8
C_{10} [$\times 10^{-12}$ erg Å^{10}]	3,041.0	2,869.0	1,415.0

accessible experimentally. In this case ion beams are accelerated and neutralized by charge exchange, yielding high-energy neutral beams (with kinetic energies ∼1,000 eV). Energetic beams interact with the target and the experimental set-up is suitable to detected small-angle differential scattering. This kind of technique pionerized by Amdur (1961), Amdur et al. (1975) and by Leonas et al. (1971), Kalinin et al. (1976) has given useful experimental information on the repulsive part of many interaction pairs, also successfully fitting experimental data with exponential-repulsive (Monchick 1959; Leonas et al. 1971; Leonas 1972) Eq. (3.37) and inverse-power-law (Amdur 1961; Amdur and Mason 1958) Eq. (3.33) potential functions. Parameters for different neutral-pair repulsive interactions are reported in Table 3.3.

Table 3.3 Potential parameters for exponential-repulsive, Eq. (3.37), and inverse-power-law, Eq. (3.33), functions fitting experimental data of repulsive interaction for different neutral pairs

Eq. (3.37) Ref. (Leonas 1972)			Eq. (3.33) Ref. (Amdur 1961)			
Interaction	A [eV]	ρ [Å^{-1}]	Interaction	d [eV]	δ	ΔR [Å]
N_2–N_2	2,290	3.160	He–He	2.884	1.79	0.52–1.02
N_2–N	620	3.310		4.712	5.94	1.27–1.59
N_2–O_2	1,430	3.020	Ne–Ne	312.075	9.99	1.76–2.13
N_2–O	11,350	5.120	Ar–Ar	28.773	4.33	1.37–1.84
N_2–NO	5,780	3.610		848.845	8.33	2.18–2.69
N–O_2	3,870	4.130	Kr–Kr	159.158	5.42	2.42–3.14
N–NO	5,333	4.210	Xe–Xe	7,052.906	7.97	3.01–3.60
O_2–O_2	820	2.850	He–Ar	62.103	7.25	1.64–2.27
O_2–O	10,250	4.850	Ne–Ar	630.392	9.18	1.91–2.44
O_2–NO	7,620	3.780	H–He	2.341	3.29	1.16–1.71
O–NO	3,140	3.950	He–N_2	74.274	7.06	1.79–2.29
NO–NO	2,160	3.260	Ar–N_2	755.223	7.78	2.28–2.83

3.3.2.2 Potentials from Spectroscopy

Accurate bound region of potential energy curves for molecular systems can be reconstructed by the Rydberg–Klein–Reese (RKR) procedure (Singh and Jain 1962; Vanderslice 1962). No special assumptions are done about the form of the potential and the energies of levels from vibrational spectroscopy are used to determine very accurately pairs of values on the potential correspond-

ing to the points of the classical inversion for the nuclear motion. However, the accessible information is limited by the highest vibrational level experimentally known, while the repulsive portion results from hypothesis on the potential form, smoothly joined to the well region.

In literature the Hulburt–Hirschfelder model potential (Rainwater et al. 1982; Biolsi et al. 1982) [Eq. (3.42)] is nowadays widely used for the flexibility of this functional form to the description of special features in the potential curve, such as the presence of secondary minima, barriers or short-range shoulders. Moreover semi-empirical relations have been proposed for the direct derivation of potential parameters (α_{HH}, β_{HH}, γ_{HH}) from the spectroscopic constants of the given molecular state (Biolsi et al. 1982)

$$\alpha_{\mathrm{HH}} = \frac{\omega_e}{2\sqrt{B_e \varphi_0}} \qquad \beta_{\mathrm{HH}} = \mathrm{d}\alpha^3 \qquad \gamma_{\mathrm{HH}} = b\alpha \tag{3.55}$$

with

$$a_0 = \frac{\omega_e^2}{4B_e} \qquad a_1 = -1 - \frac{\alpha_e \omega_e}{6B_e^2} \quad a_2 = \frac{5}{4}a_1^2 - \frac{2\omega_e \chi_e}{3B_e}$$

$$d = 1 + a_1\sqrt{\frac{\varphi_0}{a_0}} \qquad b = 2 - \frac{\frac{7}{12} - \varphi_0 \frac{a_2}{a_0}}{d}$$

φ_0 is the well depth [cm^{-1}] and ω_e and $\omega_e\chi_e$ the fundamental vibrational frequency and the first anharmonic constant, respectively, while B_e and α_e represent the rotational and the ro-vibrational coupling constants. The reliability of this approach has been demonstrated (Biolsi et al. 1982) by direct comparison with RKR potentials for some electronic terms of the C_2 molecule, and, relying on the existence of accurate compilations of spectroscopic data of electronic terms of molecular systems in literature[2], it could regarded as a tool providing a reasonable short-range description of the interaction potential. Obviously in this frame repulsive states are completely missed, being not spectroscopically detected.

3.4 Collision Integrals

3.4.1 Multi-potential Approach

The above model potentials apply to interactions evolving along a single potential energy curve, describing the change of electronic energy in the approaching of the partners, as in the case of collisions of noble gas (closed shell) atoms. In the majority of realistic systems under investigation however the interaction involves open-shell atoms that instead of a single potential entangles a number of potential energy curves, i.e. all the molecular electronic

[2] Database is available on-line at the National Institute of Standards and Technology (NIST) website http://webbook.nist.gov/chemistry/

terms arising in the coupling of the (spin and orbital) angular momenta of colliding atomic pair, theoretically predicted by the Wigner–Witmer rules (see Appendix A in Capitelli et al. 2011).

In this case the collision integral results from the weighted average of the contributions of each state, i.e.

$$\Omega_{\mathrm{av}}^{(\ell,s)\star} = \frac{\sum_i w_i \Omega_i^{(\ell,s)\star}}{\sum_i w_i} \tag{3.56}$$

w_i represents the statistical weight of the corresponding molecular electronic term. Dealing with diatomic molecules, the generic electronic term symbol for homonuclear diatomic molecule is written ${}^{(2S+1)}\Lambda$, where $(2S+1)$ is the spin multiplicity (1 for singlet, 2 for doublet, 3 for triplet, etc.) and Λ is the magnitude of the projection of the total electronic angular momentum on the molecular axis ($\Lambda = 0 \leftrightarrow \Sigma,\ 1 \leftrightarrow \Pi,\ 2 \leftrightarrow \Delta,\ \ldots$); electronic terms are twofold degenerate with the exception of nondegenerate Σ states (for details see Landau and Lifshitz 1981). The weight, w, is defined as (spin multiplicity)×(total angular momentum multiplicity).

The multi-potential approach, in either a classic or quantum frame, has been widely used in literature (Yun and Mason 1962; Capitelli and Ficocelli 1972, 1973; Rainwater et al. 1982; Biolsi et al. 1982; Levin et al. 1990; Stallcop et al. 2000, 2001; Sourd et al. 2006) and the reliability of derived collision integrals is completely determined by two elements, i.e. the *accuracy* of the relevant potential energy curves and the *completeness* of the electronic manifold. The relative weight of each term is the result of the strength of the interaction and of the degeneracy of the corresponding electronic term, thus leading to dominant contributions to the collision integral. It is worthy of note that the electronic terms associated to higher statistical weights are usually excited repulsive states, whose features could not be investigated spectroscopically, thus requiring ab initio approaches.

The C(^3P)–O(^3P) system could be, for example, considered. Collision integrals were derived in Capitelli and Ficocelli (1973) from accurate potential energy curves of all the electronic terms arising in the interaction, by fitting ab initio results with model potential, namely, the Morse function (Smith and Munn 1964) for bound and exponential decaying function (Monchick 1959) for purely repulsive states. The relevant potential parameters and the corresponding partial collision integrals are reported in Tables 3.4 and 3.5, respectively.

This approach, using model representations of states that are quite rigid and unable to reproduce special features of the interaction potentials (secondary minima or shoulders in the repulsive branch), could affect the collision integral accuracy in definite temperature ranges and therefore in the more recent literature more flexible functions have been introduced as the Hulburt–Hirschfelder (HH) model potential (Rainwater et al. 1982), used, for example, in the derivation of accurate collision integrals for binary col-

Table 3.4 Potential parameters for electronic terms in $C(^3P)$–$O(^3P)$ interaction (Capitelli and Ficocelli 1973)

Repulsive states [Eq. (3.37)]				Bound states [Eq. (3.38)]			
Term	A [eV]	ρ [Å^{-1}]		Term	C	φ_0 [eV]	σ [Å]
$2^1\Sigma^+$	2,388.0	4.83		$X^1\Sigma^+$	2.15	8.19	0.93
$2^3\Sigma^+$	5,172.0	4.81		$a'^3\Sigma^+$	2.71	3.13	1.17
$2^5\Sigma^+$	881.0	3.28		$a^3\Pi$	3.38	2.97	1.10
$1^5\Sigma^-$	1,306.0	3.41		$d^3\Delta$	3.34	2.13	1.24
$2^1\Pi$	65.0	1.66	$T \geq 18{,}000$ K	$e^3\Sigma^-$	3.53	1.81	1.26
	1,180.0	3.34	$T > 18{,}000$ K	$I^1\Sigma^-$	3.55	1.53	1.29
$2^3\Pi$	72.0	2.62	$T \geq 11{,}000$ K	$D^1\Delta$	3.48	1.44	1.30
	355.0	2.90	$T > 11{,}000$ K	$A^1\Pi$	5.52	1.11	1.20
$2^5\Pi$	964.0	3.35		$1^5\Pi$	5.92	0.44	1.45
$1^5\Delta$	1,226.0	3.40		$1^5\Sigma^+$	4.63	0.40	1.65

Table 3.5 Diffusion- and viscosity-type collision integrals as a function of temperature for $C(^3P)$–$O(^3P)$ interaction (Capitelli and Ficocelli 1973)

T [K]	$\sigma^2\Omega^{(1,1)\star}$ [Å^2]	$\sigma^2\Omega^{(2,2)\star}$ [Å^2]
2,000	6.487	7.056
4,000	5.290	5.869
6,000	4.564	5.172
8,000	4.077	4.691
10,000	3.701	4.304
15,000	3.021	3.570
20,000	2.656	3.175

lision of ground-state carbon atoms (Biolsi et al. 1982). The $C(^3P)$–$C(^3P)$ interaction evolves along 18 potential energy curves of the molecule C_2, i.e. $2^{1,5}\Sigma_g^+$, $^{1,5}\Sigma_u^-$, $2^3\Sigma_u^+$, $^3\Sigma_g^-$, $^{1,3,5}\Pi_{gu}$, $^{1,5}\Delta_g$, and $^3\Delta_u$; out of them, five states are purely repulsive: $^5\Sigma_u^-$, $^5\Pi_u$, $^5\Delta_g$, the second state of symmetries $^3\Sigma_u^+$ and $^5\Sigma_g^+$. In Biolsi et al. (1982) authors performed a comparison, in a wide temperature range, between two series of collision integrals, one set obtained by using Hulburt–Hirschfelder (HH) model potential for bound states, with potential parameters derived from accurate spectroscopic constants, and by fitting the ab initio results for repulsive states, the second set consisting of older results obtained by using the less *accommodating* Morse potential function (Biolsi and Biolsi 1979) for state with an attractive well and neglecting the contribution of $^3\Sigma_u^+$ and $^5\Sigma_g^+$ repulsive states.

In Table 3.6 the viscosity-type collision integrals in the two different calculation schemes are reported. The deviations of the averaged collision integral could be ascribed to the interplay of the different factors while considering only bound states. An almost temperature-independent relative error is found that indicates, for this system, an overestimation of collision integrals in the Morse-function model. The inclusion of missing repulsive terms accounts for a positive contribution, more effective in the high-temperature region. This analysis clarifies the critical aspects in the derivation of collision integrals in the multi-potential approach, having large effects in open-shell system interactions, characterized by a significant number of contributing terms and expected to be even larger for colliding pairs involving excited species.

Table 3.6 Viscosity-type collision integrals as a function of temperature for $C(^3P)$–$C(^3P)$ interaction obtained with a complete electronic manifold and HH potentials for bound states (Biolsi et al. 1982) (*a*), compared with older results obtained with Morse function fitting of bound states and missing some repulsive electronic terms (Biolsi and Biolsi 1979) (*b*)

T [K]	$\sigma^2\Omega^{(2,2)\star}$ [Å^2] (*a*)		$\sigma^2\Omega^{(2,2)\star}$ [Å^2] (*b*)	
	Total	Only bound	Total	Only bound
1,000	9.5400	5.0091	10.9550	6.7198
5,000	6.3116	3.4455	7.3393	4.8704
10,000	5.1913	2.9241	5.9610	4.1437
15,000	4.5207	2.5688	5.0620	3.6872
20,000	3.9958	2.2518	4.3663	3.2889
25,000	3.5765	1.9860	3.8553	2.9640

Moving to the interactions involving molecular partners, the electronic terms of the molecular system actually become potential energy surfaces, depending on an ensemble of coordinates related to the degrees of freedom of the system; however, it is still possible the use of $\varphi(r)$, i.e. a function of the coordinate along the approaching direction, thus neglecting the anisotropy of the potential due to the dependence on the relative orientation of the molecular partners, as demonstrated in Sect. 3.4.3.

3.4.2 Average Potential Approaches: Mixing Rules and Phenomenological Potential

The multi-potential approach could lead to very accurate results but for a limited number of colliding systems. Thus in literature alternative approaches have been proposed to describe in a satisfactory way the average potential energy curve of the unknown or exotic interactions.

This is the case of the so-called *mixing rules*, early suggested by Hirschfelder et al. (1966), modelling the average interaction with the Lennard–Jones potential, in Eq. (3.40), with parameters (σ, φ_0) obtained for asymmetrical interactions through simplified expressions involving well-known parameters for symmetrical colliding pairs, i.e. arithmetic mean of collision diameter and a geometric mean of the potential well depth

$$\sigma_{ij} = \tfrac{1}{2}(\sigma_{ii} + \sigma_{jj}) \qquad (\varphi_0)_{ij} = \sqrt{(\varphi_0)_{ii}(\varphi_0)_{jj}} \tag{3.57}$$

Also slightly complex relations do exist, known as the Waldman–Hagler and Halgren rules (Rat et al. 2008).

In this frame the *phenomenological approach*, developed by Pirani et al. (2004, 2006), has to be considered. The model potential can be regarded as an improvement of the Lennard–Jones potential, able to predict intermolec-

ular interactions in a variety of systems (neutral–neutral and neutral–ion). Fundamental interaction features, i.e. binding energy and equilibrium distance, enter the relevant equations as parameters and their values are determined on the basis of correlation formulas of the physical properties of colliding partners (polarizability, charge, number of electrons effective in polarization) (Liuti and Pirani 1985; Cambi et al. 1991; Cappelletti et al. 1991; Aquilanti et al. 1996).

The proposed "full-range" phenomenological potential simulating the average interaction could allow direct evaluation of internally consistent complete sets of collision integrals for different atmospheres. The validity of this approach was demonstrated in Capitelli et al. (2007) by comparing, for some benchmark systems, results obtained using the model potential with those calculated with more accurate methods (Stallcop et al. 1991, 2000, 2001; Levin and Wright 2004).

The potential has the form

$$\varphi = \varphi_0 \left[\frac{m}{n(x) - m} \left(\frac{1}{x} \right)^{n(x)} - \frac{n(x)}{n(x) - m} \left(\frac{1}{x} \right)^{m} \right] \tag{3.58}$$

where $x = r/r_e$, $n(x) = \beta + 4x^2$. For neutral–neutral and neutral–ion cases the parameter m has the value of 6 and 4, respectively. The value of β parameter, ranging from 6 to 10 depending on the hardness of interacting electronic distribution densities, could be estimated through the following empirical formula (Capitelli et al. 2007):

$$\beta = 6 + \frac{5}{(s_1 + s_2)} \tag{3.59}$$

where the subscripts 1 and 2 identify the colliding partners. The *softness* s, entering Eq. (3.59), is defined as the cubic root of the polarizability. For open-shell atoms and ions a multiplicative factor, which is the ground-state spin multiplicity, should be also considered.

For neutral–neutral systems, the phenomenological method represents the binding energy, φ_0, and the equilibrium distance, r_e, in terms of polarizabilities of the interacting partners, α, by the following correlation formulas (Liuti and Pirani 1985; Cambi et al. 1991; Pirani et al. 2001):

$$r_e = 1.767 \frac{\alpha_1^{1/3} + \alpha_2^{1/3}}{(\alpha_1 \alpha_2)^{0.095}} \tag{3.60}$$

$$\varphi_0 = 0.72 \frac{C_d}{r_e^6} \tag{3.61}$$

where r_e is given in Å, α in Å^3 and φ_0 in eV. The C_d constant (eV Å^6) is an effective long-range London coefficient

$$C_d = 15.7 \frac{\alpha_1 \alpha_2}{\left[\sqrt{\alpha_1/N_1} + \sqrt{\alpha_2/N_2}\right]} \tag{3.62}$$

where N is the effective number of electrons which contribute to the polarization of the neutral species. Previous formulas have been also extended to neutral–ion systems (Cappelletti et al. 1991; Aquilanti et al. 1996), introducing the parameter ρ, representative of the relative role of dispersion and induction attraction components in proximity to the equilibrium distance:

$$r_e = 1.767 \frac{\alpha_i^{1/3} + \alpha_n^{1/3}}{(\alpha_i \alpha_n [1 + 1/\rho])^{0.095}} \tag{3.63}$$

$$\varphi_0 = 5.2 \frac{z^2 \alpha_n}{r_e^4} [1 + \rho] \tag{3.64}$$

$$\rho = \frac{\alpha_i}{z^2 [1 + (2\alpha_i/\alpha_n)^{2/3}] \sqrt{\alpha_n}} \tag{3.65}$$

where α_n and α_i are the neutral and ionic polarizability, respectively.

In the case of phenomenological potential σ ($\varphi(\sigma)$=0) corresponds to $x_0 = \sigma/r_e$, solution of the transcendental equation

$$x_0^{(m-n(x_0))} = \frac{n(x_0)}{m} \tag{3.66}$$

In order to set results available and to favour their inclusion in transport codes, collision integrals have been fitted as a function of β with the expression

$$\ln \Omega^{(\ell,s)\star} = [a_1(\beta) + a_2(\beta)x] \frac{e^{(x-a_3(\beta))/a_4(\beta)}}{e^{(x-a_3(\beta))/a_4(\beta)} + e^{(a_3(\beta)-x)/a_4(\beta)}} + a_5(\beta) \frac{e^{(x-a_6(\beta))/a_7(\beta)}}{e^{(x-a_6(\beta))/a_7(\beta)} + e^{(a_6(\beta)-x)/a_7(\beta)}} \tag{3.67}$$

where $x = \ln T^\star$ and parameters a_i are polynomial functions of β

$$a_i(\beta) = \sum_{j=0}^{2} c_j \beta^j \tag{3.68}$$

Parameters entering Eq. (3.68) are presented in Tables 3.7 and 3.8 for neutral–ion (m=4) and neutral–neutral (m=6) interaction, respectively (Laricchiuta et al. 2007).

Table 3.7 Fitting parameters, entering Eq. (3.68), of classical transport collision integrals $\Omega^{(\ell,s)\star}$ for neutral–ion interactions ($m = 4$)

	$\Omega^{(1,1)\star}$			$\Omega^{(1,2)\star}$		
	c_0	c_1	c_2	c_0	c_1	c_2
a_1	9.851755(−01)	−2.870704(−02)	−	8.361751(−01)	−3.201292(−02)	−
a_2	−4.737800(−01)	−1.370344(−03)	−	−4.707355(−01)	−1.783284(−03)	−
a_3	7.080799(−01)	4.575312(−03)	−	1.771157(−01)	1.172773(−02)	−
a_4	−1.239439(+00)	−3.683605(−02)	−	−1.094937(+00)	−3.115598(−02)	−
a_5	−4.638467(+00)	4.418904(−01)	−1.220292(−02)	−4.976384(+00)	4.708074(−01)	−1.283818(−02)
a_6	3.841835(+00)	3.277658(−01)	−2.660275(−02)	3.645873(+00)	3.699452(−01)	−2.988684(−02)
a_7	2.317342(+00)	3.912768(−01)	−3.136223(−02)	2.428864(+00)	4.267351(−01)	−3.278874(−02)
	$\Omega^{(1,3)\star}$			$\Omega^{(1,4)\star}$		
	c_0	c_1	c_2	c_0	c_1	c_2
a_1	7.440562(−01)	−3.453851(−02)	−	6.684360(−01)	−3.515695(−02)	−
a_2	−4.656306(−01)	−2.097901(−03)	−	−4.622014(−01)	−2.135808(−03)	−
a_3	−1.465752(−01)	1.446209(−02)	−	−3.464990(−01)	1.336362(−02)	−
a_4	−1.080410(+00)	−2.712029(−02)	−	−1.054374(+00)	−3.149321(−02)	−
a_5	−5.233907(+00)	4.846691(−01)	−1.280346(−02)	−5.465789(+00)	4.888443(−01)	−1.228090(−02)
a_6	3.489814(+00)	4.140270(−01)	−3.250138(−02)	3.374614(+00)	4.602468(−01)	−3.463073(−02)
a_7	2.529678(+00)	4.515088(−01)	−3.339293(−02)	2.648622(+00)	4.677409(−01)	−3.339297(−02)
	$\Omega^{(1,5)\star}$			$\Omega^{(2,2)\star}$		
	c_0	c_1	c_2	c_0	c_1	c_2
a_1	6.299083(−01)	−3.720000(−02)	−	9.124518(−01)	−2.398461(−02)	−
a_2	−4.560921(−01)	−2.395779(−03)	−	−4.697184(−01)	−7.809681(−04)	−
a_3	−5.228598(−01)	1.594610(−02)	−	1.031053(+00)	4.069668(−03)	−
a_4	−1.124725(+00)	−2.862354(−02)	−	−1.090782(+00)	−2.413508(−02)	−
a_5	−5.687354(+00)	4.714789(−01)	−1.056602(−02)	−4.127243(+00)	4.302667(−01)	−1.352874(−02)
a_6	3.267709(+00)	5.281419(−01)	−3.678869(−02)	4.059078(+00)	2.597379(−01)	−2.169951(−02)
a_7	2.784725(+00)	4.840700(−01)	−3.265127(−02)	2.086906(+00)	2.920310(−01)	−2.560437(−02)
	$\Omega^{(2,3)\star}$			$\Omega^{(2,4)\star}$		
	c_0	c_1	c_2	c_0	c_1	c_2
a_1	8.073459(−01)	−2.581232(−02)	−	7.324117(−01)	−2.727580(−02)	−
a_2	−4.663682(−01)	−1.030271(−03)	−	−4.625614(−01)	−1.224292(−03)	−
a_3	6.256342(−01)	4.086881(−03)	−	3.315871(−01)	7.216776(−03)	−
a_4	−1.063437(+00)	−1.235489(−02)	−	−1.055706(+00)	−8.585500(−03)	−
a_5	−4.365989(+00)	4.391454(−01)	−1.314615(−02)	−4.571022(+00)	4.373660(−01)	−1.221457(−02)
a_6	3.854346(+00)	3.219224(−01)	−2.587493(−02)	3.686006(+00)	3.854493(−01)	−2.937568(−02)
a_7	2.146207(+00)	3.325620(−01)	−2.686959(−02)	2.217893(+00)	3.641196(−01)	−2.763824(−02)

(continued)

Table 3.7 (continued)

	$\Omega^{(3,3)\star}$			$\Omega^{(4,4)\star}$		
	c_0	c_1	c_2	c_0	c_1	c_2
a_1	8.402943(−01)	−2.851694(−02)	—	8.088842(−01)	−2.592379(−02)	—
a_2	−4.727437(−01)	−1.328784(−03)	—	−4.659483(−01)	−1.041599(−03)	—
a_3	4.724228(−01)	7.706027(−03)	—	6.092981(−01)	1.428402(−03)	—
a_4	−1.213660(+00)	−3.456656(−02)	—	−1.113323(+00)	−1.031574(−02)	—
a_5	−4.655574(+00)	4.467685(−01)	−1.237864(−02)	−4.349145(+00)	4.236246(−01)	−1.210668(−02)
a_6	3.817178(+00)	3.503180(−01)	−2.806506(−02)	3.828467(+00)	3.573461(−01)	−2.759622(−02)
a_7	2.313186(+00)	3.889828(−01)	−3.120619(−02)	2.138075(+00)	3.388072(−01)	−2.669344(−02)

Table 3.8 Fitting parameters, entering Eq. (3.68), of classical transport collision integrals $\Omega^{(\ell,s)\star}$ for neutral–neutral interactions ($m = 6$)

	$\Omega^{(1,1)\star}$			$\Omega^{(1,2)\star}$		
	c_0	c_1	c_2	c_0	c_1	c_2
a_1	7.884756(−01)	−2.438494(−02)	−	7.123565(−01)	−2.688875(−02)	−
a_2	−2.952759(−01)	−1.744149(−03)	−	−2.910530(−01)	−2.065175(−03)	−
a_3	5.020892(−01)	4.316985(−02)	−	4.187065(−02)	4.060236(−02)	−
a_4	−9.042460(−01)	−4.017103(−02)	−	−9.287685(−01)	−2.342270(−02)	−
a_5	−3.373058(+00)	2.458538(−01)	−4.850047(−03)	−3.598542(+00)	2.545120(−01)	−4.685966(−03)
a_6	4.161981(+00)	2.202737(−01)	−1.718010(−02)	3.934824(+00)	2.699944(−01)	−2.009886(−02)
a_7	2.462523(+00)	3.231308(−01)	−2.281072(−02)	2.578084(+00)	3.449024(−01)	−2.292710(−02)
	$\Omega^{(1,3)\star}$			$\Omega^{(1,4)\star}$		
	c_0	c_1	c_2	c_0	c_1	c_2
a_1	6.606022(−01)	−2.831448(−02)	−	6.268016(−01)	−2.945078(−02)	−
a_2	−2.870900(−01)	−2.232827(−03)	−	−2.830834(−01)	−2.361273(−03)	−
a_3	−2.519690(−01)	3.778211(−02)	−	−4.559927(−01)	3.705640(−02)	−
a_4	−9.173046(−01)	−1.864476(−02)	−	−9.334638(−01)	−1.797329(−02)	−
a_5	−3.776812(+00)	2.552528(−01)	−4.237220(−03)	−3.947019(+00)	2.446843(−01)	−3.176374(−03)
a_6	3.768103(+00)	3.155025(−01)	−2.218849(−02)	3.629926(+00)	3.761272(−01)	−2.451016(−02)
a_7	2.695440(+00)	3.597998(−01)	−2.267102(−02)	2.824905(+00)	3.781709(−01)	−2.251978(−02)
	$\Omega^{(1,5)\star}$			$\Omega^{(2,2)\star}$		
	c_0	c_1	c_2	c_0	c_1	c_2
a_1	5.956859(−01)	−2.915893(−02)	−	7.898524(−01)	−2.114115(−02)	−
a_2	−2.804989(−01)	−2.298968(−03)	−	−2.998325(−01)	−1.243977(−03)	−
a_3	−5.965551(−01)	3.724395(−02)	−	7.077103(−01)	3.583907(−02)	−
a_4	−8.946001(−01)	−2.550731(−02)	−	−8.946857(−01)	−2.473947(−02)	−
a_5	−4.076798(+00)	1.983892(−01)	−5.014065(−04)	−2.958969(+00)	2.303358(−01)	−5.226562(−03)
a_6	3.458362(+00)	4.770695(−01)	−2.678054(−02)	4.348412(+00)	1.920321(−01)	−1.496557(−02)
a_7	2.982260(+00)	4.014572(−01)	−2.142580(−02)	2.205440(+00)	2.567027(−01)	−1.861359(−02)
	$\Omega^{(2,3)\star}$			$\Omega^{(2,4)\star}$		
	c_0	c_1	c_2	c_0	c_1	c_2
a_1	7.269006(−01)	−2.233866(−02)	−	6.829159(−01)	−2.332763(−02)	−
a_2	−2.972304(−01)	−1.392888(−03)	−	−2.943232(−01)	−1.514322(−03)	−
a_3	3.904230(−01)	3.231655(−02)	−	1.414623(−01)	3.075351(−02)	−
a_4	−9.442201(−01)	−1.494805(−02)	−	−9.720228(−01)	−1.038869(−02)	−
a_5	−3.137828(+00)	2.347767(−01)	−4.963979(−03)	−3.284219(+00)	2.243767(−01)	−3.913041(−03)
a_6	4.190370(+00)	2.346004(−01)	−1.718963(−02)	4.011692(+00)	3.005083(−01)	−2.012373(−02)
a_7	2.319751(+00)	2.700236(−01)	−1.854217(−02)	2.401249(+00)	2.943600(−01)	−1.884503(−02)

(continued)

Table 3.8 (continued)

	$\Omega^{(3,3)\star}$			$\Omega^{(4,4)\star}$		
	c_0	c_1	c_2	c_0	c_1	c_2
a_1	7.468781(−01)	−2.518134(−02)	–	7.365470(−01)	−2.242357(−02)	–
a_2	−2.947438(−01)	−1.811571(−03)	–	−2.968650(−01)	−1.396696(−03)	–
a_3	2.234096(−01)	3.681114(−02)	–	3.747555(−01)	2.847063(−02)	–
a_4	−9.974591(−01)	−2.670805(−02)	–	−9.944036(−01)	−1.378926(−02)	–
a_5	−3.381787(+00)	2.372932(−01)	−4.239629(−03)	−3.136655(+00)	2.176409(−01)	−3.899247(−03)
a_6	4.094540(+00)	2.756466(−01)	−2.009227(−02)	4.145871(+00)	2.855836(−01)	−1.939452(−02)
a_7	2.476087(+00)	3.300898(−01)	−2.223317(−02)	2.315532(+00)	2.842981(−01)	−1.874462(−02)

3.4.3 Comparison Between Multi-potential and Phenomenological Approaches

A wide literature does exist on the exact multi-potential treatment of ground-state interactions relevant to hydrogen and air plasmas. The $O(^3P)$–$O(^3P)$ can be a suitable example. The momentum coupling of atomic electronic terms originates 18 molecular states ($2^{1,5}\Sigma_g^+$, $^{1,5}\Sigma_u^-$, $2^3\Sigma_u^+$, $^3\Sigma_g^-$, $^{1,3,5}\Pi_{gu}$, $^{1,5}\Delta_g$, $^3\Delta_u$) and the collision integral is defined as the weighted average of contributions from each term [see Eq. (3.56)].

The results by Yun and Mason (1962), dated 1962, were based on accurate force laws and the advancement in the theoretical study of electronic structure of O_2 molecule has been followed by an increasing accuracy in the calculation of corresponding collision integrals. The commonly adopted approach is the fitting of ab initio data using model potentials, whose $\Omega^{(\ell,s)\star}$ values are known, though quantum mechanical approaches can be also found in literature (Levin et al. 1990).

It is possible to trace the improvements either moving from a rigid classification of Morse and exponential decaying potentials, for bound and repulsive states, respectively (Capitelli and Ficocelli 1972; Laricchiuta et al. 2008) to functional forms able to accommodate peculiar potential features like double minima (Hulburt–Hirschfelder potential) (Sourd et al. 2006; André et al. 2007) or using re-evaluated ab initio potential energy curves.

In Table 3.9 theoretical diffusion- and viscosity-type collision integrals for ground-state oxygen–oxygen interaction by different authors (Yun and Mason 1962; Capitelli and Ficocelli 1972; Levin et al. 1990; André et al. 2007; Laricchiuta et al. 2008) are reported, considering the temperature interval relevant to the existence of atomic oxygen in an LTE plasma. An excellent agreement is found among the results of Capitelli and Ficocelli (1972); André et al. (2007), both based on analytical fits and the ones by Levin et al. (1990) based on quantum mechanically derived potential energy surfaces, with deviations below 4 % in the whole temperature range. Instead discrepancies within 20 % are observed in the low-temperature region with collision integrals by Laricchiuta et al. (2008), obtained following the same approach used in Capitelli and Ficocelli (1972) with updated interaction potentials. The relative difference decreases with temperature, reaching about 10 % at 20,000 K. It should be noted that different sets show quite similar values (10 % at T =2,000 K) for the relative distance from the old results by Yun and Mason (1962), this agreement being also due to compensation effects between the contributions coming from the 18 potential curves (Capitelli and Ficocelli 1972).

The case of $O(^3P)$–$O(^3P)$ interaction clarifies the critical point of the traditional approach, i.e. the availability of reliable curves for the *ensemble* of electronic terms. Thus recently a phenomenological approach has been proposed,

Table 3.9 Diffusion- and viscosity-type collision integrals for $O(^3P)$–$O(^3P)$ interaction from different authors

T[K]	$\sigma^2\Omega^{(1,1)\star}$					$\sigma^2\Omega^{(2,2)\star}$			
	(*a*)	(*b*)	(*c*)	(*d*)	(*e*)	(*b*)	(*c*)	(*d*)	(*e*)
2,000	5.27	4.69	4.84	4.81	6.01	5.45	5.58	5.57	6.97
4,000	4.39	3.98	4.00	4.07	4.88	4.66	4.67	4.74	5.74
6,000	3.90	3.58	3.57	3.63	4.26	4.21	4.20	4.26	5.06
8,000	3.58	3.30	3.27	3.33	3.84	3.90	3.88	3.94	4.59
10,000	3.34	3.09	3.05	3.11	3.53	3.67	3.64	3.69	4.24
12,000	3.15	2.93	2.87	2.94	3.28	3.49	3.44	3.50	3.97
14,000	3.00	2.79	2.72	2.79	3.08	3.34	3.28	3.34	3.74
16,000		2.68	2.59	2.67	2.91	3.21	3.14	3.20	3.55
18,000		2.58	2.48	2.56	2.77	3.10	3.02	3.08	3.38
20,000		2.49	2.38	2.47	2.64	3.00	2.91	2.98	3.24

(*a*) Yun and Mason (1962), (*b*) Capitelli and Ficocelli (1972), (*c*) Levin et al. (1990), (*d*) André et al. (2007), (*e*) Laricchiuta et al. (2008) (for results of André et al. (2007) tabulated values have been obtained by using the fitting formula in the paper by Andrè et al.)

overcoming this difficulty by considering the description of the average interaction through a modified Lennard–Jones potential (3.58).

The investigation on the applicability of the proposed methodology can proceed through the analysis of benchmark systems, such as $N(^4S)$–$N(^4S)$. According to the Witmer–Wigner rules the interaction occurs along four different potential curves corresponding to $^1\Sigma_g^+$, $^3\Sigma_u^+$, $^5\Sigma_g^+$, $^7\Sigma_u^+$ electronic terms. Following the pair valency theory we can rationalize the increase of the unbound character of the state with spin multiplicity. So while the singlet state is characterized by a strong chemical bond, the septet exhibits a repulsive potential, as can be appreciated in Fig. 3.8a, where relevant potential energy curves are reported. In the same figure the curve $<\varphi>$ is shown, resulting from the statistical average of the four potentials. This kind of averaging emphasizes the role of the repulsive states in smoothing the attractive parts of chemical bonds. The curve $<\varphi>$ for the N_2 system is compared, in Fig. 3.8b, with the one obtained with the phenomenological procedure. The comparison shows that the wells are quite similar, with a depth three orders of magnitude lower than that of the ground singlet state, and located approximately in the same internuclear distance range.

In Table 3.10 diffusion-type collision integrals, obtained integrating the classical deflection angle on the averaged and phenomenological potentials, are reported. In the same table a comparison with results from literature (Capitelli et al. 2000; Levin et al. 1990), obtained with the standard procedure, i.e. adiabatically averaging the contributions coming from the four different states, is also performed. In particular, collision integrals by Capitelli et al. (2000) result from a Morse fitting of experimental potential curves for the bound states and an exponential-repulsive function reproducing a Heitler–London calculation of septet state (Capitelli et al. 1983), while in the low-temperature region (T <1,000 K) a Lennard–Jones potential has been used. Levin et al. (1990) results are derived on the base of accurate ab initio calculations.

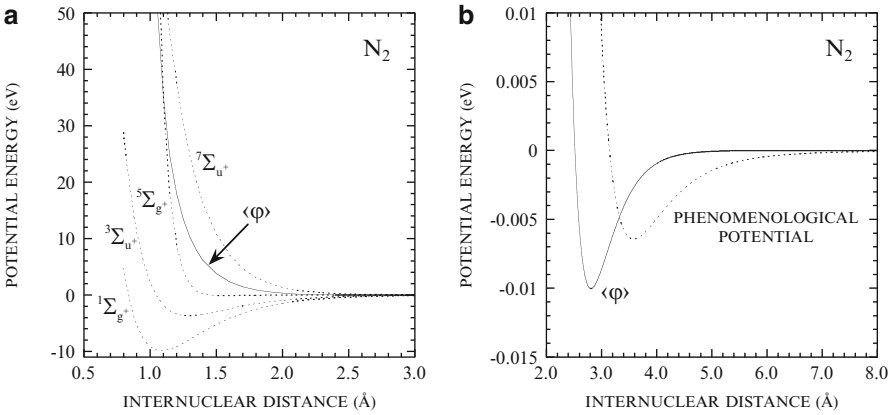

Fig. 3.8 The interaction potential energy in the N_2 system. (**a**) Potential energy curves for the electronic states correlating with $N(^4S)$–$N(^4S)$; (**b**) detail of averaged potential $< \varphi >$ (*full line*) and of phenomenological potential [Eq. (3.58)] (*dotted line*)

Table 3.10 Diffusion-type collision integrals, $\sigma^2\Omega^{(1,1)\star}$ [Å^2], as a function of temperature for $N(^4S)$–$N(^4S)$ interaction obtained with different approaches, compared with accurate theoretical results from Capitelli et al. (2000) and Levin et al. (1990)

T[K]	(*a*)	$< \varphi >$	(*b*)	(*c*)
500	7.34	5.54	7.76	7.03
1,000	6.30	4.82	6.79	5.96
2,000	5.42	4.25	5.25	5.15
4,000	4.64	3.74	4.50	4.39
5,000	4.40	3.58	4.27	4.14
6,000	4.21	3.45	4.09	3.94
8,000	3.93	3.26	3.79	3.61
10,000	3.72	3.11	3.55	3.37
15,000	3.36	2.84	3.12	2.92
20,000	3.13	2.66	2.82	2.62

(*a*) Capitelli et al. (2007), (*b*) Capitelli et al. (2000), (*c*) Levin et al. (1990)

We note a substantial agreement between data sets in literature (Capitelli et al. 2000; Levin et al. 1990). Agreement is also found when data in literature are compared with the collision integrals obtained by using the Pirani potential (column *a* in Table 3.10). In this case the differences increase with temperature, not exceeding 20 % below 15,000 K. Such behaviour indicates that the phenomenological approach describes accurately the potential well which plays a major role in the low-temperature region. The results obtained by integration of the average potential $< \varphi >$ underestimate the relevant collision integrals.

The models discussed above have been developed for isotropic interaction between colliding partners. This approach seems to be valid only for atom–atom and atom–atomic ion encounters; in fact atom–diatom dynamics develops on multidimensional surfaces and the interaction potential should take into account all the involved channels. Some authors have used classical trajectory calculation on ab initio surfaces for collisions

involving molecules (Viehland et al. 1996; Maclagan et al. 1999), considering anisotropic potentials. However, for small molecules, rapidly rotating, an isotropic potential can be assumed, as demonstrated in Stallcop et al. (2001), where ab initio multireference configuration-interaction calculations have been performed, deriving an effective angle-averaged potential for the estimation of transport cross sections of O–O_2 and N–N_2, thus reducing to a monodimensional problem.

Table 3.11 Diffusion- and viscosity-type collision integrals for $O(^3P)$-$O_2(X^3\Sigma_g^-)$ interaction from different authors

T [K]	$\sigma^2\Omega^{(1,1)\star}$			$\sigma^2\Omega^{(2,2)\star}$		
	(*a*)	(*b*)	(*c*)	(*a*)	(*b*)	(*c*)
100	13.96	13.68	13.51	15.60	15.31	14.92
200	10.46	10.32	9.99	11.60	11.49	10.91
300	9.20	9.10	8.77	10.24	10.13	9.60
400	8.52	8.39	8.15	9.53	9.39	8.93
600	7.75	7.58	7.47	8.74	8.61	8.23
800	7.28	7.09	7.08	8.26	8.13	7.83
1,000	6.95	6.74	6.81	7.92	7.78	7.56
2,000	6.03	5.70	4.59	6.96	6.71	5.31
3,000	5.54	5.15	4.24	6.44	6.09	4.93
4,000	5.22	4.78	4.00	6.09	5.67	4.67
6,000	4.78	4.29	3.68	5.60	5.13	4.31
8,000	4.48	3.96	3.45	5.27	4.78	4.07
10,000	4.26	3.71	3.29	5.02	4.50	3.88
20,000	3.63		2.80	4.30		3.33
30,000	3.29		2.53	3.91		3.03

(*a*) Capitelli et al. (2007),
(*b*) Stallcop et al. (2001),
(*c*) Capitelli et al. (2000)

Table 3.12 Diffusion- and viscosity-type collision integrals for $N(^4S)$-$N_2(X^1\Sigma_g^+)$ interaction from different authors

T [K]	$\sigma^2\Omega^{(1,1)\star}$			$\sigma^2\Omega^{(2,2)\star}$		
	(*a*)	(*b*)	(*c*)	(*a*)	(*b*)	(*c*)
100	15.03	15.04	16.31	16.76	16.56	17.99
200	11.15	11.41	12.10	12.38	12.58	13.24
300	9.75	10.10	10.65	10.86	11.21	11.65
400	9.00	9.39	9.90	10.08	10.47	10.86
600	8.16	8.57	9.08	9.21	9.68	10.02
800	7.65	8.08	8.62	8.69	9.17	9.53
1,000	7.29	7.70	8.29	8.33	8.81	9.20
2,000	6.30	6.65	5.29	7.29	7.76	6.34
3,000	5.78	6.06	4.75	6.73	7.16	5.73
4,000	5.43	5.65	4.38	6.35	6.73	5.32
6,000	4.96	5.05	3.89	5.83	6.18	4.76
8,000	4.65	4.61	3.56	5.48	5.74	4.38
10,000	4.41	4.25	3.31	5.21	5.36	4.09
20,000	3.74		2.61	4.44		3.27
30,000	3.38		2.23	4.03		2.83

(*a*) Capitelli et al. (2007),
(*b*) Stallcop et al. (2001),
(*c*) Capitelli et al. (2000)

For the $O(^3P)$–$O_2(X^3\Sigma_g^-)$ system the potential parameters suggested by this accurate procedure (σ= 3.205 [Å], φ_0/k = 80.7 [K]), which are relevant to the potential well and affect the collision integrals in the low-temperature region, are in satisfactory agreement with the phenomenological Pirani potential (Capitelli et al. 2007) (σ= 3.21 [Å], φ_0/k = 92.5 [K]) and also in reasonable agreement with experimental results (Morgan and Schiff 1964; Brunetti et al. 1981). This aspect is confirmed by the vanishing differences reported in Table 3.11 between diffusion- and viscosity-type collision integral results obtained from the phenomenological potential and from Stallcop et al. (2001) for T <5,000 K. The high-temperature region is dominated by the repulsive branch of the interaction potential and a great uncertainty exists on the behaviour of the potential for small interparticle distances. The potential proposed by Stallcop et al. (2001) is, in this region, less repulsive than the Pirani potential, explaining the increase of discrepancy between corresponding calculated collision integrals with temperature. The relative difference reaches the maximum value of 15 % for T=10,000 K. In the same table results from Capitelli et al. (2000), obtained for T <1,000 K using a

Lennard–Jones interaction potential and for $T > 2{,}000\,\mathrm{K}$ an experimental exponential-repulsive curve (the two data sets have been smoothly joined in the interval [1,000–2,000] K), have been reported, finding in general a satisfactory agreement. A good agreement is found between the present results and the corresponding ones from Stallcop et al. (2001), while it becomes less satisfactory when compared with data of Capitelli et al. (2000) for $T >$ 2,000 K.

An even better agreement is found in the case of the $\mathrm{N}(^4S)$–$\mathrm{N}_2(\mathrm{X}^1\Sigma_g^+)$ system (Table 3.12) between accurate results of Stallcop et al. (2001) and those obtained modelling the average interaction with the phenomenological potential, the relative differences remaining below 6 % in the whole temperature range. Again larger deviation is observed with respect to the collision integrals by Capitelli et al. (2000), especially in the high-temperature region ($T >$2,000 K) where differences reach about 30 %.

The procedure for estimation of elastic collision integrals in the case of neutral–ion interactions is the same already outlined for neutral–neutral collisions, thus characterized by the same drawbacks. Additionally in atom-parent-ion collisions the contribution coming from the resonant charge-transfer channel to odd-order terms should be estimated (for a detailed treatment see Chap. 4).

Also for this class of interactions the phenomenological approach has been validated for the derivation of viscosity-type and of inelastic contribution to diffusion-type collision integrals, considering benchmark systems (Capitelli et al. 2007), for example, the $\mathrm{N}(^4S)$–$\mathrm{N}^+(^3P)$ system interacting along the 12 related electronic states $^{2,4,6}\Sigma_{g,u}$, $^{2,4,6}\Pi_{g,u}$.

In Table 3.13 the viscosity-type collision integrals, not affected by the charge-transfer process, calculated with the phenomenological potential (Capitelli et al. 2007) are reported together with data in Gupta et al. (1990), Capitelli et al. (2000), Stallcop et al. (1991). Collision integrals calculated according to the Pirani potential show a reasonable agreement with Stallcop et al. (1991) and Capitelli et al. (2000) results, specially in the temperature range (5,000–20,000 K) in which N and N^+ are major species. The results in Gupta et al. (1990) are, on the contrary, higher with maximum relative difference of about 35 %.

The behaviour, in the considered temperature range, of the absolute error of data obtained with the phenomenological approach with respect to the accurate calculations, based on ab initio potentials for each interaction channel, is displayed the same by Levin et al. in Fig. 1 of Levin and Wright (2004). Levin used the effective potential in the Tang–Toennies form, which is actually a more complex function than the Pirani potential. However, it should be noted that in Levin and Wright (2004) the binding energy and the equilibrium distance, the two basic potential parameters, have been obtained using the methodology outlined above.

Same considerations apply to the case of $\mathrm{O}(^3\mathrm{P})$–$\mathrm{O}^+(^4\mathrm{S})$ collision. Atom and parent ion can interact originating $^{2,4,6}\Sigma_{g,u}$, $^{2,4,6}\Pi_{g,u}$ electronic molecular states and the corresponding $\sigma^2\Omega^{(2,2)\star}$ are presented in Table 3.14 and

Table 3.13 Viscosity-type collision integrals, $\sigma^2\Omega^{(2,2)\star}$ [Å^2], as a function of temperature for the N(^{4}S)–N$^+$(^{3}P) interaction obtained with different approaches

T[K]	(*a*)	(*b*)	(*c*)	(*d*)
500		16.41	13.25	18.54
1,000		13.27	11.32	11.65
2,000		10.50	9.55	7.88
4,000		8.33	7.85	6.09
5,000	9.32	7.74	7.32	5.72
6,000	8.64	7.26	6.90	5.45
8,000	7.67	6.48	6.26	5.09
10,000	6.99	5.84	5.79	4.83
15,000	5.91	4.66	4.99	4.41
20,000	5.25	3.87	4.46	4.13

(*a*) Gupta et al. (1990), (*b*) Stallcop et al. (1991), (*c*) Capitelli et al. (2000), (*d*) Capitelli et al. (2007)

Table 3.14 Viscosity-type collision integrals, $\sigma^2\Omega^{(2,2)\star}$ [Å^2], as a function of temperature for the O(^{3}P)–O$^+$(^{4}S) interaction obtained with different approaches

T[K]	(*a*)	(*b*)	(*c*)
500	14.78	10.19	15.22
1,000	11.14	8.73	9.58
2,000	8.72	7.40	6.50
4,000	6.94	6.09	5.05
5,000	6.39	5.65	4.74
6,000	5.95	5.29	4.53
8,000	5.26	4.73	4.23
10,000	4.75	4.31	4.02
15,000	3.92	3.61	3.67
20,000	3.41	3.18	3.45

(*a*) Stallcop et al. (1991), (*b*) Capitelli et al. (2000), (*c*) Capitelli et al. (2007)

compared with data in literature, still giving a satisfactory agreement, especially when compared with data in Capitelli et al. (2000) and Stallcop et al. (1991) in the temperature range of interest (5,000–20,000 K) and confirming that an effective potential, not directly connected with details of the interacting system in different electronic states, can be used for transport cross section prediction.

3.4.4 Electron–Neutral Interactions

In the case of electron–neutral collisions the quantum nature of the interactions is not negligible and manifests itself in the features of the energy profile of the cross section, as the low-energy peaks, due to resonances in the electron scattering, or the *Ramsauer minimum* (Gryzinski 1970). Therefore the quantum approach is required and the collision integrals are evaluated by integration of theoretical or experimental differential elastic electron-scattering cross sections (3.24).

The case of electron scattering by atomic argon could be illustrative, exhibiting a low-energy *Ramsauer minimum*. This system has been deeply studied and, combining theoretical results in the low-energy region (Bell et al. 1984) and measured elastic differential cross sections (Gibson et al. 1996; Panajotovic et al. 1997), completed at low and high scattering angles with theoretical cross sections (Nahar and Wadehra 1987), a wide energy range can be explored, allowing accurate estimation of transport cross sections and high-order collision integrals, displayed in Fig. 3.9.

A second example is represented by the elastic scattering by molecular nitrogen, exhibiting a peak structure in the energy region between 1 and 4 eV due to the capture of the electron in the resonant state $^2\Pi$ of the molecular ion N_2^-.

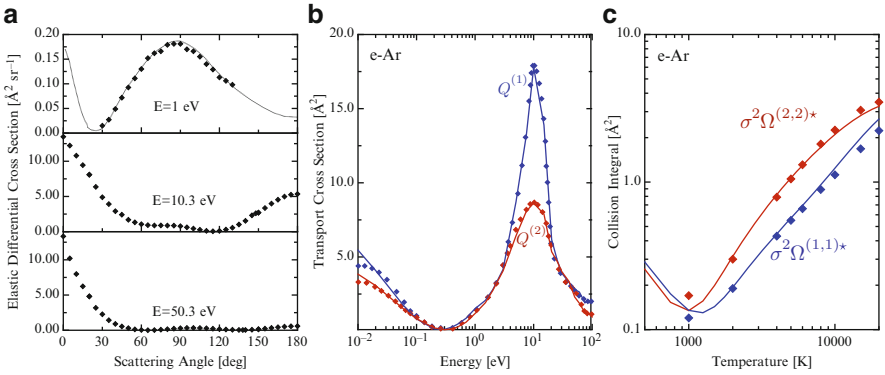

Fig. 3.9 (**a**) Differential cross sections for electron elastic scattering from Ar atoms at different electron impact energies, E=1 eV (*markers*) experimental data and (*dotted line*) results from phase-shift analysis from Gibson et al. (1996), $E = 10.3$ and 50.5 eV experimental data from Panajotovic et al. (1997). (**b**) Diffusion and viscosity transport cross sections for e-Ar system. (*markers*) (Rat et al. 2002) (*solid lines*) (Bruno et al. 2006). (**c**) Diffusion- and viscosity-type collision integrals for e-Ar interactions from Laricchiuta et al. (2009) (*solid lines*), compared with recommended data in Wright et al. (2005) (*open diamonds*)

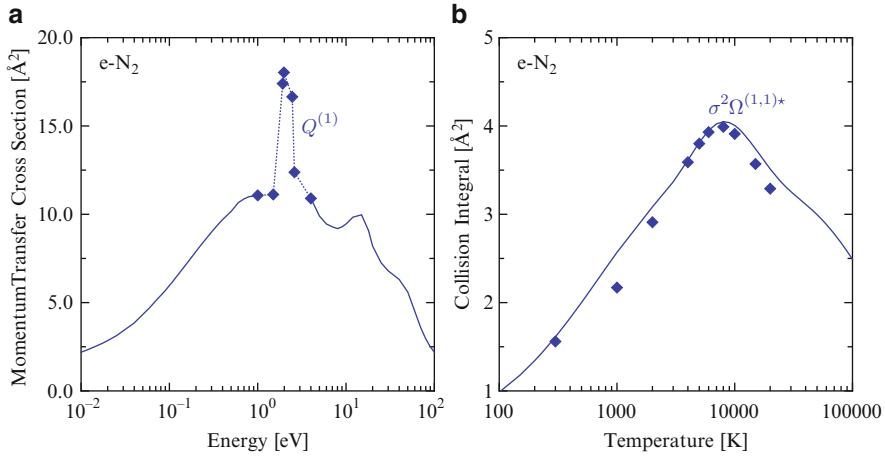

Fig. 3.10 (**a**) Recommended momentum transfer cross section (Itikawa 2006), $Q^{(1)}$, for e–N_2. (**b**) Diffusion-type collision integral as a function of temperature for e–N_2. (*solid line*) Laricchiuta et al. (2009) (*close diamonds*) recommended values from Wright et al. (2005)

The recommended values for the momentum transfer cross section, $Q^{(1)}$, displayed in Fig. 3.10, have been reviewed in Itikawa (2006) considering only an envelope of the resonance cross sections in the resonance region. The integration of transport cross sections allows the derivation of corresponding diffusion-type collision integral, presented in Fig. 3.10, where also the values recommended by Wright et al. (2005) are reported.

However, the critical point still remains the knowledge of the differential cross sections. In fact experimental data are usually available for few collision energy values, also missing extreme values of the scattering angle, and accurate theoretical results are also difficult to be retrieved for all the interactions. On the contrary the integral transport cross sections, elastic term $Q^{(0)}$ and momentum transfer $Q^{(1)}$ are found in literature for a number of systems (Itikawa 2002; Brunger and Buckman 2002; Itikawa 2006, 2009), allowing the straightforward derivation of diffusion-type collision integrals $\Omega^{(1,s)}$, but again for the higher-order viscosity-type collision integrals the $Q^{(2)}$ is not always readily available.

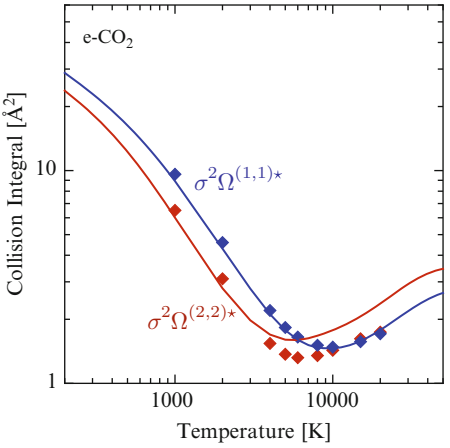

Fig. 3.11 Diffusion- and viscosity-type collision integrals for e–CO_2 interactions from Laricchiuta et al. (2009) (*solid lines*), compared with recommended data in Wright et al. (2007) (*close diamonds*)

These difficulties could be overcome by using different techniques to estimate this last from basic models or additional information. In Laricchiuta et al. (2009) the ratio Q^2/Q^1 has been determined from the known Q^1/Q^0 assuming a model angular dependence of the differential cross section:

$$\frac{1}{(1-h(E)\cos\vartheta)^2} \tag{3.69}$$

where h is here an adjustable parameter, which depends on the electron energy, obtained from the Q^1/Q^0 ratio. In extreme cases where the Q^0 cross section is also not available, according to Born scattering for a Coulomb screened potential, the h value has been fixed to

$$\frac{1}{(2\cdot 10.9\frac{Z^{2/3}}{E}+1)} \tag{3.70}$$

The approach has been demonstrated for the e–CO_2 interaction, taking the elastic and momentum transfer cross section from Itikawa (2002), giving

a satisfactory agreement with recommended data in literature as shown in Fig. 3.11.

Note that this approach can be considered as an extension of the model proposed in Longo and Capitelli (1994) for the treatment of anisotropy in elastic collisions in Monte Carlo simulations.

References

Amdur I (1961) An experimental approach to the determination of gaseous transport properties at very high temperatures. Planet Space Sci 3:228

Amdur I, Mason EA (1958) Properties of gases at very high temperatures. Phys Fluids 1(5):370–383

Amdur I, Engler MJ, Jordan JE, Mason EA (1975) Short-range He–Xe interaction from molecular-beam scattering. J Chem Phys 63(1):597–597

André P, Bussière W, Rochette D (2007) Transport coefficients of Ag-SiO_2 plasmas. Plasma Chem Plasma Process 27(4):381–403

Aquilanti V, Cappelletti D, Pirani F (1996) Range and strength of interatomic forces: dispersion and induction contributions to the bonds of dications and of ionic molecules. Chem Phys 209(2–3):299–311

Aziz RA, Slaman MJ (1990) The repulsive wall of the Ar–Ar interatomic potential reexamined. J Chem Phys 92(2):1030

Bell KL, Scott NS, Lennon MA (1984) The scattering of low-energy electrons by argon atoms. J Phys B At Mol Phys 17(23):4757

Beneventi L, Casavecchia P, Pirani F, Vecchiocattivi F, Volpi GG, Brocks G, van der Avoird A, Heijmen B, Reuss J (1991) The Ne–O_2 potential energy surface from high-resolution diffraction and glory scattering experiments and from the Zeeman spectrum. J Chem Phys 95(1):195–204

Biolsi L, Biolsi KJ (1979) Transport properties of monatomic carbon II: Contributions from excited electronic states. J Geophys Res 84(A9):5311–5318

Biolsi L, Rainwater JC, Holland PM (1982) Transport properties of monatomic carbon. J Chem Phys 77(1):448

Brunetti B, Pirani F, Vecchiocattivi F, Luzzatti E (1978) Absolute total cross sections for elastic scattering of Ne by Ar, Kr and Xe: characterization of long range interactions. Chem Phys Lett 55(3):565

Brunetti B, Liuti G, Luzzatti E, Pirani F, Vecchiocattivi F (1981) Study of the interactions of atomic and molecular oxygen with O_2 and N_2 by scattering data. J Chem Phys 74:6734

Brunetti B, Liuti G, Luzzatti E, Pirani F, Volpi GG (1983) The interaction of atomic and molecular nitrogen with argon by scattering measurements. J Chem Phys 79(1):273–277

Brunger MJ, Buckman SJ (2002) Electron-molecule scattering cross-sections. I. experimental techniques and data for diatomic molecules. Phys Rep 357(3–5):215–458

Bruno D, Catalfamo C, Laricchiuta A, Giordano D, Capitelli M (2006) Convergence of Chapman-Enskog calculation of transport coefficients of magnetized argon plasma. Phys Plasmas 13(7):072307

Cambi R, Cappelletti D, Liuti G, Pirani F (1991) Generalized correlations in terms of polarizability for van der Waals interaction potential parameter calculations. J Chem Phys 95(3):1852–1861

Capitelli M, Ficocelli E (1972) Collision integrals of oxygen atoms in different electronic states. J Phys B At Mol Phys 5(11):2066–2073

Capitelli M, Ficocelli E (1973) Collision integrals of carbon-oxygen atoms in different electronic states. J Phys B At Mol Phys 6:1819–1823

Capitelli M, Lamanna UT, Guidotti C, Arrighini GP (1983) Comment on 'spin-polarized atomic nitrogen and the $^7\Sigma_u^+$ state of N_2'. J Chem Phys 79:5210

Cappelletti D, Liuti G, Pirani F (1991) Generalization to ion—neutral systems of the polarizability correlations for interaction potential parameters. Chem Phys Lett 183(3–4):297–303

Capitelli M, Gorse C, Longo S, Giordano D (2000) Collision integrals of high-temperature air species. J Thermophys Heat Transf 14(2):259–268

Capitelli M, Cappelletti D, Colonna G, Gorse C, Laricchiuta A, Liuti G, Longo S, Pirani F (2007) On the possibility of using model potentials for collision integral calculations of interest for planetary atmospheres. Chem Phys 338(1):62–68

Capitelli M, Colonna G, D'Angola A (2011) Fundamental aspects of plasma chemical physics: thermodynamics. Springer series on atomic, optical, and plasma physics, vol 66. Springer, New York

Colonna G, Laricchiuta A (2008) General numerical algorithm for classical collision integral calculation. Comput Phys Commun 178(11):809–816

D'Angola A, Colonna G, Gorse C, Capitelli M (2008) Thermodynamic and transport properties in equilibrium air plasmas in a wide pressure and temperature range. Eur Phys J D 46(1):129–150

Devoto RS (1967) Transport coefficients of partially ionized argon. Phys Fluids 10(2):354–364

Devoto RS (1968) Transport coefficients of partially ionized hydrogen. J Plasma Phys 2(4):617–631

Geltman S (1969) Topics in atomic collision theory. Academic, New York

Gibson JC, Gulley RJ, Sullivan JP, Buckman SJ, Chan V, Burrow PD (1996) Elastic electron scattering from argon at low incident energies. J Phys B At Mol Opt Phys 29(14):3177

Gryzinski M (1970) Ramsauer effect as a result of the dynamic structure of the atomic shell. Phys Rev Lett 24:45–47

Gupta RN, Yos JM, Thompson RA, Lee KP (1990) A review of reaction and thermodynamic properties for 11-species air model for chemical and thermal non-equilibrium calculations to 30 000 K. NASA Report RP-1232

Hahn HS, Mason EA, Smith FJ (1971) Quantum transport cross sections in a completely ionized gas. Phys Fluids 14(2):278–287

Heck EL, Dickinson AS (1996) Transport and relaxation cross-sections for pure gases of linear molecules. Comput Phys Commun 95(2–3):190–220

Hirschfelder JO, Eliason MA (1957) The estimation of the transport properties for electronically excited atoms and molecules. Ann New York Acad Sci 67(9):451–461

Hirschfelder JO, Curtiss CF, Bird RB (1966) Molecular theory of gases and liquids. Wiley, New York

Itikawa Y (2002) Cross sections for electron collisions with carbon dioxide. J Phys Chem Ref Data 31(3):749–767

Itikawa Y (2006) Cross sections for electron collisions with nitrogen molecules. J Phys Chem Ref Data 35(1):31–53

Itikawa Y (2009) Cross sections for electron collisions with oxygen molecules. J Phys Chem Ref Data 38(1):1–20

Kalinin A, Dubrovitskii D (2000) The possibility of using repulsive interaction potentials for the calculation of high-temperature integrals of collisions between atoms and molecules. High Temp 38(6):848–851. Translated from Teplofizika Vysokikh Temperatur 38(6) (2000) 88–885

Kalinin A, Leonas V, Sermyagin A (1976) On the functionality of short-range potentials derived from the beam scattering data. Chem Phys Lett 39(1):191–193

Kihara T, Aono O (1963) Unified theory of relaxations in plasmas I. Basic theorem. J Phys Soc Japan 18(6):837–851

Kihara T, Taylor MH, Hirschfelder JO (1960) Transport properties for gases assuming inverse power intermolecular potentials. Phys Fluids 3(5):715–720

Landau DL, Lifshitz EM (1981) Quantum mechanics: non–relativistic theory. Butterworth–Heinemann, Oxford

Laricchiuta A, Colonna G, Bruno D, Celiberto R, Gorse C, Pirani F, Capitelli M (2007) Classical transport collision integrals for a Lennard-Jones like phenomenological model potential. Chem Phys Lett 445(4–6):133–139

Laricchiuta A, Bruno D, Capitelli M, Celiberto R, Gorse G, Pintus G (2008) Collision integrals of oxygen atoms and ions in electronically excited states. Chem Phys 344(1–2):13–20

Laricchiuta A, Bruno D, Capitelli M, Catalfamo C, Celiberto R, Colonna G, Diomede P, Giordano D, Gorse C, Longo S, Pagano D, Pirani F (2009) High temperature Mars atmosphere. Part I: Transport cross sections. Eur Phys J D 54(3):607–612

Leonas VB (1972) Studies of short-range intermolecular forces. Sov Phys Usp 15(3):266

Leonas V, Sermyagin A, Kamyshov N (1971) The short-range interaction of molecules: the experimental investigation of potential energy surfaces. Chem Phys Lett 8(3):282–284

Levin E, Wright MJ (2004) Collision integrals for ion-neutral interactions of nitrogen and oxygen. J Thermophys Heat Tran 18(1):143–147

Levin E, Partridge H, Stallcop J (1990) Collision integrals and high temperature transport properties for N-N, O-O and N-O. J Thermophys Heat Tran 4(4):469–477

Liboff RL (1959) Transport coefficients determined using the shielded Coulomb potential. Phys Fluids 2(1):40–46

Liuti G, Pirani F (1985) Regularities in van der Waals forces: correlation between the potential parameters and polarizability. Chem Phys Lett 122(3):245–250

Longo S, Capitelli M (1994) A simple approach to treat anisotropic elastic collisions in Monte Carlo calculations of the electron energy distribution function in cold plasmas. Plasma Chem Plasma Process 14:1–13

Maclagan RGAR, Viehland LA, Dickinson AS (1999) Ab initio calculation of the gas phase ion mobility of CO^+ ions in He. J Phys B At Mol Phys 32(20):4947

Mason EA (1954) Transport properties of gases obeying a modified Buckingham (expäêsix) potential. J Chem Phys 22(2):169

Mason EA (1957) Scattering of low velocity molecular beams in gases. J Chem Phys 26(3):667–677

Mason EA, Munn RJ, Smith FJ (1967) Transport coefficients of ionized gases. Phys Fluids 10(8):1827

Meeks F, Cleland T, Hutchinson K (1967) On the quantum cross sections in dilute gases. J Chem Phys 10(10):2105–2112

Monchick L (1959) Collision integrals for the exponential repulsive potential. Phys Fluids 2(6):695–700

Morgan JE, Schiff HI (1964) Diffusion coefficients of O and N atoms in inert gases. Canad J Chem 42(10):2300

Mott N, Massey H (1965) The theory of atomic collisions. Clarendon, Oxford

Murphy AB (2000) Transport coefficients of hydrogen and argon–hydrogen plasmas. Plasma Chem Plasma Process 20(3):279–297

Nahar SN, Wadehra JM (1987) Elastic scattering of positrons and electrons by argon. Phys Rev A 35:2051–2064

Neufeld PD, Janzen AR, Aziz RA (1972) Empirical equations to calculate 16 of the transport collision integrals $\Omega^{(\ell,s)\star}$ for the Lennard-Jones (12–6) potential. J Chem Phys 57(3):1100

O'Hara H, Smith F (1971) Transport collision integrals for a dilute gas. Comput Phys Commun 2(1):47–54

Panajotovic R, Filipovic D, Marinkovic B, Pejcev V, Kurepa M, Vuskovic L (1997) Critical minima in elastic electron scattering by argon. J Phys B At Mol Opt Phys 30(24):5877

Pirani F, Cappelletti D, Liuti G (2001) Range, strength and anisotropy of intermolecular forces in atom–molecule systems: an atom–bond pairwise additivity approach. Chem Phys Lett 350(3–4):286–296

Pirani F, Albertí M, Castro A, Teixidor MM, Cappelletti D (2004) Atom–bond pairwise additive representation for intermolecular potential energy surfaces. Chem Phys Lett 394(1–3):37–44

Pirani F, Maciel GS, Cappelletti D, Aquilanti V (2006) Experimental benchmarks and phenomenology of interatomic forces: open-shell and electronic anisotropy effects. Int Rev Phys Chem 25(1–2):165–199

Rainwater J, Holland P, Biolsi L (1982) Binary collision dynamics and numerical evaluation of dilute gas transport properties for potentials with multiple extrema. J Chem Phys 77(1):434–447

Rat V, André P, Aubreton J, Elchinger MF, Fauchais P, Vacher D (2002) Transport coefficients including diffusion in a two-temperature argon plasma. J Phys D Appl Phys 35(10):981–991

Rat V, Murphy AB, Aubreton J, Elchinger MF, Fauchais P (2008) Treatment of non-equilibrium phenomena in thermal plasma flows. J Phys D Appl Phys 41(18):183001

Singh NL, Jain DC (1962) The Rydberg-Klein-Rees method of constructing the true potential energy curves of diatomic molecules. Proc Phys Soc 79(2):274

Smith FJ (1967) High order collision integrals. Final Report on contract NSR 52-112-001 National Aeronautics and Space Administration

Smith F, Munn R (1964) Automatic calculation of the transport collision integrals with tables for the Morse potential. J Chem Phys 41(11):3560–3568

Sourd B, Aubreton J, Elchinger MF, Labrot M, Michon U (2006) High temperature transport coefficients in e/C/H/N/O mixtures. J Phys D Appl Phys 39(6):1105–1119

Stallcop JR, Partridge H, Levin E (1991) Resonance charge transfer, transport cross sections, and collision integrals for $N^+(^3P)$-$N(^4S)$ and $O^+(^4S)$-$O(^3P)$ interactions. J Chem Phys 95(9):6429–6439

Stallcop JR, Partridge H, Levin E (1992) Collision integrals for the interaction of the ions of nitrogen and oxygen in a plasma at high temperatures and pressures. Phys Fluids B Plasma Phys 4(2):386–391

Stallcop JR, Partridge H, Pradhan A, Levin E (2000) Potential energies and collision integrals for interactions of carbon and nitrogen atoms. J Thermophys Heat Tran 14(4):480–488

Stallcop JR, Partridge H, Levin E (2001) Effective potential energies and transport cross sections for atom-molecule interactions of nitrogen and oxygen. Phys Rev A 64(4):042722 1–12

Tang KT, Toennies JP (2003) The van der Waals potentials between all the rare gas atoms from He to Rn. J Chem Phys 118(11):4976–4983

Vanderslice JT (1962) Modification of the Rydberg-Klein-Rees method for obtaining potential curves for doublet states intermediate between Hund's cases (a) and (b). J Chem Phys 37(2):384–388

Viehland LA, Dickinson AS, Maclagan RGAR (1996) Transport coefficients for NO^+ ions in helium gas: a test of the NO^+-He interaction potential. Chem Phys 211(1–3):1–15

Wright MJ, Bose D, Palmer GE, Levin E (2005) Recommended collision integrals for transport property computations part 1: air species. AIAA J 43(12):2558–2564

Wright MJ, Hwang HH, Schwenke DW (2007) Recommended collision integrals for transport property computations part 2: Mars and Venus entries. AIAA J 45(1):281–288

Yun K, Mason E (1962) Collision integrals for the transport properties of dissociating air at high temperatures. Phys Fluids 5(4):380–386

Chapter 4
Resonant Charge Exchange in Ion-Parent–Atom Collisions: The Inelastic Contribution to Odd-Order Collision Integrals

Resonant charge-exchange cross sections are of paramount importance in affecting the diffusion-type, or more exactly the odd-order, collision integrals of ion-parent–atom collisional pairs. This process can be considered as an inelastic channel, however characterized by very high values of the cross section and therefore not negligible in the calculation of transport properties of thermal plasmas. Other kind of inelastic processes have been discussed in Chap. 1, their role being usually negligible at low temperatures (see also Chap. 10).

Some general considerations can follow from the classical-trajectory formulation. As a result of charge exchange, colliding species appear to be scattered through an angle of $(\pi - \vartheta)$, so as to lead to the expression

$$Q^{(\ell)} = 2\pi \int_0^\infty (1 - P_{\rm ex})[1 - \cos^\ell(\vartheta)] b \mathrm{d}b + 2\pi \int_0^\infty P_{\rm ex}[1 - \cos^\ell(\pi - \vartheta)] b \mathrm{d}b \quad (4.1)$$

It is straightforward that

$$\cos^\ell(\vartheta) = \cos^\ell(\pi - \vartheta) \text{ for } \ell \text{ even} \quad (4.2)$$

thus demonstrating that resonant charge-transfer processes do not affect even orders (Mason et al. 1959). Instead for ℓ odd, Eq. (4.1) reduces to

$$Q^{(\ell)} = 2\pi \int_0^\infty [1 - (1 - 2P_{\rm ex}) \cos^\ell(\vartheta)] b \mathrm{d}b \quad (4.3)$$

The probability of the process exponentially decays for large impact parameter values, while rapidly oscillates between 0 and 1 at small b. It is a common approximation (*random phase approximation*) in this case to replace $P_{\rm ex}$ by its average value, $\frac{1}{2}$, in the range of impact parameters smaller than a critical value, $b^\star$:

M. Capitelli et al., *Fundamental Aspects of Plasma Chemical Physics*, Springer Series on Atomic, Optical, and Plasma Physics 74,
DOI 10.1007/978-1-4419-8172-1_4, © Springer Science+Business Media, LLC 2013

$$
\begin{aligned}
Q^{(\ell)} &= 2\pi \int_0^{b^\star} [1 - (1 - 2P_{\rm ex})\cos^\ell(\vartheta)] b\mathrm{d}b \\
&\quad + 2\pi \int_{b^\star}^{\infty} [(1 - \cos^\ell(\vartheta)(1 - 2P_{\rm ex}) + 2P_{\rm ex}] b\mathrm{d}b \\
Q^{(\ell)} &= 2\left[\tfrac{1}{2}\pi (b^\star)^2 + 2\pi \int_{b^\star}^{\infty} P_{\rm ex} b\mathrm{d}b\right] + 2\pi \int_{b^\star}^{\infty} [(1 - \cos^\ell(\vartheta)(1 - 2P_{\rm ex})] b\mathrm{d}b \\
Q^{(\ell)} &= 2\sigma_{\rm ex} + 2\pi \int_{b^\star}^{\infty} [(1 - \cos^\ell(\vartheta)(1 - 2P_{\rm ex})] b\mathrm{d}b
\end{aligned}
\tag{4.4}
$$

The integral appearing in the last expression, accounting for the occurrence of elastic collisions, could be considered a negligible contribution to the transport cross section in the high-energy region, assessing the dominant role of resonant processes in transport. However, as already pointed out in the past (Knof et al. 1964), the low-temperature behaviour of the diffusion-type collision integral is actually governed by the polarization interaction, requiring the estimation of this elastic contribution. In the more recent literature, *effective* odd-order collision integrals are considered resulting by the geometrical mean of elastic and inelastic resonant contributions (Murphy 1995)

$$
\Omega^{(\ell,s)\star} = \sqrt{(\Omega_{\rm el}^{(\ell,s)\star})^2 + (\Omega_{\rm ex}^{(\ell,s)\star})^2} \tag{4.5}
$$

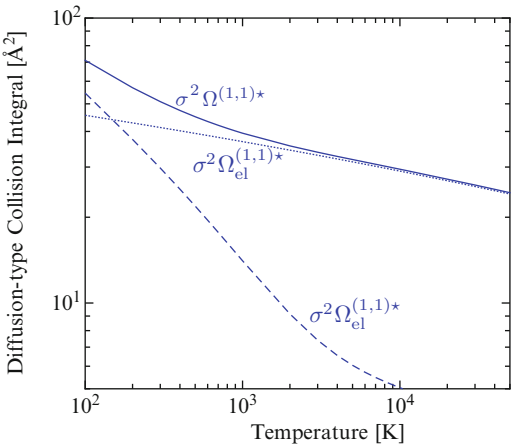

Fig. 4.1 Diffusion-type collision integrals (*solid line*) for C–C$^+$ interaction, resulting from elastic (*dashed line*) and resonant charge-exchange (*dotted line*) contributions

In Fig. 4.1 the two contributions are displayed in a wide temperature range for the C–C$^+$ interaction together with the *effective* collision integral, confirming the qualitative considerations done.

Though the inelastic contribution to the collision integral results, in principle, by the integration of the transport cross section [Eq. (3.11)], even nowadays it is widely diffuse the use of the closed forms derived in Devoto (1967). In fact if the resonant charge-exchange cross section [Å^2] shows a dependence on the relative velocity g [cm s^{-1}] of the type

$$\sqrt{2\sigma_{\mathrm{ex}}} = C - D\ln(g) \tag{4.6}$$

the collision integral assumes the form

$$\sigma^2\Omega_{\mathrm{ex}}^{(\ell,s)\star} = \frac{1}{\pi}\left\{C^2 - CDx + \left[\frac{1}{2}Dx\right]^2 + \frac{D^2}{4}\left\{\frac{\pi^2}{6} - \sum_{n=0}^{s+1}\frac{1}{n^2} + \left[\sum_{n=0}^{s+1}\frac{1}{n} - \overline{\gamma}\right]^2\right\}\right.$$
$$\left. + \frac{1}{2}D\xi[Dx - 2C] + \frac{D}{2}[D(x+\xi) - 2C]\ln\left(\frac{T}{M}\right) + \left[\frac{D}{2}\ln\left(\frac{T}{M}\right)\right]^2\right\} \tag{4.7}$$

M is the molecular weight, $x = \ln(4R)$ with R constant of perfect gas, $\overline{\gamma}$ is the Euler constant. Eq. (4.7) allows an accurate and straightforward estimation of $\Omega_{\mathrm{ex}}^{(\ell,s)}$ by a simple algebraic formula, once known, through linear regression algorithms, the C and D values.

Thus the problem reduces to the estimation of the charge-exchange cross section obtained either by crossed-beam experiments (Rutherford and Vroom, 1974; Belyaev et al. 1968) or through quantum or semiclassical approaches.

4.1 Theory of Resonant Charge-Exchange Processes

4.1.1 Quantum Approach

The resonant charge exchange in ion-parent–atom collisions is a quantum process of non-adiabatic transition between resonant states, characterized by high probability at large separation between colliders, compared to their dimension

$$\tilde{\mathrm{A}} + \mathrm{A}^+ \rightarrow \tilde{\mathrm{A}}^+ + \mathrm{A} \tag{4.8}$$

The rigorous quantum coupled-channel approach accounting for all open channels entails the solution of a complex system of coupled differential equations, requiring an high computational load and furthermore loosing the information on the mechanism. Thus usually the system is transformed in a basis of states so that the interaction is localized within a small region of distances. In this scheme the interaction is restricted to two states strongly coupled in a localized non-adiabatic region, the so-called *two state approximation*, and the resonant charge-exchange process can occur through the interaction of two distinct pathways owing to the symmetry of the quasi-molecule states. In fact, while at large distances, the molecular arrangements $\tilde{\mathrm{A}}\mathrm{A}^+$ and $\tilde{\mathrm{A}}^+\mathrm{A}$ are degenerate, as the particles approach, the exchange interaction splits the

molecular states into a pair of symmetric *gerade* and antisymmetric *ungerade* terms, with respect to the exchange of nuclei.

The wavefunction of the system can be constructed as

$$\psi(\mathbf{R},\mathbf{r}) = \psi_g(R;\mathbf{r})F_g(\mathbf{R}) + \psi_u(R;\mathbf{r})F_u(\mathbf{R}) \tag{4.9}$$

where $\mathbf{R}$ denotes the relative positions of the two atoms, $\mathbf{r}$ the complex of electronic coordinates, ψ_g and ψ_u the wavefunctions of the two adiabatic electronic states of the molecule and the $F_{g,u}$ satisfy the radial Schrödinger equations (in atomic units)

$$(\nabla_R^2 + \kappa^2 - 2\mu\varphi_{g,u})F_{g,u}(\mathbf{R}) = 0 \tag{4.10}$$

φ_g and φ_u represent the *gerade* and *ungerade* electronic terms, which in the long-range-interaction region can be expressed in the form

$$\varphi_{g,u}(R) = \varepsilon_o + U_{\rm lr} \pm \tfrac{1}{2}\Delta(R) \tag{4.11}$$

with ε_o the electronic energy component at infinite separation between nuclei, $U_{\rm lr}$ the long-range interaction, polarization and higher-order charge-induced-quadrupole interactions, and $\Delta(R)$ the *exchange interaction* potential, due to overlap of electron shells,

$$\Delta(R) = \varphi_g(R) - \varphi_u(R) = \frac{\langle\psi_g|\mathscr{H}|\psi_g\rangle}{\langle\psi_g|\psi_g\rangle} - \frac{\langle\psi_u|\mathscr{H}|\psi_u\rangle}{\langle\psi_u|\psi_u\rangle} \tag{4.12}$$

The charge-exchange differential cross sections can be written, assuming the nuclei distinguishable, in terms of the scattering amplitudes associated to the collisional pathways along gerade and ungerade interaction potentials

$$\frac{{\rm d}\sigma_{\rm ex}}{{\rm d}\Omega} = |f_{\rm ex}(\vartheta)|^2 = \tfrac{1}{4}|f_g(\vartheta) - f_u(\vartheta)|^2 \tag{4.13}$$

However being the particles, or better ionic cores, identical a different treatment is required. The total differential cross section, accounting for the proper nuclear spin statistics, has the form (Krstič and Schultz 1999; Cohen and Schneider 1975)

$$\begin{aligned}\frac{{\rm d}\sigma_{\rm el}}{{\rm d}\Omega} = \tfrac{1}{4}\big[&x|f_g(\vartheta) + f_g(\pi-\vartheta) + f_u(\vartheta) - f_u(\pi-\vartheta)|^2 \\ &+(1-x)|f_g(\vartheta) - f_g(\pi-\vartheta) + f_u(\vartheta) + f_u(\pi-\vartheta)|^2\big]\end{aligned} \tag{4.14}$$

with $x = (s+1)/(2s+1)$ for nuclear spin s integer and $x = s/(2s+1)$ for s semi-integer.

Expanding the scattering amplitudes in partial waves and performing the angular integration it leads to the total scattering cross section as

$$\sigma = \sigma_{\rm d} + \sigma_{\rm ex} + \sigma_{\rm i} \tag{4.15}$$

σ_{d} and σ_{ex} represent the cross sections due to direct elastic scattering and to charge exchange, respectively, while σ_{i} is the term due to the interference. At relatively high collision energies the scattering amplitudes are peaked at ϑ=0, the interference is minimal and the classical limit is attained (Krstič and Schultz 1999). In this frame the charge-exchange cross sections could be expressed in terms of the phase shifts, as done for elastic transport cross sections in the case of neutral collisions [Eqs. (3.25) and (3.26)]

$$\sigma_{\mathrm{d}} = \frac{\pi}{\kappa^2}\sum_{n=0}^{\infty}(2n+1)[2\sin^2\eta_g^n + 2\sin^2\eta_u^n - \sin^2(\eta_g^n - \eta_u^n)] \tag{4.16}$$

$$\sigma_{\mathrm{ex}} = \frac{\pi}{\kappa^2}\sum_{n=0}^{\infty}(2n+1)\sin^2(\eta_g^n - \eta_u^n) \tag{4.17}$$

The phase shifts can be obtained using the semiclassical Wentzel–Kramers–Brillouin (WKB) approximation (3.29).

In colliding systems involving open-shell atoms, the resonant charge-exchange process usually occurs through more than one pair of *gerade–ungerade* states and the relevant cross section can be obtained by averaging the partial contributions with suitable statistical weights.

4.1.2 Asymptotic Approach

Considering the nature of the resonant (and quasi-resonant) processes at low collision energies, characterized by low probability of transitions among states adiabatically correlated with initial and final states and occurring at large separation between colliders, an alternative theoretical approach has been developed many years ago by soviet scientists (Smirnov 1973; Nikitin and Smirnov 1978; Firsov 1951), i.e. the *asymptotic approach*. The method is fundamentally based on the idea of expanding the cross section in terms of small parameter connected to the geometry of the collision.

The wavefunction of the system is expressed, in a semiclassical time-dependent frame, in the basis of the electronic states of the quasi-molecule

$$\Psi(t) = a_g(t)\psi_g \exp\left[-\frac{\imath}{\hbar}\int_{-\infty}^{t}\varphi_g \mathrm{d}t'\right] + a_u(t)\psi_u \exp\left[-\frac{\imath}{\hbar}\int_{-\infty}^{t}\varphi_u \mathrm{d}t'\right] \tag{4.18}$$

$$\begin{aligned}\imath\hbar\frac{\mathrm{d}a_g}{\mathrm{d}t} &= c_{gu}a_u \exp\left[-\frac{\imath}{\hbar}\int^{t}(\varphi_g - \varphi_u)\mathrm{d}t'\right]\\ \imath\hbar\frac{\mathrm{d}a_u}{\mathrm{d}t} &= c_{ug}a_g \exp\left[-\frac{\imath}{\hbar}\int^{t}(\varphi_u - \varphi_g)\mathrm{d}t'\right]\end{aligned} \tag{4.19}$$

$c_{gu} = \langle \varphi_g - \imath h\partial/\partial t|\varphi_u\rangle$ represents the matrix element of the non-adiabatic coupling operator and $a_{g,u}$ are the probability amplitudes.

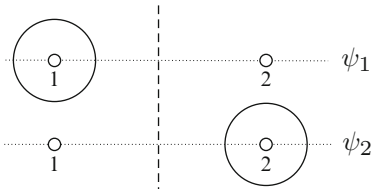

Fig. 4.2 Electron in the field of two identical ionic cores. Reflection in the symmetry plane corresponds to the transformation of $\psi_1 \rightarrow \psi_2$ and vice versa

In the region of large separation between the ionic cores the *gerade* and *ungerade* terms can be obtained by linear combination of the wavefunctions corresponding to the electron located in the field of one of the two ionic cores (Fig. 4.2)

$$\varphi_{gu} = \tfrac{1}{\sqrt{2}}(\psi_1 \pm \psi_2) \tag{4.20}$$

The initial condition, before the interaction, is chosen to correspond to the electron located in the field of the first nucleus $\Psi(t = -\infty) = \psi_1$. After the interaction the probability of electron transition to the state ψ_2, i.e. the probability of resonant charge exchange, is given by Bates et al. (1953)

$$P_{\text{ex}} = \lim_{t\to\infty} |\langle \Psi(t)|\psi_2\rangle|^2 = \sin^2 \int_{-\infty}^{+\infty} \frac{(\varphi_g - \varphi_u)}{2\hbar} \mathrm{d}t \tag{4.21}$$

$$\sigma_{\text{ex}} = 2\pi \int_0^{\infty} P_{\text{ex}}(b) b \mathrm{d}b = 2\pi \int_0^{\infty} \sin^2 \zeta b \mathrm{d}b \text{ with } \zeta = \int_{-\infty}^{+\infty} \frac{\Delta(R)\mathrm{d}t}{2\hbar} \tag{4.22}$$

The laws governing the classical motion of nuclei in the collision [Eq. (3.3)] allow to transform the time integral to a spatial integration along the trajectory, further simplified considering that the process takes place at large internuclear distances where the interaction potential is rather ineffective in deflecting straight-line trajectories

$$\zeta(b) = \frac{1}{\hbar} \int_{R_c}^{+\infty} \frac{(\varphi_g - \varphi_u)}{g\sqrt{1 - \frac{\varphi_{g,u}}{E} - \frac{b^2}{R^2}}} \mathrm{d}R = \frac{1}{\hbar} \int_b^{+\infty} \frac{\Delta(R)}{g\sqrt{R^2 - b^2}} R \mathrm{d}R \tag{4.23}$$

Due to the fact that the exchange interaction potential has a decreasing exponential character at large distances, the integral in Eq. (4.22) can be estimated in the *random phase approximation*

$$\sigma_{\text{ex}} = 2\pi \left[\int_0^{b^\star} \sin^2 \zeta(b) b \mathrm{d}b + \int_{b^\star}^{\infty} \sin^2 \zeta(b) b \mathrm{d}b \right] \tag{4.24}$$

In the early Firsov approach (Firsov 1951) the exchange cross section results from the relations

$$\sigma_{\mathrm{ex}} = \tfrac{1}{2}\pi b^{\star 2} \text{ with } \zeta(b^{\star}) = \tfrac{1}{\pi} \tag{4.25}$$

The exchange interaction potential expressed in the functional form $\Delta = A\exp(-\alpha R)$ allows the condition on the phase ζ to be reduced to the solution of a transcendental equation

$$\zeta(b^{\star}) = \frac{1}{\hbar g}\int_{b^{\star}}^{+\infty}\frac{\Delta(R)R\mathrm{d}R}{\sqrt{R^2-(b^{\star})^2}} = \frac{1}{\hbar g}\left(\frac{\pi b^{\star}}{2\alpha}\right)^{\frac{1}{2}}\Delta(b^{\star}) = \frac{1}{\pi} \tag{4.26}$$

Therefore it could be concluded that, once the accurate energy values for the g–u pairs are known, the exchange interaction can be straightforwardly derived as the energy difference of these electronic terms in the asymptotic region approaching the molecular-ion-system dissociation [Eq. (4.12)]. Unfortunately, despite the large advances achieved in computational quantum chemistry, this region of internuclear separation is still accessible at high level of accuracy only using perturbative approaches to include corrections (Møller–Plasset method (Szabó and Ostlund 1996)). These considerations justify the deviations observed in results obtained in the past, following this approach, with respect to more recent accurate ones (see next section for a detailed comparison in benchmark systems), and also the further formulation due to Smirnov (1973) and Nikitin and Smirnov (1978), to give an accurate expression to the exchange interaction potential, based on the asymptotic form of the wavefunction for the electron transferred in the resonant process.

The g–u splitting is demonstrated to be expressed by a surface integral (Nikitin and Smirnov 1978)

$$\Delta = \varphi_g - \varphi_u = \frac{\hbar^2}{2m}\int_V \varphi_g\nabla^2\varphi_u - \varphi_u\nabla^2\varphi_g\mathrm{d}\mathbf{r} = \frac{\hbar^2}{m}\int_S \psi_2\frac{\partial\psi_1}{\partial z} - \psi_1\frac{\partial\psi_2}{\partial z}\mathrm{d}s \tag{4.27}$$

the surface S coincides with the symmetry plane perpendicular to the z axis joining the nuclei. Moving to cylindrical coordinates (ρ,ϕ,z) with origin at the inversion point of the molecular system and considering spherically symmetric electron wavefunctions

$$\psi_1 = \psi(r) = \psi\left(\sqrt{(z+\tfrac{R}{2})^2+\rho^2}\right)\ \ \psi_2 = \psi(r) = \psi\left(\sqrt{(z-\tfrac{R}{2})^2+\rho^2}\right) \tag{4.28}$$

it leads to Nikitin and Smirnov (1978)

$$\begin{aligned}\Delta = \frac{\hbar^2}{m}\int_0^{2\pi}\mathrm{d}\phi\int_0^{\infty}\rho\mathrm{d}\rho\psi\left(\sqrt{(z-\tfrac{R}{2})^2+\rho^2}\right)\tfrac{\partial}{\partial z}\psi\left(\sqrt{(z+\tfrac{R}{2})^2+\rho^2}\right)\\ -\psi\left(\sqrt{(z-\tfrac{R}{2})^2+\rho^2}\right)\tfrac{\partial}{\partial z}\psi\left(\sqrt{(z-\tfrac{R}{2})^2+\rho^2}\right) = \tfrac{\pi\hbar^2}{m}R\psi^2\left(\tfrac{R}{2}\right)\end{aligned} \tag{4.29}$$

The resonance interaction is therefore determined by the wavefunction of the electron in the quasi-molecule, in the field of action of one of the

two ionic cores, and, being the distance between the nuclei large, it can be conveniently expressed in terms of the atomic wavefunction in its asymptotic form ($r\gamma \gg 1$)

$$\Re(r) = \mathcal{A}\, r^{\left(\frac{1}{\gamma}-1\right)}\, e^{-\gamma r} \tag{4.30}$$

$-\frac{\gamma^2}{2}$ is the binding energy of the valence electron (in atomic units), and $\mathcal{A}$ is the so-called *asymptotic parameter*. The most accurate way to evaluate the $\mathcal{A}$ parameter is tailoring the long-range asymptotic representation of the electron wavefunction with that calculated by the Hartree–Fock method, describing the behaviour of the electron in the vicinity of the parent nucleus.

The general expression for that depends on the scheme of orbital and spin angular momentum summation in atom and ion core. The most proper scheme for light atoms is *LS coupling*: in this frame the fine-structure splitting for an ion and the parent atom is negligible in comparison to the energy difference for various angular momentum projections of the valence electron onto the molecular axis. This allows, also neglecting transitions among different terms, the separate consideration of states with different total spin of a quasi-molecule. Then the quantum numbers of the molecular ion are the atomic quantum numbers L, S, M_L, and M_S and the relevant quantum numbers of the ion core are ℓ, s, m, and m_s. In such a scheme the orbital and spin angular momenta of the valence electron ℓ_e and $1/2$ are summed up with the corresponding angular momenta of the ion core ℓ and s into the atomic angular momenta L and S; thereafter the atomic spin S and the spin of the ion core s are summed into the total spin of the molecular ion S_M. Due to neglecting of the spin–orbit interaction the exchange interaction potential does not depend on the total spin of a quasi-molecule S_M. In the frame of this scheme the general expression for the exchange interaction potential has the following form (Smirnov 1973; Nikitin and Smirnov 1978):

$$\Delta(\ell_e\mu, \ell m, LM_L) = n_e (G^{LS}_{\ell s})^2\, \frac{S_M+\frac{1}{2}}{2s+1} \begin{bmatrix} \ell_e & \ell & L \\ \mu & m & m+\mu \end{bmatrix} \begin{bmatrix} \ell_e & \ell & L \\ \mu & M_L-\mu & M_L \end{bmatrix} \Delta_{\ell_e\mu} \tag{4.31}$$

n_e is the number of valence electrons, $G^{LS}_{\ell s}(\ell_e, n_e)$ is the *genealogical* or *Racah coefficient* (Smirnov 2001), which is responsible for formation of the atom from the parent ion and electron, the expression in the squared brackets is the Clebsch–Gordan coefficient, which is responsible for summation of electron and ion angular momenta into the atom orbital angular momentum, μ is the projection of the orbital angular momentum of the valence electron on the axis of the quasi-molecule and $\Delta_{\ell_e\mu}$ is the partial single-electron exchange interaction potential, determined by the following relation:

$$\Delta_{\ell_e\mu} = \mathcal{A}^2 R^{\left(\frac{2}{\gamma}-1\right)}\, e^{\left(-R\gamma-\frac{1}{\gamma}\right)}\, \frac{(2\ell_e+1)(\ell_e+|\mu|)!}{(\ell_e-|\mu|)!|\mu|!(R\gamma)^{|\mu|}} \tag{4.32}$$

A remarkable consequence of the exchange interaction potential expressed in Eq. (4.31), i.e. in the frame of the *one-electron approximation*, is the onset of selection rules, governing the process

$$|L - \ell| \leq \ell_e; \qquad |S - s| \leq \tfrac{1}{2} \tag{4.33}$$

thus predicting zero probability for transitions violating conditions in Eq. (4.33). For these transitions the process could be possible only through different mechanisms involving the simultaneous exchange of two electrons, characterized by a relatively low probability.

In the further formulation (Smirnov 1973; Nikitin and Smirnov 1978) the critical impact parameter is obtained requiring that in the expansion of the integral in the asymptotic region $[b^\star,\infty]$ in Eq. (4.24), the terms linear in $b^\star$ must vanish (Nikitin and Smirnov 1978). This results in the following transcendental equation:

$$\zeta(b^\star) = \tfrac{1}{2} e^{-\overline{\gamma}} = 0.28 \tag{4.34}$$

and in the case of an s-electron (ℓ_e=0,μ=0) transferred between two structureless cores

$$\begin{aligned} \zeta(b^\star) &= \frac{1}{\hbar g}\left(\frac{\pi b^\star}{2\gamma}\right)^{\frac{1}{2}} \Delta(b^\star) \\ &= \frac{1}{\hbar g}\left(\frac{\pi}{2\gamma}\right)^{\frac{1}{2}} \mathcal{A}^2 (b^\star)^{\frac{2}{\gamma}-\frac{1}{2}} e^{-\gamma b^\star - 1/\gamma} = 0.28 \end{aligned} \tag{4.35}$$

Extensive calculations have been done by Smirnov (2001) on the resonant charge exchange in parent-atom-ion systems for all the elements in the periodic table (see Fig. 4.3). For oxygen and nitrogen systems more recent calculations have been performed (Kosarim and Smirnov, 2005; Kosarim et al. 2006) accounting also for different momentum-coupling schemes in the analysis of the interaction hierarchy and resulting in lower absolute values of the resonant cross sections. Data reported in Table 4.3 could be regarded as upper limits to more accurate values and could be particularly useful in absence of other information on the relevant cross sections.

4.2 $N(^4S)$–$N^+(^3P)$ and $O(^3P)$–$O^+(^4S)$ Charge-Exchange Cross Sections: Two Case Studies

The independent treatment of resonant charge-exchange channels, associated to the different g–u pairs of electronic terms arising in the interaction of open-shell atoms, can be illustrated considering the case of $N(^4S)$–$N^+(^3P)$ system, widely investigated in literature by different authors in different theoretical

Period	Group I	Group II	Group III	Group IV	Group V	Group VI	Group VII	Group VIII
1	1.008 $1s\ ^2S_{1/2}$ $_1$**H** 1.000 6.12 2.00 4.82 Hydrogen 3.65	$1s^2\ ^1S_0$ 4.003 3.4 1.344 $_2$**He** 2.7 2.87 2.1 Helium						
2	6.491 $2s\ ^2S_{1/2}$ $_3$**Li** 0.630 26 0.82 22 Lithium 18	9.012 $2s^2\ ^1S_0$ $_4$**Be** 0.828 13 1.6 10 Berillium 8.2	2p $^2P_{1/2}$ 10.81 13 0.781 $_5$**B** 11 0.88 8.5 Boron	$2p^2\ ^3P_0$ 12.011 9.9 0.910 $_6$**C** 8.6 1.3 6.9 Carbon	$2p^3\ ^4S_{3/2}$ 14.007 7.6 1.034 $_7$**N** 6.2 1.5 5.0 Nitrogen	$2p^4\ ^3P_2$ 15.999 8.1 1.000 $_8$**O** 6.6 1.3 5.3 Oxygen	$2p^5\ ^2P_{3/2}$ 18.998 6.0 1.132 $_9$**F** 4.9 1.6 4.0 Fluorine	$2p^6\ ^1S_0$ 20.179 4.1 1.259 $_{10}$**Ne** 3.3 1.8 2.6 Neon
3	22.990 $3s\ ^2S_{1/2}$ $_{11}$**Na** 0.615 31 0.74 26 Sodium 21	24.305 $3s^2\ ^1S_0$ $_{12}$**Mg** 0.750 18 1.3 15 Magnesium 12	3p $^2P_{1/2}$ 26.982 22 0.663 $_{13}$**Al** 19 0.61 15 Aluminium	$3p^2\ ^3P_0$ 28.086 18 0.774 $_{14}$**Si** 15 1.1 12 Silicon	$3p^3\ ^4S_{3/2}$ 30.974 13 0.878 $_{15}$**P** 11 1.6 9.2 Phosphorus	$3p^4\ ^3P_2$ 32.06 12 0.873 $_{16}$**S** 10 1.1 8.4 Sulfur	$3p^5\ ^2P_{3/2}$ 35.453 10 0.976 $_{17}$**Cl** 8.4 1.8 6.9 Chlorine	$2p^6\ ^1S_0$ 39.948 7.0 1.076 $_{18}$**Ar** 5.8 2.0 4.7 Argon
4	39.098 $4s\ ^2S_{1/2}$ $_{19}$**K** 0.565 40 0.52 34 Potassium 28	40.08 $4s^2\ ^1S_0$ $_{20}$**Ca** 0.670 25 0.95 21 Calsium 17	4p $^2P_{1/2}$ 69.72 24 0.664 $_{31}$**Ga** 20 0.60 16 Gallium	$4p^2\ ^3P_0$ 72.59 21 0.762 $_{32}$**Ge** 18 1.3 15 Germanium	$4p^3\ ^4S_{3/2}$ 74.922 16 0.850 $_{33}$**As** 13 1.6 11 Arsenic	$4p^4\ ^3P_2$ 78.96 16 0.847 $_{34}$**Se** 13 1.5 11 Selenium	$4p^5\ ^2P_{3/2}$ 79.904 12 0.932 $_{35}$**Br** 10 1.8 8.2 Bromine	$4p^6\ ^1S_0$ 83.80 9.0 1.014 $_{36}$**Kr** 7.5 2.1 6.2 Krypton
5	85.468 $5s\ ^2S_{1/2}$ $_{37}$**Rb** 0.554 45 0.48 38 Rubidium 32	87.62 $5s^2\ ^1S_0$ $_{38}$**Sr** 0.647 29 0.86 25 Strontium 20	5p $^2P_{1/2}$ 114.82 26 0.652 $_{49}$**In** 22 0.58 18 Indium	$5p^2\ ^3P_0$ 118.69 23 0.735 $_{50}$**Sn** 19 1.0 16 Tin	$5p^3\ ^4S_{3/2}$ 121.75 20 0.797 $_{51}$**Sb** 17 1.7 14 Antimony	$5p^4\ ^3P_2$ 127.60 19 0.814 $_{52}$**Te** 16 1.6 13 Tellurium	$5p^5\ ^2P_{3/2}$ 126.90 16 0.876 $_{53}$**I** 13 1.9 11 Iodine	$5p^6\ ^1S_0$ 131.29 12 0.944 $_{54}$**Xe** 10 2.2 8.2 Xenon
6	132.90 $6s\ ^2S_{1/2}$ $_{55}$**Cs** 0.535 51 0.41 44 Cesium 36	137.33 $6s^2\ ^1S_0$ $_{56}$**Ba** 0.619 35 0.78 29 Barium 25	6p $^2P_{1/2}$ 204.38 24 0.670 $_{81}$**Tl** 21 0.55 17 Thallium	$6p^2\ ^3P_0$ 207.2 24 0.738 $_{82}$**Pb** 20 1.1 17 Lead	$6p^3\ ^4S_{3/2}$ 208.98 26 0.732 $_{83}$**Bi** 22 1.4 19 Bismuth	$6p^4\ ^3P_2$ [209] 21 0.788 $_{84}$**Po** 18 1.5 15 Polonium	$6p^5\ ^2P_{3/2}$ [210] 20 0.813 $_{85}$**At** 17 1.9 15 Astatine	$6p^6\ ^1S_0$ [222] 15 0.889 $_{86}$**Rn** 12 2.3 10 Radon
z 7	[223] $7s\ ^2S_{1/2}$ $_{87}$**Fr** 0.542 53 0.49 45 Francium 38	226.02 $7s^2\ ^1S_0$ $_{88}$**Ra** 0.623 35 0.78 30 Radium 25						

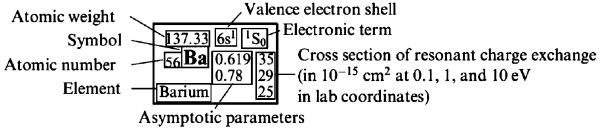

Fig. 4.3 Asymptotic resonant charge-exchange cross sections in ion-parent–atom (ground-state) collisions for elements of the periodical table, adapted from Smirnov (2001)

frames. The Wigner–Witmer rules predict for the ground-state parent-atom-ion interaction six pairs, i.e. ${}^{2,4,6}\Sigma_{gu}^+$ and ${}^{2,4,6}\Pi_{gu}$. The effective resonance cross section results from the averaging of partial contributions due to different channels, with the statistical weight of the electronic terms

$$\sigma_{\rm ex} = \sum_n \frac{w_n \sigma_{\rm ex}^n}{w_n} \tag{4.36}$$

In the pioneering paper by Knof et al. (1964) the cross section was estimated in the semiclassical Firsov approach [Eqs. (4.25) and (4.26)] and the g–u splittings were estimated from accurate RKR experimental energy curves, where available, and from ab initio results obtained in the frame of the valence-bond formalism, deriving the ratios of splittings for the different pairs. Later on, Stallcop (1971), by improving the Knof approach and by neglecting the multiple exchange integrals in the Heitler–London scheme, was able to produce the following equations linking the potential splittings of the N_2^+ potentials:

$$\Delta E_{gu} = \begin{cases} \frac{2}{3}\mathcal{W}_1 & \text{for } {}^2\Sigma_{gu}^+ \text{ and } {}^2\Pi_{gu} \\ \frac{4}{3}\mathcal{W}_1 & \text{for } {}^4\Sigma_{gu}^+ \text{ and } {}^4\Pi_{gu} \\ 2\mathcal{W}_1 & \text{for } {}^6\Sigma_{gu}^+ \text{ and } {}^6\Pi_{gu} \end{cases} \tag{4.37}$$

where

$$\begin{aligned} \mathcal{W}_1(\Sigma) = {} & \langle \pi_A^+ \pi_B^+ \pi_A^- \pi_B^- \sigma_A | \mathscr{H} | \pi_A^+ \pi_B^+ \pi_A^- \pi_B^- \sigma_B \rangle \\ & - E_\infty S_\sigma - 4\ell_3 - 2g_2 S_\sigma + 2q_1 S_\pi \end{aligned} \tag{4.38}$$

$$\begin{aligned} \mathcal{W}_1(\Pi) = {} & \langle \sigma_A \sigma_B \pi_A^+ \pi_B^+ \pi_A^- | \mathscr{H} | \sigma_A \sigma_B \pi_A^+ \pi_B^+ \pi_B^- \rangle \\ & - E_\infty S_\pi - 2(\ell_1 + \ell_2) - (2g_1 - q_2) S_\pi + q_1 S_\sigma \end{aligned} \tag{4.39}$$

$\mathscr{H}$ is the hamiltonian operator defined as

$$\mathscr{H} = -\sum_i \tfrac{1}{2}\nabla_i^2 + \frac{Z_A}{r_{iA}} + \frac{Z_B}{r_{iB}} + \sum_{j>i} \frac{1}{r_{ij}} + \frac{Z_A Z_B}{R_{AB}} \tag{4.40}$$

where Z_A=Z_B=3 (i.e. only p-electrons are considered). The orbitals σ and π represent combination of $2p$ atomic orbitals, i.e. σ=p_z and $\pi^\pm$=$2^{-1/2}(p_x \pm p_y)$, while other symbols are associated to overlap and two-electron integrals

$$\begin{gathered} S_\sigma = \langle \sigma_A | \sigma_B \rangle \qquad S_\pi = \langle \pi_A^+ | \pi_B^+ \rangle \\ \ell_1 = \langle \pi_A^+ \pi_A^- | r_{12}^{-1} | \pi_A^- \pi_B^+ \rangle \quad \ell_2 = \langle \pi_A^+ \sigma_A | r_{12}^{-1} | \sigma_A \pi_B^+ \rangle \quad \ell_3 = \langle \pi_A^+ \sigma_A | r_{12}^{-1} | \sigma_B \pi_A^+ \rangle \\ g_1 = \langle \pi_A^+ \sigma_A | r_{12}^{-1} | \sigma_A \pi_A^+ \rangle \qquad g_2 = \langle \pi_A^+ \pi_A^- | r_{12}^{-1} | \pi_A^- \pi_A^+ \rangle \\ q_1 = \langle \pi_A^+ \sigma_B | r_{12}^{-1} | \sigma_A \pi_B^+ \rangle \qquad q_2 = \langle \pi_A^+ \pi_B^- | r_{12}^{-1} | \pi_A^- \pi_B^+ \rangle \end{gathered}$$

$E_\infty = -6.255952$ au represents the sum of the energies of the free atom and ion that, in turn, have been calculated as the difference of the energy corresponding to the complete atom (or ion) and the energy of the core configuration, $E(1s^2\ 2s^2) = -50.89545$ au.

Capitelli and Devoto (1973) used relations (4.37), in combination with the experimental splittings for doublet Σ and Π electronic terms, to obtain charge-transfer cross sections. Their values were much lower than the charge-transfer cross sections derived from molecular beam experiments and of unpublished Yos (1965) results based on the ab initio Heitler–London method, i.e. the valence-bond approach. It was then decided to perform an ab initio Heitler–London calculation of the Σ states of N–N^+ potentials. The following wavefunctions were written (Capitelli et al. 1977b):

$$
\begin{aligned}
|^2\Sigma_{gu}\rangle = {} & \tfrac{1}{\sqrt{6}}|0,0,\tfrac{15}{4},-\tfrac{1}{2}\rangle_{N_A}|1,0,2,1\rangle_{N_B^+} - \tfrac{1}{\sqrt{3}}|0,0,\tfrac{15}{4},\tfrac{1}{2}\rangle_{N_A}|1,0,2,0\rangle_{N_B^+} \\
& + \tfrac{1}{\sqrt{2}}|0,0,\tfrac{15}{4},\tfrac{3}{2}\rangle_{N_A}|1,0,2,-1\rangle_{N_B^+} \pm \Big[\tfrac{1}{\sqrt{6}}|0,0,\tfrac{15}{4},-\tfrac{1}{2}\rangle_{N_B}|1,0,2,1\rangle_{N_A^+} \\
& - \tfrac{1}{\sqrt{3}}|0,0,\tfrac{15}{4},\tfrac{1}{2}\rangle_{N_B}|1,0,2,0\rangle_{N_A^+} + \tfrac{1}{\sqrt{2}}|0,0,\tfrac{15}{4},\tfrac{3}{2}\rangle_{N_B}|1,0,2,-1\rangle_{N_A^+}\Big]
\end{aligned}
\tag{4.41}
$$

$$
\begin{aligned}
|^4\Sigma_{gu}\rangle = {} & -\sqrt{\tfrac{8}{15}}|0,0,\tfrac{15}{4},-\tfrac{1}{2}\rangle_{N_A}|1,0,2,1\rangle_{N_B^+} + \tfrac{1}{\sqrt{15}}|0,0,\tfrac{15}{4},\tfrac{1}{2}\rangle_{N_A}|1,0,2,0\rangle_{N_B^+} \\
& + \sqrt{\tfrac{2}{5}}|0,0,\tfrac{15}{4},\tfrac{3}{2}\rangle_{N_A}|1,0,2,-1\rangle_{N_B^+} \pm \Big[-\sqrt{\tfrac{8}{15}}|0,0,\tfrac{15}{4},-\tfrac{1}{2}\rangle_{N_B}|1,0,2,1\rangle_{N_A^+} \\
& + \tfrac{1}{\sqrt{15}}|0,0,\tfrac{15}{4},\tfrac{1}{2}\rangle_{N_B}|1,0,2,0\rangle_{N_A^+} + \sqrt{\tfrac{2}{5}}|0,0,\tfrac{15}{4},\tfrac{3}{2}\rangle_{N_B}|1,0,2,-1\rangle_{N_A^+}\Big]
\end{aligned}
\tag{4.42}
$$

$$
\begin{aligned}
|^6\Sigma_{gu}\rangle = {} & \sqrt{\tfrac{3}{10}}|0,0,\tfrac{15}{4},-\tfrac{1}{2}\rangle_{N_A}|1,0,2,1\rangle_{N_B^+} + \sqrt{\tfrac{3}{5}}|0,0,\tfrac{15}{4},\tfrac{1}{2}\rangle_{N_A}|1,0,2,0\rangle_{N_B^+} \\
& + \tfrac{1}{\sqrt{10}}|0,0,\tfrac{15}{4},\tfrac{3}{2}\rangle_{N_A}|1,0,2,-1\rangle_{N_B^+} \pm \Big[\sqrt{\tfrac{3}{10}}|0,0,\tfrac{15}{4},-\tfrac{1}{2}\rangle_{N_B}|1,0,2,1\rangle_{N_A^+} \\
& + \sqrt{\tfrac{3}{5}}|0,0,\tfrac{15}{4},\tfrac{1}{2}\rangle_{N_B}|1,0,2,0\rangle_{N_A^+} + \tfrac{1}{\sqrt{10}}|0,0,\tfrac{15}{4},\tfrac{3}{2}\rangle_{N_B}|1,0,2,-1\rangle_{N_A^+}\Big]
\end{aligned}
\tag{4.43}
$$

The $\pm$ sign refers to symmetric (*gerade*) or anti-symmetric (*ungerade*) states, while the ket atomic states, $|\ \rangle_{N_A}$, centred on the nuclei A and B, are eigenfunctions of the operators $(\mathcal{L}^2, \mathcal{L}_z, \mathcal{S}^2, \mathcal{S}_z)$, associated to the squared modulus and the axial component of the orbital angular and spin momenta.

The determinantal wavefunctions $|\ldots\rangle_N$ are described in terms of a minimal STO (*Slater-type orbital*) basis set, obtaining energies for ground-state configuration of the nitrogen atom and ion, $N(^4S) = -54.26512\,\text{au}$ and $N^+(^3P) = -53.78174\,\text{au}$, leading to a value for the ionization potential of 13.5 eV, to be compared with the experimental value of 14.54 eV.

The energy associated with each molecular state should, in general, be obtained by solving a secular problem. In the present case, however, the problem is trivial, because, for symmetry reasons, the secular matrix factorizes in unidimensional blocks. The energy of a given state is, therefore, simply given by the expression

$$E(R) = \frac{< \Psi | \mathscr{H} | \Psi >}{< \Psi | \Psi >} \tag{4.44}$$

where Ψ represents the wavefunction of the electronic molecular state given in Eqs. (4.41)–(4.43) and $\mathscr{H}$ is the complete hamiltonian operator

$$\begin{aligned} \mathscr{H} = & -\tfrac{1}{2} \sum_{i \in A} \nabla_i^2 - \sum_{i \in A} \frac{Z_A}{r_{iA}} + \tfrac{1}{2} \sum_{i,j \in A} \frac{1}{r_{ij}} - \tfrac{1}{2} \sum_{i \in B} \nabla_i^2 - \sum_{i \in B} \frac{Z_B}{r_{iB}} \\ & + \tfrac{1}{2} \sum_{i,j \in B} \frac{1}{r_{ij}} - \sum_{i \in B} \frac{Z_A}{r_{iA}} - \sum_{i \in A} \frac{Z_B}{r_{iB}} + \tfrac{1}{2} \sum_{i \in A, j \in B} \frac{1}{r_{ij}} \end{aligned} \tag{4.45}$$

The algebra involved in the development of the matrix elements between determinantal wavefunctions can be found in classical textbooks (McWeeny and Sutcliffe 1969). All relevant integrals, including multiple-exchange integrals, were calculated by Gauss and Gauss–Laguerre quadrature formulae. The splittings for Σ_{gu} states were found to fulfill the relation

$$[\Delta E_{gu}]_{\text{sextet}} = \tfrac{3}{2} [\Delta E_{gu}]_{\text{quartet}} = 3 [\Delta E_{gu}]_{\text{doublet}} \tag{4.46}$$

as put in evidence by Stallcop (1971) and Yos (1965) on a semi-empirical base.

Also the splitting of Π pairs were evaluated by using the Stallcop approach (Stallcop 1971) and a quantum mechanical calculation of the $\mathcal{W}_1$ energy. At the same time this approximation was also used for the Σ states. The results of complete Heitler–London calculation, case (a), of Σ states and approximate Heitler–London calculation, case (b), for Σ and Π states are reported in Table 4.1 in the form of exponential representation of g–u splittings.

The corresponding charge-transfer cross sections, obtained through Eqs. (4.25) and (4.26), are reported in Fig. 4.4 and compared with the experimental molecular beam results. We can note that the ab initio Heitler–London Σ contributions averaged with the approximate Π state contributions are still below the experimental charge-exchange cross sections, while a better agreement was found with the approximate calculations for Σ and Π splittings.

Due to the relevance of N–N^+ resonant charge-exchange process in affecting the transport properties of air plasmas, the NASA group decided to calculate all electronic molecular terms arising in the interaction, of N_2^+ potentials by using the complete-active-space self-consistent field (CASSCF) approach with a $(4s3p1d)$ Gaussian basis set (Stallcop et al. 1985). A comparison of the CASSCF g–u splittings for Σ and Π pairs with the approximate Heitler–London calculations shows large differences in the two sets of results (Fig. 4.5). These discrepancies however do not propagate in the charge-exchange cross section, being the differences below 15%, as appreciable in Fig. 4.5. It should be noted that CASSCF results were found in closer agreement with experiments (Belyaev et al. 1968) and the comparison is even better including a *tail* energy-dependent correction, accounting for

Table 4.1 Parameters, A[eV] and α[Å^{-1}], of exponential decay functional form of g–u splitting for Σ and Π pairs of N_2^+ system, by different authors

Reference	$^2\Sigma_{g,u}$		$^4\Sigma_{g,u}$		$^6\Sigma_{g,u}$		$^2\Pi_{g,u}$	
	A	α	A	α	A	α	A	α
(a)	372.0	2.428	646.0	2.429	977.0	2.430		
(b)	1,660.0	2.577					703.0	2.990
(c)	1,890.0	3.650					104.0	2.486
(d)	81.6	1.778					31.0	2.026
(e)	42.1	1.920					296.0	3.140
(f)	25.1	1.586					111.0	2.510

(a) Accurate results in Capitelli et al. (1977b), (b) Approximate results in Capitelli et al. (1977b), (c) Capitelli and Devoto (1973), (d) Yos (1965), (e) Andersen and Thulstrup (1973) and Thulstrup and Andersen (1975), (f) Cartwright and Dunning (1975)

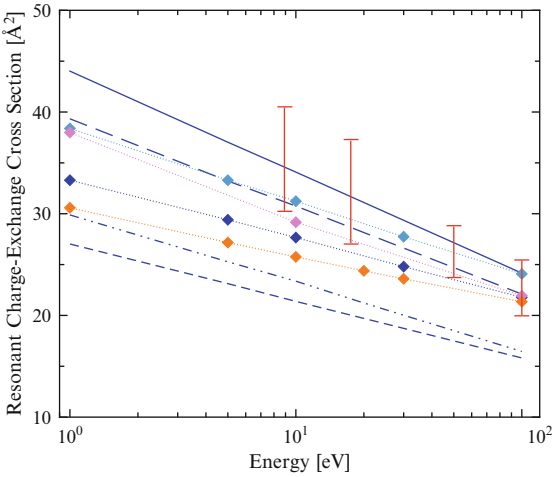

Fig. 4.4 Resonant charge-exchange cross section as a function of energy from Capitelli et al. (1977b). (*Thick solid line*) calculated with the potentials of Yos (1965), (*short-dashed line*) calculated with the potentials of Capitelli and Devoto (1973), (*dashed–dotted line*) calculated with the potentials of Andersen and Thulstrup (1973); Thulstrup and Andersen (1975), (*long-dashed line*) calculated with the potentials of Cartwright and Dunning (1975), (*cyan diamonds*) case (a) Σ pairs, (*blue diamonds*) case (b) $\Sigma + \Pi$ pairs, (*orange diamonds*) (Knof et al. 1964), (*pink diamonds*) (Duman and Smirnov 1974), (*red bars*) experimental results (Belyaev et al. 1968)

the estimation of resonant cross section in the *random phase approximation* [see Eq. (4.24)]. In a subsequent paper by the NASA group (Stallcop et al. 1991) calculated a new complete set of potential curves by combining available experimental data with accurate potentials at a CASSCF level. Authors presented arguments about the accuracy of their potential energy curves, not significantly improved by high-order ab initio approaches,

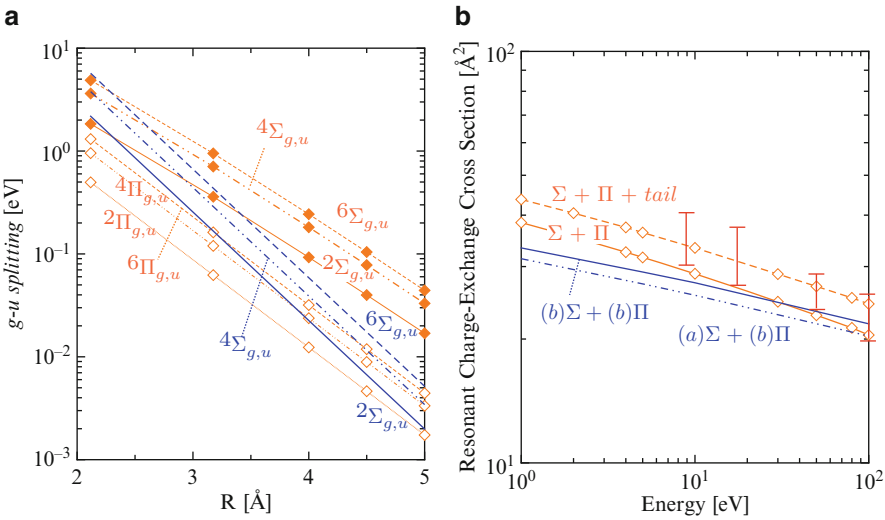

Fig. 4.5 (**a**) g–u splitting for Σ and Π pairs. (*dashed and full lines*) Σ pairs, case (*a*) (Capitelli et al. 1977b); (*dashed and full with markers*) Σ and Π pairs, CASSCF approach (Stallcop et al. 1985). (**b**) Resonant charge-exchange cross sections as a function of energy. (*lines*) (Capitelli et al. 1977b), (*lines with markers*) CASSCF approach including a tail correction (Stallcop et al. 1985), (*red bars*) experimental results (Belyaev et al. 1968)

i.e. multi-reference configuration interaction plus quadruples corrections (MRCI+Q). The charge-exchange cross sections were obtained in a quantum frame from WKB phase shifts (3.29). The new charge-exchange cross sections are again reported in Fig. 4.6. They are in agreement with the experimental results presenting also an increase of the cross section at very low energy this behaviour being absent in all other results. This behaviour was ascribed to the role of polarizability (Knof et al. 1964) not present in all other calculations.

Apparently the last calculation of charge-exchange cross sections and the corresponding diffusion-type collision integrals tabulated by the NASA group (Stallcop et al. 1991) can be considered as benchmark values for similar calculations. In this context two series of data recently obtained in the frame of the asymptotic approach (Kosarim et al. 2006; Eletskii et al. 2004) should be also referenced. The asymptotic resonant charge-exchange cross sections differ by the choice of the scheme of orbital and spin momentum coupling. Again we note a satisfactory agreement with the results of the NASA group thus emphasizing that this approach can be used with a fair amount of confidence for the calculation of charge-exchange cross sections involving excited states (see Chap. 5).

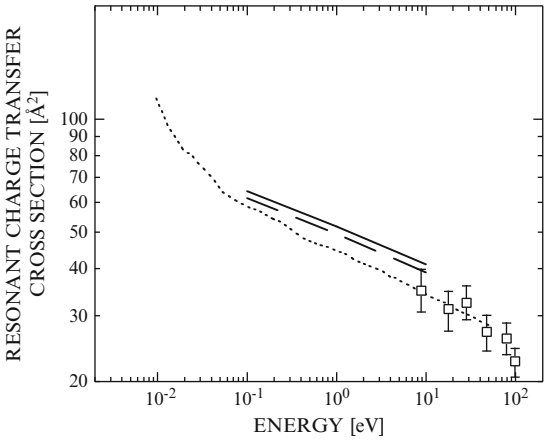

Fig. 4.6 Comparison of the cross section for the resonant charge-exchange process in $N(^4S)$–$N^+(^3P)$ collisions, as a function of collision energy, by different authors. (*Continuous line*) (Kosarim et al. 2006), (*dashed line*) (Eletskii et al. 2004), (*dotted line*) (Stallcop et al. 1991). Experimental results (Belyaev et al. 1968) are also reported with error bars

The diffusion-type collision integrals, obtained by integration of resonant charge-exchange cross sections calculated with different theoretical approaches (Capitelli et al. 1977a; Stallcop et al. 1991; Eletskii et al. 2004; Kosarim et al. 2006) or from experiments (Belyaev et al. 1968), are reported in Table 4.2.

Inspection of the results shows a satisfactory agreement between the reported calculations emphasizing also that the *asymptotic approach* can be considered as an upper limit to the value of the transport cross sections. It should be also noted that the pioneering results by Knof et al. (1964) and of Capitelli and Devoto (1973) underestimate the corresponding diffusion-type collision integrals.

The second case study is the $O(^3P)$–$O^+(^4S)$ system. The first attempts made by Knof et al. (1964) ended in the underestimation of charge-exchange cross sections as compared with the more recent results by NASA group (Stallcop et al. 1991). As in the case of nitrogen, the potential energy curves of all the electronic terms arising in the interaction of ground-state O–O^+ collisional pair were derived by mixing experimental information and the CASSCF method, while phase shifts were estimated in the WKB approximation for the calculation of the charge-exchange cross section.

A comparison of these values with two series of results obtained in the asymptotic approach (Eletskii et al. 2004; Kosarim and Smirnov 2005) is shown in Fig. 4.7. The asymptotic cross sections are higher than the NASA results especially in the case of the more recent series (Kosarim and Smirnov 2005), with discrepancies up to 40%. Experimental results by Rutherford and

Table 4.2 Inelastic contribution to diffusion-type collision integrals, $\sigma^2\Omega_{ex}^{(1,1)\star}$ [Å^2], as a function of temperature for the N(^{4}S)–N$^+$(^{3}P) interaction obtained with different approaches

T[K]	(*a*)	(*b*)	(*c*)	(*d*)	(*e*)
500		38.17	40.6	38.88	40.61
1,000		34.27	37.5	36.52	38.17
2,000	22.62	31.39	34.5	34.24	35.81
3,000		29.95	32.8	32.94	34.46
4,000	21.42	29.00	31.6	32.03	33.52
5,000		28.30	30.7	31.34	32.80
6,000	20.74	27.73	30.0	30.78	32.22
8,000	20.26	26.86	28.9	29.90	31.31
10,000	19.90	26.19	28.1	29.23	30.61
14,000	19.35	25.20	26.8	28.23	29.58
18,000	18.95	24.48	25.9	27.50	28.50
20,000	18.78	24.18	25.5	27.19	28.50
30,000		23.05	24.0	26.04	27.30
40,000		22.28	23.0	25.23	26.46
50,000		21.70	22.3	24.61	25.82

(*a*) Capitelli et al. (1977a) based on Heitler–London potentials in Capitelli et al. (1977b), (*b*) Stallcop et al. (1991), (*c*) Results in Capitelli et al. (2000) from experiments (Belyaev et al. 1968), (*d*) Eletskii et al. (2004), (*e*) Kosarim et al. (2006)

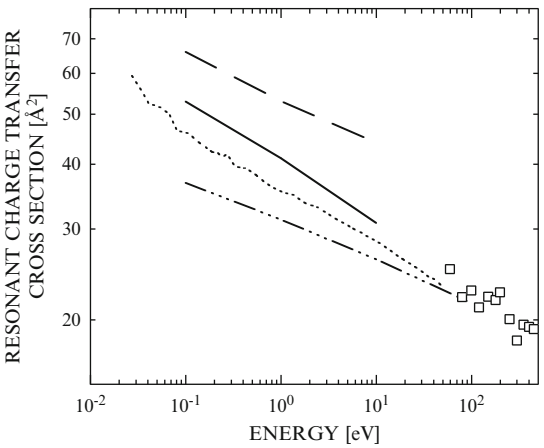

Fig. 4.7 Comparison of the cross section for the resonant charge-exchange process in $O(^3P)$–$O^+(^4S)$ collisions, as a function of collision energy, by different authors. (*Dashed–dotted line*) (Knof et al. 1964), (*dashed line*) (Kosarim and Smirnov 2005), (*continuous line*) (Eletskii et al. 2004), (*dotted line*) (Stallcop et al. 1991). Experimental results (Rutherford and Vroom 1974) are also reported

Vroom (1974) are also reported, showing that different approaches seem to converge for relatively high collision energies, results by Kosarim and Smirnov (2005) still overestimating the resonant charge-exchange cross section.

Table 4.3 Inelastic contribution to diffusion-type collision integrals, $\sigma^2 \Omega_{ex}^{(1,1)\star}$ [Å^2], as a function of temperature for the O(^{3}P)–O$^+$(^{4}S) interaction obtained with different approaches

T[K]	(*a*)	(*b*)	(*c*)	(*d*)	(*e*)
500	21.25	29.64	28.88	33.43	41.27
1,000	20.17	26.96	27.16	31.08	38.98
2,000	19.11	24.88	25.49	28.82	36.76
4,000	18.07	23.11	23.87	26.64	34.60
5,000	17.75	22.60	23.36	25.96	33.92
6,000	17.48	22.21	22.95	25.41	33.37
8,000	17.07	21.60	22.31	24.55	32.51
10,000	16.75	21.13	21.82	23.89	31.85
20,000	15.78	19.72	20.33	21.91	29.84
30,000	15.22	18.90	19.48	20.80	28.70
40,000	14.83	18.32	18.89	20.02	27.90
50,000	14.53	17.89	18.43	19.43	27.29

(*a*) Knof et al. (1964), (*b*) Stallcop et al. (1991), (*c*) Results in Capitelli et al. (2000) from experiments (Rutherford and Vroom 1974), (*d*) Eletskii et al. (2004), (*e*) Kosarim and Smirnov (2005)

The corresponding diffusion-type collision integrals are reported in Table 4.3, showing deviations of the asymptotic results up to 35% with respect to quantum ones (Stallcop et al. 1991).
This last point merits some comments. The asymptotic results of Kosarim and Smirnov (2005) are more accurate than the corresponding ones in Eletskii et al. (2004), the reverse being true when comparing the theoretical results with the experimental ones (Rutherford and Vroom 1974). However, more recent experimental results (Lindsay et al. 2001; Lindsay and Stebbings 2005) in the energy range 0.5–5 keV, extrapolated to the low-energy region, yield a value of charge-exchange cross section of 71 Å^2 at 0.1 eV, very close to the value by Smirnov and Kosarim at the same energy (66 Å^2). A further theoretical study should be welcome to shed light on the actual value for the cross section of this important process.

Before ending this section it is important to point out that the resonant charge-exchange processes should be taken into account in principle in each symmetric collision involving an ionic species encountering its neutral parent, i.e. sharing the same ionic core, as in the case of $O_2(^3\Sigma_g^-)$–$O_2^+(X^2\Pi_g)$ and $N_2(^1\Sigma_g^+)$–$N_2^+(^2\Sigma_g^+)$ systems, experimentally investigated by different authors (Berry 1948; Stebbings et al. 1963; Moran et al. 1974; Kobayashi 1975). A full multi-state impact parameter model has been developed (Flannery et al. 1973; Moran et al. 1974), accounting for the anisotropy of the potential surface due to the orientation of molecules in different colliding geometries and for the vibrational energy content of the molecule in its ground electronic state. This approach was shown to be predictive, as shown in Fig. 4.8, where also the theoretical results obtained in the asymptotic approach, successfully extended to the case of diatomic collisions in Yevseyev et al. (1982), are displayed.
In Table 4.4 inelastic contribution to diffusion-type collision integrals, due to resonant process, is reported for interactions relevant to the Earth atmosphere. These results have been derived in Capitelli et al. (2000) through

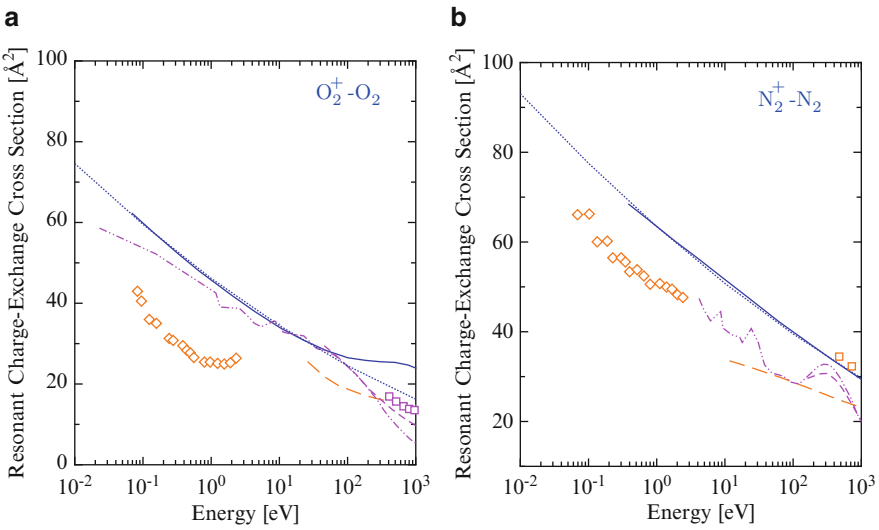

Fig. 4.8 Resonant charge-exchange cross sections in molecular systems by different authors. (**a**) O_2^+–O_2 (*solid line*) asymptotic approach (Yevseyev et al. 1982), (*dashed–dotted line*) low-energy approximation (Moran et al. 1974), (*short-dashed line*) multi-state approach (Moran et al. 1974), compared with experimental results (*diamonds*) (Kobayashi 1975), (*squares*) (Moran et al. 1974), (*long-dashed line*) (Stebbings et al. 1963), (*dotted line*) fit in (Capitelli et al. 2000). (**b**) N_2^+–N_2 (*solid line*) asymptotic approach (Yevseyev et al. 1982), (*dashed–dotted line*) low-energy approximation (Flannery et al. 1973), (*short-dashed line*) multi-state approach (Flannery et al. 1973), compared with experimental results (*diamonds*) (Kobayashi 1975), (*squares*) (Berry 1948), (*long-dashed line*) (Stebbings et al. 1963), (*dotted line*) fit in (Capitelli et al. 2000)

a closed form (Devoto 1967) fitting theoretical (Yevseyev et al. 1982) and experimental (Rutherford and Vroom 1974) cross sections.

4.3 Resonant Exchange in Multiply-Charged-Ion–Parent-Atom Collisions

Cross sections for multiple resonant charge exchange, i.e. the process

$$\tilde{\mathrm{A}} + \mathrm{A}^{q+} \rightarrow \tilde{\mathrm{A}}^{q+} + \mathrm{A} \tag{4.47}$$

have been evaluated in the frame of the asymptotic approach [Eq. (4.35)] estimating the exchange interaction potential with the expression

$$\Delta(b^\star) = \tfrac{8}{e} I b^\star \exp\left(-\gamma b^\star\right) \tag{4.48}$$

setting in place of ionization potential, I, the corresponding values for double and triple ionizations, as suggested in Miller et al. (2002).

Table 4.4 Inelastic contribution to diffusion-type collision integrals, $\sigma^2 \Omega_{ex}^{(1,1)\star}$ [Å^2], as a function of temperature for molecular-ion–parent-molecule interactions from Capitelli et al. (2000)

T[K]	O_2–O_2^-	O_2^+–O_2	N_2^+–N_2	NO^+–NO
100	19.62	44.18	55.85	43.63
500	17.38	37.62	49.07	37.31
1,000	16.46	34.95	46.28	34.74
2,000	15.57	32.39	43.58	32.27
4,000	14.70	29.92	40.96	29.88
6,000	14.20	28.52	39.46	28.53
8,000	13.85	27.55	38.42	27.59
10,000	13.59	26.81	37.62	26.87
20,000	12.78	24.56	35.18	24.70
30,000	12.31	23.30	33.80	23.47
40,000	11.99	22.42	32.83	22.62
50,000	11.74	21.75	32.09	21.97

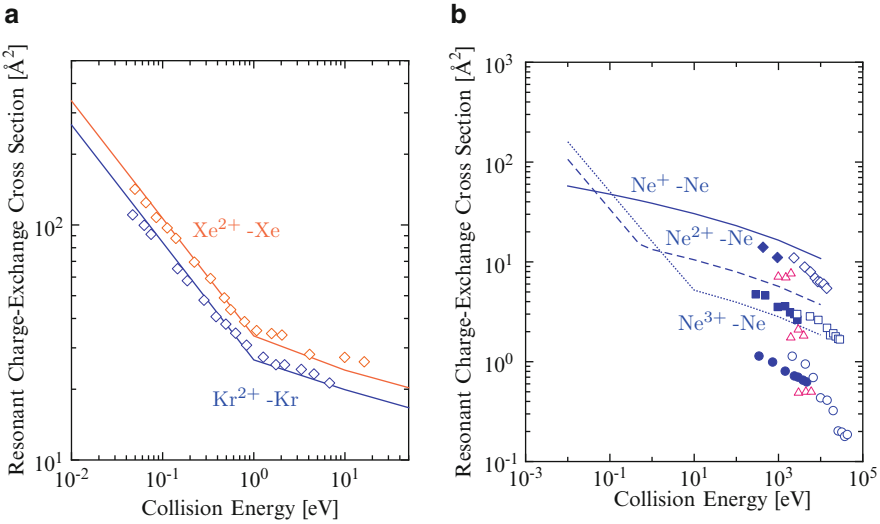

Fig. 4.9 (**a**) Double resonant charge-exchange cross section for rare-gases collisional pairs, i.e. Xe^{2+}–Xe and Kr^{2+}–Kr. (*solid lines*) Asymptotic approach, (*open diamonds*) experimental results (Okuno et al. 1978)). (**b**) Single to multiple resonant charge-exchange cross section for Ne^{q+}–Ne. (*solid lines*) Asymptotic approach compared with experimental results, (*close diamonds*) (Latypov et al. 1969), (*open diamonds*)(Flaks and Solv'ev 1958), (*close squares*) (Latypov et al. 1969), (*open squares*) (Flaks and Solv'ev 1958), (*open circles*) (Latypov et al. 1969), (*closed circles*) (Flaks and Filippenko 1960), (*open triangles*) (Kaneko et al. 1981)

In the low collision energy domain σ_{ex} should be corrected for the contribution of elastic scattering to the resonant charge-transfer processes: the polarization interaction potential acts modifying the particle trajectories and the cross section should be evaluated as half of the probability of orbiting (Duman et al. 1982). The correction, negligible for a single-electron process, could be relevant at low temperatures, for atom-multiply charged

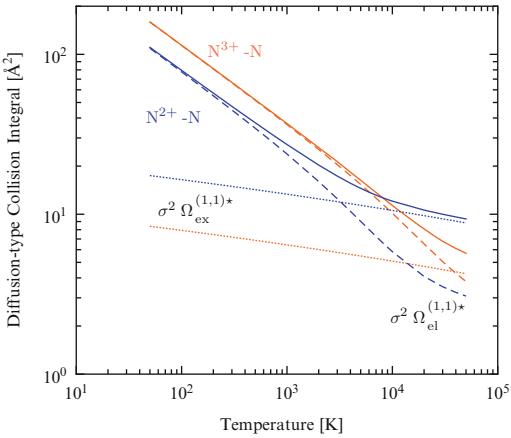

Fig. 4.10 Diffusion-type collision integrals (*solid line*) for N–N^{q+} interactions with $q = 2$ and 3, resulting from elastic (phenomenological approach) (*dashed line*) and resonant charge-exchange (asymptotic approach) (*dotted line*) contributions

ion interactions, due to a square dependence of the capture cross section on the ion charge (Okuno et al. 1978). The asymptotic results have been compared with experiments for rare-gas colliding systems in Fig. 4.9, showing the reliability of this approach.

In the estimation of diffusion-type collision integrals, actually the elastic contribution already accounts for the strong polarization interaction and correction terms have not been included. The resonant inelastic contribution decreases with the ion charge, as the ionization potential for the removal of two or more electrons increases, becoming negligible for $q > 3$, while the polarization term becomes dominant, as appreciable in Fig. 4.10, where results for N^{q+}–N interactions are reported.

References

Andersen A, Thulstrup EW (1973) Configuration interaction studies of the low-lying quartet states of N_2^+. J Phys B: At Mol Phys 6(8):L211

Bates DR, Massey HSW, Stewart AL (1953) Inelastic collisions between atoms. I. General theoretical considerations. Proc R Soc Lond A 216:437–458

Belyaev YN, Brezhnev BG, Erastov EM (1968) Resonant charge transfer of low energy carbon and nitrogen ions. Sov Phys JETP 27(6):924

Berry HW (1948) Secondary electron emission by fast neutral molecules and neutralization of positive ions. Phys Rev 74:848–849

Capitelli M, Devoto RS (1973) Transport coefficients of high-temperature nitrogen. Phys Fluids 16(11):1835

Capitelli M, Gorse C, Fauchais P (1977a) Transport coefficients of high temperature N_2-H_2 mixtures. J Phys 38(6):653

Capitelli M, Lamanna UT, Guidotti C, Arrighini GP (1977b) The gerade-ungerade splitting of N_2^+ potentials: effects on the resonant charge transfer cross sections of nitrogen atoms. Chem Phys 19:269

Capitelli M, Gorse C, Longo S, Giordano D (2000) Collision integrals of high-temperature air species. J Thermophys Heat Transf 14(2):259–268

Cartwright DC, Dunning TH Jr (1975) New electronic states of N_2^+. J Phys B: At Mol Phys 8(6):L100

Cohen JS, Schneider B (1975) Collisions of $Ne^*(3s)$ and Ne^+ with Ne: Excitation and charge transfer, elastic scattering, and diffusion. Phys Rev A 11:884–892

Devoto RS (1967) Transport coefficients of partially ionized argon. Phys Fluids 10(2):354–364

Duman EL, Smirnov BM (1974) Teplofizika Vysokikh Temperatur 12:502

Duman EL, Yevseyev AV, Eletskii AV, Radtsig AA, Smirnov BM (1982) Charge exchange processes, vol 3532/12. I. V. Kurchatov Atomic Energy Institute, Moscow

Eletskii AV, Capitelli M, Celiberto R, Laricchiuta A (2004) Resonant charge exchange and relevant transport cross sections for excited states of oxygen and nitrogen atoms. Phys Rev A 69(4):042718/1–8

Firsov OB (1951) JETP (in russian) 21:1001

Flaks IP, Filippenko LG (1960) Sov Phys JETP 4:1005–1013

Flaks IP, Solv'ev ES (1958) Sov Phys JETP 3:564–576

Flannery MR, Cosby PC, Moran TF (1973) Molecular charge transfer: Experimental and theoretical investigation of the role of incident-ion vibrational states in N_2^+-N_2 and CO^+-CO collisions. J Chem Phys 59(10):5494–5510

Kaneko Y, Iwai T, Ohtani S, Okuno K, Kobayashi N, Tsurubuchi S, Kimura M, Tawara H (1981) Symmetric resonance multiple charge transfer of Ne^{q+} and Ar^{q+} ($q \leq 4$). J Phys B: At Mol Phys 14(5):881

Knof H, Mason EA, Vanderslice JT (1964) Interaction energies, charge exchange cross sections, and diffusion cross sections for N^+-N and O^+-O collisions. J Chem Phys 40(12):3548–3553

Kobayashi N (1975) Low energy ion-neutral reactions. VI. Ar^++Ar, N_2^++N_2, O_2^++O_2 and CO^++CO. J Phys Soc Japan 38(2):519–523

Kosarim AV, Smirnov BM (2005) Electron terms and resonant charge exchange involving oxygen atoms and ions. J Exp Theor Phys 101(4):611–627

Kosarim AV, Smirnov BM, Capitelli M, Celiberto R, Laricchiuta A (2006) Resonant charge exchange involving electronically excited states of nitrogen atoms and ions. Phys Rev A 74(6):062707

Krstić PS, Schultz DR (1999) Elastic scattering and charge transfer in slow collisions: isotopes of H and H^+ colliding with isotopes of H and with He. J Phys B: At Mol Phys 32(14):3485–3509

Latypov ZZ, Fedorenko NV, Flaks IP, Shaporenko AA (1969) Symmetric resonance, charge exchange of multichanged ions. Sov Phys JETP 28(3):439–442

Lindsay BG, Stebbings RF (2005) Charge transfer cross sections for energetic neutral atom data analysis. J Geophys Res 110(A12):A12213

Lindsay BG, Sieglaff DR, Smith KA, Stebbings RF (2001) Charge transfer of keV O^+ ions with atomic oxygen. J Geophys Res 106(A5):8197–8203

Mason EA, Vanderslice JT, Yos JM (1959) Transport properties of high-temperature multicomponent gas mixtures. Phys Fluids 2(6):688–694

McWeeny R, Sutcliffe BT (1969) Methods of molecular quantum mechanics. Academic, London

Miller JS, Pullins S, Lavandier DJ, hui Chiu Y, Dressler RA (2002) Xenon charge exchange cross sections for electrostatic thruster models. J Appl Phys 91(3):984–991

Moran TF, Flannery MR, Cosby PC (1974) Molecular charge transfer. II. Experimental and theoretical investigation of the role of incident-ion vibrational states in O_2^+-O_2 and NO^+-NO collisions. J Chem Phys 61(4):1261–1273

Murphy AB (1995) Transport coefficients of air, argon-air, nitrogen-air, and oxygen-air plasmas. Plasma Chem Plasma P 15(2):279

Nikitin EE, Smirnov BM (1978) Quasiresonant processes in slow collisions. Sov Phys Uspekhi 21(2):95–116

Okuno K, Koizumi T, Kaneko Y (1978) Symmetric resonance double charge transfer in Kr^{++}+Kr and Xe^{++}+Xe systems. Phys Rev Lett 40(26):1708–1710

Rutherford JA, Vroom DA (1974) The reaction of atomic oxygen with several atmospheric ions. J Chem Phys 61(7):2514–2519

Smirnov BM (1973) Asymptotic methods in theory of atomic collisions. Atomizdat, Moskva (in russian)

Smirnov BM (2001) Atomic structure and the resonant charge exchange process. Phys Usp 44(3):221–253

Stallcop JR (1971) N_2^+ potential-energy curves. J Chem Phys 54(6):2602–2605

Stallcop J, Partridge H, Levin E (1985) N^+-N long-range interaction energies and resonant charge exchange. Phys Rev A 32(1):639–642

Stallcop JR, Partridge H, Levin E (1991) Resonance charge transfer, transport cross sections, and collision integrals for $N^+(^3P)$-$N(^4S)$ and $O^+(^4S)$-$O(^3P)$ interactions. J Chem Phys 95(9):6429–6439

Stebbings RF, Turner BR, Smith ACH (1963) Charge transfer in oxygen, nitrogen, and nitric oxide. J Chem Phys 38(9):2277–2279

Szabó A, Ostlund NS (1996) Modern quantum chemistry: Introduction to advanced electronic structure theory. Dover, New York

Thulstrup EW, Andersen A (1975) Configuration interaction studies of bound, low-lying states of N_2^-, N_2, N_2^+ and N_2^{2+}. J Phys B: At Mol Phys 8(6):965

Yevseyev AV, Radtsig AA, Smirnov BM (1982) The asymptotic theory of resonance charge exchange between diatomics. J Phys B: At Mol Phys 15(23):4437–4452

Yos JM (1965) vol RAD-TF 65-7. AVCO Corporation, Wilmington

Chapter 5
Collision Integrals for Interactions Involving Excited Species

The role of electronically excited states (EES) in affecting transport coefficients started with the pioneering paper (Hirschfelder and Eliason 1957), where it was predicted a significant increase of the collision integral with the principal quantum number, based on the semi-empirical relation for the collision diameter

$$\sigma = 2\bar{r} + 1.8 \qquad \bar{r} = \frac{\mathrm{n}^\star}{2}\frac{2\mathrm{n}^\star+1}{Z-S}a_0$$

$\bar{r}$ being the mean electron radius, $\mathrm{n}^\star$ the effective principal quantum number, Z the atomic number and S the screening constant in the Slater orbital wavefunction.

This analysis, while overestimating the transport cross section, does not account for the resonant processes of excitation- and charge-exchange in collisions involving excited atoms or ion-parent atoms that actually have been demonstrated to be dramatically affected by the quantum state of colliding partners.

The excited state issue is still an open problem, being the dependence of collision integrals on the quantum state of chemical species largely unknown. In the following the construction of a consistent collision integral database for interactions relevant to atomic hydrogen plasma is demonstrated, considering $\mathrm{H}^\star(\mathrm{n})$ excited species up to $\mathrm{n} = 12$, thus allowing the investigation on transport coefficient from atmospheric to high-pressure regimes with a suitable *cutoff* criterion for the truncation of internal partition function and for the inclusion of excited states in the reaction scheme (see Chap. 7). Diffusion- and viscosity-type collision integrals have been fitted with suitable analytical functions in the temperature range [10,000–25,000 K], where excited atomic species do exist in an LTE plasma, while higher orders, i.e. (ℓ, s) with $s > \ell$ were derived through recurrence relation in Eq. (3.16).

M. Capitelli et al., *Fundamental Aspects of Plasma Chemical Physics*,
Springer Series on Atomic, Optical, and Plasma Physics 74,
DOI 10.1007/978-1-4419-8172-1_5, © Springer Science+Business Media, LLC 2013

A collision-integral database for interactions involving electronically excited atoms, relevant to LTE atomic air plasma, is far from being complete; however, a review of the acquired results on both *low-* and *high-lying* excited states for nitrogen and oxygen is presented.

5.1 Electronically Excited H*(n) Atom Interactions

5.1.1 The Symmetric H(n)–H(n) *Interactions*

Diffusion- and viscosity-type collision integrals for the symmetric H(n)–H(n) interactions, up to n = 5, have been obtained by integrating the corresponding momentum transfer and viscosity cross sections obtained, in a quantum phase-shift approach, by integration of accurate ab initio CI potential energy curves (Celiberto et al. 1998) of a limited number of electronic terms. Data have been extrapolated up to n = 12 modelling the dependence on the principal quantum number, in a reduced energy scale, i.e. $\mathrm{n}' = 2 - \frac{1}{\mathrm{n}^2}$, with the equation

$$\Omega^{(\ell,\ell)\star}_{\mathrm{H(n)-H(n)}} = \exp\left(a_1 + \exp\left(-a_2 \mathrm{n}' + a_3\right)\right) \tag{5.1}$$

Collision integrals have been fitted against temperature with the simple equation

$$\Omega^{(\ell,\ell)\star}_{\mathrm{H(n)-H(n)}}(T) = b_1\, T^{b_2} \tag{5.2}$$

The relevant parameters, b_i, have been reported in Tables 5.1 and 5.2.

Table 5.1 Fitting coefficients, b_i, for temperature dependence of diffusion-type collision integrals [Eq. (5.2)] for H(n)–H(n) interactions up to n = 12

(n,n)	b_1	b_2
(1,1)	1.886 (3)*	−7.312 (−1)
(2,2)	7.144 (4)	−1.013 (0)
(3,3)	3.218 (4)	−8.561 (−1)
(4,4)	5.808 (4)	−8.992 (−1)
(5,5)	6.983 (4)	−9.114 (−1)
(6,6)	4.767 (4)	−8.584 (−1)
(7,7)	4.579 (4)	−8.493 (−1)
(8,8)	4.452 (4)	−8.431 (−1)
(9,9)	4.364 (4)	−8.388 (−1)
(10,10)	4.299 (4)	−8.356 (−1)
(11,11)	4.251 (4)	−8.332 (−1)
(12,12)	4.214 (4)	−8.314 (−1)

$^\star(3) \equiv 10^3$

Table 5.2 Fitting coefficients, b_i, for temperature dependence of viscosity-type collision integrals [Eq. (5.2)] for H(n)–H(n) interactions up to n = 12

(n,n)	b_1	b_2
(1,1)	4.976 (2)	−5.688 (−1)
(2,2)	3.471 (4)	−9.033 (−1)
(3,3)	4.385 (4)	−8.664 (−1)
(4,4)	3.854 (4)	−8.246 (−1)
(5,5)	3.384 (4)	−7.963 (−1)
(6,6)	3.216 (4)	−7.828 (−1)
(7,7)	2.976 (4)	−7.691 (−1)
(8,8)	2.961 (4)	−7.655 (−1)
(9,9)	2.804 (4)	−7.572 (−1)
(10,10)	2.759 (4)	−7.537 (−1)
(11,11)	2.786 (4)	−7.538 (−1)
(12,12)	2.690 (4)	−7.489 (−1)

5.1.2 Excitation Exchange

The study of the excitation exchange in collisions of excited hydrogen atoms, i.e. the process

$$\tilde{\mathrm{H}}(\mathrm{n}) + \mathrm{H}(^2S) \rightarrow \tilde{\mathrm{H}}(^2S) + \mathrm{H}(\mathrm{n}),$$

has been investigate in the past by different authors (Watanabe 1965; Nakamura and Matsuzawa 1967; Matsuzawa and Nakamura 1967; Capitelli et al. 1974), focusing on ($\mathrm{n} = 2, 3\ \ell = 0, 1, 2$) states.

In Capitelli et al. (1974) the electronic terms arising in the interaction H(3ℓ)–H($1s$) were calculated in the frame of the Heitler–London method and improving the estimation of correlation energy in the asymptotic region of dissociation, through a configuration interaction procedure among states of the same symmetry. The resonant excitation-exchange cross sections, governed by the exchange interaction potential, were estimated for each *gerade–ungerade* pair in the Firsov approach, already illustrated in Chap. 4, and reported in Table 5.3, together with corresponding values for H(2n)–H($1s$) and H(3n)–H($1s$) interactions, obtained with the PSS (perturbed stationary state) method in Nakamura and Matsuzawa (1967) and Matsuzawa and Nakamura (1967).

Table 5.3 Partial resonant excitation-exchange cross sections for each $g - u$ pair in H(3ℓ)–H($1s$) interaction

Collision pair	Term	A [eV]	α [Å^{-1}]	$\sigma_{\mathrm{ex}}^{(n\ell)}$[Å^2]($E = 0.1$ eV)	1 eV	5 eV	10 eV	Multiplicity
H($3s$)–H($1s$)	$^1\Sigma_{g,u}$	85.25	1.725	52.4	40.4	32.8	29.8	1
	$^3\Sigma_{g,u}$	20.92	1.307	70.8	52.4	41.1	36.6	3
H($3p$)–H($1s$)	$^1\Sigma_{g,u}$	10.81	1.251	66.1	47.5	36.2	31.8	1
	$^3\Sigma_{g,u}$	11.48	1.505	44.2	31.6	23.9	20.9	3
	$^1\Pi_{g,u}$	52.92	1.568	58.4	44.6	35.8	32.3	2
	$^3\Pi_{g,u}$	25.09	1,307	74.0	55.1	43.5	38.9	6
H($3d$)–H($1s$)	$^1\Sigma_{g,u}$	7.19	1.392	46.4	32.4	24.0	20.8	1
	$^3\Sigma_{g,u}$	17.28	1.596	43.1	31.3	24.1	21.3	3
	$^1\Pi_{g,u}$	13.40	1.338	60.0	43.5	33.4	29.4	2
	$^3\Pi_{g,u}$	18.99	1.505	50.3	36.9	28.6	25.3	6
	$^1\Delta_{g,u}$	85.17	1.779	48.9	37.7	30.6	27.8	2
	$^3\Delta_{g,u}$	77.58	1.734	50.8	39.0	31.7	28.7	6
H(3n)–H($1s$)			$\langle\sigma_{\mathrm{ex}}\rangle$	56.2	41.8	32.8	29.3	
H(2n)–H($1s$)			$\langle\sigma_{\mathrm{ex}}\rangle$	722.0	229.0	96.0	70.0	

Average values for H(3n)–H($1s$) (Capitelli et al. 1974) and H(2n)–H($1s$) (Nakamura and Matsuzawa 1967; Matsuzawa and Nakamura 1967) interactions are also reported

These results showed interestingly that in the case of exchange of excitation, differently from charge exchange, increasing the principal quantum number of the excited atomic partner reduces the process probability and this aspect could be better appreciated in inspection of Fig. 5.1 where results obtained in Capitelli et al. (2002) for the complete matrix of asymmetric interactions, up to $\mathrm{n} = 11$, $\mathrm{m} = 12$, are displayed. It is evident that the processes characterized

by higher cross sections are those corresponding to mono-quantum excitation, while the values decrease for multi-quantum transitions (n → m = n + 2, n + 3, ...).

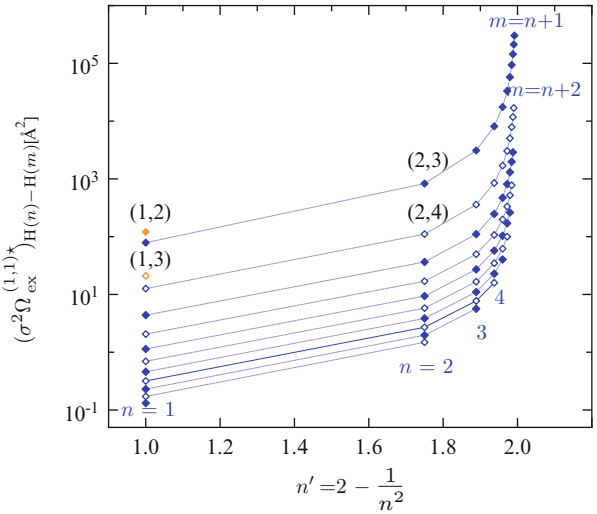

Fig. 5.1 Resonant excitation-exchange diffusion-type collision integrals for H(n)–H(m) interactions, as function of the principal quantum number of atomic partner (in the reduced energy scale n′) at $T = 10,000\,\text{K}$ (Capitelli et al. 2002) (*orange diamonds*) (Capitelli et al. 1974; Nakamura and Matsuzawa 1967; Matsuzawa and Nakamura 1967)

Actually in Capitelli et al. (2002) the approach for the cross section estimation was different, recalling the equation for $s - p$ (allowed) transitions in Watanabe (1965)

$$\sigma_{\text{ex}} = 3.36\pi\mu_{sp}^2 e^2 \frac{1}{\hbar g} \tag{5.3}$$

where g is the relative velocity of colliding atoms, related to collision energy, and μ_{sp} the dipole moment matrix element between s and p electronic states. Mean excitation transfer cross sections for other kinds of allowed interactions ($p - d$, $d - f$, $f - g$, ...) were estimated using a scaling procedure, through G functions (Hirschfelder et al. 1966)

$$\frac{\sigma_{1s-2p}}{G_{1s-2p}} = \frac{\sigma_{\text{n}d-mf}}{G_{\text{n}d-mf}} \tag{5.4}$$

$$G(\text{n}, \ell; \text{m}, \ell - 1) = \frac{1}{a_0^2}\left[\int_0^\infty \text{d}r\; r^3 R_{\text{n},\ell} R_{\text{m},\ell-1}\right]^2 \tag{5.5}$$

where R is the radial wavefunction for atomic hydrogen. The allowed transitions, coupling different atomic states characterized by different values assumed by the orbital quantum number ℓ, which give a contribution to the H(n)–H(m) interaction, have been weighted in an averaging procedure, where the statistical weight was the number of molecular electronic states correlating with specified asymptotic atomic states

$$\sigma_{\mathrm{ex}}^{\mathrm{nm}} = \frac{\sum_i \omega_i \sigma_i}{\sum_i \omega_i} \tag{5.6}$$

The temperature dependence of the excitation transfer contribution to the diffusion-type collision integral $\sigma^2 \Omega_{\mathrm{ex}}^{(1,1)}$ is reproduced using a logarithmic relation

$$\sigma^2 \Omega^{(1,1)\star}(T) = d_1 + d_2 \ln(T) \tag{5.7}$$

The elastic contribution to diffusion-type collision integrals is estimated by arithmetic average of the corresponding contributions for symmetric H(n)–H(n) and H(m)–H(m) interactions, not affected by resonant excitation-exchange processes, according to the simple formula

$$\sigma^2 \Omega_{\mathrm{H(n)-H(m)}}^{(1,1)\star} = \tfrac{1}{2}\left(\sigma^2 \Omega_{\mathrm{H(n)-H(n)}}^{(1,1)\star} + \sigma^2 \Omega_{\mathrm{H(m)-H(m)}}^{(1,1)\star}\right) \tag{5.8}$$

In general excitation transfer process dominates the diffusion-type collision integrals; the elastic contribution starts being predominant for large differences in the i–j values.

Equation (5.8) is extended also to the estimation of viscosity-type collision integrals, whose temperature behaviour is described through the simple power relation

$$\sigma^2 \Omega^{(2,2)\star}(T) = e_1 T^{e_2} \tag{5.9}$$

Fitting parameters entering Eqs. (5.7) and (5.9) are reported in Tables 5.4 and 5.5, respectively.

5.1.3 Resonant Charge Exchange

The resonant charge-exchange process in hydrogen–proton collisions involving excited atomic partners

$$\tilde{\mathrm{H}}(\mathrm{n}) + \mathrm{H}^+ \rightarrow \tilde{\mathrm{H}}^+ + \mathrm{H}(\mathrm{n})$$

has been deeply investigated in literature since from the past (Dalgarno and Yadav 1953; Bates and Reid 1968, 1969; Malaviya 1970) due to its fundamental relevance in many fields from astrophysics to transport.

Resonant cross sections in H^+–H(n) interactions, up to n = 5, were obtained, in the frame of the Firsov approach (see Chap. 4), estimating the

Table 5.4 Fitting coefficients, d_i, entering Eq. (5.7) for temperature dependence of diffusion-type collision integrals, $\sigma^2\Omega_{\rm ex}^{(1,1)\star}$, for single quantum excitation transitions in H(n)–H(m) interactions

(n,m)	d_1	d_2
(1,2)	3.709 (2)	−3.178 (1)
(2,3)	3.913 (3)	−3.353 (2)
(3,4)	1.460 (4)	−1.251 (3)
(4,5)	3.829 (4)	−3.281 (3)
(5,6)	8.256 (4)	−7.074 (3)
(6,7)	1.568 (5)	−1.344 (4)
(7,8)	2.720 (5)	−2.330 (4)
(8,9)	4.411 (5)	−3.780 (4)
(9,10)	6.758 (5)	−5.814 (4)
(10,11)	1.000 (6)	−8.573 (4)
(11,12)	1.425 (6)	−1.221 (5)

Table 5.5 Fitting coefficients, e_i, entering Eq. (5.9) for temperature dependence of viscosity-type collision integrals, $\sigma^2\Omega^{(2,2)\star}$, for single quantum excitation transitions in H(n)–H(m) interactions

(n,m)	e_1	e_2
(1,2)	2.947 (3)	−6.690 (−1)
(2,3)	4.002 (4)	−8.832 (−1)
(3,4)	3.953 (4)	−8.403 (−1)
(4,5)	3.532 (4)	−8.076 (−1)
(5,6)	3.332 (4)	−7.905 (−1)
(6,7)	3.090 (4)	−7.758 (−1)
(7,8)	2.937 (4)	−7.662 (−1)
(8,9)	2.910 (4)	−7.624 (−1)
(9,10)	2.817 (4)	−7.569 (−1)
(10,11)	2.717 (4)	−7.514 (−1)
(11,12)	2.744 (4)	−7.515 (−1)

g–u splittings from accurate potential energy curves of relevant electronic terms (Capitelli and Lamanna 1974). Partial contributions for different g–u pairs are reported in Table 5.6.

The comparison of the average cross sections, retaining the dependence on the principal quantum number n, with those obtained, for n = 2 and 3, by Bates (Bates and Reid 1968, 1969), by using a *two-state* approach, also reported in Table 5.6, shows a substantial agreement, confirming the reliability of the asymptotic approach when the accurate long-range behaviour of potential energy curves for *gerade* and *ungerade* electronic terms is available.

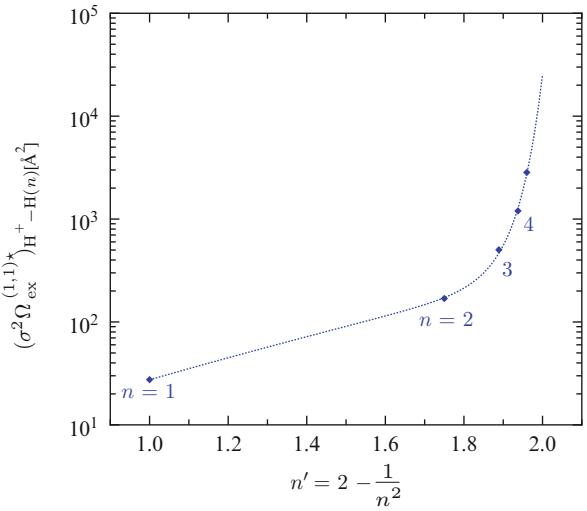

Fig. 5.2 Resonant charge-exchange diffusion-type collision integrals for H(n)–H^+ interactions, as function of the principal quantum number of atomic partner (in the reduced energy scale n′) at $T = 10,000$ K (Capitelli et al. 2002)

Table 5.6 Resonant charge-exchange cross sections, partial contributions due to different (gu) pairs with statistical weight and average values, in H(n)–H$^+$ collisions

State	A [eV]	α [Å^{-1}]	Δr [a_0]	$\sigma^i_{\rm ex}(E)$ [Å^2]				ω_i	(nℓ)
				$E = 0.1$ eV	1.0	5.0	10.0		
$^2\Sigma_{gu}$	111.4	1.65	6–15	60.7	47.3	38.8	35.4	1	1s
$^2\Sigma_{gu}$	6.5	0.77	5–24	170	123	94	82	2	2s
$^2\Sigma_{gu}$	40.7	0.50	13–20	675	528	438	398	2	2p
$^2\Pi_{gu}$	16.5	0.62	7–20	347	262	208	187	4	2p
			$\langle\sigma_{\rm ex}\rangle_{n=2}$	384.8	293.8	237.0	213.5		
			$\langle\sigma_{\rm ex}\rangle^{(a)}_{n=2}$	380	248	208	191		
$^2\Sigma_{gu}$	2.4	0.58	8–36	254	176	128	111	2	3s
$^2\Sigma_{gu}$	5.8	0.30	9–30	1,403	1,045	823	739	2	3p
$^2\Sigma_{gu}$	26.8	0.27	18–60	2,524	1,990	1,648	1,508	2	3d
$^2\Pi_{gu}$	4.8	0.43	10–30	577	422	326	286	4	3p
$^2\Pi_{gu}$	13.5	0.30	10–54	1,638	1,257	1,020	927	4	3d
$^2\Delta_{gu}$	10	0.40	10–48	852	641	514	459	4	3d
			$\langle\sigma_{\rm ex}\rangle_{n=3}$	1,146.1	872.3	702.1	633.6		
			$\langle\sigma_{\rm ex}\rangle^{(a)}_{n=3}$	1,033.0	845.0	716.0	662.0		
$^2\Sigma_{gu}$	0.79	0.43	1–36	353	226	156	129	2	4s
$^2\Sigma_{gu}$	1.41	0.20	1–40	2,512	1,814	1,375	1,204	2	4p
$^2\Sigma_{gu}$	6.3	0.19	16–80	3,784	2,875	2,315	2,091	2	4d
$^2\Sigma_{gu}$	87.3	0.20	40–112	5,576	4,527	3,862	3,587	2	4f
$^2\Pi_{gu}$	1.4	0.32	1–40	852	590	433	372	4	4p
$^2\Pi_{gu}$	3.4	0.22	8–72	2,499	1,847	1,450	1,293	4	4d
$^2\Pi_{gu}$	11.5	0.18	24–106	4,941	3,846	3,151	2,862	4	4f
$^2\Delta_{gu}$	1.42	0.22	1–28	2,057	1,460	1,094	957	4	4d
$^2\Delta_{gu}$	4.5	0.19	12–80	3,662	2,756	2,196	1,967	4	4f
$^2\Phi_{gu}$	2.6	0.23	6–64	2,160	1,567	1,213	1,069	4	4f
			$\langle\sigma_{\rm ex}\rangle_{n=4}$	2,785.4	2,098.4	1,673.9	1,503.2		
$^2\Sigma_{gu}$	0.38	0.35	1–40	448	273	176	140	2	5s
$^2\Sigma_{gu}$	0.77	0.17	1–50	3,067	2,126	1,557	1,347	2	5p
$^2\Sigma_{gu}$	1.38	0.13	10–90	6,450	4,783	3,693	3,264	2	5d
$^2\Sigma_{gu}$	7.1	0.13	40–120	9,823	7,693	6,231	5,652	2	5f
$^2\Sigma_{gu}$	89.4	0.14	70–160	12,435	10,048	8,690	8,094	2	5g
$^2\Pi_{gu}$	0.73	0.25	1–40	1,161	780	555	470	4	5p
$^2\Pi_{gu}$	0.57	0.09	1–35	11,612	8,831	6,633	5,841	4	5d
$^2\Pi_{gu}$	5.1	0.15	27–120	6,430	4,923	3,925	3,617	4	5f
$^2\Pi_{gu}$	19.6	0.13	50–140	11,078	8,831	7,367	6,777	4	5g
$^2\Delta_{gu}$	0.79	0.19	1.25–50	2,267	1,558	1,144	981	4	5d
$^2\Delta_{gu}$	1.19	0.12	11.25–80	6,818	5,101	3,925	3,468	4	5f
$^2\Delta_{gu}$	5.2	0.12	35–120	9,798	7,475	6,035	5,465	4	5g
$^2\Phi_{gu}$	0.88	0.16	1.25–60	3,816	2,639	2,034	1,710	4	5f
$^2\Phi_{gu}$	1.13	0.11	8.75–100	8,831	6,633	5,101	4,578	4	5g
$^2\Gamma_{gu}$	1.18	0.15	1.25–90	4,245	3,039	2,267	2,034	4	5g
			$\langle\sigma_{\rm ex}\rangle_{n=5}$	6,573.4	4,981.7	3,932.8	3,535.2		

$^{(a)}$Results of Bates and Reid (1968, 1969) for n = 2, 3 are also reported

The contribution of resonant charge exchange to diffusion-type collision integrals was estimated in Capitelli and Lamanna (1974) and Capitelli et al. (2002) through Eq. (4.7) and the dependence on temperature (see Fig. 5.2), in the interval [10,000–25,000 K], and on the principal quantum number is described with the following analytical function:

$$\sigma^2\Omega^{(1,1)\star}(T,\mathrm{n}) = \exp\left[f_1(\mathrm{n}')^{f_2}(T')^{f_3} + \exp\left(f_4\mathrm{n}' - f_5\right)\right] \tag{5.10}$$

with $T' = T/1,000$ and parameters $f_1 = 3.519$, $f_2 = 0.77$, $f_3 = -2.732 \times 10^{-2}$, $f_4 = 15.9$ and $f_5 = 30.3$.

The elastic contribution is estimated with a *polarization* model potential, characterized by closed form for corresponding collision integrals [Eqs. (3.36)], which can be straightforwardly extended to interactions of proton with excited atomic partners, considering the dependence of the polarizability, $\alpha_{\mathrm{pol}}^{\mathrm{H(n)}}$ on the principal quantum number

$$\alpha_{\mathrm{pol}} = \tfrac{1}{8} a_0^3 \mathrm{n}^4 [17\mathrm{n}^2 - 3(\mathrm{n}_1 - \mathrm{n}_2)^2 - 9m^2 + 19] \tag{5.11}$$

n_1 and n_2 being the *parabolic quantum numbers*, defined as

$$\begin{cases} \mathrm{n}_1 = \mathrm{n} - \ell - 1 \\ \mathrm{n}_2 = \ell - |m| \end{cases} \Rightarrow \mathrm{n}_1 - \mathrm{n}_2 = \mathrm{n} - 2\ell - 1 - |m| \tag{5.12}$$

The resonant charge-exchange collision integral dominates the *effective* diffusion-type collision integral, derived with Eq. (4.5), the polarization contribution not exceeding 10%.

In Capitelli and Lamanna (1974) also viscosity-type collision integrals for interaction H^+–H(n) up to $\mathrm{n} = 5$ were calculated, these results being extrapolated to $\mathrm{n} = 12$ with a suitable function of the principal quantum number and of the temperature, having the same form adopted for diffusion-type collision integrals

$$\sigma^2 \Omega^{(2,2)\star}(T, \mathrm{n}) = \exp\left[g_1 (\mathrm{n}')^{g_2} (T')^{g_3} + \exp\left(g_4 \mathrm{n}' - g_5\right)\right] \tag{5.13}$$

with $T' = T/1,000$ and parameters $g_1 = 4.0349$, $g_2 = 0.9$, $g_3 = -0.3442$, $g_4 = 15.6$ and $g_5 = 30.25$.

5.1.4 Electron-H(n) Interactions

In the case of electron interaction with excited atomic hydrogen, diffusion-type collision integrals for different values of the principal quantum number have been derived by direct integration [Eq. (3.11)] of corresponding momentum transfer cross sections for elastic electron scattering by H(n) atoms, in Ignjatović and Mihajlov (1997), calculated in the frame of the partial wave method. Cross sections $[a_0^2]$ have been fitted as a function of energy E [eV] and of the principal quantum number n by the following expression:

$$Q^{(1)} = \frac{A}{E} \ln\left[1 + B\mathrm{n}^4 E^2\right] \left[1 + C \exp\left(-D\sqrt{E}\right)\right] \tag{5.14}$$

the relevant parameters being reported in Table 5.7.

The temperature dependence of diffusion-type collision integrals Fig. 5.3 has been fitted with a power function

$$\sigma^2 \Omega^{(1,1)\star}(T) = h_1 T^{h_2} \tag{5.15}$$

the relevant parameters being reported in Table 5.8.

Viscosity-type collision integrals for e-H(n) interactions would require the calculation of higher momenta of elastic scattering cross section, not available when the database was created. Thus the equality $\sigma^2 \Omega^{(1,1)\star} = \sigma^2 \Omega^{(2,2)\star}$ was assumed.

Table 5.7 Fitting coefficients, entering Eq. (5.14) for temperature dependence of elastic cross section in e-H(n) interactions

n	A	B	C	D
1	528.6	0.019	18.68	0.73
2	755.6	0.038	34.04	1.51
3	757.2	0.047	32.04	7.81
4	772.7	0.037	23.73	8.60
5	798.6	0.030	11.08	7.58
6	821.3	0.026	5.43	6.39
7	846.6	0.022	4.00	4.93
8	861.5	0.021	3.56	6.41
9	862.3	0.020	3.28	5.43
10	862.3	0.019	3.28	5.43

Table 5.8 Fitting coefficients, h_i, entering Eq. (5.15), for temperature dependence of diffusion-type collision integrals for e-H(n) interactions

n	h_1	h_2
1	4.946 (3)	−0.721
2	8.347 (5)	−1.129
3	7.317 (6)	−1.279
4	2.858 (7)	−1.386
5	7.561 (7)	−1.462
6	1.611 (8)	−1.520
7	3.440 (8)	−1.582
8	4.105 (8)	−1.590
9	6.952 (8)	−1.634
10	9.519 (8)	−1.658

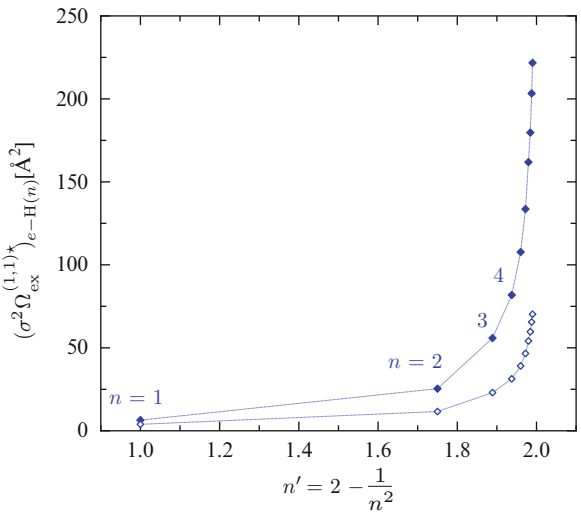

Fig. 5.3 Diffusion-type collision integrals for e-H(n) interactions, as function of the principal quantum number of atomic partner (in the reduced energy scale n′) at different temperatures "(Capitelli et al. 2004)" T = 10,000 K, "T=20,000 K"

5.2 Electronically Excited He(n)–He^+ Interactions

Very recently the charge-exchange process

$$He^\star + He^+(^2S) \rightarrow He^+(^2S) + He^\star$$

involving singlet and triplet helium excited states up to n = 5 has been investigated, estimating cross sections in the frame of classical theory and quantum asymptotic approach (Kosarim et al. 2012). The classical and asymptotic approaches correspond to a different character of the process, so that the classical approach assumes, in the course of the collision, effective transitions between states close in energy, whereas the asymptotic approach ignores these transitions.

According to the asymptotic theory (Chap. 4), the cross sections of resonant charge exchange is averaged over the momentum projection of the electron onto the molecular axis at closest approach of nuclei in collision

$$\sigma_{n\ell} = \frac{\sigma_{n\ell 0} + 2\sum_\mu \sigma_{n\ell\mu}}{2\ell + 1} \tag{5.16}$$

where $\sigma_{n\ell\mu}$ is the cross section for indicated quantum numbers of the transferring electron. Evidently, for a strongly excited atom, the elliptic electron quantum numbers describe the process better than the spherical ones. Table 5.9 gives the averaged values for different collision energies.

Further averaging over the different electronic states of excited helium atoms characterized by the same principal quantum number, properly accounting for statistical weight of different terms, allows to study the dependence on n of resonant charge transfer cross sections, reported in Table 5.10.

It is worth noting that the present $He^\star$–He^+ averaged cross sections are close to the corresponding values for the $H^\star$(n)–H^+ interaction pair, as it can be appreciated in Fig. 5.4, where results for helium system obtained in the asymptotic approach have been compared with results for hydrogen (Capitelli et al. 1974), derived with the Firsov approach (Firsov 1951). Note also that the charge-exchange cross sections for interaction involving excited $H^\star$ atoms are in close agreement with the two-state quantum approach by Bates (Bates and Reid 1968) and multistate results for n = 2 by Malaviya (1970) (see Sect. 5.1.3).

Diffusion-type collision integrals are governed in the high-temperature region by resonant processes, as it can be appreciated in Table 5.11 where values, obtained from the average resonant charge transfer cross sections in Table 5.10, are reported for He(n)–He^+ interactions.

The classical approach can be used also to estimate the dependence of resonant charge transfer cross sections on principal quantum number of $He^{+\star}$ for the process

$$He^{+\star} + He^{2+} \rightarrow He^{2+} + He^{+\star}$$

Table 5.9 Averaged values of asymptotic cross sections of resonant charge exchange in He*–He$^+$ collisions

Electron shell	σ_{ex} [Å^2]		
	$E = 0.1$ eV	1 eV	10 eV
$1s^2$ ($^1S_0$)	33	26	20
$1s2s(2^3S)$	300	250	200
$1s2s(2^1S)$	400	330	270
$1s2p(2^3P)$	370	310	240
$1s2p(2^1P)$	420	350	280
$1s3s(3^3S)$	1,300	1,100	950
$1s3s(3^1S)$	1,600	1,400	1,200
$1s3p(3^3P)$	1,500	1,300	1,100
$1s3p(3^1P)$	1,700	1,400	1,200
$1s3d(3^{1,3}D)$	1,400	1,200	950
$1s4s(4^3S)$	3,900	3,400	2,900
$1s4s(4^1S)$	4,500	4,000	3,400
$1s4p(4^3P)$	4,300	3,800	3,200
$1s4p(4^1P)$	4,600	4,000	3,500
$1s4d(4^{1,3}D)$	4,100	3,600	3,100
$1s4f(4^{1,3}F)$	3,400	2,900	2,400
$1s5s(5^3S)$	9,100	8,100	7,200
$1s5s(5^1S)$	10,200	9,200	8,200
$1s5p(5^3P)$	9,800	8,700	7,700
$1s5p(5^1P)$	10,400	9,300	8,200
$1s5d(5^{1,3}D)$	9,500	8,400	7,500
$1s5f(5^{1,3}F)$	8,400	7,500	6,600
$1s5g(5^{1,3}G)$	7,000	6,100	5,200

Table 5.10 Resonant charge transfer cross section [Å^2] for ion–parent-atom interactions involving excited helium atoms, with principal quantum number n = 2–5

n	$E = 0.1$ eV	1 eV	10 eV
1	33	26	20
2	390	320	260
3	1,400	1,200	1,000
4	3,800	3,300	2,800
5	8,400	7,400	6,500

Table 5.11 Inelastic contribution to diffusion-type collision integrals, due to resonant charge transfer, for He(n)–He$^+$ interactions, with principal quantum number n

T	$\sigma^2\Omega^{(1,1)\star}_{\mathrm{He(n)-He^+}}$ [Å^2]				
	n = 1	n = 2	n = 3	n = 4	n = 5
1,000	18.1	219.9	807.7	2,210.9	4,942.6
2,000	16.9	207.2	768.7	2,113.4	4,758.2
4,000	15.6	194.8	730.6	2,018.1	4,577.2
6,000	14.9	187.8	708.8	1,963.4	4,473.0
8,000	14.5	182.9	693.5	1,925.1	4,399.8
10,000	14.1	179.1	681.7	1,895.6	4,343.4
20,000	13.0	167.7	645.9	1,805.4	4,170.6
30,000	12.3	161.1	625.4	1,753.7	4,071.2
40,000	11.9	156.6	611.0	1,717.4	4,001.3
50,000	11.5	153.1	600.0	1,689.6	3,947.6
100,000	10.5	142.5	566.4	1,604.5	3,782.9

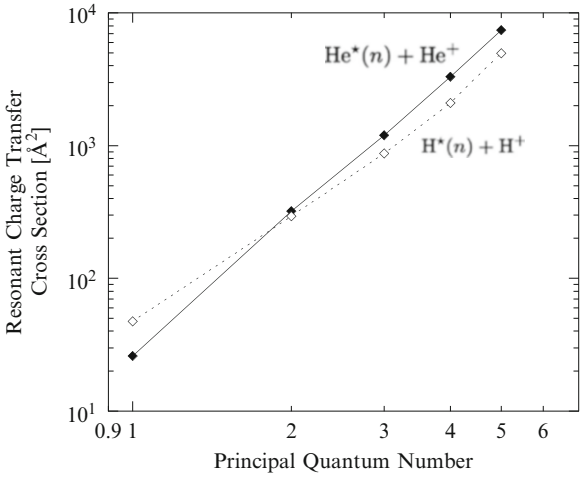

Fig. 5.4 Asymptotic resonant charge transfer cross section as a function of principal quantum number of excited atomic partner in $He^{\star}(n)$–$He^{+}(^2S)$ interactions, at collision energy $E = 1\,eV$, compared with corresponding theoretical results for $H^{\star}(n)$–H^{+} (Capitelli et al. 1974)

which can be considered as a benchmark system for comparison with Coulomb interactions. In the diabatic limit the temperature-independent cross section can be estimated through the n scaling relation

$$\sigma_{ct} = \frac{32\pi n^4}{Z^2} a_o^2, \tag{5.17}$$

Ze being the charge of the multi-charge ionic cores interacting.

Usually for interactions involving ionic species only the elastic Coulomb contribution is considered. However in this scheme the inelastic contribution could be estimated as $\sigma^2\Omega^{(1,1)\star} = \frac{2\sigma_{ct}}{\pi}$, and inspection of Fig. 5.5, where the diffusion-type collision integrals for excited states in $He^{+}(n)$–He^{2+} interactions are compared with the Coulomb collision integral, shows that it could significantly affect the actual value of $\sigma^2\Omega^{(1,1)\star}$. These results open to question the impact of including inelastic resonant charge-exchange channels in the estimation of transport coefficients in highly ionized regimes.

5.3 Electronically Excited N(n)–N^{+}(n) and O(n)–O^{+}(n) Interactions

For air species, namely, oxygen and nitrogen atoms and ions, the investigation was focused on the so-called *low-lying* excited states, i.e. states sharing the same electronic configuration of the ground term (Capitelli and Ficocelli

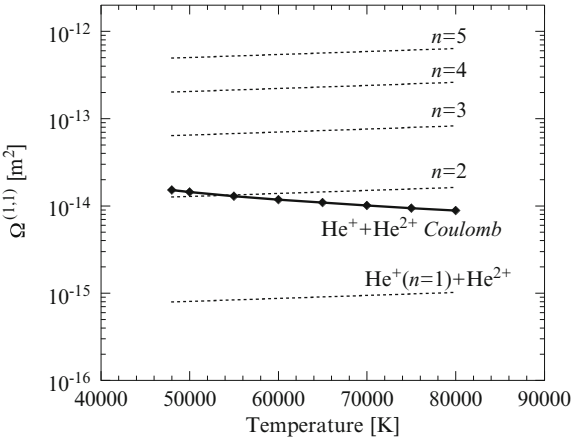

Fig. 5.5 Diffusion-type collision integrals, $\Omega^{(1,1)} = \sqrt{[k_B T\pi/2\mu]}\sigma^2\Omega^{(1,1)\star}$, for He$^+$(n)–He^{2+} interactions. Inelastic contributions due to resonant charge-transfer for excited states (*dotted lines*) and elastic contribution (*markers*)

1972; Sourd et al. 2007a,b; Laricchiuta et al. 2008). Collision integrals have been estimated as weighted averages of different electronic states, considering also the contribution due to inelastic channels which affect the odd-order terms (Kosarim and Smirnov 2005; Kosarim et al. 2006). The dependence on electronic excitation of colliding partners was actually weak; however, the paper by Eletskii (Eletskii et al. 2004), estimating the charge-exchange contribution in highly excited state interactions, demonstrated that greater effects are to be expected increasing the principal quantum number.

Reference should be done to the early work in this field by different authors (Nyeland and Mason 1967; Capitelli and Ficocelli 1972, 1973; Capitelli 1975; Capitelli et al. 1977), attempting the accurate calculation of diffusion and viscosity-type collision integrals for interactions involving the ground and the *low-lying* excited states of nitrogen and oxygen atoms [N(^{4}S,^{2}P,^{2}D), O(^{3}P,^{1}D,^{1}S)] and ions [N$^+$(^{3}P,^{1}D,^{1}S), O$^+$(^{4}S,^{2}P,^{2}D)]. Recently a complete revision of old results for oxygen system has been performed (Laricchiuta et al. 2008), based on accurate ab initio interaction potentials for valence states. The inelastic contribution to odd-order collision integrals due to resonant charge-exchange processes in ion–parent-atom collisions has been evaluated from the corresponding cross sections recalculated in the framework of the asymptotic theory (Eletskii et al. 2004; Kosarim and Smirnov 2005; Kosarim et al. 2006) considering different momentum coupling schemes. An attempt to study the effects of excited species in an LTE nitrogen plasma can be found in recent papers by Aubreton et al. (Sourd et al. 2007a,b), however restricted to dissociative regime, i.e. neutral atom interactions.

In the cited references, collision integrals have been obtained in the traditional multi-potential approach, thus requiring the accurate knowledge of a huge number of electronic terms increasing the quantum state of colliding

partners. In the case of $N_2^\star$ and $N_2^{+\star}$ excited systems only some electronic terms are available from ab initio calculations or from spectroscopic data models, reflecting the theoretical and experimental limits in studying excited states.

In this context the phenomenological approach could represent a valuable tool, allowing the derivation of complete and internally consistent sets of collision integrals. The potential functional form is the same adopted for describing the interaction between not excited species, this choice is justified considering that low-lying excited states are characterized by physical properties quite similar to the ground state and by small energy separation (Laricchiuta et al. 2009). In the next sections we will discuss more in details the previous considerations.

5.3.1 Low-Lying Excited States

The phenomenological approach (Chap. 3), already validated in the case of ground-state interactions (Capitelli et al. 2007), has been used for estimating the elastic collision integrals for $N^\star$–$N^{+\star}$ and $O^\star$–$O^{+\star}$ low-lying interactions.

Table 5.12 Polarizability values [Å^3] for nitrogen and oxygen atoms and ions in ground and electronically excited states

Atom	α_{pol}	Ion	α_{pol}
$N(^4S)$ (a)	1.1	$N^+(^3P)$ (a)	0.55
$N(^2D)$ (b)	1.1657	$N^+(^1D)$ (c)	0.527
$N(^2P)$ (b)	1.2232	$N^+(^1S)$ (c)	0.585
$O(^3P)$ (a)	0.80	$O^+(^4S)$ (a)	0.279
$O(^1D)$ (b)	0.8039	$O^+(^2D)$ (c)	0.352
$O(^1S)$ (b)	0.8371	$O^+(^2P)$ (c)	0.371

(a) Miller and Bederson (1977), (b) Nesbet (1977), (c) Fraga and Saxena (1972)

In Table 5.12 polarizability values for relevant species, needed in the estimation of potential parameters through correlation formulas, are reported.

Reduced collision integrals, $\Omega^{(\ell,s)\star}$, have been calculated, up to order (4,4), over a wide range of reduced temperatures and fitted as a function of both temperature and β parameter (Laricchiuta et al. 2007), allowing the estimation of collision integrals on the base of the *tuplet* (r_e,φ_0,β,m) completely characterizing the physical system.

Table 5.13 Parameters of phenomenological potential for interactions relevant to nitrogen and oxygen excited states

Interaction	φ_0 [meV]	r_e [Å]	β	Interaction	φ_0 [meV]	r_e [Å]	β	m
N(^{4}S)	6.432	3.583	6.605	O(^{3}P)	5.763	3.423	6.898	6
N(^{4}S) N(^{2}D)	6.550	3.598	6.802	O(^{3}P) O(^{1}D)	5.772	3.424	7.346	6
N(^{2}P)	6.646	3.611	6.798	O(^{1}S)	5.846	3.434	7.341	6
N(^{2}D) N(^{2}D)	6.675	3.613	7.188	O(^{1}D) O(^{1}D)	5.781	3.425	8.689	6
N(^{2}P)	6.777	3.625	7.178	O(^{1}S)	5.855	3.435	8.671	6
N(^{2}P) N(^{2}P)	6.884	3.638	7.169	O(^{1}S) O(^{1}S)	5.933	3.445	8.653	6
N(^{4}S)	94.581	2.956	6.759	O(^{3}P)	93.447	2.689	6.926	4
N^+(^{3}P) N(^{2}D)	98.213	2.969	7.096	O^+(^{4}S) O(^{1}D)	93.736	2.690	7.411	4
N(^{2}P)	101.31	2.981	7.088	O(^{1}S)	96.162	2.699	7.406	4
N(^{4}S)	95.687	2.943	7.013	O(^{1}D)	87.540	2.754	8.135	4
N^+(^{1}D) N(^{2}D)	99.344	2.957	7.717	O^+(^{2}D) O(^{3}P)	87.264	2.753	7.191	4
N(^{2}P)	102.46	2.968	7.697	O(^{1}S)	89.861	2.763	8.124	4
N(^{4}S)	93.006	2.975	7.007	O(^{3}P)	85.922	2.768	7.184	4
N^+(^{1}S) N(^{2}D)	96.603	2.988	7.700	O^+(^{2}P) O(^{1}D)	86.195	2.769	8.112	4
N(^{2}P)	99.670	2.999	7.681	O(^{1}S)	88.494	2.778	8.101	4
O(^{3}P)	5.989	3.507	6.723	O(^{3}P)	6.133	3.537	7.015	6
N(^{4}S) O(^{1}D)	6.001	3.508	6.988	N(^{2}P) O(^{1}D)	6.146	3.538	7.629	6
O(^{1}S)	6.098	3.517	6.986	O(^{1}S)	6.252	3.547	7.623	6
O(^{3}P)	6.069	3.523	7.023					6
N(^{2}D) O(^{1}D)	6.081	3.524	7.648					6
O(^{1}S)	6.184	3.533	7.641					6
N(^{4}S)	113.879	2.764	6.742	O(^{3}P)	76.475	2.886	6.954	4
O^+(^{4}S) N(^{2}D)	117.956	2.779	7.060	N^+(^{3}P) O(^{1}D)	76.729	2.887	7.476	4
N(^{2}P)	121.427	2.791	7.052	O(^{1}S)	78.870	2.895	7.470	4
N(^{4}S)	106.835	2.827	6.902	O(^{3}P)	77.451	2.873	7.392	4
O^+(^{2}D) N(^{2}D)	110.746	2.841	7.422	N^+(^{1}D) O(^{1}D)	77.707	2.874	8.878	4
N(^{2}P)	114.077	2.853	7.408	O(^{1}S)	79.864	2.882	8.857	4
N(^{4}S)	105.308	2.841	6.898	O(^{3}P)	75.084	2.905	7.381	4
O^+(^{2}P) N(^{2}D)	109.183	2.855	7.412	N^+(^{1}S) O(^{1}D)	75.336	2.906	8.831	4
N(^{2}P)	112.485	2.867	7.398	O(^{1}S)	77.454	2.915	8.811	4

In Table 5.13 parameters of phenomenological potential for interactions relevant to atomic and ionic nitrogen and oxygen excited states are reported, exhibiting a regular trend, dominated by the increase of polarizability corresponding to electronic excitation, with the exception of the β value, strongly influenced by the change in spin multiplicity of excited states.

Viscosity-type collision integrals for O–O* interactions are plotted in Fig. 5.6 together with two series of data available in literature (Capitelli and Ficocelli 1972; Laricchiuta et al. 2008), based on the traditional multi-potential approach. Being the (2,2) term not affected by resonant excitation exchange in asymmetric collisions, the observed deviations could give indication of the accuracy of the proposed procedure. In general a satisfactory agreement is found between data sets in the considered temperature range [2,000–20,000 K], being the percentage relative error confined below 25% with respect to Laricchiuta et al. (2008). The error analysis should also take into account that the traditional multi-potential procedure, including all electronic-term contributions, is based in Capitelli and Ficocelli (1972)

and Laricchiuta et al. (2008) on a rigid classification of repulsive (decaying exponential function) and bound (Morse function) states that could affect data accuracy.

The proposed phenomenological approach does not account for the contributions to odd-ℓ collision integrals coming from inelastic channels, represented by the resonant charge-exchange and excitation-exchange processes occurring in ion–parent-atom and asymmetric atom–atom interactions, respectively.

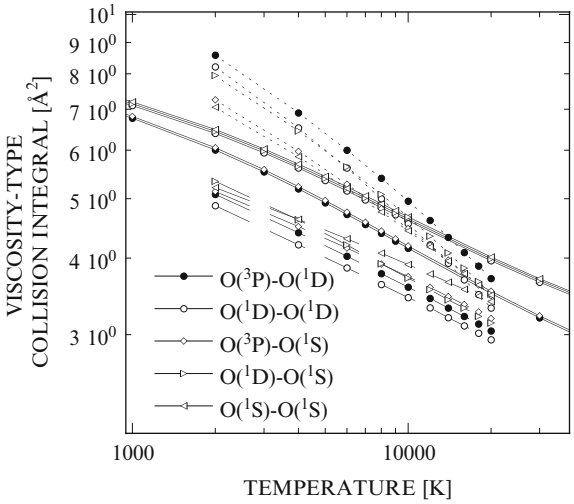

Fig. 5.6 Viscosity-type collision integrals for O–O* interactions (*continuous lines*) from phenomenological approach, compared with results in Capitelli and Ficocelli (1972) (*dashed lines*) and Laricchiuta et al. (2008) (*dotted lines*)

Diffusion-type transport cross sections for different interactions involving *low-lying* (LL) excited states have been derived from accurate resonant charge-exchange cross sections, calculated in the frame of the asymptotic approach, reconsidering the hierarchy of interactions and averaging over momentum projections with appropriate momentum coupling scheme (Kosarim and Smirnov 2005; Kosarim et al. 2006). As it can be appreciated in Fig. 5.7, the diffusion-type collision integrals for interactions involving LL states present peculiar features. The values corresponding to $^2D - ^3P$ and $^2P - ^3P$ interactions are lower than those involving the ground state, i.e. $^4S - ^3P$, the reverse being true for other interactions, although in general a weak dependence is observed on the excitation energy of the collisional pair. It is worth noting that the asymptotic approach is a one-electron-transfer theory, thus predicting a null probability for some resonant processes involving low-lying excited atoms, i.e. N(^4S)–N$^+$(^1D), N(^4S)–N$^+$(^1S) and N(^2D)–N$^+$(^1S), classified as

forbidden. This results in collision integrals for these interactions retaining only the elastic contribution and thus characterized by much lower values.

Older results, obtained in Capitelli (1977) in the Firsov approach and also reported in Fig. 5.7, though underestimating the resonant charge-exchange contribution due to the poor accuracy of the *gerade–ungerade* splitting at large distances, correctly predict the significant reduction of cross section corresponding to forbidden one-electron transitions in the asymptotic frame. Moreover the comparison of theoretical charge-exchange cross sections for oxygen system with measurements by Lindsay (Lindsay et al. 2001) for the ground-state interaction $O(^3P)$–$O^+(^4S)$ and for the average interaction with low-lying excited states of the $O^{+\star}$ ion shows clearly that the ratio of the corresponding values is largely satisfactory (see Fig. 5.8).

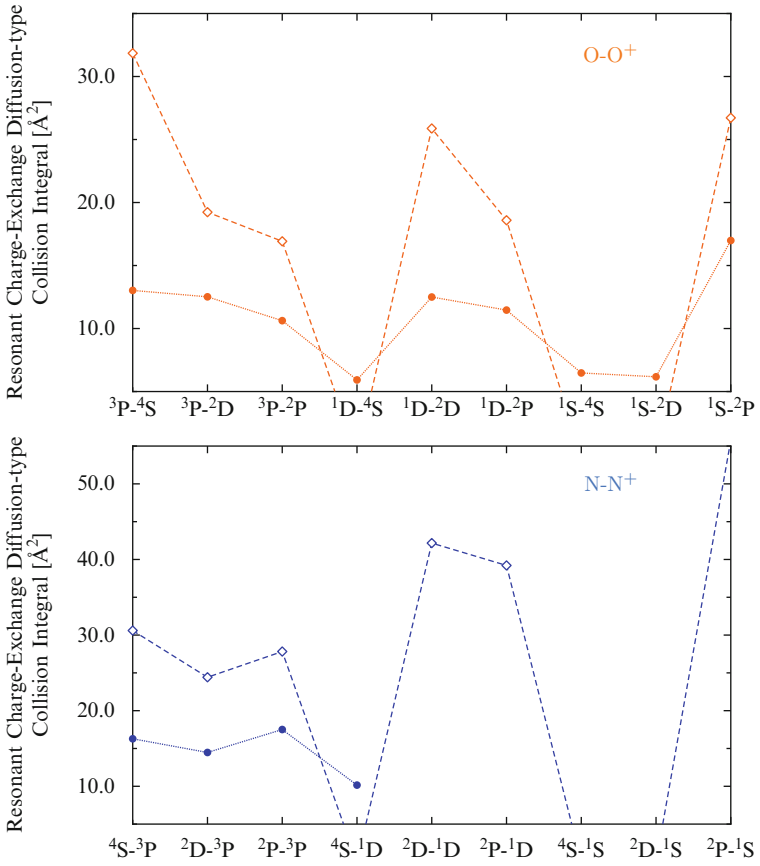

Fig. 5.7 Resonant charge-exchange diffusion-type collision integrals for interaction involving ground and LL excited states of atom and ion for nitrogen (Kosarim et al. 2006) and oxygen (Kosarim and Smirnov 2005) systems, at the temperature $T = 10,000$ K, compared with results in Capitelli (1977) (*solid line–close markers*)

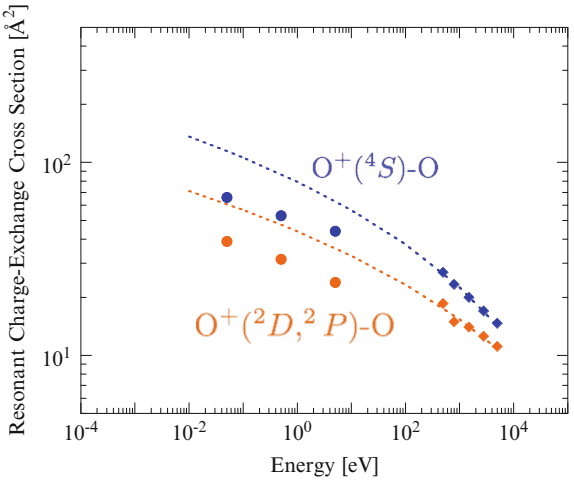

Fig. 5.8 Resonant charge-exchange cross sections for interactions involving ground and LL excited states of oxygen ion (Kosarim and Smirnov 2005) in $O(^3P)$–$O^{+\star}$ (*close circles*) compared with high-energy experimental results in Lindsay et al. (2001) (the *dotted line* represents the low-energy extrapolation of the fit given by Lindsay)

Resonant contribution to odd-order collision integrals for relevant interactions has been fitted with the following equation:

$$\sigma^2 \Omega_{\mathrm{ex}}^{(\ell,s)\star} = d_1 + d_2 x + d_3 x^2 \tag{5.18}$$

with $x = \ln(T)$. d_i coefficients are presented in Table 5.14, with reference in literature to corresponding resonant charge-exchange cross sections.

Concerning excitation-exchange processes, few references can be found in literature (Nyeland and Mason 1967; Sourd et al. 2007a; Capitelli and Ficocelli 1972, 1973) and new calculations have been performed, based on the estimation of gerade–ungerade energy splitting between electronic terms of the same symmetry, $\Delta\varphi = \varphi_g - \varphi_u$, within an asymptotic approach.

The excitation exchange cross section is defined as

$$\sigma_{\mathrm{ex}} = \frac{\pi R_0^2}{2} \tag{5.19}$$

R_0 is the solution of the transcendental equation

$$\frac{1}{g}\sqrt{\frac{\pi R_0}{2\gamma}}\Delta\varphi = 0.28 \tag{5.20}$$

where $\gamma = \alpha_i + \beta_i$, $-\alpha_i^2/2$ and $-\beta_i^2/2$ being the binding energies of the two valence electrons transferring from one atomic core to the other.

The electronic exchange interaction with excitation transfer, in atomic transitions forbidden via electric dipole, is found in literature with an analytical form (Hadinger et al. 1994)

Table 5.14 Fitting coefficients, entering Eq. (11.2), for $\sigma^2\Omega_{\rm ex}^{(\ell,s)\star}$ in ion–parent-atom collisions

	(ℓ,s)	d_1	d_2	d_3		(ℓ,s)	d_1	d_2	d_3
N$^+$(^{3}P)–N(^{4}S) (*a*)	(1,1)	65.8423	−4.5492	7.8608(−2)	N$^+$(^{3}P)–N(^{2}D) (*a*)	(1,1)	57.7292	−4.3834	8.3266(−2)
	(1,2)	64.3259	−4.4969	7.8619(−2)		(1,2)	56.2676	−4.3278	8.3258(−2)
	(1,3)	63.2015	−4.4575	7.8613(−2)		(1,3)	55.1845	−4.2858	8.3238(−2)
	(1,4)	62.3098	−4.4260	7.8606(−2)		(1,4)	54.3258	−4.2521	8.3206(−2)
	(1,5)	61.5722	−4.3997	7.8601(−2)		(1,5)	53.6194	−4.2250	8.3252(−2)
N$^+$(^{3}P)–N(^{2}P) (*a*)	(1,1)	68.9054	−5.4518	0.1079(0)	N$^+$(^{1}D)–N(^{2}D) (*a*)	(1,1)	87.0737	−5.7506	9.4982(−2)
	(1,2)	67.0876	−5.3797	0.1079(0)		(1,2)	85.1572	−5.6873	9.4987(−2)
	(1,3)	65.7434	−5.3259	0.1079(0)		(1,3)	83.7344	−5.6396	9.4972(−2)
	(1,4)	64.6773	−5.2825	0.1079(0)		(1,4)	82.6065	−5.6016	9.4974(−2)
	(1,5)	63.7972	−5.2468	0.1079(0)		(1,5)	81.6749	−5.5705	9.5006(−2)
N$^+$(^{1}D)–N(^{2}P) (*a*)	(1,1)	86.6184	−6.1552	0.1094(0)	N$^+$(^{1}S)–N(^{2}P) (*a*)	(1,1)	110.8355	−6.9958	0.1104(0)
	(1,2)	84.5658	−6.0819	0.1094(0)		(1,2)	108.5029	−6.9220	0.1104(0)
	(1,3)	83.0473	−6.0278	0.1094(0)		(1,3)	106.7730	−6.8669	0.1104(0)
	(1,4)	81.8405	−5.9837	0.1094(0)		(1,4)	105.4002	−6.8229	0.1104(0)
	(1,5)	80.8430	−5.9471	0.1094(0)		(1,5)	104.2624	−6.7859	0.1104(0)
O$^+$(^{4}S)–O(^{3}P) (*b*)	(1,1)	64.7044	−4.1936	6.7974(−2)	O$^+$(^{2}D)–O(^{3}P) (*b*)	(1,1)	45.5286	−3.4609	6.5796(−2)
	(1,2)	63.3075	−4.1485	6.7991(−2)		(1,2)	44.3750	−3.4172	6.5810(−2)
	(1,3)	62.2707	−4.1146	6.8000(−2)		(1,3)	43.5215	−3.3844	6.5815(−2)
	(1,4)	61.4470	−4.0872	6.7986(−2)		(1,4)	42.8448	−3.3582	6.5829(−2)
	(1,5)	60.7663	−4.0646	6.7987(−2)		(1,5)	42.2860	−3.3365	6.5845(−2)
O$^+$(^{2}D)–O(^{1}D) (*b*)	(1,1)	59.6379	−4.4205	8.1955(−2)	O$^+$(^{2}P)–O(^{3}P) (*b*)	(1,1)	40.1251	−3.0553	5.8192(−2)
	(1,2)	58.1643	−4.3657	8.1945(−2)		(1,2)	39.1085	−3.0170	5.8223(−2)
	(1,3)	57.0729	−4.3248	8.1951(−2)		(1,3)	38.3530	-2.9875	5.8201(−2)
	(1,4)	56.2083	−4.2921	8.1958(−2)		(1,4)	37.7560	−2.9643	5.8207(−2)
	(1,5)	55.4918	−4.2645	8.1933(−2)		(1,5)	37.2601	−2.9444	5.8171(−2)
O$^+$(^{2}P)–O(^{1}D) (*b*)	(1,1)	45.0371	−3.4968	6.7913(−2)	O$^+$(^{2}P)–O(^{1}S) (*b*)	(1,1)	60.4547	−4.4004	8.0107(−2)
	(1,2)	43.8724	−3.4517	6.7926(−2)		(1,2)	58.9883	−4.3472	8.0118(−2)
	(1,3)	43.0088	−3.4175	6.7907(−2)		(1,3)	57.9017	−4.3071	8.0118(−2)
	(1,4)	42.3257	−3.3906	6.7931(−2)		(1,4)	57.0393	−4.2748	8.0099(−2)
	(1,5)	41.7612	−3.3680	6.7928(−2)		(1,5)	56.3270	−4.2482	8.0109(−2)

(*a*) Kosarim et al. (2006), (*b*) Kosarim and Smirnov (2005)

$$\Delta\varphi = (2\ell_1+1)(2\ell_2+1)\mathcal{A}^2\mathcal{B}^2 R^{(2/\alpha_i)+(2/\beta_i)-1/(\alpha_i+\beta_i)-1}\exp\left(-(\alpha_i+\beta_i)R\right)I(\alpha_i,\beta_i)$$

$$I(\alpha_i,\beta_i) = \frac{(\alpha_i+\beta_i)^{(1/\alpha_i)+(1/\beta_i)-1/(\alpha_i+\beta_i)}}{\alpha_i^{1+1/\beta_i}\beta_i^{1+1/\alpha_i}2^{(1/\alpha_i)+(1/\beta_i)+1/(\alpha_i+\beta_i)+2}}\exp\left[-\frac{1}{2}\left(\frac{1}{\alpha_i}+\frac{1}{\beta_i}\right)\right]\Gamma\left[\frac{1}{(\alpha_i+\beta_i)}\right]$$
$$\int_0^1 \mathrm{d}x\,(1-x)^{(1/\alpha_i)+(1/\beta_i)-1/(\alpha_i+\beta_i)}(1+x)^{1/(\alpha_i+\beta_i)}\exp\left[\frac{1}{2}x\left(\frac{1}{\alpha_i}+\frac{1}{\beta_i}\right)\right] \quad (5.21)$$

$|\ell_1, m_1>$ e $|\ell_2, m_2>$ are the quantum numbers associated with the eigenvalue of angular momentum and to the axial projection for the two electrons undergoing exchange. $\mathcal{A}$ and $\mathcal{B}$ are the coefficients entering the asymptotic formula of electronic wavefunctions for valence orbitals (Eletskii et al. 2004) and Γ is the Gamma function.

Cross sections are obtained including in Eq. (5.21) terms with null axial projection ($\ell = 1$, $m = 0$), representing the main contribution (Chibisov and Janev 1988). Excitation-exchange contribution to odd-order collision integrals has been fitted again with Eq. (5.18), with d_i coefficients given in Table 5.15.

Table 5.15 Fitting coefficients, entering Eq. (5.18), for $\sigma^2\Omega_{\mathrm{ex}}^{(\ell,s)\star}$ in asymmetric atom–atom collisions

	(ℓ,s)	d_1	d_2	d_3		(ℓ,s)	d_1	d_2	d_3
$N(^4S)$–$N(^2D)$	(1,1)	31.5961	−1.8580	2.7332(−2)	$N(^4S)$–$N(^2P)$	(1,1)	32.9761	−1.9830	2.9808(−2)
	(1,2)	30.9767	−1.8396	2.7314(−2)		(1,2)	32.3161	−1.9634	2.9824(−2)
	(1,3)	30.5173	−1.8261	2.7322(−2)		(1,3)	31.8263	−1.9487	2.9842(−2)
	(1,4)	30.1516	−1.8150	2.7319(−2)		(1,4)	31.4361	−1.9367	2.9840(−2)
	(1,5)	29.8486	−1.8057	2.7301(−2)		(1,5)	31.1130	−1.9267	2.9830(−2)
$N(^2D)$–$N(^2P)$	(1,1)	35.7731	−2.1781	3.3162(−2)	$O(^3P)$–$O(^1D)$	(1,1)	27.8104	−1.8819	3.1851(−2)
	(1,2)	35.0466	−2.1558	3.3155(−2)		(1,2)	27.1844	−1.8610	3.1874(−2)
	(1,3)	34.5087	−2.1396	3.3178(−2)		(1,3)	26.7188	−1.8449	3.1861(−2)
	(1,4)	34.0787	−2.1257	3.3138(−2)		(1,4)	26.3499	−1.8322	3.1860(−2)
	(1,5)	33.7258	−2.1151	3.3164(−2)		(1,5)	26.0439	−1.8215	3.1855(−2)
$O(^3P)$–$O(^1S)$	(1,1)	33.7682	−2.1791	3.5187(−2)	$O(^1D)$–$O(^1S)$	(1,1)	39.3236	−2.4460	3.8046(−2)
	(1,2)	33.0403	−2.1553	3.5161(−2)		(1,2)	38.5091	−2.4209	3.8066(−2)
	(1,3)	32.5011	−2.1375	3.5144(−2)		(1,3)	37.9035	−2.4017	3.8058(−2)
	(1,4)	32.0735	−2.1235	3.5151(−2)		(1,4)	37.4222	−2.3862	3.8038(−2)
	(1,5)	31.7202	−2.1119	3.5160(−2)		(1,5)	37.0237	−2.3733	3.8018(−2)

The asymptotic approach predicts higher values than those obtained by the evaluation of gerade–ungerade splitting from potential energy curves (Nyeland and Mason 1967; Sourd et al. 2007a; Capitelli and Ficocelli 1972, 1973); however, the direct estimation could be affected by the lower accuracy characterizing the region of large internuclear distances, where the process takes place favourably.

As generally observed, the inelastic contribution is significantly higher with respect to the elastic one, especially in the high-temperature region, dominating the temperature dependence of the diffusion-type collision integral and, consequently, also its dependence on the electronic excitation of colliding partners.

5.3.2 High-Lying Excited States

The only attempt to estimate the charge-exchange cross sections in ion-parent–atom collisions involving nitrogen and oxygen atoms in highly excited (*hl*) states (n >2) is in Eletskii et al. (2004), where the theoretical frame is the asymptotic approach and results show an $n^4 - n^5$ dependence on the principal quantum number of the atomic valence shell.

The state-selected results are reported in Tables 5.16 and 5.17.

Corresponding diffusion-type collision integrals for interactions involving HL states, exhibit an n^5 dependence on the principal quantum number as shown in Fig. 5.9, where the interactions O(HL)–$O^+(^4S)$ and N(HL)–$N^+(^3P)$ are displayed as a function of the excitation of the atomic partner.

Table 5.16 The partial and averaged magnitudes of the resonant charge-exchange cross section (10^{-16} cm^2), calculated for excited states of nitrogen

State	Λ	I	E [eV] 0.1	1.0	10.0
			g [10^5 cm/s] 1.66	5.24	16.6
N(^4S) (γ = 1.034)	0	1/2	65.9	52.7	40.8
		3/2	73.3	60.0	47.8
		5/2	79.5	65.2	52.1
	1	1/2	47.0	36.7	27.9
		3/2	53.8	43.0	33.0
		5/2	57.9	46.6	36.4
		σ_{ex}	61.5	49.5	39.0
N($^2D_{3/2,5/2}$) (γ = 0.945)	0	1/2	62.2	50.8	39.5
		3/2	72.0	56.0	43.8
	1	1/2	36.3	23.3	15.9
		3/2	42.9	28.5	20.0
		σ_{ex}	50.0	36.1	27.2
N($^2P_{1/2,3/2}$) (γ = 0.898)	0	1/2	65.7	53.9	38.4
		3/2	75.7	61.9	46.7
	1	1/2	39.0	29.3	18.7
		3/2	44.6	33.4	23.6
		σ_{ex}	52.8	41.2	29.0
N($2p^2 3s\ ^2P$) (γ = 0.53)	0	1/2	404	332	265
		3/2	438	374	307
		σ_{ex}	426	361	293
N($2p^2 4s\ ^2P$) (γ = 0.344)	0	1/2	2,690	2,400	2,130
		3/2	2,870	2,580	2,270
		σ_{ex}	2,800	2,520	2,220
N($2p^2 5s\ ^2P$) (γ = 0.25)	0	1/2	4,900	4,300	3,710
		3/2	5,290	4,670	4,090
		σ_{ex}	5,160	4,540	3,970
N($2p^2 3s\ ^4P$) (γ = 0.556)	0	1/2	201	149	100
		3/2	233	179	129
		5/2	274	216	161
		σ_{ex}	249	192	140
N($2p^2 4s\ ^4P$) (γ = 0.35)	0	1/2	1,770	1,520	1,300
		3/2	1,910	1,660	1,440
		5/2	2,000	1,750	1,520
		σ_{ex}	1,930	1,690	1,460
N($2p^2 5s\ ^4P$) (γ = 0.26)	0	1/2	4,310	3,780	3,260
		3/2	4,680	4,090	3,590
		5/2	4,850	4,290	3,760
		σ_{ex}	4,710	4,140	3,620

Table 5.17 The partial and averaged magnitudes of the resonant charge-exchange cross section (10^{-16} cm^2), calculated for excited states of oxygen

State	Λ	I	E (eV) 0.1	1.0	10.0
			g (10^5 cm/s) 1.55	4.9	15.5
O(^3P) ($\gamma = 1.0$)	0	1/2	56.7	44.8	32.6
		3/2	63.8	51.3	39.5
		5/2	69.8	56.1	43.8
	1	1/2	39.0	29.0	21.1
		3/2	45.2	35.3	25.7
		5/2	49.8	38.7	28.8
		σ_{ex}	52.9	41.1	30.8
O($2p^3 3s\ ^5S$) ($\gamma = 0.573$)	0	1/2	308	255	207
		3/2	344	286	233
		5/2	365	306	254
		7/2	381	320	268
		σ_{ex}	367	312	261
O($2p^3 4s\ ^5S$) ($\gamma = 0.34$)	0	1/2	1,890	1,640	1,390
		3/2	2,060	1,800	1,530
		5/2	2,160	1,890	1,630
		7/2	2,240	1,970	1,700
		σ_{ex}	2,150	1,870	1,620
O($2p^3 5s\ ^5S$) ($\gamma = 0.26$)	0	1/2	4,240	3,710	3,200
		3/2	4,590	4,000	3,520
		5/2	4,780	4,170	3,690
		7/2	4,940	4,290	3,840
		σ_{ex}	4,750	4,150	3,660
O($2p^3 3s\ ^3S$) $\gamma = 0.549$)	0	1/2	360	300	246
		3/2	400	336	276
		5/2	423	357	298
		σ_{ex}	412	350	291

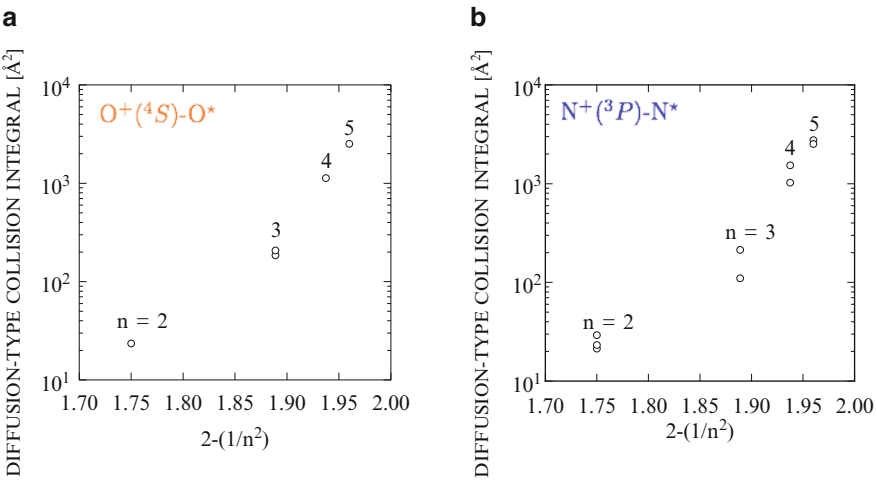

Fig. 5.9 Dependence on principal quantum number (reduced energy scale) of inelastic contribution to diffusion-type collision integrals in N*–N$^+$(^3P) and O*–O$^+$(^4S) interactions, involving excited atomic partner, at $T = 10,000$ K. Different electronic states of N and O atoms arising from the same electronic configuration have been considered

References

Bates DR, Reid RHG (1968) Electronic eigenenergies of the hydrogen molecular ion. Advances in atomic and molecular physics, vol 4. Academic, New York, pp 13–35

Bates DR, Reid RHG (1969) Resonance charge transfer between protons and excited hydrogen atoms. I. Quantal two-state approximation. J Phys B: At Mol Phys 2(8):851

Capitelli M (1975) Charge transfer from low-lying excited states: effects on reactive thermal conductivity. J Plasma Phys 14(2):365–371

Capitelli M (1977) Transport coefficients of partially ionized gases. J Phys Supp Colloque C3 (Paris) 38(8):C3 227–C3 237

Capitelli M, Ficocelli E (1972) Collision integrals of oxygen atoms in different electronic states. J Phys B: At Mol Phys 5(11):2066–2073

Capitelli M, Ficocelli E (1973) Collision integrals of carbon-oxygen atoms in different electronic states. J Phys B: At Mol Phys 6:1819–1823

Capitelli M, Lamanna U (1974) Collision integrals of electronically excited states and transport coefficients of thermal plasmas. J Plasma Phys 12:71–79

Capitelli M, Guidotti C, Lamanna U (1974) Potential energy curves and excitation transfer cross sections of excited hydrogen atoms. J Phys B: At Mol Phys 7(13):1683

Capitelli M, Lamanna UT, Guidotti C, Arrighini GP (1977) The gerade-ungerade splitting of N_2^+ potentials: effects on the resonant charge transfer cross sections of nitrogen atoms. Chem Phys 19:269

Capitelli M, Celiberto R, Gorse C, Laricchiuta A, Minelli P, Pagano D (2002) Electronically excited states and transport properties of thermal plasmas: the reactive thermal conductivity. Phys Rev E 66(1):016403/1–8

Capitelli M, Celiberto R, Gorse C, Laricchiuta A, Pagano D, Traversa P (2004) Transport properties of local thermodynamic equilibrium hydrogen plasmas including electronically excited states. Phys Rev E 69(2):026412

Capitelli M, Cappelletti D, Colonna G, Gorse C, Laricchiuta A, Liuti G, Longo S, Pirani F (2007) On the possibility of using model potentials for collision integral calculations of interest for planetary atmospheres. Chem Phys 338(1):62–68

Celiberto R, Lamanna UT, Capitelli M (1998) Elastic, diffusion, and viscosity cross sections for collisions involving excited atomic hydrogen. Phys Rev A 58:2106–2114

Chibisov MI, Janev RK (1988) Asymptotic exchange interactions in ion-atom systems. Phys Rep (Review Section of Physics Letters) 166(1):1–87

Dalgarno A, Yadav HN (1953) Electron capture II: Resonance capture from hydrogen atoms by slow protons. P Phys Soc A 66(2):173

Eletskii AV, Capitelli M, Celiberto R, Laricchiuta A (2004) Resonant charge exchange and relevant transport cross sections for excited states of oxygen and nitrogen atoms. Phys Rev A 69(4):042718/1–8

Firsov OB (1951) JETP (in russian) 21:1001
Fraga S, Saxena KMS (1972) Hartree-Fock values of energies, interaction constants, and atomic properties for excited states with p^n configurations of the negative ions, neutral atoms, and first positive ions from boron to bromine. Atom Data 4(3):255–267
Hadinger G, Hadinger G, Bouty O, Frécon MA (1994) Asymptotic calculation of the exchange interaction between two long-range interacting atoms with open valence shells of any type. Phys Rev A 50(2):1927–1930
Hirschfelder JO, Eliason MA (1957) The estimation of the transport properties for electronically excited atoms and molecules. Ann NY Acad Sci 67(9):451–461
Hirschfelder JO, Curtiss CF, Bird RB (1966) Molecular theory of gases and liquids. Wiley, New York
Ignjatović LJM, Mihajlov AA (1997) Interaction of electrons with atoms in ground and excited states; potential of interaction, momentum transfer cross-sections. Contrib Plasm Phys 37(4):309–326
Kosarim AV, Smirnov BM (2005) Electron terms and resonant charge exchange involving oxygen atoms and ions. J Exp Theor Phys 101(4):611–627
Kosarim AV, Smirnov BM, Capitelli M, Celiberto R, Laricchiuta A (2006) Resonant charge exchange involving electronically excited states of nitrogen atoms and ions. Phys Rev A 74(6):062707
Kosarim AV, Smirnov BM, Laricchiuta A, Capitelli M (2012) Resonant charge-exchange involving excited helium atoms and reactive transport of LTE helium plasma. Phys Plasmas 19(6):062309
Laricchiuta A, Colonna G, Bruno D, Celiberto R, Gorse C, Pirani F, Capitelli M (2007) Classical transport collision integrals for a Lennard-Jones like phenomenological model potential. Chem Phys Lett 445(4–6):133–139
Laricchiuta A, Bruno D, Capitelli M, Celiberto R, Gorse G, Pintus G (2008) Collision integrals of oxygen atoms and ions in electronically excited states. Chem Phys 344(1–2):13–20
Laricchiuta A, Pirani F, Colonna G, Bruno D, Gorse C, Celiberto R, Capitelli M (2009) Collision integrals for interactions involving atoms in electronically excited states. J Phys Chem A 113(52):15250–15256
Lindsay BG, Sieglaff DR, Smith KA, Stebbings RF (2001) Charge transfer of keV O^+ ions with atomic oxygen. J Geophys Res 106(A5):8197–8203
Malaviya V (1970) Resonance charge transfer between protons and excited hydrogen atoms. III. Quantal eight-state approximation. J Phys B: At Mol Phys 3(11):1492
Matsuzawa M, Nakamura H (1967) Collisional excitation transfer between hydrogen atoms. II. H($2s$)+ H($1s$)→H($1s$)+ H($2s$). J Phys Soc Japan 22(2):392–398
Miller T, Bederson B (1977) Atomic and molecular polarizabilities-A review of recent advances. In: Bates DR, Bederson B (eds) Advances in Atomic and Molecular Physics, vol 13. Academic, New York

Nakamura H, Matsuzawa M (1967) Collisional excitation transfer between hydrogen atoms. I. H($2p$)+ H($1s$)→H($1s$)+ H($2p$). J Phys Soc Japan 22(1):248–256

Nesbet RK (1977) Atomic polarizabilities for ground and excited states of C, N, and O. Phys Rev A 16(1):1–5

Nyeland C, Mason EA (1967) Adiabatic excitation transfer in gases: Effects on transport. Phys Fluids 10(5):985–991

Sourd B, André P, Aubreton J, Elchinger MF (2007a) Influence of the excited states of atomic nitrogen N(^2D) and N(^2P) on the transport properties of nitrogen. Part I: Atomic nitrogen properties. Plasma Chem Plasma P 27(1):35–50

Sourd B, André P, Aubreton J, Elchinger MF (2007b) Influence of the excited states of atomic nitrogen N(^2D), N(^2P) and N(R) on the transport properties of nitrogen. Part II: Nitrogen plasma properties. Plasma Chem Plasma P 27(2):225–240

Watanabe T (1965) Collisional excitation transfer of $S - P$ type between identical atoms. Phys Rev 138:A1573–A1581

Chapter 6
Vibrational Excitation and Transport Properties of Reacting Gases: Beyond the Eucken Approximation

In Chap. 1 we have introduced the Eucken approximation as a useful tool to calculate the thermal conductivity contribution of the internal states of molecules. In the case of vibration a closed form appears as a result of the following hypotheses:

1. All the vibrational excited states have the same elastic cross sections independently of the vibrational quantum number of the molecule.
2. The vibrational distribution is well described by a Boltzmann law at a given temperature.
3. Inelastic energy exchange processes play a minor role.

The most critical point is the assumption (2) due to non-equilibrium vibrational distributions existing under different conditions which include cold plasmas, shock wave, nozzle and boundary layer flows. In these reacting mixtures, in fact, the coupling between chemical and vibrational kinetics produces strong non-equilibrium vibrational distributions, which can modify the transport coefficients. A generalized formulation of the Enskog expansion can be used to describe this situation (Nagnibeda and Kustova 2009; Brun 2009). The model assumes that the relaxation times for the chemical and vibrational modes are much longer than the relaxation times for the translational and rotational ones. Therefore, the chemical composition of the system and the populations of the vibrational levels of the molecules are treated as macroscopic parameters on the same ground as temperature and hydrodynamic velocity: their evolution on a macroscopic timescale is governed by kinetic equations coupled with the system of fluid dynamic equations. As a consequence, the transport coefficients derived in this way depend on all these macroscopic parameters so that the method allows the explicit inclusion of the non-equilibrium situation in the calculation. In these conditions a state-to-state approach is necessary in order to get the information on the concentrations and the gradients of the different vibrational levels entering the transport equations. In this chapter we will present different numerical

M. Capitelli et al., *Fundamental Aspects of Plasma Chemical Physics*,
Springer Series on Atomic, Optical, and Plasma Physics 74,
DOI 10.1007/978-1-4419-8172-1_6, © Springer Science+Business Media, LLC 2013

examples (Bruno et al. 1999, 2001; Kustova et al. 2002) illustrating the state of the art on these topics. A more detailed discussion is contained in the recent book by Nagnibeda and Kustova (2009).

6.1 Theory

We use the model developed by Kustova and Nagnibeda (1998), with particular attention to the evaluation of the heat flux and corresponding transport coefficients. To lowest-order approximation, the distribution functions are the equilibrium Maxwell–Boltzmann distribution over velocities and rotational energy and a non-equilibrium distribution over vibrational energy and chemical species. To this order of approximation, the equations for the macroscopic parameters n_{ci}, $\boldsymbol{v}$ and T (the level populations, the hydrodynamic velocity and gas temperature, respectively), are the nonviscous Euler equations. The diffusion velocity is written as

$$\boldsymbol{V}_{ci} = -\sum_{dk} D_{ci}^{dk} \boldsymbol{d}_{dk} - D_{ci}^{T} \nabla \ln T$$

(D_{ci}^{dk}, diffusion coefficients; D_{ci}^{T}, thermal diffusion coefficients) and the heat flux

$$\boldsymbol{q} = -\lambda' \nabla T - p \sum_{ci} D_{ci}^{T} \boldsymbol{d}_{ci} + \sum_{ci} \left(\tfrac{5}{2} k_{\mathrm{B}} T + < E_j^{ci} >_{\mathrm{rot}} + E_i^c + E^c \right) n_{ci} \boldsymbol{V}_{ci}$$

(λ', thermal conductivity), where $< E_j^{ci} >_{\mathrm{rot}}$ is the average rotational energy associated with molecules of species c in the vibrational level i, E_i^c is the vibrational energy of molecules of species c in the vibrational level i and E^c is the formation energy for molecules of species c.
The quantity

$$\boldsymbol{d}_{ci} = \nabla\left(\frac{n_{ci}}{n}\right) + \left(\frac{n_{ci}}{n} - \frac{\rho_{ci}}{\rho}\right) \nabla \ln p$$

involves the gradients of the vibrational level populations (the subscript c refers to the chemical species and i refers to the vibrational level). In this way, the system of transport coefficients is enlarged to include diffusion coefficients for every vibrational level.

The transport coefficients in these formulas are expressed in terms of the macroscopic parameters and the collision integrals.

If we suppose that the collision integrals do not depend on the vibrational level of the particles, the system of transport coefficients is further simplified:

$$
\begin{aligned}
&D_{ci}^{ci} && \text{different for every vibrational level}\\
&D_c^c = D_{ci}^{ck} && i \neq k\\
&D_c^d = D_{ci}^{dk} && c \neq d\\
&D_c^T && \text{different for every chemical species}
\end{aligned}
$$

For a binary mixture of molecules and their atoms, taking into account that the diffusion driving forces satisfy (1 refers to molecules, 2 to atoms)

$$\sum_i \boldsymbol{d}_{1i} + \boldsymbol{d}_2 = \boldsymbol{d}_1 + \boldsymbol{d}_2 = 0 \tag{6.1}$$

we get the following final expression for the diffusion velocities and the heat flux:

$$
\begin{aligned}
\boldsymbol{V}_{1i} &= -D_{1i}^{1i}\boldsymbol{d}_{1i} - D_1^1 \sum_{k\neq i} \boldsymbol{d}_{1k} - D_1^2\boldsymbol{d}_2 - D_1^T \nabla \log p\\
&= (D_1^1 - D_{1i}^{1i})\boldsymbol{d}_{1i} + (D_1^1 - D_1^2)\boldsymbol{d}_2 - D_1^T \nabla \log p\\
\boldsymbol{V}_2 &= -D_2^2\boldsymbol{d}_2 - D_2^1\boldsymbol{d}_1 - D_2^T \nabla \log p\\
\boldsymbol{q} &= -\lambda' \nabla T - p(D_1^T \boldsymbol{d}_1 + D_2^T \boldsymbol{d}_2)\\
&\quad + \sum_{ci} \left(\tfrac{5}{2} k_{\mathrm{B}} T + < E_j^{ci} >_{\mathrm{rot}} + E_i^c + E_c\right) n_{ci} \boldsymbol{V}_{ci} = -\lambda_{\mathrm{tot}} \nabla T
\end{aligned}
\tag{6.2}
$$

Assuming that thermal diffusion is a small effect, we can distinguish two contributions to the heat flux: the flux due to conduction, i.e. the Fourier term, describes the transport of energy due to the collisions of the rapid type. Due to our assumption that these collisions are independent of the vibrational level, this term does not depend on the particular vibrational distribution of the molecules but only on the chemical composition of the gas mixture; the second term describes the convective contribution, due to the diffusion of all vibrational levels. As we will see, this term is strongly modified by the vibrational non-equilibrium and cannot be described by an internal thermal conductivity coefficient as in the usual Eucken description of polyatomic gases (Hirschfelder et al. 1966).

6.2 Cooling Flow

We have applied the model to the calculation of the transport properties in a model flow. The macroscopic parameters are derived by a direct simulation Monte Carlo method (DSMC) simulation of an N–N_2 mixture (Bruno et al. 1998); we use just a rough model of the system that gives a qualitative insight into the dynamics of the vibrational distributions. The model

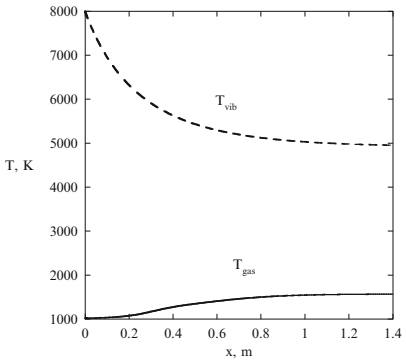

Fig. 6.1 Evolution of gas and vibrational temperatures along the flow

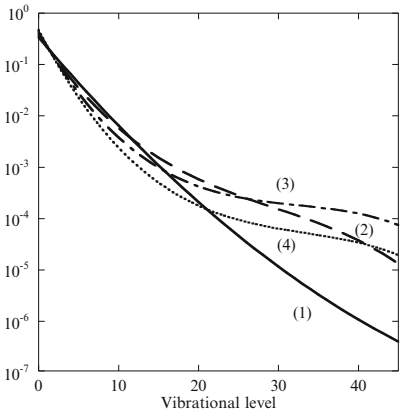

Fig. 6.2 Evolution of the vibrational distribution function at different points along the flow. (1) $x = 0\,\mathrm{m}$; (2) $x = 0.2\,\mathrm{m}$; (3) $x = 0.5\,\mathrm{m}$; (4) $x = 1.4\,\mathrm{m}$

implements a state-to-state vibrational kinetics with simple rate coefficients. The particles are treated as hard spheres as far as the total cross section is concerned; no difference between atoms and molecules in this respect is considered; the dissociation process is described by a simple ladder-climbing model (Capitelli and Molinari 1980; Capitelli 1986). The initial situation is strongly non-equilibrium: the vibrational levels are distributed according to the Boltzmann distribution at $T_{\mathrm{vib}} = 8,000\,\mathrm{K}$, the gas temperature is $T_{\mathrm{gas}} = 1,000\,\mathrm{K}$, and the gas is in steady flow at $v = 10^5\,\mathrm{cm/s}$ and is considered to be made only by molecules; the relaxation is followed for a time $\Delta t = 1.4\,\mathrm{ms}$. In Fig. 6.1 we show the behaviour of the temperatures T_{gas}, T_{vib}. The latter is defined by

$$T_{\mathrm{vib}} = \frac{1}{k_{\mathrm{B}}} \frac{E_1^1 - E_0^1}{\ln\left(n_{10}/n_{11}\right)} \tag{6.3}$$

The gas has a high-energy content stored in the vibrational degrees of freedom; during relaxation, due to the anharmonicity of the molecule vibrations and to the low gas temperature, the vibration–vibration (VV) energy exchanges are much faster than vibration–translation (VT) ones so that high-lying plateau in the vibrational distribution function (VdF) builds up (see Fig. 6.2).

The long plateau present at location (3), i.e. $x = 0.5$ m, is therefore the result of the VV up pumping model (Capitelli and Molinari 1980; Capitelli 1986) followed at location (4), $x = 1.4$ m, by VT relaxation from atomic nitrogen.

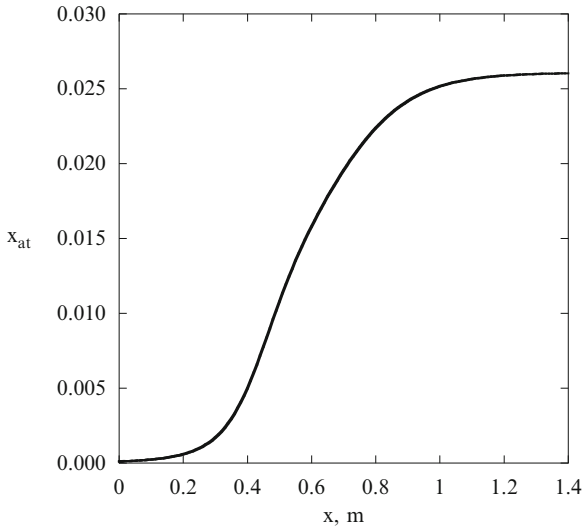

Fig. 6.3 Evolution of the system chemical composition

In Fig. 6.3 we report the evolution of the composition of an N_2/N mixture, in particular the behaviour of the molar fraction of atomic nitrogen is reported as a function of the distance along the flow. These data are used as input for a calculation of the heat flux in the flow. We report the different contributions to the total heat conductivity as they appear in Eq. (6.2). We thus distinguish a Fourier term, due to the energy exchanges during rapid collisions; a term due to the thermal diffusion; and a convection term due to particle diffusion. The latter can be further split in the sum over molecules plus the term concerning the diffusion of atoms.

Figure 6.4 shows that there is a great contribution to the conductivity due to molecular diffusion, this term being directly influenced by vibrational non-equilibrium. In Fig. 6.5 we compare the latter quantity from the calculations for the same quantity obtained when considering vibrational distributions at the vibrational temperature T_{vib}. We see that with this assumption the theory completely fails to reproduce the correct behaviour.

It is interesting to show how the different vibrational levels contribute to the total convective term of molecular diffusion. According to Bruno et al. (1999) this term can be re-written as

$$-\mathcal{D}_{\text{mol}} \sum_{\text{mol}} H_{ci} \nabla(n_{ci}) = -\nabla T \sum_{\text{mol}} \lambda_i \tag{6.4}$$

We now analyse the different contributions of all levels to this term; we can roughly distinguish two regions in the flow. In the beginning, at distances less than 0.5 m, the plateau in the distribution builds up; in Fig. 6.6 we show the comparison between terms of the form $\sum_{i=i_1}^{i_2} \lambda_i$, calculated for the two cases.

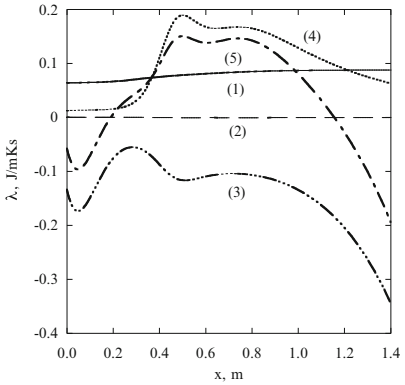

Fig. 6.4 Different contributions to the total heat conductivity. (1) Fourier part; (2) thermal diffusion part; (3) molecular diffusion; (4) atomic diffusion; (5) total thermal conductivity

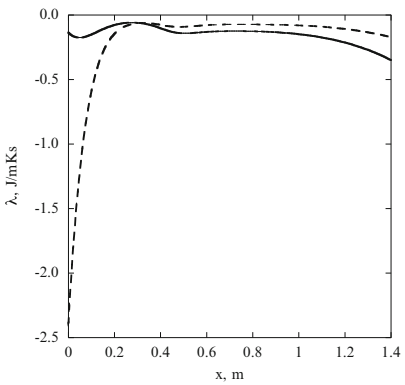

Fig. 6.5 Convective contribution to the thermal conductivity, due to molecules. (*full line*) non-equilibrium vibrational distributions; (*dashed line*) Boltzmann-like distributions at T_{vib}

The contribution coming from the 0–8 levels (Fig. 6.6a) presents the same qualitative trend for the equilibrium and non-equilibrium cases. A different behaviour is presented by the intermediate levels $i = 9$–22 (Fig. 6.6b), which in one case are populated and in the other depopulated following the decreasing vibrational temperature; also, the upper-lying levels (Fig. 6.6c), which do not contribute to the flux in the Boltzmann-like case, give a substantial contribution in the non-equilibrium case. In the second region, the relaxation slows down as the established quasi-stationary distribution slowly relaxes due to VT energy transfers (in particular, those due to collisions with atoms). In this case, the level kinetics can be better approximated by a Boltzmann-like behaviour for levels 0–8 (Fig. 6.6a′). The intermediate levels (9–22) present large differences for equilibrium and non-equilibrium cases (Fig. 6.6b′). Finally the high-lying levels (23–45), in the non-equilibrium case, still give an important contribution to the thermal conductivity, being practically zero for the equilibrium case (Fig. 6.6c′). Therefore, the transport coefficients essentially depend on the shape of the VdF and on the level kinetics so that only a "state-to-state" approach that explicitly takes into account the details of the VdF can give the correct results.

The results reported in the different figures are a clear example of the inadequacy of the second hypothesis of Eucken approach in estimating the vibrational contribution to the heat flow in the presence of strongly non-equilibrium conditions. It is also interesting to note that the results reported in Fig. 6.6a-c′ are a little affected by the introduction of the transport cross sections depending on the vibrational quantum number (Gorbachev et al. 1997) as shown by Bruno et al. (1999).

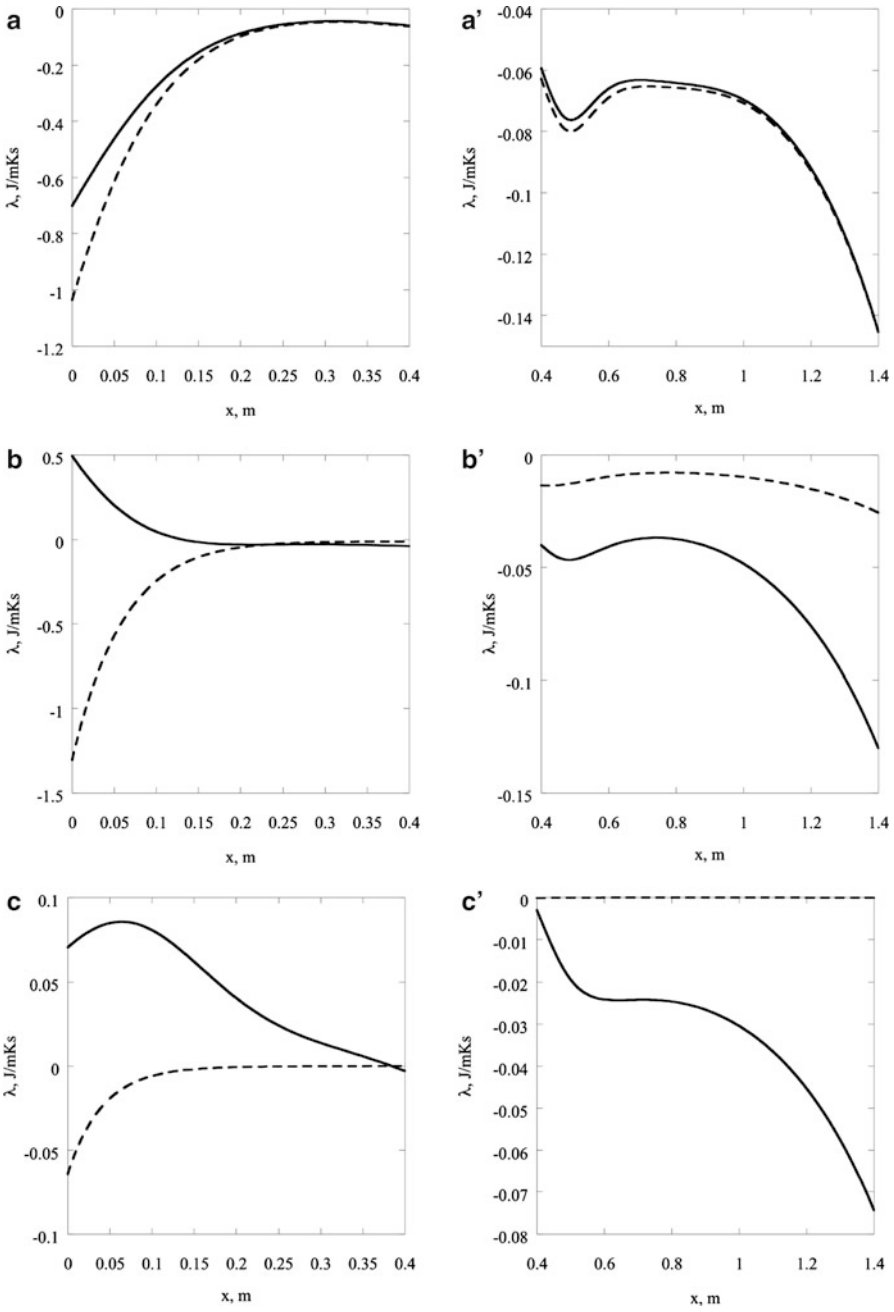

Fig. 6.6 Selected level contributions to the heat conductivity in the first (**a**, **b**, **c**) and second (**a′**, **b′**, **c′**) regions of the flow, considering non-equilibrium vibrational (*full lines*) and Boltzmann-like distributions (*dashed lines*) at T_{vib}. (a and a′) contribution of levels $i = 0$–8, (b and b′) $i = 9$–22 and (c and c′) $i = 23$–45

6.3 Nozzle Flow

As a second case study we present the transport properties in a model nozzle flow (Bruno et al. 2001), considering three different reservoir conditions:

- Nitrogen mixture, pressure $p = 1\,\text{bar}$, temperature $T = 8,000\,\text{K}$
- Nitrogen mixture, pressure $p = 100\,\text{bar}$, temperature $T = 8,000\,\text{K}$
- Oxygen mixture, pressure $p = 1\,\text{bar}$, temperature $T = 6,000\,\text{K}$

The nozzle flow calculations were performed by Colonna et al. (1999) for one metre long, parabolic nozzle having cylindrical symmetry and the nozzle profile dependence

$$r(x) = 3.5x^2 - 3.5x + 1 \tag{6.5}$$

with x in metres ($x_{\text{throat}} = 0.5\,\text{m}$). The nozzle flow equations were solved in a quasi-one-dimensional approximation, with no consideration of viscous effects. Besides the simplified modelling of the fluid dynamics, the model included a detailed description of the state-to-state vibrational kinetics (Colonna et al. 1999).

In Fig. 6.7a–c we show the behaviour of the temperatures T_{gas}, T_{vib} along the nozzle in the three cases: we see that the gas temperature suddenly drops to low values after the throat of the nozzle, due to the rapid expansion into the vacuum; but the vibrational temperature lags behind since the relaxation of the vibrational modes is much slower. During relaxation, recombination of atomic species pumps vibrational quanta on the top of the vibrational ladder. These quanta are redistributed (especially at low translational temperatures) by VV (vibration–vibration) and VT (vibration-translation) energy transfer processes, leading to the strong non-equilibrium vibrational distributions.

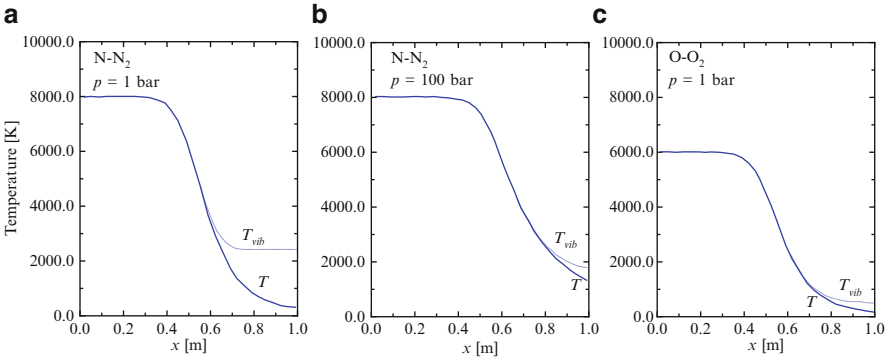

Fig. 6.7 Evolution of gas temperature and vibrational temperature along the flow. (**a**) N_2–N, p =1 bar, $T = 8,000\,\text{K}$; (**b**) N_2–N, $p = 100\,\text{bar}$, $T = 8,000\,\text{K}$; (**c**) O_2–O, $p = 1\,\text{bar}$, $T = 6,000\,\text{K}$

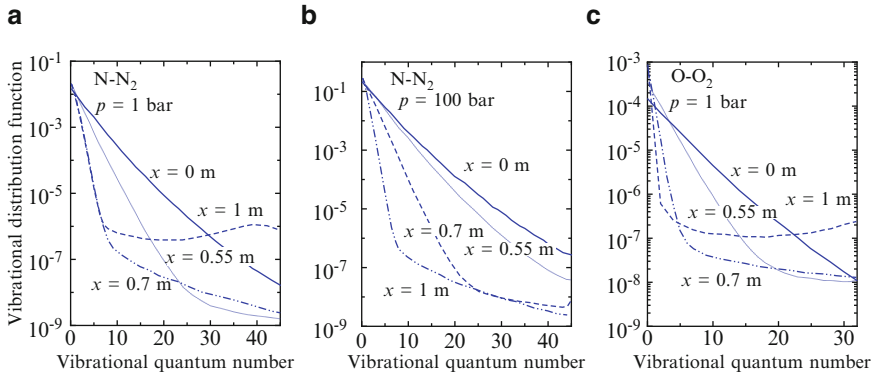

Fig. 6.8 Evolution of the VdF at different points along the flow. (**a**) N_2–N, $p = 1$ bar, $T = 8,000$ K; (**b**) N_2–N, $p = 100$ bar, $T = 8,000$ K; (**c**) O_2–O, $p = 1$ bar, $T = 6,000$ K

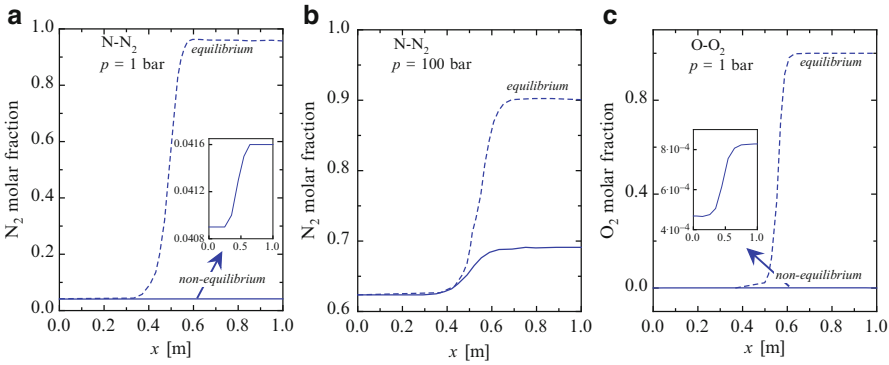

Fig. 6.9 Evolution of the system chemical composition. (**a**) N_2–N, $p = 1$ bar, T=8,000 K; (**b**) N_2–N, $p = 100$ bar, $T = 8,000$ K; (**c**) O_2–O, $p = 1$ bar, $T = 6,000$ K (*dashed line*) equilibrium, (*continuous line*) non-equilibrium

This can be seen in Fig. 6.8a–c.

In Fig. 6.9a–c we show the evolution of the system composition for the cases discussed, as compared to the composition of a system in chemical equilibrium at the same temperature. Before the expansion the gas has a high degree of dissociation. After the expansion, due to the low gas temperature, the atoms slowly recombine through the upper vibrational levels; however, the pressure after the nozzle throat ($x = 0.5$ m) is very low and the global recombination is very inefficient. In all cases we see that the chemical reactions are nearly frozen shortly after the nozzle throat. We note however that the small recombination is sufficient to create the non-equilibrium vibrational distributions reported in Fig. 6.8.

In particular we can see that the first vibrational levels of the distributions cool down as a function of the nozzle coordinate, presenting overpopulated tails as a result of the recombination process. Note also that the high pressure

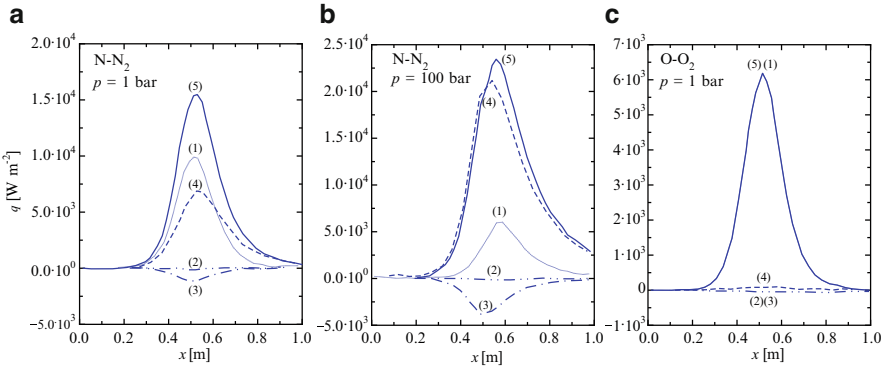

Fig. 6.10 Different contributions to the total heat flux. (1) Fourier term; (2) thermal diffusion; (3) molecular diffusion; (4) atomic diffusion; (5) total heat flux. (**a**) N_2–N, $p = 1$ bar, $T = 8,000$ K; (**b**) N_2–N, $p = 100$ bar, $T = 8,000$ K; (**c**) O_2–O, $p = 1$ bar, $T = 6,000$ K

decreases the initial concentration of atomic nitrogen in the first two cases, while this species is dominant in the oxygen case. As a consequence we should observe a major role of the diffusion of vibrational levels for case b as compared with the corresponding results for case a and case c. This point can be appreciated by looking at Fig. 6.10a–c where the different contributions to the heat flux have been reported as a function of the nozzle coordinate. In general the atom diffusion term dominates the other contributions specially for case c. On the other hand for case b the diffusion of vibrational energy is as important as the Fourier term. It should be also noted that in the three cases the results obtained by assuming a Boltzmann distribution at T_{vib} are close to the corresponding state-to-state results due to the fact that the tails of the distributions are in any case strongly underpopulated as compared with the first few vibrational levels in all cases. The differences between Boltzmann and state-to-state results reach a maximum value of 3 % for case b.

6.4 Boundary-Layer Flow

As a third example we report the heat transfer contributions in the boundary layer of a re-entering body in an $O_2(i)$/O mixture (Kustova et al. 2002; Armenise et al. 2006).

To evaluate state-to-state distributions in the boundary layer around a re-entering body, the equations for the vibrational level populations and atomic number density have been coupled with fluid dynamic equations, and some simplifications have been carried out. A stationary flow in the vicinity of the stagnation point has been considered, and boundary-layer equations

have been obtained using the Lees–Dorodnitsyn coordinate transformation (Kustova et al. 2002):

$$\xi = \int_0^x \rho_e v_e \mathrm{d}x \qquad \eta = \frac{v_e}{\sqrt{2\xi}} \int_0^y \rho \mathrm{d}y.$$

Introducing these variables, one can write the boundary-layer equations in the one-dimensional form:

$$c_i'' + f^\star Sc^\star c_i' = S_i, \quad i = 0, \ldots, 33 \tag{6.6}$$

$$\vartheta'' + f^\star Pr^\star \vartheta' = S_T \tag{6.7}$$

where Eq. (6.6) for $i = 0, \ldots, 32$ is the equation for the mass fractions of vibrationally excited O_2 molecules, $i = 33$ corresponds to atomic mass fraction c_O, Eq. (6.7) is the energy conservation equation ($\vartheta = T/T_{\mathrm{gas}}$, T_{gas} being the gas temperature at the boundary layer edge, the definition of ϑ should not be confused with symbol used in Chap. 8) and $f^\star$ is the *stream function* that, in the vicinity of the stagnation point, can be approximated by a polynomial in η (Armenise et al. 1996). The derivatives have been done with respect to the surface normal coordinate η.

In Eqs. (6.6) and (6.7) the left-hand side describe the diffusive and convection terms. The Schmidt and Prandtl numbers are supposed to be constant: $Sc^\star = 0.49$ and $Pr^\star = 0.71$. The source terms S_i and S_T describe, respectively, vibrational energy exchanges and dissociation–recombination processes in the gas phase as well as at the surface. Among vibrational energy exchanges only the single quantum ones have been retained (Armenise et al. 2000)

$$\begin{aligned} O_2(i) + O_2(k) &\rightleftharpoons O_2(i-1) + O_2(k+1) \\ O_2(i) + O_2 &\rightleftharpoons O_2(i-1) + O_2 \\ O_2(i) + O &\rightleftharpoons O_2(i-1) + O \\ O_2(i) + wall &\rightarrow O_2(i-1) + wall \end{aligned}$$

According to the ladder-climbing model (Kustova et al. 2002), the pseudo-level located just above the last bound level of a molecule has been introduced, and it has been supposed that dissociation and recombination proceed only through this level. Finally, dissociation and recombination reactions in the gas phase are treated as VV and VT energy exchange processes involving the pseudo-level. Recombination and dissociation at the catalytic surface are described by two main mechanisms (Cacciatore et al. 1999; Armenise et al. 2000):

- Eley–Rideal mechanism

$$O + O@wall \rightleftharpoons O_2(i) + wall \tag{6.8}$$

- Langmuir–Hinshelwood mechanism

$$\mathrm{O@}wall + \mathrm{O@}wall \rightleftharpoons \mathrm{O}_2(i) + wall \tag{6.9}$$

where O@*wall* is an atom adsorbed at the surface.

Another possible mechanism

$$\mathrm{O}_2(i) + wall \rightleftharpoons \mathrm{O} + \mathrm{O} \tag{6.10}$$

has also been taken into account.

To solve the problem we need appropriate boundary conditions for Eqs. (6.6) and (6.7). At the external edge of the boundary layer, the gas temperature is fixed as a parameter T_{gas}, and the level populations are supposed to follow the thermal equilibrium Boltzmann distribution with the gas temperature T_{gas}. On the surface the gas temperature is also fixed at $T = T_w$. In the present case study $T_{\mathrm{gas}} = 7,000\,\mathrm{K}$, $T_w = 1,000\,\mathrm{K}$ and $p = 0.01\,\mathrm{bar}$.

The corresponding equation for c_i and c_{O} at the wall read (Armenise et al. 2000)

$$\left.\frac{\partial c_i}{\partial \eta}\right|_w = -\frac{\gamma_i}{\mathcal{D}}\sqrt{\frac{k_{\mathrm{B}}T}{2\pi m}}c_{\mathrm{O}} + \gamma_{\mathrm{diss}}c_i - \gamma_{\mathrm{deact}}c_i + \gamma_{\mathrm{deact}}c_{i+1} \quad i = 0,\ldots,32 \tag{6.11}$$

$$\left.\frac{\partial c_{\mathrm{O}}}{\partial \eta}\right|_w = \frac{\sum_i \gamma_i}{\mathcal{D}}\sqrt{\frac{k_{\mathrm{B}}T}{2\pi m}}c_{\mathrm{O}} - \sum_i \gamma_{\mathrm{diss}}c_i \tag{6.12}$$

where recombination coefficient γ_i represents the ratio of the flux of atoms recombining on the surface to the flux of atoms impinging the surface; the diffusion coefficient $\mathcal{D}$ is assumed to be independent of the vibrational level number. Note that in the right-hand sides of Eqs. (6.11) and (6.12) the first term is from recombination at the surface, the second one is due to heterogeneous dissociation, and the third and fourth ones in Eq. (6.11) are caused by deactivation at the wall. Details for the homogeneous and heterogeneous rates are discussed in Kustova et al. (2002).

Equations (6.6) and (6.7) for c_i, c_{O}, ϑ with boundary conditions in Eqs. (6.11) and (6.12) have been solved numerically using a finite difference method (Armenise et al. 2000). The variables c_i, c_{O}, ϑ as well as their gradients have been found along the coordinate η. Then, this solution has been inserted into the kinetic transport theory algorithm (Kustova and Nagnibeda 1998) to compute the diffusion and heat conductivity coefficients and the total heat flux.

First, let us consider the reduced O_2 level populations n_i/n versus vibrational quantum number i for different values of coordinate η ($\eta = 0$ at the surface, $\eta = 8$ at the external edge of the boundary layer) (see Fig. 6.11). The selective pumping of high-lying vibrational levels by heterogeneous recombination is well evident near the surface ($\eta = 0, 0.1, 0.2$), the

discontinuity of level population at $\eta = 0$ being due to the molecular dynamic data used in the model. The overpopulation of vibrational levels is reflected on the different components of heat flux reported in Fig. 6.12a.

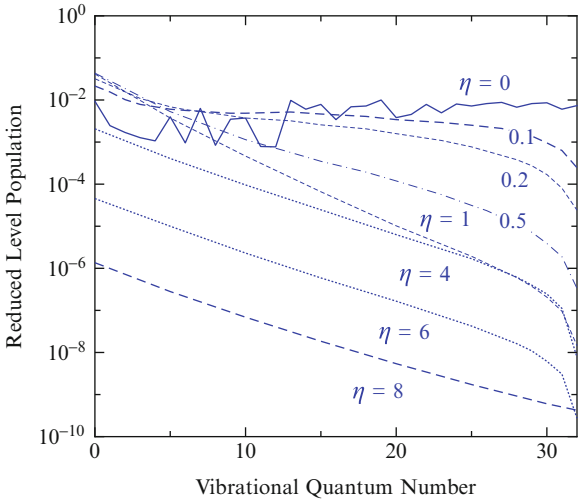

Fig. 6.11 Reduced level populations n_i/n as functions of the vibrational quantum number at different η

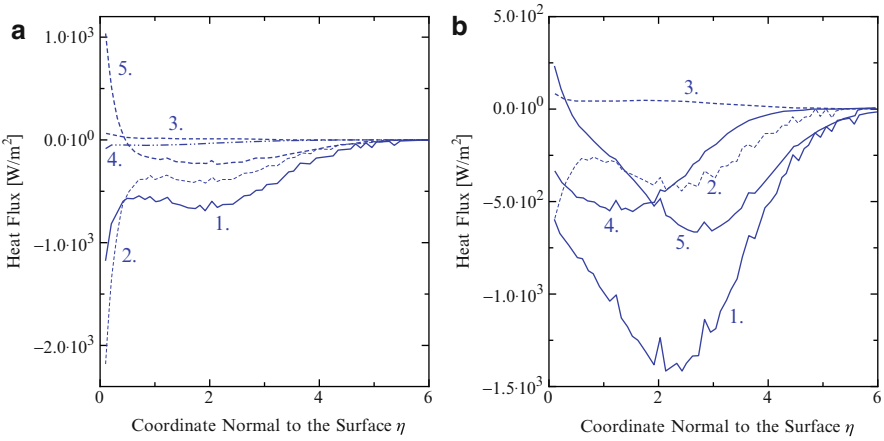

Fig. 6.12 Contribution of various processes to the heat flux: including (**a**) or neglecting (**b**) processes (6.9) and (6.10). Curves 1 total heat flux; 2 Fourier flux; 3 flux caused by thermal diffusion; 4 flux caused by mass diffusion of atoms; 5 flux caused by diffusion of vibrational energy

Again, among the diffusion processes, one can distinguish thermal diffusion, mass diffusion of chemical species and diffusion of vibrational energy by excited molecules. Inspection of Fig. 6.12a shows that the heat flux is scarcely affected by thermal diffusion (its maximum contribution does not exceed 6 % in the vicinity of the surface and then decreases to 3 %). The influence of mass diffusion of atoms is also small, and the main role in the heat transfer belongs to heat conductivity (Fourier term) and diffusion of vibrational energy. Near the wall a competition of these two processes is observed. The diffusion of vibrational energy becomes more important when the influence of processes (6.9) and (6.10) are neglected in the model as it can be appreciated in Fig. 6.12b.

Similar results are found for non-catalytic surfaces when the plateaux are formed by the gas-phase recombination even though in this case, depending on the initial conditions, the concentration of molecules is rather small to affect the heat flux.

References

Armenise I, Capitelli M, Colonna G, Gorse C (1996) Nonequilibrium vibrational kinetics in the boundary layer of re-entering bodies. J Thermophys Heat Transf 10(3):397–405

Armenise I, Capitelli M, Gorse C, Cacciatore M, Rutigliano M (2000) Non equilibrium vibrational kinetics of a O_2/O mixtures hitting a catalytic surface. J Spacecr Rockets 37(3):318–323

Armenise I, Barbato M, Capitelli M, Kustova E (2006) State to state catalytic models, kinetics and transport in hypersonic boundary layers. J Thermophys Heat Transf 20(3):465–476

Brun R (2009) Introduction to Reactive Gas Dynamics. Oxford University Press, Oxford

Bruno D, Capitelli M, Longo S (1998) DSMC modelling of vibrational and chemical kinetics for a reacting gas mixture. Chem Phys Lett 289:141

Bruno D, Capitelli M, Kustova E, Nagnibeda E (1999) Non-equilibrium vibrational distributions and transport coefficients of $N_2(v)$–N mixtures. Chem Phys Lett 308:463–472

Bruno D, Capitelli M, Cervellera V, Longo S (2001) Calculation of transport coefficients with vibrational nonequilibrium. J Thermophys Heat Transf 15(1):70–75

Cacciatore M, Rutigliano M, Billing GD (1999) Eley-Rideal and Langmuir-Hinshelwood recombination coefficients for oxygen on silica surfaces. J Thermophys Heat Transf 13(2):195–203

Capitelli M (ed) (1986) Non-equilibrium vibrational kinetics. In: Topics in current physics, vol 36. Springer, Berlin

Capitelli M, Molinari E (1980) Kinetics of dissociation processes in plasmas in the low and intermediate pressure range. Top Curr Chem 90:59–109

Colonna G, Tuttafesta M, Capitelli M, Giordano D (1999) Non-Arrhenius NO formation rate in one-dimensional nozzle airflow. J Thermophys Heat Transf 13:372

Gorbachev YE, Gordillo-Vàzquez FJ, Kunc JA (1997) Diameters of rotationally and vibrationally excited diatomic molecules. Physica A: Stat Mech Appl 247(1–4):108–120

Hirschfelder JO, Curtiss CF, Bird RB (1966) Molecular theory of gases and liquids. Wiley, New York

Kustova E, Nagnibeda E, Armenise I, Capitelli M (2002) Nonequilibrium kinetics and heat transfer in O_2/O mixtures near catalytic surfaces. J Thermophys Heat Transf 16(2):238–244

Kustova EV, Nagnibeda EA (1998) Transport properties of a reacting gas mixture with strong vibrational and chemical nonequilibrium. Chem Phys 233(1):57–75

Nagnibeda E, Kustova E (2009) Non-equilibrium reacting gas flows: kinetic theory of transport and relaxation processes. Springer series heat and mass transfer. Springer, Berlin

Chapter 7
Electronically Excited States and Transport Properties of Thermal Plasmas

In this chapter we try to elucidate the role of electronically excited states (EES) in affecting the transport properties of high-temperature high-pressure thermal plasmas. This topic started many years ago when one of us showed the dependence of transport coefficients on the *cutoff* criterion used in truncating the electronic partition function of atomic species with large consequences in the equilibrium composition and thermodynamic properties to be inserted in the transport equations (Capitelli 1972). Soon after it was recognized that electronically excited states affect the transport properties not only acting on the plasma composition but also through their transport cross sections, dramatically depending on the principal quantum number. These cross sections were then inserted in the Butler–Brokaw equation for calculating the role of excited states in the transport of internal and reactive contribution to the thermal conductivity (Capitelli 1974). In this case an *unusual* effect was discovered, i.e. the role of excited states, while very important in affecting the internal and reactive contributions when the excited states were considered as inert species in the relevant equation, tends to disappear when a more complex model was inserted in the Butler–Brokaw equation. These ideas were then extended to the calculation of translational thermal conductivity and of viscosity of hydrogen thermal plasma once obtained a set of viscosity-type collision integrals for the relevant interactions involving excited states (Capitelli and Lamanna 1974). Recently a more complete set of transport cross sections of electronically excited states (see Chap. 5) of atomic hydrogen has been used in combination with different transport equation approaches to better understand the EES role (Capitelli et al. 2002, 2003, 2004).

These ideas are being also extended to nitrogen and oxygen plasmas. In this case a large effort has been devoted to the excitation-transfer and charge-transfer cross sections of *low-lying* and *high-lying* electronically excited states (Capitelli 1975; Eletskii et al. 2004; Kosarim et al. 2006) (see Chap. 5), which allows us to estimate the role of excited states on these more complicated systems making use of the lessons learned for hydrogen plasmas.

M. Capitelli et al., *Fundamental Aspects of Plasma Chemical Physics*,
Springer Series on Atomic, Optical, and Plasma Physics 74,
DOI 10.1007/978-1-4419-8172-1_7, © Springer Science+Business Media, LLC 2013

These points will be widely exposed in this chapter which is subdivided into five sections, the first three dedicated to atomic hydrogen plasmas, the other ones to air plasmas. In particular Sect. 7.1 is dedicated to the dependence of transport coefficients on electronically excited states, whose concentration is taken in a parametric form. Section 7.2 focusses on the influence of electronically excited states on the internal and reactive contributions, while Section 7.3 investigates the role of adopted cutoff criterion.

Finally Sects. 7.4 and 7.5 introduce new models to take into account excited states in the transport equations trying to avoid the state-to-state approach. Numerical examples for complex plasma systems are discussed, while Section 7.3 investigates the role of adopted cutoff criterion.

7.1 EES and Transport Properties of Hydrogen Plasma: A Parametric Study

In this section we investigate the role of electronically excited states in affecting the transport properties of H_2 plasmas in the temperature range 10,000–30,000 K and in the pressure range 1–1,000 atm. The main species are H(n) ($n \leq 12$), $H^+$and electrons, being H_2 and H_2^+ species important only in a restricted temperature range at p=1000 atm. Saha and Boltzmann laws have been used for calculating the equilibrium plasma composition and the concentration of excited states of atomic hydrogen with different principal quantum number n (see Capitelli et al. 2002, 2003, 2004). In general we have considered up to n=12 electronically excited states; at high pressure we have reduced the number of excited states to seven to partially take into account the decrease of the number of electronically excited states with increasing the pressure as discussed in Capitelli et al. (2002, 2003, 2004).

Transport coefficients have been calculated by using the third approximation of the Chapman–Enskog method for the electron component and the first non-vanishing approximation for heavy components (i.e. the first approximation for viscosity and the second one for the contribution of the heavy components to the thermal conductivity) (Devoto 1968), while an extension of Butler–Brokaw equation is used for calculating the internal and reactive contributions to the thermal conductivity (Butler and Brokaw 1957; Brokaw 1960; Hirschfelder et al. 1966).

7.1.1 Thermal Conductivity

The total thermal conductivity λ_{tot} of an LTE plasma has been calculated by adding the different contributions, i.e.

$$\lambda_{tot} = \lambda_h + \lambda_e + \lambda_{int} + \lambda_r \tag{7.1}$$

where the members on the right-hand side of the equation represent in the order the translational contribution of heavy particles, the translational contribution of electrons, the contribution of internal degrees of freedom and the reactive thermal conductivity.

The first term can be expressed in the second approximation of the Chapman–Enskog method according to the following equation (Hirschfelder et al. 1966)

$$\lambda_h = 4 \begin{vmatrix} L_{11} & \dots & L_{1\nu} & x_1 \\ \vdots & & \vdots & \vdots \\ L_{\nu 1} & \dots & L_{\nu\nu} & x_\nu \\ x_1 & \dots & x_\nu & 0 \end{vmatrix} \Bigg/ \begin{vmatrix} L_{11} & \dots & L_{1\nu} \\ \vdots & & \vdots \\ L_{\nu 1} & \dots & L_{\nu\nu} \end{vmatrix} \tag{7.2}$$

$$\begin{aligned} L_{ii} &= -\frac{4x_i^2}{\lambda_{ii}} - \sum_{j \neq i} \frac{2x_i x_j [\frac{15}{2} m_i^2 + \frac{25}{4} m_j^2 - 3m_j^2 B_{ij}^\star + 4m_i m_j A_{ij}^\star]}{(m_i + m_j)^2 A_{ij}^\star \lambda_{ij}} \\ L_{ij} &= \frac{2x_i x_j m_i m_j}{(m_i + m_j)^2 A_{ij}^\star \lambda_{ij}} \left[\tfrac{55}{4} - 3B_{ij}^\star - 4A_{ij}^\star\right] \qquad i \neq j \end{aligned} \tag{7.3}$$

where x_i and m_i are, respectively, molar fraction and molar mass of the ith species, $A_{ij}^\star$ and $B_{ij}^\star$ are given in Eq. (3.15) and

$$\lambda_{\mathrm{ij}} = 0.0832 \frac{\sqrt{T(m_i + m_j)/(2m_i m_j)}}{\sigma_{ij}^2 \Omega_{ij}^{\star(2,2)}} \qquad [\mathrm{W\ m^{-1} K^{-1}}] \tag{7.4}$$

The order of the determinant is controlled by the number of chemical species (ν) considered in the calculation. In the present case we consider up to 15 species (H_2, H^+, e, H(n)).

Figure 7.1a reports the ratio λ_h^a/λ_h^u i.e. the ratio between the translational thermal conductivity values calculated with the *abnormal* (a) cross sections (λ_h^a) and the corresponding results calculated with the *usual* (u) cross sections (λ_h^u) as a function of temperature for different pressures.

The *abnormal* cross sections include the dependence of transport cross section on the quantum state of interacting atomic species, i.e. on the principal quantum number, while in the *usual* case the ground-state transport cross section values are used also for describing the interaction involving excited species (see Chap. 5).

The small effect observed at p=1 atm is due to a compensation effect between diagonal and off-diagonal terms in the whole representation of the translational thermal conductivity of the heavy components [see Eq. (7.2)], this compensation disappearing when considering only the diagonal terms in Eq. (7.2). In this case in fact the relative error reaches a value of 160 % when comparing the translational thermal conductivity calculated with the two sets of collision integrals. This compensation disappears at high pressure as a result of the shifting of the ionization equilibrium towards higher tempera-

tures where excited states are more easily populated. The results of Fig. 7.1a have been obtained by considering in all cases 12 excited states. However as already pointed out the number of excited states to be considered in the partition function should decrease with increasing the pressure. As in Capitelli et al. (2002, 2003, 2004), applying a very simple *cutoff* criterion, i.e. the *confined atom approximation*, we have estimated to n=7 the maximum principal quantum number to be considered at 100 atm. As expected the differences in λ_h^a/λ_h^u strongly decrease when reducing the total number of excited states (see the dotted line in Fig. 7.1a).

Let us now consider the effect of excited states on the translational thermal conductivity of free electrons. In this case we have used the third approximation of the Chapman–Enskog method. The relevant equation can be written as (Devoto 1967a; Capitelli et al. 2004)

$$\lambda_e = \tfrac{75}{8} n_e^2 k_B \left(\frac{2\pi k_B T_e}{m_e}\right)^{1/2} \frac{q^{22}}{q^{11}q^{22} - (q^{12})^2} \tag{7.5}$$

where

$$q^{11} = 8\sqrt{2} n_e^2 \overline{Q}_{ee}^{(2,2)\star} + 8 \sum_{j=1}^{\nu-1} n_j n_e \left[\tfrac{25}{4} \overline{Q}_{ej}^{(1,1)\star} - 15\overline{Q}_{ej}^{(1,2)\star} + 12\overline{Q}_{ej}^{(1,3)\star}\right]$$

$$q^{12} = 8\sqrt{2} n_e^2 \left(\tfrac{7}{4} \overline{Q}_{ee}^{(2,2)\star} - 2\overline{Q}_{ee}^{(2,3)\star}\right) + 8 \sum_{j=1}^{\nu-1} n_j n_e \left[\tfrac{175}{16} \overline{Q}_{ej}^{(1,1)\star} - \tfrac{315}{8} \overline{Q}_{ej}^{(1,2)\star} + 57\overline{Q}_{ej}^{(1,3)\star} - 30\overline{Q}_{ej}^{(1,4)\star}\right]$$

$$q^{22} = 8\sqrt{2} n_e^2 \left[\tfrac{77}{16} \overline{Q}_{ee}^{(2,2)\star} - 7\overline{Q}_{ee}^{(2,3)\star} + 5\overline{Q}_{ee}^{(2,4)\star}\right] + 8 \sum_{j=1}^{\nu-1} n_j n_e \left[\tfrac{1225}{64} \overline{Q}_{ej}^{(1,1)\star} - \tfrac{735}{8} \overline{Q}_{ej}^{(1,2)\star} + \tfrac{399}{2} \overline{Q}_{ej}^{(1,3)\star} - 210\overline{Q}_{ej}^{(1,4)\star} + 90\overline{Q}_{ej}^{(1,5)\star}\right]$$

where m_e, T_e, and n_e represent the electron mass, the temperature and the density of electrons respectively, and $\overline{Q}_{ij}^{(\ell,s)\star} = \pi\sigma^2 \Omega_{ij}^{(\ell,s)\star}$.

In this case the presence of excited states affects only the interaction of electrons with H(n). Figure 7.1b reports the ratio λ_e^a/λ_e^u calculated with the two sets of collision integrals as a function of temperature at different pressures, showing a minor effect of EES due to the weak dependence of e-H(n) collision integrals on the principal quantum number.

Let us now examine the reactive thermal conductivity. The reactive thermal conductivity, which describes the transport of chemical enthalpy through temperature gradients, can be calculated by the general theory of the diffusion fluxes (Hirschfelder et al. 1966) assuming a compact form under the hypothesis of local chemical equilibrium along the temperature gradient. For a system of μ independent chemical (dissociation, ionization) reactions and ν chemical species, the Brokaw equation assumes the form (Brokaw 1960; Hirschfelder et al. 1966).

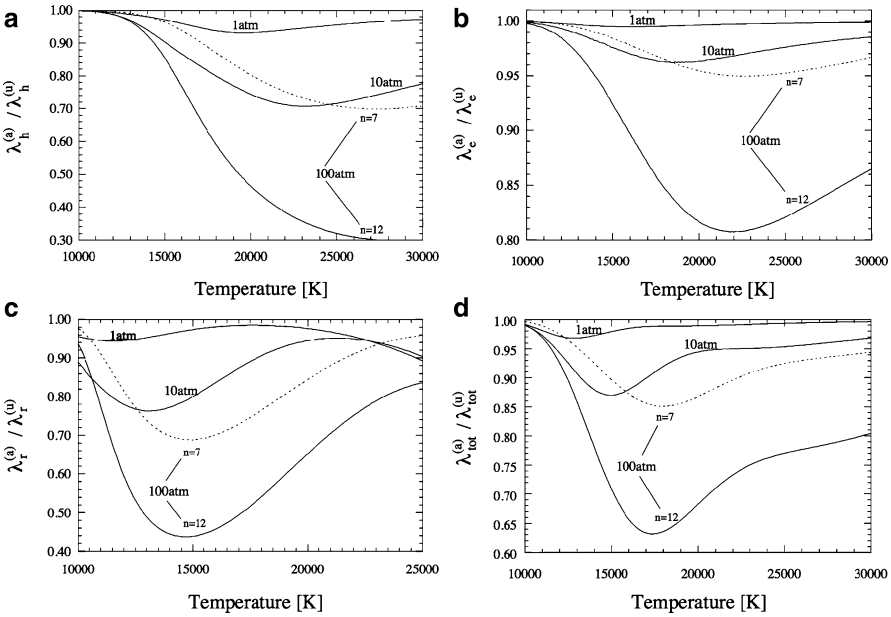

Fig. 7.1 Ratio between transport coefficients calculated by using *abnormal (a)* and *usual* (u) collision integrals, as a function of temperature, at different pressures and for different number of atomic levels. (**a**) Translational thermal conductivity of heavy particles; (**b**) translational thermal conductivity of electrons; (**c**) reactive thermal conductivity; (**d**) total thermal conductivity

$$\lambda_r = -\frac{1}{k_B T^2} \begin{vmatrix} A_{11} & \dots & A_{1\mu} & \Delta H_1 \\ \vdots & & \vdots & \vdots \\ A_{\mu 1} & \dots & A_{\mu\mu} & \Delta H_\mu \\ \Delta H_1 & \dots & \Delta H_\mu & 0 \end{vmatrix} \Bigg/ \begin{vmatrix} A_{11} & \dots & A_{1\mu} \\ \vdots & & \vdots \\ A_{\mu 1} & \dots & A_{\mu\mu} \end{vmatrix} \tag{7.6}$$

where:

$$A_{ij} = \sum_{k=1}^{\nu-1} \sum_{l=k+1}^{\nu} \frac{k_B T}{\mathcal{D}_k^l p} x_k x_l \left(\frac{a_{ik}}{x_k} - \frac{a_{il}}{x_l} \right) \left(\frac{a_{jk}}{x_k} - \frac{a_{jl}}{x_l} \right) \tag{7.7}$$

ΔH_i represents the variation of enthalpy associated with ith reaction, p is the total pressure, T the temperature in Kelvin, $\mathcal{D}_i^j$ is the binary diffusion coefficient of the ij pair, x_i is the molar fraction of ith component in the mixture and a_{ij} is the stoichiometric coefficient of jth species in the ith reaction.

The first 12 electronic states have been included in the ionization scheme as well as the dissociation reaction (i.e. we consider $\mu = 13$ independent chemical (1 dissociation, 12 ionizations) reactions and $\nu = 15$ independent chemical species), i.e.

$$\begin{aligned} \mathrm{H(1)} &\leftrightarrows \mathrm{H}^+ + e \\ \mathrm{H(2)} &\leftrightarrows \mathrm{H}^+ + e \\ &\vdots \\ \mathrm{H(n)} &\leftrightarrows \mathrm{H}^+ + e \end{aligned}$$

Again we compare the *abnormal* and *usual* results. Before the analysis we want to point out that Eq. (7.6) represents indeed the transport of *reactive* and *internal* contributions. The internal term in fact can be considered in this approach as the result of excitation reactions

$$\begin{aligned} \mathrm{H(1)} &\leftrightarrows \mathrm{H(2)} \\ \mathrm{H(2)} &\leftrightarrows \mathrm{H(3)} \\ &\vdots \\ \mathrm{H(11)} &\leftrightarrows \mathrm{H(12)} \end{aligned}$$

which are not independent for the state-to-state ionization reactions (see also the end of Sect. 7.1).

We start our analysis by considering in Eq. (7.6) only the diagonal terms, an approximation which is known to work very well for reactive neutral gases, when transport cross sections of different species are similar. In this case the reactive thermal conductivity for an atmospheric hydrogen plasma strongly depends on the choice of cross sections. This behaviour disappears at p=1 atm when we calculate Eq. (7.6) inserting also the off-diagonal terms. In this case a sort of compensation between diagonal and off-diagonal terms arises having as a consequence the practical coincidence of the two cases, confirming the results of Capitelli (1974).

This kind of compensation disappears with increasing pressure (see Fig. 7.1c). For the higher pressure examined in the present study, using the complete Eq. (7.6) and the same number of electronically excited states (again up to n = 12), a difference up to factor 2 in the results can be appreciated. At high pressure this difference decreases if seven excited states (n_{max}=7) are considered.

Total thermal conductivity calculated according to the two sets of collision integrals is reported in Fig. 7.1d as the ratio $\lambda^a_{tot}/\lambda^u_{tot}$ as a function of temperature for different pressures. The relative error in this case assumes the values of 3 %, 15 % and 60 % for p=1, 10, 100 atm, respectively, the last error becomes 18 % when inserting seven excited states.

7.1.2 Viscosity

The influence of electronically excited states on the viscosity has been obtained by using the first approximation of the Chapman–Enskog method which assumes a form very similar to Eq. (7.2) (Hirschfelder et al. 1966).

$$\eta = -\begin{vmatrix} H_{11} & \dots & H_{1\nu} & x_1 \\ \vdots & & \vdots & \vdots \\ H_{\nu 1} & \dots & H_{\nu\nu} & x_\nu \\ x_1 & \dots & x_\nu & 0 \end{vmatrix} \Bigg/ \begin{vmatrix} H_{11} & \dots & H_{1\nu} \\ \vdots & & \vdots \\ H_{\nu 1} & \dots & H_{\nu\nu} \end{vmatrix} \tag{7.8}$$

The elements of the determinant assume the following form (Hirschfelder et al. 1966):

$$\begin{aligned} H_{ii} &= \frac{x_i^2}{\eta_{ii}} + \sum_{j=1, j\neq i}^{\nu} \frac{2x_i x_j}{\eta_{ij}} \frac{m_i m_j}{(m_i + m_j)^2} \left(\frac{5}{3A_{ij}^\star} + \frac{m_j}{m_i} \right) \\ H_{ij} &= -\frac{2x_i x_j}{\eta_{ij}} \frac{m_i m_j}{(m_i + m_j)^2} \left(\frac{5}{3A_{ij}^\star} - 1 \right) \qquad i \neq j \end{aligned} \tag{7.9}$$

$$\eta_{ij} = 2.6693 \times 10^{-6} \frac{\sqrt{2(m_i m_j)T/(m_i + m_j)}}{\sigma_{ij}^2 \Omega_{ij}^{(2,2)\star}} \qquad [\text{Kg m}^{-1}\text{s}^{-1}] \tag{7.10}$$

The results are in line with those discussed for the heavy-particle translational contribution to the total thermal conductivity. In particular Fig. 7.2 reports the ratio η^a/η^u as a function of temperature for different pressures. As in the case of translational thermal conductivity the viscosity values

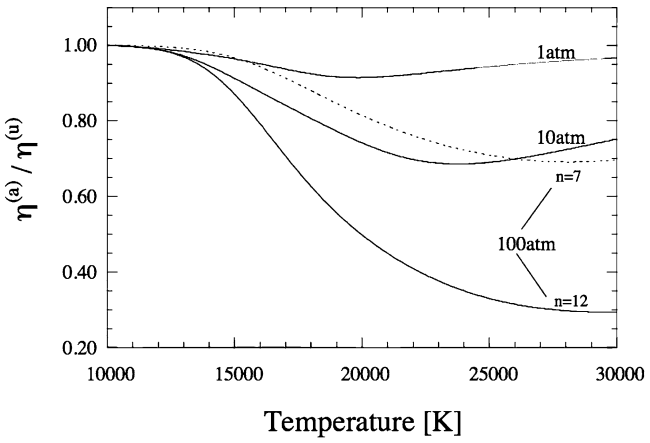

Fig. 7.2 Ratio between the viscosity values calculated by using *abnormal (a)* and *usual (u)* collision integrals, as a function of temperature, at different pressures and for different number of atomic levels

calculated with the *abnormal* cross sections are less than the corresponding values calculated with the *usual* cross sections. The maximum relative error in this case assumes the values of 9 %, 48 % and 250 % for p=1, 10, and 100 atm, respectively, the last error becoming 18 % when inserting seven excited states.

Again we observe larger deviations when the off-diagonal terms in the viscosity equation are neglected in the calculation. As an example at 1 atm the maximum error increases from 9 % to 100 % (Capitelli et al. 2004).

7.1.3 Electrical Conductivity

The electrical conductivity (Fig. 7.3) has been calculated by using the third approximation of the Chapman–Enskog method which can be written as (Devoto 1967a)

$$\sigma_e = \tfrac{3}{2} e^2 n_e^2 \frac{(2\pi/k_B m_e T)^{\frac{1}{2}}}{|q|} \begin{vmatrix} q^{11} & q^{12} \\ q^{21} & q^{22} \end{vmatrix} \tag{7.11}$$

where

$$|q| = \begin{vmatrix} q^{00} & q^{01} & q^{02} \\ q^{10} & q^{11} & q^{12} \\ q^{20} & q^{21} & q^{22} \end{vmatrix} \tag{7.12}$$

and

$$q^{00} = 8 n_e \sum_{j=1}^{\nu-1} n_j \overline{Q}_{ej}^{(1,1)\star}$$

$$q^{01} = q^{10} = 8 n_e \sum_{j=1}^{\nu-1} n_j \left[\tfrac{5}{2} \overline{Q}_{ej}^{(1,1)\star} - 3 \overline{Q}_{ej}^{(1,2)\star} \right]$$

$$q^{02} = q^{20} = 8 n_e \sum_{j=1}^{\nu-1} n_j \left[\tfrac{35}{8} \overline{Q}_{ej}^{(1,1)\star} - \tfrac{21}{2} \overline{Q}_{ej}^{(1,2)\star} + 6 \overline{Q}_{ej}^{(1,3)\star} \right]$$

It should be noted that Eq. (7.11) completely neglects the ion contribution to the electrical conductivity, which indeed are accounted for in the general theory reported in this book.

The presence of electronically excited states can affect σ_e through the collisions e-H(n). The trend of the electrical conductivity follows that one described for the contribution of electrons to the thermal conductivity as can be appreciated in Fig. 7.3 where we have reported σ_e^a/σ_e^u. The relative error calculated as before increases from 1 % at 1 atm to 45 % at 100 atm. The last error reduces to 10 % when only seven states are considered. The results at 1 atm are similar to those reported by Ignjatović and Mihajlov (1997), being however different at 10 atm. This is probably due to the simplified equation

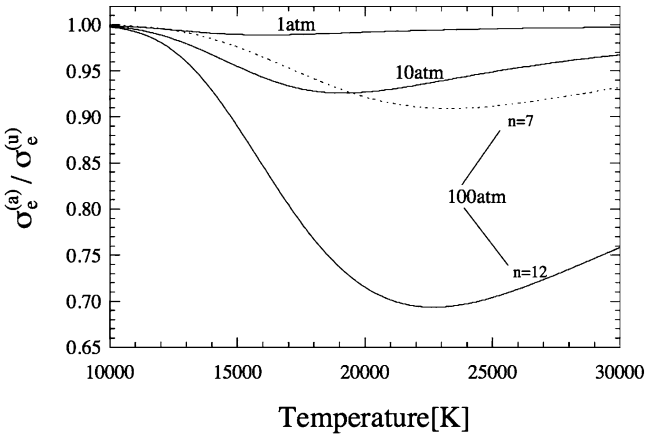

Fig. 7.3 Ratio between the electrical conductivity values calculated by using *abnormal (a)* and *usual (u)* collision integrals, as a function of temperature, at different pressures and for different number of atomic levels

used in Ignjatović and Mihajlov (1997) for the calculation of the electrical conductivity.

The accuracy of the presented results depends on the adopted set of collision integrals for excited states as well as on the number of excited states existing in the plasma.

These points need some comments. Let us consider first the most important interactions which affect our results. In the case of heavy-particle components (translational thermal conductivity and viscosity) the viscosity-type collision integrals for the interaction H(n)–H^+ have a large role in affecting the results. These collision integrals have been obtained by extrapolating to n >5 the collision integrals calculated in Capitelli and Lamanna (1974) by adiabatically averaging the contribution coming from the different potential curves arising in a particular collision. In turn the potential curves of H_2^+ are exact being the hydrogen molecular ion one of the few examples treated exactly by quantum mechanics. The problem in this case is the extrapolation of the results to higher n. A different way to calculate the viscosity-type collision integrals should be by using the polarizability model taking into account the dependence of the polarizability on the principal quantum number. The corresponding viscosity-type collision integrals are much higher than those based on the H_2^+ potential energy curves, having large effects on the plasma viscosity, as reported in Capitelli et al. (2004).

The contribution of electrons to the thermal and electrical conductivity depends on the collision integrals for the interaction *e*-H(n). The quantum mechanical calculation of the momentum transfer cross sections performed by Ignjatović and Mihajlov 1997 seems adequate to the present aim.

In this case however we have neglected in the transport cross sections the effects due to inelastic and reactive collisions which strongly increase with n.

In the reported cases the translational thermal conductivity of heavy particles and the viscosity have been derived in the first non-vanishing approximation of the Chapman–Enskog method, while for the translational thermal conductivity of electrons and the electrical conductivity the third approximation has been used. Higher approximations, also accounting for the presence of excited states, have been extensively discussed in Singh et al. (2008, 2010) and Sharma et al. (2011) and reported in Chap. 8.

7.2 The Transport of Internal and Reactive Contributions: A Decoupled Scheme

The starting point of this approach (Bruno et al. 2007a,b) is the convective heat flux describing the transport of enthalpy due to diffusion. It is defined by:

$$\boldsymbol{q} = \sum_i n_i H_i \boldsymbol{V}_i = -(\lambda_r + \lambda_{int}) \cdot \nabla T \tag{7.13}$$

where H_i is the enthalpy carried by i-type particles, $\boldsymbol{V}_i$ the diffusion velocity and λ_r, λ_{int} are the reactive and internal thermal conductivity, respectively. It is further assumed that (Meador, Jr. and Staton 1965):

- Thermal diffusion is negligible.
- Total pressure is uniform.
- There are not non-electromagnetic forces acting on the plasma.
- The plasma is quasi neutral.
- The plasma is in thermal and chemical equilibrium.
- The total current density equals zero (i.e. the ambipolar diffusion regime has been established).

Under these assumptions, the diffusion velocities read

$$\boldsymbol{V}_i = -\sum_j D_i^j \boldsymbol{d}_j \tag{7.14}$$

where

$$\boldsymbol{d}_j = \nabla\left(\frac{n_i}{n}\right) - \frac{n_i}{n}\frac{e_i \boldsymbol{E}'}{k_\mathrm{B} T} \tag{7.15}$$

and $\boldsymbol{E}'$ is the ambipolar electric field. In particular, in Eq. (7.14) the sum over atomic levels read

$$\sum_{\mathrm{n}=1}^{\mathrm{n}_{max}} D_i^{\mathrm{n}} \boldsymbol{d}_H + \sum_{\mathrm{n}=1}^{\mathrm{n}_{max}} \frac{n_{\mathrm{n}}}{n} D_i^{\mathrm{n}} \frac{E_{\mathrm{n}} - E_H}{k_\mathrm{B} T^2} \nabla T. \tag{7.16}$$

The gradients of the species concentrations are then expressed in terms of the equilibrium constant and the ambipolar electric field in terms of the gradient of the temperature (Meador, Jr. and Staton 1965). Now, the second term on the RHS of Eq. (7.16) does not vanish also in the case that no chemical reaction occurs and it is therefore recognized as the term producing the internal thermal conductivity.

In Sect. 7.1 the internal and reactive contributions were mixed together and the overall effect was barely noticeable, especially at low pressure. We wish to show that, indeed, the effect of EES is by no means negligible and that it produces in the two coefficients modifications of opposite signs that compensate in the thermal equilibrium case.

The plasma composition is obtained under a global equilibrium assumption of the H(n), H^+ and e system:

1. The concentration of the species present (H, H^+, e) is obtained by solving the Saha equation.
2. The concentration of EES satisfies a Boltzmann distribution.
3. H_2 and H_2^+ species are neglected.

The maximum number of allowed EES is determined by the confined atom (CA) model:

$$a_0 \mathrm{n}_{max}^2 \leq n^{-1/3} \tag{7.17}$$

where a_0 is the Bohr radius, n_{max} the maximum allowed principal quantum number and n the particle density. The number of EES actually used in calculations, however, never exceeds 12. This restriction only affects calculations at p=1 atm where n_{max}=12 is used throughout. Calculations are carried out to the second non-vanishing approximation in Sonine polynomials (see Chap. 1).

In order to understand how the EES cross sections affect these coefficients rewrite the convective heat flux, Eq. (7.13),

$$\begin{aligned} \boldsymbol{q}_{r+int} = {} & n_e \tfrac{5}{2} k_\mathrm{B} T \boldsymbol{V}_e + n_e \left[\tfrac{5}{2} k_\mathrm{B} T + 1\right] \boldsymbol{V}_e \\ & + \sum_\mathrm{n} n_\mathrm{n} \left[\tfrac{5}{2} k_\mathrm{B} T + E_\mathrm{n}\right] \boldsymbol{V}_\mathrm{n} \end{aligned} \tag{7.18}$$

$$\begin{aligned} \sum_\mathrm{n} n_\mathrm{n} \left[\tfrac{5}{2} k_\mathrm{B} T + E_\mathrm{n}\right] \boldsymbol{V}_\mathrm{n} = {} & \left[\tfrac{5}{2} k_\mathrm{B} T + E_\mathrm{H}\right] \cdot n_\mathrm{H} \boldsymbol{V}_\mathrm{H} \\ & + \sum_\mathrm{n} n_\mathrm{n} \left[E_\mathrm{n} - E_\mathrm{H}\right] \boldsymbol{V}_\mathrm{n} \end{aligned} \tag{7.19}$$

The diffusion velocities are made up of two contributions

$$\boldsymbol{V}_j = \underbrace{-D_j^e \boldsymbol{d}_e - D_j^{\mathrm{H}^+} \boldsymbol{d}_{\mathrm{H}^+} - D_j^\mathrm{H} \boldsymbol{d}_\mathrm{H}}_{\boldsymbol{z}_j} \underbrace{- \sum_{\mathrm{n}=1}^{\mathrm{n}_{max}} \frac{n_\mathrm{n}}{n} D_j^\mathrm{n} \frac{E_\mathrm{n} - E_\mathrm{H}}{k_\mathrm{B} T^2} \nabla T}_{\boldsymbol{y}_j} \tag{7.20}$$

Recalling that

$$\boldsymbol{V}_i \equiv \boldsymbol{V}_{ion} = \boldsymbol{V}_{electrons} \equiv \boldsymbol{V}_e \tag{7.21}$$

and

$$\sum_{\mathrm{n}} n_{\mathrm{n}} \boldsymbol{V}_{\mathrm{n}} = n_{\mathrm{H}} \boldsymbol{V}_{\mathrm{H}} \approx -n_e \boldsymbol{V}_e \tag{7.22}$$

we arrive at:

$$\boldsymbol{q}_{int} = \underbrace{n_e \boldsymbol{y}_e \tfrac{5}{2} k_{\mathrm{B}} T}_{i_1} \underbrace{+ n_e \boldsymbol{y}_{\mathrm{H}^+} (I - E_{\mathrm{H}})}_{i_2} \underbrace{+ \sum_{\mathrm{n}} n_{\mathrm{n}} (E_{\mathrm{n}} - E_{\mathrm{H}}) \boldsymbol{y}_{\mathrm{n}}}_{i_3} \tag{7.23}$$

$$\boldsymbol{q}_r = \underbrace{n_e \boldsymbol{z}_e \tfrac{5}{2} k_{\mathrm{B}} T}_{r_1} \underbrace{+ n_e \boldsymbol{z}_{\mathrm{H}^+} (I - E_{\mathrm{H}})}_{r_2} \underbrace{+ \sum_{\mathrm{n}} n_{\mathrm{n}} (E_{\mathrm{n}} - E_{\mathrm{H}}) \boldsymbol{z}_{\mathrm{n}}}_{r_3} \tag{7.24}$$

7.2.1 Internal Thermal Conductivity

If equal cross sections are considered for all EES:

$$\sum_{\mathrm{n}=1}^{\mathrm{n}_{max}} \tfrac{n_{\mathrm{n}}}{n} D_i^{\mathrm{n}} \tfrac{E_{\mathrm{n}} - E_{\mathrm{H}}}{k_{\mathrm{B}} T^2} = \begin{cases} 0 & i = \mathrm{H}^+, e \\ (D_i^i - D_i^j) \tfrac{n_i}{n} \tfrac{E_i - E_{\mathrm{H}}}{k_{\mathrm{B}} T^2} & i = \mathrm{n}; \mathrm{n} = 1, \ldots, \mathrm{n}_{max}, \\ & j = \mathrm{m}; \mathrm{m} \neq \mathrm{n} \end{cases} \tag{7.25}$$

that gives for the internal thermal conductivity:

$$\lambda_{int} = \tfrac{n_{\mathrm{H}}}{n} (D_{\mathrm{H}}^{\mathrm{H}} - D_{\mathrm{n}}^{\mathrm{m}}) n_{\mathrm{H}} c^{\mathrm{int}} \begin{cases} \mathrm{n} = 1, \ldots, \mathrm{n}_{max} \\ \mathrm{m} \neq \mathrm{n} \end{cases} \tag{7.26}$$

where $c^{\mathrm{int}} = [\bar{E}^2 - E_{\mathrm{H}}^2]/k_{\mathrm{B}} T^2$ is the *internal specific heat* per particle.

Equation (7.26) is the extension of Eucken formula to a multicomponent mixture. In the *usual* case, therefore, the internal thermal conductivity is proportional to the internal specific heat.

Figure 7.4 shows the internal thermal conductivity of equilibrium hydrogen plasma at different pressures, calculated with (*abnormal*) and without (*usual*) different cross sections for EES. It increases with increasing pressure as the population of EES increases and it becomes of comparable value as the reactive term at high pressure. Note that the effect of EES cross sections on this coefficient can be dramatic. Figure 7.4, however, shows also some puzzling features: the increase of some cross sections should decrease the diffusion coefficients. According to Eq. (7.26), the *abnormal* internal thermal conductivity should be correspondingly smaller. The effect of EES cross

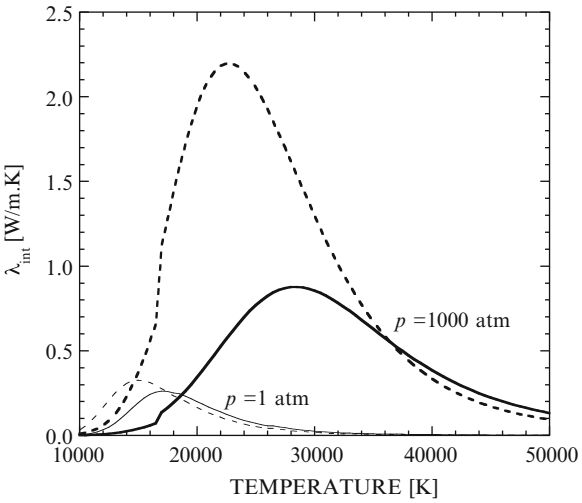

Fig. 7.4 Internal thermal conductivity of equilibrium hydrogen plasma at different pressures. (*solid lines*) *abnormal*, (*dashed lines*) *usual*

sections, instead, is to reduce the coefficient below the *usual* value at low temperatures and above it at high temperatures.

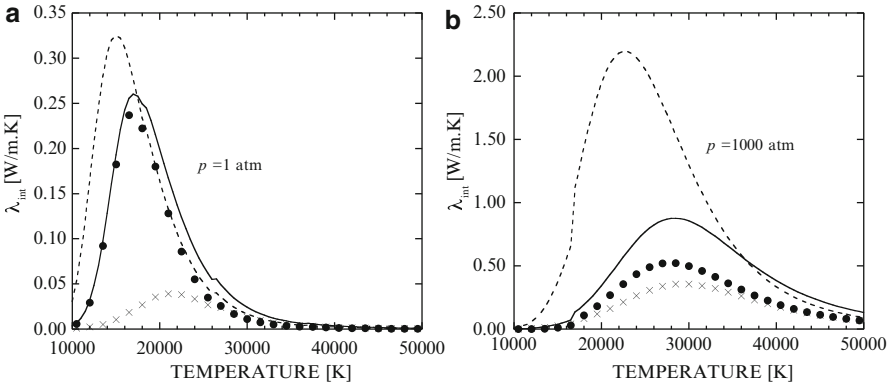

Fig. 7.5 Contributions to internal thermal conductivity of equilibrium hydrogen plasma at different pressures. (**a**) p=1 atm, (**b**) p=1,000 atm. For the definition of the different terms, see text, Eq. (7.23). (*solid line*) *abnormal*, (*closed circles*) $i_1 + i_2$, (*crosses*) i_3, (*dashed line*) *usual*

In order to understand these features we rewrite Eq. (7.23) for the *usual* case:

$$\boldsymbol{q}_{int} = \sum_{\mathrm{n}} n_{\mathrm{n}}(E_{\mathrm{n}} - E_{\mathrm{H}})\boldsymbol{y}_{\mathrm{n}} \tag{7.27}$$

This is obviously equivalent to Eq. (7.26): the internal thermal conductivity corresponds to the Eucken formula (i.e. self diffusion times internal specific heat). In the *abnormal* case this term is lower due to the large EES cross sections that make the diffusion velocities of high EES smaller. This effect is however counterbalanced by the presence of the terms i_1 and i_2 in Eq. (7.23), which are absent in the *usual* case. These additional terms read

$$n_e \boldsymbol{y}_e \tfrac{5}{2} k_\mathrm{B} T + n_e \boldsymbol{y}_{\mathrm{H}^+} \ (I - E_\mathrm{H}) = \frac{n_e}{n} \sum_\mathrm{n} \ (E_\mathrm{n} - E_\mathrm{H}) \frac{D_e^\mathrm{n} \frac{5}{2} k_\mathrm{B} T + D_{\mathrm{H}^+}^\mathrm{n} (I - E_\mathrm{H})}{k_\mathrm{B} T^2} \nabla T \tag{7.28}$$

In this formula, all diffusion coefficients are negative and low-lying levels ($E_\mathrm{n} < E_\mathrm{H}$) give a positive contribution; the diffusion coefficients of higher levels are smaller (in absolute value) with respect to the *usual* case so that overall the term increases the internal conductivity: the electronic energy of high levels, not being diffused away, acts as if the internal specific heat had increased. At high temperature, when the ionization fraction is large, this effect can become dominant and the *abnormal* coefficient is greater than the *usual* one. The different contributions to the internal thermal conductivity of equilibrium hydrogen plasma are reported in Fig. 7.5a, b for two plasma pressures.

7.2.2 Reactive Thermal Conductivity

Figure 7.6 shows the reactive thermal conductivity of equilibrium hydrogen plasma at different pressures. The two sets of curves refer to *usual* and *abnormal* values.

We note that:

- The reactive thermal conductivity decreases with increasing pressure. This happens because at higher pressure ionization shifts to higher temperatures where the term $\frac{\Delta H}{k_\mathrm{B} T^2} = \frac{I + \frac{5}{2} k_\mathrm{B} T - E_\mathrm{H}}{k_\mathrm{B} T^2}$ is lower.
- Although the EES cross sections are larger than the ground state ones, the *abnormal* coefficient can be larger than the *usual* one.
- The coefficient is not dramatically dependent on EES cross sections even at high pressure, when the population of EES is significant.
- Overall, the curves follow the behavior predicted by equation

$$\lambda_r = p \frac{\Delta H^2}{{k_\mathrm{B}}^2 T^3} \frac{n_e n_\mathrm{H}}{(n_e + n_\mathrm{H})^2} D_{\mathrm{H}^+}^\mathrm{H} \tag{7.29}$$

and peak when the reaction has the maximum temperature gradient.

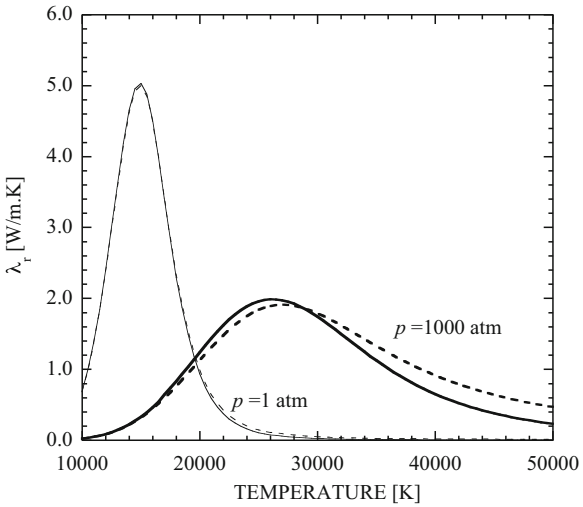

Fig. 7.6 Reactive thermal conductivity of equilibrium hydrogen plasma at different pressures. (*solid lines*) *abnormal*, (*dashed lines*) *usual*

In the *usual* case, $\boldsymbol{y}_e = \boldsymbol{y}_{\mathrm{H}^+} = 0, \boldsymbol{z}_e = \boldsymbol{V}_e = \boldsymbol{V}_{\mathrm{H}^+} = \boldsymbol{z}_{\mathrm{H}^+}$ and $r_3 = 0$ so that

$$\boldsymbol{q}_r = n_e \boldsymbol{V}_e \Delta H \tag{7.30}$$

The reactive thermal conductivity can therefore be seen as the reaction enthalpy carried by the ion diffusion, in accord with Butler and Brokaw expression. In the *abnormal* case this term is suppressed due to the increase of atom–proton cross sections. From inspection of Eq. (7.20) we also note that, for each given species j, $\boldsymbol{z}_j$ has a weaker dependence on EES compared to $\boldsymbol{y}_j$. In $\boldsymbol{z}_j$, in fact, atomic diffusion enters through

$$D_j^{\mathrm{H}} = \sum_{\mathrm{n}=1}^{\mathrm{n}_{max}} \frac{n_{\mathrm{n}}}{n} D_j^{\mathrm{n}} \tag{7.31}$$

In $\boldsymbol{y}_j$, instead, atomic diffusion is weighted with the energy content of each state: the importance of high-lying levels is therefore increased. In the *abnormal* case, in addition, the term r_3 does not vanish and balances the previous effect so that the overall effect is small. This latter term describes the difference of the actual atomic diffusion with respect to the average term $n_{\mathrm{H}} E_{\mathrm{H}} \boldsymbol{z}_{\mathrm{H}} = -n_e E_{\mathrm{H}} \boldsymbol{z}_{\mathrm{H}^+}$. Higher levels diffuse with lower velocity, since they have higher cross sections and their contribution to r_3 is smaller than in the *usual* case. This unbalance causes the sum not to vanish.

As a result, an effective atomic energy is transported, which is less than the actual one (and the transported reaction enthalpy thus bigger). At its maximum, this effect can be more important than the decrease due to smaller

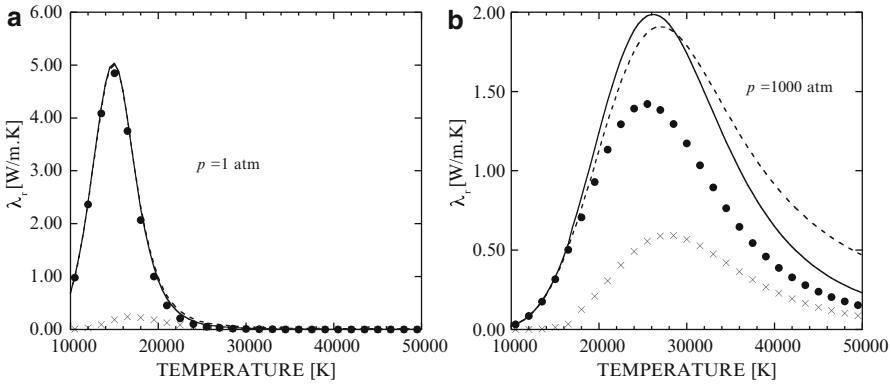

Fig. 7.7 Contributions to reactive thermal conductivity of equilibrium hydrogen plasma at different pressures. (**a**) p=1 atm, (**b**) p=1,000 atm. For the definition of the different terms see text, Eq. (7.24). (*solid line*) *abnormal*, (*closed circles*) $r_1 + r_2$, (*crosses*) r_3, (*dashed line*) *usual*

ionic diffusion and the *abnormal* coefficient is bigger than the *usual* one. At high temperature, when the atomic fraction becomes small, the first effect dominates again. Figure 7.7a, b illustrates this by comparing the different contributions to the reactive thermal conductivity for the *abnormal* and *usual* cases at two different pressures.

The extent to which EES cross sections affect the calculation of the convective contribution (internal and reactive) to the thermal conductivity in atomic hydrogen thermal plasmas is summarized in Fig. 7.8 that reports the percentage relative difference between *abnormal* and *usual* values of this quantity, normalized to the *abnormal* value, for different plasma pressures.

The results of the present work can be therefore summarized as follows:

- The internal thermal conductivity due to atomic electronic energy is a considerable fraction of the convective thermal conductivity, this ratio increasing with pressure.
- EES cross sections affect in a dramatic and nontrivial way both the internal and reactive thermal conductivities.
- The changes produced by EES cross sections affect the two coefficients in opposite ways so that the changes on their sum are somewhat reduced. This, in particular, explains the partial compensation apparent in the results of Capitelli (1974).

It is worth noting that the sum of $\lambda_r + \lambda_{int}$ yields values in close agreement with those reported in Sect. 7.1, obtained by using the Brokaw equation (see Fig. 7.9). The Brokaw results have been calculated by including n_{max} levels, with n_{max} chosen to be close to the value predicted with the CA model as done in this section (i.e. n_{max}=12, 7 and 4 at p=1, 100 and 1,000 atm, respectively). The differences in the *usual* values at p=1,000 atm can be ascribed

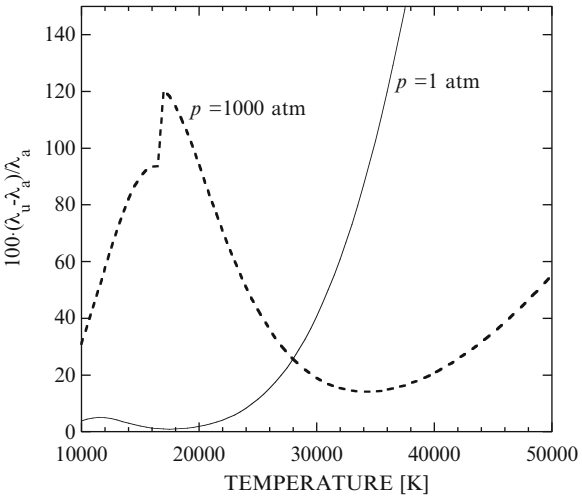

Fig. 7.8 Percentage relative difference between *abnormal* and *usual* values of *convective* (internal and reactive) thermal conductivities for equilibrium hydrogen plasma at different pressures. (*solid line*) p=1 atm, (*dashed line*) p=1,000 atm

to small differences in n_{max} selected in the parametric study with respect to the CA model.

7.3 EES and Transport Coefficients: The Dependence on the *Cutoff* Criterion

The results reported in Sects. 7.1 and 7.2 have been obtained either by parametrizing the number of excited states or by using the *confined atom* approximation for calculating the number of EES. In this section we want to show how the most used models of equilibrium thermodynamics affect the reported results (Bruno et al. 2008), emphasizing the central role played by the adopted *cutoff* criterion for the truncation of electronic partition function of atomic species (atomic hydrogen for the considered system).

We report data obtained by the following models:

1. The *ground-state model* (GS), completely disregarding the EES presence as well as any perturbation of the ionization energy, i.e. the so-called *lowering* of the ionization potential.
2. The *confined atom approximation* (CA), considering only EES with a classical radius not exceeding the inter-particle distance (as before the lowering of ionization potentials is neglected).
3. The *Debye–Hückel theory* (SSCP ≡ static screened Coulomb potential), truncating the series for the internal partition functions to the term

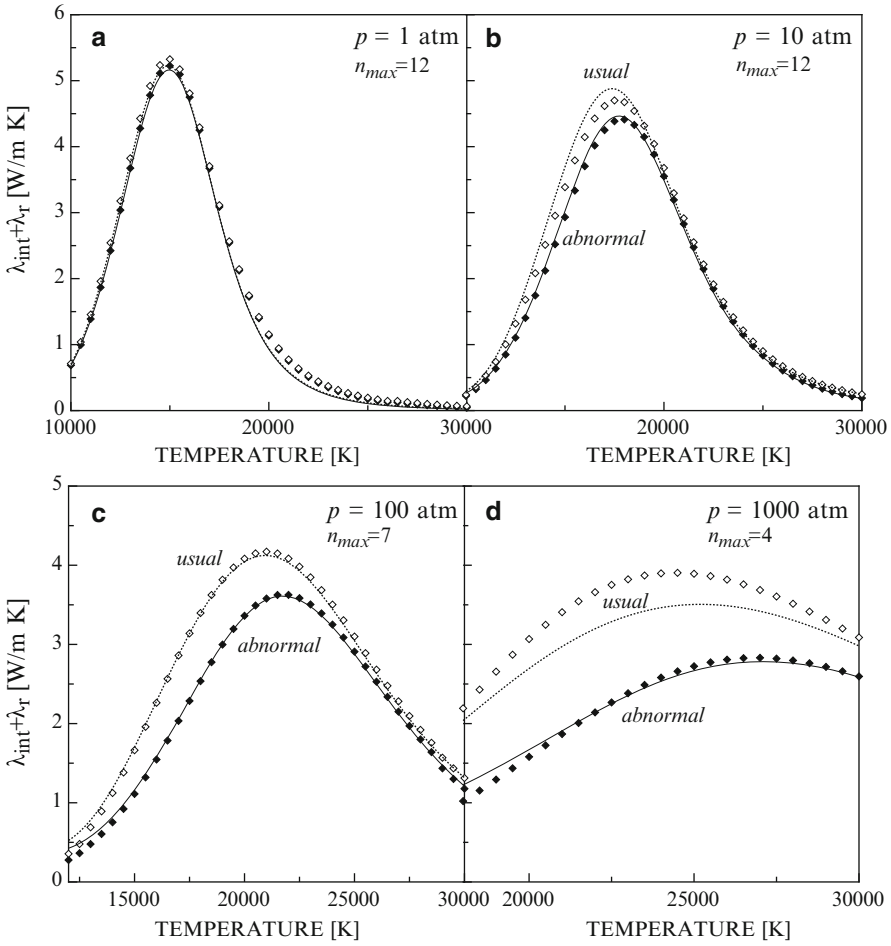

Fig. 7.9 Internal plus reactive contributions to thermal conductivity of equilibrium hydrogen plasma at different pressures. (*open markers*) case *usual* in Bruno et al. (2007a); (*close markers*) case *abnormal* in Bruno et al. (2007a); (*dotted line*) case *usual* in Capitelli et al. (2004); (*solid line*) case *abnormal* in Capitelli et al. (2004). (In the case (*d*) the actual number of states included in Bruno et al. (2007a) is n_{max}=5)

corresponding to electronically excited levels of atoms with energy above the corrected ionization potential predicted by the same theory (in this case the lowered ionization potentials enter the equations for equilibrium constants, becoming an important factor in determining the *ionization degree* of the equilibrium plasma, especially at high pressure).

The presentation of results is made by considering two groups of values coming from:

(*i*) GS and CA models either using *usual* or *abnormal* cross sections
(*ii*) CA and SSCP models either using *usual* or *abnormal* cross sections

The differences of the results in the (*i*) category are due to the number of excited states introduced in the atomic hydrogen partition function (0 for GS), without any compensation due to the inclusion of the lowering of the ionization potential (absent in both cases). On the other hand the differences of the results in the (*ii*) category come from the different number of electronic states inserted in the CA and SSCP models as well as in the presence of the lowering of the ionization potential in the SSCP model.

We limit our analysis to plasma viscosity, electrical conductivity and the sum of reactive and internal contributions to the thermal conductivity. The translational thermal conductivity of heavy components behaves like the viscosity while the electron thermal conductivity behaves like the electrical conductivity.

Values of the viscosity for two extreme conditions (p=1 and 1,000 atm) have been reported in Fig. 7.10a–d for the different adopted models. Comparison of the results reported in Fig. 7.10a, c shows the differences between GS and CA models using *usual* (Fig. 7.10a) and *abnormal* (Fig. 7.10c) transport cross sections.

The differences between GS and CA models in the first case (Fig. 7.10a) are well evident at p=1,000 atm, practically disappearing at 1 atm. At high pressure the ionization reaction is slowed down and the differences can be attributed to the increase of atom concentration in the CA model. This in turn is due to the dependence of the electronic partition function on the adopted *cutoff* model. The use of *abnormal* cross sections (Fig. 7.10c) while being uneffective on GS values strongly alters the CA values as a consequence of the large increase of transport cross sections as a function of principal quantum number. It is worth noting that the use of *abnormal* cross sections reverses the behaviour of GS and CA values, in particular CA values become much lower than the corresponding GS values. The insensitivity of the 1 atm values is due to the predominance of the ionization reaction over the excitation of electronic states.

Let us now compare CA and SSCP values calculated by using *usual* (Fig. 7.10b) and *abnormal* (Fig. 7.10d) transport cross sections. In the first case (Fig. 7.10b) large differences can be observed at p=1,000 atm due to the combined effect of the increase of the atom concentration due to the higher number of excited levels in the CA model as compared with the SSCP one and to neglecting of the lowering of the ionization potential in the CA model. Use of *abnormal* cross sections (Fig. 7.10d) reduces the differences between CA and SSCP models because they act preferentially on CA values which present higher electronic state concentrations.

Let us consider now the dependence of electrical conductivity on the different models. Figure 7.11a–d reports the corresponding results in the same order as the viscosity. To understand these results we must remind that the electrical conductivity depends on the electron density and on the interaction

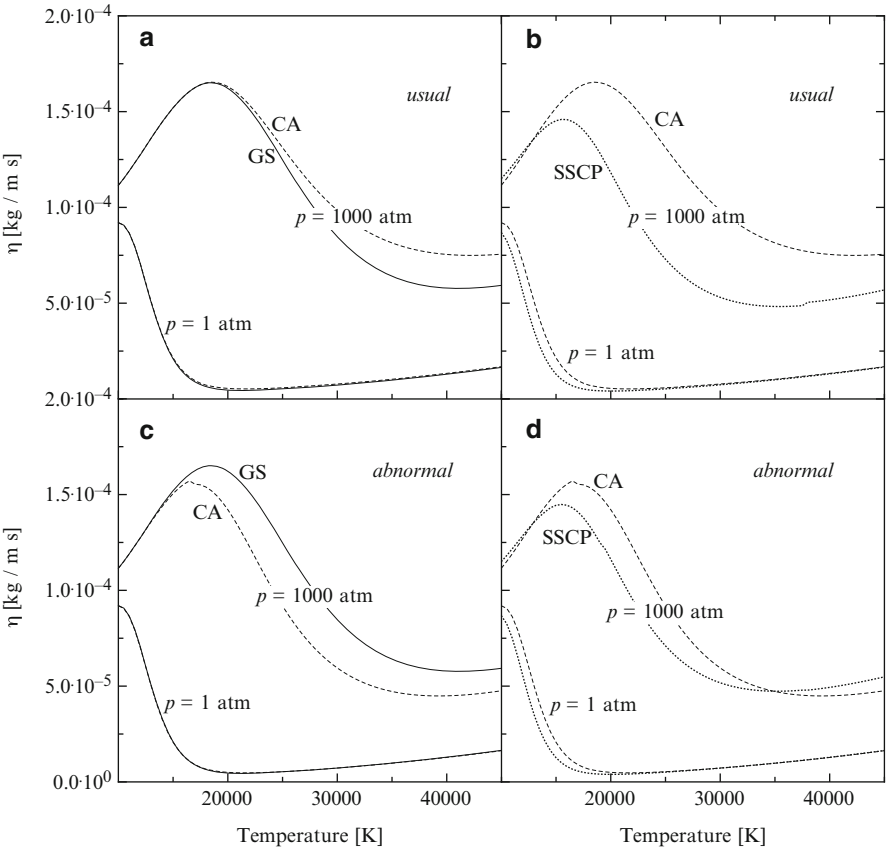

Fig. 7.10 Viscosity of equilibrium hydrogen plasma at different pressures. (*solid line*: GS; *dashed line*: CA; *dotted line*: SSCP)

of free electrons with themselves and with H(n) and protons H^+. Concerning the electron density we can say that it increases with the decrease of electronic partition function and with the increase of the lowering of the ionization potential. In the case of *usual* cross sections we should expect the following hierarchy:

$$(\sigma_e)_{\mathrm{CA}} < (\sigma_e)_{\mathrm{GS}} < (\sigma_e)_{\mathrm{SSCP}}$$

This hierarchy is well reproduced in the results of Fig. 7.11a, b especially at high pressure. On the other hand the introduction of *abnormal* cross sections is such to decrease the CA model electrical conductivity acting on the *e*-H(n) transport cross sections having a minor effect on SSCP values and a null effect of GS values. This explains the differences in the models reported in Fig. 7.11c, d.

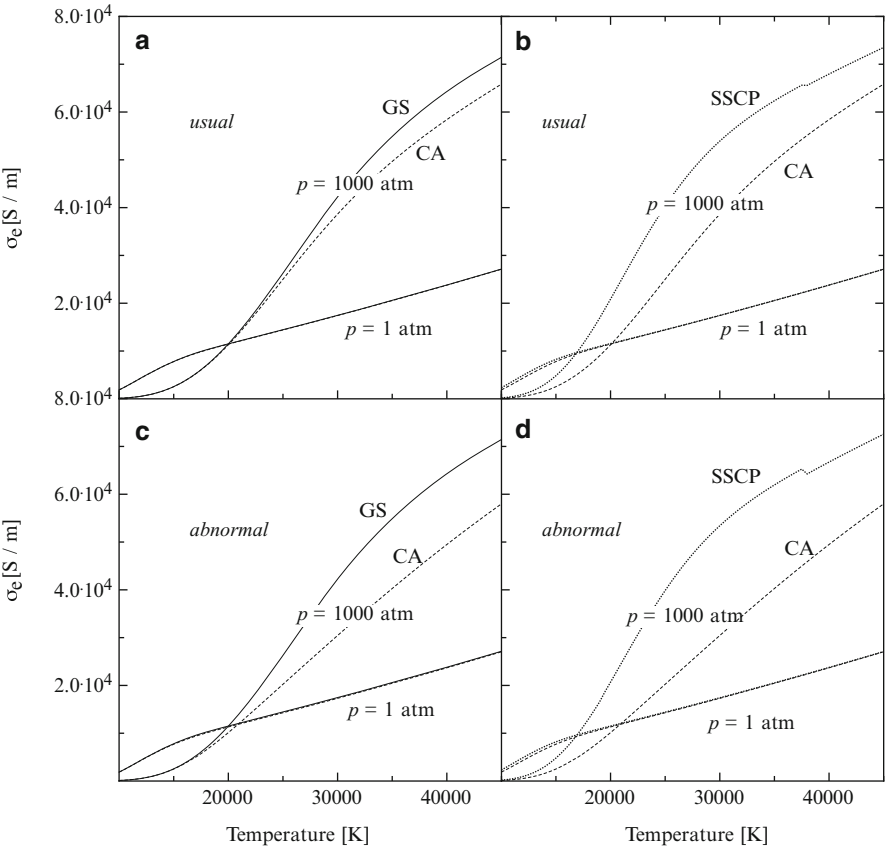

Fig. 7.11 Electrical conductivity of equilibrium hydrogen plasma at different pressures. (*solid line*: GS; *dashed line*: CA; *dotted line*: SSCP)

Finally we analyse the quantity $\lambda_r + \lambda_{int}$ reported in Fig. 7.12a–d calculated according to the different thermodynamic models. Keeping in mind the results reported in the previous section we can say that λ_r values do not depend too much on the model used, contrary to the situation for λ_{int}. Moreover in this last case in the atomic hydrogen plasma λ_{int}=0 for GS model so that one can expect that the GS $\lambda_r + \lambda_{int}$ values will represent the lower limit of the quantity, the CA results representing the upper limit. This behaviour is largely satisfied when comparing the different results using the *usual* transport cross sections (Fig. 7.12a, b). The use of *abnormal* cross sections (Fig. 7.12c, d) not only produces a large decrease of $\lambda_r + \lambda_{int}$ values but also a different role of the various *cutoff* criteria in affecting the relevant values.

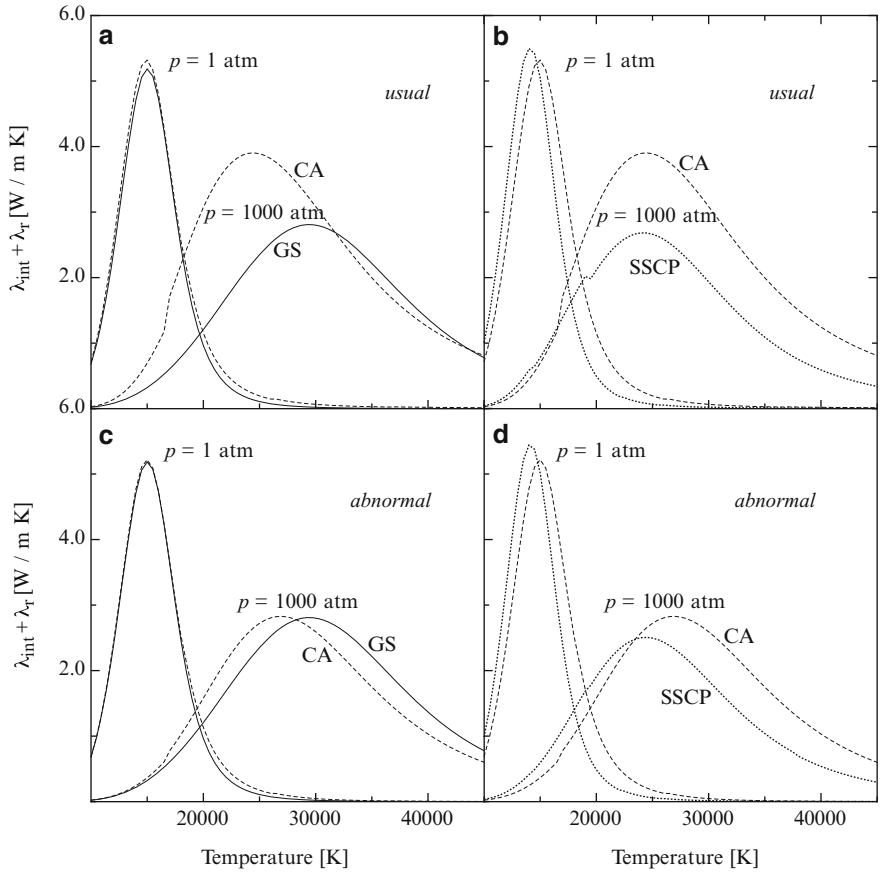

Fig. 7.12 Internal plus reactive contributions to thermal conductivity of equilibrium hydrogen plasma at different pressures. (*solid line*: GS; *dashed line*: CA; *dotted line*: SSCP)

7.4 The Role of Electronically Excited States in Complicated Mixtures: Beyond the State-to-State Approach

In the previous sections we have discussed the role of electronically excited states in affecting the transport properties of hydrogen plasmas. Both models presented are based on a state-to-state approach, i.e. each electronic state of the atomic hydrogen is considered as a new species with its own transport cross sections.

Extension of these ideas to more complicated systems (e.g. planetary atmospheres) presents some difficulties, especially for the presence of two kinds of electronically excited states in these media, i.e. *low-lying* excited states

and *high-lying* excited states, with electronic configurations characterized by principal quantum number higher than the ground state. In this last case the coupling of angular and spin angular momenta yields a multitude of electronic states, whose behaviour can be different with respect to the hydrogen-like systems. Simplified models urge to be developed to take into account the role of electronically excited states in affecting the transport properties of planetary plasmas, with particular attention to air plasmas. Such models have been recently developed for the reactive thermal conductivity of LTE nitrogen and helium plasmas (Capitelli et al. 2012; Kosarim et al. 2012).

The reactive thermal conductivity was calculated by using a closed form (Brokaw equation) with a diffusion-type cross section for the interactions N–N^+ obtained by averaging in a *parallel* scheme the relevant transport cross sections, i.e.

$$\begin{aligned}\left\langle \frac{1}{\Omega^{(1,1)\star}} \right\rangle_{\text{parallel}} &= \frac{1}{Q_{\text{N}}^{int}} \Bigg[\underbrace{g(^4S)(\Omega^{(1,1)\star}_{\text{N}(^4S)-\text{N}^+(^3P)})^{-1}}_{ground} \\ &\quad + g(^2D)(\Omega^{(1,1)\star}_{\text{N}(^2D)-\text{N}^+(^3P)})^{-1} e^{-E(\text{N}(^2D))/k_{\text{B}}T} \\ &\quad + \underbrace{g(^2P)(\Omega^{(1,1)\star}_{\text{N}(^2P)-\text{N}^+(^3P)})^{-1} e^{-E(\text{N}(^2P))/k_{\text{B}}T}}_{low-lying} \\ &\quad + \underbrace{\sum_{\text{n}=3}^{\text{n}_{max}} g^{\star}_{\text{n}} (\Omega^{(1,1)\star}_{\text{N}^\star-\text{N}^+(^3P)})^{-1} e^{-E(\text{N}^\star)/k_{\text{B}}T}}_{high-lying} \Bigg] \\ &\propto \frac{1}{n_{\text{N}}} \Bigg[\underbrace{n_{\text{N}(^4S)} \mathcal{D}^{\text{N}^+(^3P)}_{\text{N}(^4S)}}_{ground} \\ &\quad + \underbrace{n_{\text{N}(^2D)} \mathcal{D}^{\text{N}^+(^3P)}_{\text{N}(^2D)} + n_{\text{N}(^2P)} \mathcal{D}^{\text{N}^+(^3P)}_{\text{N}(^2P)}}_{low-lying} \\ &\quad + \underbrace{\sum_{\text{n}=3}^{\text{n}_{max}} n_{\text{N}^\star} \mathcal{D}^{\text{N}^+(^3P)}_{\text{N}^\star}}_{high-lying} \Bigg] = \langle \mathcal{D}^{\text{N}^+}_{\text{N}} \rangle \end{aligned} \tag{7.32}$$

E and g being the energy and the degeneracy of electronic levels, respectively.

Considering a system like helium, with no low-lying excited states, the large increase of diffusion-type collision integrals, due to the effectiveness of resonant charge-transfer processes, makes the contribution to the average vanishingly small, thus leading to an oversimplified form for the reactive thermal conductivity of the first ionization reaction (Kosarim et al. 2012)

$$\lambda_r \simeq \frac{p}{k_{\text{B}}T} \mathcal{D}^{\text{He}^+}_{\text{He(n=1)}} \frac{x_{\text{He(n=1)}} x_{\text{He}^+}}{(x_{\text{He(n=1)}} + x_{\text{He}^+})^2} \frac{\Delta H^2}{k_{\text{B}}T^2} \tag{7.33}$$

This approach gives results in agreement with the corresponding ones obtained by the state-to-state approach (Capitelli et al. 2012). On the other hand the averaging of diffusion-type collision integrals in a *serial* scheme, i.e.

$$\langle \Omega^{(1,1)\star} \rangle_{\text{serial}} = \frac{1}{Q_{\text{N}}^{int}} \Big[\; g(^4S)\Omega^{(1,1)\star}_{\text{N}(^4S)-\text{N}^+(^3P)} \tag{7.34}$$

$$+ g(^2D)\Omega^{(1,1)\star}_{\text{N}(^2D)-\text{N}^+(^3P)} e^{-E(\text{N}(^2D))/k_{\text{B}}T} + g(^2P)\Omega^{(1,1)\star}_{\text{N}(^2P)-\text{N}^+(^3P)} e^{-E(\text{N}(^2P))/k_{\text{B}}T} + \sum_{\text{n}=3}^{\text{n}_{max}} g^{\star}_{\text{n}} \Omega^{(1,1)\star}_{\text{N}^\star-\text{N}^+(^3P)} e^{-E(\text{N}^\star)/k_{\text{B}}T} \Big] \tag{7.35}$$

is such to completely destroy the reactive thermal conductivity, contrary to what is observed in the state-to-state approach. These considerations lead to the conclusion that the *parallel* approach to the diffusion transport coefficients is equivalent to completely disregard the presence of high-lying excited states in the reactive thermal conductivity. These points, here considered only qualitatively, will be further analysed in the next section, where results for the internal and reactive thermal conductivities of nitrogen plasmas obtained in the frame of different models are reported. On the other hand in the last section of this chapter *serial*-averaging models will be discussed, for the estimation of the role of electronically excited states in determining the viscosity, the translational thermal conductivity of electrons and the electrical conductivity of plasmas.

7.4.1 The Reactive and Internal Thermal Conductivities of a Nitrogen Plasma

The nitrogen plasma is composed of the following species: N_2, N_2^+, $N(^4S)$, $N(^2D)$, $N(^2P)$, $N(\text{HL})$, $N^+(^3P)$, $N^+(^1D)$, $N^+(^1S)$, $N^+(\text{HL})$, N^{2+}, N^{3+}, N^{4+}, N^{5+} and e. Chemical equilibrium is established via the following set of reactions:

$$\begin{cases} \text{N}_2 \leftrightarrows 2\text{N} & (r1) \quad \text{N}_2^+ \leftrightarrows 2\text{N} - e & (r2) \\ \text{N}(^2D) \leftrightarrows \text{N}(^4S) & (r3) \quad \text{N}(^2P) \leftrightarrows \text{N}(^4S) & (r4) \quad \text{N}(\text{HL}) \leftrightarrows \text{N}(^4S) & (r5) \\ \text{N}^+(^3P) \leftrightarrows \text{N}(^4S) - e & (r6) \quad \text{N}^+(^1D) \leftrightarrows \text{N}(^4S) - e & (r7) \quad \text{N}^+(^1S) \leftrightarrows \text{N}(^4S) - e & (r8) \\ & & \text{N}^+(\text{HL}) \leftrightarrows \text{N}(^4S) - e & (r9) \end{cases}$$

$\text{N}(\text{HL})$ and $\text{N}^+(\text{HL})$ represent lumped excited states, which include the population of excited states with principal quantum number $\text{n} \geqslant 3$. The population of all excited states follows a Boltzmann distribution at the given temperature, while the equilibrium composition is calculated by statistical thermodynamics. To this end the electronic partition functions

of atomic species are obtained adopting a self-consistent pressure- and temperature-dependent *cutoff* criterion, in high-ionization-degree regimes determined by the Griem method (D'Angola et al. 2008; Capitelli et al. 2011).

7.4.1.1 Transport Coefficient Calculation

The internal and reactive thermal conductivities have been obtained in the frame of the Chapman–Enskog method of solution of the Boltzmann equation (Hirschfelder et al. 1966). The internal thermal conductivity is usually calculated using the Eucken correction (Ferziger and Kaper 1972) and the reactive thermal conductivity following (Butler and Brokaw 1957).

Both formulations, however, correspond to lowest order Chapman–Enskog approximations. In order to overcome this limitation, a more general approach to the calculation of these quantities has been derived based on the state-to-state kinetic theory of transport (Nagnibeda and Kustova 2009) and on the extension to high Chapman–Enskog approximations of the Stefan–Maxwell relations (Kolesnikov and Tirskiy 1984).

The main ideas of the derivation are described here.

Consider a mixture of n^C species $X_c, c = 1, \ldots, n^C$, each with a set of internal energy levels $i = 1, \ldots, L_c$. A state-to-state approach considers each internal level as a separate species and the heat flux reads

$$\boldsymbol{q} = -\lambda' \nabla T - p \sum_{c=1}^{n^C} \sum_{i=1}^{L_c} D_{ci}^T \boldsymbol{d}_{ci} + \sum_{c=1}^{n^C} \sum_{i=1}^{L_c} \left(\tfrac{5}{2} k_\mathrm{B} T + E_i^c + E_c \right) n_{ci} \boldsymbol{V}_{ci} \quad (7.36)$$

where E_i^c is the energy of the internal level and E_c is the formation energy.

Assume now that the plasma is in thermal and chemical equilibrium. The convective part of the heat flux vector will then be shown to be proportional to the temperature gradient:

$$\boldsymbol{q}_{conv} \equiv \sum_{c=1}^{n^C} \sum_{i=1}^{L_c} \left(\tfrac{5}{2} k_\mathrm{B} T + E_i^c + E_c \right) n_{ci} \boldsymbol{V}_{ci} = -(\lambda_{int} + \lambda_r) \nabla T \quad (7.37)$$

We start by writing the expression for the diffusion velocities:

$$\boldsymbol{V}_{ci} = -\sum_{d=1}^{n^C} \sum_{k=1}^{L_d} D_{ci}^{dk} \boldsymbol{d}_{dk} - D_{ci}^T \nabla \ln T \quad (7.38)$$

where D_{ci}^{dk} and D_{ci}^T are diffusion and thermal diffusion coefficients, respectively. The *diffusion driving forces*, $\boldsymbol{d}_{ci}$, are

$$\boldsymbol{d}_{ci} = \nabla\left(\frac{n_{ci}}{n}\right) + \left(\frac{n_{ci}}{n} - \frac{\rho_{ci}}{\rho}\right)\nabla \ln p - \frac{\rho_{ci}}{p}\left(\boldsymbol{b}_{ci} - \sum_{dk}\frac{\rho_{dk}}{\rho}\boldsymbol{b}_{dk}\right) \tag{7.39}$$

where $\boldsymbol{b}_{ci}$ are external forces per unit mass. We then assume that these forces are restricted to the action of the electric field and that the plasma is electrically neutral (the ambipolar diffusion case is discussed in Meador, Jr. and Staton 1965). Since each chemical species in different internal levels has the same mass and electric charge and internal level populations are constrained by the thermal equilibrium assumption, the above expression simplifies to

$$\boldsymbol{d}_{ci} = \frac{n_{ci}}{n}\boldsymbol{d}_c + \frac{n_{ci}}{n}\left[\frac{E_i^c}{k_{\mathrm{B}}T}\right]'\nabla \ln T \tag{7.40}$$

where

$$\boldsymbol{d}_c = \nabla\left(\frac{n_c}{n}\right) + \left(\frac{n_c}{n} - \frac{\rho_c}{\rho}\right)\nabla \ln p - \frac{n_c}{n}\frac{e_c\boldsymbol{E}}{k_{\mathrm{B}}T} \tag{7.41}$$

$$\left[\frac{E_i^c}{k_{\mathrm{B}}T}\right]' \equiv \frac{E_i^c}{k_{\mathrm{B}}T} - \langle\frac{E_j^c}{k_{\mathrm{B}}T}\rangle_j \tag{7.42}$$

and $\langle \ldots \rangle_j$ means thermal average over internal levels.

Since our aim is to lump together species in different internal states that share the same collision integrals (and to treat internal states with different collision integrals as separate species) we assume that the collision integrals involving a chemical species c are independent of the internal state of that species. As a consequence, the diffusion and thermal diffusion coefficient sets can be simplified:

$$D_{ci}^T = D_c^T, \quad i = 1, \ldots, L_c \tag{7.43}$$

$$D_{ci}^{dk} = D_c^d, \quad c \neq d \tag{7.44}$$

$$D_{ci}^{cj} = \tilde{D}_c^c, \quad i \neq j \tag{7.45}$$

$$\tilde{D}_c^c\left(1 - \frac{n_{ci}}{n_c}\right) + D_{ci}^{ci}\frac{n_{ci}}{n_c} = D_c^c, \quad i = 1, \ldots, L_c \tag{7.46}$$

After some algebra, the convective heat flux, Eq. (7.37), can be written as

$$\boldsymbol{q}_{conv} = \sum_{c=1}^{n^C}\left(\tfrac{5}{2}k_{\mathrm{B}}T + \langle E_i^c\rangle_i + E_c\right)n_c\boldsymbol{V}_c - \lambda_{int}\nabla T \tag{7.47}$$

$$\lambda_{int} = \sum_{c=1}^{n^C}\frac{n_c}{n}\left(D_c^c - \tilde{D}_c^c\right)n_c c_c^{\mathrm{int}} \tag{7.48}$$

where $\boldsymbol{V}_c = \sum_{i=1}^{L_c} \frac{n_{ci}}{n_c} \boldsymbol{V}_{ci}$ and c_c^{int} are internal specific heats:

$$\frac{c_c^{\text{int}}}{k_{\text{B}}} = \langle \left(\frac{E_i^c}{k_{\text{B}} T} \right)^2 \rangle_i - \langle \frac{E_i^c}{k_{\text{B}} T} \rangle_i^2 \tag{7.49}$$

The linear systems required for the calculation of the diffusion coefficients in Eq. (7.48) can easily be derived and are completely analogous to those required for the calculation of diffusion and thermal diffusion coefficients, involving the knowledge of collision integrals for the species in the plasma. To the lowest Chapman–Enskog approximation, this approach yields the usual Eucken correction to the translational thermal conductivity.

The first sum in Eq. (7.47), instead, gives rise to the reactive thermal conductivity and is discussed in the following section.

Concerning the reactive thermal conductivity, first, we write the elemental conservation laws as

$$\sum_{c=1}^{n^C} a_c^s x_c \boldsymbol{V}_c = 0 \quad s = 1, \ldots, n^S \tag{7.50}$$

where $X_s, \quad s = 1, \ldots, n^S$ are the elements (including electrons) that compose each chemical species via

$$X_c = \sum_{s=1}^{n^S} a_c^s X_s \quad c = 1, \ldots, n^C \tag{7.51}$$

Now, among the chemical reactions that keep the system in chemical equilibrium, choose a linearly independent set:

$$\sum_{c=1}^{n^C} b_c^r X_c = 0 \quad r = 1, \ldots, n^R \tag{7.52}$$

so that $n^C = n^S + n^R$.

For each of these reactions, the van't Hoff equation can be used to link the concentration gradients to the temperature gradient:

$$\sum_{c=1}^{n^C} b_c^r \nabla \ln x_c = \frac{\Delta H_r}{k_{\text{B}} T^2} \nabla T, \quad r = 1, \ldots, n^R \tag{7.53}$$

where

$$\Delta H_r = \sum_{c=1}^{n^C} b_c^r H_c, \quad r = 1, \ldots, n^R \tag{7.54}$$

$$H_c = \tfrac{5}{2} k_{\text{B}} T + \langle E_i^c \rangle_i + E_c, \quad c = 1, \ldots, n^C \tag{7.55}$$

From Eq. (7.41), we express ∇x_c in terms of $\boldsymbol{d}_c$ and substitute in Eq. (7.53) to obtain

$$\sum_{c=1}^{n^C} b_c^r \frac{\boldsymbol{d}_c}{x_c} - \nabla \ln p \sum_{c=1}^{n^C} b_c^r \left(1 - \frac{m_c}{m}\right) + \frac{\boldsymbol{E}}{k_\mathrm{B} T} \sum_{c=1}^{n^C} b_c^r e_c = \frac{\Delta H_r}{k_\mathrm{B} T^2} \nabla T, \quad r = 1, \ldots, n^R \tag{7.56}$$

We further assume that the pressure is constant, i.e. $\nabla p = 0$, and use the property of chemical reactions to conserve electric charge:

$$\sum_{c=1}^{n^C} b_c^r e_c = 0, \quad r = 1, \ldots, n^R \tag{7.57}$$

We can then write Eqs. (7.50) and (7.53) as

$$\sum_{c=1}^{n^C} a_c^s x_c \boldsymbol{V}_c = 0 \quad s = 1, \ldots, n^S \tag{7.58}$$

$$\sum_{c=1}^{n^C} b_c^r \frac{\boldsymbol{d}_c}{x_c} = \frac{\Delta H_r}{k_\mathrm{B} T^2} \nabla T, \quad r = 1, \ldots, n^R \tag{7.59}$$

The diffusion driving forces are related to the diffusion velocities via the diffusion and thermal diffusion coefficients. These are the extension of the Stefan–Maxwell relations to any Chapman–Enskog order (Kolesnikov and Tirskiy 1984). The full system to be solved is thus

$$\sum_{c=1}^{n^C} a_c^s x_c \mathbf{g}_c^0 = 0 \quad s = 1, \ldots, n^S \tag{7.60}$$

$$\sum_{c=1}^{n^C} \sum_q \boldsymbol{g}_c^q \left(\sum_{d=1}^{n^C} b_d^r A_{dc}^{0q} \right) = -\tfrac{4}{25} \frac{\Delta H_r}{k_\mathrm{B} T} \frac{\nabla T}{p}, \quad r = 1, \ldots, n^R \tag{7.61}$$

$$\sum_{d=1}^{n^C} \sum_q A_{cd}^{pq} \boldsymbol{g}_d^q = \tfrac{2}{5} \delta_{p1} \frac{\nabla T}{p}, \quad c = 1, \ldots, n^C, \quad p \geqslant 1 \tag{7.62}$$

$$\boldsymbol{V}_c = \boldsymbol{g}_c^0, \quad c = 1, \ldots, n^C \tag{7.63}$$

The reactive thermal conductivity can then be obtained from the defining relation:

$$-\lambda_r \nabla T = \sum_{c=1}^{n^C} n_c H_c \boldsymbol{V}_c \tag{7.64}$$

It is worth pointing out that, in this scheme, each chemical species contributes to λ_{int}, Eq. (7.48), with its own internal specific heat and to λ_r, Eq. (7.64), with its enthalpy and *average* internal energy. For the plasma under study, this means λ_{int} will show the transport of rotational and vibrational energy of molecular N_2 and N_2^+ species, whereas the transport of electronic excitation energy of *low-* and *high-lying* N and N^+ species will go into λ_r.

7.4.1.2 Internal and Reactive Thermal Conductivities

Several calculations have been performed (Bruno et al., 2012) according to different assumptions on the relevant transport cross sections:

- *Usual*: transport cross sections for the interactions with excited states are set equal to those with the ground state, i.e. $\Omega_{N(HL)-N(^4S)} = \Omega_{N(^2P)-N(^4S)} = \Omega_{N(^2D)-N(^4S)} = \Omega_{N(^2D)-N(^2P)} = \Omega_{N(^4S)-N(^4S)}$ (see also Kustova and Puzyreva (2009)) and $\Omega_{N(^2P)-N^+(^3P)} = \Omega_{N(^2D)-N^+(^3P)} = \Omega_{N(^4S)-N^+(^3P)}$.
- *Abnormal 1* (without high-lying states): In this approach all the above equalities are relaxed introducing the actual values of the transport cross sections for low-lying states. The transport cross sections involving high-lying excited states are set equal to the corresponding values involving the highest low-lying state, i.e. $\Omega_{N(HL)-N^+(^3P)} = \Omega_{N(^2P)-N^+(^3P)}$.
- *Abnormal 2* (with high-lying states): In this scheme the high-lying collision integrals due to the inelastic contribution of the resonant charge-exchange processes have been increased by a factor 100, simulating the expected dramatic dependence of diffusion-type collision integrals on the principal quantum number of excited atomic collisional partner, i.e. $\Omega_{N(HL)-N^+(^3P)} = 100 \times \Omega_{N(^2P)-N^+(^3P)}$. Among the calculations in this work, this is the only case where an estimation of the transport cross sections involving high-lying states is required.
- *Abnormal 3* (simplified): The molar fraction of high-lying excited states of both N and N^+ is set to zero, in the hypothesis that their effect on the reactive thermal conductivity could be reproduced through the reduction of the molar fraction of the ground state.

Figure 7.13a, b reports the internal and thermal conductivities calculated according to the four models above, at the pressure of 1,000 bar in the temperature range 5,000–30,000 K. It is useful, at this stage, to recall that the internal thermal conductivity contains only the contribution due to the vibrational and rotational degrees of freedom since the transport of electronic energy is contained in the reactive term (see also Capitelli (1975, 1977)). In particular the transport of the electronic states $N(^2D)$, $N(^2P)$ and N (HL) is directly accounted for in reactions $(r3)$–$(r5)$, while the transport of the internal energies of N^+ ions (i.e. (^1D), (^1S) and (HL) states) is indirectly accounted for in reactions $(r6)$–$(r9)$.

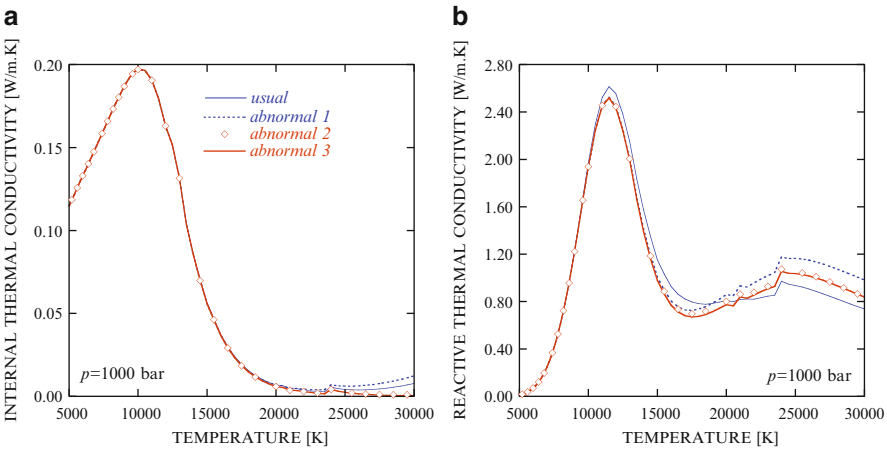

Fig. 7.13 (**a**) Internal and (**b**) reactive thermal conductivities as a function of temperature for LTE nitrogen plasma at p=1,000 bar obtained by different approaches. (*thin solid line*) *usual*, (*dotted line*) *abnormal 1*, (*close diamonds*) *abnormal 2*, (*thick solid line*) *abnormal 3*

Let us first consider the internal thermal conductivity in Fig. 7.13a. In this case the peak at about 10,000 K is due to the excitation of the internal degrees of freedom of molecular nitrogen, while the strong decrease of λ_{int} from 10,000 K is the consequence of the progressive transformation of molecules in atoms. After 20,000 K the internal contribution is practically zero because the transport of electronic excitation goes into the reactive contribution. It should also be noted that the internal thermal conductivity does not depend in this scheme on the adopted model, i.e. the results from *usual* and *abnormal* models are practically the same. For the reactive thermal conductivity (Fig. 7.13b) we can note that the *usual* values are higher than the *abnormal* values up to the onset of the ionization regime, at $T \approx 17,000\,K$. The differences in this case are due to the transport of the *low-lying* excited states of the nitrogen atom (i.e. reactions $(r3)$–$(r5)$). The transport cross sections of the N(^2D) and N(^2P) states with N(^4S) in the *usual* model are lower than the corresponding values adopted in the *abnormal 1* model: in the former case, in fact, the excitation transfer contribution to the diffusion-type collision integrals has been neglected. As a consequence, the *usual* approach overestimates the reactive thermal conductivity by about 10 % in the dissociation regime.

In the ionization regime plasma equilibrium is governed by reactions $(r5)$–$(r8)$ that include also the contribution of EES of both atoms and ions. In this temperature range the *usual* approximation yields much lower (up to 30 %) λ_r values than those obtained from the *abnormal 1* model.

The large discrepancy is attributed to differences in the transport of low-lying excited atoms in the two models. While the *abnormal 1* model correctly accounts for the different transport cross sections of ground and low-lying ex-

cited atoms, in the *usual* model all the nine interactions among the ground and LL states of the nitrogen atom and ion are dominated by the resonant charge-exchange process, determining an underestimation of the corresponding reactive contributions.

The *abnormal 1* model properly takes into account the role of low-lying electronically excited states and is therefore superior to the *usual* model. Nonetheless, high-lying excited states are not well described because the actual diffusion-type cross sections of high-lying states enormously increase as a function of principal quantum number (Capitelli et al. 1974; Eletskii et al. 2004; Kosarim et al. 2012). In order to account approximately for the increase of charge-exchange cross sections with the principal quantum number, we assume that the high-lying excited states colliding with $N^+(^3P)$ have diffusion-type collision integrals 100 times higher than those used in the *abnormal 1* model. This choice (*abnormal 2*) leads to λ_r values between the *usual* and *abnormal 1* results.

Finally, the results from the *abnormal 3* model practically coincide with those of *abnormal 2* model thus confirming that neglecting high-lying excited states in the transport equations reproduces with sufficient accuracy the results of more sophisticated models. The latter that explicitly account for the dramatic dependence of charge-exchange cross sections with the principal quantum number obviously require the knowledge of a larger set of transport cross sections.

This conclusion is confirmed by the results obtained at different pressures (1–1,000 bar). Figure 7.14a, b display the λ_{int} and λ_r values at p=1 bar. The results follow the same trends discussed above, the discrepancy between the *abnormal 1* and the *usual* approaches reaching 15 % in the ionization regime. This is due to a smaller population of excited species. Note however that at $T = 10,000\,K$, the more correct *abnormal 1* model gives values of λ_r 23 % lower than the *usual* values, reflecting the effect of the transport cross sections in reactions $(r3)$–$(r4)$.

Internal and reactive thermal conductivities for the *abnormal 3* model are reported in Table 7.1 for different pressures. The temperature range explored is limited to the regions of the first ionization equilibrium, where information on transport cross sections for interactions involving excited species is available.

These results can be regarded as an improvement in the vast literature on the estimation of the reactive and internal contributions to the thermal conductivity of nitrogen plasma (Wang et al. 2011, 2012; Aubreton et al. 1998; Murphy 1995; Capitelli et al. 2012).

Note also that the reported effect will increase if use is made of the Fermi criterion for truncating the electronic partition functions of the atomic species. In the latter case, in fact, a larger concentration of *high-lying* excited states is expected and therefore a bigger role of electronically excited states in affecting λ_r (Bruno et al. 2008).

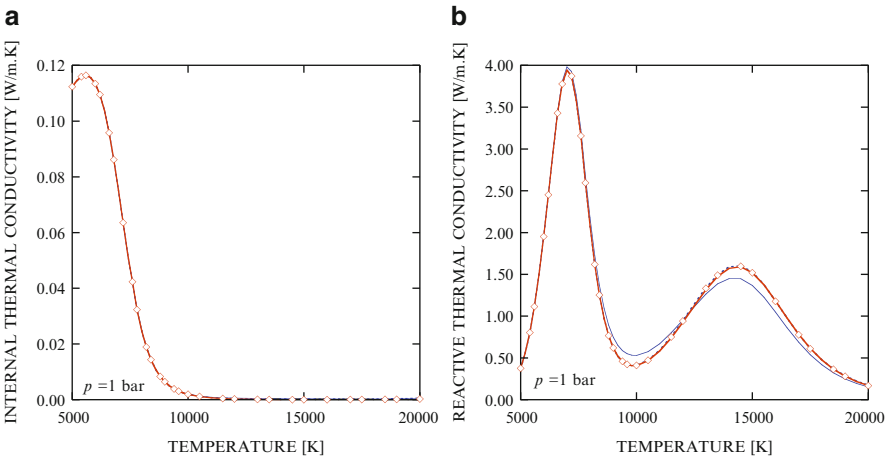

Fig. 7.14 (**a**) Internal and (**b**) reactive thermal conductivities as a function of temperature for LTE nitrogen plasma at p=1 bar obtained by different approaches. (*thin solid line*) *usual*, (*dotted line*) *abnormal 1*, (*close diamonds*) *abnormal 2*, (*thick solid line*) *abnormal 3*

7.5 Further Simplified Models

Different models can be proposed for the reactive and internal thermal conductivities of a nitrogen plasma. The model that takes into account, to a given extent, both low-lying and high-lying excited states is the one that, while considering as independent species the low-lying excited states of nitrogen atoms and ions, completely disregards the presence of high-lying excited states. However this model fails in describing the translational thermal conductivities of both heavy particles and electrons, the viscosity and the electrical conductivity. In fact for these transport coefficients the *parallel* averaging of viscosity-type cross sections yields unsatisfactory results as demonstrated in the following.

7.5.1 Electrical Conductivity

It has been already shown that the reactive thermal conductivity of an LTE plasma, including the role of electronically excited states, can be reduced, in the case of the first ionization equilibrium, to the usual Brokaw equation with the only prescription of entering the molar fraction of atoms in the ground state, instead of the total molar fraction for the atomic species (Eq. (7.33)). Analogously in the temperature region of the second ionization equilibrium a similar expression can be written, entering the molar fraction of the ion in

Table 7.1 Internal and reactive thermal conductivities as a function of temperature for LTE nitrogen plasma at different pressures, obtained with the model *abnormal 3*

	p=1 bar		10 bar		100 bar		1,000 bar	
T [K]	λ_{int}	λ_r	λ_{int}	λ_r	λ_{int}	λ_r	λ_{int}	λ_r
5,000	1.124(−01)	3.759(−01)	1.141(−01)	1.203(−01)	1.146(−01)	3.817(−02)	1.148(−01)	1.209(−02)
5,200	1.145(−01)	5.593(−01)	1.173(−01)	1.802(−01)	1.182(−01)	5.731(−02)	1.185(−01)	1.816(−02)
5,400	1.159(−01)	8.036(−01)	1.203(−01)	2.615(−01)	1.217(−01)	8.344(−02)	1.221(−01)	2.646(−02)
5,600	1.164(−01)	1.114(+00)	1.229(−01)	3.688(−01)	1.251(-01)	1.182(−01)	1.257(−01)	3.752(−02)
5,800	1.157(−01)	1.501(+00)	1.252(−01)	5.065(−01)	1.284(−01)	1.633(−01)	1.293(−01)	5.193(−02)
6,000	1.134(−01)	1.952(+00)	1.270(−01)	6.786(−01)	1.315(−01)	2.205(−01)	1.330(−01)	7.032(−02)
6,200	1.095(−01)	2.452(+00)	1.282(−01)	8.882(−01)	1.345(−01)	2.918(−01)	1.366(−01)	9.337(−02)
6,400	1.036(−01)	2.962(+00)	1.287(−01)	1.137(+00)	1.374(−01)	3.790(−01)	1.402(−01)	1.218(−01)
6,600	9.580(−02)	3.429(+00)	1.283(−01)	1.423(+00)	1.400(−01)	4.836(−01)	1.438(−01)	1.562(−01)
6,800	8.617(−02)	3.779(+00)	1.268(−01)	1.742(+00)	1.423(−01)	6.069(−01)	1.474(−01)	1.974(−01)
7,000	7.518(−02)	3.942(+00)	1.242(−01)	2.084(+00)	1.443(−01)	7.500(−01)	1.511(−01)	2.461(−01)
7,200	6.353(−02)	3.873(+00)	1.204(−01)	2.435(+00)	1.460(−01)	9.132(−01)	1.548(−01)	3.028(−01)
7,400	5.204(−02)	3.580(+00)	1.152(−01)	2.772(+00)	1.472(−01)	1.096(+00)	1.584(−01)	3.681(−01)
7,600	4.232(−02)	3.156(+00)	1.087(−01)	3.068(+00)	1.479(−01)	1.296(+00)	1.622(−01)	4.426(−01)
7,800	3.234(−02)	2.593(+00)	1.010(−01)	3.295(+00)	1.480(−01)	1.512(+00)	1.659(−01)	5.265(−01)
8,000	2.484(−02)	2.075(+00)	9.227(−02)	3.425(+00)	1.475(−01)	1.739(+00)	1.696(−01)	6.201(−01)
8,200	1.893(−02)	1.619(+00)	8.285(−02)	3.438(+00)	1.462(−01)	1.971(+00)	1.732(−01)	7.233(−01)
8,400	1.438(−02)	1.253(+00)	7.344(−02)	3.334(+00)	1.440(−01)	2.200(+00)	1.768(−01)	8.358(−01)
8600	1.094(−02)	9.719(−01)	6.350(−02)	3.120(+00)	1.410(−01)	2.418(+00)	1.804(−01)	9.571(−01)
8,800	8.365(−03)	7.657(−01)	5.437(−02)	2.828(+00)	1.371(−01)	2.614(+00)	1.837(−01)	1.089(+00)
9,000	6.433(−03)	6.197(−01)	4.601(−02)	2.492(+00)	1.323(−01)	2.778(+00)	1.869(−01)	1.222(+00)
9,200	4.990(−03)	5.210(−01)	3.858(−02)	2.146(+00)	1.274(−01)	2.887(+00)	1.898(−01)	1.364(+00)
9,400	3.899(−03)	4.578(−01)	3.217(−02)	1.818(+00)	1.201(−01)	2.969(+00)	1.923(−01)	1.509(+00)
9,600	3.074(−03)	4.220(−01)	2.673(−02)	1.524(+00)	1.130(−01)	2.984(+00)	1.945(−01)	1.654(+00)
9,800	2.441(−03)	4.071(−01)	2.219(−02)	1.273(+00)	1.053(−01)	2.941(+00)	1.961(−01)	1.798(+00)
10,000	1.945(−03)	4.084(−01)	1.843(−02)	1.066(+00)	9.732(−02)	2.845(+00)	1.971(−01)	1.938(+00)
10,500	1.148(−03)	4.674(−01)	1.169(−02)	7.151(−01)	7.727(−02)	2.427(+00)	1.964(−01)	2.245(+00)
11,000	6.926(−04)	5.832(−01)	7.604(−03)	5.443(−01)	5.905(−02)	1.901(+00)	1.906(−01)	2.451(+00)
11,500	4.300(−04)	7.400(−01)	5.053(−03)	4.828(−01)	4.418(−02)	1.421(+00)	1.792(−01)	2.519(+00)
12,000	2.965(−04)	9.275(−01)	3.423(−03)	4.908(−01)	3.276(−02)	1.057(+00)	1.631(−01)	2.437(+00)
13,000	9.228(−05)	1.316(+00)	1.632(−03)	6.247(−01)	1.804(−02)	6.644(−01)	1.316(−01)	1.991(+00)
14,000	2.995(−05)	1.572(+00)	9.522(−04)	8.512(−01)	1.010(−02)	5.575(−01)	8.570(−02)	1.392(+00)
15,000	8.575(−06)	1.519(+00)	4.904(−04)	1.092(+00)	5.697(−03)	5.934(−01)	5.593(−02)	9.784(−01)
16,000	2.336(−06)	1.183(+00)	2.198(−04)	1.281(+00)	3.300(−03)	6.919(−01)	3.666(−02)	7.686(−01)
17,000	6.911(−07)	7.838(−01)	8.951(−05)	1.353(+00)	1.865(−03)	8.252(−01)	2.331(−02)	6.812(−01)
18,000	5.152(−07)	4.757(−01)	3.516(−05)	1.277(+00)	1.043(−03)	9.585(−01)	1.483(−02)	6.756(−01)
19,000	1.196(−06)	2.816(−01)	9.466(−06)	1.079(+00)	1.102(−03)	1.082(+00)	9.368(−03)	7.146(−01)
20,000	3.649(−06)	1.696(−01)	5.188(−06)	8.443(−01)	5.761(−04)	1.137(+00)	5.943(−03)	7.747(−01)
22,000	–	–	–	–	1.371(−04)	1.076(+00)	2.871(−03)	8.558(−01)
24,000	–	–	–	–	4.067(−05)	8.517(−01)	4.287(−03)	1.055(+00)
26,000	–	–	–	–	–	–	1.551(−03)	1.016(+00)
28,000	–	–	–	–	–	–	6.188(−04)	9.358(−01)
30,000	–	–	–	–	–	–	4.133(−04)	8.377(−01)

the ground state. This choice is reasonable in absence of low-lying excited states, i.e. for high-temperature helium plasmas. Extension of these ideas to other transport coefficients can be problematic. As an example the electrical conductivity of a partially ionized gas, taking into account electronically excited states, cannot be reduced to the simple form of reactive thermal conductivity, i.e. by considering only the ground-state concentration of neutral atoms in the electron–atom operator.

Figure 7.15 reports the electrical conductivity of atomic hydrogen plasma calculated by using three assumptions, i.e. (1) *usual* approximation, i.e. the transport cross sections for e-H interactions are independent of the principal quantum number; (2) the approximation *abnormal 1*, i.e. transport cross

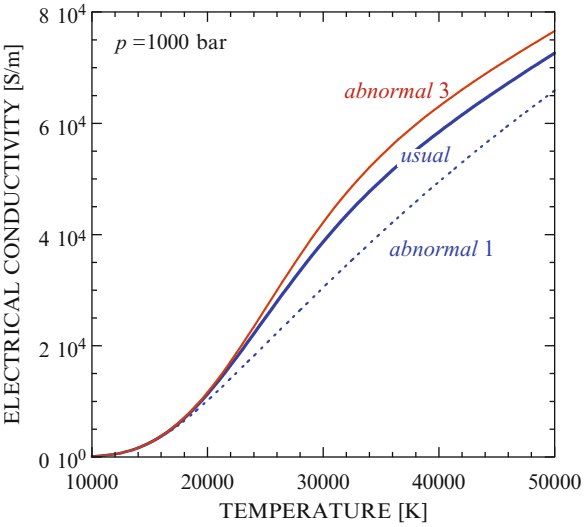

Fig. 7.15 Electrical conductivity as a function of temperature for LTE hydrogen plasma, at p=1,000 bar, obtained by different approaches. (*thick solid line*) *usual*, (*dotted line*) *abnormal 1*, (*thin solid line*) *abnormal 3*

sections for e-H*(n) interactions dependent on the principal quantum number of the excited atom; (3) the approximation *abnormal 3*, where the density of excited atomic species is set equal to zero. Inspection of Fig. 7.15 shows that the last hypothesis overestimates the electrical conductivity as compared with the results coming from the other two models. Although reported results have been obtained in the third approximation of the Chapman–Enskog approximation, a rationalization of the observed trend could be obtained from a simple mathematical treatment dealing with the equation of σ_e in the first approximation (Sharma et al. 2011)

$$\sigma_e = \tfrac{3}{2} e^2 n_e^2 \left[\frac{2\pi}{m_e k_B T_e}\right]^{1/2} \frac{1}{q_{00}} \tag{7.65}$$

with

$$q_{00} = 8 n_e \sum_{j=1}^{\nu-1} n_j \pi \sigma^2 \Omega_{ej}^{(1,1)} \tag{7.66}$$

where the index ν moves on heavy species, i.e. H and H$^+$.

In the frame of the three models the term q_{00} can be rewritten in different forms

$$q_{00}^{usual} = 8 n_e (n_H \pi \sigma^2 \Omega_{eH}^{(1,1)} + n_{H^+} \pi \sigma^2 \Omega_{eH^+}^{(1,1)}) \tag{7.67}$$

$$q_{00}^{abnormal1} = 8n_e(n_{\mathrm{H}}(1)\pi\sigma^2\Omega_{e\mathrm{H}(1)}^{(1,1)} + n_{\mathrm{H}}(2)\pi\sigma^2\Omega_{e\mathrm{H}(2)}^{(1,1)} + \ldots + n_{\mathrm{H}(\mathrm{n}_{max})}\pi\sigma^2\Omega_{e\mathrm{H}(\mathrm{n}_{max})}^{(1,1)} + n_{\mathrm{H}^+}\pi\sigma^2\Omega_{e\mathrm{H}^+}^{(1,1)}) \tag{7.68}$$

$$q_{00}^{abnormal3} = 8n_e(n_{\mathrm{H}(1)}\pi\sigma^2\Omega_{e\mathrm{H}(1)}^{(1,1)} + n_{\mathrm{H}^+}\pi\sigma^2\Omega_{e\mathrm{H}^+}^{(1,1)}) \tag{7.69}$$

We can understand that the following inequalities hold

$$q_{00}^{abnormal3} < q_{00}^{usual} < q_{00}^{abnormal1} \tag{7.70}$$

thus generating the trend reported in Fig. 7.15.

To avoid the state-to-state formulation of the electrical conductivity, $q_{00}^{abnormal1}$ can be written as

$$\begin{aligned} q_{00}^{abnormal1} &= 8n_e n_{\mathrm{H}}\left(\frac{n_{\mathrm{H}(1)}}{n_{\mathrm{H}}}\pi\sigma^2\Omega_{e\mathrm{H}(1)}^{(1,1)} + \frac{n_{\mathrm{H}(2)}}{n_{\mathrm{H}}}\pi\sigma^2\Omega_{e\mathrm{H}(2)}^{(1,1)} + \ldots + \frac{n_{\mathrm{H}(\mathrm{n}_{max})}}{n_{\mathrm{H}}}\pi\sigma^2\Omega_{e\mathrm{H}(\mathrm{n}_{max})}^{(1,1)} + \frac{n_{\mathrm{H}^+}}{n_{\mathrm{H}}}\pi\sigma^2\Omega_{e\mathrm{H}^+}^{(1,1)}\right) \\ &= 8n_e(n_{\mathrm{H}}\langle\pi\sigma^2\Omega_{e\mathrm{H}}^{(1,1)}\rangle_{serial} + n_{\mathrm{H}^+}\pi\sigma^2\Omega_{e\mathrm{H}^+}^{(1,1)}) \end{aligned} \tag{7.71}$$

The quantity $\langle\pi\sigma^2\Omega_{e\mathrm{H}}^{(1,1)}\rangle_{\mathrm{serial}}$ represents an averaged transport cross section which can be calculated once the transport cross sections of each quantum state and the relevant Boltzmann factors are known. When the state-selected information is not available a simplified *two-level* system could be considered, consisting of the ground state and a lumped excited state, whose transport cross section can be set, to a first approximation, equal to Coulomb cross section. A better approximation can be obtained by scaling ground cross sections with the known dependence of transport cross sections on the principal quantum number for the atomic hydrogen system. Difficulties in any case will arise when trying to extend these considerations to higher approximations of the Chapman Enskog method for the electrical conductivity.

7.5.2 Viscosity

Plasma viscosity depends to a given extent on the presence of electronically excited states through their higher viscosity transport cross sections as compared with the ground state. *Abnormal* and *usual* values of the viscosity of a high-pressure plasma have been reported in Fig. 7.16 as a function of temperature. These values have been obtained by using the first approximation of the Chapman–Enskog method. The Fermi criterion (CA model) has been used for the *cutoff* of the partition function. Inspection of Fig. 7.16 clearly shows the role of excited states in reducing the plasma viscosity. In the same

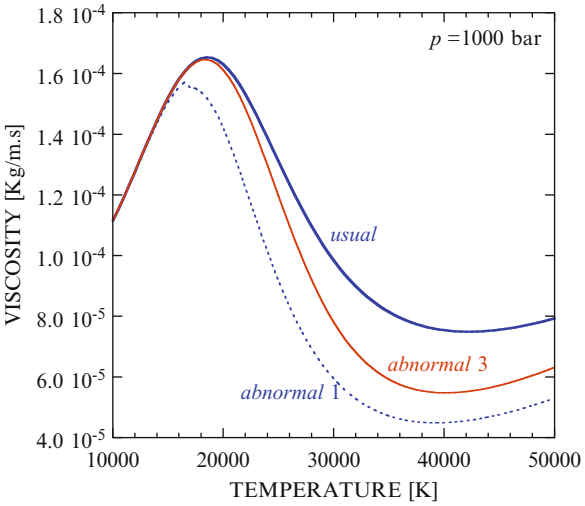

Fig. 7.16 Viscosity as a function of temperature for LTE hydrogen plasma, at p=1,000 bar, obtained by different approaches. (*thick solid line*) *usual*, (*dotted line*) *abnormal 1*, (*thin solid line*) *abnormal 3*

figure we have reported viscosity values calculated by eliminating the concentration of electronically excited states in the viscosity equation. Qualitatively the new viscosity values follow the trend of *abnormal 1* viscosity, the maximum deviation being of the order of 27 %.

To understand the results we use the Wilke equation (Wilke 1950) for the viscosity of a mixture, even though this equation is only a crude representation of the first-order Chapman–Enskog results:

$$\eta = \sum_{i=1}^{\nu-1} \frac{x_i \eta_i}{\phi_i} \tag{7.72}$$

with ϕ_i expressed in terms of the coefficient $A^\star$ (Eq. (3.15)), i.e.

$$\phi_i = \tfrac{6}{5} A^\star_{ij} \frac{k_B T}{p m_i} \frac{\eta_i}{\mathcal{D}_i^j} \tag{7.73}$$

Setting $\phi_{\mathrm{H}(1)}$=$\phi_{\mathrm{H}(2)}$=$\phi_{\mathrm{H}(\mathrm{n}_{max})}$=$\phi_{\mathrm{H}^+}$=1 the viscosity can be written as a Dalton law

$$\eta = x_{\mathrm{H}(1)}\eta_{\mathrm{H}(1)} + x_{\mathrm{H}(2)}\eta_{\mathrm{H}(2)} + \ldots + x_{\mathrm{H}(\mathrm{n}_{max})}\eta_{\mathrm{H}(\mathrm{n}_{max})} + x_{\mathrm{H}^+}\eta_{\mathrm{H}^+} \tag{7.74}$$

The approximation to the *abnormal 3* viscosity, i.e. the cancellation of the contribution of excited states, can be considered satisfactory due to the decrease of the viscosity with the increase of i. This means that a good

approximation to the estimation of excited states in affecting the plasma viscosity is to eliminate them from relevant equations. A further simplification could be the reduction of the electronic manifold to a two-level system, the ground and a lumped excited state,

$$\eta = x_{\mathrm{H}(1)}\eta_{\mathrm{H}(1)} + x_{\mathrm{H}^\star(\mathrm{n})}\eta_{\mathrm{H}^\star(\mathrm{n})} + x_{\mathrm{H}^+}\eta_{\mathrm{H}^+} \tag{7.75}$$

assigning to the lumped electronic state either the transport cross section corresponding to the Coulomb interaction, i.e. $\eta_{\mathrm{H}^\star(\mathrm{n})} \propto 1/\Omega^{(2,2)\star}_{\mathrm{H}^\star(\mathrm{n})-\mathrm{H}^\star(\mathrm{n})} \sim 1/\Omega^{(2,2)\star}_{\mathrm{H}^+-\mathrm{H}^+}$, or using the scaling relations that hold for atomic hydrogen.

7.5.3 Translational Thermal Conductivity

In a plasma the translational thermal conductivity can be separated into two contributions one due to free electrons and the other due to heavy components. The form of the thermal conductivity due to electrons mimes the corresponding equation for the electrical conductivity. The consideration made for the first approximation of electrical conductivity can be applied to the first non-vanishing equation for the electron thermal conductivity. In this case no simple way to take into account the excited states can be found. Only an average transport cross section of the type previously discussed can be used to avoid the state-to-state calculations. At the same time the translational thermal conductivity due to heavy components can be manipulated as in the case of the viscosity by eliminating the electronically excited states in the relevant equation.

References

Aubreton J, Elchinger MF, Fauchais P (1998) New method to calculate thermodynamic and transport properties of a multi-temperature plasma: application to N_2 plasma. Plasma Chem Plasma P 18(1):1–27

Brokaw RS (1960) Thermal conductivity of gas mixtures in chemical equilibrium. II. J Chem Phys 32(4):1005–1006

Bruno D, Capitelli M, Catalfamo C, Laricchiuta A (2007a) Transport of internal electronic energy in atomic hydrogen thermal plasmas. Phys Plasmas 14:072308

Bruno D, Laricchiuta A, Capitelli M, Catalfamo C (2007b) Effect of electronic excited states on transport in magnetized hydrogen plasma. Phys Plasmas 14:022303

Bruno D, Capitelli M, Catalfamo C, Laricchiuta A (2008) Cutoff criteria of electronic partition functions and transport properties of atomic hydrogen thermal plasmas. Phys Plasmas 15:112306

Bruno D, Colonna G, Laricchiuta A, Capitelli M (2012) Reactive and internal contributions to the thermal conductivity of local thermodynamic equilibrium nitrogen plasma: The effect of electronically excited states. Phys Plasmas 19: 122309

Butler JN, Brokaw RS (1957) Thermal conductivity of gas mixtures in chemical equilibrium. J Chem Phys 26(6):1636–1643

Capitelli M (1972) Cut-off criteria of electronic partition functions and transport properties of thermal plasmas. J Plasma Phys 7:99–106

Capitelli M (1974) The influence of excited states on the reactive thermal conductivity of an LTE hydrogen plasma. Zeitschrift für Naturforschung A (Astrophysik, Physik und Physikalische Chemie) 29:953–954

Capitelli M (1975) Charge transfer from low-lying excited states: effects on reactive thermal conductivity. J Plasma Phys 14(2):365–371

Capitelli M (1977) Transport coefficients of partially ionized gases. Journal de Physique Supplemént Colloque C3 (Paris) 38(8):C3 227– C3 237

Capitelli M, Lamanna U (1974) Collision integrals of electronically excited states and transport coefficients of thermal plasmas. J Plasma Phys 12:71–79

Capitelli M, Guidotti C, Lamanna U (1974) Potential energy curves and excitation transfer cross sections of excited hydrogen atoms. J Phys B: Atomic Mol Phys 7(13):1683

Capitelli M, Celiberto R, Gorse C, Laricchiuta A, Minelli P, Pagano D (2002) Electronically excited states and transport properties of thermal plasmas: the reactive thermal conductivity. Phys Rev E 66(1):016403/1–8

Capitelli M, Laricchiuta A, Pagano D, Traversa P (2003) Electronically excited states and transport properties of thermal plasmas: the viscosity. Chem Phys Lett 379:490–494

Capitelli M, Celiberto R, Gorse C, Laricchiuta A, Pagano D, Traversa P (2004) Transport properties of local thermodynamic equilibrium hydrogen plasmas including electronically excited states. Phys Rev E 69(2):026412

Capitelli M, Colonna G, D'Angola A (2011) Fundamental aspects of plasma chemical physics: Thermodynamics. Springer series on atomic, optical, and plasma physics, vol 66. Springer, New York

Capitelli M, Armenise I, Bisceglie E, Bruno D, Celiberto R, Colonna G, D'Ammando G, De Pascale O, Esposito F, Gorse C, Laporta V, Laricchiuta A (2012) Thermodynamics, transport and kinetics of equilibrium and non-equilibrium plasmas: a state-to-state approach. Plasma Chem Plasma P 32(3):427–450

D'Angola A, Colonna G, Gorse C, Capitelli M (2008) Thermodynamic and transport properties in equilibrium air plasmas in a wide pressure and temperature range. Eur Phys J D 46(1):129–150

Devoto RS (1967a) Simplified expressions for the transport properties of ionized monatomic gases. Phys Fluids 10(10):2105–2112

Devoto RS (1967b) Transport coefficients of partially ionized argon. Phys Fluids 10(2):354–364

Devoto RS (1968) Transport coefficients of partially ionized hydrogen. J Plasma Phys 2(4):617–631
Eletskii AV, Capitelli M, Celiberto R, Laricchiuta A (2004) Resonant charge exchange and relevant transport cross sections for excited states of oxygen and nitrogen atoms. Phys Rev A 69(4):042718/1–8
Ferziger JH, Kaper HG (1972) Mathematical theory of transport processes in gases. North-Holland, Amsterdam
Hirschfelder JO, Curtiss CF, Bird RB (1966) Molecular theory of gases and liquids. Wiley, New York
Ignjatović LJM, Mihajlov AA (1997) Interaction of electrons with atoms in ground and excited states; potential of interaction, momentum transfer cross-sections. Contrib Plasm Phys 37(4):309–326
Kolesnikov AF, Tirskiy GA (1984) The Stefan-Maxwell equations for diffusion fluxes in a magnetic field. Fluid Dynamics (translated from Russian) Plenum 19:643
Kosarim AV, Smirnov BM, Capitelli M, Celiberto R, Laricchiuta A (2006) Resonant charge exchange involving electronically excited states of nitrogen atoms and ions. Phys Rev A 74(6):062707
Kosarim AV, Smirnov BM, Laricchiuta A, Capitelli M (2012) Resonant charge-exchange involving excited helium atoms and reactive transport of LTE helium plasma. Phys Plasmas 19(6):062309
Kustova EV, Puzyreva LA (2009) Transport coefficients in nonequilibrium gas-mixture flows with electronic excitation. Phys Rev E 80:046407
Meador, Jr WE, Staton LD (1965) Electrical and thermal properties of plasmas. Phys Fluids 8(9):1694–1703
Murphy AB (1995) Transport coefficients of air, argon-air, nitrogen-air, and oxygen-air plasmas. Plasma Chem Plasma P 15(2):279
Nagnibeda E, Kustova E (2009) Non-equilibrium reacting gas flows: kinetic theory of transport and relaxation processes. Springer series heat and mass transfer. Springer, Berlin
Sharma R, Singh G, Singh K (2011) Higher-order contributions to transport coefficients in two-temperature hydrogen thermal plasma. Phys Plasmas 18(6):063504
Singh G, Sharma R, Singh K (2008) Effect of excited states on higher-order contributions to electron transport in hydrogen thermal plasmas. J Phys D: Appl Phys 41(22):225203
Singh K, Singh G, Sharma R (2010) Role of electronic excitation on thermodynamic and transport properties of argon and argon-hydrogen plasmas. Phys Plasmas 17(7):072309
Wang WZ, Rong MZ, Yan JD, Murphy AB, Spencer JW (2011) Thermophysical properties of nitrogen plasmas under thermal equilibrium and non-equilibrium conditions. Phys Plasmas 18(11):113502

Wang WZ, Rong MZ, Yan JD, Wu Y (2012) The reactive thermal conductivity of thermal equilibrium and non-equilibrium plasmas: application to nitrogen. IEEE T Plasma Sci DOI 10.1109/TPS.2012.2185717

Wilke CR (1950) A viscosity equation for gas mixtures. J Chem Phys 18(4):517–519

Chapter 8
Transport Properties of Multi-temperature Plasmas

The rigorous kinetic theory developed in Chap. 1 could be extended to multi-temperature plasmas. This approach however has several disadvantages when applied to concrete situations. An alternative is to use simplified approaches based on decoupling the Boltzmann equation for the electron component from the corresponding ones describing the heavy particles. This approach, due in particular to the pioneering work of Devoto (1967a,b), uses the same equations developed in Chap. 1 for the electron thermal conductivity, λ_e, and the electrical conductivity, σ_e, of the plasma as well as the translational thermal conductivity of the heavy particles and the viscosity. The electron component is calculated at the electron temperature, T_e, while the heavy-particle translational temperature, T_h, must be used for λ_h and η. The reactive and internal contributions on the other hand are calculated by modifying the Butler–Brokaw and Eucken approaches. In particular the reactive contribution, λ_r, has been reformulated by adapting the Butler–Brokaw to two-temperature plasmas (Bonnefoi 1983; Bonnefoi et al. 1985; Aubreton et al. 1986).

A problem in any case arises, in the theory reformulation, linked to the definition of the composition and of the thermodynamic properties to be inserted in the relevant transport equations. This is due to the numerous existing Saha equations coming from the different thermodynamic constraints used for defining the multi-temperature equilibrium (Giordano and Capitelli 1995, 2001; Capitelli et al. 2011). It is in fact well known that the application of the Gibbs potential for obtaining the multi-temperature equilibrium gives results different from those obtained by using the entropy maximization as equilibrium criterion. This point will be widely analysed in Sect. 8.1 discussing the relevant results obtained in different formulations of Saha equilibrium. In Sect. 8.2 recent attempts are reported to a new formulation of transport equations for multi-temperature plasmas by using essentially the maximization of entropy to get the equilibrium composition as well as the temperature derivatives of the partial pressures of the relevant species entering the reactive contribution.

M. Capitelli et al., *Fundamental Aspects of Plasma Chemical Physics*,
Springer Series on Atomic, Optical, and Plasma Physics 74,
DOI 10.1007/978-1-4419-8172-1_8, © Springer Science+Business Media, LLC 2013

8.1 The Devoto and Bonnefoi Approaches

The transport properties of multi-temperature plasmas have been for long time calculated according to theories first developed by Devoto and then extended by Bonnefoi (Bonnefoi 1983; Bonnefoi et al. 1985; Aubreton et al. 1986) to non-equilibrium plasma. The original idea was to decouple the Boltzmann equation for free electrons from the corresponding ones for heavy particles. In this case the translational thermal conductivity is given by the sum of the contributions due to electrons and to heavy components, i.e.

$$\lambda = \lambda_h + \lambda_e \tag{8.1}$$

The corresponding equations have been reported in Chap. 7. A different level of approximation is used for the calculation of the two terms; in general the second approximation of the Chapman–Enskog method is used for λ_h and the third one for λ_e. A similar approach is used for calculating the viscosity and the electrical conductivity of the multi-temperature plasma. In particular the viscosity which depends on heavy particles is calculated by the first non-vanishing Chapman–Enskog approximation while the third approximation is used for σ_e, which in turn depends on the electron component (see Chap. 7 for the relevant equations).

The reactive thermal conductivity for two-temperature plasmas was worked out by Bonnefoi starting from the total heat flux vector for a multi-temperature plasma, resulting from the reactive flux of electrons and of heavy particles

$$\boldsymbol{q}_r = \boldsymbol{q}_r^e + \boldsymbol{q}_r^h = -\lambda_r^e \cdot \nabla T_e - \lambda_r^h \cdot \nabla T_h \tag{8.2}$$

being the gradients of the two temperatures connected by the relation

$$\nabla T_e = \vartheta \nabla T_h$$

where $\vartheta = T_e/T_h$ is the ratio of electron and heavy-particle temperatures.

It follows

$$\boldsymbol{q}_r = -\left[\lambda_r^e + \frac{\lambda_r^h}{\vartheta}\right] \nabla T_e = -\lambda_r \nabla T_e \tag{8.3}$$

Let us consider a system of ν chemical components and define j the number of elementary components, i.e. the minimal basis of chemical species that allows to derive all other components through M independent reactions, being $M = \nu - j$.

The stoichiometric coefficient of the ith component in the mth reaction, a_{mi}, entering the balance relation with chemical potential μ_i

$$\sum_{i=1}^{\nu} a_{mi}\mu_i = 0 \qquad m = 1, \ldots, M \tag{8.4}$$

could be redefined in the minimal chemical basis as

$$\sum_{i=1}^{j} \alpha_{mi}\mu_i - \mu_m = 0 \qquad m = 1, \ldots, M \tag{8.5}$$

where the index i runs over the independent chemical components and the index m, running over independent chemical reactions, represents also the non-independent chemical component generated in the reaction.

To clarify this point a practical example is considered here of an atomic nitrogen plasma system of ν=5 components, i.e. e, N, N^+, N^{2+}, N^{3+}, with M=3 independent chemical reactions of ionization:

$$\begin{cases} \mathrm{N} & \leftrightarrow \mathrm{N}^+ + e \\ \mathrm{N}^+ & \leftrightarrow \mathrm{N}^{2+} + e \\ \mathrm{N}^{2+} & \leftrightarrow \mathrm{N}^{3+} + e \end{cases} \tag{8.6}$$

The system of Eq. 8.4 has the form

$$\begin{cases} a_{\mathrm{N}}\mu_{\mathrm{N}} - a_{\mathrm{N}^+}\mu_{\mathrm{N}^+} - a_e\mu_e & = \mu_{\mathrm{N}} - \mu_{\mathrm{N}^+} - \mu_e & = 0 \\ a_{\mathrm{N}^+}\mu_{\mathrm{N}^+} - a_{\mathrm{N}^{2+}}\mu_{\mathrm{N}^{2+}} - a_e\mu_e & = \mu_{\mathrm{N}^+} - \mu_{\mathrm{N}^{2+}} - \mu_e & = 0 \\ a_{\mathrm{N}^{2+}}\mu_{\mathrm{N}^{2+}} - a_{\mathrm{N}^{3+}}\mu_{\mathrm{N}^{3+}} - a_e\mu_e & = \mu_{\mathrm{N}^{2+}} - \mu_{\mathrm{N}^{3+}} - \mu_e & = 0 \end{cases} \tag{8.7}$$

with stoichiometric coefficients a_{mi} assuming values ± 1 or 0 for the considered ionization equilibria. Moving to the minimal chemical basis representation, we have $j = \nu - M$=5-3=2 independent chemical components that are naturally chosen to be $\{e$,N$\}$, leading to equilibria rewritten in the form

$$\begin{cases} \mathrm{N} - e & \leftrightarrow \mathrm{N}^+ \\ \mathrm{N} - 2e & \leftrightarrow \mathrm{N}^{2+} \\ \mathrm{N} - 3e & \leftrightarrow \mathrm{N}^{3+} \end{cases} \tag{8.8}$$

and to a new system of balancing equations

$$\begin{cases} \alpha_{\mathrm{N}}\mu_{\mathrm{N}} - \alpha_e\mu_e - \alpha_{\mathrm{N}^+}\mu_{\mathrm{N}^+} & = \mu_{\mathrm{N}} - \mu_e - \mu_{\mathrm{N}^+} & = 0 \\ \alpha_{\mathrm{N}}\mu_{\mathrm{N}} - \alpha_e\mu_e - \alpha_{\mathrm{N}^{2+}}\mu_{\mathrm{N}^{2+}} & = \mu_{\mathrm{N}^+} - 2\mu_e - \mu_{\mathrm{N}^{2+}} & = 0 \\ \alpha_{\mathrm{N}}\mu_{\mathrm{N}} - \alpha_e\mu_e - \alpha_{\mathrm{N}^{3+}}\mu_{\mathrm{N}^{3+}} & = \mu_{\mathrm{N}^{2+}} - 3\mu_e - \mu_{\mathrm{N}^{3+}} & = 0 \end{cases} \tag{8.9}$$

Coming back to the general approach, the Bonnefoi treatment allows to write the M equations in the form

$$a_{m1}\vartheta\nabla\ln p_1 + \sum_{\ell=2}^{j} a_{m\ell}\nabla\ln p_\ell + \sum_{i=1}^{M} a_{mi}\nabla\ln p_i = \frac{\vartheta\Delta H_m^\star}{k_{\mathrm{B}}T_e^2}\nabla T_e \quad m = 1, \ldots, M \tag{8.10}$$

with p_i and $\Delta H_m^\star$ the partial pressure of the ith component and the enthalpy variation in the mth reaction (the subscript 1 refers to electrons). It should be pointed out that this equation comes from the differentiation of the equilibrium constant of a two-temperature plasma described by the

Potapov method (i.e. minimization of the free energy). The reactive thermal conductivity assumes the form

$$\lambda_r(T_e) = -\frac{\vartheta}{k_{\mathrm{B}} T_e^2} \begin{vmatrix} 0 & n_1 \Delta H_1 & \dots & n_M \Delta H_M \\ \Delta H_1^\star & A_{11} & \dots & A_{1M} \\ \vdots & \vdots & \ddots & \vdots \\ \Delta H_M^\star & A_{M1} & \dots & A_{MM} \end{vmatrix} \begin{vmatrix} A_{11} & \dots & A_{1M} \\ \vdots & \ddots & \vdots \\ A_{M1} & \dots & A_{MM} \end{vmatrix}^{-1} \tag{8.11}$$

The variation of enthalpy $\Delta H_m^\star$ and ΔH_m, entering the determinants in Eq. (8.11), is associated to the reaction schemes in the natural and in the minimal chemical basis representations, i.e. recalling the nitrogen plasma example:

$$\begin{cases} \Delta H_1^\star = a_{\mathrm{N}} H_{\mathrm{N}} - a_{\mathrm{N}^+} H_{\mathrm{N}^+} - a_e H_e & = H_{\mathrm{N}} - H_{N^+} - H_e \\ \Delta H_2^\star = a_{\mathrm{N}^+} H_{\mathrm{N}^+} - a_{\mathrm{N}^{2+}} H_{\mathrm{N}^{2+}} - a_e H_e & = H_{\mathrm{N}^+} - H_{\mathrm{N}^{2+}} - H_e \\ \Delta H_3^\star = a_{\mathrm{N}^{2+}} H_{\mathrm{N}^{2+}} - a_{\mathrm{N}^{3+}} H_{\mathrm{N}^{3+}} - a_e H_e & = H_{\mathrm{N}^{2+}} - H_{\mathrm{N}^{3+}} - H_e \end{cases} \tag{8.12}$$

$$\begin{cases} \Delta H_1 = \alpha_{\mathrm{N}} H_{\mathrm{N}} - \alpha_e H_e - \alpha_{\mathrm{N}^+} H_{\mathrm{N}^+} & = H_{\mathrm{N}} - H_e - H_{\mathrm{N}^+} \\ \Delta H_2 = \alpha_{\mathrm{N}} H_{\mathrm{N}} - \alpha_e H_e - \alpha_{\mathrm{N}^{2+}} H_{\mathrm{N}^{2+}} & = H_{\mathrm{N}^+} - 2H_e - H_{\mathrm{N}^{2+}} \\ \Delta H_3 = \alpha_{\mathrm{N}} H_{\mathrm{N}} - \alpha_e H_e - \alpha_{\mathrm{N}^{3+}} H_{\mathrm{N}^{3+}} & = H_{\mathrm{N}^{2+}} - 3H_e - H_{\mathrm{N}^{3+}} \end{cases} \tag{8.13}$$

The systems in Eqs. (8.12) and (8.13) can be expressed in a compact form

$$\Delta H_m^\star = \sum_{i=1}^{\nu} a_{mi} H_i \qquad \text{and} \qquad \Delta H_m = \sum_{i=1}^{j} \alpha_{mi} H_i - H_m \tag{8.14}$$

The A_{mn} coefficients have the form

$$\begin{aligned} A_{mn} = {} & \frac{a_{n1}\vartheta}{\mathcal{D}_e^e} \alpha_{m1} \frac{x_n}{x_1} \\ & + \sum_{i=2}^{j} a_{ni} \frac{x_n}{\mathcal{D}_i^n} + \sum_{i=2}^{j} \sum_{k=2}^{\nu} a_{ni} \alpha_{mi} \frac{x_n}{x_i} \frac{x_k}{\mathcal{D}_i^k} - \sum_{i=2}^{j} \sum_{k=2}^{\nu} a_{nk} \alpha_{mk} \frac{x_n}{\mathcal{D}_i^k} \\ & + \sum_{i=j+1}^{\nu} a_{ni} \frac{x_n}{\mathcal{D}_i^n} - \sum_{i=j+1}^{\nu} \sum_{k=2}^{\nu} a_{ni} \alpha_{mk} \frac{x_n}{\mathcal{D}_i^k} - \sum_{k=2}^{\nu} a_{nn} \frac{x_k}{\mathcal{D}_n^k} \end{aligned} \tag{8.15}$$

where x_i represents the molar fraction of the ith component and $\mathcal{D}_i^j$ the binary diffusion coefficients.

Results obtained basically with this method (i.e. Devoto and Bonnefoi) have been reported for atmospheric N_2, H_2 and O_2 plasmas (Casavola et al.

1998; Capitelli et al. 2001, 2002). For all these systems we have considered only the dissociation and the first ionization reactions

$$A_2 \Leftrightarrow 2A$$

$$A \Leftrightarrow A^+ + e$$

We apply the Gibbs criterion to a two-temperature plasma, T_h characterizing translational and internal degrees of freedom (molecules, atoms and ions) and T_e characterizing the translational energy of free electrons. Under these conditions we obtain for the equilibrium constants of the dissociation and ionization reactions the following equations:

$$K_n = \frac{n_A^2}{n_{A_2}} = \left[\frac{(\pi m_A k_B T_h)^{3/2}}{(2)^{3/2} h_P{}^3} \frac{(Q_A^{el})^2}{Q_{A_2}^{rot} Q_{A_2}^{vib} Q_{A_2}^{el}}\right] \exp\left(-\frac{E_D}{k_B T_h}\right) \tag{8.16}$$

$$\left[\frac{n_{A^+}}{n_A}\right]^{\frac{1}{\vartheta}} n_e = \frac{(2\pi m_e k_B T_e)^{3/2}}{h_P{}^3} Q_e^{int} \left[\frac{Q_{A^+}^{int}(T_h)}{Q_A^{int}(T_h)}\right]^{\frac{1}{\vartheta}} \exp\left(-\frac{E_I}{k_B T_e}\right) \tag{8.17}$$

where E_D and E_I represent the dissociation and ionization energies and $\vartheta = T_e/T_h$ is the ratio between translational temperature of free electrons and the temperature of heavy particles (including ions). To get the composition we must couple Eqs. (8.16),(8.17) with the conservation equation for the total pressure and with the electro-neutrality condition. Once obtained the composition we can get through the methods of statistical thermodynamics the properties of the mixture. In the present example, as already anticipated, the thermodynamic properties of single species (translational and internal) are calculated at the gas temperature T_h, while the free electron properties are calculated at T_e. Before examining the results (Casavola et al. 1998) we want to remind that for one temperature plasma ϑ=1 the dissociation process is well separated from the ionization, while increasing the parameter ϑ we should observe a shift of the ionization equilibrium towards the dissociation one.

This point can be better appreciated by looking at Fig. 8.1 where we have reported the electron density as a function of translational temperature for different ϑ values. We can see that the maximum of electron density shifts towards lower translational temperatures with the increase of ϑ. For ϑ=2.5 the maximum of electron density occurs at about T_h=7,000 K. On the other hand the maximum of the atom number density tends to disappear with increasing ϑ, i.e. the atomic ionization equilibrium is such to transform the chemical reactions into

$$N_2 \Leftrightarrow 2N^+ + 2e,$$

i.e. the dissociation reaction practically disappears.

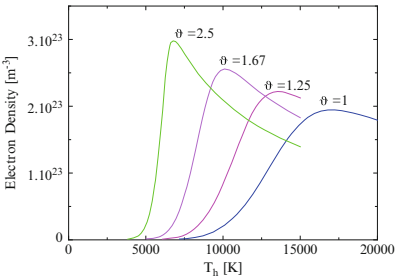

Fig. 8.1 Electron density versus T_h of N_2 plasma at different ϑ values

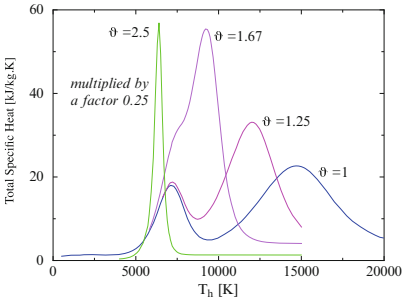

Fig. 8.2 Total specific heat versus T_h of N_2 plasma at different ϑ values

This is well evident looking at the behaviour of the total specific heat as a function of the translational temperatures at different ϑ values (see Fig. 8.2). Looking at the equilibrium curve for ϑ=1 we easily recognize two well-separated peaks, the first one due to the dissociation reaction and the second one due to the ionization reaction. The increase of ϑ is such to shift the ionization peak towards lower translational temperatures as well as to destroy the peak due to the dissociation reaction. At ϑ=2.5 we observe only one peak due to the ionization reaction. These simple considerations will help in the understanding of transport properties of two-temperature plasmas. We can write as usual the total thermal conductivity as

$$\lambda_{tot} = \lambda_{tr} + \lambda_{int} + \lambda_r \tag{8.18}$$

In turn the translational term can be split, as anticipated according to the well-known Devoto treatment, in two components, one due to free electrons (λ_e) and the other one to heavy particles (λ_h), i.e.

$$\lambda_{tr} = \lambda_e + \lambda_h \tag{8.19}$$

The results we are showing have been calculated by using the second approximation of the Chapman–Enskog method for λ_h and the third approximation for λ_e. Moreover the collision integrals entering in λ_h have been calculated at the gas temperature, while those entering in λ_e at T_e. λ_{int} have been calculated by using the Eucken approximation with the relevant collision integrals entering in it calculated at T_h. Finally λ_r has been calculated by the Bonnefoi equation inserting in it collision integrals calculated at T_h. In this equation electron–heavy-particle collision integrals have been calculated at T_e.

All the contributions will depend on the behaviour of the concentrations of the different species as a function of ϑ. So the shift of the ionization reaction as a function of ϑ will propagate its effects on λ_h by anticipating its maximum as a consequence of the higher concentrations of ions with their strong Coulomb

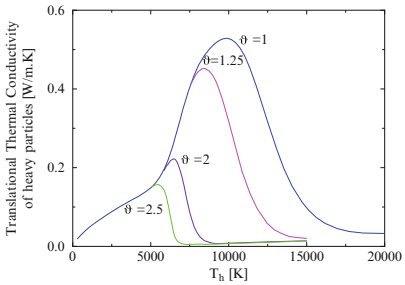

Fig. 8.3 Heavy-particle translational thermal conductivity versus T_h of N_2 plasma at different ϑ values

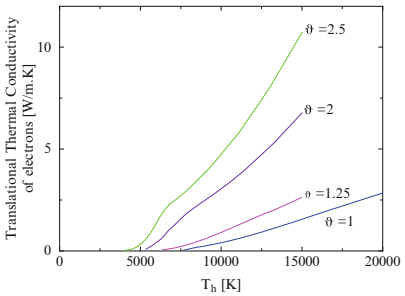

Fig. 8.4 Electron translational thermal conductivity versus T_h of N_2 plasma at different ϑ values

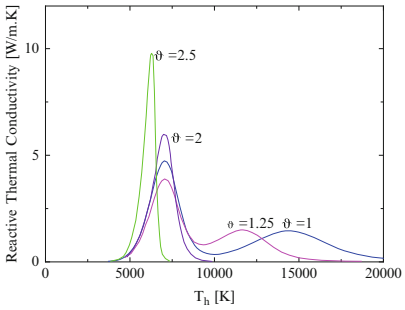

Fig. 8.5 Reactive thermal conductivity versus T_h of N_2 plasma at different ϑ values

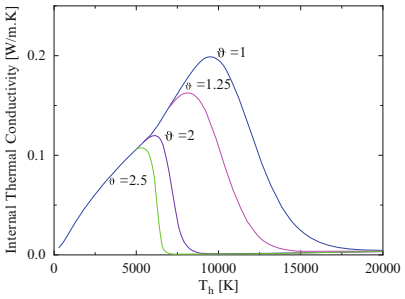

Fig. 8.6 Internal thermal conductivity versus T_h of N_2 plasma at different ϑ values

cross sections. On the other hand we can expect an anticipation of the onset of the importance of λ_e due to the corresponding trend of electron density. These points can be understood by looking at Figs. 8.3 and 8.4 where we have reported λ_h and λ_e for a nitrogen plasma as a function of T_h at different ϑ values.

Figures 8.5 and 8.6 report the trend of the reactive thermal conductivity λ_r and of λ_{int}. The behaviour of the reactive thermal conductivity closely follows the overlapping of the ionization reaction with the dissociation one; in particular passing from ϑ=1 to 2.5 we can observe the progressive disappearance of the dissociation peak which is substituted by the ionization one. To understand the trend of the internal contribution we must remind that in the present results this contribution comes from the rotational and vibrational contributions of nitrogen molecules as well as from the low-lying excited states of atomic nitrogen. Keeping in mind this point we can understand the trend of λ_{int} for the equilibrium case, i.e. ϑ=1. We see that in this case λ_{int} increases up to T=10,000 K presenting an abrupt decay from T=10,000 K on. In this temperature range we observe the progressive

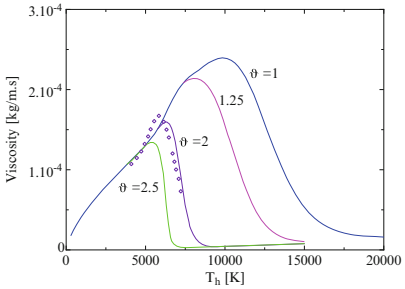

Fig. 8.7 Viscosity of N_2 plasma versus T_h of N_2 plasma at different ϑ values. For ϑ=2 the comparison with results by Aubreton et al. (1998), at p=1 bar, (*markers*) is shown

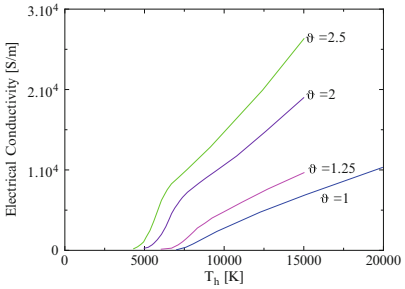

Fig. 8.8 Electrical conductivity of N_2 plasma versus T_h of N_2 plasma at different ϑ values

substitution of the ro-vibrational energy transport with the transport of low-lying excited states of atomic nitrogen. The increase of ϑ accelerates the ionization equilibrium, thus destroying the transport of internal energy of both atomic and molecular nitrogen.

Let us consider the behaviour of the viscosity of multi-temperature plasmas reported in Fig. 8.7. The mixture viscosity depends on heavy-particle collisions (electrons due to their mass are not a viscous fluid) and as such presents a trend very similar to λ_h. On the same arguments the electrical conductivity trend is very similar to λ_e strongly depending on the behaviour of electron density (see Fig. 8.8). A good agreement is found with the viscosity results by Aubreton et al. (1998) (Fig. 8.7), while the agreement of λ_{tot} with the corresponding results in the same reference is less satisfactory (Fig. 8.9). Discrepancies are probably due to the differences in the calculation of electronic partition function (at T_h in Casavola et al. 1998, while at T_e in Aubreton et al. 1998).

The results reported in the previous pages have been plotted as a function of translational temperature of heavy components. The same results can be plotted as a function of electron temperature getting similar trends (see Fig. 8.10). In particular Fig. 8.10a reports the reactive thermal conductivity of the nitrogen plasma as a function of T_e for different ϑ values. We can note that the peak due to the dissociation present at ϑ=1 and 1.25 disappears from ϑ=2 on merging itself with the corresponding ionization peak. This behaviour is reflected on the total thermal conductivity (in Fig. 8.10b), which presents only one peak for ϑ=2 and 3, as a result of the convolution of dissociation and ionization peaks. Finally Fig. 8.10c reports the viscosity as a function of T_e, whose trend tends to merge to the same values after the relevant maxima.

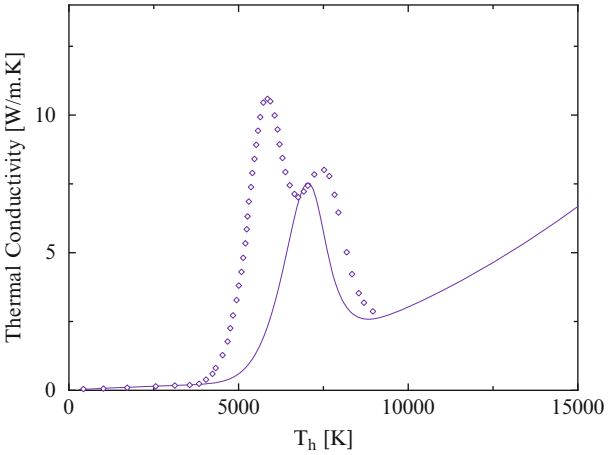

Fig. 8.9 Total thermal conductivity of nitrogen plasma at atmospheric pressure, as a function of T_h, for ϑ=2 (*solid lines*) compared with results by Aubreton et al. (1998), at p=1 bar (*markers*)

As a second example we report results for hydrogen plasmas comparing them with those by Boulos et al. (1994), the last obtained by using the same method with some differences in the temperature at which is calculated the internal partition function of atomic and molecular species. The relevant results are reported as a function of electron temperature in Fig. 8.11a–c for an atmospheric two-temperature hydrogen plasma composed by the following species: H_2, H^+, H and electrons. In particular Fig. 8.11a reports the different contributions of the total thermal conductivity as a function of electron temperature for ϑ =2 compared with the results by Boulos et al. 1994. The agreement between the results is rather satisfactory with the exception of the internal thermal conductivity which is much larger in the case of Boulos et al. results. This is probably due to the fact that our results have been obtained by using the Eucken approximation and imposing the diffusion cross sections of excited states calculated by the charge-transfer cross sections of ground state. Moreover the internal partition function is calculated at T_h in Capitelli et al. (2001, 2002) while at T_e in Boulos et al. (1994). Inspection of the figure shows the net distinction between the peak due to the dissociation process from that one of the ionization. Dissociation peak occurs at about T_e=7,000 K (i.e. T_h=3,500 K) while the ionization peak occurs at about T_e=15,000 K. The mutual influence between the reactive thermal conductivity of the dissociation and ionization peaks can be observed from Fig. 8.11b where we report λ_r as a function of T_e for ϑ=1,2,3. The dissociation peak is shifted at higher electron temperatures passing from ϑ=1 to 3 presenting also a strong decrease in its maximum. On the other hand the ionization peak is also shifted at higher T_e with the increase of ϑ presenting however higher values of the corresponding ionization peak. Also in this case a satisfactory

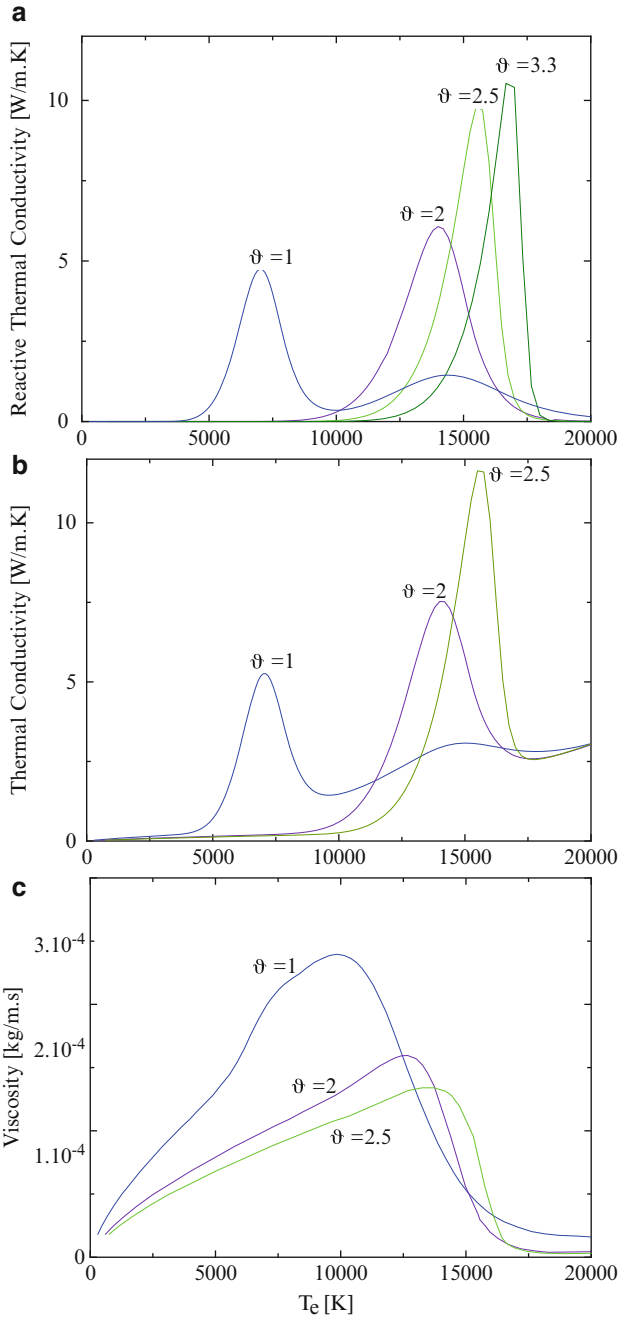

Fig. 8.10 Transport coefficients for atmospheric N_2 plasma as a function of electron temperature for different ϑ values. (**a**) Reactive thermal conductivity, (**b**) total thermal conductivity and (**c**) viscosity

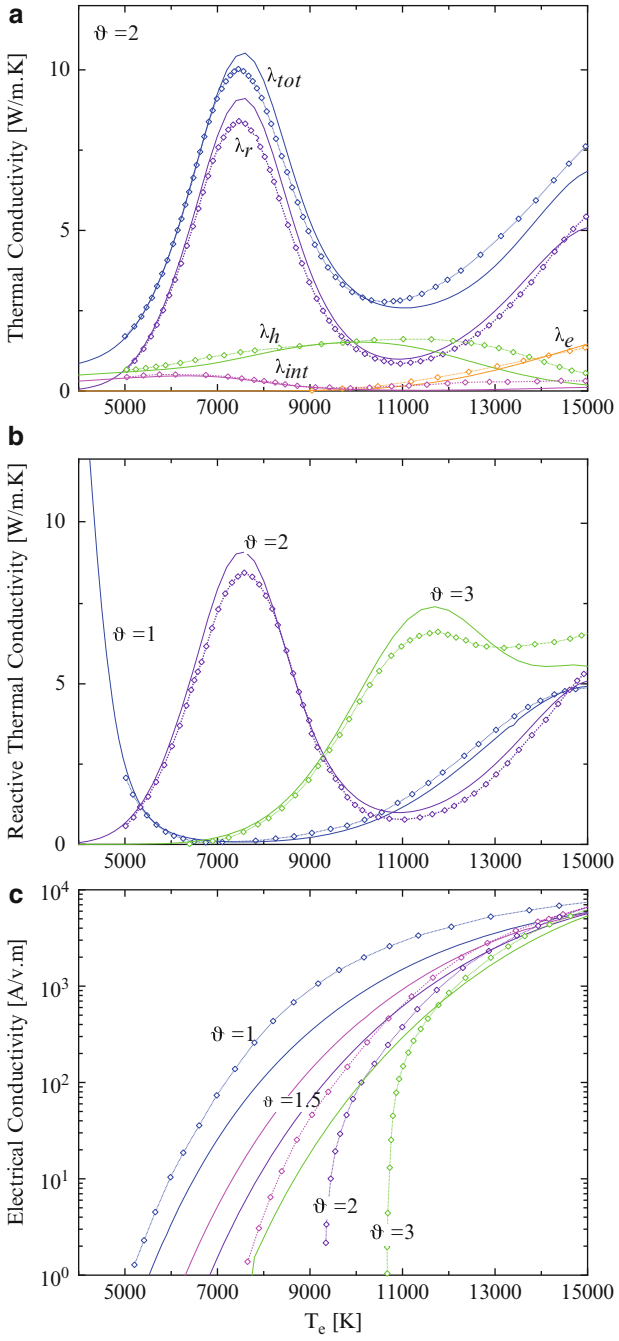

Fig. 8.11 (**a**) Thermal conductivity components of two-temperature hydrogen plasma for $\vartheta = 2$. (**b**) Reactive thermal conductivity of two-temperature hydrogen plasma for different values of ϑ. (**c**) Electrical conductivity of two-temperature hydrogen plasma for different values of ϑ. (*solid lines*) (Capitelli et al. 2001, 2002) (p=1 atm), (*dotted lines with markers*) (Boulos et al. 1994) (p=1 bar)

agreement is found with the Boulos et al. results. The situation drastically changes when comparing the present electrical conductivity values with the corresponding ones of Boulos et al. (Fig. 8.11c). In this case only a qualitative agreement is present in the two sets of results probably due also to the insertion of H_2^+ ion in the Boulos results as well as to different transport cross sections used in these cases.

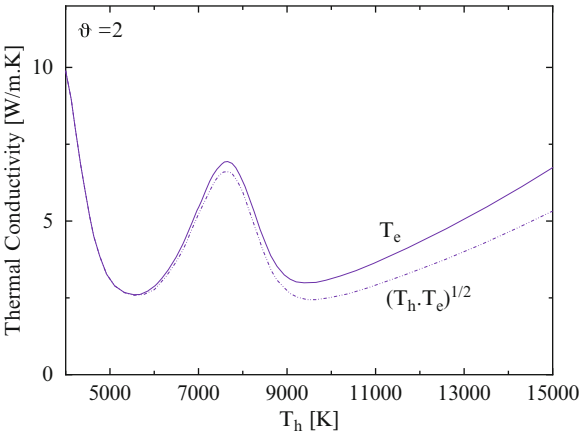

Fig. 8.12 Total thermal conductivity of hydrogen plasma at atmospheric pressure, as a function of T_h, for ϑ=2. Collision integrals for electron–heavy-particle interactions evaluated at T_e (*solid line*) and $(T_e T_h)^{1/2}$ (*dashed–dotted line*)

Before ending this section we want to show the dependence of the total thermal conductivity of a two-temperature H_2 plasmas on the choice of the temperature at which the collision integrals between electrons and heavy particles are calculated. The results as far reported have been calculated at T_e; an alternative choice could be $(T_e T_h)^{1/2}$. This last choice increases the corresponding e–e and e–ion Coulomb collision integrals decreasing at the same time the corresponding transport properties (in particular λ_e and σ_e). Figure 8.12 reports the total thermal conductivity calculated with the two choices of collision integrals at ϑ=2. We can see a large dependence of the corresponding total thermal conductivity on the choice of temperature at which the electron–atom, electron–ion and electron–electron collision integrals are calculated.

The reported results have been obtained by inserting in the relevant transport equations the thermodynamic properties (composition and partial pressure derivatives) obtained minimizing the Gibbs potential. Alternative methods however are used in the literature to get the thermodynamic properties depending on the thermodynamic criterion (minimization of Gibbs potential, maximization of entropy) and on the constraints used in the different methods. We report in the following the transport coefficients for two-temperature

H_2 plasmas obtained by using different two-temperature Saha equations in the Bonnefoi and Devoto approach. In particular we consider the following different Saha equations for the ionization reaction of atomic hydrogen, T_{el} being the temperature characterizing the distribution of electronic levels:

- Minimization of Gibbs potential with $T_h = T_{el} \neq T_e$

$$\left[\frac{n_{H^+}}{n_H}\right]^{\frac{1}{\vartheta}} n_e = \frac{(2\pi m_e k_B T_e)^{3/2}}{h_P{}^3} Q_e^{int} \left[\frac{Q_{H^+}^{int}(T_h)}{Q_H^{int}(T_h)}\right]^{\frac{1}{\vartheta}} \exp\left(-\frac{E_I}{k_B T_e}\right) \quad (8.20)$$

- Minimization of Gibbs potential with $T_h \neq T_{el} = T_e$

$$\left[\frac{n_{H^+}}{n_H}\right]^{\frac{1}{\vartheta}} n_e = \frac{(2\pi m_e k_B T_e)^{3/2}}{h_P{}^3} Q_e^{int} \left[\frac{Q_{H^+}^{int}(T_e)}{Q_H^{int}(T_e)}\right] \exp\left(-\frac{E_I}{k_B T_e}\right) \quad (8.21)$$

- Maximization of entropy with $T_h \neq T_{el} = T_e$

$$\left[\frac{n_{H^+}}{n_H}\right] n_e = \frac{(2\pi m_e k_B T_e)^{3/2}}{h_P{}^3} Q_e^{int} \left[\frac{Q_{H^+}^{int}(T_e)}{Q_H^{int}(T_e)}\right] \exp\left(-\frac{E_I}{k_B T_e}\right) \quad (8.22)$$

- Maximization of entropy with $T_h = T_{el} \neq T_e$

$$\left[\frac{n_{H^+}}{n_H}\right] n_e = \frac{(2\pi m_e k T_e)^{3/2}}{h_P{}^3} Q_e^{int} \left[\frac{Q_{H^+}^{int}(T_h)}{Q_H^{int}(T_h)}\right] \exp\left(-\frac{E_I}{k_B T_h}\right) \quad (8.23)$$

where Q_e^{int}=2 and $Q_{H^+}^{int}$=1, the nuclear partition function of H^+ is not considered, cancelling with the corresponding one for H. Comparison of the different equilibrium equations for our case study (i.e. H_2 plasmas) shows differences in both the exponential ϑ factor disappearing in the equations, which derive from the maximization of entropy as well as on the different temperatures appearing in the partition function and in the exponential term. Again we note that all exponential terms contain the electron temperature with the exception of Eq. (8.23) which contains the heavy-particle temperature. This difference should have strong consequences in the relevant results. It should be noted that Eq. (8.22) is nowadays the most used equation for the two-temperature plasmas based on the "kinetic" idea that electrons are responsible of the ionization equilibrium as well as of the excitation one, i.e. mixing thermodynamic and kinetic concepts being a little contradictory (Capitelli et al. 2011). Before illustrating the results we want to warn the reader that we will present them in a different way as compared with our previous case study. The presentation of results taken from Capitelli et al. (2001) is made either as a function of T_h (in the range 2,500–10,000 K) keeping constant T_e=10,000 K or as a function of T_e (in the range 8,000–30,000 K) at constant T_h=8,000 K, thus meaning that the different plots are made at different ϑ values rather than at fixed ϑ as done in the previous presentation.

In the first case only the electron density is strongly affected by the choice of the different equations while atomic and molecular hydrogen densities scarcely depend on this choice (Capitelli et al. 2011). In any case electron and ion densities keep values well below the corresponding values for atomic and molecular hydrogen (at T_h=T_e=10,000 K the electron density is a factor 100 less than atom density). As a consequence only the transport coefficients which depend on the electron density (i.e. λ_e and electrical conductivity σ_e) will be affected by the choice of the equilibrium constants. This is indeed the case as can be appreciated by looking at Fig. 8.13a, where we have reported σ_e versus T_h at T_e=10,000 K for an atmospheric hydrogen plasma calculated inserting in the transport equations the compositions coming from Eqs. (8.20)-(8.23). No appreciable change is observed by using Eqs. (8.20),(8.21), while the use of Eq. (8.22) strongly increases the electrical conductivity. On the other hand use of Eq. (8.23) is such to strongly underestimate the electrical conductivity as a consequence of the exponential factor calculated at T_h (see Eq. (8.23)). All the σ_e curves converge to the same values for the one-temperature case, i.e. T_h=T_e=10,000 K.

Let us consider now the results obtained as a function of T_e for T_h=8,000 K. In this case the influence of T_e can play an important role when $T_e \geq 2T_h$, i.e. from 15,000 K on. This is indeed the case as shown in Fig. 8.13b, where we have reported the total thermal conductivity calculated by inserting in the transport equations the different compositions coming from Eqs. (8.20)–(8.23). Inspection of the results shows that Eqs. (8.20) and (8.21) give practically the same results, while an appreciable change is observed when using the maximization of entropy in the form of Eq. (8.22). Again we note that use of Eq. (8.23) does not allow the onset of the ionization reaction yielding a total thermal conductivity basically given by the atomic hydrogen contribution.

The results reported in Fig. 8.13b suffer to some extent the fact that the use of Bonnefoi theory for λ_r is correct only when use is made of Eq. (8.20). This point will be analysed in the next section when other theoretical approaches for the reactive thermal conductivity will be introduced and used.

8.2 Beyond the Devoto and Bonnefoi Approaches

The results reported in the previous pages have been obtained by essentially decoupling the electron component from the heavy ones as well as by calculating the reactive thermal conductivity by using the Bonnefoi approach. This last approach has been derived by following the old Butler–Brokaw approach, inserting in it composition and partial pressure derivatives from the minimization of the Gibbs potential. More recently other schemes have been proposed to improve these results. We refer in particular to the Rat et al. (2002c, 2008) approach for calculating diffusion coefficients, viscosity, electrical conductivity and translational thermal conductivity and to the theory of

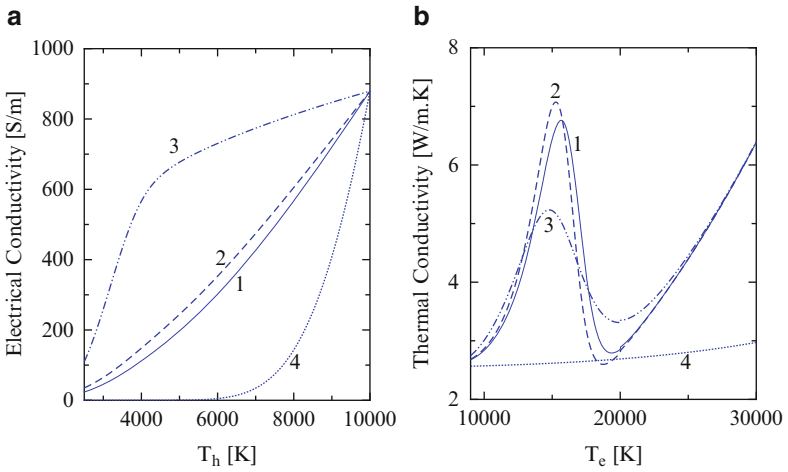

Fig. 8.13 Transport coefficients of H_2 plasma, corresponding to different Saha equations. (1) Eq. (8.20), (2) Eq. (8.21), (3) Eq. (8.22), (4) Eq. (8.23). (**a**) Electrical conductivity versus T_h at T_e=10,000 K, (**b**) total thermal conductivity versus T_e at T_h=8,000 K

Chen and Li (2003) (Li and Chen 2001) for the reactive thermal conductivity (see also Bose et al. 1985).

8.2.1 The Rat Approach

Following the approach by Rat et al. (2002c, 2008) no decoupling between electrons and heavy particles is allowed so that the diffusion velocity is written as

$$\boldsymbol{V}_i = \frac{n}{n_i \rho k_B T_i} \sum_{j=1}^{N} m_j (D_i^j \boldsymbol{d}_j + D_i^{\vartheta,j} g_j \nabla \ln \vartheta) - \frac{D_i^T}{n_i m_i} \nabla \ln T_h - \frac{D_i^{\vartheta\star}}{n_i m_i} \nabla \ln \vartheta \tag{8.24}$$

From this one can build up a set of new expressions for transport coefficients and coupling terms in the mass, momentum and energy flux definitions. These equations have been applied to an Ar/H_2 plasma for different ϑ values and compared with the Bonnefoi results based on the Devoto approach. Large differences were found both in the electrical conductivity and in the electron translational thermal conductivity pushing the authors to conclude that the Devoto approach cannot be used. The reported differences are probably due to the different two-temperature equilibrium compositions used by Rat et al. and by Bonnefoi. The first in fact used the maximization of the entropy contrary to the Bonnefoi approach based on the minimization of

Gibbs potential. This point becomes clear when comparing the results of the two approaches (Devoto 1967a; Rat et al. 2002a) using the same two-temperature equilibrium composition as recently shown by Colombo et al. (2008, 2009, 2011). In this case in fact the comparison of the transport values obtained by the two transport methods, i.e. Devoto and Rat approaches, are made by using the same two-temperature equilibrium composition derived from entropy maximization. In this case an excellent agreement (Colombo et al. 2011) has been reported for the total thermal conductivity, for the viscosity and the electrical conductivity (Fig. 8.14) for a CO_2 plasma in a wide temperature range. Note also the two methods also produce an excellent agreement in the viscosity values because this quantity depends on heavy particles rather than on electrons. Some differences are found in some multicomponent diffusion coefficients. These results indicate that the Devoto approach, i.e. the decoupling between heavy particles and electron distribution functions can be used with a fair amount of confidence in the calculation of two-temperature plasma transport coefficients(λ_e, λ_h and σ_e) once selected the appropriate two-temperature Saha equation.

Note also that Colombo et al. (2011) calculate the total thermal conductivity by using the Devoto approach for λ_e and λ_h and the Rat approach for λ_r.

8.2.2 The Reactive Thermal Conductivity: The Chen and Li Approach

The thermal conductivity values reported in the previous sections have been obtained by using the Devoto approach for all quantities but the reactive thermal conductivity obtained by Bonnefoi method which uses the non-equilibrium composition from the Potapov method (i.e. the minimization of Gibbs potential) (Potapov 1966). Basically the same approach is followed by Chen and Li (2003) (Li and Chen 2001), who however use the maximization of entropy to get the equilibrium compositions and their derivatives entering the transport equation. The theory was first applied to the case of an argon plasma composed by four components (Ar, Ar^+, Ar^{2+} and electrons, with the index j moving from 1 to 4) and two independent reactions (r=2) describing the first and second ionization process, i.e.

$$\begin{aligned} Ar &\Leftrightarrow Ar^+ + e \\ Ar^+ &\Leftrightarrow Ar^{2+} + e \end{aligned}$$

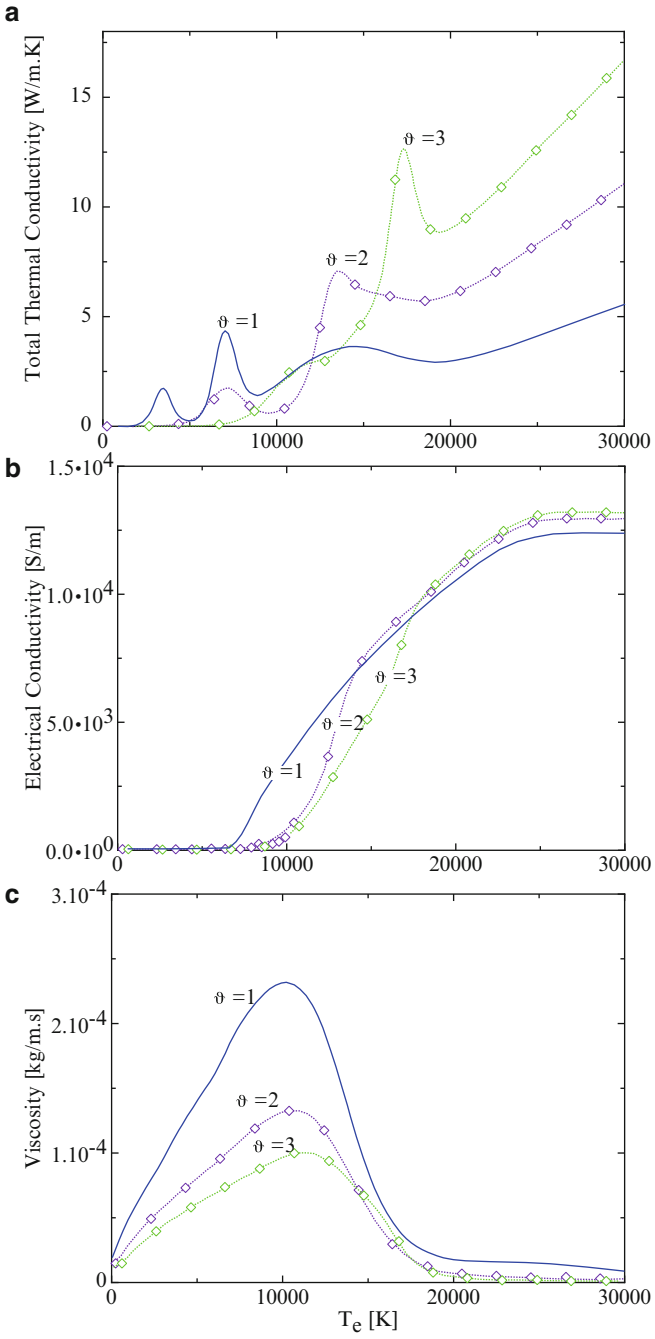

Fig. 8.14 Transport coefficients of two-temperature CO_2 mixture for different values of $\vartheta = T_e/T_h$. (**a**) Total thermal conductivity, (**b**) electrical conductivity and (**c**) viscosity. For ϑ=2 and 3 results obtained with simplified Devoto approach (*markers*) (Devoto 1967a) and with non-simplified theory by Rat et al. (2002a) are compared

The heat flux was then written as

$$\begin{aligned}\boldsymbol{q}_r &= -\sum_{r=1}^{2} \Delta H_r^{\star} \boldsymbol{\Psi}_r \\ &= -\sum_{r=1}^{2} \frac{n}{\rho k_{\mathrm{B}} T_h} \Delta H_r^{\star} \sum_{j=1}^{4} \frac{T_h}{T_j} m_j D_{rj}^{a} \nabla p_j \end{aligned} \tag{8.25}$$

where p_j is the partial pressure of the jth species, $\Delta H_r^{\star}$ and D_{rj}^{a} are, respectively, the reaction enthalpy change, for the rth reaction, and the ambipolar diffusion coefficient defined in terms of ordinary diffusion coefficients (Li and Chen 2001). The gradient of each partial pressure can be expressed as

$$\nabla p_j = \frac{\partial p_j}{\partial T_e} \nabla T_e + \frac{\partial p_j}{\partial T_h} \nabla T_h \qquad (j = 1 - 4) \tag{8.26}$$

Equation (8.25) therefore becomes

$$\begin{aligned}\boldsymbol{q}_r &= -\sum_{r=1}^{2} \frac{n}{\rho k_{\mathrm{B}} T_h} \Delta H_r^{\star} \left(\sum_{j=1}^{3} m_j D_{rj}^{a} \frac{\partial p_j}{\partial T_e} + \frac{T_h}{T_e} m_e D_{re}^{a} \frac{\partial p_e}{\partial T_e} \right) \nabla T_e \\ &\quad -\sum_{r=1}^{2} \frac{n}{\rho k_{\mathrm{B}} T_h} \Delta H_r^{\star} \left(\sum_{j=1}^{3} m_j D_{rj}^{a} \frac{\partial p_j}{\partial T_h} + \frac{T_h}{T_e} m_e D_{re}^{a} \frac{\partial p_e}{\partial T_h} \right) \nabla T_h \\ &= \lambda_{re} \nabla T_e + \lambda_{rh} \nabla T_h \end{aligned} \tag{8.27}$$

where

$$\lambda_{re} = -\sum_{r=1}^{2} \frac{n}{\rho k_{\mathrm{B}} T_h} \Delta H_r^{\star} \left(\sum_{j=1}^{3} m_j D_{rj}^{a} \frac{\partial p_j}{\partial T_e} + \frac{T_h}{T_e} m_e D_{re}^{a} \frac{\partial p_e}{\partial T_e} \right) \tag{8.28}$$

$$\lambda_{rh} = -\sum_{r=1}^{2} \frac{n}{\rho k_{\mathrm{B}} T_h} \Delta H_r^{\star} \left(\sum_{j=1}^{3} m_j D_{rj}^{a} \frac{\partial p_j}{\partial T_h} + \frac{T_h}{T_e} m_e D_{re}^{a} \frac{\partial p_e}{\partial T_h} \right) \tag{8.29}$$

can be defined as the reactive thermal conductivity due to electrons and to the heavy particles. The reactive thermal conductivity defined with respect to the gradient of heavy-particle temperature can be then written as

$$\lambda_r = (\lambda_{rh} + \vartheta \lambda_{re}) \tag{8.30}$$

The partial derivatives appearing in Eqs. (8.28)–(8.29) can be obtained by the set of Saha equations, by the Dalton law and by the quasi-neutrality condition. These quantities strongly depend on the selected Saha equations. An alternative method to get the partial pressure derivatives is to obtain them by numerical differentiation of the non-equilibrium composition.

Equations (8.28)–(8.29) are nowadays widely used in the literature in combination with the maximization of entropy to get all the necessary thermodynamic quantities (Ghorui et al. 2007a, 2008; Colombo et al. 2008, 2009, 2011; Wang et al. 2011, 2012). The reason can be ascribed to the easy insertion of the equations in the fluid dynamics of two-temperature plasmas (Ghorui et al. 2007b).

Let us now discuss the most important results obtained by Chen and Li on the reactive thermal conductivity of a two-temperature argon plasma. Figure 8.15 reports the relevant results for ϑ=5 calculated with the following hypotheses:

Case 1. Two-temperature Saha equation from the minimization of the Gibbs potential [Potapov equation (Potapov 1966), i.e. Eq. (8.20)] and reactive thermal conductivity from Hsu (1982)

Case 2. Two-temperature Saha equation from the minimization of the Gibbs potential (Potapov equation) and reactive thermal conductivity from $\lambda_r = (\lambda_{rh} + \vartheta\lambda_{re})$

Case 3. Two-temperature Saha equation from the entropy maximization of the Gibbs potential [van de Sanden equation (van de Sanden et al. 1989), i.e. Eq. (8.22)] and reactive thermal conductivity from Hsu (1982)

Case 4. Two-temperature Saha equation from the entropy maximization of the Gibbs potential (van de Sanden equation) and reactive thermal conductivity from $\lambda_r = (\lambda_{rh} + \vartheta\lambda_{re})$

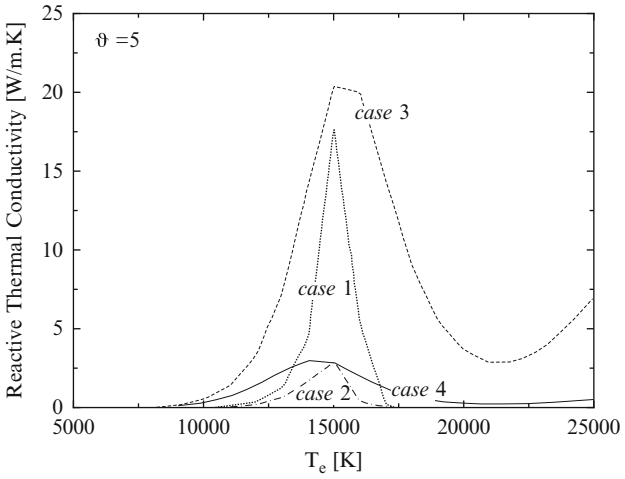

Fig. 8.15 Comparison of the calculated values of the reactive thermal conductivity of the two-temperature argon plasma at atmospheric pressure for the four different cases reported in the text (Chen and Li 2003)

Inspection of the Fig. 8.15 shows strong differences in the values obtained in the four examined cases, the more reliable results according to Chen and Li are those calculated for case 4. The results reported for cases 1 and 3 can be ruled off because they are obtained by using a reactive transport equation which is valid only for one-temperature plasma (i.e. the Butler–Brokaw one). The differences in the results of cases 2 and 4, obtained by using the same correct reactive transport equation, derive from a different choice of the two-temperature Saha equation (minimization of Gibbs potential against maximization of the entropy). This choice introduces large differences in the λ_r results, these differences tending to decrease at low values of the ϑ parameter. Similar results have been recently derived by Wang et al. (2012) for the reactive thermal conductivity of a nitrogen plasma. These authors basically extend the Chen and Li theory to nitrogen plasmas comparing the results with the corresponding ones obtained by using the Potapov criterion (Potapov 1966). Inspection of Fig. 8.16 emphasizes the differences of the relevant values. In particular the use of Potapov equilibrium (*case B*) underestimates the values of λ_r as compared with the van de Sanden theory (*case A*) (van de Sanden et al. 1989), confirming the results reported by Chen and Li for argon.

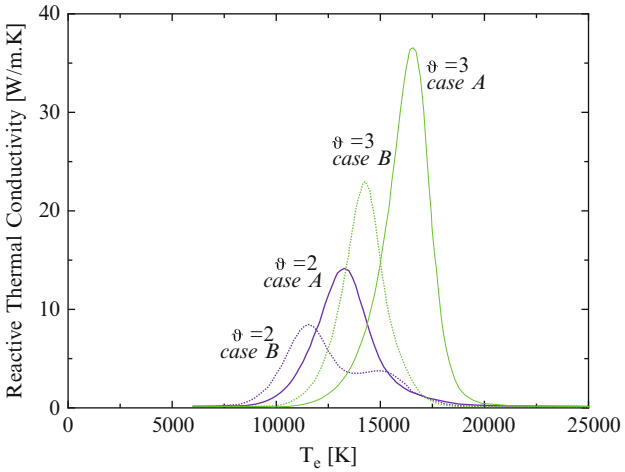

Fig. 8.16 Comparison of the calculated values of the reactive thermal conductivity of the two-temperature nitrogen plasma at atmospheric pressure for ϑ=2 and 3 in cases A and B (see text for details) (Wang et al. 2012)

The Chen and Li approach is presently used by different authors. Ghorui et al. (2008) in fact have reported an extended study of the transport coefficients of two-temperature N_2–O_2 plasmas for different N_2/O_2 ratios and different pressures. The results were obtained by using:

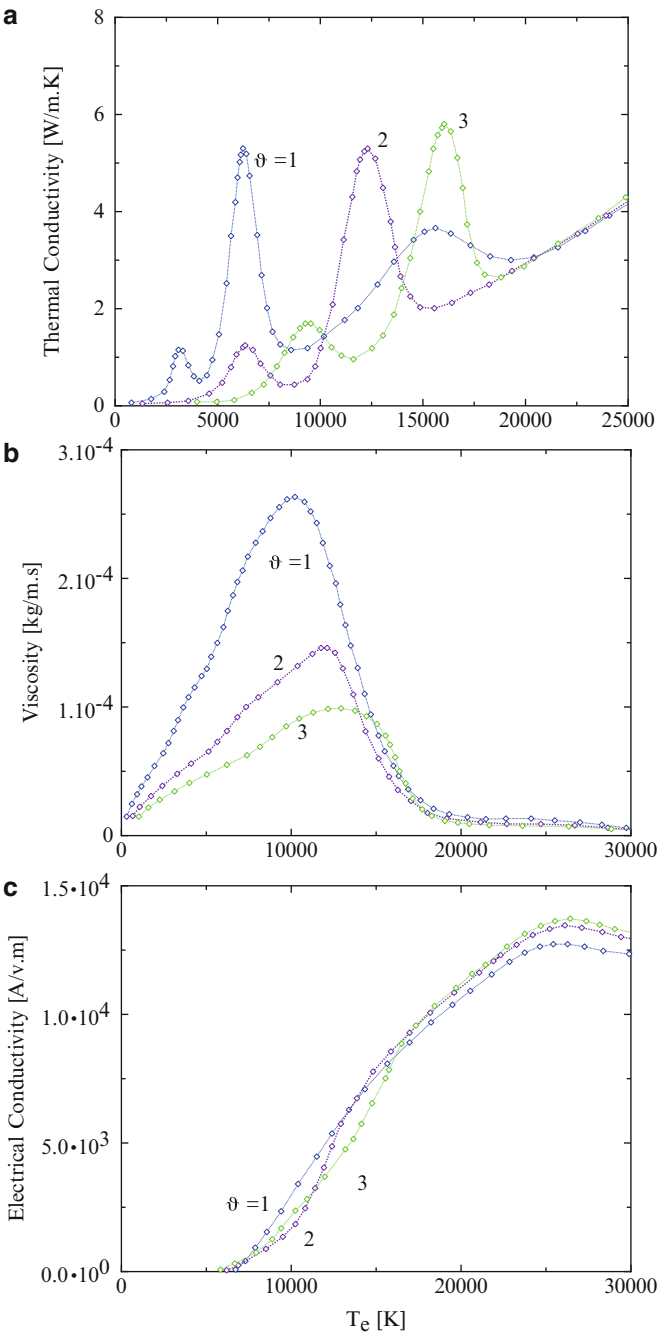

Fig. 8.17 Transport properties of two-temperature air plasma for different values of $\vartheta = T_e/T_h$ at p=1 atm for N_2–O_2 mixture (80:20) (Ghorui et al. 2008). (**a**) Total thermal conductivity, (**b**) viscosity, (**c**) electrical conductivity

(*i*) The van de Sanden equation for the two-temperature Saha equation (i.e. the maximization of entropy)
(*ii*) The Devoto approach for the viscosity, the translational thermal conductivity of heavy particles and of electrons, and the electrical conductivity
(*iii*) The Bose approach for calculating the reactive thermal conductivity (i.e. the same approach used by Chen and Li)

This last term differs, as already pointed out, from the Bonnefoi approach for the calculation of the relevant pressure gradients derived from the van de Sanden approach rather than from the Potapov one. The reactive thermal conductivity from the dissociation process is indeed the same. A sample of results are reported in Fig. 8.17, which respectively show the behaviour of the total thermal conductivity, the viscosity and the electrical conductivity for a N_2–O_2 80/20 % atmospheric air mixture for different ϑ values. The trends of the different quantities follow those already discussed in the previous sections. A peculiarity is however present in the case of N_2–O_2 mixture linked to the O_2/O dissociation peak. This peak moves with the increase of ϑ without merging with the ionization peak as observed in the case of N_2/N system.

In particular the viscosity and the electrical conductivity are very similar to those reported for CO_2 in Fig. 8.14c, thus meaning that the CO_2 and air plasmas should behave in a similar way (see Capitelli et al. 2011). The behaviour of the total thermal conductivity is indeed different for CO_2 and N_2–O_2 plasmas, being the results by Ghorui et al. lower than the corresponding ones by Colombo et al.

The same problem occurs when comparing the total thermal conductivity calculated by Ghorui et al. (2008) with the corresponding results reported by Wang et al. (2011) for nitrogen. The differences are probably due to the fact at Ghorui et al. define their total reactive thermal conductivity without ϑ, i.e.

$$\lambda_r = (\lambda_{rh} + \lambda_{re}) \tag{8.31}$$

8.3 Concluding Remarks and Perspectives

We have reported in this chapter results of transport coefficients of two-temperature plasmas obtained according to different approaches. The results strongly depend on the thermodynamic model used in the calculation of the multi-temperature equilibrium composition to be inserted in the transport equations. Nowadays the method first developed by van de Sanden et al. (1989), i.e. the maximization of entropy, seems to be preferred by the literature even though we want to remind the still open problem associated with the multiplicity of Saha equations coming from a correct use of thermodynamics (Giordano and Capitelli, 1995, 2001; Capitelli et al., 2011).

An alternative could be to use a kinetic approach to calculate the composition of two-temperature plasmas, as described by Rat and Aubreton (Rat et al. 2002b, 2008) with results largely different from the corresponding ones obtained by the two-temperature Saha equation especially in the ionization regime.

The stationary kinetic calculation (Rat et al. 2002b; Richley and Tuma 1982; Hingana 2010) solves a set of differential equations for the relevant forward and reverse processes occurring in the plasma (Ar–H_2 in this case). The kinetic coefficients entering the kinetic equations are expressed in an Arrhenius-type form with different temperatures (T_e, T_h, T_{exc}, i.e. electron, heavy-particle and excitation temperatures) entering the forward reactions, while the reverse process coefficients are calculated by micro-reversibility using a two-temperature Saha equation (maximization of entropy). Details can be found in Rat et al. (2002b) (see also Hingana 2010). As an example Fig. 8.18 reports the total thermal conductivity calculated according the stationary kinetic model (λ_T^{kin}) with the corresponding ones calculated with the two-temperature thermodynamic model (λ_T^{th}) for ϑ=1.6 and 2. For ϑ=1.6 a good agreement is found in the two approaches in the dissociation region, while for ϑ=2 the two theories give a different dissociation peak. Furthermore for a temperature range 8,000–11,000 K the kinetic method leads to an ionization delay of argon atoms, $\lambda_T^{kin} < \lambda_T^{th}$, while for T_e >11,000 K an avalanche phenomenon of the argon ionization is such to reverse the calculated values, i.e. $\lambda_T^{kin} > \lambda_T^{th}$.

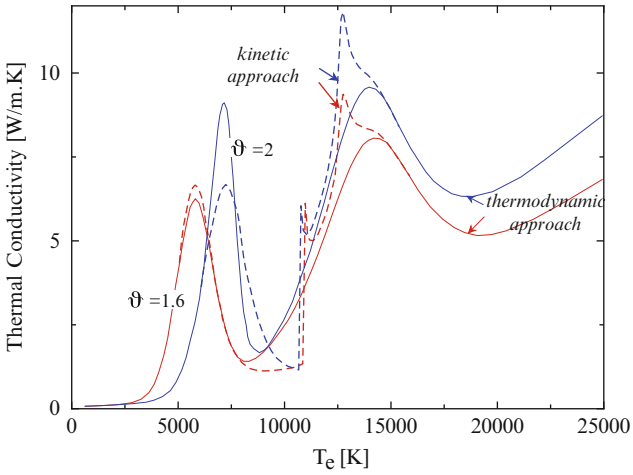

Fig. 8.18 Total thermal conductivity of atmospheric-pressure Ar–H_2 (50 mol.%) mixture with electron temperature using compositions calculated by the stationary kinetic calculation (*dashed lines*) and the equilibrium constant method (*solid lines*) for ϑ=1.6 and 2

The kinetic approach has been also used by Nemchinsky (2005) to separate the electron and heavy-particle contributions of the reactive thermal conductivity in the dissociation regime of a non-equilibrium nitrogen plasma. At the same time the reactive thermal conductivity obtained by Eqs. (8.28)–(8.29) are nowadays preferred to the Bonnefoi approach even though an accurate comparison between the relevant equations is still lacking. An accurate comparison of the Bonnefoi approach and that one of Chen and Li should be welcome also to shed light on the different reactive transport equations in the literature which in some cases are the same equations with different names.

Finally we want to remind that the results reported in this section have calculated the internal thermal conductivity with the Eucken approximation introducing in the relevant equations diffusion coefficients in the *usual* approximation for the transport cross sections. Of course the problems associated with the insertion of the *abnormal* cross sections discussed in Chap. 7 should be taken into account also in the two-temperature situations. This is more and more true at high ϑ values when the ionization equilibrium is shifted at very high temperatures allowing the excitation of electronic states of atoms without losing them in the ionization process. This point has been reported by Wang et al. (2011), which have shown that for ϑ=20 the internal contribution to the thermal conductivity dominates all the other contributions implying the importance of a correct treatment of the internal thermal conductivity as in Chap. 7. In this case however caution should be exercised when using two-temperature transport theories because we can meet situations typical of cold plasmas where the electron energy distribution function is far from being Maxwellian, as well as the vibrational and in some cases rotational distributions are far from the Boltzmann ones. In this case the Chapman–Enskog method for solving the Boltzmann equation can give erroneous results.

References

Aubreton J, Bonnefoi C, Mexmain JM (1986) Calcul de propriétés thermodynamiques et des coefficients de transport dans un plasma Ar-O_2 en non-équilibre thermodynamique et à la pression atmosphérique. Revue de Physique Appliquèe (Paris) 21(6):365–376

Aubreton J, Elchinger MF, Fauchais P (1998) New method to calculate thermodynamic and transport properties of a multi-temperature plasma: application to N_2 plasma. Plasma Chem Plasma P 18(1):1–27

Bonnefoi C (1983) Contribution to the study of methods to solve the Boltzmann's equation in a two temperature plasma: Ar-H_2 mixture (in french). State thesis, University of Limoges, France

Bonnefoi C, Aubreton J, Mexmain JM (1985) New approach taking into account elastic and inelastic processes for transport properties of two temperature plasmas. Zeitschrift für Naturforschung A (Astrophysik, Physik und Physikalische Chemie) 40a:885–891

Bose TK, Kannappan D, Seeniraj RV (1985) On reactive heat conduction for multiple ionized two-temperature argon plasma. Heat Mass Transf 19:3–8

Boulos MI, Fauchais P, Pfender E (1994) Thermal plasmas: fundamentals and applications, vol 1. Plenum Press, New York

Capitelli M, Colonna G, Gorse C, Minelli P, Pagano D, Giordano D (2001) Two-temperature saha equations: Effects on thermophysical properties of hydrogen plasmas. AIAA paper pp 2001–3018

Capitelli M, Colonna G, Gorse C, Minelli P, Pagano D, Giordano D (2002) Two-temperature Saha equations. effects on thermophysical properties of H_2 plasmas. J Thermophys Heat Transf 16(3):469–472

Capitelli M, Colonna G, D'Angola A (2011) Fundamental aspects of plasma chemical physics: Thermodynamics. Springer series on atomic, optical, and plasma physics, vol 66. Springer, New York

Casavola A, Cascarano C, Milella A, Minelli P, Mininni R, Pagano D, Sardella E, Capitelli M, Colonna G, Gorse C (1998) Problems in the determination of thermodynamic and transport properties of multi-temperature plasmas. Proceedings of 3rd European Symposium on Aerothermodynamics for Space Vehicles, Noordwijk 24–26 november 1998 ESA SP-426:357–363

Chen X, Li HP (2003) The reactive thermal conductivity for a two-temperature plasma. Int J Heat Mass Transf 46(8):1443–1454

Colombo V, Ghedini E, Sanibondi P (2008) Thermodynamic and transport properties in non-equilibrium argon, oxygen and nitrogen thermal plasmas. Prog Nucl Energ 50(8):921–933

Colombo V, Ghedini E, Sanibondi P (2009) Two-temperature thermodynamic and transport properties of argon-hydrogen and nitrogen-hydrogen plasmas. J Phys D: Appl Phys 42(5):055213

Colombo V, Ghedini E, Sanibondi P (2011) Two-temperature thermodynamic and transport properties of carbon-oxygen plasmas. Plasma Sources Sci T 20(3):035003

Devoto RS (1967a) Simplified expressions for the transport properties of ionized monatomic gases. Phys Fluids 10(10):2105–2112

Devoto RS (1967b) Transport coefficients of partially ionized argon. Phys Fluids 10(2):354–364

Ghorui S, Heberlein J, Pfender E (2007a) Thermodynamic and transport properties of two-temperature oxygen plasmas. Plasma Chem Plasma P 27:267–291

Ghorui S, Heberlein JVR, Pfender E (2007b) Non-equilibrium modelling of an oxygen-plasma cutting torch. J Phys D: Appl Phys 40(7):1966–1976

Ghorui S, Heberlein JVR, Pfender E (2008) Thermodynamic and transport properties of two-temperature nitrogen-oxygen plasma. Plasma Chem Plasma P 28(4):553–582

Giordano D, Capitelli M (1995) Two-temperature Saha equation: A misunderstood problem. J Thermophys Heat Transf 9:803–804

Giordano D, Capitelli M (2001) Nonuniqueness of the two-temperature Saha equation and related considerations. Phys Rev E 65:016401

Hingana H (2010) Contribution à l'étude des propriétés des plasmas à deux températures : application à l'argon et l'air (in french). PhD thesis, Universitè de Toulouse, France

Hsu KC (1982) A self-consistent model for the high intensity free-burning argon arc. PhD thesis, Department of Mechanical Engineering, University of Minnesota, USA

Li HP, Chen X (2001) Diffusion in two-temperature partially ionized gases. Chinese Phys Lett 18(4):547–549

Nemchinsky V (2005) Dissociation reactive thermal conductivity in a two-temperature plasma. J Phys D: Appl Phys 38(20):3825

Potapov A (1966) Chemical equilibrium of multitemperature systems. High Temp 4:48

Rat V, André P, Aubreton J, Elchinger M, Fauchais P, Lefort A (2002a) Two-temperature transport coefficients in argon-hydrogen plasmas I: Elastic processes and collision integrals. Plasma Chem Plasma P 22:453–474

Rat V, André P, Aubreton J, Elchinger M, Fauchais P, Lefort A (2002b) Two-temperature transport coefficients in argon-hydrogen plasmas II: Inelastic processes and influence of composition. Plasma Chem Plasma P 22:475–493

Rat V, André P, Aubreton J, Elchinger MF, Fauchais P, Vacher D (2002c) Transport coefficients including diffusion in a two-temperature argon plasma. J Phys D: Appl Phys 35(10):981–991

Rat V, Murphy AB, Aubreton J, Elchinger MF, Fauchais P (2008) Treatment of non-equilibrium phenomena in thermal plasma flows. J Phys D: Appl Phys 41(18):183001

Richley E, Tuma DT (1982) On the determination of particle concentrations in multitemperature plasmas. J Phys 53(12):8537–8542

van de Sanden MCM, Schram PPJM, Peeters AG, van der Mullen JAM, Kroesen GMW (1989) Thermodynamic generalization of the saha equation for a two-temperature plasma. Phys Rev A 40(9):5273

Wang WZ, Rong MZ, Yan JD, Murphy AB, Spencer JW (2011) Thermophysical properties of nitrogen plasmas under thermal equilibrium and non-equilibrium conditions. Phys Plasmas 18(11):113502

Wang WZ, Rong MZ, Yan JD, Wu Y (2012) The reactive thermal conductivity of thermal equilibrium and non-equilibrium plasmas: application to nitrogen. IEEE T. Plasma Sci. DOI 10.1109/TPS.2012.2185717

Chapter 9
Transport Properties in the Presence of Magnetic Fields

The presence of the magnetic field breaks the isotropy of the gas system because velocities in a plane normal to the field are modified, while velocities parallel to it are not. As a result, the transport coefficients turn into tensors with three (five in the case of viscosity) independent components. In a frame of reference where the x axis has the direction of the magnetic field the transport coefficients (but the viscosity) are written as:

$$\mathbf{A} = \begin{pmatrix} A^{\parallel} & 0 & 0 \\ 0 & A^{\perp} & -A^{\mathrm{t}} \\ 0 & A^{\mathrm{t}} & A^{\perp} \end{pmatrix} \tag{9.1}$$

where $A^{\parallel}$, $A^{\perp}$ and A^{t} denote the *parallel*, *perpendicular* and *transverse* components of the relevant transport coefficient, respectively.

$A^{\parallel}$ does not depend on the magnetic field; $A^{\perp}$ reduces to the parallel component when $B \to 0$; A^{t} vanishes when $B \to 0$. The *electron Hall parameter* is the governing parameter that controls the extent to which the magnetic field effectively perturbs the electron trajectories. This is defined as

$$\beta_{\mathrm{e}} = \omega_{\mathrm{e}} \tau_{\mathrm{e}} \tag{9.2}$$

where $\omega_{\mathrm{e}} = eB/m_{\mathrm{e}}$ is the electron Larmor frequency and τ_{e} is the mean collision time for electron collisions. When β_{e} is of order 1 the electron transport properties are mainly controlled by the magnetic field and the importance of the collisions decreases. At high field strengths the plasma behaves like an inviscid fluid and the components affected by the field vanish. Due to their masses, the heavy components are affected at much larger field strengths. At the field strengths considered, up to several Tesla, the effect on the charged heavy components is barely noticeable, except at very low pressures.

Many papers are available in literature on the introduction of the magnetic field in the Boltzmann equation (Devoto 1969; Montgomery and Tidman 1964; Balescu 1963; Braginskii 1965; Schweitzer and Mitchner 1967;

M. Capitelli et al., *Fundamental Aspects of Plasma Chemical Physics*, Springer Series on Atomic, Optical, and Plasma Physics 74,
DOI 10.1007/978-1-4419-8172-1_9, © Springer Science+Business Media, LLC 2013

Chmieleski and Ferziger 1967a, b; Kolesnikov and Tirskiy 1984; Zhdanov 2002). In this chapter we limit to recent results obtained in our lab in thermal plasmas, while the recent work by Colonna and Capitelli 2008 can be used as a guide to understand the role of magnetic fields in affecting the transport properties of electrons under non-equilibrium conditions.

To this end, a complete computational scheme has been developed for the calculation of transport coefficients of partially ionized gas under the action of the magnetic field. The tensorial transport coefficients can be calculated to any desired level of approximation, provided the required collision integrals are available. Also, ionization non-equilibrium can be taken into account in a straightforward manner. However, we recall that this formalism is applicable only when thermal equilibrium can be assumed, so that, in particular, the electron and heavy-particle average kinetic energies are equal.

9.1 Theory

The transport coefficients in the presence of a magnetic field follow the lines discussed in Chap. 1 (see also Bruno et al. 2008; Giordano 2002) with the introduction of the magnetic field in the relevant equations. The following transport coefficients have been considered:

- Diffusion coefficients
- Thermal diffusion coefficients
- Thermal conductivity
- Viscosity

In terms of these coefficients, the flux vectors of mass, electric charge, and energy are written as follows:

1. Mass Diffusion Fluxes
   Taking into account the properties of diffusion and thermal diffusion coefficients, Eq. (1.127), and the expression for the diffusion velocities, Eq. (1.75), the mass diffusion fluxes, $\boldsymbol{J}_j = \rho_j \boldsymbol{V}_j$, can be conveniently written as

$$\boldsymbol{J}_j = -\frac{\rho_j}{p} \sum_{k \in S} \boldsymbol{D}_{\boldsymbol{j}}^{\boldsymbol{k}} \cdot \boldsymbol{x}_k - \frac{1}{T} \rho_j \boldsymbol{D}_{\boldsymbol{j}}^{\boldsymbol{T}} \cdot \nabla T \qquad j = 1, \ldots, n^s \tag{9.3}$$

   where the diffusion driving force is expressed as

$$\boldsymbol{x}_j = \nabla p_j - \frac{e_j}{m_j} \rho_j (\boldsymbol{E} + \boldsymbol{v} \times \boldsymbol{B}) \qquad j = 1, \ldots, n^s \tag{9.4}$$

   In Eqs. (9.3) and (9.4) ρ, p, p_j, e_j, m_j and ρ_e denote, respectively, total mass density, pressure, partial pressure of the jth component, electric

charge of the jth component, molecular mass of the jth component and electric charge density.
$\boldsymbol{D_j^k}$ and $\boldsymbol{D_j^T}$ represent the diffusion and thermal diffusion coefficients. These are tensors of rank 3:

$$\boldsymbol{D_j^k} = \begin{pmatrix} (\boldsymbol{D_j^k})^{\parallel} & 0 & 0 \\ 0 & (\boldsymbol{D_j^k})^{\perp} & -(\boldsymbol{D_j^k})^t \\ 0 & (\boldsymbol{D_j^k})^t & (\boldsymbol{D_j^k})^{\perp} \end{pmatrix} \tag{9.5}$$

$$\boldsymbol{D_j^T} = \begin{pmatrix} (\boldsymbol{D_j^T})^{\parallel} & 0 & 0 \\ 0 & (\boldsymbol{D_j^T})^{\perp} & -(\boldsymbol{D_j^T})^t \\ 0 & (\boldsymbol{D_j^T})^t & (\boldsymbol{D_j^T})^{\perp} \end{pmatrix} \tag{9.6}$$

2. Conduction Current Density
Conduction current density, in Eq. (1.93), can be written as

$$\boldsymbol{j}_e = -\sum_{j\in S} \boldsymbol{\sigma_e}_j^p \cdot \nabla p_j + \boldsymbol{\sigma_e} \cdot (\boldsymbol{E} + \boldsymbol{v} \times \boldsymbol{B}) - \boldsymbol{\sigma_e}^T \cdot \nabla T \tag{9.7}$$

where we have defined

Presso-electrical conductivity coefficients:

$$\boldsymbol{\sigma_e}_j^p = \frac{1}{p} \sum_{k\in S} n_k e_k \boldsymbol{D_j^k} \tag{9.8}$$

Electrical conductivity coefficients:

$$\boldsymbol{\sigma_e} = \frac{1}{p} \sum_{j,k\in S} n_j e_j \boldsymbol{D_j^k} n_k e_k \tag{9.9}$$

Thermo-electrical conductivity coefficients:

$$\boldsymbol{\sigma_e}^T = \frac{1}{T} \sum_{j\in S} n_j e_j \boldsymbol{D_j^T} \tag{9.10}$$

3. Heat Flux
The heat flux, in Eq. (1.80), can be written as

$$\begin{aligned} \boldsymbol{q} &= \sum_{j\in S} \frac{H_j}{m_j} \boldsymbol{J}_j - \sum_{j\in S} \boldsymbol{D_j^T} \cdot \boldsymbol{x}_j - \boldsymbol{\lambda}' \cdot \nabla T \\ &= -\sum_{j\in S} \boldsymbol{\lambda}_j^p \cdot \nabla p_j + \boldsymbol{\lambda}^E \cdot (\boldsymbol{E} + \boldsymbol{v} \times \boldsymbol{B}) - \boldsymbol{\lambda} \cdot \nabla T \end{aligned} \tag{9.11}$$

where the partial thermal conductivity is

$$\boldsymbol{\lambda}' = \begin{pmatrix} (\boldsymbol{\lambda}')^{\parallel} & 0 & 0 \\ 0 & (\boldsymbol{\lambda}')^{\perp} & -(\boldsymbol{\lambda}')^{t} \\ 0 & (\boldsymbol{\lambda}')^{t} & (\boldsymbol{\lambda}')^{\perp} \end{pmatrix} \tag{9.12}$$

and we have defined
True thermal conductivity:

$$\boldsymbol{\lambda} = \boldsymbol{\lambda}' + \frac{1}{T}\sum_{j\in S} n_j H_j \boldsymbol{D_j^T} \tag{9.13}$$

Presso-thermal conductivity coefficients:

$$\boldsymbol{\lambda}_j^p = \boldsymbol{D_j^T} + \frac{1}{p}\sum_{k\in S} n_k H_k \boldsymbol{D_j^k} \tag{9.14}$$

Electrothermal conductivity coefficients:

$$\boldsymbol{\lambda}^E = \sum_{j\in S}\left[n_j e_j \boldsymbol{D_j^T} + \frac{1}{p} n_j H_j \sum_{k\in S} n_k e_k \boldsymbol{D_j^k}\right] \tag{9.15}$$

4. Pressure Tensor

The pressure tensor, Eq. (1.76), is now given by

$$\mathbb{P} = (p - \kappa \partial_{\boldsymbol{r}} \cdot \boldsymbol{v} - p^{rel})\mathbb{I} - 2\boldsymbol{\eta} : \mathbb{S} \tag{9.16}$$

The viscosity coefficient $\boldsymbol{\eta}$ is a 4th-rank tensor with five independent components (de Groot and Mazur 1984; McCourt et al. 1990).

Note that the bulk viscosity, κ, vanishes when the internal structure of particles is neglected. The linear dependence of the components of the pressure tensor on those of the traceless symmetric part of the velocity gradient ($\mathbb{S}$) is explained in de Groot and Mazur (1984).

9.2 Results

9.2.1 Argon Plasma

Equations in the theoretical Sect. 9.1 have been used to calculate the transport properties of argon plasmas as a function of the magnetic field for two extreme conditions, i.e. fully ionized and weakly ionized gases (Bruno et al. 2006, 2008).

It is the electron component that is affected by the magnetic field at the considered field strengths ($B \approx 1\,\mathrm{T}$). Therefore, the transverse component is non-negligible only if the ionization degree is substantial. The electron-argon collision cross sections are smaller than the Coulomb cross sections at the same temperature, so that, for a given magnetic field strength, the electron Hall parameter is larger and the effect of the magnetic field correspondingly enhanced when these collisions contribute to transport. In Fig. 9.1 the ratio of transverse-to-parallel components of the true thermal conductivity as a function of magnetic field is reported for the two cases. For weakly ionized plasma, the Hall parameter does not significantly change with temperature and the maximum effect ($\beta_e \sim 1$) is attained for $B \sim 0.1\,\mathrm{T}$. The transverse component stays very much smaller than the parallel one for this case. On the contrary, in the fully ionized case, the cross sections are larger and decrease strongly with increasing temperature. The curves are shifted to higher B values but, because the electron component is large enough, the effect in absolute values is much stronger in this case.

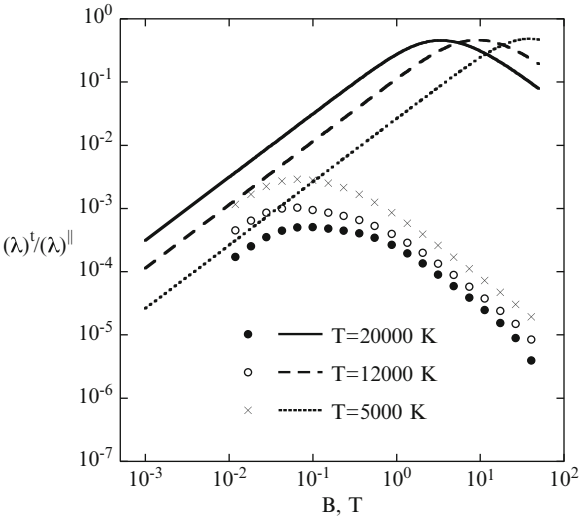

Fig. 9.1 Ratio of transverse to parallel components of the true thermal conductivity as a function of magnetic field at $p = 1\,\mathrm{atm}$ for different temperature values (Bruno et al. 2008). Fully ionized (*lines*) and weakly ionized gas (*symbols*)

As clearly noted, the magnetic field affects mainly the electron component; therefore, we shall expect a much bigger effect on the electrical conductivity, that is essentially due to electron diffusion.

The absolute values of the transverse components of the electrical conductivity in the two cases, reproduce the behaviour of the transverse components of the true thermal conductivity and the same considerations apply. However,

the effect of the magnetic field is for σ_e relatively stronger as can be appreciated in Fig. 9.2. Even at low ionization degrees, the transverse component is comparable to the parallel component.

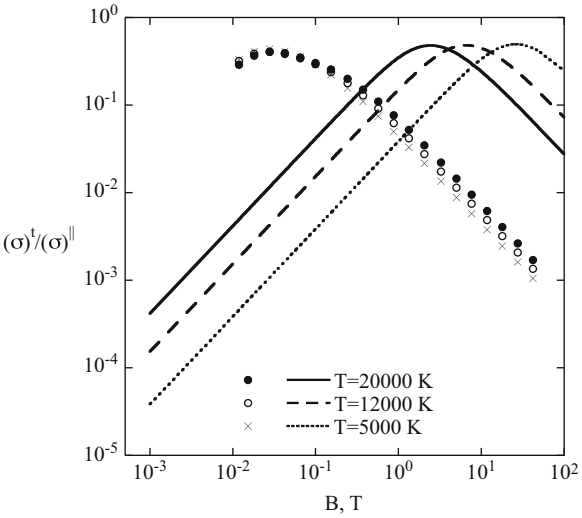

Fig. 9.2 Ratio of transverse to parallel components of the electrical conductivity of argon plasma as a function of magnetic field at $p = 1$ atm, for different temperature values (Bruno et al. 2008). Fully ionized (*lines*) and weakly ionized gas (*symbols*)

The convergence of the transverse components shows a similar qualitative trend as that of the parallel component. The presence of the magnetic field speeds up the approach to convergence for the equilibrium case (Bruno et al. 2008). When the electron Hall parameter is large enough to affect the transport coefficients appreciably, the role of the collisions decreases correspondingly and the convergence in enhanced, as it can be appreciated in Fig. 9.3 (Bruno et al. 2006).

9.2.2 Air Plasma

Figure 9.4 shows the transverse-to-parallel ratio for the thermal conductivity coefficients as a function of temperature for equilibrium air plasma at p=1 atm, $B = 1$ T (Bruno et al. 2011). This ratio is significant for the translational coefficient as soon as the electron contribution becomes important. It increases around 10,000 K even if the Hall parameter is decreasing in this zone. Then, the electron contribution dominates and the transverse-to-parallel ratio follows the Hall parameter. The internal thermal conductivity, instead, is due to heavy particle diffusion and is therefore less sensitive to the magnetic field. Note also that, since the internal thermal conductivity

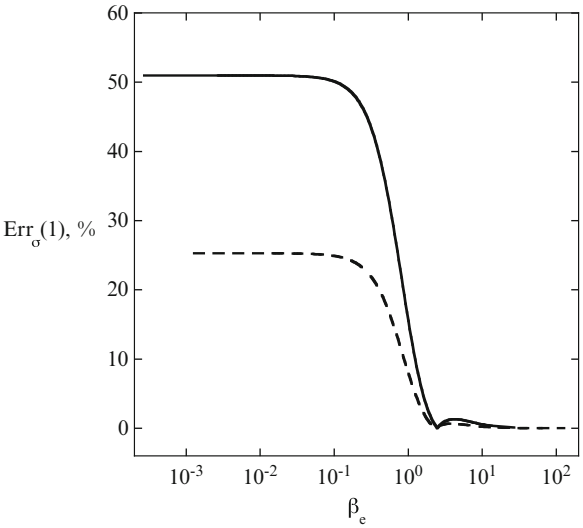

Fig. 9.3 Percentage error of the first approximation of the transverse component of the electrical conductivity with respect to the fifth one for argon plasma as a function of the electron Hall parameter for the fully ionized plasma (*continuous line*) at T=20,000 K and for the weakly ionized plasma (*dashed line*) at T=2,000 K (Bruno et al. 2006)

is mainly contributed by positive ion diffusion, its transverse component has the opposite sign as compared to the translational coefficient. This is best seen in Fig. 9.5 that reports the transverse-to-parallel ratio for the thermal conductivity coefficients as a function of magnetic field for equilibrium air plasma at $p = 1\,\text{atm}$, $T = 25,000\,\text{K}$. While the ratio for the translational coefficient shows the usual behaviour and peaks at about 0.5 for $B \approx 2\,\text{T}$, the corresponding value for the internal and reactive thermal conductivities requires much stronger fields and is negative.

Figure 9.6 reports the components of the electrical conductivity of equilibrium air plasma at $p = 1\,\text{atm}$, $B = 1\,\text{T}$. For this coefficient, which is mainly due to electron transport, the magnetic field is very effective and anisotropy effects are very strong. The figure also reports the approximations obtained by

$$\sigma_e^{\perp} = \sigma_e^{\parallel} \frac{1}{1+\beta_e^2} \tag{9.17}$$

$$\sigma_e^{t} = \sigma_e^{\parallel} \frac{\beta_e}{1+\beta_e^2} \tag{9.18}$$

The figure shows that, while the approximations work at very low temperature (when the Hall parameter is small enough), they give completely wrong results in the general case. The effect of the magnetic field is shown in Fig. 9.7, where the transverse-to-parallel ratio is shown in equilibrium air

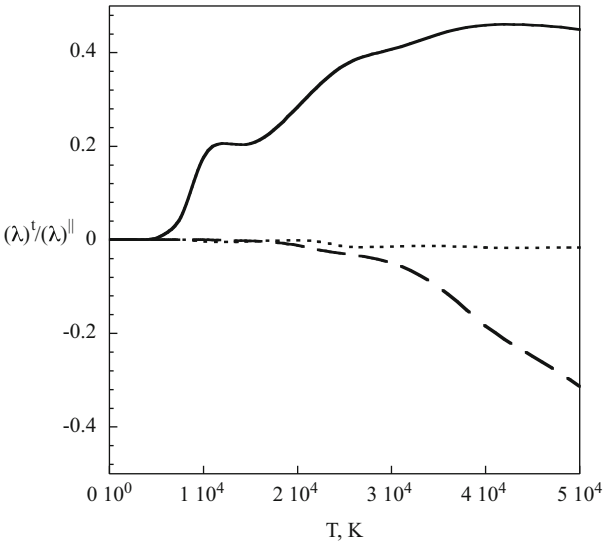

Fig. 9.4 Transverse-to-parallel ratio of thermal conductivities for equilibrium air plasma as a function of temperature, at $p = 1$ atm, B=1 T (Bruno et al. 2011). True thermal conductivity (*solid line*), internal thermal conductivity (*dashed line*) and reactive thermal conductivity (*dotted line*)

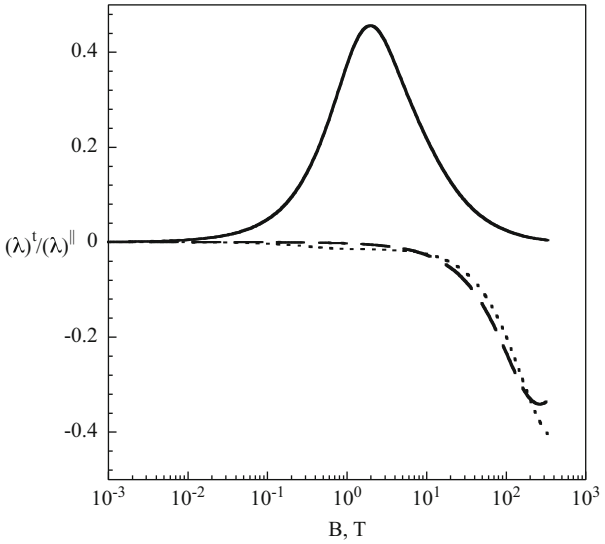

Fig. 9.5 Transverse-to-parallel ratio of thermal conductivities for equilibrium air plasma as a function of magnetic field, at $p = 1$ atm, $T = 25,000$ K (Bruno et al. 2011). True thermal conductivity (*solid line*), internal thermal conductivity (*dashed line*) and reactive thermal conductivity (*dotted line*)

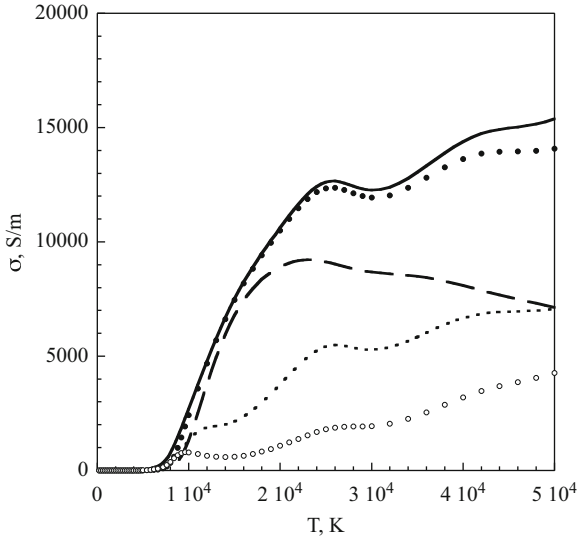

Fig. 9.6 Electrical conductivity components for equilibrium air plasma as a function of temperature, at $p = 1\,\text{atm}$, $B = 1\,\text{T}$ (Bruno et al. 2011). Parallel component (*solid line*), perpendicular component (*dashed line*) and transverse (*dotted line*). (*full symbols*) Eq. (9.17), (*open symbols*) Eq. (9.18)

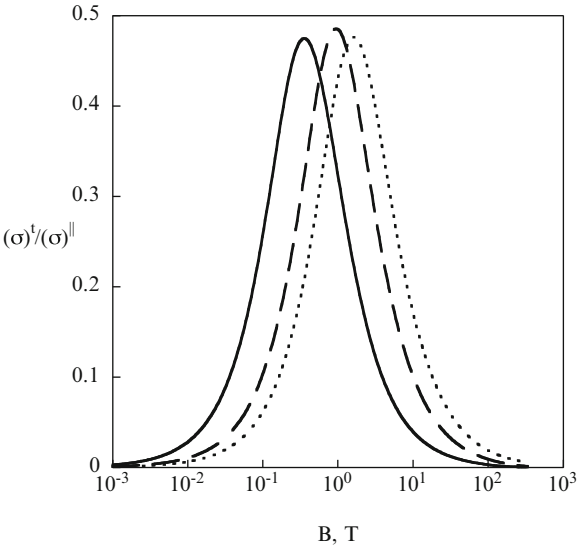

Fig. 9.7 Transverse-to-parallel ratio of electrical conductivity for equilibrium air plasma as a function of magnetic field, at $p = 1\,\text{atm}$ (Bruno et al. 2011). T=4,600 K (*solid line*), T=10,000 K (*dashed line*) and T=25,000 K (*dotted line*)

plasma at $p = 1\,\text{atm}$ and at three different temperatures. Irrespective of the plasma composition, the electrical conductivity is produced by the electrons, so that the behaviour of the transverse-to-parallel ratio is the same in all cases. The differences are due to differences in the electron Hall parameter.

Figure 9.8 reports the transverse-to-parallel ratio of the shear viscosity of equilibrium air plasma at $p = 1\,\text{atm}$, $B = 1\,\text{T}$. Since viscosity is due to heavy particles, the effect of the magnetic field is negligible reaching 2 % at 50,000 K. Since in this case the governing Hall parameter is very small, the transverse components can be determined with sufficient accuracy from first-order approximations, similar to Eqs. (9.17) and (9.18).

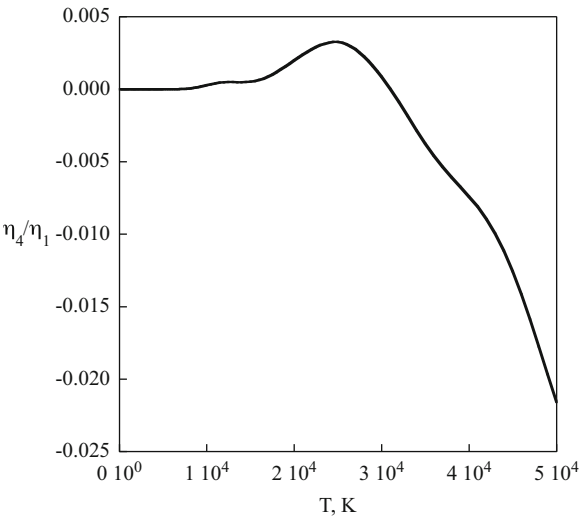

Fig. 9.8 Transverse-to-parallel ratio of shear viscosity for equilibrium air plasma as a function of temperature, at $p = 1\,\text{atm}$, $B = 1\,\text{T}$ (Bruno et al. 2011)

9.2.3 Hydrogen Plasma

In Fig. 9.9 the transverse component of the multicomponent diffusion coefficient, $\boldsymbol{D}_{\text{H}}^{\text{H}^+}$, is plotted as a function of the magnetic field strength for a hydrogen plasma at $p = 1\,\text{atm}$ and $T = 50,000\,\text{K}$. The two curves report the results for the *usual* and *abnormal* coefficients, respectively (Bruno et al. 2007) (see also Chapt. 7). As expected, both curves increase as the magnetic field increases. As the electron Hall parameter becomes of order 1, however, the contribution due to electron collisions vanishes and the effect is much

stronger when the EES cross sections are taken into account. This is due to the fact, already mentioned, that H(n)–H^+ transport cross sections have a stronger dependence on principal quantum number than H(n)–e ones. It can also be noticed that the presence of EES cross sections slows down the effect of the magnetic field. This will become more evident in the discussion of the electrical conductivity, where electron transport is the dominant phenomenon.

Let us now consider the influence of EES on another diffusion coefficient. Figure 9.10 reports the parallel component of the $\boldsymbol{D}_{H^+}^{H^+}$ diffusion coefficient for equilibrium hydrogen plasma at $p = 1$ atm. Without excited states, this coefficient, after a maximum, strongly decreases with increasing temperature. Increasing the pressure shifts this behaviour to higher temperatures. The decrease of the coefficient with the increase of gas temperature is mainly due to the increase of the proton concentration; the decrease of the coefficient is therefore due to the very effective, as compared to H(1)–H^+ ones, Coulomb collisions. The coefficient must reach the limiting value of 3.3×10^{-6} [m^2/s] of the fully ionized gas in both cases. However, the presence of EES is such to dramatically affect the decrease of the coefficient as a result of the increase of the diffusion cross sections H(n)–H^+. Small concentrations of excited states

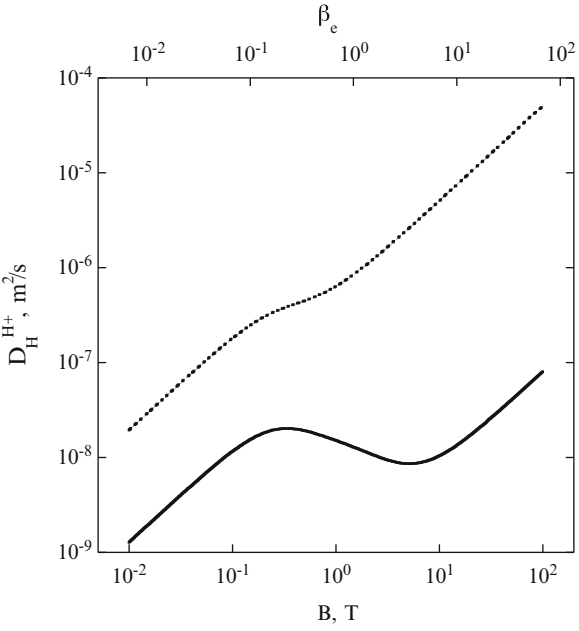

Fig. 9.9 Transverse component of the atom-proton diffusion coefficient as a function of the magnetic field. Equilibrium hydrogen plasma at $p = 1$ atm, T=50,000 K (Bruno et al. 2007). *Abnormal* (*solid line*) and *usual* (*dotted line*)

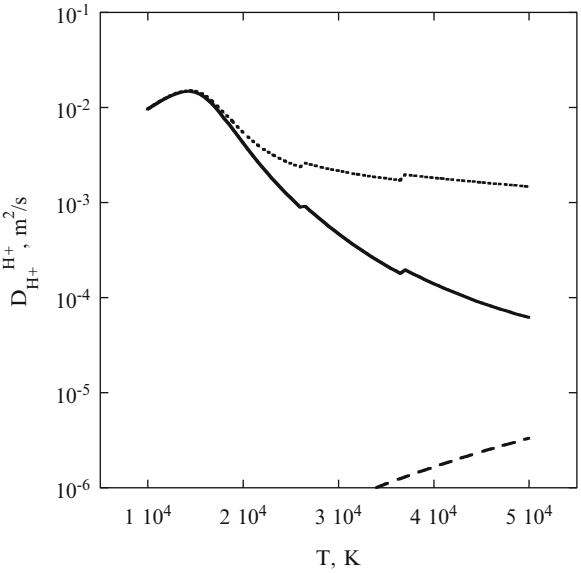

Fig. 9.10 Parallel component of the proton-proton diffusion coefficient as a function of the temperature. Equilibrium hydrogen plasma at $p = 1$ atm, (Bruno et al. 2007). *Abnormal* (*solid line*) and *usual* (*dotted line*) Fully ionized case (*dashed line*)

combined with their enormous cross sections (see Chap. 5) are able to obscure the role of Coulomb collisions in affecting the $\boldsymbol{D}^{\mathrm{H}^+}_{\mathrm{H}^+}$ diffusion coefficient.

At variance from the diffusion coefficients discussed so far, the electron-electron diffusion coefficient, $\boldsymbol{D}^{\mathbf{e}}_{\mathbf{e}}$, is dominated by interactions of the plasma constituents with the electron component. The particular property of the $\boldsymbol{D}^{\mathbf{e}}_{\mathbf{e}}$ diffusion coefficient to depend only on electron collision processes allows us to discuss in more detail the effect of the magnetic field in the whole range of the relevant Hall parameter. To this end, we remind that the plasma electrical conductivity is expressed in terms of the multicomponent diffusion coefficients as follows:

$$\boldsymbol{\sigma_e} = \frac{1}{p} \sum_{j,k \in S} n_j e_j \boldsymbol{D}^{\boldsymbol{k}}_{\boldsymbol{j}} n_k e_k \approx \frac{n_e e^2}{k_{\mathrm{B}} T} \boldsymbol{D}^{\mathbf{e}}_{\mathbf{e}} \tag{9.19}$$

The last equality neglects terms of order $m_{\mathrm{e}}/m_{\mathrm{H}}$ and is therefore accurate for our purposes. When a magnetic field is present, the scenario is modified in different ways depending on the value of the electron Hall parameter. Focusing on the transverse component of the electrical conductivity, we recall that this component vanishes for very small and very strong magnetic fields, i.e.

$$\sigma^t_e \sim \begin{cases} \sigma^{\parallel}_e \cdot \beta_{\mathrm{e}} & \beta_{\mathrm{e}} \ll 1 \\ \sigma^{\parallel}_e \cdot \beta_{\mathrm{e}}^{-1} & \beta_{\mathrm{e}} \gg 1 \end{cases} \tag{9.20}$$

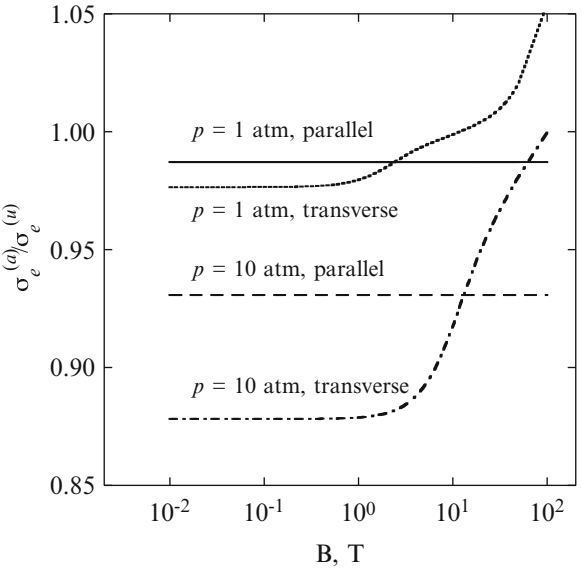

Fig. 9.11 *Abnormal*-to-*usual* ratio for the parallel and the transverse components of the electrical conductivity as a function of the magnetic field for two plasma equilibrium conditions ($p = 1$ atm, T=16,500 K; $p = 10$ atm, T=20,000 K) (Bruno et al. 2007)

Figure 9.11 reports the ratio of *abnormal*-to-*usual* values for the parallel and transverse components of the electrical conductivity for two cases: (i) $p = 1$ atm, T=16,500 K, and (ii) $p = 10$ atm, T=20,000 K. At each pressure, the temperature is such to maximize the effect of the EES cross sections. Now, pressure and temperature being assigned, the composition of the plasma and the populations of EES are determined by the equilibrium condition, as well as the values of the collision integrals and of the mean collision times for each species. The first consequence is that the difference on the parallel component between the *abnormal* and *usual* values is a constant, independent of the magnetic field strength. Another consequence is that, for the same value of the magnetic field, the *abnormal* electron Hall parameter is smaller than the corresponding *usual* value, i.e.

$$\frac{\beta_e^{(a)}}{\beta_e^{(u)}} = \frac{\tau_e^{(a)}}{\tau_e^{(u)}} = f(p,T) \leq 1 \tag{9.21}$$

This fact, together with Eq. (9.20), explains the curves of Fig. 9.11 . At small fields, where the transverse component has a linear increase with β_e, the *abnormal*-to-*usual* ratios have a fixed value, smaller than the corresponding value relative to the parallel component. As the effect of the magnetic field becomes noticeable (the *abnormal* electron Hall parameter is 1 at $B = 10.5$ T

in case (i) and at $B = 48\,\mathrm{T}$ in case (ii), respectively) the transverse electrical conductivity has a more complicated dependence on the electron Hall parameter. After a maximum at $\beta_e \approx 1$ the transverse component starts decreasing and tends towards the asymptotic behaviour of Eq. (9.20). As a consequence, the *abnormal* transport coefficients have a slower decrease and the *abnormal*-to-*usual* ratios increase with increasing magnetic field, reaching values greater than 1.

References

Balescu R (1963) Statistical mechanics of charged particles. Interscience, New York

Braginskii SI (1965) Transport processes in a plasma. In: M. Leontovich (ed) Reviews of plasma physics, vol 1. Consultants Bureau, New York

Bruno D, Catalfamo C, Laricchiuta A, Giordano D, Capitelli M (2006) Convergence of Chapman-Enskog calculation of transport coefficients of magnetized argon plasma. Phys Plasmas 13(7):072307

Bruno D, Laricchiuta A, Capitelli M, Catalfamo C (2007) Effect of electronic excited states on transport in magnetized hydrogen plasma. Phys Plasmas 14:022303

Bruno D, Laricchiuta A, Capitelli M, Catalfamo C, Giordano D (2008) Transport properties of partially ionized argon in a magnetic field. J Thermophys Heat Transf 22:424–433

Bruno D, Capitelli M, Catalfamo C, Giordano D (2011) Transport properties of high-temperature air in a magnetic field. Phys Plasmas 18(1):012308

Chmieleski RM, Ferziger JH (1967a) Transport properties of a nonequilibrium partially ionised gas. Phys Fluids 10(2):364

Chmieleski RM, Ferziger JH (1967b) Transport properties of a nonequilibrium partially ionised gas in a magnetic field. Phys Fluids 10(12):2520

Colonna G, Capitelli M (2008) Boltzmann and Master Equations for magnetohydrodynamics in weakly ionized gases. J Thermophys Heat Transf 22(3):414–423

Devoto RS (1969) Heat and diffusion fluxes in a multicomponent ionized gas in a magnetic field. I. general expressions. Zeitschrift für Naturforschung A (Astrophysik, Physik und Physikalische Chemie) 24:967

Giordano D (2002) Hypersonic-flow governing equations with electromagnetic fields. AIAA paper pp 2002–2165

de Groot SR, Mazur P (1984) Non-equilibrium thermodynamics. In: Dover Books on Physics. Dover, New York

Kolesnikov AF, Tirskiy GA (1984) The Stefan-Maxwell equations for diffusion fluxes in a magnetic field. Fluid Dynamics (translated from Russian) Plenum 19:643

McCourt RF, Beenakker JJM, Köhler WE, Kuscer I (1990) Non equilibrium phenomena in polyatomic gases. Clarendon, Oxford

Montgomery DC, Tidman DA (1964) Plasma kinetic theory. McGraw-Hill, New York

Schweitzer S, Mitchner M (1967) Electrical conductivity of a partially ionised gas in a magnetic field. Phys Fluids 10(4):799

Zhdanov VM (2002) Transport processes in multicomponent plasma. Taylor and Francis, London

Chapter 10
Some Problems in the Calculation of Transport Properties of Partially Ionized Gases

In this chapter we discuss several problems to be taken into account when trying to calculate the transport coefficients of thermal plasmas to reach an adequate accuracy of the results. Some problems are discussed in other chapters of this book, dealing in particular with the different methods used in the calculation of transport cross sections (Chaps. 3 and 4), with the role of electronically excited states in affecting the transport properties (Chap. 5) as well as the different Saha equations in affecting the results in two-temperature plasmas (Chap. 8).

The first problem we consider in this chapter is the selection of the order of approximation of the Chapman–Enskog method to be used in the relevant applications. This problem, after the pioneering papers of Devoto (1967a,b), has been recently reexamined by Bruno et al. (2006) and by Singh et al. (2009) (Singh and Singh 2006; Sharma et al. 2011), where also the convergence in two-temperature plasmas is studied. In this context, the selected transport cross sections are important in determining the convergence of the method. The second problem is linked to the selection of a consistent database of transport cross sections especially for the calculation of transport properties of plasma mixtures for which an appropriate data set of transport cross sections does not exist. A case study of air plasmas, based on the transport cross sections presented in Chaps. 3 and 4, is discussed here, with the aim to understand if the so-called *phenomenological approach* can be used for unknown mixtures. The third problem deals with the role of inelastic processes in affecting the transport coefficients, with particular attention to rotational and vibrational energy exchange processes. In addition we briefly examine the role of quantum effects, a problem which can become very important at low temperature and high pressure, ending with a comparison of present results with existing experiments.

M. Capitelli et al., *Fundamental Aspects of Plasma Chemical Physics*,
Springer Series on Atomic, Optical, and Plasma Physics 74,
DOI 10.1007/978-1-4419-8172-1_10,

10.1 The Convergence of the Chapman–Enskog Method

10.1.1 Translational Thermal Conductivity

The convergence of the Chapman–Enskog method has been recently re-examined by Bruno et al. (2006) for an LTE argon plasma up to the fifth approximation by including both electron and heavy-particle components.

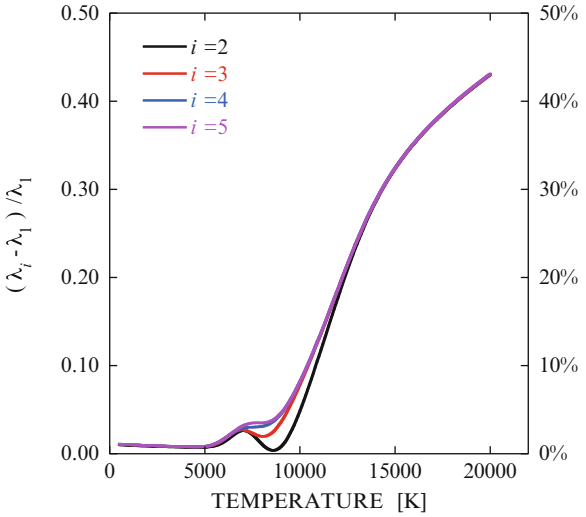

Fig. 10.1 Relative deviation of translation thermal conductivity, λ, calculated in the ith approximation with respect to the first non-vanishing approximation

The results have been reported in Fig. 10.1 in the form $([\lambda]_i - [\lambda]_1)/[\lambda]_1$, i.e. the difference between the translational thermal conductivity values calculated according to the ith approximation and the corresponding ones calculated according to the first non-vanishing approximation, the differences being normalized to the first approximation values. Appreciable ionization starts at T >8,000 K, and, therefore, we can ideally divide the temperature axis in a region where neutral species prevail (300< T <8,000 K) and a second region, for T >8000 K, where electrons start becoming the majority species. In the first region, dominated by neutrals, convergence is reached quickly, with the exception of a narrow zone 5,000< T <8,000 K, where the fifth approximation is required. This behaviour is due to the Ramsauer effect in the electron scattering from argon atoms, which dramatically affects the convergence of electron component distribution function. This effect is in any case very small because the total translational thermal conductivity in this temperature range is dominated by the neutral component which does not present convergence problems. The small Ramsauer effect disappears in the

ionization region where electron–electron and electron–ion collisions dominate the translational thermal conductivity. In this case however we have serious convergence problems due to the difference in the electron–heavy-particle masses which slows down the convergence of the Chapman Enskog method. In this case we should use at least the second approximation of the Chapman–Enskog method (the third one in Devoto formulation). Inspection of Fig. 10.1 shows that no differences between the approximations i=2 to 5 do exist far from the Ramsauer effect region, implying that this approximation can be used with a fair amount of confidence with the gases which do not present the Ramsauer effect. The shown results treat electrons and heavy particle at the same level even though, as it will appear soon, electrons are the main reason of the slow convergence of the Chapman–Enskog method in the partial ionization range so that a possible decoupling of distribution functions for electrons and neutrals generates a different level of approximation in the two components.

10.1.2 Viscosity

The convergence of the Chapman–Enskog method for viscosity in equilibrium and non-equilibrium argon plasmas has been investigated by Bruno et al. (2006) up to the sixth approximation. The results have been reported in Fig. 10.2 again in the form $(\eta_i - \eta_1)/\eta_1$.

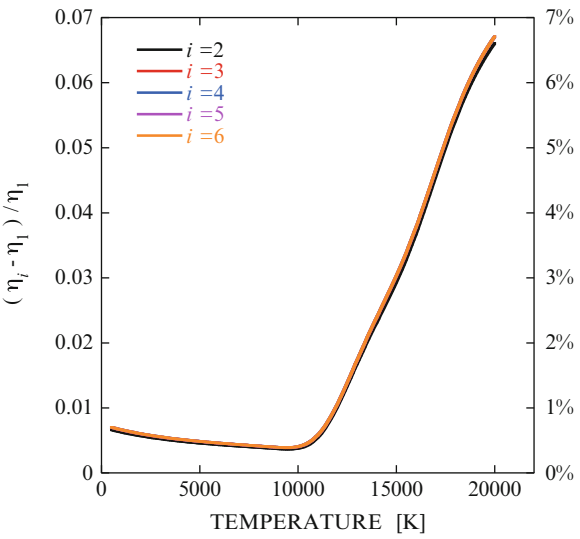

Fig. 10.2 Relative deviation of argon plasma viscosity calculated in the ith approximation with respect to the first non-vanishing approximation

Keeping in mind that only for T >8,000 K ionization equilibrium starts, we can understand that in the neutral region the first approximation gives results very similar to the sixth one, while for higher temperatures the first approximation gives values within 7 % of the sixth one. In this case no differences between the approximations i=2 to 6 can be noted. As a result for a partially ionized gas the second approximation should be used to obtain very accurate viscosity values, while the first approximation is excellent for calculating viscosity values for a neutral gas. This statement is confirmed also for strong non-equilibrium conditions characterized by weakly and fully ionized situations in the whole temperature range 500–20,000 K (Bruno et al. 2006). These conclusions are in line with the pioneering work of Devoto (1967a). Note also that the previous results contain both electrons and heavy-particle components. Neglecting electrons in the viscosity equation yields differences not higher of 0.9 % so that the viscosity of a plasma can be written as

$$\eta = \eta_e + \eta_h \simeq \eta_h \tag{10.1}$$

This conclusion also explains that the Ramsauer effect practically does not affect the viscosity dominated by heavy-particle collisions. Nowadays the most used formula for the calculation of the viscosity of a partially ionized LTE plasma is the first approximation which reads, for a ν-component mixture, in the Hirschfelder et al. (1966) formalism as

$$\eta_1 = -\begin{vmatrix} H_{11} & \dots & H_{1\nu} & x_1 \\ \vdots & & \vdots & \\ H_{n1} & \dots & H_{\nu\nu} & x_\nu \\ x_1 & x_\nu & 0 & \end{vmatrix} \cdot \begin{vmatrix} H_{11} & \dots & H_{1\nu} \\ \vdots & & \vdots \\ H_{\nu 1} & \dots & H_{\nu\nu} \end{vmatrix}^{-1} \tag{10.2}$$

$$H_{ii} = \frac{x_i^2}{[\eta_i]_1} + \sum_{j=1, j\neq i}^{\nu} \frac{2x_i x_j}{(m_i + m_j)} \frac{k_B T}{p[\mathcal{D}_i^j]_1} \left[1 + \tfrac{3}{5} \frac{m_j}{m_i} A_{ij}^\star\right] \tag{10.3}$$

$$H_{ij} = -\frac{2x_i x_j}{(m_i + m_j)} \frac{k_B T}{p[\mathcal{D}_i^j]_1} \left[1 - \tfrac{3}{5} A_{ij}^\star\right] \tag{10.4}$$

Equation 10.2 can be expanded as

$$\eta_1 = \sum_{i=1}^{\nu} \frac{x_i^2}{H_{ii}} - \sum_{i=1}^{\nu} \sum_{j=1, j\neq i}^{\nu} \frac{x_i x_j H_{ij}}{H_{ii} H_{jj}} + \dots \tag{10.5}$$

The first term, which can be derived by assuming all off-diagonal elements null, H_{ij}=0, i.e. $A_{ij}^\star = \frac{5}{3}$, will be referred to as the first approximation to the actual first approximation of the Chapman–Enskog method, while the first two terms as the second approximation (first and second approximations here defined should not be confused with previous definitions).

Thus

$$[\eta_f]_1 = \sum_{i=1}^{\nu} \frac{x_i^2}{H_{ii}} \tag{10.6}$$

$$[\eta_s]_1 = \sum_{i=1}^{\nu} \frac{x_i^2}{H_{ii}} - \sum_{i=1}^{\nu} \sum_{j=1, j\neq i}^{\nu} \frac{x_i x_j H_{ij}}{H_{ii} H_{jj}} \tag{10.7}$$

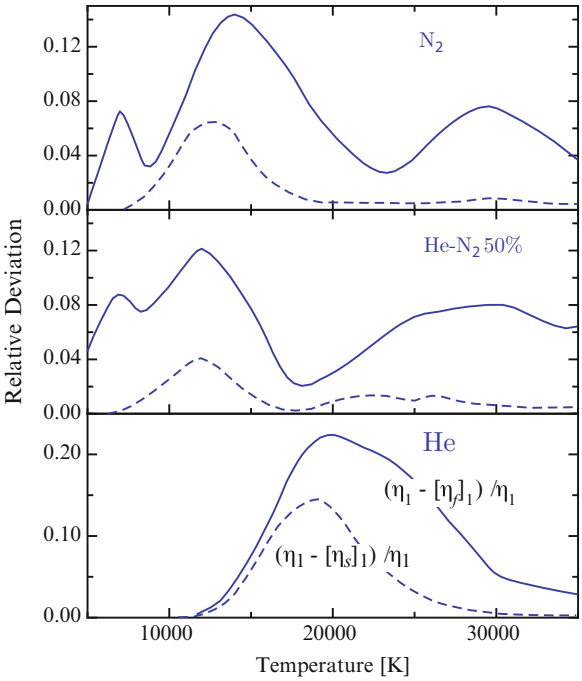

Fig. 10.3 Relative deviations of viscosity values calculated with Eqs. (10.6) (*solid lines*) and (10.7) (*dashed lines*) with respect to Eq. (10.2) for different atmospheric plasmas (Capitelli 1972)

In Fig. 10.3 the percentage relative deviation of Eqs. (10.6) and (10.7) with respect to Eq. (10.2) have been plotted as a function of the temperature for different plasmas. It can be seen that the convergence for mixtures is generally better than for the single-component plasmas. In order to explain this behaviour, let us consider the range of the first ionization, where the largest deviations are observed (Capitelli 1972). The main reason of the slow convergences of Eqs. (10.6) and (10.7) with respect to Eq. (10.2) can be ascribed, for both pure and mixed plasmas, to the fact that the off-diagonal elements H_{ij} cannot be neglected as compared with diagonal ones H_{ii}, when the ij pair represents an ion–parent-atom interaction, $A–A^+$. In fact in this case

the resonant charge-exchange mechanism increases diffusion-type collision integrals, without affecting the viscosity-type ones, thus leading to small $A^{\star}_{ij}$ values in Eq. (10.2) for A–A^+ interactions (see Chap. 4).

The charge-exchange contribution is negligible in atom–ion hetero-interactions, i.e. A–B^+, B–A^+, having a non-resonant character, so that for mixed plasmas off-diagonal elements are less important in determining the convergence of the approximations.

10.1.3 Electrical Conductivity

The convergence of the Chapman–Enskog method of the electrical conductivity can be understood by looking at Fig. 10.4, where we have reported, for an LTE atmospheric argon plasma, the quantity $([\sigma_e]_i - [\sigma_e]_1)/[\sigma_e]_1$, i.e. the differences of the electrical conductivity values calculated according to the ith approximation and the corresponding ones calculated according to the first approximation, the differences being normalized to the first approximation values.

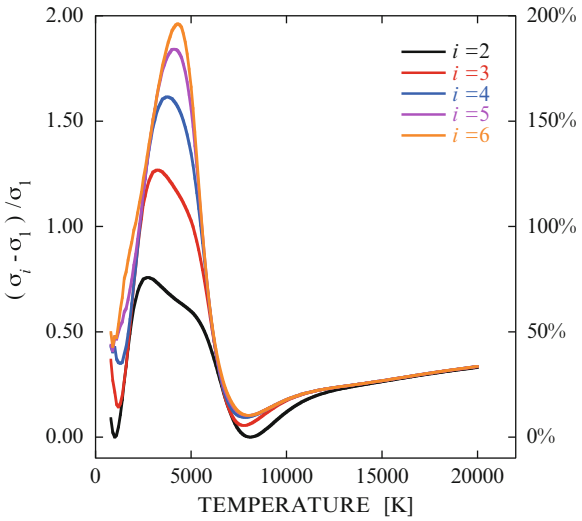

Fig. 10.4 Relative deviation of argon plasma electrical conductivity calculated in the ith approximation with respect to the first non-vanishing approximation

Inspection of the figure shows two distinct regions, the first one from room temperature to approximately 7,000 K dominated by e-Ar collisions, the second region, from 7,000 K on, dominated by e-Ar^+ and e-e collisions. In the low-temperature region, affected by the quantum mechanical Ramsauer effect, we recover the slow convergence of the Chapman–Enskog method for

the electron properties (Devoto 1967a). In this case in fact also the sixth Chapman–Enskog approximation is still far from a complete convergence. On the other hand in the region of partial and total ionization the second approximation (the third in Devoto formulation) seems sufficient to yield accurate results. Again the non-equilibrium situations confirm these conclusions (Bruno et al. 2006).

10.1.4 The Separation Between Electron and Heavy-Particle Contributions

Devoto 1967a showed that the translational thermal conductivity of an argon plasma could be written as the sum of two components, one due to the electrons (λ_e) and the other one due to the heavy components (λ_h), i.e.

$$\lambda = \lambda_e + \lambda_h \tag{10.8}$$

A comparison between *exact* λ values, i.e. values obtained treating electron and heavy particle as a coupled system as those shown in the previous section, and *approximate* values, i.e. those obtained by using Eq. (10.8), shows differences not larger than 0.1 %, when use is made of the third approximation. The decoupling scheme is a very useful tool because it allows a high-order approximation for the electron component and a lower one for the heavy particles. Nowadays it is common to use the third approximation for the electron component and the second one (the first non-vanishing approximation) for heavy particles, i.e.

$$\lambda = [\lambda_e]_3 + [\lambda_h]_2 \tag{10.9}$$

In the case of argon plasmas the Ramsauer effect demands a higher approximation for the electron contribution, while for gases not presenting this effect, Eq. (10.9) well describes the translational thermal conductivity. This point can be understood from Fig. 10.5a where the Devoto results (Devoto 1967a) for λ_e have been plotted in the form $([\lambda_e]_i - [\lambda_e]_{i-1})/[\lambda_e]_{i-1}$ as a function of temperature. The Ramsauer effect and the inadequacy of the third approximation for the calculation of the contribution of electrons to the thermal conductivity are well evident especially in the low-temperature region.

Values from Eq. (10.9) depend to a given extent also on the used transport cross sections for charged–charged collisions. Figure 10.5b reports the ratio $([\lambda_e]_3 + [\lambda_h]_2)/[\lambda]_2$ for an atmospheric nitrogen plasma (Capitelli 1970, 1977; Capitelli et al. 1996), obtained by calculating the transport cross sections of charged-particle interactions with the closed forms of Liboff (1959), including and neglecting the $\mathcal{O}(1)$ terms in the relevant equations (see Chap. 3). We can see that the differences between the third and the second approximations

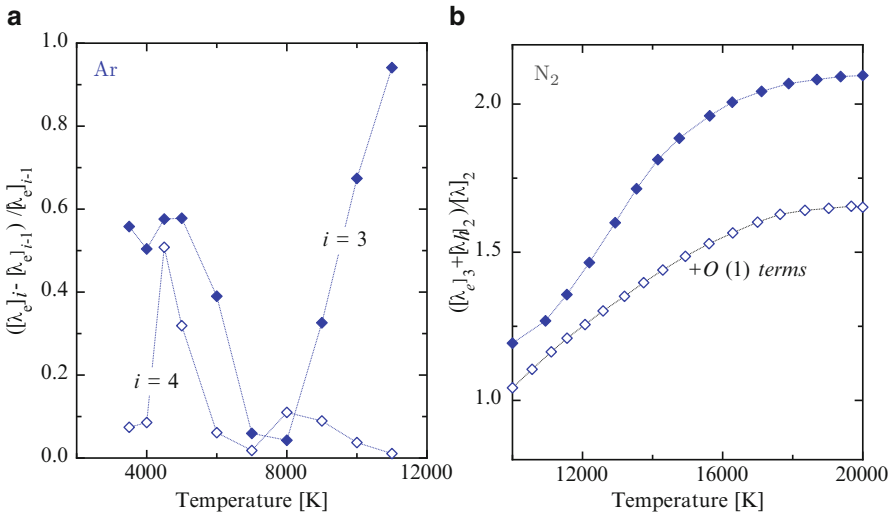

Fig. 10.5 (a) Relative deviation of translational thermal conductivity of electrons for argon plasma at p=1 atm, calculated in the ith approximation with respect to the i-1th approximation (Devoto 1967a). i=4 (*open markers*), i=3 (*close markers*). (b) Ratio of the third approximation of thermal conductivity to the second, $([\lambda_e]_3 + [\lambda_h]_2)/[\lambda]_2$ as a function of temperature for an LTE nitrogen plasma at p=1 atm, neglecting (*close markers*) or including (*open markers*) $\mathcal{O}(1)$ terms in Coulomb collision integrals (Capitelli 1977; Capitelli et al. 1996)

strongly increase when the $\mathcal{O}(1)$ terms of the Liboff equations are neglected, thus warning on the importance of using the same cross sections when discussing the convergence of the Chapman–Enskog method.

Attempts also to reduce the complexity of $[\lambda_h]_2$ follow the same lines discussed for the viscosity, obtaining also similar results (Capitelli 1972). These approximations work better as compared with the viscosity because the translational thermal conductivity of heavy components presents values lower than the corresponding contribution of electrons and of the reactive thermal conductivity in the temperature range where the relevant approximations to $[\lambda_h]_2$ are open to criticism.

10.1.5 Singh et al. Results

In a recent series of papers Singh et al. (2009) (Singh and Singh 2006; Sharma et al. 2011) have studied the convergence problems of $[\lambda_e]_i$ and $[\sigma_e]_i$ for equilibrium and non-equilibrium conditions. They used a formalism, that can be reduced to the Devoto one, presenting also the possibility of further simplifications for complicated systems. Basically they write the following equations:

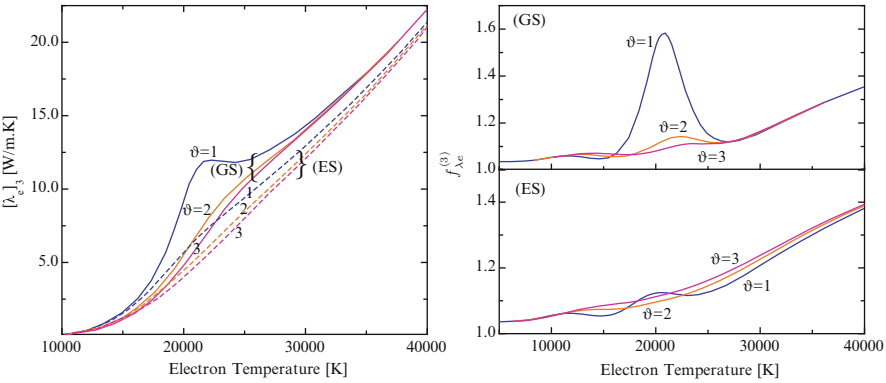

Fig. 10.6 (*left*) Thermal conductivity versus electron temperature for both ground-state (GS) (*solid lines*) and excited state (ES) (*dashed lines*) hydrogen thermal plasma at $p = 100$ atm, for different values of the non-equilibrium parameter ϑ. (*right*) Variation of third-order contribution to thermal conductivity $f^{(3)}_{\lambda_e}$ with electron temperature for the ground state (GS) and for the excited state (ES) hydrogen thermal plasma at $p = 100$ atm (Sharma et al. 2011)

$$[\lambda_e]_i = [\lambda_e]_1 f^i_{\lambda_e} \tag{10.10}$$

$$[\sigma_e]_i = [\sigma_e]_1 f^i_{\sigma_e} \tag{10.11}$$

i.e. the ith approximation is seen equal to the first one times a factor f accounting for the deviation to the first approximation for both the translational thermal conductivity of electrons and the electrical conductivity. Closed forms for these factors can be found in Sharma et al. (2011). They apply their method to atomic hydrogen plasmas considering different effects due to

- The presence of excited states (see Chap. 7)
- non-equilibrium multi-temperature plasmas (see Chap. 8).

Interesting results have been obtained at p=100 atm for the third approximation of the translational thermal conductivity of free electrons calculated at different values of ϑ, the ratio of electron–heavy-particle temperatures, in the presence excited state (ES) and in the absence (GS) of excited states. The results, derived using the maximization of entropy, i.e. van de Sanden equation (Eq. (8.22)) (van de Sanden et al. 1989), are reported in Fig. 10.6. This figure shows the effect of excited states in affecting the translational thermal conductivity passing from ϑ=1 to ϑ=3 and the corresponding third-order corrections for the three cases in the GS approximation showing the strong dependence of this factor on the ϑ values. This factor also depends on the presence of excited states which smooth the maximum present in the previous figure, thus emphasizing the role of the different interactions in the convergence problem. Comparison of these results with the corresponding ones at p=1 atm shows that non-equilibrium factor strongly increases with decreasing pressure.

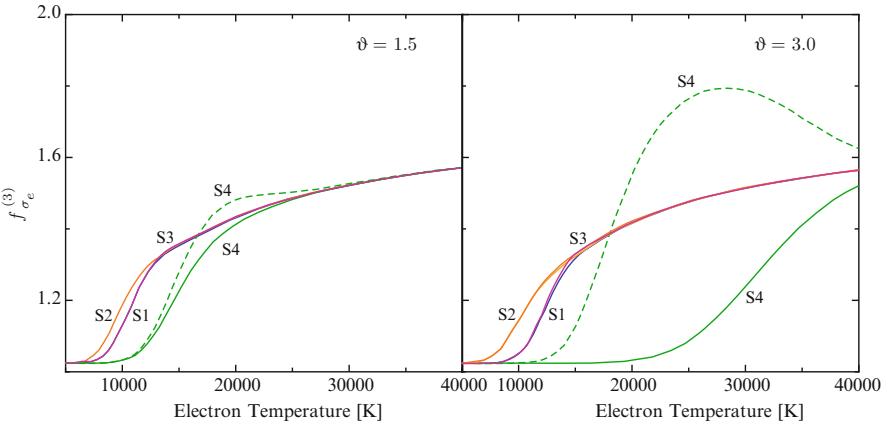

Fig. 10.7 Variation of third-order contribution to electrical conductivity $f_\sigma^{(3)}$ with electron temperature using different Saha equations for GS (*solid lines*) and ES (*dashed lines*) hydrogen thermal plasmas at p=1 atm (*left*), ϑ=1.5 and (*right*) ϑ=3. (Sharma et al. 2011). Curves S_1–S_4 correspond to Saha Eqs. (8.20)–(8.23), respectively

The second example we want to show is the dependence of the third-order coefficient to electrical conductivity on the adopted Saha equation and on the presence of excited states. This quantity is reproduced in Fig. 10.7 for ϑ=1.5 and 3.0. In general, excited states do not change the convergence factor in all the reported cases with the exception of non-equilibrium Saha equation described by Eq. (8.23). Moreover we can see that in the three cases the convergence factor decreases with ϑ changing from 1.5 to 3. On the other hand the use of Saha equation (8.23) has a large role in affecting the convergence factor in the presence of electronically excited states, this role becoming extremely important for ϑ=3.

10.2 Transport Cross Section Data Set

Transport properties of thermal plasmas strongly depend on the selection of accurate and reliable sets of transport cross sections to be inserted in the transport equations. Several papers do exist in literature devoted to the sensitivity analysis of transport coefficients to transport cross sections and presenting comparisons of results obtained by using different set of collision integrals (Capitelli and Devoto 1973; Murphy 1995; Capitelli et al. 2000c; Murphy 2000; Capitelli et al. 2000a; D'Angola et al. 2008; Rat et al. 2008). In this section a systematic comparison is reported of air plasma transport coefficients obtained with two sets of collision integrals, the first one based on multi-potential approach (Capitelli et al. 2000c), while the second constructed on a phenomenological approach, recently proposed in literature (Laricchiuta et al. 2009; Capitelli et al. 2007).

The translational thermal conductivity of free electrons, λ_e, and the electrical conductivity, σ_e, have been evaluated in the third approximation of the Chapman–Enskog method, while the first non-vanishing approximation has been used for the translational thermal conductivity of heavy particles, λ_h, and of the viscosity, η. The Eucken approximation and the Butler–Brokaw equation have been used for the calculation of the internal thermal conductivity, λ_{int}, and of the reactive one, λ_r. The thermodynamic properties of air thermal plasmas entering in the transport equations have been obtained by using the statistical thermodynamics (Capitelli et al. 2011), i.e. by an accurate determination of partition functions of relevant species. In particular the electronic partition functions of atomic (neutral and ionized) species have been obtained by applying a suitable *cutoff* criterion to complete sets of energy levels (observed plus missing). Basically the Fermi criterion has been adopted at low ionization degrees, switching to the Griem criterion when the electron density becomes sufficiently high (Capitelli et al. 2000a; D'Angola et al. 2008, 2011).

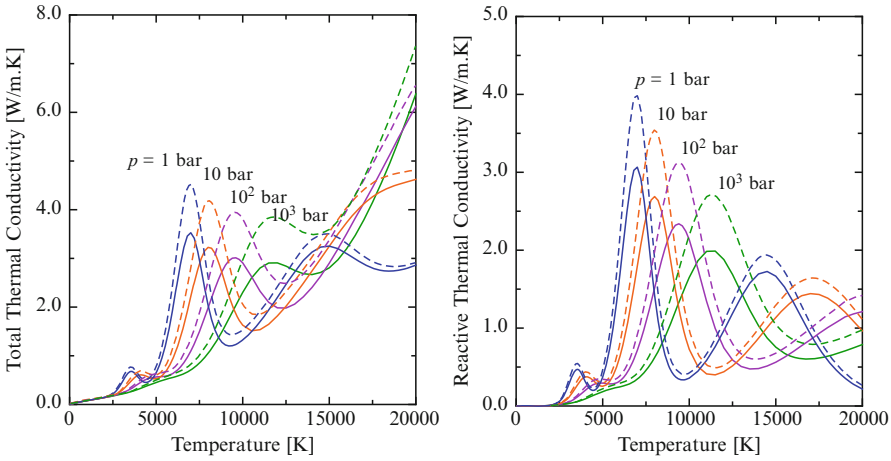

Fig. 10.8 Total thermal conductivity (*left*) and reactive thermal conductivity (*right*) of air plasma as a function of temperature, at different pressures. Collision integral data set (*a*)(*dashed lines*) and (*b*)(*solid lined*)

Figure 10.8 reports the total thermal conductivity ($\lambda = \lambda_h + \lambda_e + \lambda_{int} + \lambda_r$) and its reactive component (λ_r) obtained by using the code in D'Angola et al. (2011, 2008), including in the transport equations the collision integrals of the older data set (*a*) (Capitelli et al. 2000c), compared with transport coefficients recently re-evaluated in the phenomenological approach (*b*) (Laricchiuta et al. 2009). A general satisfactory agreement is observed, though non-negligible differences arise, also in the different contributions, always less than 25 % except for the onset of the translational thermal conductivity, where higher deviations are found at T=7,000 K.

The reactive thermal conductivity has been calculated by the rigorous Butler–Brokaw equation (Brokaw 1960; Butler and Brokaw 1957). Inspection of the results at p=1 bar shows three different maxima: the first one due to the dissociation reaction of O_2 (i.e. $O_2 \leftrightarrow 2O$), the second one due the molecular nitrogen dissociation ($N_2 \leftrightarrow 2N$) and the third one due the convolution of the ionization reactions of atomic nitrogen and atomic oxygen (i.e. $N \leftrightarrow N^+ + e$ and $O \leftrightarrow O^+ + e$). These maxima shift to high temperature with the increase of the pressure. To rationalize the differences (less than 25 %) arising in the results by using the two data sets, we remind that, to a first approximation, the reactive thermal conductivity is determined by the diffusion coefficients, related to the corresponding diffusion-type collision integrals by an inverse dependence, i.e. $\mathcal{D}_i^j \propto 1/\Omega_{ij}^{(1,1)\star}$. Thus, the first maximum depends on $\Omega_{O-O_2}^{(1,1)\star}$, the second maximum on $\Omega_{N-N_2}^{(1,1)\star}$ and the third one on $\Omega_{O-O^+}^{(1,1)\star}$ and $\Omega_{N-N^+}^{(1,1)\star}$. In all these cases the diffusion-type collision integrals, reported in Capitelli et al. (2000c), are lower than the corresponding ones reported in the more recent compilation (Laricchiuta et al. 2009) generating the differences of Fig. 10.8. Note however that the N–N^+ and O–O^+ interactions of Capitelli et al. (2000c) were based on the high-energy experimental charge-transfer cross sections of Belyaev et al. (1968), while the most recent data are based on theoretical values from the asymptotic theory (Kosarim et al. 2006; Kosarim and Smirnov 2005) (see Chap. 4).

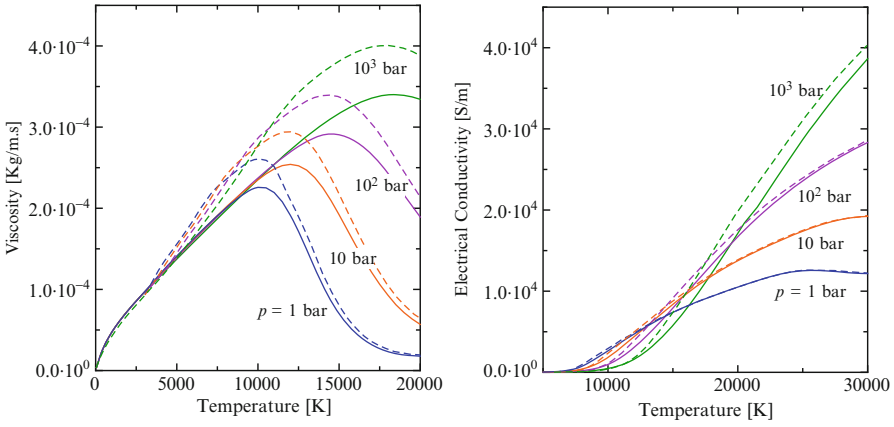

Fig. 10.9 Viscosity (*left*) and electrical conductivity (*right*) of air plasma as a function of temperature, at different pressures. Collision integral data set (a)(*dashed lines*) and (*b*)(*solid lined*)

In Fig. 10.9 viscosity and electrical conductivity are displayed. Deviations less than 20 % are observed in the viscosity, either in the dissociation or partial ionization regimes, being the values calculated with the transport cross sections from the phenomenological approach lower than the corresponding

values obtained by using the database of Capitelli et al. (2000c). In this last case the neutral–neutral interaction were obtained by using an experimental repulsive potential for T >2,000 K and a Lennard-Jones potential for T <1,000 K. On the other hand the corresponding N–N_2 and O–O_2 transport cross sections, calculated by using ab initio potentials (Stallcop et al. 2001), are close to the corresponding value from phenomenological approach. A similar situation holds for the viscosity-type collision integrals for N–N^+ and O–O^+ interactions, i.e. the collision integrals for the set (a) are lower than the corresponding ones for the set (b), thus generating the differences reported in Fig. 10.9.

To rationalize the behaviour of the electrical conductivity it must be reminded that it mainly depends on electron–neutral interactions, i.e. e-N_2, e-O_2, e-N, e-O, as well as on electron–electron and electron–ion interactions. The Coulomb interactions tend to dominate as soon as the concentration of electrons becomes about one order of magnitude lower than the corresponding ones for neutral species. This condition rapidly occurs for p=1–10 bar, while at very high pressures, p=10^2-10^3 bar, neutral species keep their role in a wider temperature range. As a result, at high temperature, for p=1 bar, we observe differences less than 5 % in the values of translational thermal conductivity of electrons calculated with the two sets of transport cross sections, because these results are determined by the electron–electron and electron–ion transport cross sections, evaluated with the same shielded Coulomb potential. On the other hand, at p=10^3 bar, differences of 20 % can be observed due to the corresponding deviations in the e-N_2, e-O_2, e-N, e-O transport cross sections between the two databases.

This analysis could be extended also to the components of the thermal conductivity, not reported here, just recalling that the internal thermal conductivity behaves like the reactive thermal conductivity, the translational thermal conductivity of heavy particles like the viscosity and the translational thermal conductivity of free electrons like the electrical conductivity (see D'Angola et al. 2012).

Transport coefficients tend to converge for high values of the electron density (T >20,000 K) regardless the database used for heavy-particle interactions, due to the dominant role of Coulomb interaction between charged particles. Actually in the high-temperature region, other sources of discrepancy are connected to the adopted values for Coulomb collision integrals. Nowadays the accurate Hahn and Mason (Hahn et al. 1971) transport cross sections are widely used; however, a problem still exists in the practical application linked to the definition of the Debye length, in fact including or neglecting ion density yields different results as can be observed in Fig. 10.10 where the effect on the electrical conductivity is shown. Differences could arise also when the well-known Liboff formulae (Liboff 1959) are used, in fact Coulomb collision integrals, estimated including high-order corrections $\mathcal{O}(1)$ in Eq. (3.49), are lower than values by Hahn and Mason, thus resulting in higher values for derived transport coefficients, as it can be appreciated in Fig. 10.10, for electrical

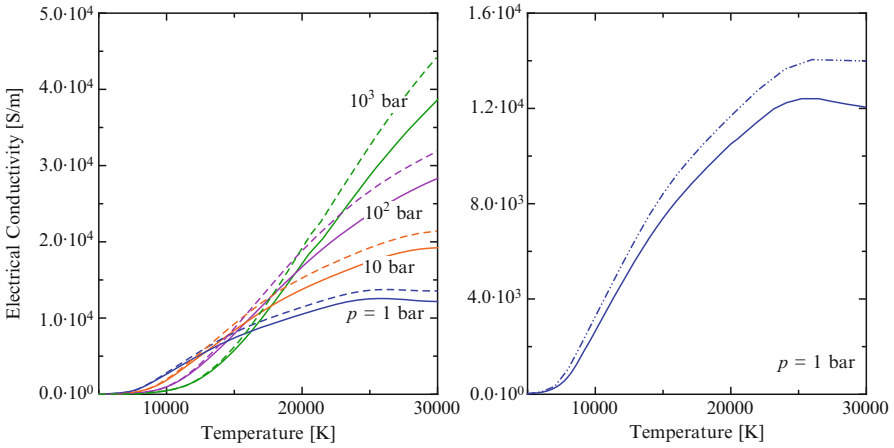

Fig. 10.10 (*left*) Electrical conductivity of air plasma as a function of temperature, at different pressures, including (*solid lines*) or neglecting (*dotted lines*) the ion density in the calculation of Debye length (collision integral data set (*right*)). (*right*) Electrical conductivity of air plasma as a function of temperature, at p=1 bar, by using different values for the Coulomb interaction collision integrals. (*solid line*) (Hahn et al. 1971), (*dashed-dotted line*) Liboff formulae (Liboff 1959)

conductivity of air plasmas, and expected for the total thermal conductivity. On the other hand we can note that use of the Liboff formulae without taking into account the $\mathcal{O}(1)$ terms leads to an increase of the corresponding cross sections, producing a corresponding decrease of transport coefficients. Therefore use of Liboff formulae (Liboff 1959) truncated to the dominant $\ln\left[\frac{2\lambda_D}{b_0}\right]$ term yields transport cross sections in better agreement with the more accurate Hahn and Mason numerical results. Moreover the fourth approximation of the Chapman–Enskog method in combination with Liboff transport cross sections for Coulomb interactions, not including $\mathcal{O}(1)$ terms, reproduces, in the completely ionized gas regime, the Spitzer and Härm results (Spitzer and Härm 1953) based on the Fokker–Planck equation (Devoto 1967b).

This point, exalted when two-temperature plasmas are considered, should be further investigated in light of the numerous efforts done in the past on the topic (Devoto 1968).

10.3 Inelastic Processes

The study of the influence of inelastic processes on the transport properties of atomic and molecular gases began with the formal description of the kinetic problem by Chang and Uhlenbeck (1951). Later, Mason and Monchick (1962) put the equations in a more compact form, trying to emphasize the

close connection of the collision integrals calculated by taking into account inelastic processes with the familiar ones, obtained considering only elastic processes.

Let us denote with $\frac{d\sigma_{ij}^{kl}}{d\Omega}(g \to g', \vartheta, \phi)$ the differential scattering cross section for the process

$$\boldsymbol{g} = \boldsymbol{v} - \boldsymbol{v}_1 \to \boldsymbol{v}' - \boldsymbol{v}_1' = \boldsymbol{g}' \qquad E_i^q \to E_k^q \qquad E_j^{q'} \to E_l^{q'} \tag{10.12}$$

i.e. for the process involving species q and q' initially in the internal states i and j and after the collision in internal states k and l. $\boldsymbol{g}$ and $\boldsymbol{g}'$ are the relative velocities before and after the collision, and ϑ and ϕ are, respectively, the polar and azimuthal angles, describing the relative orientation of the relative-velocity vectors. After different manipulations the diffusion- and viscosity-type collision integrals can be written as

$$\Omega^{(\ell,s)} = \frac{1}{Q_q Q_{q'}} \sum_{ijkl} \int_0^\infty \mathrm{d}\gamma \int_0^{2\pi} \mathrm{d}\phi \int_0^\pi \sin\vartheta d\vartheta \gamma^3 e^{(-\gamma^2 - \epsilon_i + \epsilon_j)} \frac{\mathrm{d}\sigma_{ij}^{kl}}{\mathrm{d}\Omega} A^{(\ell,s)} \tag{10.13}$$

with

$$A^{(1,1)} = (\gamma^2 - \gamma\gamma' \cos\vartheta) \tag{10.14}$$

$$A^{(2,2)} = [\gamma^4 \sin^2\vartheta + \tfrac{1}{3}(\Delta\epsilon)^2 - \tfrac{1}{2}(\Delta\epsilon)^2 \sin^2\vartheta] \tag{10.15}$$

where $\gamma^2 = (m_{qq'} g^2)/(2k_\mathrm{B}T)$, $\epsilon_i = E_i^q/k_\mathrm{B}T$, $\Delta\epsilon = \epsilon_k + \epsilon_l - \epsilon_i - \epsilon_j$ and Q_q is the internal partition function of q-th species. The Eq. (10.13) reduces, in the limit of elastic collision, to Eq. (3.11). In fact in this case we have $\gamma = \gamma'$ and $\Delta\epsilon$=0 and we retrieve exactly the elastic collision expressions provided that all internal states have the same elastic cross section, that is, $\sigma_{ij}^{kl} = \sigma_{el}$ for all i, j. If σ_{ij}^{kl} varies with i, j the classical expression is still obtained provided each quantum state is counted as a different molecular species. This last procedure has been adopted to estimate the influence of electronically excited states on transport properties. In this case both the diffusion- and viscosity-type collision integrals depend on the specific quantum number so that we are obliged to consider them as a separate species in the mixture. The elastic cross section involving vibrational states depends on the vibrational quantum number. As an example, the total elastic cross section for e-$N_2(v)$ interaction strongly decreases (Chandra and Temkin 1976) with the vibrational quantum number v.

Let us now consider the effect of inelastic cross sections on transport cross sections (see also Chap. 1). A lot of work has been done in this field, especially concerning the rotational degree of freedom (Chandra and Temkin 1976; Gianturco et al. 1991, 1994; Dickinson and Lee 1986; Parker and Pack 1978; Billing and Wang 1992; Wang and Billing 1992).

Classical and quantum scattering theories have been used for calculating the differential scattering cross sections for the process

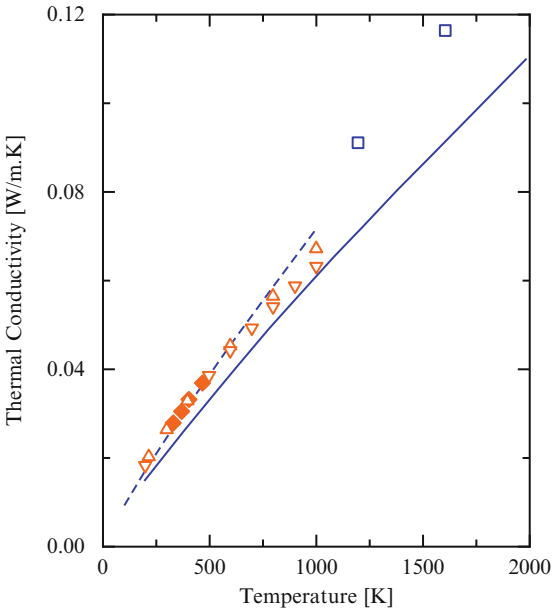

Fig. 10.11 Thermal conductivity of N_2 as a function of temperature. (*solid line*) semiclassical, (*dashed line*) classical rigid rotor, and (*open squares*) classical vibrating-rotor results, compared with experimental results (*down triangles*) (Touloukian 1970), (*up triangles*) (Shashkov et al. 1985), (*close diamonds*) (Haarman 1973)

$$M_2(i) + M_2(j) \rightarrow M_2(k) + M_2(l)$$

where i, j, k, l denote quantum states (rotational levels). These cross sections are then averaged in the collision integrals according to Eq. (10.13). In general, the use of the inelastic rotational cross sections does not change dramatically the collision integrals. A difference up to 6 % has been observed between viscosity-type collision integrals calculated with and without insertion of inelastic processes, the latter being larger. More important in this kind of calculation is the dependence of the collision integrals on the potential energy surface used in the scattering problem, as shown by Nyeland and Billing (1988). The effect of inelastic vibrational collisions in the calculation of the transport properties of air components is more complicated. Nyeland and Billing (1988) have tried to estimate this effect by using the same semiclassical treatment used for rotational states. The results show that the viscosity-type collision integrals for the rigid rotor are larger than the corresponding values for the vibrating rotor. In this case the two nitrogen molecules were allowed to have $1/2\hbar\omega$ energy each one. This result, however, gives greater values of transport coefficients, in disagreement with the experimental results (Touloukian 1970; Shashkov et al. 1985; Haarman 1973) (see Fig. 10.11).

A large effort has been also dedicated to understand the contribution of rotational states by using quantum scattering theories. The problem of using vibrational inelastic processes remains of great actuality, especially when the vibrational distribution of molecules is far from the Boltzmann one (see Chap. 6). The effect of inelastic vibrational collisions on the thermal conductivity of nitrogen has been studied by Billing and Wang (1992), in the frame of coupled semiclassical vibro-rotational treatment. The differences are in any case small. It should be noted the Eucken approximation gives approximately the same results.

Fox (1970) considered the role of the first electronic excitation of argon and lithium in affecting the diffusion coefficients of e-Ar, e-Li pairs. Insertion of inelastic cross section decreases the diffusion coefficient by approximately 15 % for argon and 8 % for lithium (see Fig. 10.12), in a temperature range where these collisions lose their importance as compared to electron–electron and electron–ion collisions. As a consequence the electrical conductivity for LTE argon and lithium plasmas was only affected by these collisions for no more than 1 %.

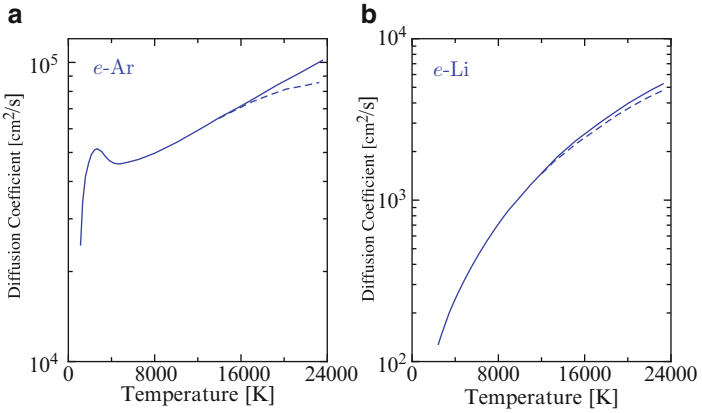

Fig. 10.12 Binary diffusion coefficient for electrons in neutral argon (a) and lithium (b) vapour at p=1 atm (Fox 1970). (*solid lines*) elastic collisions, (*dashed lines*) including inelastic electronic excitation channel

These results however can change for systems characterized by processes with low-energy threshold such as resonant vibrational excitation. In this case one should expect an important role of inelastic collisions in affecting the transport coefficients similarly of what happens in cold plasmas (Capitelli et al. 2000b).

10.4 Quantum Effects

The effectiveness of quantum effects can be estimated considering a model potential for the collisional-pair interaction, e.g. the well-known Lennard-Jones (12-6) potential (see Chap. 3). The diffusion-type cross section can be written in reduced form as (Imam-Rahajoe et al. 1965)

$$Q^{(1)\star} = \frac{Q^{(1)}}{\pi\sigma^2} = \left(\frac{\Lambda^{\star 2}}{\pi^2 E^\star}\right) \sum_\ell (\ell+1) \sin^2(\eta_{\ell+1} - \eta_\ell) \tag{10.16}$$

where $\Lambda^\star = h_{\text{P}}/\sigma(2\mu\varphi_0)^{1/2}$ is the quantum parameter which governs the magnitude of the quantum effects, $E^\star = E/\varphi_0$ is the reduced energy, and ℓ is the angular momentum quantum number. In turn the phase shifts are obtained by the solution of the radial wavefunction equation describing the scattering problem. The diffusion-type collision integrals are then obtained by integrating the cross sections on Maxwell distribution functions of the velocity. The classical behaviour is obtained in the limit $\Lambda^\star = 0$. As shown in Imam-Rahajoe et al. (1965), quantum effects are important for a reduced temperatures $T^\star = k_{\text{B}}T/\varphi_0 < 4$ and for $\Lambda^\star > 1$. As an example in the case of H_2–D_2 collisions $\Lambda^\star = 1.5$ and the corrections are very small for all reduced temperature range, while in the case of He–He $\Lambda^\star = 2.9$ and the quantum corrections are well evident for $T < 100$ K. In the interaction among air components the reduced mass and the depth of the attractive potentials reduce the $\Lambda^\star$ values, thus reducing the importance of quantum effects in this kind of collisions (Levin et al. 1994). Note, however, that in the electron–atom and electron–molecule cases the reduced mass corresponds to that one of the electron and the quantum corrections are very important because of the increased values of $\Lambda^\star$. Quantum corrections for attractive and repulsive screened Coulomb potentials have been considered by Hahn et al. (1971). These corrections increase with increasing $E^\star\Lambda^{\star 2}$ values, being in any case small for thermal plasma conditions.

10.5 Comparison with Experiments

A comparison of theoretical and experimental transport coefficients of plasmas suffers to some extent from the fact that no experiments have been attempted recently that could improve the measurements done forty years ago. On the other hand the theoretical results, while constantly improved in these last years, do not differ significantly with respect to old values, mainly because compensation effects occur in the different approaches. As a result the comparison between theory and experiments follows qualitatively the same lines discussed in the early papers (Capitelli and Devoto 1973; Capitelli et al. 1977). The situation however from the point of view of theory is nowadays

well assessed so that the differences between theoretical and experimental values can be ascribed to the partial lack of LTE (local thermodynamic equilibrium) conditions in the so-called thermal plasmas as well as in the possible errors in the measurements. Keeping in mind these considerations, different case studies, namely, hydrogen, nitrogen and air equilibrium plasmas, are here examined in detail.

Figure 10.13 reports a comparison of the theoretical transport coefficients (Bruno et al. 2010) with available experimental values, i.e. the total thermal conductivity and the electrical conductivity obtained in Popović and Konjević (1976) correcting for the radial temperature distribution. The agreement for both quantities can be considered satisfactory even though the comparison of the theoretical results with older experimental values (Plantikow and Steinberger 1970; Morris et al. 1970) reviewed in Bauder and Maecker (1971) is less satisfactory

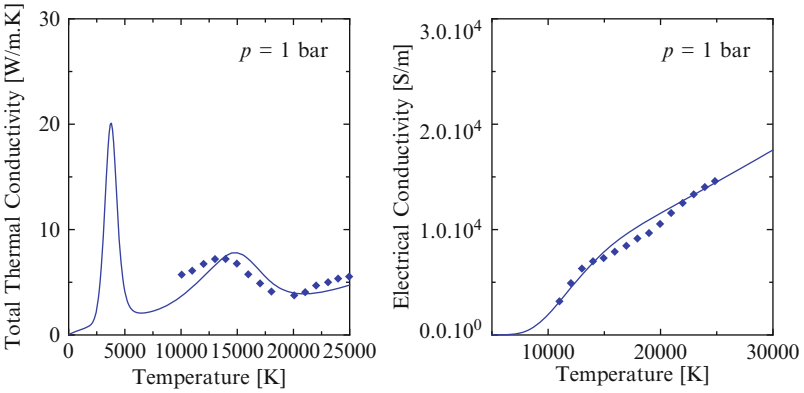

Fig. 10.13 Comparison of theoretical total thermal conductivity and electrical conductivity for equilibrium hydrogen plasma, at p=1 bar, with experiments. (*solid line*) (Bruno et al. 2010), (*close diamonds*) (Popović and Konjević 1976)

Figure 10.14 reports a comparison of the theoretical results calculated with the potentials derived as a subsystem of Mars database and the experimental results obtained by different authors. All the measurements have been corrected in some way for the transport of energy via radiation in the arc-heated gas. The corrective method employed by Asinovsky et al. (1971) appears to be the best: they measured the effective conductivity in arcs of different radii and extrapolated to zero radius where the effect of radiation vanishes. The agreement between theoretical and experimental results is indeed satisfactory especially taking into account the error bars reported in Capitelli and Devoto (1973) for the thermal conductivity and those of Schreiber et al. (1971) for the viscosity. The agreement is indeed very good for the electrical conductivity.

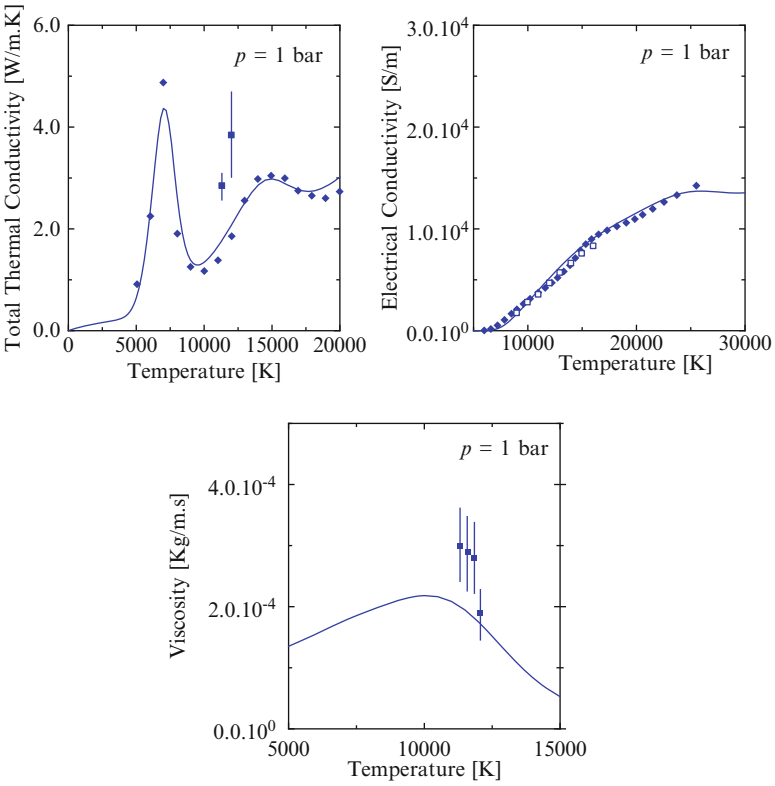

Fig. 10.14 Comparison of theoretical total thermal conductivity, electrical conductivity and viscosity for equilibrium nitrogen plasma, at p=1 bar, with experiments. (*solid line*) (Bruno et al. 2012), (*close diamonds*) (Hermann and Schade 1970, (*close squares*) (Schreiber et al. 1972, 1971), (*open squares*) (Asinovsky et al. 1971)

Finally, Fig. 10.15 compares theoretical and experimental thermal conductivity and electrical conductivity values for equilibrium air plasmas. Two series of theoretical results (D'Angola et al. 2008, 2012) are reported, obtained including two sets of transport cross sections discussed in Sect. 10.2.

A good agreement is found for the experimental electrical conductivity with both data sets of transport cross sections. The agreement between experimental and theoretical results seems to privilege the use of the old database of transport cross sections than the more recent calculations. This is more and more true in the region of nitrogen dissociation. We can see in fact that the largest difference occurs at about 7,000 K, dominated by the reactive thermal conductivity of nitrogen. In this case the results depend on the $\sigma^2\Omega^{(1,1)\star}$ of the N–N_2 interaction pair, which, according to our analysis, should be better described by our recent calculations. These data in fact are in good agreement with the quantum mechanical calculations of Stallcop et al. (2001), as it can be appreciated in Fig. 10.16. Probably the two sets of theoretical

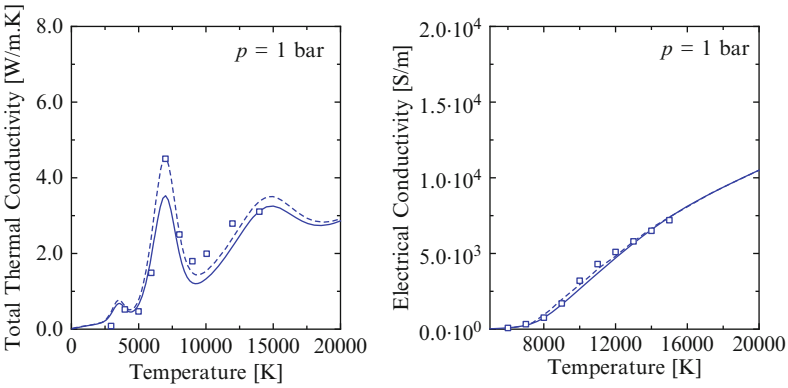

Fig. 10.15 Comparison of theoretical total thermal conductivity and electrical conductivity for equilibrium air plasma, at p=1 bar, with experiments. (*solid line*) (D'Angola et al. 2012) with transport cross section data set in Laricchiuta et al. (2007), (*dashed line*) (D'Angola et al. 2008) with transport cross section data set in Capitelli et al. (2000c), (*open squares*) (Asinovsky et al. 1971)

results become compatible with the experimental ones once taken into account possible error bars of the experimental values. Note that the present status of theoretical and experimental results seems to definitively rule out older theoretical values (Yos 1965; Bacri and Raffanel 1987, 1989; Hansen 1960), which however are still widely used in fluid dynamics codes.

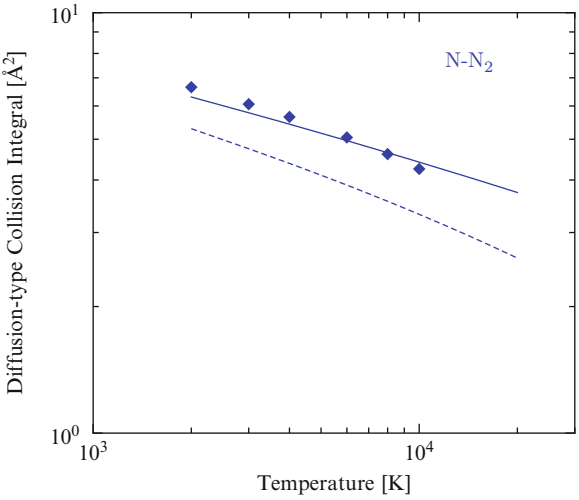

Fig. 10.16 Diffusion-type collision integrals for N–N_2 interaction. (*solid line*) (Laricchiuta et al. 2007), (*dashed line*) (Capitelli et al. 2000c), (*closed markers*) (Stallcop et al. 2001)

References

Asinovsky E, Kirillin A, Pakhomov E, Shabashov V (1971) Experimental investigation of transport properties of low-temperature plasma by means of electric arc. P IEEE 59(4):592–601

Bacri J, Raffanel S (1987) Calculation of some thermodynamic properties of air plasmas: Internal partition functions, plasma composition, and thermodynamic functions. Plasma Chem Plasma Process 7(1):53–87

Bacri J, Raffanel S (1989) Calculation of transport coefficients of air plasmas. Plasma Chem Plasma P 9(1):133–154

Bauder U, Maecker H (1971) The determination of transport properties from arc experiments: Methods and results. P IEEE 59(4):588–592

Belyaev YN, Brezhnev BG, Erastov EM (1968) Resonant charge transfer of low energy carbon and nitrogen ions. Sov Phys JETP 27(6):924

Billing GD, Wang L (1992) Semiclassical calculations of transport coefficients and rotational relaxation of nitrogen at high temperatures. J Phys Chem 96(6):2572–2575

Brokaw RS (1960) Thermal conductivity of gas mixtures in chemical equilibrium. II. J Chem Phys 32(4):1005–1006

Bruno D, Catalfamo C, Laricchiuta A, Giordano D, Capitelli M (2006) Convergence of Chapman-Enskog calculation of transport coefficients of magnetized argon plasma. Phys Plasmas 13(7):072307

Bruno D, Catalfamo C, Capitelli M, Colonna G, De Pascale O, Diomede P, Gorse C, Laricchiuta A, Longo S, Giordano D, Pirani F (2010) Transport properties of high-temperature Jupiter atmosphere components. Phys Plasmas 17(11):112315

Butler JN, Brokaw RS (1957) Thermal conductivity of gas mixtures in chemical equilibrium. J Chem Phys 26(6):1636–1643

Capitelli M (1970) Problems of determination of transport properties of argon-nitrogen mixtures at one atmosphere between 5 000 K and 15 000 K. Quaderni dell'Ingegnere Chimico Italiano 6:94–103

Capitelli M (1972) Simplified expressions for the calculation of the contribution of the heavy components to the transport coefficients of partially ionized gases. Zeitschrift für Naturforschung A (Astrophysik, Physik und Physikalische Chemie) 27:809–812

Capitelli M (1977) Transport coefficients of partially ionized gases. Journal de Physique Supplemént Colloque C3 (Paris) 38(8):C3 227–C3 237

Capitelli M, Devoto RS (1973) Transport coefficients of high-temperature nitrogen. Phys Fluids 16(11):1835

Capitelli M, Gorse C, Fauchais P (1977) Transport coefficients of high temperature N_2-H_2 mixtures. J de Physique 38(6):653

Capitelli M, Celiberto R, Gorse C, Giordano D (1996) Transport properties of high temperature air components: a review. Plasma Chem Plasma P 16:S267-S302

Capitelli M, Colonna G, Gorse C, D'Angola A (2000a) Transport properties of high temperature air in local thermodynamic equilibrium. Eur Phys J D 11(2):279–289

Capitelli M, Ferreira CM, Gordiets BF, Osipov R (2000b) Plasma kinetics in atmospheric gases. Springer, New York

Capitelli M, Gorse C, Longo S, Giordano D (2000c) Collision integrals of high-temperature air species. J Thermophys Heat Transf 14(2):259–268

Capitelli M, Cappelletti D, Colonna G, Gorse C, Laricchiuta A, Liuti G, Longo S, Pirani F (2007) On the possibility of using model potentials for collision integral calculations of interest for planetary atmospheres. Chem Phys 338(1):62–68

Capitelli M, Colonna G, D'Angola A (2011) Fundamental aspects of plasma chemical physics: Thermodynamics. Springer series on atomic, optical, and plasma physics, vol 66. Springer, New York

Bruno D, Colonna G, Laricchiuta A, Capitelli M (2012) Reactive and internal contributions to the thermal conductivity of local thermodynamic equilibrium nitrogen plasma: The effect of electronically excited states. Phys Plasmas 19: 122309

Chandra N, Temkin A (1976) NASA Techn Note D-8347

Chang WCS, Uhlenbeck GE (1951) Transport Phenomena in Polyatomic Gases. report CM-681 University of Michigan Engineering Research

D'Angola A, Colonna G, Gorse C, Capitelli M (2008) Thermodynamic and transport properties in equilibrium air plasmas in a wide pressure and temperature range. Eur Phys J D 46(1):129–150

D'Angola A, Colonna G, Gorse C, Capitelli M (2011) Thermodynamic properties of high temperature air in local thermodynamic equilibrium: II accurate analytical expression for electron molar fractions. Eur Phys J D 65(3):453–457

D'Angola A, Colonna G, Bonomo A, Bruno D, Laricchiuta A, Capitelli M (2012) A phenomenological approach for the transport properties of air plasmas. Eur Phys J D 66: 205

Devoto RS (1967a) Simplified expressions for the transport properties of ionized monatomic gases. Phys Fluids 10(10):2105–2112

Devoto RS (1967b) Transport coefficients of partially ionized argon. Phys Fluids 10(2):354–364

Devoto RS (1968) Transport coefficients of partially ionized hydrogen. J Plasma Phys 2(4):617–631

Dickinson AS, Lee MS (1986) Classical trajectory calculations for anisotropy-dependent cross sections for He-N_2 mixtures. J Phys B: Atom Mol Phys 19(19):3091

Fox RL (1970) Effect of inelastic collisions on electron transport coefficients. Phys Fluids 13(6):1480

Gianturco FA, Serna S, Sanna N (1991) Dynamical decoupling in the quantum calculations of transport coefficients. I - coupled state results for He-N_2 gaseous mixtures. Mol Phys 74(5):1071

Gianturco FA, Serna S, Sanna N (1994) An improved He-CO interaction potential from a multiproperty analysis. Mol Phys 81(2):421

Haarman JW (1973) Thermal conductivity measurements of He, Ne, Ar, Kr, N_2 and CO_2 with a transient hot wire method. AIP Conf Proc 11(1):193–202

Hahn HS, Mason EA, Smith FJ (1971) Quantum transport cross sections in a completely ionized gas. Phys Fluids 14(2):278–287

Hansen C (1960) vol TR-R50. Technical Rep. NASA, Ames Research Center, Ames, Iowa

Hermann W, Schade E (1970) Transportfunktionen von stickstoff bis 26000 K. Zeitschrift für Physik A Hadrons and Nuclei 233:333–350

Hirschfelder JO, Curtiss CF, Bird RB (1966) Molecular theory of gases and liquids. Wiley, New York

Imam-Rahajoe S, Curtiss CF, Bernstein RB (1965) Numerical evaluation of quantum effects on transport cross sections. J Chem Phys 42(2):530–536

Kosarim AV, Smirnov BM (2005) Electron terms and resonant charge exchange involving oxygen atoms and ions. J Exp Theor Phys 101(4):611–627

Kosarim AV, Smirnov BM, Capitelli M, Celiberto R, Laricchiuta A (2006) Resonant charge exchange involving electronically excited states of nitrogen atoms and ions. Phys Rev A 74(6):062707

Laricchiuta A, Colonna G, Bruno D, Celiberto R, Gorse C, Pirani F, Capitelli M (2007) Classical transport collision integrals for a Lennard-Jones like phenomenological model potential. Chem Phys Lett 445(4–6):133–139

Laricchiuta A, Bruno D, Capitelli M, Catalfamo C, Celiberto R, Colonna G, Diomede P, Giordano D, Gorse C, Longo S, Pagano D, Pirani F (2009) High temperature Mars atmosphere. Part I: Transport cross sections. Eur Phys J D 54(3):607–612

Levin E, Schwenke DW, Stallcop JR, Partridge H (1994) Comparison of semiclassical and quantum-mechanical methods for the determination of transport cross sections. Chem Phys Lett 227(6):669

Liboff RL (1959) Transport coefficients determined using the shielded Coulomb potential. Phys Fluids 2(1):40–46

Mason EA, Monchick L (1962) Heat conductivity of polyatomic and polar gases. J Chem Phys 36(6):1622–1639

Morris JC, Rudis RP, Yos JM (1970) Measurements of electrical and thermal conductivity of hydrogen, nitrogen, and argon at high temperatures. Phys Fluids 13(3):608–617

Murphy AB (1995) Transport coefficients of air, argon-air, nitrogen-air, and oxygen-air plasmas. Plasma Chem Plasma P 15(2):279

Murphy AB (2000) Transport coefficients of hydrogen and argon–hydrogen plasmas. Plasma Chem Plasma P 20(3):279–297

Nyeland C, Billing GD (1988) Transport coefficients of diatomic gases: Internal-state analysis for rotational and vibrational degrees of freedom. J Phys Chem 92:1752

Parker GA, Pack RT (1978) Rotationally and vibrationally inelastic scattering in the rotational IOS approximation. ultrasimple calculation of total (differential, integral, and transport) cross sections for nonspherical molecules. J Chem Phys 68(4):1585

Plantikow U, Steinberger S (1970) Elektrische und thermische leitfähigkeit von wasserstoff bis 27 000 K. Zeitschrift für Physik A Hadrons and Nuclei 109:231

Popović S, Konjević N (1976) On the thermal conductivity of hydrogen at elevated temperatures. Zeitschrift für Naturforschung A (Astrophysik, Physik und Physikalische Chemie) 31:1042

Rat V, Murphy AB, Aubreton J, Elchinger MF, Fauchais P (2008) Treatment of non-equilibrium phenomena in thermal plasma flows. J Phys D: Appl Phys 41(18):183001

Schreiber PW, II AMH, Benedetto KR (1971) Argon and nitrogen plasma viscosity measurements. Phys Fluids 14(12):2696–2702

Schreiber PW, II AMH, Benedetto KR (1972) Measurement of nitrogen plasma transport properties. AIAA J 10(5):670–6747

Sharma R, Singh G, Singh K (2011) Higher-order contributions to transport coefficients in two-temperature hydrogen thermal plasma. Phys Plasmas 18(6):063504

Shashkov AG, Abramenko TN, Aleinikova VI (1985) Determination of the true thermal conductivities of helium and nitrogen at atmospheric pressure and temperatures from the normal boiling points to 6700 K. J Eng Phys Thermophys 49:818–827

Singh G, Singh K (2006) Estimation of higher-order contribution to viscosity of hydrogen plasmas including electronically excited states. Phys Plasmas 13(12):122309

Singh G, Singh K, Sharma R (2009) Estimation of higher-order contributions to viscosity in thermal plasmas: role of unlike interactions. Phys Plasmas 16:114507

Spitzer L, Härm R (1953) Transport phenomena in a completely ionized gas. Phys Rev 89(5):977–981

Stallcop JR, Partridge H, Levin E (2001) Effective potential energies and transport cross sections for atom-molecule interactions of nitrogen and oxygen. Phys Rev A 64(4):042722 1–12

Touloukian YS (1970) Thermophysical properties of matter. IFI/Plenum, New York

van de Sanden MCM, Schram PPJM, Peeters AG, van der Mullen JAM, Kroesen GMW (1989) Thermodynamic generalization of the saha equation for a two-temperature plasma. Phys Rev A 40(9):5273

Wang L, Billing GD (1992) Rotational relaxation and transport coefficients for gaseous hydrogen chloride. J Chem Soc Faraday T 88(2):163

Yos JM (1965) vol RAD-TF 65-7. AVCO Coporation, Wilmington, Massachusetts (USA)

Chapter 11
Transport Properties of High Temperature Planetary Atmospheres

In this chapter we report in graphical and tabular form the transport properties of high-temperature planetary atmospheres (Earth, Mars and Jupiter) in a wide range of temperature and pressure.[1] We are using the basic equations for the transport equations illustrated in Chap. 1 as well as transport cross sections databases calculated according to the methods reported in Chaps. 3 and 4. We limit our transport data to LTE (local thermodynamic equilibrium) situations leaving to future editions extensive tables including several important features discussed in the present volume (two-temperature plasmas, inclusion of vibrational and electronically excited states, magnetic field role). The relevant data together with the corresponding thermodynamic data (Capitelli et al. 2011) can be used with a fair amount of confidence in several applications of plasma and laser–plasma dynamics. It should be noted that we have also reported tables of thermodynamic properties of planetary atmospheres at 1,000 bar, missing in Capitelli et al. (2011).

11.1 Basic Equations

Transport coefficients of high-temperature planetary atmospheres have been calculated according to the following hypotheses (Devoto 1967; Capitelli et al. 1976; Capitelli 1977; Capitelli et al. 2000a; D'Angola et al. 2008):

- The translational thermal conductivity of the plasma is considered as the sum of the contributions due to heavy particles and free electrons, i.e. $\lambda_{tr} = \lambda_h + \lambda_e$. λ_h is calculated in the first non-vanishing approximation of the Chapman–Enskog (CE) method, while the third approximation is used for λ_e.

[1] The pressure is given in bar, though throughout the book, also atm units are used for results taken from literature, the conversion factor being 1 bar=0.987 atm.

M. Capitelli et al., *Fundamental Aspects of Plasma Chemical Physics*,
Springer Series on Atomic, Optical, and Plasma Physics 74,
DOI 10.1007/978-1-4419-8172-1_11, © Springer Science+Business Media, LLC 2013

- The viscosity of the plasma is decoupled in the sum of heavy particle and free electron contributions, the last term being neglected. The heavy-particle viscosity is calculated according to the first CE approximation.
- The electrical conductivity is limited to the electron contribution and calculated in the third CE approximation.
- The compact Brokaw approximation has been used for the calculation of the reactive thermal conductivity.
- The Eucken approximation in the form

$$\lambda_{int} = \frac{1}{T} \sum_{j=1}^{\nu} \frac{x_j \frac{(c^P \mathrm{int})_j}{k_\mathrm{B}}}{\sum_{i=1}^{\nu} \frac{x_i}{p\mathcal{D}_i^j}} \tag{11.1}$$

  is used for the calculation of the internal thermal conductivity. This approach is used for the calculation of transport properties of Earth and Mars atmospheres. On the other hand for Jupiter the results have been obtained with the equivalent approach described in Chaps. 1 and 2, however not separating electron and heavy-particle contributions in the translational thermal conductivity and viscosity. Moreover in the Jupiter case both electrons and ions are inserted in the calculation of the Debye length. In particular the second non-vanishing approximation has been used for λ and η (i.e. the third and the second approximations in the Devoto formulation, respectively).

Once selected the transport equations, appropriate transport collision integrals and thermodynamic properties of the species forming the high-temperature mixture must be entered. The recent database of Mars atmosphere (Laricchiuta et al. 2009) has been also used for air (Bruno et al. 2011; D'Angola et al. 2012), the Earth atmosphere components being a sub-system of Mars atmosphere. Collision integrals relevant to Jupiter component interactions have been recently reviewed in Bruno et al. (2010).

Finally equilibrium compositions and thermodynamic properties entering in the transport equations are those tabulated in the recently published book by Capitelli et al. (2011) (here results for the three atmospheres at p=1,000 bar are reported also to complete the database of thermodynamic properties). Briefly these data have been obtained by accurate values of internal partition functions; in the case of monatomic species (neutral and ionized) a self-consistent *cutoff* criterion, based on the interplay of Griem and Fermi criteria, has been used over complete sets of energy levels (observed and missing) of the relevant atomic species (Capitelli et al. 2000a; D'Angola et al. 2008). Accurate values of equilibrium compositions and thermodynamic properties of the species forming the mixture are inserted in the transport equations overestimating the role of electronic excitation in affecting the transport coefficients, calculated inserting the ground-state transport cross sections. This decision can be justified with the still poor existence of complete databases including the dependence of the transport cross sections on

the quantum state of the colliding species, despite the efforts done in this book. The progress in this direction is increasing and we hope to report more accurate values, including the role of electronically excited states, possibly in a second edition of the book. Note also that some caution should be exercised when using these data at very high pressure and low temperature when the concept of binary collision is open to criticism (D'Angola et al. 2012).

11.2 Collision Integrals

11.2.1 Mars and Earth Interactions

Collision integrals for neutral–neutral and ion–neutral interactions involving atomic and polyatomic species and multiply-charged ions have been calculated, modelling the interactions in the frame of the phenomenological approach (see Chap. 3).

Polarizabilities have been taken from literature (Hirschfelder et al. 1966; Miller and Bederson 1977; Das et al. 1992; Hati and Datta 1995, 1996) or estimated through an empirical formula (Alagia et al. 2004) for neutral and unstable ionic gaseous species, for which no experimental and/or theoretical information is available. For polyatomic species an "effective atomic polarizability-in-molecule" approach (van Duijnen and Swart 1998; Ewig et al. 2002; Gavezzotti 2003) has been adopted. In Table 11.1 the polarizability values for Mars atmosphere species have been reported. In Tables 11.2–11.4 the parameters for the phenomenological potential in neutral and neutral–ion interactions have been presented, whose values allow the direct estimation of the corresponding collision integrals through fitting relations Eqs. (3.67) and (3.68) (see Sect. 3.4.2).

Inelastic contributions to odd-order collision integrals due to resonant charge-exchange processes in ion–parent-neutral interactions have been fitted with the following formula:

$$\sigma^2 \Omega_{\mathrm{ex}}^{(\ell,s)\star} = d_1 + d_2 x + d_3 x^2 \tag{11.2}$$

where $x = \ln(T)$. Table 11.5 reports fitting parameters for different systems, together with the references in literature for resonant charge-exchange cross sections. For ion–parent-atom interactions results obtained in the framework of the asymptotic theory (Nikitin and Smirnov 1978; Smirnov 2001) have been considered and parameters listed, in the table, as well as those for oxygen and nitrogen systems, for which cross sections data have recently been updated (Kosarim and Smirnov 2005; Kosarim et al. 2006). In Capitelli et al. (2000b) $\sigma^2 \Omega^{(1,s)\star}$ values were derived, from multi-state impact parameter cross sections (Flannery et al. 1973; Moran et al. 1974), for molecule–molecular-ion systems relevant to Earth atmosphere, i.e. N_2–N_2^+,

O_2–O_2^+, O_2–O_2^-, NO–NO^+ (see Table 9 of Capitelli et al. 2000b). CO–CO^+ interaction has been included, using resonant cross sections by Yevseyev et al. (1982), obtained by extending the asymptotic theory to diatoms, while for C_2–C_2^+ and CN–CN^+ collision integrals have been assumed equal to C–C^+ and CO–CO^+, respectively. Resonant charge-transfer processes involving triatomic species have not been considered yet.

In Table 11.4 parameters for atom–multiply-charged ion interactions, modeled with the phenomenological potential, are reported. The depth of the potential well was found to be of the order of eV or even tens of eV in some cases, due to the strength of induction fields, which characterize these kinds of interactions. As for singly charged ions, the contribution of inelastic resonant processes has been estimated. Corresponding cross sections for multiple resonant charge exchange have been evaluated in the framework of the asymptotic approach (see Section 4.3). Adopting the functional form of Eq. (11.2), fitting coefficients for considered colliding systems are reported in Table 11.6.

In the case of electron–neutral species interactions, the approaches outlined in Section 3.4.4 have been used, in particular:

- CO_2 momentum transfer and elastic cross sections from Itikawa (2002) (for energies lower than 1 eV the elastic cross section is considered equal to the momentum transfer one).
- CO elastic and momentum transfer from Chandra (1977).
- C elastic cross section from Thomas and Nesbet (1975b) and Coulomb screening with $Z = 6$ for the calculation of Q^2.
- N_2O elastic and momentum transfer from Winstead and McKoy (1998) for energies greater than 1.5 eV due to the better resolution of the resonance region, while for lower energies data are from Biagi (2012) and the momentum transfer cross section is considered equal to the elastic one.
- O_3 elastic momentum transfer from Biagi (2012) and Coulomb screening with average Z for the calculation of Q^2.

For air species, i.e. N, O, N_2, O_2 and NO, new calculations have been performed that represent an extension of the database for electron–neutral collisions for Earth atmosphere species (Capitelli et al. 2000b):

- As regards the nitrogen molecule, the momentum transfer cross section is the one by Itikawa (2006), whereas the corrections Q^2/Q^1 and Q^3/Q^1 have been obtained by integrating the differential cross sections recommended by Brunger and Buckman (2002). From 0.55 to 10 eV the differential cross sections were taken from Sun et al. (1995), while for energies above 10 eV from Gote and Ehrhardt (1995).
- For the e–O_2 interaction we used the momentum transfer cross section from Phelps (2007) below 0.5 eV, while above 0.5 eV we used the one from Itikawa et al. (1989). For the DCS data, we used the ones of Sullivan et al. (1995), recommended by Brunger and Buckman (2002), below 30 eV, while above 30 eV we used the ones of Shyn and Sharp (1982).

- For the e–NO interaction the momentum transfer is the one of Hayashi (1989), while the Q^2/Q^1 and Q^3/Q^1 corrections were obtained by integrating the DCS of Mojarrabi et al. (1995), again following the recommendations of Brunger and Buckman (2002).
- As regards the e–O collision, we have used the Q^2 and Q^1 cross sections of Thomas and Nesbet (1975a). Additional points at 20, 45 and 100 eV were obtained by integrating the differential cross sections of Blaha and Davis (1975). The Q^3/Q^1 ratio was deduced from the known Q^2/Q^1 by assuming the model angular dependence of the differential cross section in Eq. (3.69).
- The e–N collision integrals were calculated using the total and differential elastic cross section of Thomas and Nesbet (1975c) with $\Delta = 0.575$ eV below 2 eV and the results of Blaha and Davis for higher energies (Blaha and Davis 1975).

For electron–argon interaction high-order collision integrals have been derived by integration of experimental differential elastic scattering cross sections (see Bruno et al. 2006).

Electron–molecule systems, whose transport cross sections are not available, have been modeled considering the corresponding collision integrals equal to known interactions. Collision integrals have been fitted, as a function of $x = \ln(T)$, using the following formula, which is slightly different from the one proposed in the previous work (Capitelli et al. 2000b) due to the additional parameter g_{10}:

$$\sigma^2 \Omega^{(\ell,s)\star} = \frac{g_3 x^{g_6} \exp\left[(x-g_1)/g_2\right]}{\exp\left[(x-g_1)/g_2\right] + \exp\left[-(x-g_1)/g_2\right]} + g_7 \exp\left[-\left(\frac{x-g_8}{g_9}\right)^2\right] + g_4 + g_{10} x^{g_5} \tag{11.3}$$

Fitting coefficients g_j, entering Eq. (11.3), are presented in Table 11.7, for relevant interaction in the Mars atmosphere.

Table 11.1 Polarizability values (Å^3) for Mars atmosphere species

Ar (^{1}S)	1.64	N^{2+} (^{2}P)	0.284	N_2	1.75	C_3	3.60
Ar^+ (^{2}P)	0.919	N^{3+} (^{1}S)	0.209	N_2^+	1.75	N_3	2.70
Ar^{2+} (^{3}P)	0.391	N^{4+} (^{2}S)	0.201	N_2^-	7.00	O_3	3.21
Ar^{3+} (^{4}S)	0.231	N^- (^{3}P)	4.41	O_2	1.60	O_3^-	6.42
Ar^{4+} (^{3}P)	0.294	O (^{3}P)	0.80	O_2^+	0.80	C_2N	3.3
C (^{3}P)	1.76	O^+ (^{4}S)	0.279	O_2^-	6.40	CO_2	2.91
C^+ (^{2}P)	0.79	O^{2+} (^{3}P)	0.228	CN	2.1	CO_2^+	1.46
C^{2+} (^{1}S)	0.368	O^{3+} (^{2}P)	0.182	CN^+	1.05	CO_2^-	11.64
C^{3+} (^{2}S)	0.289	O^{4+} (^{1}S)	0.164	CN^-	4.20	C_2O	3.2
C^{4+} (^{1}S)	0.003	O^- (^{2}P)	3.256	CO	1.95	NO_2	3.02
C^- (^{4}S)	5.13	C_2	2.4	CO^+	0.98	N_2O	3.03
N (^{4}S)	1.1	C_2^+	1.2	NO	1.70	N_2O^+	1.52
N^+ (^{3}P)	0.55	C_2^-	4.8	NO^+	0.85	CNO	2.9

Table 11.2 Parameters of phenomenological potential for neutral–neutral interactions (m =6) relevant to Mars atmosphere

	β	φ_0 (meV)	r_e (Å)		β	φ_0 (meV)	r_e (Å)		β	φ_0 (meV)	r_e (Å)
Ar–Ar	8.12	11.603	3.794	O–C_2N	7.17	8.840	3.895	CO–O_3	7.84	16.409	4.044
Ar–C	7.04	9.289	3.813	O–CO_2	7.19	9.270	3.842	CO–C_2N	7.83	15.127	4.054
Ar–N	6.94	8.505	3.695	O–C_2O	7.17	8.995	3.882	CO–CO_2	7.87	15.418	4.011
Ar–O	7.26	7.821	3.629	O–NO_2	7.18	9.529	3.857	CO–C_2O	7.84	15.277	4.043
Ar–C_2	7.99	11.955	3.906	O–N_2O	7.18	9.298	3.859	CO–NO_2	7.86	15.908	4.024
Ar–N_2	8.10	11.508	3.812	O–CNO	7.19	9.105	3.841	CO–N_2O	7.85	15.576	4.025
Ar–O_2	8.13	11.780	3.787	C_2–C_2	7.87	12.954	4.006	CO–CNO	7.87	15.166	4.010
Ar–CN	8.03	11.834	3.865	C_2–N_2	7.97	11.991	3.922	NO–NO	8.09	11.845	3.813
Ar–CO	8.06	11.869	3.843	C_2–O_2	7.99	12.062	3.901	NO–C_3	7.83	14.538	4.055
Ar–NO	8.11	11.721	3.804	C_2–CN	7.91	12.608	3.969	NO–N_3	7.93	14.485	3.954
Ar–C_3	7.84	14.299	4.048	C_2–CO	7.93	12.507	3.950	NO–O_3	7.87	15.916	4.013
Ar–N_3	7.94	14.288	3.945	C_2–NO	7.97	12.125	3.915	NO–C_2N	7.86	14.581	4.023
Ar–O_3	7.88	15.686	4.006	C_2–C_3	7.74	15.923	4.134	NO–CO_2	7.91	14.976	3.979
Ar–C_2N	7.87	14.354	4.016	C_2–N_3	7.83	15.328	4.041	NO–C_2O	7.87	14.757	4.012
Ar–CO_2	7.92	14.765	3.971	C_2–O_3	7.78	16.982	4.096	NO–NO_2	7.89	15.451	3.992
Ar–C_2O	7.88	14.534	4.005	C_2–C_2N	7.77	15.803	4.105	NO–N_2O	7.89	15.106	3.993
Ar–NO_2	7.90	15.233	3.984	C_2–CO_2	7.81	15.922	4.064	NO–CNO	7.91	14.719	3.978
Ar–N_2O	7.90	14.888	3.985	C_2–C_2O	7.78	15.909	4.095	C_3–C_3	7.63	20.118	4.246
Ar–CNO	7.92	14.510	3.970	C_2–NO_2	7.80	16.430	4.076	C_3–N_3	7.71	18.969	4.164
C–C	6.69	7.861	3.832	C_2–N_2O	7.79	16.123	4.077	C_3–O_3	7.66	21.260	4.212
C–N	6.65	6.884	3.717	C_2–CNO	7.81	15.681	4.063	C_3–C_2N	7.65	19.841	4.220
C–O	6.78	6.125	3.653	N_2–N_2	8.07	11.443	3.829	C_3–CO_2	7.69	19.805	4.185
C–C_2	7.01	9.984	3.924	N_2–O_2	8.11	11.665	3.805	C_3–C_2O	7.66	19.928	4.211
C–N_2	7.04	9.314	3.831	N_2–CN	8.01	11.825	3.881	C_3–NO_2	7.68	20.486	4.195
C–O_2	7.04	9.364	3.807	N_2–CO	8.04	11.831	3.860	C_3–N_2O	7.68	20.111	4.196
C–CN	7.02	9.748	3.883	N_2–NO	8.08	11.635	3.821	C_3–CNO	7.69	19.504	4.184
C–CO	7.03	9.679	3.861	N_2–C_3	7.83	14.410	4.061	N_3–N_3	7.80	18.392	4.075

C–NO	7.04	9.409	3.823	N_2–N_3	7.92	14.282	3.960	N_3–O_3	7.74	20.470	4.127
C–C_3	6.97	12.028	4.063	N_2–O_3	7.87	15.700	4.020	N_3–C_2N	7.74	18.869	4.136
C–N_3	7.00	11.650	3.962	N_2–C_2N	7.86	14.430	4.030	N_3–CO_2	7.77	19.127	4.097
C–O_3	6.98	12.783	4.021	N_2–CO_2	7.90	14.772	3.986	N_3–C_2O	7.74	19.033	4.126
C–C_2N	6.98	11.959	4.031	N_2–C_2O	7.87	14.590	4.019	N_3–NO_2	7.76	19.780	4.108
C–CO_2	6.99	12.058	3.987	N_2–NO_2	7.89	15.237	3.998	N_3–N_2O	7.76	19.362	4.109
C–C_2O	6.98	12.037	4.020	N_2–N_2O	7.89	14.908	3.999	N_3–CNO	7.77	18.807	4.096
C–NO_2	6.99	12.408	4.000	N_2–CNO	7.90	14.526	3.984	O_3–O_3	7.69	22.900	4.177
C–N_2O	6.99	12.193	4.001	O_2–O_2	8.14	11.972	3.780	O_3–C_2N	7.69	21.104	4.185
C–CNO	6.99	11.891	3.986	O_2–CN	8.04	11.964	3.859	O_3–CO_2	7.72	21.334	4.148
N–N	6.61	6.432	3.583	O_2–CO	8.07	12.017	3.836	O_3–C_2O	7.70	21.273	4.176
N–O	6.72	5.989	3.507	O_2–NO	8.12	11.895	3.797	O_3–NO_2	7.71	22.089	4.159
N–C_2	6.91	8.639	3.821	O_2–C_3	7.85	14.397	4.043	O_3–N_2O	7.71	21.619	4.160
N–N_2	6.94	8.424	3.715	O_2–N_3	7.95	14.454	3.940	O_3–CNO	7.72	20.971	4.147
N–O_2	6.94	8.633	3.687	O_2–O_3	7.89	15.862	4.000	C_2N–C_2N	7.68	19.620	4.194
N–CN	6.92	8.597	3.774	O_2–C_2N	7.88	14.474	4.011	C_2N–CO_2	7.71	19.677	4.157
N–CO	6.93	8.642	3.750	O_2–CO_2	7.93	14.931	3.965	C_2N–C_2O	7.69	19.732	4.184
N–NO	6.94	8.578	3.706	O_2–C_2O	7.89	14.667	3.999	C_2N–NO_2	7.70	20.353	4.167
N–C_3	6.88	10.069	3.977	O_2–NO_2	7.91	15.407	3.979	C_2N–N_2O	7.70	19.963	4.168
N–N_3	6.91	10.171	3.864	O_2–N_2O	7.91	15.048	3.980	C_2N–CNO	7.72	19.369	4.156
N–O_3	6.89	11.032	3.930	O_2–CNO	7.93	14.667	3.964	CO_2–CO_2	7.75	19.911	4.119
N–C_2N	6.89	10.141	3.941	CN–CN	7.95	12.342	3.931	CO_2–C_2O	7.72	19.839	4.147
N–CO_2	6.90	10.461	3.892	CN–CO	7.98	12.288	3.910	CO_2–NO_2	7.74	20.599	4.130
N–C_2O	6.89	10.272	3.929	CN–NO	8.02	11.986	3.874	CO_2–N_2O	7.74	20.166	4.131
N–NO_2	6.90	10.757	3.906	CN–C_3	7.78	15.350	4.102	CO_2–CNO	7.75	19.577	4.118
N–N_2O	6.90	10.528	3.908	CN–N_3	7.87	14.964	4.005	C_2O–C_2O	7.70	19.858	4.175
N–CNO	6.90	10.293	3.891	CN–O_3	7.81	16.524	4.062	C_2O–NO_2	7.71	20.522	4.158
O–O	6.90	5.763	3.423	CN–C_2N	7.81	15.294	4.071	C_2O–N_2O	7.71	20.117	4.159

(continued)

Table 11.2 (continued)

	β	φ_0 (meV)	r_e (Å)		β	φ_0 (meV)	r_e (Å)		β	φ_0 (meV)	r_e (Å)
O–C_2	7.21	7.630	3.765	CN–CO_2	7.85	15.515	4.029	C_2O–CNO	7.72	19.521	4.146
O–N_2	7.25	7.677	3.651	CN–C_2O	7.82	15.425	4.061	NO_2–NO_2	7.73	21.319	4.141
O–O_2	7.26	7.978	3.621	CN–NO_2	7.83	16.008	4.042	NO_2–N_2O	7.73	20.866	4.142
O–CN	7.23	7.696	3.715	CN–N_2O	7.83	15.688	4.043	NO_2–CNO	7.74	20.249	4.129
O–CO	7.24	7.805	3.689	CN–CNO	7.85	15.270	4.028	N_2O–N_2O	7.73	20.432	4.143
O–NO	7.26	7.862	3.641	CO–CO	8.00	12.264	3.889	N_2O–CNO	7.74	19.831	4.130
O–C_3	7.16	8.699	3.933	CO–NO	8.05	12.011	3.852	CNO–CNO	7.75	19.253	4.117
O–N_3	7.20	9.051	3.812	CO–C_3	7.80	15.145	4.085				
O–O_3	7.17	9.744	3.883	CO–N_3	7.89	14.885	3.987				

Table 11.3 Parameters of phenomenological potential for neutral–ion interactions (m =4) relevant to Mars atmosphere

	β	φ_0 (meV)	r_e (Å)		β	φ_0 (meV)	r_e (Å)		β	φ_0 (meV)	r_e (Å)
Ar–Ar^+	7.60	107.619	3.213	C^+–NO	7.64	114.191	3.174	N^-–CO	6.81	83.948	3.864
Ar–C^+	7.65	111.596	3.165	C^+–C_3	7.48	179.641	3.388	N^-–NO	6.82	75.124	3.839
Ar–C^-	6.62	69.986	3.907	C^+–N_3	7.54	151.876	3.300	N^-–C_3	6.77	133.758	3.998
Ar–N^+	7.37	121.840	3.054	C^+–O_3	7.50	168.151	3.352	N^-–N_3	6.79	108.169	3.930
Ar–N^-	6.82	72.941	3.833	C^+–C_2N	7.50	170.870	3.360	N^-–O_3	6.78	123.067	3.970
Ar–O^+	7.32	144.355	2.869	C^+–CO_2	7.53	158.768	3.322	N^-–C_2N	6.78	125.585	3.976
Ar–O^-	7.21	79.018	3.694	C^+–C_2O	7.50	167.847	3.351	N^-–CO_2	6.79	114.440	3.947
Ar–C_2^+	8.23	100.970	3.303	C^+–NO_2	7.52	162.269	3.333	N^-–C_2O	6.78	122.786	3.969
Ar–C_2^-	7.74	71.280	3.874	C^+–N_2O	7.52	162.583	3.334	N^-–NO_2	6.79	117.647	3.955
Ar–N_2^+	8.10	92.224	3.440	C^+–CNO	7.53	158.446	3.321	N^-–N_2O	6.79	117.936	3.956
Ar–N_2^-	7.62	64.057	4.067	C^-–N	6.45	49.483	3.850	N^-–CNO	6.79	114.146	3.946
Ar–O_2^+	8.37	111.259	3.168	C^-–O	6.52	37.012	3.815	O–O^+	6.93	93.447	2.689
Ar–O_2^-	7.65	65.747	4.020	C^-–C_2	6.61	95.555	3.975	O–O^-	6.87	43.565	3.581
Ar–CN^+	8.28	104.243	3.257	C^-–N_2	6.62	73.901	3.917	O–C_2^+	7.30	60.395	3.153
Ar–CN^-	7.79	73.905	3.810	C^-–O_2	6.62	68.542	3.903	O–C_2^-	7.12	37.930	3.779
Ar–CO^+	8.30	105.976	3.234	C^-–CN	6.61	85.856	3.949	O–N_2^+	7.25	53.609	3.302
Ar–NO^+	8.35	109.651	3.188	C^-–CO	6.61	80.822	3.936	O–N_2^-	7.06	32.911	3.993
Ar–O_3^-	7.65	65.687	4.021	C^-–NO	6.62	72.132	3.912	O–O_2^+	7.35	68.365	3.008
Ar–CO_2^+	8.16	96.339	3.373	C^-–C_3	6.59	130.318	4.064	O–O_2^-	7.08	34.062	3.940
Ar–CO_2^-	7.45	54.791	4.361	C^-–N_3	6.60	104.808	3.999	O–CN^+	7.32	62.936	3.104
Ar–N_2O^+	8.15	95.412	3.387	C^-–O_3	6.60	119.641	4.037	O–CN^-	7.14	39.814	3.709
Ar^+–C	6.90	112.671	3.231	C^-–C_2N	6.60	122.153	4.043	O–CO^+	7.32	64.280	3.079
Ar^+–N	6.82	82.229	3.121	C^-–CO_2	6.60	111.044	4.015	O–NO^+	7.34	67.123	3.029
Ar^+–O	7.06	65.552	3.056	C^-–C_2O	6.60	119.360	4.036	O–O_3^-	7.08	34.021	3.942
Ar^+–C_2	7.52	137.023	3.313	C^-–NO_2	6.60	114.238	4.023	O–CO_2^+	7.28	56.798	3.229
Ar^+–N_2	7.59	112.256	3.229	C^-–N_2O	6.60	114.526	4.024	O–CO_2^-	6.99	26.859	4.318
Ar^+–O_2	7.61	105.894	3.207	C^-–CNO	6.60	110.752	4.014	O–N_2O^+	7.27	56.078	3.245

(continued)

Table 11.3 (continued)

	β	φ_0 (meV)	r_e (Å)		β	φ_0 (meV)	r_e (Å)		β	φ_0 (meV)	r_e (Å)
Ar^+–CN	7.55	126.096	3.277	N–N^+	6.76	94.581	2.956	O^+–C_2	7.26	179.105	2.979
Ar^+–CO	7.57	120.323	3.257	N–N^-	6.55	51.979	3.772	O^+–N_2	7.31	149.866	2.887
Ar^+–NO	7.59	110.167	3.222	N–O^+	6.74	113.879	2.764	O^+–O_2	7.32	142.301	2.862
Ar^+–C_3	7.44	174.594	3.433	N–O^-	6.70	57.183	3.625	O^+–CN	7.28	166.240	2.939
Ar^+–N_3	7.50	147.240	3.347	N–C_2^+	6.96	76.403	3.215	O^+–CO	7.29	159.422	2.918
Ar^+–O_3	7.46	163.272	3.398	N–C_2^-	6.86	50.572	3.815	O^+–NO	7.31	147.385	2.879
Ar^+–C_2N	7.46	165.951	3.406	N–N_2^+	6.94	68.714	3.358	O^+–C_3	7.21	223.056	3.110
Ar^+–CO_2	7.48	154.028	3.368	N–N_2^-	6.83	44.559	4.020	O^+–N_3	7.25	191.095	3.016
Ar^+–C_2O	7.46	162.972	3.397	N–O_2^+	6.99	85.406	3.074	O^+–O_3	7.22	209.848	3.071
Ar^+–NO_2	7.47	157.476	3.379	N–O_2^-	6.84	45.950	3.970	O^+–C_2N	7.22	212.975	3.080
Ar^+–N_2O	7.47	157.786	3.380	N–CN^+	6.97	79.275	3.167	O^+–CO_2	7.24	199.043	3.040
Ar^+–CNO	7.48	153.711	3.367	N–CN^-	6.87	52.798	3.748	O^+–C_2O	7.22	209.497	3.070
C–C^+	6.91	116.739	3.182	N–CO^+	6.98	80.793	3.143	O^+–NO_2	7.23	203.076	3.051
C–C^-	6.48	74.253	3.918	N–NO^+	6.98	84.004	3.095	O^+–N_2O	7.23	203.438	3.053
C–N^+	6.82	127.234	3.073	N–O_3^-	6.84	45.901	3.971	O^+–CNO	7.24	198.672	3.038
C–N^-	6.59	77.281	3.845	N–CO_2^+	6.95	72.333	3.288	O^-–C_2	7.16	105.541	3.773
C–O^+	6.80	150.358	2.888	N–CO_2^-	6.78	37.113	4.331	O^-–N_2	7.20	83.124	3.706
C–O^-	6.76	83.492	3.707	N–N_2O^+	6.95	71.517	3.303	O^-–O_2	7.21	77.499	3.689
C–C_2^+	7.07	105.878	3.320	N^+–O	6.95	76.475	2.886	O^-–CN	7.18	95.557	3.744
C–C_2^-	6.94	75.579	3.886	N^+–C_2	7.32	153.147	3.159	O^-–CO	7.19	90.340	3.728
C–N_2^+	7.04	96.958	3.456	N^+–N_2	7.36	126.792	3.071	O^-–NO	7.20	81.270	3.701
C–N_2^-	6.90	68.161	4.077	N^+–O_2	7.38	119.996	3.048	O^-–C_3	7.11	140.719	3.873
C–O_2^+	7.10	116.394	3.186	N^+–CN	7.34	141.535	3.121	O^-–N_3	7.15	114.990	3.800
C–O_2^-	6.91	69.900	4.030	N^+–CO	7.35	135.391	3.101	O^-–O_3	7.13	130.003	3.843
C–CN^+	7.08	109.221	3.275	N^+–NO	7.37	124.562	3.064	O^-–C_2N	7.12	132.530	3.850
C–CN^-	6.96	78.267	3.822	N^+–C_3	7.25	192.956	3.284	O^-–CO_2	7.14	121.321	3.818
C–CO^+	7.08	110.992	3.252	N^+–N_3	7.30	163.987	3.194	O^-–C_2O	7.13	129.720	3.842

C–NO^+	7.09	114.749	3.206	N^+–O_3	7.27	180.973	3.248	O^-–NO_2	7.13	124.552	3.827
C–O_3^-	6.91	69.839	4.032	N^+–C_2N	7.27	183.808	3.256	O^-–N_2O	7.13	124.843	3.828
C–CO_2^+	7.05	101.154	3.389	N^+–CO_2	7.29	171.182	3.217	O^-–CNO	7.14	121.024	3.817
C–CO_2^-	6.85	58.583	4.368	N^+–C_2O	7.27	180.655	3.247	C_2–C_2^+	8.08	129.606	3.400
C–N_2O^+	7.05	100.208	3.404	N^+–NO_2	7.28	174.835	3.229	C_2–C_2^-	7.65	96.999	3.944
C^+–N	6.84	85.700	3.070	N^+–N_2O	7.28	175.163	3.230	C_2–N_2^+	7.97	119.971	3.531
C^+–O	7.08	68.625	3.004	N^+–CNO	7.29	170.846	3.216	C_2–N_2^-	7.54	88.851	4.127
C^+–C_2	7.57	141.499	3.266	N^-–O	6.65	39.119	3.734	C_2–O_2^+	8.21	141.118	3.270
C^+–N_2	7.64	116.317	3.181	N^-–C_2	6.80	98.846	3.905	C_2–O_2^-	7.56	90.777	4.082
C^+–O_2	7.66	109.839	3.158	N^-–N_2	6.82	76.923	3.844	C_2–CN^+	8.12	133.247	3.356
C^+–CN	7.60	130.394	3.229	N^-–O_2	6.82	71.471	3.829	C_2–CN^-	7.69	99.914	3.883
C^+–CO	7.61	124.524	3.209	N^-–CN	6.81	89.046	3.878	C_2–CO^+	8.14	135.183	3.334
C_2–NO^+	8.19	139.306	3.289	N_2^-–C_2O	7.48	112.317	4.182	CN^-–CNO	7.65	115.244	3.925
C_2–O_3^-	7.56	90.710	4.083	N_2^-–NO_2	7.49	107.240	4.170	CO–CO^+	8.23	118.592	3.278
C_2–CO_2^+	8.02	124.490	3.467	N_2^-–N_2O	7.49	107.525	4.171	CO–NO^+	8.28	122.468	3.232
C_2–CO_2^-	7.39	78.022	4.405	N_2^-–CNO	7.50	103.793	4.162	CO–O_3^-	7.61	76.250	4.048
C_2–N_2O^+	8.01	123.469	3.481	O_2–O_2^+	8.38	109.505	3.162	CO–CO_2^+	8.10	108.466	3.414
C_2^+–N_2	8.20	105.476	3.319	O_2–O_2^-	7.65	64.343	4.016	CO–CO_2^-	7.42	64.489	4.379
C_2^+–O_2	8.24	99.295	3.297	O_2–CN^+	8.29	102.544	3.251	CO–N_2O^+	8.08	107.495	3.428
C_2^+–CN	8.13	118.948	3.364	O_2–CN^-	7.80	72.427	3.806	CO^+–NO	8.29	108.506	3.243
C_2^+–CO	8.16	113.324	3.345	O_2–CO^+	8.31	104.264	3.228	CO^+–C_3	7.98	172.535	3.453
C_2^+–NO	8.22	103.445	3.312	O_2–NO^+	8.36	107.910	3.182	CO^+–N_3	8.10	145.338	3.367
C_2^+–C_3	7.93	166.349	3.516	O_2–O_3^-	7.65	64.285	4.018	CO^+–O_3	8.03	161.276	3.418
C_2^+–N_3	8.04	139.586	3.432	O_2–CO_2^+	8.17	94.697	3.367	CO^+–C_2N	8.01	163.940	3.426
C_2^+–O_3	7.97	155.265	3.482	O_2–CO_2^-	7.46	53.516	4.359	CO^+–CO_2	8.07	152.086	3.388
C_2^+–C_2N	7.96	157.887	3.490	O_2–N_2O^+	8.16	93.776	3.382	CO^+–C_2O	8.03	160.978	3.417

(continued)

Table 11.3 (continued)

	β	φ_0 (meV)	r_e (Å)		β	φ_0 (meV)	r_e (Å)		β	φ_0 (meV)	r_e (Å)
C_2^+–CO_2	8.01	146.222	3.453	O_2^+–CN	8.26	130.029	3.233	CO^+–NO_2	8.05	155.514	3.399
C_2^+–C_2O	7.97	154.972	3.481	O_2^+–CO	8.30	124.168	3.213	CO^+–N_2O	8.05	155.822	3.400
C_2^+–NO_2	7.99	149.595	3.464	O_2^+–NO	8.36	113.850	3.178	CO^+–CNO	8.07	151.771	3.387
C_2^+–N_2O	7.99	149.898	3.465	O_2^+–C_3	8.03	179.211	3.391	NO–NO^+	8.34	112.223	3.197
C_2^+–CNO	8.01	145.912	3.452	O_2^+–N_3	8.15	151.482	3.304	NO–O_3^-	7.64	67.774	4.027
C_2^-–N_2	7.73	75.225	3.885	O_2^+–O_3	8.08	167.736	3.356	NO–CO_2^+	8.15	98.767	3.381
C_2^-–O_2	7.75	69.824	3.870	O_2^+–C_2N	8.07	170.450	3.364	NO–CO_2^-	7.45	56.693	4.365
C_2^-–CN	7.68	87.255	3.918	O_2^+–CO_2	8.12	158.365	3.326	NO–N_2O^+	8.13	97.830	3.396
C_2^-–CO	7.70	82.192	3.904	O_2^+–C_2O	8.08	167.431	3.355	NO^+–C_3	8.02	177.163	3.409
C_2^-–NO	7.74	73.442	3.880	O_2^+–NO_2	8.11	161.860	3.337	NO^+–N_3	8.14	149.603	3.322
C_2^-–C_3	7.55	131.830	4.034	O_2^+–N_2O	8.10	162.175	3.338	NO^+–O_3	8.06	165.757	3.374
C_2^-–N_3	7.62	106.284	3.968	O_2^+–CNO	8.12	158.043	3.325	NO^+–C_2N	8.05	168.456	3.382
C_2^-–O_3	7.58	121.147	4.007	O_2^-–CN	7.59	81.243	4.058	NO^+–CO_2	8.11	156.443	3.344
C_2^-–C_2N	7.57	123.661	4.013	O_2^-–CO	7.61	76.313	4.046	NO^+–C_2O	8.07	165.455	3.373
C_2^-–CO_2	7.61	112.536	3.985	O_2^-–NO	7.64	67.834	4.025	NO^+–NO_2	8.09	159.918	3.355
C_2^-–C_2O	7.58	120.865	4.006	O_2^-–C_3	7.48	125.277	4.165	NO^+–N_2O	8.09	160.230	3.356
C_2^-–NO_2	7.60	115.735	3.993	O_2^-–N_3	7.54	99.912	4.104	NO^+–CNO	8.11	156.124	3.343
C_2^-–N_2O	7.60	116.024	3.994	O_2^-–O_3	7.50	114.631	4.139	C_3–O_3^-	7.47	125.205	4.166
C_2^-–CNO	7.61	112.242	3.984	O_2^-–C_2N	7.49	117.132	4.145	C_3–CO_2^+	7.87	160.758	3.581
N_2–N_2^+	8.07	96.569	3.455	O_2^-–CO_2	7.52	106.090	4.119	C_3–CO_2^-	7.32	111.342	4.469
N_2–N_2^-	7.60	67.822	4.077	O_2^-–C_2O	7.50	114.352	4.139	C_3–N_2O^+	7.86	159.654	3.594
N_2–O_2^+	8.34	115.973	3.185	O_2^-–NO_2	7.51	109.260	4.127	N_3–O_3^-	7.54	99.843	4.106
N_2–O_2^-	7.63	69.557	4.029	O_2^-–N_2O	7.51	109.546	4.127	N_3–CO_2^+	7.98	134.328	3.498
N_2–CN^+	8.25	108.813	3.273	O_2^-–CNO	7.52	105.800	4.118	N_3–CO_2^-	7.37	86.710	4.422
N_2–CN^-	7.77	77.908	3.821	CN–CN^+	8.18	122.461	3.320	N_3–N_2O^+	7.97	133.282	3.512
N_2–CO^+	8.27	110.581	3.250	CN–CN^-	7.73	90.083	3.856	O_3–O_3^-	7.50	114.561	4.141

N_2–NO^+	8.32	114.331	3.204	CN–CO^+	8.20	124.326	3.297	O_3–CO_2^+	7.92	149.806	3.547
N_2–O_3^-	7.63	69.496	4.031	CN–NO^+	8.24	128.290	3.252	O_3–CO_2^-	7.34	100.917	4.449
N_2–CO_2^+	8.14	100.759	3.388	CN–O_3^-	7.59	81.179	4.060	O_3–N_2O^+	7.90	148.724	3.560
N_2–CO_2^-	7.44	58.269	4.368	CN–CO_2^+	8.07	113.996	3.432	O_3^-–C_2N	7.49	117.061	4.147
N_2–N_2O^+	8.12	99.814	3.402	CN–CO_2^-	7.41	69.070	4.388	O_3^-–CO_2	7.52	106.020	4.121
N_2^+–O_2	8.11	90.611	3.434	CN–N_2O^+	8.06	113.007	3.446	O_3^-–C_2O	7.50	114.281	4.140
N_2^+–CN	8.01	109.610	3.498	CN^+–CO	8.21	116.766	3.301	O_3^-–NO_2	7.51	109.189	4.128
N_2^+–CO	8.04	104.158	3.480	CN^+–NO	8.26	106.754	3.266	O_3^-–N_2O	7.51	109.475	4.129
N_2^+–NO	8.08	94.610	3.448	CN^+–C_3	7.96	170.377	3.474	O_3^-–CNO	7.52	105.730	4.120
N_2^+–C_3	7.83	155.892	3.642	CN^+–N_3	8.08	143.338	3.389	C_2N–CO_2^+	7.91	152.396	3.555
N_2^+–N_3	7.92	129.700	3.562	CN^+–O_3	8.01	159.183	3.439	C_2N–CO_2^-	7.33	103.355	4.454
N_2^+–O_3	7.87	145.030	3.609	CN^+–C_2N	8.00	161.831	3.448	C_2N–N_2O^+	7.89	151.308	3.568
N_2^+–C_2N	7.86	147.597	3.617	CN^+–CO_2	8.05	150.046	3.410	CO_2–CO_2^+	7.95	140.876	3.519
N_2^+–CO_2	7.90	136.182	3.582	CN^+–C_2O	8.01	158.886	3.438	CO_2–CO_2^-	7.35	92.642	4.433
N_2^+–C_2O	7.87	144.742	3.608	CN^+–NO_2	8.03	153.454	3.421	CO_2–N_2O^+	7.94	139.814	3.533
N_2^+–NO_2	7.89	139.480	3.592	CN^+–N_2O	8.03	153.760	3.422	CO_2^+–C_2O	7.92	149.516	3.546
N_2^+–N_2O	7.89	139.777	3.593	CN^+–CNO	8.05	149.732	3.409	CO_2^+–NO_2	7.94	144.206	3.529
N_2^+–CNO	7.90	135.879	3.581	CN^-–CO	7.75	84.964	3.841	CO_2^+–N_2O	7.94	144.505	3.530
N_2^-–O_2	7.62	62.671	4.064	CN^-–NO	7.78	76.100	3.816	CO_2^+–CNO	7.95	140.570	3.518
N_2^-–CN	7.57	79.391	4.105	CN^-–C_3	7.59	134.870	3.977	CO_2^-–C_2O	7.34	100.645	4.448
N_2^-–CO	7.58	74.507	4.093	CN^-–N_3	7.66	109.258	3.909	CO_2^-–NO_2	7.35	95.703	4.439
N_2^-–NO	7.61	66.119	4.072	CN^-–O_3	7.62	124.175	3.949	CO_2^-–N_2O	7.35	95.980	4.440
N_2^-–C_3	7.45	123.222	4.207	CN^-–C_2N	7.61	126.694	3.955	CO_2^-–CNO	7.35	92.362	4.433
N_2^-–N_3	7.51	97.933	4.149	CN^-–CO_2	7.64	115.539	3.926	C_2O–N_2O^+	7.91	148.434	3.560
N_2^-–O_3	7.48	112.596	4.183	CN^-–C_2O	7.62	123.893	3.948	NO_2–N_2O^+	7.93	143.136	3.543
N_2^-–C_2N	7.47	115.091	4.189	CN^-–NO_2	7.63	118.750	3.934	N_2O–N_2O^+	7.93	143.435	3.544
N_2^-–CO_2	7.50	104.083	4.163	CN^-–N_2O	7.63	119.039	3.935	N_2O^+–CNO	7.94	139.509	3.532

Table 11.4 Parameters of phenomenological potential for neutral–multiply-charged ion interactions (m =4) relevant to Mars atmosphere

	β	φ_0 (meV)	r_e (Å)		β	φ_0 (meV)	r_e (Å)		β	φ_0 (meV)	r_e (Å)
Ar–Ar^{2+}	7.48	753.338	2.624	C–C^{2+}	7.15	805.275	2.625	N^{2+}–O	7.22	533.935	2.388
Ar–Ar^{3+}	7.38	2,718.805	2.313	C–C^{3+}	7.01	2,614.482	2.379	N^{2+}–C_2	7.88	1,064.249	2.638
Ar–Ar^{4+}	7.58	5,444.026	2.243	C–C^{4+}	7.33	17,972.179	1.690	N^{2+}–N_2	7.98	880.011	2.559
Ar–C^{2+}	8.64	770.263	2.608	C–N^{2+}	7.01	883.085	2.560	N^{2+}–O_2	8.01	832.821	2.537
Ar–C^{3+}	8.00	2,502.004	2.363	C–N^{3+}	7.19	2,941.739	2.308	N^{2+}–CN	7.93	982.843	2.604
Ar–C^{4+}	9.78	17,502.973	1.671	C–N^{4+}	7.04	6,550.181	2.178	N^{2+}–CO	7.95	939.915	2.585
Ar–N^{2+}	8.01	845.610	2.543	C–O^{2+}	6.92	952.875	2.508	N^{2+}–NO	7.99	864.511	2.552
Ar–N^{3+}	8.82	2,819.168	2.292	C–O^{3+}	7.05	3,088.233	2.279	N^{2+}–C_3	7.76	1,345.742	2.751
Ar–N^{4+}	8.13	6,277.300	2.163	C–O^{4+}	7.20	7,037.770	2.139	N^{2+}–N_3	7.85	1,140.551	2.670
Ar–O^{2+}	7.66	913.271	2.491	C^{2+}–N	7.03	595.208	2.520	N^{2+}–O_3	7.79	1,260.654	2.718
Ar–O^{3+}	8.16	2,961.338	2.263	C^{2+}–O	7.43	480.732	2.457	N^{2+}–C_2N	7.78	1280.764	2.726
Ar–O^{4+}	8.90	6,750.649	2.123	C^{2+}–C_2	8.43	975.039	2.702	N^{2+}–CO_2	7.82	1,191.348	2.690
Ar^{2+}–C	6.86	787.784	2.641	C^{2+}–N_2	8.60	802.401	2.624	N^{2+}–C_2O	7.79	1,258.401	2.717
Ar^{2+}–N	6.79	581.253	2.537	C^{2+}–O_2	8.65	758.322	2.603	N^{2+}–NO_2	7.81	1,217.184	2.701
Ar^{2+}–O	7.00	468.867	2.474	C^{2+}–CN	8.50	898.656	2.668	N^{2+}–N_2O	7.81	1,219.507	2.702
Ar^{2+}–C_2	7.42	954.919	2.717	C^{2+}–CO	8.54	858.441	2.650	N^{2+}–CNO	7.82	1,188.974	2.689
Ar^{2+}–N_2	7.47	784.957	2.639	C^{2+}–NO	8.62	787.916	2.617	N^{3+}–O	7.48	1,795.779	2.145
Ar^{2+}–O_2	7.49	741.593	2.619	C^{2+}–C_3	8.22	1,240.280	2.812	N^{3+}–C_2	8.59	3,532.983	2.381
Ar^{2+}–CN	7.44	879.697	2.684	C^{2+}–N_3	8.37	1,046.771	2.733	N^{3+}–N_2	8.78	2,931.689	2.306
Ar^{2+}–CO	7.45	840.108	2.665	C^{2+}–O_3	8.28	1,159.933	2.780	N^{3+}–O_2	8.84	2,777.315	2.286
Ar^{2+}–NO	7.48	770.706	2.633	C^{2+}–C_2N	8.27	1,178.910	2.788	N^{3+}–CN	8.67	3,267.570	2.349
Ar^{2+}–C_3	7.34	1,216.383	2.827	C^{2+}–CO_2	8.33	1,094.596	2.753	N^{3+}–CO	8.71	3,127.439	2.331
Ar^{2+}–N_3	7.39	1,025.592	2.748	C^{2+}–C_2O	8.28	1,157.808	2.779	N^{3+}–NO	8.80	2,880.999	2.300
Ar^{2+}–O_3	7.36	1,137.141	2.795	C^{2+}–NO_2	8.31	1,118.940	2.763	N^{3+}–C_3	8.35	4,447.643	2.487
Ar^{2+}–C_2N	7.36	1,155.854	2.803	C^{2+}–N_2O	8.31	1,121.131	2.764	N^{3+}–N_3	8.52	3,781.380	2.411
Ar^{2+}–CO_2	7.38	1,072.727	2.768	C^{2+}–CNO	8.33	1,092.359	2.752	N^{3+}–O_3	8.42	4,171.657	2.456
Ar^{2+}–C_2O	7.36	1,135.045	2.794	C^{3+}–N	6.92	1,939.107	2.280	N^{3+}–C_2N	8.40	4,236.922	2.463
Ar^{2+}–NO_2	7.37	1,096.725	2.778	C^{3+}–O	7.22	1,570.498	2.221	N^{3+}–CO_2	8.47	3,946.551	2.430

Ar^{2+}–N_2O	7.37	1,098.884	2.779	C^{3+}–C_2	7.88	3,159.366	2.451	N^{3+}–C_2O	8.42	4,164.343	2.455
Ar^{2+}–CNO	7.38	1,070.523	2.767	C^{3+}–N_2	7.98	2,605.254	2.378	N^{3+}–NO_2	8.45	4,030.498	2.440
Ar^{3+}–C	6.82	2,838.249	2.329	C^{3+}–O_2	8.01	2,463.638	2.358	N^{3+}–N_2O	8.45	4,038.046	2.441
Ar^{3+}–N	6.76	2,118.979	2.229	C^{3+}–CN	7.92	2,914.306	2.419	N^{3+}–CNO	8.48	3,938.835	2.429
Ar^{3+}–O	6.95	1,724.045	2.168	C^{3+}–CO	7.94	2,785.217	2.402	N^{4+}–O	7.26	3,999.056	2.024
Ar^{3+}–C_2	7.32	3,415.174	2.402	C^{3+}–NO	7.99	2,558.722	2.371	N^{4+}–C_2	7.99	7,866.435	2.248
Ar^{3+}–N_2	7.37	2,828.453	2.328	C^{3+}–C_3	7.75	4,009.013	2.554	N^{4+}–N_2	8.10	6,527.807	2.177
Ar^{3+}–O_2	7.38	2,678.033	2.308	C^{3+}–N_3	7.84	3,389.350	2.480	N^{4+}–O_2	8.14	6,184.121	2.158
Ar^{3+}–CN	7.34	3,156.038	2.370	C^{3+}–O_3	7.79	3,751.858	2.524	N^{4+}–CN	8.04	7,275.574	2.217
Ar^{3+}–CO	7.35	3,019.319	2.352	C^{3+}–C_2N	7.78	3,812.612	2.531	N^{4+}–CO	8.07	6,963.605	2.201
Ar^{3+}–NO	7.37	2,779.051	2.321	C^{3+}–CO_2	7.82	3,542.601	2.499	N^{4+}–NO	8.11	6,414.954	2.171
Ar^{3+}–C_3	7.25	4,309.877	2.507	C^{3+}–C_2O	7.79	3,745.053	2.523	N^{4+}–C_3	7.85	9,902.376	2.348
Ar^{3+}–N_3	7.30	3,657.905	2.432	C^{3+}–NO_2	7.81	3,620.585	2.508	N^{4+}–N_3	7.95	8,419.388	2.276
Ar^{3+}–O_3	7.27	4,039.657	2.476	C^{3+}–N_2O	7.81	3,627.600	2.509	N^{4+}–O_3	7.89	9,288.111	2.319
Ar^{3+}–C_2N	7.27	4,103.540	2.484	C^{3+}–CNO	7.82	3,535.436	2.498	N^{4+}–C_2N	7.88	9,433.377	2.326
Ar^{3+}–CO_2	7.29	3,819.414	2.451	C^{4+}–N	7.17	15,013.919	1.571	N^{4+}–CO_2	7.92	8787.056	2.294
Ar^{3+}–C_2O	7.27	4,032.500	2.476	C^{4+}–O	7.71	13,220.922	1.498	N^{4+}–C_2O	7.89	9,271.833	2.318
Ar^{3+}–NO_2	7.28	3,901.530	2.460	C^{4+}–C_2	9.37	20,141.268	1.774	N^{4+}–NO_2	7.91	8,973.914	2.304
Ar^{3+}–N_2O	7.28	3,908.915	2.461	C^{4+}–N_2	9.71	17,933.987	1.688	N^{4+}–N_2O	7.91	8,990.715	2.304
Ar^{3+}–CNO	7.29	3,811.867	2.450	C^{4+}–O_2	9.81	17,341.015	1.665	N^{4+}–CNO	7.92	8,769.880	2.294
Ar^{4+}–C	6.89	5,690.301	2.258	C^{4+}–CN	9.51	19,185.464	1.737	O–O^{2+}	7.08	582.243	2.334
Ar^{4+}–N	6.82	4,212.898	2.165	C^{4+}–CO	9.59	18,669.409	1.717	O–O^{3+}	7.28	1,898.102	2.115
Ar^{4+}–O	7.05	3,408.157	2.108	C^{4+}–NO	9.74	17,740.597	1.680	O–O^{4+}	7.50	4,340.629	1.983
Ar^{4+}–C_2	7.50	6,884.416	2.326	C^{4+}–C_3	8.98	23,255.695	1.894	O^{2+}–C_2	7.58	1,143.841	2.588
Ar^{4+}–N_2	7.56	5,670.091	2.256	C^{4+}–N_3	9.25	21,012.589	1.808	O^{2+}–N_2	7.65	949.628	2.507
Ar^{4+}–O_2	7.58	5,360.040	2.238	C^{4+}–O_3	9.09	22,341.759	1.859	O^{2+}–O_2	7.67	899.746	2.485
Ar^{4+}–CN	7.53	6,347.159	2.296	C^{4+}–C_2N	9.06	22,559.718	1.868	O^{2+}–CN	7.61	1,058.128	2.553
Ar^{4+}–CO	7.54	6,064.284	2.279	C^{4+}–CO_2	9.18	21,580.723	1.830	O^{2+}–CO	7.62	1,012.866	2.534

(continued)

Table 11.4 (continued)

	β	φ_0 (meV)	r_e (Å)		β	φ_0 (meV)	r_e (Å)		β	φ_0 (meV)	r_e (Å)
Ar^{4+}–NO	7.57	5,568.201	2.250	C^{4+}–C_2O	9.09	22,317.262	1.859	O^{2+}–NO	7.65	933.250	2.500
Ar^{4+}–C_3	7.42	8,749.317	2.423	C^{4+}–NO_2	9.15	21,866.257	1.841	O^{2+}–C_3	7.49	1,439.140	2.702
Ar^{4+}–N_3	7.48	7,388.897	2.353	C^{4+}–N_2O	9.14	21,891.830	1.842	O^{2+}–N_3	7.55	1,224.045	2.620
Ar^{4+}–O_3	7.44	8,184.564	2.395	C^{4+}–CNO	9.18	21,554.371	1.829	O^{2+}–O_3	7.51	1,350.045	2.668
Ar^{4+}–C_2N	7.44	8,317.966	2.402	N–N^{2+}	6.92	657.586	2.453	O^{2+}–C_2N	7.51	1,371.115	2.676
Ar^{4+}–CO_2	7.46	7,725.197	2.371	N–N^{3+}	7.06	2,202.680	2.207	O^{2+}–CO_2	7.53	1,277.372	2.640
Ar^{4+}–C_2O	7.44	8,169.622	2.394	N–N^{4+}	6.94	4,904.828	2.082	O^{2+}–C_2O	7.51	1,347.684	2.667
Ar^{4+}–NO_2	7.45	7,896.367	2.380	N–O^{2+}	6.84	713.953	2.400	O^{2+}–NO_2	7.53	1,304.474	2.651
Ar^{4+}–N_2O	7.45	7,911.767	2.381	N–O^{3+}	6.95	2,321.715	2.177	O^{2+}–N_2O	7.52	1,306.911	2.652
Ar^{4+}–CNO	7.46	7,709.472	2.370	N–O^{4+}	7.07	5,301.792	2.042	O^{2+}–CNO	7.53	1,274.881	2.640
O^{3+}–C_2	8.02	3,699.210	2.353	O^{3+}–CO_2	7.95	4,125.578	2.403	O^{4+}–NO	8.87	6,895.523	2.131
O^{3+}–N_2	8.14	3,077.832	2.278	O^{3+}–C_2O	7.92	4,349.809	2.428	O^{4+}–C_3	8.40	10,544.095	2.311
O^{3+}–O_2	8.17	2,917.988	2.257	O^{3+}–NO_2	7.94	4,212.030	2.412	O^{4+}–N_3	8.58	8,997.273	2.238
O^{3+}–CN	8.07	3,425.161	2.321	O^{3+}–N_2O	7.94	4,219.802	2.413	O^{4+}–O_3	8.47	9,904.145	2.281
O^{3+}–CO	8.10	3,280.326	2.303	O^{3+}–CNO	7.95	4,117.629	2.402	O^{4+}–C_2N	8.46	10,055.579	2.289
O^{3+}–NO	8.15	3,025.360	2.271	O^{4+}–C_2	8.65	8,418.840	2.210	O^{4+}–CO_2	8.53	9,381.359	2.257
O^{3+}–C_3	7.88	4,641.196	2.460	O^{4+}–N_2	8.85	7,014.239	2.138	O^{4+}–C_2O	8.47	9,887.172	2.281
O^{3+}–N_3	7.98	3,955.387	2.383	O^{4+}–O_2	8.91	6,652.541	2.118	O^{4+}–NO_2	8.51	9,576.405	2.266
O^{3+}–O_3	7.92	4,357.335	2.429	O^{4+}–CN	8.74	7,799.642	2.179	O^{4+}–N_2O	8.51	9,593.938	2.267
O^{3+}–C_2N	7.91	4,424.490	2.436	O^{4+}–CO	8.78	7,472.221	2.162	O^{4+}–CNO	8.53	9,363.425	2.256

Table 11.5 Fitting coefficients, entering Eq. (11.2), for $\sigma^2 \Omega_{\rm ex}^{(\ell,s)\star}$ in neutral–ion interactions, from resonant charge-transfer cross sections of different authors

	(ℓ, s)	d_1	d_2	d_3		(ℓ, s)	d_1	d_2	d_3
N–N^+ (a)	(1,1)	65.8423	−4.5492	7.8608(−2)	Ar–Ar^+(c)	(1,1)	68.6279	−4.3366	6.8542(−2)
	(1,2)	64.3259	−4.4969	7.8619(−2)		(1,2)	67.1824	−4.2908	6.8533(−2)
	(1,3)	63.2015	−4.4575	7.8613(−2)		(1,3)	66.1106	−4.2568	6.8542(−2)
	(1,4)	62.3098	−4.4260	7.8606(−2)		(1,4)	65.2603	−4.2297	6.8562(−2)
	(1,5)	61.5722	−4.3997	7.8601(−2)		(1,5)	64.5529	−4.2062	6.8523(−2)
O–O^+(b)	(1,1)	64.7044	−4.1936	6.7974(−2)	C–C^+(d)	(1,1)	65.8583	−4.8063	8.7735(−2)
	(1,2)	63.3075	−4.1485	6.7991(−2)		(1,2)	64.2555	−4.7476	8.7729(−2)
	(1,3)	62.2707	−4.1146	6.8000(−2)		(1,3)	63.0684	−4.7037	8.7724(−2)
	(1,4)	61.4470	−4.0872	6.7986(−2)		(1,4)	62.1279	−4.6687	8.7729(−2)
	(1,5)	60.7663	−4.0646	6.7987(−2)		(1,5)	61.3500	−4.6395	8.7730(−2)
					CO–CO^+(e)	(1,1)	85.0889	−5.5980	9.2122(−2)
						(1,2)	83.2212	−5.5362	9.2097(−2)
						(1,3)	81.8376	−5.4902	9.2105(−2)
						(1,4)	80.7381	−5.4530	9.2078(−2)
						(1,5)	79.8298	−5.4225	9.2091(−2)

(a) (Kosarim et al. 2006), (b) (Kosarim and Smirnov 2005), (c) (Smirnov 2001), (d) (Nikitin and Smirnov 1978), (e) (Yevseyev et al. 1982)

Table 11.6 Fitting coefficients, entering Eq. (11.2), for $\sigma^2\Omega_{\rm ex}^{(\ell,s)\star}$ in neutral–multiply-charged ion interactions

	(ℓ,s)	d_1	d_2	d_3		(ℓ,s)	d_1	d_2	d_3
C–C^{2+}	(1,1)	28.9720	−2.0977	3.7982(−2)	N–N^{2+}	(1,1)	23.6264	−1.6989	3.0557(−2)
	(1,2)	28.2735	−2.0727	3.8003(−2)		(1,2)	23.0587	−1.6782	3.0541(−2)
	(1,3)	27.7555	−2.0537	3.8004(−2)		(1,3)	22.6398	−1.6631	3.0550(−2)
	(1,4)	27.3449	−2.0386	3.8011(−2)		(1,4)	22.3082	−1.6511	3.0565(−2)
	(1,5)	27.0044	−2.0256	3.7986(−2)		(1,5)	22.0323	−1.6407	3.0555(−2)
C–C^{3+}	(1,1)	12.3615	−0.8950	1.6208(−2)	N–N^{3+}	(1,1)	11.3843	−0.8184	1.4708(−2)
	(1,2)	12.0640	−0.8844	1.6219(−2)		(1,2)	11.1116	−0.8088	1.4725(−2)
	(1,3)	11.8434	−0.8765	1.6232(−2)		(1,3)	10.9103	−0.8016	1.4733(−2)
	(1,4)	11.6670	−0.8697	1.6210(−2)		(1,4)	10.7496	−0.7956	1.4726(−2)
	(1,5)	11.5216	−0.8641	1.6197(−2)		(1,5)	10.6156	−0.7903	1.4705(−2)
Ar–Ar^{2+}	(1,1)	25.6354	−1.7611	3.0263(−2)	O–O^{2+}	(1,1)	21.5699	−1.5419	2.7577(−2)
	(1,2)	25.0475	−1.7407	3.0249(−2)		(1,2)	21.0551	−1.5233	2.7562(−2)
	(1,3)	24.6123	−1.7256	3.0254(−2)		(1,3)	20.6754	−1.5098	2.7582(−2)
	(1,4)	24.2671	−1.7135	3.0251(−2)		(1,4)	20.3727	−1.4986	2.7577(−2)
	(1,5)	23.9816	−1.7035	3.0259(−2)		(1,5)	20.1227	−1.4893	2.7564(−2)
Ar–Ar^{3+}	(1,1)	13.2224	−0.9084	1.5613(−2)	O–O^{3+}	(1,1)	10.1289	−0.7238	1.2929(−2)
	(1,2)	12.9179	−0.8975	1.5581(−2)		(1,2)	9.8879	−0.7153	1.2936(−2)
	(1,3)	12.6945	−0.8899	1.5593(−2)		(1,3)	9.7098	−0.7090	1.2952(−2)
	(1,4)	12.5166	−0.8838	1.5607(−2)		(1,4)	9.5669	−0.7036	1.2936(−2)
	(1,5)	12.3694	−0.8786	1.5604(−2)		(1,5)	9.4498	−0.6992	1.2930(−2)

Table 11.7 Fitting coefficients, entering Eq. (11.3), for $\sigma^2\Omega^{(\ell,s)\star}$ in electron–neutral interactions

	(ℓ, s)	g_1	g_2	g_3	g_4	g_5
e–Ar	(1,1)	8.8972699(+00)	1.5224377(+00)	2.4749525(+00)	−2.0999602(+00)	−1.0000000(+00)
	(1,2)	8.3023850(+00)	1.4606183(+00)	2.3444186(+00)	−2.4467102(+00)	−1.0000000(+00)
	(1,3)	7.9620769(+00)	1.3082040(+00)	2.1990363(+00)	−2.3822774(+00)	−1.0000000(+00)
	(1,4)	7.7277052(+00)	1.1680935(+00)	2.0557289(+00)	−2.2105696(+00)	−1.0000000(+00)
	(1,5)	7.5366571(+00)	1.0787061(+00)	1.9828179(+00)	−2.1278210(+00)	−1.0000000(+00)
	(2,2)	8.2815471(+00)	1.2189631(+00)	2.4126978(+00)	−2.5194275(+00)	−1.0000000(+00)
	(2,3)	7.9623178(+00)	1.1969767(+00)	2.3930747(+00)	−2.6403058(+00)	−1.0000000(+00)
	(2,4)	7.7185195(+00)	1.1616956(+00)	2.3352034(+00)	−2.6316705(+00)	−1.0000000(+00)
	(3,3)	8.0588828(+00)	1.3129979(+00)	2.5357454(+00)	−2.7659195(+00)	−1.0000000(+00)
e–C	(1,1)	8.6639477(+00)	2.2504916(+00)	9.1785843(+02)	−7.0109479(−03)	2.7782979(+00)
	(1,2)	8.2658158(+00)	2.2895873(+00)	3.6106073(+02)	−4.2809613(−03)	3.0370217(+00)
	(1,3)	7.9285892(+00)	2.7157052(+00)	4.5517545(+02)	−2.4068061(−01)	1.5918309(+00)
	(1,4)	7.9205710(+00)	2.8337855(+00)	1.6537720(+03)	−1.2297969(+00)	9.1430191(−01)
	(1,5)	7.9405463(+00)	2.5511666(+00)	4.8770342(+03)	−1.4703291(+00)	7.0332825(−01)
	(2,2)	8.2749792(+00)	2.7208384(+00)	1.3775072(+02)	−2.4227513(−02)	2.5376418(+00)
	(2,3)	7.8723708(+00)	2.9765929(+00)	1.4660357(+02)	−1.5204273(−01)	1.9011370(+00)
	(2,4)	7.8589366(+00)	3.0478637(+00)	5.2005446(+02)	−7.0272252(−01)	1.2756528(+00)
	(3,3)	7.9216890(+00)	2.8810891(+00)	3.0253221(+02)	−2.5189030(−01)	1.6414080(+00)

(continued)

Table 11.7 (continued)

	(ℓ, s)	g_1	g_2	g_3	g_4	g_5
e–CO	(1,1)	6.0038560(+00)	1.0742443(+00)	2.2460591(+00)	1.0801813(+00)	−1.5849157(+00)
	(1,2)	5.7673817(+00)	8.0546342(−01)	1.9228408(+00)	1.2581547(+00)	−1.1772175(+00)
	(1,3)	5.4791376(+00)	8.6338863(−01)	2.5082567(+00)	7.5823348(−01)	−1.4824169(+00)
	(1,4)	5.2498641(+00)	7.6461445(−01)	2.1814973(+00)	1.3243593(+00)	−1.7332682(+00)
	(1,5)	5.0671796(+00)	7.0732108(−01)	2.0015308(+00)	1.6182404(+00)	−1.9194912(+00)
	(2,2)	6.3520032(+00)	1.3943704(+00)	1.4925516(+00)	2.9117186(+00)	−3.0005496(+00)
	(2,3)	6.2868123(+00)	8.8268789(−01)	9.3543620(−01)	3.5472292(+00)	−3.4240038(+00)
	(2,4)	6.1711567(+00)	6.2655153(−01)	7.0153609(−01)	3.8222601(+00)	−3.8138544(+00)
	(3,3)	5.6938002(+00)	7.0140212(−01)	1.4041403(+00)	2.6725563(+00)	−3.2672416(+00)
$e–O_3$	(1,1)	1.2085049(+01)	−6.7073828(−01)	1.9000000(+00)	0.0000000(+00)	0.0000000(+00)
	(1,2)	1.2072024(+01)	−1.0408204(+00)	1.9000000(+00)	0.0000000(+00)	0.0000000(+00)
	(1,3)	1.1957946(+01)	−1.4409899(+00)	1.9000000(+00)	0.0000000(+00)	0.0000000(+00)
	(1,4)	1.1744211(+01)	−1.7671914(+00)	1.9000000(+00)	0.0000000(+00)	0.0000000(+00)
	(1,5)	1.1526836(+01)	−1.8339480(+00)	1.9000000(+00)	0.0000000(+00)	0.0000000(+00)
	(2,2)	1.2141978(+01)	−7.3395660(−01)	1.9000000(+00)	0.0000000(+00)	0.0000000(+00)
	(2,3)	1.2169044(+01)	−1.0856385(+00)	1.9000000(+00)	0.0000000(+00)	0.0000000(+00)
	(2,4)	1.2102398(+01)	−1.4253014(+00)	1.9000000(+00)	0.0000000(+00)	0.0000000(+00)
	(3,3)	1.2114249(+01)	−1.3360779(+00)	1.9000000(+00)	0.0000000(+00)	0.0000000(+00)

$e–CO_2$	(1,1)	6.3659775(+00)	−1.6943062(+00)	3.9912327(+02)	2.6382895(−01)	0.0000000(+00)
	(1,2)	6.3257018(+00)	−1.3367194(+00)	5.5996421(+02)	9.2140558(−01)	0.0000000(+00)
	(1,3)	6.1685846(+00)	−1.2033017(+00)	5.7296000(+02)	1.0546831(+00)	0.0000000(+00)
	(1,4)	5.9989562(+00)	−1.1407959(+00)	5.2161995(+02)	1.1029885(+00)	0.0000000(+00)
	(1,5)	5.8356957(+00)	−1.1134046(+00)	4.5006704(+02)	1.0997464(+00)	0.0000000(+00)
	(2,2)	6.3233873(+00)	−1.2961264(+00)	5.8340151(+02)	1.1790882(+00)	0.0000000(+00)
	(2,3)	6.1674479(+00)	−1.1564207(+00)	6.0601309(+02)	1.3226214(+00)	0.0000000(+00)
	(2,4)	6.0057342(+00)	−1.0832880(+00)	5.6600726(+02)	1.3792131(+00)	0.0000000(+00)
	(3,3)	6.1675648(+00)	−1.1843222(+00)	5.8569699(+02)	1.1670117(+00)	0.0000000(+00)
$e–N_2O$	(1,1)	1.0000000(−02)	1.9785329(+01)	9.5923867(+03)	−2.6193278(+03)	−8.5956159(−01)
	(1,2)	1.0000000(−02)	1.9418943(+01)	1.0008392(+04)	−2.7592746(+03)	−8.7616574(−01)
	(1,3)	1.0000000(−02)	1.9132706(+01)	1.0435247(+04)	−2.8943302(+03)	−8.8655129(−01)
	(1,4)	1.0000000(−02)	1.8871800(+01)	1.0507527(+04)	−2.9200628(+03)	−8.8852119(−01)
	(1,5)	1.0000000(−02)	1.8626320(+01)	1.0285087(+04)	−2.8570210(+03)	−8.8542694(−01)
	(2,2)	1.0000000(−02)	1.9079110(+01)	1.0321796(+04)	−2.8471850(+03)	−8.7396712(−01)
	(2,3)	1.0000000(−02)	1.9269516(+01)	1.2135338(+04)	−3.3848730(+03)	−8.9801865(−01)
	(2,4)	1.0000000(−02)	1.9000124(+01)	1.2862612(+04)	−3.5999692(+03)	−9.0357060(−01)
	(3,3)	1.0000000(−02)	1.9220291(+01)	1.1251798(+04)	−3.1300232(+03)	−8.9254007(−01)

(continued)

Table 11.7 (continued)

	(ℓ, s)	g_6	g_7	g_8	g_9	g_{10}
e–Ar	(1,1)	0.0000000(+00)	2.2908023(+00)	1.0598130(+01)	−9.5311431(−01)	1.4563107(+01)
	(1,2)	0.0000000(+00)	2.7946739(+00)	1.0332759(+01)	−9.2951788(−01)	1.5600366(+01)
	(1,3)	0.0000000(+00)	3.0721525(+00)	1.0113820(+01)	−8.9258310(−01)	1.4639558(+01)
	(1,4)	0.0000000(+00)	3.2696470(+00)	9.9309667(+00)	−8.6123322(−01)	1.3284529(+01)
	(1,5)	0.0000000(+00)	3.4224305(+00)	9.7747672(+00)	−8.3694730(−01)	1.2496435(+01)
	(2,2)	0.0000000(+00)	2.0930911(+00)	1.0332509(+01)	1.1471789(+00)	1.6882429(+01)
	(2,3)	0.0000000(+00)	2.2899014(+00)	1.0105058(+01)	1.1339640(+00)	1.6766113(+01)
	(2,4)	0.0000000(+00)	2.4303103(+00)	9.9182703(+00)	1.1244871(+00)	1.6102658(+01)
	(3,3)	0.0000000(+00)	3.3679099(+00)	1.0150131(+01)	9.3747185(−01)	1.7323673(+01)
e–C	(1,1)	−1.8982327(+00)	4.6188070(+00)	7.7388422(+00)	1.0205910(+00)	−7.0109479(−03)
	(1,2)	−1.5182681(+00)	5.1592160(+00)	7.4373319(+00)	9.3784288(−01)	−4.2809613(−03)
	(1,3)	−1.4394052(+00)	5.4562628(+00)	7.2005312(+00)	8.3224778(−01)	−2.4068061(−01)
	(1,4)	−1.9549443(+00)	5.6696597(+00)	7.0116924(+00)	7.7329930(−01)	−1.2297969(+00)
	(1,5)	−2.5255855(+00)	5.8687095(+00)	6.8407794(+00)	7.4954768(−01)	−1.4703291(+00)
	(2,2)	−9.1918369(−01)	5.2227684(+00)	7.4462819(+00)	9.4776453(−01)	−2.4227513(−02)
	(2,3)	−8.5530036(−01)	5.5788638(+00)	7.2054718(+00)	8.4383284(−01)	−1.5204273(−01)
	(2,4)	−1.3689873(+00)	5.8107660(+00)	7.0145109(+00)	7.8422181(−01)	−7.0272252(−01)
	(3,3)	−1.2022384(+00)	5.5067052(+00)	7.2034784(+00)	8.3722322(−01)	−2.5189030(−01)

e–CO	(1,1)	0.0000000(+00)	2.6286214(+00)	8.7159919(+00)	9.5246509(−01)	2.1584298(+01)
	(1,2)	0.0000000(+00)	2.9709666(+00)	8.4272639(+00)	8.3650016(−01)	1.0133651(+01)
	(1,3)	0.0000000(+00)	3.1700001(+00)	8.2014113(+00)	7.6172201(−01)	1.8025400(+01)
	(1,4)	0.0000000(+00)	3.3418610(+00)	7.9472608(+00)	8.1415109(−01)	1.8025400(+01)
	(1,5)	0.0000000(+00)	3.5333921(+00)	7.7667522(+00)	8.0531174(−01)	1.8025400(+01)
	(2,2)	0.0000000(+00)	2.7642243(+00)	8.5536931(+00)	7.6174072(−01)	1.5000000(+02)
	(2,3)	0.0000000(+00)	3.0791882(+00)	8.3308981(+00)	6.8253560(−01)	1.5000000(+02)
	(2,4)	0.0000000(+00)	3.3500568(+00)	8.1452572(+00)	6.2868640(−01)	1.5000000(+02)
	(3,3)	0.0000000(+00)	3.1846923(+00)	8.2584247(+00)	7.4036146(−01)	1.5000000(+02)
$e–O_3$	(1,1)	2.8539711(−01)	3.3292083(+03)	−3.3729721(+00)	3.9524568(+00)	0.0000000(+00)
	(1,2)	3.0285426(−01)	1.1098273(+02)	2.3937919(+00)	2.1601142(+00)	0.0000000(+00)
	(1,3)	3.2663645(−01)	5.2815458(+01)	3.4457978(+00)	1.5724752(+00)	0.0000000(+00)
	(1,4)	3.5233499(−01)	4.1107153(+01)	3.7008669(+00)	1.3090511(+00)	0.0000000(+00)
	(1,5)	3.6473106(−01)	3.6839102(+01)	3.7373397(+00)	1.1758627(+00)	0.0000000(+00)
	(2,2)	3.1744234(−01)	1.0904948(+02)	2.4361965(+00)	2.1361187(+00)	0.0000000(+00)
	(2,3)	3.3233547(−01)	5.2684389(+01)	3.4531193(+00)	1.5661535(+00)	0.0000000(+00)
	(2,4)	3.5012930(−01)	4.1152025(+01)	3.6978710(+00)	1.3123366(+00)	0.0000000(+00)
	(3,3)	3.2817125(−01)	5.2782625(+01)	3.4476640(+00)	1.5708891(+00)	0.0000000(+00)

(continued)

Table 11.7 (continued)

	(ℓ, s)	g_6	g_7	g_8	g_9	g_{10}
e–CO_2	(1,1)	−1.4292437(+00)	2.4166822(+00)	1.1167191(+01)	1.6169381(+00)	0.0000000(+00)
	(1,2)	−1.8012100(+00)	1.9126827(+00)	1.0811667(+01)	1.2420486(+00)	0.0000000(+00)
	(1,3)	−1.9088543(+00)	1.8676215(+00)	1.0573825(+01)	1.1317427(+00)	0.0000000(+00)
	(1,4)	−1.9149185(+00)	1.8841041(+00)	1.0382419(+01)	1.0708859(+00)	0.0000000(+00)
	(1,5)	−1.8682495(+00)	1.9377125(+00)	1.0221046(+01)	1.0400131(+00)	0.0000000(+00)
	(2,2)	−1.8359502(+00)	2.2994549(+00)	1.1021182(+01)	1.3727000(+00)	0.0000000(+00)
	(2,3)	−1.9556685(+00)	2.2438324(+00)	1.0774206(+01)	1.2526391(+00)	0.0000000(+00)
	(2,4)	−1.9822257(+00)	2.2499255(+00)	1.0580831(+01)	1.1933787(+00)	0.0000000(+00)
	(3,3)	−1.9273639(+00)	2.0678167(+00)	1.0705193(+01)	1.2355301(+00)	0.0000000(+00)
e–N_2O	(1,1)	−3.7224483(−01)	1.7590138(+00)	9.0269678(+00)	−7.0604469(−01)	−2.6193278(+03)
	(1,2)	−3.7225348(−01)	2.2684615(+00)	8.7254170(+00)	−6.3539884(−01)	−2.7592746(+03)
	(1,3)	−3.7259752(−01)	2.6734135(+00)	8.4978555(+00)	−5.8138057(−01)	−2.8943302(+03)
	(1,4)	−3.7359357(−01)	2.9971072(+00)	8.3162465(+00)	−5.3888775(−01)	−2.9200628(+03)
	(1,5)	−3.7496271(−01)	3.2607371(+00)	8.1642188(+00)	−5.0622369(−01)	−2.8570210(+03)
	(2,2)	−3.7370535(−01)	6.8673343(−01)	7.3362402(+00)	−2.3731632(−01)	−2.8471850(+03)
	(2,3)	−3.7057553(−01)	2.5282546(+00)	8.5626187(+00)	5.4825651(−01)	−3.3848730(+03)
	(2,4)	−3.7138652(−01)	2.8523910(+00)	8.3774808(+00)	5.1059199(−01)	−3.5999692(+03)
	(3,3)	−3.7143810(−01)	2.6622684(+00)	8.5290715(+00)	5.7117683(−01)	−3.1300232(+03)

	(ℓ, s)	g_1	g_2	g_3	g_4	g_5
e–O	(1,1)	8.4272724(+00)	1.5114426(+00)	1.8515287(+02)	5.1923435(−01)	0.0000000(+00)
	(1,2)	8.8104856(+00)	1.4638292(+00)	4.6284537(+05)	3.4721927(−01)	0.0000000(+00)
	(1,3)	8.7209499(+00)	1.6025253(+00)	1.7347857(+05)	2.5782606(−01)	0.0000000(+00)
	(1,4)	8.5791555(+00)	1.6974863(+00)	9.3716661(+04)	1.6125373(−01)	0.0000000(+00)
	(1,5)	8.4079354(+00)	1.7417063(+00)	6.6900888(+04)	7.6528761(−02)	0.0000000(+00)
	(2,2)	8.5895173(+00)	1.1543620(+00)	1.1397656(+07)	5.1127498(−01)	0.0000000(+00)
	(2,3)	8.4019947(+00)	1.1520014(+00)	1.1681715(+07)	4.5650827(−01)	0.0000000(+00)
	(2,4)	8.2004011(+00)	1.1443707(+00)	9.6043123(+06)	4.2229855(−01)	0.0000000(+00)
	(3,3)	7.9654594(+00)	1.1821958(+00)	4.9627266(+04)	5.6671305(−01)	0.0000000(+00)
e–N	(1,1)	5.8254006(+00)	−6.1358276(−01)	4.6947975(−10)	0.0000000(+00)	−1.9000000(+00)
	(1,2)	5.6035615(+00)	−5.4460457(−01)	5.3579631(−10)	0.0000000(+00)	−1.9000000(+00)
	(1,3)	5.4230088(+00)	−4.9686275(−01)	6.7403110(−10)	0.0000000(+00)	−1.9000000(+00)
	(1,4)	5.2477084(+00)	−4.5868521(−01)	4.1056388(−10)	0.0000000(+00)	−1.9000000(+00)
	(1,5)	5.1018556(+00)	−4.3139316(−01)	3.5987258(−10)	0.0000000(+00)	−1.9000000(+00)
	(2,2)	5.5683614(+00)	−5.4215959(−01)	8.7754486(−11)	0.0000000(+00)	−1.9000000(+00)
	(2,3)	5.3873634(+00)	−4.9481075(−01)	9.9406630(−11)	0.0000000(+00)	−1.9000000(+00)
	(2,4)	5.2118627(+00)	−4.5534815(−01)	5.0851876(−11)	0.0000000(+00)	−1.9000000(+00)
	(3,3)	5.4142881(+00)	−4.9733458(−01)	5.1258839(−10)	0.0000000(+00)	−1.9000000(+00)

(continued)

Table 11.7 (continued)

	(ℓ, s)	g_1	g_2	g_3	g_4	g_5
$e–O_2$	(1,1)	7.8588787(+00)	1.8369546(+00)	3.5693172(+02)	2.8223244(−02)	0.0000000(+00)
	(1,2)	7.6482114(+00)	1.7644092(+00)	6.6540159(+02)	4.3786142(−03)	0.0000000(+00)
	(1,3)	7.4713949(+00)	1.6999137(+00)	1.0582978(+03)	−1.1775249(−02)	0.0000000(+00)
	(1,4)	7.3195193(+00)	1.6438407(+00)	1.5323704(+03)	−2.3221479(−02)	0.0000000(+00)
	(1,5)	7.1872618(+00)	1.5993805(+00)	2.0917705(+03)	−3.8643508(−02)	0.0000000(+00)
	(2,2)	8.6050316(+00)	1.9234429(+00)	2.4007545(+04)	−6.1447421(−01)	0.0000000(+00)
	(2,3)	8.4198162(+00)	1.9466632(+00)	2.0484698(+04)	−7.5126150(−01)	0.0000000(+00)
	(2,4)	8.2684322(+00)	1.9702143(+00)	1.6867520(+04)	−8.6114910(−01)	0.0000000(+00)
	(3,3)	7.6919894(+00)	1.8118510(+00)	1.0798292(+03)	−8.5419626(−02)	0.0000000(+00)
$e–N_2$	(1,1)	8.6647417(+00)	−2.8470816(+00)	2.4974553(−03)	3.7435842(−01)	0.0000000(+00)
	(1,2)	9.2427216(+00)	−3.1087179(+00)	2.9946282(−02)	−1.2250469(−01)	0.0000000(+00)
	(1,3)	1.0916068(+01)	−3.6802640(+00)	6.9820942(−01)	−2.3577425(+00)	0.0000000(+00)
	(1,4)	1.2183894(+01)	−4.2550219(+00)	3.0322926(+00)	−6.0542005(+00)	0.0000000(+00)
	(1,5)	1.3185789(+01)	−4.8168341(+00)	6.7403385(+00)	−1.0660674(+01)	0.0000000(+00)
	(2,2)	1.1057870(+01)	−2.0428465(+00)	1.3399913(−01)	−6.2499744(−01)	0.0000000(+00)
	(2,3)	1.1097560(+01)	−2.0628663(+00)	3.0772770(−01)	−1.1293145(+00)	0.0000000(+00)
	(2,4)	1.0916044(+01)	−2.0870247(+00)	3.5408884(−01)	−1.1863700(+00)	0.0000000(+00)
	(3,3)	1.2168592(+01)	−2.6164186(+00)	1.5868230(+00)	−3.5877170(+00)	0.0000000(+00)

e–NO	(1,1)	−2.8293464(+00)	1.5622863(+01)	9.5242325(+02)	−3.2162905(+02)	4.1010211(−01)
	(1,2)	−2.7835540(+00)	1.7932672(+01)	1.2663247(+03)	−6.2354687(+02)	5.6193400(−01)
	(1,3)	1.6372178(+01)	5.3192532(+00)	3.5244399(+04)	−3.7753003(+01)	3.4490100(+00)
	(1,4)	1.7513152(+01)	9.6046452(+00)	7.0747112(+03)	−1.6412975(+02)	2.2583084(+00)
	(1,5)	1.8114157(+01)	1.3573935(+01)	5.7001312(+03)	−3.6998837(+02)	1.8295712(+00)
	(2,2)	8.3572298(+00)	4.6952991(+00)	4.8893334(+02)	1.0084118(+03)	1.7306059(−02)
	(2,3)	6.9188668(−04)	1.4492179(+01)	7.2127752(+02)	−2.0803768(+02)	5.9137721(−01)
	(2,4)	2.9393554(−04)	1.2082965(+01)	3.8699104(+02)	−5.3850473(+01)	5.8338089(−01)
	(3,3)	1.6408711(+01)	6.3271130(+00)	1.4455880(+04)	−4.7514382(+01)	3.0925093(+00)
	(ℓ, s)	g_6	g_7	g_8	g_9	g_{10}
e–O	(1,1)	−2.4753262(+00)	4.5551320(−01)	1.1183108(+01)	1.3284135(+00)	0.0000000(+00)
	(1,2)	−5.8325613(+00)	7.2600394(−01)	1.1019551(+01)	1.4157571(+00)	0.0000000(+00)
	(1,3)	−5.3356533(+00)	7.0492042(−01)	1.0823475(+01)	1.3369725(+00)	0.0000000(+00)
	(1,4)	−5.0345906(+00)	7.2049861(−01)	1.0657225(+01)	1.3166940(+00)	0.0000000(+00)
	(1,5)	−4.8849034(+00)	7.6169177(−01)	1.0514777(+01)	1.3291704(+00)	0.0000000(+00)
	(2,2)	−7.0781870(+00)	1.4301510(+00)	1.0160031(+01)	1.2547808(+00)	0.0000000(+00)
	(2,3)	−7.1333167(+00)	1.4773336(+00)	9.9422415(+00)	1.2229175(+00)	0.0000000(+00)
	(2,4)	−7.1138747(+00)	1.5482109(+00)	9.7503828(+00)	1.2182253(+00)	0.0000000(+00)
	(3,3)	−4.9155056(+00)	1.3172987(+00)	9.8246972(+00)	1.3776101(+00)	0.0000000(+00)

(continued)

Table 11.7 (continued)

	(ℓ, s)	g_6	g_7	g_8	g_9	g_{10}
e–N	(1,1)	1.4568706(+01)	2.0801421(+00)	1.0511520(+01)	2.0320525(+00)	7.0000000(+00)
	(1,2)	1.4907928(+01)	2.1420027(+00)	1.0057131(+01)	2.3400382(+00)	7.0000000(+00)
	(1,3)	1.5125600(+01)	2.1934504(+00)	9.7252286(+00)	2.4094586(+00)	7.0000000(+00)
	(1,4)	1.5766290(+01)	2.2238493(+00)	9.5040311(+00)	2.3875410(+00)	7.0000000(+00)
	(1,5)	1.6153823(+01)	2.2526053(+00)	9.2275803(+00)	2.4952532(+00)	7.0000000(+00)
	(2,2)	1.5775236(+01)	2.9194982(+00)	9.5472258(+00)	2.1393001(+00)	7.0000000(+00)
	(2,3)	1.6076010(+01)	3.0104698(+00)	9.2214353(+00)	2.1882147(+00)	7.0000000(+00)
	(2,4)	1.6844386(+01)	3.0592425(+00)	8.9702707(+00)	2.2246032(+00)	7.0000000(+00)
	(3,3)	1.5326933(+01)	2.8132158(+00)	9.5154236(+00)	2.4166467(+00)	7.0000000(+00)
$e–O_2$	(1,1)	−2.2467312(+00)	5.0707449(−01)	1.0843859(+01)	1.0487624(+00)	0.0000000(+00)
	(1,2)	−2.5567984(+00)	6.3599773(−01)	1.0597054(+01)	1.0651801(+00)	0.0000000(+00)
	(1,3)	−2.8012345(+00)	7.4937898(−01)	1.0396702(+01)	1.0989618(+00)	0.0000000(+00)
	(1,4)	−3.0058803(+00)	8.4916205(−01)	1.0228012(+01)	1.1421074(+00)	0.0000000(+00)
	(1,5)	−3.1834745(+00)	9.4024864(−01)	1.0082742(+01)	1.1927295(+00)	0.0000000(+00)
	(2,2)	−3.9000941(+00)	1.0229813(+00)	1.0482913(+01)	1.1035341(+00)	0.0000000(+00)
	(2,3)	−3.8356592(+00)	1.0450625(+00)	1.0262712(+01)	1.0484238(+00)	0.0000000(+00)
	(2,4)	−3.7539962(+00)	1.0494037(+00)	1.0079267(+01)	9.9980198(−01)	0.0000000(+00)
	(3,3)	−2.7486271(+00)	9.4853921(−01)	1.0377500(+01)	1.1136931(+00)	0.0000000(+00)

e–N_2	(1,1)	3.6373136(+00)	4.2807542(−01)	8.9937032(+00)	6.4208483(−01)	0.0000000(+00)
	(1,2)	2.4738237(+00)	5.9874800(−01)	8.6867502(+00)	6.1223806(−01)	0.0000000(+00)
	(1,3)	1.1027690(+00)	8.0170671(−01)	8.4501962(+00)	6.2738810(−01)	0.0000000(+00)
	(1,4)	6.1008698(−01)	8.9617529(−01)	8.2816052(+00)	5.9781149(−01)	0.0000000(+00)
	(1,5)	4.0773619(−01)	9.4738178(−01)	8.1408417(+00)	5.6174043(−01)	0.0000000(+00)
	(2,2)	1.6080129(+00)	7.1921263(−01)	8.5357712(+00)	9.3300209(−01)	0.0000000(+00)
	(2,3)	1.2832611(+00)	7.9799880(−01)	8.3126680(+00)	9.4017592(−01)	0.0000000(+00)
	(2,4)	1.2387612(+00)	8.2247892(−01)	8.1024810(+00)	9.4113201(−01)	0.0000000(+00)
	(3,3)	7.2392521(−01)	8.7107617(−01)	8.5009936(+00)	6.9264029(−01)	0.0000000(+00)
e–NO	(1,1)	5.6798247(−02)	8.7924482(−01)	8.7622132(+00)	9.3677536(−01)	−2.2749385(+02)
	(1,2)	−4.5835203(−06)	1.0031122(+00)	8.4650903(+00)	8.4983082(−01)	−1.0814810(+02)
	(1,3)	−1.4927515(+00)	1.1851607(+00)	8.2549115(+00)	8.6733305(−01)	−1.9185125(−02)
	(1,4)	−5.4036053(−01)	1.2525764(+00)	8.0726285(+00)	8.0052616(−01)	−1.0243770(+00)
	(1,5)	−2.7287725(−01)	1.2779459(+00)	7.9214785(+00)	7.3053658(−01)	−4.9373914(+00)
	(2,2)	−9.8587087(−01)	8.5811919(−01)	8.5897447(+00)	9.2261791(−01)	−9.9824283(+02)
	(2,3)	1.5846610(−01)	1.0862450(+00)	8.3869998(+00)	9.9033699(−01)	−1.5856733(+02)
	(2,4)	2.5072363(−01)	1.1311315(+00)	8.2300353(+00)	9.3272837(−01)	−1.3619490(+02)
	(3,3)	−1.2051174(+00)	1.1362137(+00)	8.2751838(+00)	8.7079571(−01)	−4.3852555(−02)

11.2.2 Jupiter Interactions

11.2.2.1 H–H, H–H_2, H_2–H_2

For these systems accurate collision integral calculations have been performed by Stallcop et al. (1996, 1998) based on ab initio potential energy surfaces, considering an angular averaged potential for anisotropic atom–diatom and diatom–diatom collisions. For H–H_2 and H_2–H_2 data have been tabulated up to $T = 20,000\,\mathrm{K}$; therefore, in the high-temperature region, dominated by the short-range interaction, collision integrals have been calculated by integration of a repulsive potential used in Gorse and Capitelli (2001) and based on experimental data.
A full-range fitting expression [Eq. (11.4)], merging the low- and high-temperature data sets, has been used. The sigmoidal form is the same already used for the phenomenological case, though in this case, the dimensional $\sigma^2\Omega^{(\ell,s)\star}$ is obtained directly as a function of $x = \ln(T)$:

$$\sigma^2\Omega^{(\ell,s)\star} = [a_1 + a_2 x]\frac{\exp[(x-a_3)/a_4]}{\exp[(x-a_3)/a_4] + \exp[(a_3-x)/a_4]} + a_5\frac{\exp[(x-a_6)/a_7]}{\exp[(x-a_6)/a_7] + \exp[(a_6-x)/a_7]} \tag{11.4}$$

Fitting coefficients a_i are reported in Table 11.8.

11.2.2.2 H–He, He–He, H^-–He, H–He^+, He–He^+

The existence of weakly bound states of H^-–He molecular ion, where the H–He neutral molecule itself is either unbound or barely bound, has been theoretically investigated (Li and Lin 1999; Olson and Liu 1980). The interaction potentials, merging short-range repulsive and long-range weakly attractive ab initio results by different authors (Li and Lin 1999; Meyer and Frommhold 1994; Olson and Liu 1980), have been fitted with Hulburt–Hirschfleder functions. Optimised potential parameters are ($\varphi_0 = 6.14\ 10^{-4}\,\mathrm{eV}$, $r_e = 3.524\,\text{Å}$, $\alpha_{\mathrm{HH}} = 6.2613, \beta_{\mathrm{HH}} = 3.6046, \gamma_{\mathrm{HH}} = 0.8732$) for the H–He system and ($\varphi_0 = 6.22\ 10^{-4}\,\mathrm{eV}$, $r_e = 6.15\,\text{Å}$, $\alpha_{\mathrm{HH}} = 3.8, \beta_{\mathrm{HH}} = 7.9166, \gamma_{\mathrm{HH}} = 3.2832$) for H^-–He.

The potential for the He–He interaction has been taken from accurate theoretical results in literature, also providing a fitting formula, combining repulsive and attractive components (Hurly and Mehl 2007).

For the H–He^+ interaction the Hulburt–Hirschfelder fitting of the accurate ab initio potential by Aubreton et al. (2004a) has been considered ($\varphi_0 = 2.040\,\mathrm{eV}$, $r_e = 0.7743\,\text{Å}$, $\alpha_{\mathrm{HH}} = 2.1243, \beta_{\mathrm{HH}} = -0.3528, \gamma_{\mathrm{HH}} = -1.7676$) and collision integrals derived by integration.

The accurate ab initio potential energy curves for the $^2\Sigma_{gu}$ electronic terms, arising in the He–He^+ interaction have been fitted by Hulburt–Hirschfelder potential ($\varphi_0 = 2.4730\,\text{eV}$, $r_e = 1.081\,\text{Å}$, $\alpha_{HH} = 2.23, \beta_{HH} = 0.2205, \gamma_{HH} = 4.3890$) and modified repulsive potential ($\varphi_0 = 359.0\,\text{eV}$, $a = 4.184\,\text{Å}^{-1}$, $b = -0.649\,\text{Å}^{-2}$, $c = 0.08528\,\text{Å}^{-3}$) in Aubreton et al. (2004b). The effective collision integrals results from the usual averaging procedure [Eq. (3.56)].

In Table 11.8 the fitting coefficients, a_i, entering Eq. (11.4) are reported.

11.2.2.3 He^{2+}–He, He^{2+}–H, He^{2+}–H_2

Collision integrals for interactions involving the He^{2+} dication have been derived in the framework of a polarization model (Chap. 3), polarizability values being reported in Table 11.9.

11.2.2.4 H^+–H, H^+–H_2, H^+–He

Accurate potential energy curves are available for the two electronic terms, $^2\Sigma_g^+$ and $^2\Sigma_u^+$, of the H_2^+ system (Sharp 1970) correlating with H(^2S)-H^+, allowing the rigorous multi-potential procedure. The gerade term has been fitted with the Hulburt–Hirschfelder potential ($\varphi_0 = 2.791\,\text{eV}$, $r_e = 1.060\,\text{Å}$, $\alpha_{HH} = 1.28, \beta_{HH} = -0.5, \gamma_{HH} = -2.0$) while the modified Morse potential proposed in Sourd et al. (2006) ($\varphi_0 = 3.018\,\text{eV}$, $r_e = 1.058\,\text{Å}$, $\beta_0 = 1.3870\,\text{Å}^{-1}, \beta_1 = 0.0135, \beta_2 = 0.0117$) has been adopted for the ungerade state.

The H^+–H_2 and H^+–He systems have been studied by Krstič and Schultz (1999, 2003) within the frame of a quantum approach, obtaining accurate diffusive and viscosity transport cross sections in the energy range [0.1–20 eV] and [0.1–100 eV], respectively. The derivation of collision integrals is straightforward by integration in Eq. (3.11) however, the lower energy limit does not allow the $\sigma^2\Omega^{(\ell,s)\star}$ estimation at low temperatures.

In order to estimate the transport cross sections, $Q^{(\ell)}$, for $E \leq 0.1\,\text{eV}$, the long-range potential for the H^+–He, has been described by a polarization model [Eq. (3.34)], while the potential surface for H_3^+ in the limit of H^+–H_2 dissociation (Krstič 2002) has been fitted with a Hulburt–Hirschfelder potential ($\varphi_0 = 4.78\,\text{eV}$, $r_e = 0.73291\,\text{Å}$, $\alpha_{HH} = 1.3767, \beta_{HH} = -0.590, \gamma_{HH} = -1.653$). The $\sigma^2\Omega^{(3,3)\star}$ values, required by the adopted approximation in the Chapman–Enskog method, for H^+–H_2 have been calculated by the Hulburt–Hirschfelder potential and in the case of H^+–He interaction have been set equal to $\sigma^2\Omega^{(1,1)\star}$. Collision integrals have been fitted by using the expression in Eq. (11.4) and a_i coefficients given in Table 11.10.

Table 11.8 Fitting coefficients, entering Eq. (11.4), for $\sigma^2\Omega^{(\ell,s)\star}$ in heavy-particle interactions from different authors

	(ℓ, s)	a_1	a_2	a_3	a_4	a_5	a_5	a_7
H–H (a)	(1,1)	15.09506044	−1.25710008	9.57839369	−3.80371463	0.98646613	9.25705877	−0.93611707
	(1,2)	14.14566908	−1.17057105	9.02830724	−3.00779776	0.74653903	9.10299040	−0.68184353
	(1,3)	13.39722075	−1.09886403	8.50097335	−2.86025395	0.85345727	8.90666490	−0.67571329
	(1,4)	12.97073246	−1.06479185	8.18885522	−2.78105132	0.89401865	8.73403138	−0.65658782
	(1,5)	12.69248000	−1.04857945	7.97861283	−2.73621289	0.90816787	8.57840253	−0.63732002
	(2,2)	22.08948804	−1.85066626	8.50932055	−7.66943974	0.77454531	9.69545318	−0.62104466
	(2,3)	17.94703897	−1.42488999	7.66669340	−4.76239721	1.26783524	9.53716768	−0.73914215
	(2,4)	18.78590499	−1.59291967	7.97734302	−5.66814860	1.01816360	9.32328437	−0.60882006
	(3,3)	13.82986524	−1.01454290	7.48970759	−3.27628187	2.08225623	9.21388055	−1.32086596
H–H_2 (b)	(1,1)	12.49063970	−1.14704753	8.76515503	−3.52921496	0.32874932	12.77040465	−3.04802967
	(1,2)	12.02124035	−1.19514025	8.76515503	−3.45192920	0.45922882	12.77040465	−2.29080329
	(1,3)	11.69204285	−1.24240232	8.76515503	−3.49608019	0.63354264	12.77040465	−2.29080329
	(1,4)	11.45792771	−1.29677120	8.76515503	−3.64478512	0.85298582	12.77040465	−2.29080329
	(1,5)	11.00483923	−1.27212994	8.76515503	−3.51537463	0.85298582	12.77040465	−2.29080329
	(2,2)	7.45048892	−1.43326160	9.59201391	−1.35066206	7.15859874	9.88881724	−1.39484886
	(2,3)	10.84507417	−1.42859529	9.20889644	−1.29890434	3.37747184	9.83307970	−1.30321649
	(2,4)	11.55088396	−1.41480945	8.98739895	−1.39880703	2.32276221	9.89142509	−1.26804718
	(3,3)	−15.25288758	−1.39293852	9.59147724	−1.62599901	28.71128123	9.68396961	−1.63186985

H_2–H_2 (a)	(1,1)	24.00841090	−1.61027553	3.88885724	−8.89043396	0.44260972	8.88408687	−1.05402226
	(1,2)	23.02146328	−1.70509850	3.88885724	−10.46929121	0.36330166	8.26405726	−1.02331842
	(1,3)	21.17218602	−1.57714612	3.88885724	−9.72209606	0.59112956	8.15580488	−1.46063978
	(1,4)	20.05416161	−1.51326919	3.88885724	−9.38278743	0.70004430	8.00952510	−1.57063623
	(1,5)	19.06639058	−1.45577823	3.88885724	−9.14716131	0.81250655	7.85268967	−1.66995743
	(2,2)	27.54387526	−1.98253166	3.88885724	−12.91940775	0.34707960	8.72131306	−0.88296275
	(2,3)	26.22527642	−1.94538819	3.88885724	−13.40557645	0.40398208	8.42662474	−0.96878644
	(2,4)	24.59185702	−1.83729737	3.88885724	−12.78050876	0.62739891	8.27557505	−1.33071440
	(3,3)	24.57128293	−1.80855250	3.88885724	−11.86035430	0.36590658	8.38682707	−1.00746362
He–He (c)	(1,1)	14.66352146	−4.63010743	8.0	−15.40279240	16.26563367	4.0	5.06175281
	(1,2)	13.27609410	−2.44958217	8.0	−13.15623577	6.06716329	4.0	4.36702795
	(1,3)	12.25725957	−1.82548388	8.0	−11.79884311	3.47017274	4.0	3.88325561
	(1,4)	11.63440137	−1.61085155	8.0	−11.05638573	2.66723974	4.0	3.62035139
	(1,5)	11.22090805	−1.52094326	8.0	−10.60144544	2.36315549	4.0	3.48035253
	(2,2)	15.98872720	−4.31593080	8.0	−15.52249873	14.35288253	4.0	4.80040319
	(2,3)	14.82825809	−2.53225662	8.0	−14.04985907	6.10575500	4.0	4.17133518
	(2,4)	13.94776984	−1.89501662	8.0	−13.05297802	3.40674382	4.0	3.65268182
	(3,3)	14.07571785	−2.58722648	8.0	−13.68401223	6.53996034	4.0	4.28596613

(continued)

Table 11.8 (continued)

	(ℓ, s)	a_1	a_2	a_3	a_4	a_5	a_5	a_7
He–H (d)	(1,1)	10.06955597	−0.78208832	8.90551185	−4.17119119	76.18192207	−2.53113293	−2.89309888
	(1,2)	7.19869772	−0.68092029	9.54561159	−3.73700195	76.18192207	−8.84268703	−7.48001507
	(1,3)	6.55743323	−0.71505725	9.75769768	−3.90437553	76.18192207	−11.7792635	−9.63359232
	(1,4)	6.35904452	−0.73482728	9.66498209	−4.00054192	76.18192207	−13.1043859	−10.4621344
	(1,5)	6.25347577	−0.74253418	9.51511012	−4.02417882	76.18192207	−13.6296726	−10.6948126
	(2,2)	11.79267184	−0.91854409	9.46049069	−4.15691291	76.18192207	−2.52045886	−2.67556855
	(2,3)	9.11713279	−0.82598144	10.00526403	−3.68708893	76.18192207	−10.9038647	−8.42960742
	(2,4)	8.55265897	−0.88142795	10.32649048	−3.83898513	76.18192207	−15.7314905	−11.8299368
	(3,3)	8.45675669	−0.74217526	9.61034137	−3.82155303	76.18192207	−8.95019085	−7.14064928
$He–H^-$ (d)	(1,1)	16.83383128	−1.40086033	9.03792344	−3.76712840	76.18192207	0.0128648	−2.87368310
	(1,2)	11.26280636	−1.02780542	9.48063008	−2.93672204	50.16628602	0.0128648	−4.15375249
	(1,3)	8.49517155	−0.88101058	9.91582728	−2.56415853	45.66368787	0.0128648	−4.89901464
	(1,4)	6.92882973	−0.78943626	10.13073161	−2.45943130	43.96165902	0.0128648	−5.28289363
	(1,5)	5.99889967	−0.73327723	10.17888281	−2.44506151	42.80471500	0.0128648	−5.47961017
	(2,2)	18.96022395	−1.59117471	9.72963354	−3.60520521	72.97489590	0.0128648	−3.19508067
	(2,3)	14.24553114	−1.27240767	9.96040497	−2.85245325	56.52153525	0.0128648	−4.18966597
	(2,4)	11.68946064	−1.13472411	10.21270634	−2.43973469	52.00801821	0.0128648	−4.81326828
	(3,3)	13.37723617	−1.18163311	9.67449296	−3.11159621	53.82204847	0.0128648	−4.03136340

H–He$^+$ (e)	(1,1)	7.26019648	−0.45830355	8.75289388	−1.05196080	7.88022406	5.84488923	−2.83633436
	(1,2)	5.31621068	−0.25198722	8.39297559	−0.93572327	8.72583156	5.65613996	−2.63420758
	(1,3)	4.17730650	−0.13011997	8.12931880	−0.85589802	9.22623392	5.50181035	−2.54217036
	(1,4)	3.17455995	−0.00742372	7.90685901	−0.80603726	9.70796087	5.34685366	−2.47598237
	(1,5)	1.68374817	0.19151490	7.70176676	−0.76610507	10.49889283	5.20973048	−2.40196402
	(2,2)	4.47457332	−0.22703750	9.11487604	−0.84002241	13.68381322	4.46462878	−3.36880863
	(2,3)	3.75792422	−0.14961184	8.85486132	−0.77896426	13.27800873	4.46462878	−3.22466335
	(2,4)	2.98401159	−0.06111433	8.63912765	−0.74591089	13.14184555	4.46462878	−3.11327610
	(3,3)	11.80660156	−1.03306109	8.70928231	−1.32152742	7.24503625	4.46462878	−3.57325027
He–He$^+$ (f)	(1,1)	23.80276836	−1.53417198	7.14997977	−3.74339421	2.24179600	8.83793442	−0.99003900
	(1,2)	22.57798208	−1.37458298	6.71823986	−3.53660052	2.18797641	8.56245919	−0.88202165
	(1,3)	21.77686866	−1.29515584	6.44908263	−3.42650635	2.18797641	8.32964088	−0.88202165
	(1,4)	21.11384220	−1.22362410	6.23671845	−3.33679994	2.18797641	8.14201577	−0.88202165
	(1,5)	20.64796097	−1.18639584	6.07978682	−3.28123742	2.18797641	7.98030797	−0.88202165
	(2,2)	30.01038539	−1.71614435	5.80735212	−4.49537445	2.18797641	9.31326960	−0.88202165
	(2,3)	29.62345576	−1.80193239	5.65162107	−4.53517495	2.18797641	9.07520846	−0.88202165
	(2,4)	29.31400621	−1.84347108	5.48758712	−4.55520888	2.18797641	8.87814997	−0.88202165
	(3,3)	25.03330307	−1.29500767	6.24002334	−3.72851310	2.18797641	8.65029782	−0.88202165

(a) (Stallcop et al. 1998), (b) (Stallcop et al. 1996), (c) (Hurly and Mehl 2007), (d) (Li and Lin 1999; Olson and Liu 1980), (e) (Aubreton et al. 2004a), (f) (Aubreton et al. 2004b)

Table 11.9 Polarizability values (Å^3) for Jupiter atmosphere species

He	0.205
H_2	0.81
H	0.6668
He^+	0.03
H^-	27.0
H_2^+	0.424
H_3^+	0.4663

11.2.2.5 Phenomenological Interactions

The phenomenological approach has been adopted for the other interactions relevant to Jupiter atmosphere. Polarizability values for Jupiter species, taken from literature (Miller and Bederson 1977; Magnasco and Ottonelli 1999; Olney et al. 1997; Gorfinkiel and Tennyson 2004) or estimated through an empirical formula (Alagia et al. 2004) as for H^-, have been reported in Table 11.9 and potential parameters for different interactions, needed for bi-dimensional fit, presented in Table 11.11.

Table 11.12 reports fitting parameters entering Eq. (11.2) for $\sigma^2\Omega_{ex}^{(\ell,s)\star}$ in different systems, together with the references in literature for resonant charge-exchange cross sections. For ion–parent-atom interactions experimental results have been considered (Rundel et al. 1979; Huels et al. 1990). The cross section for the double charge transfer in He–He^{2+} collisions has been theoretically derived in Janev et al. (1987). In the case of H–H^+ accurate charge-transfer cross sections have been obtained by Krstič and Schultz (1999) by quantum approach. H_2–H_2^+ interaction has been included, using resonant cross sections by Yevseyev et al. (1982), obtained by extending the asymptotic theory to diatoms. For H–H^- interaction the experimental cross sections by Huels et al. (1990) have been used, which compares well with theoretical results obtained in the framework of the asymptotic theory (Davidović and Janev 1969) and with a perturbed-stationary-states approach (Dalgarno and McDowell 1956).

Collision integrals for electron–neutral species interactions have been calculated by straightforward integration based on the corresponding transport cross sections, $Q^\ell(E)$ as functions of electron energy.

Electronic scattering from hydrogen atoms has been deeply investigated theoretically (Bray et al. 1991; Gupta and Mathur 1980) finding an excellent agreement with absolute crossed-beam measurements (Williams 1975b,a). The diffusion-type collision integral has been calculated here by integration of the momentum transfer cross section by Gorse and Capitelli (2001), whereas the corrections $Q^{(2)}/Q^{(1)}$ and $Q^{(3)}/Q^{(1)}$ have been obtained by integrating the elastic differential cross sections by Bray et al. (1991) for the low-energy range [0.582–30 eV] and by Gupta and Mathur (1980) for energies above 50 eV.

Table 11.10 Fitting coefficients, entering Eq. (11.4), for $\sigma^2\Omega^{(\ell,s)\star}$ in H^+–neutral interactions

	(ℓ,s)	a_1	a_2	a_3	a_4	a_5	a_5	a_7
H^+–H	(1,1)	46.68783791	−0.33303803	4.25686770	−2.03851201	14.98170958	8.59618369	−1.65616736
	(1,2)	46.68783791	−0.33303803	3.92217635	−2.00886829	14.98170958	8.24501842	−1.65616736
	(1,3)	46.68783791	−0.33303803	3.65740159	−2.01434735	14.98170958	7.97534885	−1.65616736
	(1,4)	46.68783791	−0.33303803	3.43102576	−2.04002032	14.98170958	7.76086951	−1.65616736
	(1,5)	46.68783791	−0.33303803	3.23079831	−2.07543755	14.98170958	7.58613195	−1.65616736
	(2,2)	46.68783791	−0.33303803	4.10212490	−1.85454858	14.98170958	8.86285119	−1.65616736
	(2,3)	46.68783791	−0.33303803	3.89701552	−1.76267951	14.98170958	8.61913831	−1.65616736
	(2,4)	46.68783791	−0.33303803	3.73496748	−1.69596577	14.98170958	8.41234103	−1.65616736
	(3,3)	46.68783791	−0.33303803	3.95678840	−2.00381603	15.72150840	8.30656354	−1.79347178
H^+–H_2 (*a*)	(1,1)	21.26444082	−1.66425043	9.43954208	−1.18521519	17.72506447	5.16010621	−2.45568134
	(1,2)	22.04614090	−1.82881022	9.15603332	−1.09802478	16.51669691	4.84818012	−2.34842201
	(1,3)	22.20902097	−1.90013155	8.91515513	−1.04865323	15.76252584	4.62340367	−2.26445563
	(1,4)	22.03893787	−1.91163206	8.70196666	−1.02144928	15.03274560	4.48334473	−2.16080985
	(1,5)	21.58227738	−1.87980396	8.51589918	−1.00037698	14.35787253	4.41475379	−2.05912196
	(2,2)	16.29263601	−1.32780746	10.00998032	−0.70566506	17.72506447	5.16010621	−2.45568134
	(2,3)	15.17470368	−1.24428548	9.70964984	−0.61129207	17.72506447	4.99747949	−2.45568134
	(2,4)	14.08165081	−1.15372544	9.48976675	−0.58297710	17.72506447	4.89671501	−2.45568134
	(3,3)	11.21674909	−0.56122635	9.08694827	−1.28700668	25.96742671	4.83728681	−2.37965195
H^+–He (*b*)	(1,1)	2.71952379	−0.04746783	8.74213997	−0.88498112	91.77715465	2.49590845	−2.82208634
	(1,2)	0.90687201	0.18953042	8.34680329	−0.81094456	67.45506771	2.84282065	−2.68838648
	(1,3)	−1.51856588	0.53435861	7.99486464	−0.78866372	53.68311327	3.16719614	−2.55404045
	(1,4)	−4.74037779	1.00045484	7.68664217	−0.76331244	45.61529587	3.46378279	−2.42943739
	(1,5)	−7.26104273	1.37303488	7.46364505	−0.72571710	41.33193035	3.63435585	−2.34213326
	(2,2)	−3.94194326	0.73466954	8.79837656	−0.85969721	76.18192207	2.86197842	−2.85970495
	(2,3)	−5.23082562	0.92841556	8.50739551	−0.83699163	63.85598616	3.05252604	−2.75743238
	(2,4)	−6.28592988	1.09364996	8.27457168	−0.81943409	56.74233232	3.16129013	−2.68295935
	(3,3)	2.71952379	−0.04746783	8.74213997	−0.88498112	91.77715465	2.49590845	−2.82208634

(a) (Krstič and Schultz 2003), (b) (Krstič and Schultz 1999)

Table 11.11 Parameters of phenomenological potential for interactions relevant to Jupiter atmosphere

	β	φ_0 (meV)	r_e (Å)	m
He–H_2	9.29	1.865	3.189	6
He–H_2^+	9.73	30.664	2.574	4
He–H_3^+	9.66	29.471	2.606	4
H–H^-	7.05	15.151	4.975	4
H–H_2^+	8.00	73.104	2.769	4
H–H_3^+	7.98	70.982	2.797	4
H_2–H^-	7.27	18.896	4.962	4
H_2–He^+	9.22	177.500	2.223	4
H_2–H_2^+	8.97	83.283	2.809	4
H_2–H_3^+	8.93	80.981	2.838	4

The momentum transfer cross section $Q^{(1)}$ for e–H_2 interaction by Brunger and Buckman (2002) has been integrated, including low-($E < 0.01$ eV) and high-energy ($E > 25$ eV) data by Biagi (2012). The corrections to higher momentum transport cross sections, $Q^{(2)}/Q^{(1)}$ and $Q^{(3)}/Q^{(1)}$, have been obtained by integrating the elastic differential cross sections by Shyn and Sharp (1981); Brunger and Buckman (2002).

For e–He interaction the momentum transfer and elastic cross sections were taken from Biagi (2012) and the Q^2/Q^1 and Q^3/Q^1 ratios were deduced from the known Q^1/Q^0 by assuming a model angular dependence of the differential cross section (see Chap. 3).

Electron–neutral interaction collision integrals have been fitted, as a function of $x = \ln(T)$, using a slightly different formula with respect to that given in Eq. (11.3), i.e.

$$\sigma^2 \Omega^{(\ell,s)\star} = \frac{g_3 x^{g_5} \exp\left[(x-g_1)/g_2\right]}{\exp\left[(x-g_1)/g_2\right] + \exp\left[-(x-g_1)/g_2\right]} + g_6 \exp\left[-\left(\frac{x-g_7}{g_8}\right)^2\right] + g_4 \tag{11.5}$$

Fitting coefficients g_j, entering Eq. (11.5), are presented in Table 11.13, for relevant interaction in the Jupiter atmosphere.

11.3 Transport Coefficients

11.3.1 Earth

The thermodynamic model considered for Earth atmosphere (x_{N_2}:x_{O_2} = 80:20) includes 19 chemical species, i.e. N, O, N_2, O_2, NO, N^+, N^{2+}, N^{3+}, N^{4+}, O^+, O^{2+}, O^{3+}, O^{4+}, O^-, N_2^+, O_2^+, O_2^-, NO^+ and electrons, (see Capitelli et al. 2011). The transport cross section database for relevant interactions is derived from the Mars one (Laricchiuta et al. 2009). We have already compared the relevant transport coefficients with the corresponding ones obtained some years ago (Capitelli et al. 2000b), finding a satisfactory agreement (D'Angola et al. 2012) (see also Chap. 10). The present data should

Table 11.12 Fitting coefficients, entering Eq. (11.2), for $\sigma^2\Omega_{\rm ex}^{(\ell,s)\star}$ in neutral-ion interactions (to be added to the elastic contribution in order to obtain the effective odd-order collision integrals)

	(ℓ,s)	d_1	d_2	d_3		(ℓ,s)	d_1	d_2	d_3
He–He^+ (*a*)	(1,1)	38.6185	−3.1289	6.3410(−2)	He–He^{2+} (*d*)	(1,1)	12.1147	−0.9650	1.9236(−2)
	(1,2)	37.5764	−3.0869	6.3429(−2)		(1,2)	11.7937	−0.9524	1.9245(−2)
	(1,3)	36.8042	−3.0551	6.3424(−2)		(1,3)	11.5550	−0.9426	1.9229(−2)
	(1,4)	36.1948	−3.0302	6.3459(−2)		(1,4)	11.3658	−0.9347	1.9223(−2)
	(1,5)	35.6877	−3.0085	6.3422(−2)		(1,5)	11.2103	−0.9283	1.9218(−2)
H–H^- (*b*)	(1,1)	363.2187	−39.8121	1.0922	H_2–H_2^+ (*e*)	(1,1)	38.2368	−3.8755	9.8299(−2)
	(1,2)	349.9484	−39.0841	1.0922		(1,2)	36.9454	−3.8101	9.8307(−2)
	(1,3)	340.1784	−38.5383	1.0922		(1,3)	35.9923	−3.7608	9.8299(−2)
	(1,4)	332.4694	−38.1009	1.0922		(1,4)	35.2418	−3.7220	9.8329(−2)
	(1,5)	326.1197	−37.7370	1.0922		(1,5)	34.6202	−3.6888	9.8306(−2)
H–H^+ (*c*)	(1,1)	63.5437	−5.0093	9.8797(−2)					
	(1,2)	61.8730	−4.9431	9.8766(−2)					
	(1,3)	60.6364	−4.8936	9.8767(−2)					
	(1,4)	59.6591	−4.8544	9.8785(−2)					
	(1,5)	58.8493	−4.8213	9.8776(−2)					

(a) (Rundel et al. 1979), (b) (Huels et al. 1990), (c) (Krstič and Schultz 1999), (d) (Janev et al. 1987), (e) (Yevseyev et al. 1982)

Table 11.13 Fitting coefficients, entering Eq. (11.5), for $\sigma^2\Omega^{(\ell,s)\star}$ in electron–neutral interactions

	(ℓ,s)	g_1	g_2	g_3	g_4
e–He (a)	(1,1)	10.59136372(+00)	−1.52697125(+00)	2.18892432(−02)	−17.3791485(+00)
	(1,2)	10.38275022(+00)	−1.47464657(+00)	6.90741396(−02)	−3.37723956(+00)
	(1,3)	10.21366567(+00)	−1.44621765(+00)	0.15768321(+00)	−0.40718547(+00)
	(1,4)	10.06183007(+00)	−1.41920632(+00)	0.26516138(+00)	−0.15710196(+00)
	(1,5)	9.92613479(+00)	−1.39377540(+00)	0.37258117(+00)	−8.83214413(−02)
	(2,2)	11.02594479(+00)	−2.75226422(+00)	0.25837224(+00)	−1.80065315(+00)
	(2,3)	10.95544093(+00)	−2.24065670(+00)	1.42500349(+00)	−0.65562457(+00)
	(2,4)	10.68567439(+00)	−2.03462360(+00)	1.47732284(+00)	−0.44873292(+00)
	(3,3)	10.27636518(+00)	−1.60869251(+00)	0.18373753(+00)	−0.44953771(+00)
e–H (b)	(1,1)	10.35291134(+00)	−1.58301162(+00)	12.45844036(+00)	−0.23285190(+00)
	(1,2)	10.09959930(+00)	−1.50068352(+00)	12.54524872(+00)	−7.29529868(−02)
	(1,3)	9.84443341(+00)	−1.42568830(+00)	12.97194554(+00)	−9.24067489(−02)
	(1,4)	9.65959253(+00)	−1.38293428(+00)	13.18865311(+00)	−6.34310879(−02)
	(1,5)	9.50113220(+00)	−1.36043711(+00)	13.23885240(+00)	−4.44172748(−02)
	(2,2)	10.33445440(+00)	−1.44880911(+00)	12.08534341(+00)	−1.86163984(−02)
	(2,3)	10.08612484(+00)	−1.39070408(+00)	12.39823810(+00)	−3.26532858(−02)
	(2,4)	9.89312188(+00)	−1.34820033(+00)	12.63138071(+00)	−1.96030794(−02)
	(3,3)	9.99023294(+00)	−1.41457896(+00)	12.53875975(+00)	−2.82169003(−02)
e–H_2 (c)	(1,1)	7.61552567(+00)	−1.31152238(+00)	1.08767030(+00)	−8.58478684(−02)
	(1,2)	7.82045948(+00)	−1.28509145(+00)	0.84661899(+00)	7.30252753(−03)
	(1,3)	7.91713411(+00)	−1.18533267(+00)	0.77902584(+00)	4.56053378(−02)
	(1,4)	7.86089850(+00)	−1.10926763(+00)	0.77235681(+00)	5.98096935(−02)
	(1,5)	7.76607601(+00)	−1.06076517(+00)	0.78630351(+00)	6.51985996(−02)
	(2,2)	8.44904482(+00)	−0.85941165(+00)	0.45608703(+00)	−3.28370076(−02)
	(2,3)	8.28235333(+00)	−0.77764787(+00)	0.39162611(+00)	3.15214680(−02)
	(2,4)	8.14899029(+00)	−0.71893844(+00)	0.33943549(+00)	8.34297336(−02)
	(3,3)	8.09697330(+00)	−1.08367568(+00)	0.67651715(+00)	5.92335717(−02)

	(ℓ, s)	g_5	g_6	g_7	g_8
e–He (*a*)	(1,1)	1.99019765(+00)	19.13183426(+00)	−3.87345716(+00)	52.39042000(+00)
	(1,2)	1.54430366(+00)	36.06175647(+00)	−115.629356(+00)	82.85050640(+00)
	(1,3)	1.22119154(+00)	36.06175647(+00)	−41.6895622(+00)	24.95446099(+00)
	(1,4)	1.01178482(+00)	36.06175647(+00)	−27.9895600(+00)	16.41208651(+00)
	(1,5)	0.87073597(+00)	36.06175647(+00)	−21.8337945(+00)	12.72530780(+00)
	(2,2)	1.11428478(+00)	36.06175647(+00)	−41.1176569(+00)	27.16469738(+00)
	(2,3)	0.31741278(+00)	36.06175647(+00)	−9.11869898(+00)	5.60148399(+00)
	(2,4)	0.25766199(+00)	36.06175647(+00)	−3.57516627(+00)	2.96346809(+00)
	(3,3)	1.13659747(+00)	36.06175647(+00)	−42.9018487(+00)	25.63994176(+00)
e–H (*b*)	(1,1)	5.36628573(−02)	−5.34372929(+00)	9.35561752(+00)	−2.15463427(+00)
	(1,2)	4.37301268(−02)	−5.73166847(+00)	9.09798179(+00)	−2.13265127(+00)
	(1,3)	2.32754987(−02)	−5.71948057(+00)	8.83259870(+00)	−2.05797013(+00)
	(1,4)	1.11968653(−02)	−5.77977010(+00)	8.64525855(+00)	−2.02715634(+00)
	(1,5)	7.88864536(−03)	−5.83593794(+00)	8.49000000(+00)	−2.01418763(+00)
	(2,2)	3.30723152(−02)	−6.45649277(+00)	9.15932646(+00)	−2.13494419(+00)
	(2,3)	1.75287406(−02)	−6.48186913(+00)	8.90783546(+00)	−2.08119318(+00)
	(2,4)	4.55766915(−03)	−6.50687636(+00)	8.71405704(+00)	−2.04690115(+00)
	(3,3)	2.70547916(−02)	−6.11376507(+00)	8.89657156(+00)	−2.09400530(+00)
e–H_2 (*c*)	(1,1)	0.60307406(+00)	5.01125522(+00)	9.07403916(+00)	1.92416429(+00)
	(1,2)	0.77338688(+00)	4.59038620(+00)	8.92912750(+00)	1.72315372(+00)
	(1,3)	0.84160605(+00)	4.29393447(+00)	8.81056581(+00)	1.59949292(+00)
	(1,4)	0.86441504(+00)	4.18795370(+00)	8.67601998(+00)	1.53347205(+00)
	(1,5)	0.86956793(+00)	4.14851371(+00)	8.54553153(+00)	1.49396365(+00)
	(2,2)	0.88418654(+00)	3.62672485(+00)	9.45483919(+00)	1.67160237(+00)
	(2,3)	0.98366646(+00)	3.59756557(+00)	9.25577830(+00)	1.57423504(+00)
	(2,4)	1.07846844(+00)	3.56463327(+00)	9.10019221(+00)	1.49404727(+00)
	(3,3)	0.86030007(+00)	4.05861889(+00)	9.00694175(+00)	1.62336471(+00)

(a) (Biagi 2012), (b) (Bray et al. 1991; Gupta and Mathur 1980), (c) (Shyn and Sharp 1981; Brunger and Buckman 2002)

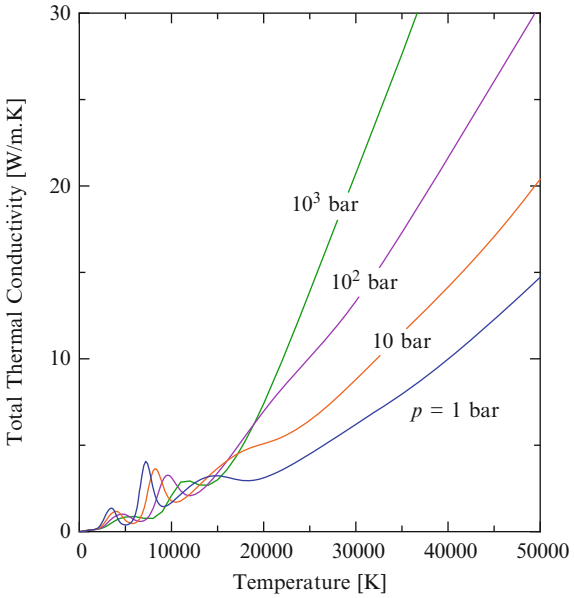

Fig. 11.1 Total thermal conductivity of Mars plasma as a function of temperature, at different pressures

compare satisfactory also calculating the transport properties by using the transport cross sections from NASA database (Wright et al. 2005). The transport properties of air have been extensively discussed in Chap. 10, so that here we limit to numerical values as a function of temperature at different pressures. Tables 11.14–11.17 report numerical values of transport coefficients for different pressures, while Table 11.18reports thermodynamic properties of air mixture at p=1,000 bar.

11.3.2 Mars

The thermodynamic model used for the high-temperature Mars atmosphere (x_{CO_2}:x_{N_2}:x_{Ar}:x_{O_2}=95.3:2.7:1.6:0.4) has been discussed in detail in Capitelli et al. (2011, 2005) and used by Bruno et al. at 1 bar (Bruno et al. 2011) and either by d'Angola et al. at different pressures (Colonna et al. 2013). Fifty-three species, including C, N, O, C_2, N_2, O_2, CN, CO, NO, C_3, N_3, O_3, C_2N, CO_2, C_2O, NO_2, N_2O, CNO, Ar, C^+, C^{2+}, C^{3+}, C^{4+}, C^-, N^+, N^{2+}, N^{3+}, N^{4+}, N^-, O^+, O^{2+}, O^{3+}, O^{4+}, O^-, C_2^+, C_2^-, N_2^+, N_2^-, O_2^+, O_2^-, CN^+, CN^-, CO^+, NO^+, O_3^-, CO_2^+, CO_2^-, N_2O^+, Ar^+, Ar^{2+}, Ar^{3+}, Ar^{4+} and electrons, have been considered in the transport calculations. The transport cross sections database has been previously discussed. A sample of results for the total thermal conductivity is reported in Fig. 11.1. The different peaks

Table 11.14 Transport coefficients for Earth atmosphere at $p = 1\,\text{bar}$

T (K)	σ_e (S/m)	η (Kg/m.s)	λ_e (W/m.K)	λ_h (W/m.K)	λ_{int} (W/m.K)	λ_r (W/m.K)	λ_{tot} (W/m.K)
100	0.00(+00)	6.84(−06)	0.00(+00)	7.41(−03)	2.64(−03)	0.00(+00)	1.00(−02)
200	0.00(+00)	1.31(−05)	0.00(+00)	1.42(−02)	5.11(−03)	0.00(+00)	1.93(−02)
300	0.00(+00)	1.91(−05)	0.00(+00)	2.07(−02)	7.47(−03)	0.00(+00)	2.81(−02)
400	0.00(+00)	2.45(−05)	0.00(+00)	2.65(−02)	9.81(−03)	0.00(+00)	3.63(−02)
500	0.00(+00)	2.93(−05)	0.00(+00)	3.17(−02)	1.23(−02)	3.26(−09)	4.41(−02)
600	3.86(−38)	3.36(−05)	2.41(−43)	3.64(−02)	1.51(−02)	9.86(−08)	5.15(−02)
700	1.19(−31)	3.75(−05)	9.05(−37)	4.06(−02)	1.81(−02)	1.09(−06)	5.87(−02)
800	8.86(−27)	4.11(−05)	8.00(−32)	4.45(−02)	2.12(−02)	6.43(−06)	6.57(−02)
900	5.42(−23)	4.45(−05)	5.69(−28)	4.81(−02)	2.43(−02)	2.51(−05)	7.24(−02)
1,000	5.66(−20)	4.76(−05)	6.80(−25)	5.15(−02)	2.74(−02)	7.34(−05)	7.90(−02)
1,500	4.35(−11)	6.17(−05)	8.74(−16)	6.68(−02)	4.18(−02)	1.65(−03)	1.10(−01)
2,000	9.44(−07)	7.41(−05)	2.60(−11)	8.02(−02)	5.46(−02)	9.59(−03)	1.44(−01)
2,500	3.69(−04)	8.56(−05)	1.19(−08)	9.30(−02)	6.61(−02)	5.93(−02)	2.18(−01)
3,000	1.98(−02)	9.68(−05)	7.02(−07)	1.08(−01)	7.50(−02)	2.53(−01)	4.36(−01)
3,500	3.24(−01)	1.08(−04)	1.26(−05)	1.29(−01)	7.85(−02)	4.69(−01)	6.76(−01)
4,000	2.28(+00)	1.20(−04)	9.98(−05)	1.53(−01)	7.95(−02)	3.10(−01)	5.42(−01)
4,500	8.91(+00)	1.31(−04)	4.50(−04)	1.72(−01)	8.35(−02)	2.01(−01)	4.57(−01)
5,000	2.41(+01)	1.41(−04)	1.45(−03)	1.90(−01)	8.94(−02)	3.72(−01)	6.53(−01)
6,000	9.19(+01)	1.62(−04)	7.56(−03)	2.38(−01)	1.00(−01)	1.70(+00)	2.05(+00)
7,000	2.56(+02)	1.82(−04)	2.31(−02)	3.24(−01)	1.14(−01)	3.07(+00)	3.53(+00)
8,000	7.51(+02)	2.00(−04)	6.86(−02)	4.11(−01)	1.38(−01)	1.42(+00)	2.04(+00)
9,000	1.63(+03)	2.16(−04)	1.66(−01)	4.62(−01)	1.62(−01)	4.32(−01)	1.22(+00)

(continued)

Table 11.14 (continued)

T (K)	σ_e (S/m)	η (Kg/m.s)	λ_e (W/m.K)	λ_h (W/m.K)	λ_{int} (W/m.K)	λ_r (W/m.K)	λ_{tot} (W/m.K)
10,000	2.65(+03)	2.26(−04)	3.10(−01)	4.83(−01)	1.73(−01)	3.58(−01)	1.32(+00)
11,000	3.69(+03)	2.19(−04)	4.86(−01)	4.58(−01)	1.73(−01)	5.85(−01)	1.70(+00)
12,000	4.70(+03)	1.91(−04)	6.85(−01)	3.79(−01)	1.61(−01)	9.69(−01)	2.19(+00)
13,000	5.67(+03)	1.49(−04)	9.02(−01)	2.75(−01)	1.42(−01)	1.40(+00)	2.72(+00)
14,000	6.58(+03)	1.05(−04)	1.13(+00)	1.83(−01)	1.19(−01)	1.69(+00)	3.13(+00)
15,000	7.39(+03)	7.03(−05)	1.36(+00)	1.18(−01)	1.03(−01)	1.67(+00)	3.25(+00)
16,000	8.12(+03)	4.63(−05)	1.60(+00)	7.76(−02)	8.75(−02)	1.34(+00)	3.10(+00)
17,000	8.77(+03)	3.17(−05)	1.83(+00)	5.42(−02)	7.12(−02)	9.23(−01)	2.88(+00)
18,000	9.38(+03)	2.36(−05)	2.07(+00)	4.19(−02)	5.66(−02)	5.85(−01)	2.75(+00)
19,000	9.95(+03)	1.95(−05)	2.32(+00)	3.60(−02)	4.64(−02)	3.58(−01)	2.76(+00)
20,000	1.05(+04)	1.77(−05)	2.57(+00)	3.39(−02)	4.05(−02)	2.17(−01)	2.86(+00)
22,000	1.15(+04)	1.68(−05)	3.11(+00)	3.36(−02)	2.61(−02)	9.58(−02)	3.27(+00)
24,000	1.23(+04)	1.71(−05)	3.67(+00)	3.46(−02)	2.19(−02)	8.26(−02)	3.81(+00)
26,000	1.26(+04)	1.56(−05)	4.20(+00)	3.15(−02)	2.16(−02)	1.50(−01)	4.41(+00)
28,000	1.23(+04)	1.23(−05)	4.69(+00)	2.46(−02)	2.29(−02)	2.68(−01)	5.00(+00)
30,000	1.22(+04)	9.02(−06)	5.19(+00)	1.79(−02)	2.25(−02)	3.39(−01)	5.57(+00)
35,000	1.30(+04)	5.08(−06)	6.79(+00)	1.04(−02)	1.65(−02)	1.80(−01)	7.00(+00)
40,000	1.43(+04)	4.45(−06)	8.77(+00)	9.32(−03)	1.16(−02)	8.21(−02)	8.88(+00)
45,000	1.49(+04)	3.69(−06)	1.07(+01)	7.69(−03)	8.21(−03)	1.29(−01)	1.09(+01)
50,000	1.53(+04)	2.75(−06)	1.27(+01)	5.75(−03)	6.51(−03)	1.29(−01)	1.29(+01)

Table 11.15 Transport coefficients for Earth atmosphere at $p = 10\,\text{bar}$

T (K)	σ_e (S/m)	η (Kg/m.s)	λ_e (W/m.K)	λ_h (W/m.K)	λ_{int} (W/m.K)	λ_r (W/m.K)	λ_{tot} (W/m.K)
100	0.00(+00)	6.84(−06)	0.00(+00)	7.41(−03)	2.64(−03)	0.00(+00)	1.00(−02)
200	0.00(+00)	1.31(−05)	0.00(+00)	1.42(−02)	5.11(−03)	0.00(+00)	1.93(−02)
300	0.00(+00)	1.91(−05)	0.00(+00)	2.07(−02)	7.47(−03)	0.00(+00)	2.81(−02)
400	0.00(+00)	2.45(−05)	0.00(+00)	2.65(−02)	9.81(−03)	0.00(+00)	3.63(−02)
500	0.00(+00)	2.93(−05)	0.00(+00)	3.17(−02)	1.23(−02)	3.26(−09)	4.41(−02)
600	3.87(−39)	3.36(−05)	2.38(−44)	3.64(−02)	1.51(−02)	9.86(−08)	5.15(−02)
700	1.20(−32)	3.75(−05)	9.12(−38)	4.06(−02)	1.81(−02)	1.09(−06)	5.87(−02)
800	9.08(−28)	4.11(−05)	8.20(−33)	4.45(−02)	2.12(−02)	6.43(−06)	6.57(−02)
900	5.77(−24)	4.45(−05)	6.06(−29)	4.81(−02)	2.43(−02)	2.51(−05)	7.24(−02)
1,000	6.43(−21)	4.76(−05)	7.74(−26)	5.15(−02)	2.74(−02)	7.34(−05)	7.90(−02)
1,500	8.60(−12)	6.17(−05)	1.73(−16)	6.68(−02)	4.18(−02)	1.63(−03)	1.10(−01)
2,000	2.51(−07)	7.41(−05)	6.91(−12)	8.02(−02)	5.46(−02)	7.59(−03)	1.42(−01)
2,500	1.07(−04)	8.56(−05)	3.44(−09)	9.28(−02)	6.63(−02)	2.85(−02)	1.88(−01)
3,000	5.91(−03)	9.66(−05)	2.10(−07)	1.06(−01)	7.67(−02)	1.03(−01)	2.85(−01)
3,500	1.04(−01)	1.07(−04)	4.03(−06)	1.21(−01)	8.44(−02)	2.57(−01)	4.62(−01)
4,000	8.57(−01)	1.18(−04)	3.73(−05)	1.40(−01)	8.84(−02)	3.74(−01)	6.02(−01)
4,500	4.09(+00)	1.30(−04)	2.04(−04)	1.62(−01)	9.08(−02)	3.16(−01)	5.69(−01)
5,000	1.29(+01)	1.40(−04)	7.53(−04)	1.82(−01)	9.45(−02)	2.53(−01)	5.30(−01)
6,000	5.90(+01)	1.61(−04)	4.79(−03)	2.20(−01)	1.06(−01)	6.40(−01)	9.71(−01)
7,000	1.59(+02)	1.81(−04)	1.60(−02)	2.73(−01)	1.22(−01)	1.80(+00)	2.21(+00)
8,000	3.78(+02)	2.01(−04)	4.00(−02)	3.54(−01)	1.45(−01)	2.69(+00)	3.23(+00)
9,000	9.27(+02)	2.19(−04)	9.92(−02)	4.38(−01)	1.71(−01)	1.76(+00)	2.47(+00)

(continued)

Table 11.15 (continued)

T (K)	σ_e (S/m)	η (Kg/m.s)	λ_e (W/m.K)	λ_h (W/m.K)	λ_{int} (W/m.K)	λ_r (W/m.K)	λ_{tot} (W/m.K)
10,000	1.87(+03)	2.35(−04)	2.16(−01)	4.96(−01)	1.89(−01)	7.28(−01)	1.63(+00)
11,000	3.05(+03)	2.48(−04)	3.95(−01)	5.31(−01)	1.98(−01)	4.12(−01)	1.54(+00)
12,000	4.36(+03)	2.54(−04)	6.29(−01)	5.42(−01)	2.08(−01)	4.39(−01)	1.82(+00)
13,000	5.70(+03)	2.47(−04)	9.09(−01)	5.18(−01)	2.02(−01)	6.21(−01)	2.25(+00)
14,000	7.05(+03)	2.25(−04)	1.23(+00)	4.57(−01)	1.88(−01)	8.65(−01)	2.74(+00)
15,000	8.37(+03)	1.92(−04)	1.57(+00)	3.75(−01)	1.61(−01)	1.14(+00)	3.25(+00)
16,000	9.63(+03)	1.55(−04)	1.94(+00)	2.91(−01)	1.51(−01)	1.35(+00)	3.73(+00)
17,000	1.08(+04)	1.21(−04)	2.32(+00)	2.20(−01)	1.40(−01)	1.44(+00)	4.12(+00)
18,000	1.19(+04)	9.31(−05)	2.70(+00)	1.66(−01)	1.26(−01)	1.38(+00)	4.38(+00)
19,000	1.29(+04)	7.15(−05)	3.08(+00)	1.27(−01)	1.04(−01)	1.20(+00)	4.52(+00)
20,000	1.37(+04)	5.69(−05)	3.46(+00)	1.02(−01)	9.29(−02)	9.65(−01)	4.62(+00)
22,000	1.53(+04)	4.09(−05)	4.23(+00)	7.66(−02)	6.61(−02)	5.43(−01)	4.91(+00)
24,000	1.67(+04)	3.51(−05)	5.02(+00)	6.85(−02)	4.83(−02)	2.94(−01)	5.43(+00)
26,000	1.80(+04)	3.35(−05)	5.85(+00)	6.71(−02)	4.05(−02)	1.85(−01)	6.14(+00)
28,000	1.89(+04)	3.29(−05)	6.68(+00)	6.66(−02)	4.06(−02)	1.76(−01)	6.96(+00)
30,000	1.92(+04)	3.09(−05)	7.48(+00)	6.25(−02)	4.41(−02)	2.53(−01)	7.84(+00)
35,000	1.89(+04)	1.94(−05)	9.40(+00)	3.86(−02)	4.64(−02)	5.40(−01)	1.00(+01)
40,000	1.97(+04)	1.21(−05)	1.17(+01)	2.46(−02)	3.59(−02)	4.12(−01)	1.22(+01)
45,000	2.12(+04)	9.84(−06)	1.45(+01)	2.04(−02)	2.82(−02)	2.09(−01)	1.48(+01)
50,000	2.22(+04)	8.43(−06)	1.74(+01)	1.76(−02)	1.98(−02)	2.10(−01)	1.76(+01)

Table 11.16 Transport coefficients for Earth atmosphere at $p = 100\,\text{bar}$

T (K)	σ_e (S/m)	η (Kg/m.s)	λ_e (W/m.K)	λ_h (W/m.K)	λ_{int} (W/m.K)	λ_r (W/m.K)	λ_{tot} (W/m.K)
100	0.00(+00)	6.84(−06)	0.00(+00)	7.41(−03)	2.64(−03)	0.00(+00)	1.00(−02)
200	0.00(+00)	1.31(−05)	0.00(+00)	1.42(−02)	5.11(−03)	0.00(+00)	1.93(−02)
300	0.00(+00)	1.91(−05)	0.00(+00)	2.07(−02)	7.47(−03)	0.00(+00)	2.81(−02)
400	0.00(+00)	2.45(−05)	0.00(+00)	2.65(−02)	9.81(−03)	0.00(+00)	3.63(−02)
500	0.00(+00)	2.93(−05)	0.00(+00)	3.17(−02)	1.23(−02)	3.26(−09)	4.41(−02)
600	3.87(−40)	3.36(−05)	2.80(−45)	3.64(−02)	1.51(−02)	9.86(−08)	5.15(−02)
700	1.20(−33)	3.75(−05)	9.12(−39)	4.06(−02)	1.81(−02)	1.09(−06)	5.87(−02)
800	9.10(−29)	4.11(−05)	8.22(−34)	4.45(−02)	2.12(−02)	6.43(−06)	6.57(−02)
900	5.81(−25)	4.45(−05)	6.10(−30)	4.81(−02)	2.43(−02)	2.51(−05)	7.24(−02)
1,000	6.53(−22)	4.76(−05)	7.85(−27)	5.15(−02)	2.74(−02)	7.34(−05)	7.90(−02)
1,500	1.02(−12)	6.17(−05)	2.06(−17)	6.68(−02)	4.18(−02)	1.62(−03)	1.10(−01)
2,000	4.11(−08)	7.41(−05)	1.13(−12)	8.02(−02)	5.46(−02)	6.95(−03)	1.42(−01)
2,500	2.24(−05)	8.56(−05)	7.24(−10)	9.27(−02)	6.64(−02)	1.86(−02)	1.78(−01)
3,000	1.42(−03)	9.65(−05)	5.04(−08)	1.05(−01)	7.72(−02)	4.75(−02)	2.30(−01)
3,500	2.69(−02)	1.07(−04)	1.04(−06)	1.17(−01)	8.68(−02)	1.10(−01)	3.15(−01)
4,000	2.41(−01)	1.18(−04)	1.05(−05)	1.32(−01)	9.44(−02)	2.03(−01)	4.29(−01)
4,500	1.31(+00)	1.28(−04)	6.50(−05)	1.48(−01)	9.99(−02)	2.78(−01)	5.27(−01)
5,000	4.90(+00)	1.39(−04)	2.82(−04)	1.67(−01)	1.04(−01)	2.93(−01)	5.65(−01)
6,000	3.02(+01)	1.60(−04)	2.40(−03)	2.05(−01)	1.13(−01)	3.23(−01)	6.44(−01)
7,000	9.48(+01)	1.80(−04)	9.85(−03)	2.45(−01)	1.28(−01)	7.14(−01)	1.10(+00)
8,000	2.17(+02)	1.99(−04)	2.62(−02)	2.96(−01)	1.49(−01)	1.51(+00)	1.99(+00)
9,000	4.57(+02)	2.19(−04)	5.77(−02)	3.66(−01)	1.78(−01)	2.26(+00)	2.86(+00)

(continued)

Table 11.16 (continued)

T (K)	σ_e (S/m)	η (Kg/m.s)	λ_e (W/m.K)	λ_h (W/m.K)	λ_{int} (W/m.K)	λ_r (W/m.K)	λ_{tot} (W/m.K)
10,000	9.61(+02)	2.37(−04)	1.23(−01)	4.46(−01)	2.04(−01)	2.14(+00)	2.91(+00)
11,000	1.85(+03)	2.54(−04)	2.48(−01)	5.15(−01)	2.19(−01)	1.34(+00)	2.33(+00)
12,000	3.06(+03)	2.69(−04)	4.46(−01)	5.66(−01)	2.26(−01)	7.46(−01)	1.98(+00)
13,000	4.53(+03)	2.82(−04)	7.22(−01)	6.00(−01)	2.31(−01)	5.07(−01)	2.06(+00)
14,000	6.16(+03)	2.90(−04)	1.08(+00)	6.19(−01)	2.27(−01)	4.80(−01)	2.40(+00)
15,000	7.92(+03)	2.91(−04)	1.50(+00)	6.17(−01)	2.19(−01)	5.62(−01)	2.90(+00)
16,000	9.73(+03)	2.82(−04)	2.00(+00)	5.93(−01)	2.17(−01)	6.98(−01)	3.51(+00)
17,000	1.15(+04)	2.67(−04)	2.53(+00)	5.52(−01)	2.03(−01)	8.51(−01)	4.14(+00)
18,000	1.33(+04)	2.43(−04)	3.12(+00)	4.93(−01)	1.70(−01)	1.01(+00)	4.80(+00)
19,000	1.50(+04)	2.16(−04)	3.75(+00)	4.30(−01)	1.59(−01)	1.14(+00)	5.48(+00)
20,000	1.67(+04)	1.89(−04)	4.39(+00)	3.69(−01)	1.47(−01)	1.21(+00)	6.12(+00)
22,000	1.98(+04)	1.42(−04)	5.71(+00)	2.71(−01)	1.22(−01)	1.18(+00)	7.29(+00)
24,000	2.24(+04)	1.09(−04)	7.04(+00)	2.09(−01)	9.83(−02)	9.72(−01)	8.32(+00)
26,000	2.47(+04)	8.93(−05)	8.36(+00)	1.73(−01)	8.04(−02)	7.12(−01)	9.33(+00)
28,000	2.66(+04)	7.96(−05)	9.67(+00)	1.57(−01)	7.15(−02)	5.11(−01)	1.04(+01)
30,000	2.83(+04)	7.48(−05)	1.10(+01)	1.50(−01)	6.98(−02)	3.94(−01)	1.16(+01)
35,000	3.12(+04)	7.06(−05)	1.44(+01)	1.44(−01)	1.02(−01)	3.89(−01)	1.50(+01)
40,000	3.10(+04)	5.09(−05)	1.74(+01)	1.02(−01)	1.12(−01)	8.34(−01)	1.85(+01)
45,000	3.15(+04)	3.57(−05)	2.08(+01)	7.16(−02)	9.63(−02)	9.11(−01)	2.19(+01)
50,000	3.28(+04)	2.73(−05)	2.47(+01)	5.55(−02)	7.34(−02)	6.96(−01)	2.56(+01)

Table 11.17 Transport coefficients for Earth atmosphere at $p = 1,000$ bar

T (K)	σ_e (S/m)	η (Kg/m.s)	λ_e (W/m.K)	λ_h (W/m.K)	λ_{int} (W/m.K)	λ_r (W/m.K)	λ_{tot} (W/m.K)
100	0.00(+00)	6.84(−06)	0.00(+00)	7.41(−03)	2.64(−03)	0.00(+00)	1.00(−02)
200	0.00(+00)	1.31(−05)	0.00(+00)	1.42(−02)	5.11(−03)	0.00(+00)	1.93(−02)
300	0.00(+00)	1.91(−05)	0.00(+00)	2.07(−02)	7.47(−03)	0.00(+00)	2.81(−02)
400	0.00(+00)	2.45(−05)	0.00(+00)	2.65(−02)	9.81(−03)	0.00(+00)	3.63(−02)
500	0.00(+00)	2.93(−05)	0.00(+00)	3.17(−02)	1.23(−02)	3.26(−09)	4.41(−02)
600	3.87(−41)	3.36(−05)	0.00(+00)	3.64(−02)	1.51(−02)	9.86(−08)	5.15(−02)
700	1.20(−34)	3.75(−05)	9.13(−40)	4.06(−02)	1.81(−02)	1.09(−06)	5.87(−02)
800	9.10(−30)	4.11(−05)	8.22(−35)	4.45(−02)	2.12(−02)	6.43(−06)	6.57(−02)
900	5.81(−26)	4.45(−05)	6.10(−31)	4.81(−02)	2.43(−02)	2.51(−05)	7.24(−02)
1,000	6.54(−23)	4.76(−05)	7.87(−28)	5.15(−02)	2.74(−02)	7.34(−05)	7.90(−02)
1,500	1.05(−13)	6.17(−05)	2.11(−18)	6.68(−02)	4.18(−02)	1.62(−03)	1.10(−01)
2,000	4.55(−09)	7.41(−05)	1.25(−13)	8.02(−02)	5.46(−02)	6.75(−03)	1.42(−01)
2,500	2.90(−06)	8.56(−05)	9.36(−11)	9.27(−02)	6.64(−02)	1.54(−02)	1.74(−01)
3,000	2.19(−04)	9.65(−05)	7.77(−09)	1.05(−01)	7.74(−02)	2.93(−02)	2.11(−01)
3,500	4.82(−03)	1.07(−04)	1.87(−07)	1.16(−01)	8.76(−02)	5.35(−02)	2.57(−01)
4,000	4.86(−02)	1.17(−04)	2.11(−06)	1.28(−01)	9.68(−02)	9.15(−02)	3.17(−01)
4,500	2.94(−01)	1.27(−04)	1.46(−05)	1.41(−01)	1.05(−01)	1.39(−01)	3.85(−01)
5,000	1.22(+00)	1.37(−04)	6.97(−05)	1.55(−01)	1.12(−01)	1.85(−01)	4.53(−01)
6,000	1.02(+01)	1.57(−04)	7.94(−04)	1.87(−01)	1.24(−01)	2.46(−01)	5.58(−01)
7,000	4.14(+01)	1.77(−04)	4.30(−03)	2.22(−01)	1.38(−01)	3.45(−01)	7.09(−01)
8,000	1.07(+02)	1.97(−04)	1.37(−02)	2.60(−01)	1.57(−01)	6.21(−01)	1.05(+00)
9,000	2.35(+02)	2.16(−04)	3.36(−02)	3.06(−01)	1.85(−01)	1.10(+00)	1.62(+00)

(continued)

Table 11.17 (continued)

T (K)	σ_e (S/m)	η (Kg/m.s)	λ_e (W/m.K)	λ_h (W/m.K)	λ_{int} (W/m.K)	λ_r (W/m.K)	λ_{tot} (W/m.K)
10,000	4.64(+02)	2.35(−04)	6.99(−02)	3.63(−01)	2.19(−01)	1.65(+00)	2.30(+00)
11,000	8.79(+02)	2.54(−04)	1.37(−01)	4.30(−01)	2.50(−01)	1.98(+00)	2.80(+00)
12,000	1.59(+03)	2.72(−04)	2.58(−01)	5.01(−01)	2.69(−01)	1.88(+00)	2.91(+00)
13,000	2.66(+03)	2.88(−04)	4.55(−01)	5.66(−01)	2.75(−01)	1.46(+00)	2.75(+00)
14,000	4.08(+03)	3.03(−04)	7.43(−01)	6.20(−01)	2.74(−01)	1.03(+00)	2.67(+00)
15,000	5.78(+03)	3.17(−04)	1.13(+00)	6.61(−01)	2.55(−01)	7.55(−01)	2.81(+00)
16,000	7.74(+03)	3.28(−04)	1.63(+00)	6.92(−01)	2.42(−01)	6.29(−01)	3.20(+00)
17,000	9.90(+03)	3.36(−04)	2.24(+00)	7.12(−01)	2.33(−01)	6.04(−01)	3.79(+00)
18,000	1.22(+04)	3.40(−04)	2.96(+00)	7.21(−01)	2.19(−01)	6.39(−01)	4.54(+00)
19,000	1.46(+04)	3.39(−04)	3.79(+00)	7.19(−01)	1.99(−01)	7.07(−01)	5.41(+00)
20,000	1.71(+04)	3.34(−04)	4.70(+00)	7.05(−01)	1.88(−01)	7.89(−01)	6.38(+00)
22,000	2.16(+04)	3.19(−04)	6.56(+00)	6.66(−01)	1.48(−01)	9.35(−01)	8.31(+00)
24,000	2.69(+04)	2.84(−04)	9.00(+00)	5.83(−01)	1.02(−01)	1.05(+00)	1.07(+01)
26,000	3.08(+04)	2.60(−04)	1.12(+01)	5.30(−01)	9.41(−02)	1.12(+00)	1.29(+01)
28,000	3.50(+04)	2.33(−04)	1.36(+01)	4.72(−01)	8.53(−02)	1.05(+00)	1.52(+01)
30,000	3.86(+04)	2.11(−04)	1.60(+01)	4.28(−01)	8.31(−02)	9.46(−01)	1.75(+01)
35,000	4.60(+04)	1.81(−04)	2.20(+01)	3.68(−01)	1.11(−01)	7.42(−01)	2.32(+01)
40,000	5.03(+04)	1.66(−04)	2.77(+01)	3.39(−01)	1.64(−01)	8.67(−01)	2.91(+01)
45,000	5.24(+04)	1.43(−04)	3.33(+01)	2.89(−01)	1.97(−01)	1.31(+00)	3.51(+01)
50,000	5.35(+04)	1.17(−04)	3.90(+01)	2.36(−01)	2.00(−01)	1.68(+00)	4.11(+01)

Table 11.18 Thermodynamic properties for Earth atmosphere at $p = 1,000$ bar

T (K)	ρ (kg/m^3)	h (kJ/kg)	c_p (J/kg.K)
100	3.465(+03)	1.008(+02)	1.009(+03)
200	1.733(+03)	2.018(+02)	1.011(+03)
300	1.155(+03)	3.029(+02)	1.015(+03)
400	8.663(+02)	4.045(+02)	1.027(+03)
500	6.930(+02)	5.074(+02)	1.045(+03)
600	5.775(+02)	6.122(+02)	1.068(+03)
700	4.950(+02)	7.193(+02)	1.093(+03)
800	4.331(+02)	8.288(+02)	1.117(+03)
900	3.850(+02)	9.406(+02)	1.140(+03)
1,000	3.465(+02)	1.055(+03)	1.159(+03)
1,500	2.310(+02)	1.651(+03)	1.270(+03)
2,000	1.733(+02)	2.296(+03)	1.346(+03)
2,500	1.386(+02)	2.982(+03)	1.437(+03)
3,000	1.155(+02)	3.712(+03)	1.537(+03)
3,500	9.874(+01)	4.492(+03)	1.670(+03)
4,000	8.590(+01)	5.337(+03)	1.834(+03)
4,500	7.556(+01)	6.261(+03)	2.005(+03)
5,000	6.696(+01)	7.267(+03)	2.140(+03)
6,000	5.358(+01)	9.451(+03)	2.309(+03)
7,000	4.399(+01)	1.181(+04)	2.698(+03)
8,000	3.674(+01)	1.462(+04)	3.676(+03)
9,000	3.071(+01)	1.843(+04)	5.213(+03)
10,000	2.545(+01)	2.372(+04)	6.802(+03)
11,000	2.096(+01)	3.052(+04)	7.529(+03)
12,000	1.745(+01)	3.806(+04)	6.993(+03)
13,000	1.491(+01)	4.516(+04)	5.921(+03)
14,000	1.312(+01)	5.122(+04)	5.110(+03)
15,000	1.181(+01)	5.641(+04)	4.924(+03)
16,000	1.078(+01)	6.131(+04)	5.125(+03)
17,000	9.911(+00)	6.636(+04)	5.549(+03)
18,000	9.148(+00)	7.170(+04)	6.172(+03)
19,000	8.488(+00)	7.724(+04)	6.666(+03)
20,000	7.843(+00)	8.355(+04)	7.049(+03)
22,000	6.695(+00)	9.793(+04)	7.824(+03)
24,000	5.749(+00)	1.136(+05)	8.668(+03)
26,000	4.959(+00)	1.311(+05)	8.746(+03)
28,000	4.322(+00)	1.486(+05)	8.547(+03)
30,000	3.809(+00)	1.660(+05)	8.011(+03)
35,000	2.938(+00)	2.056(+05)	7.849(+03)
40,000	2.385(+00)	2.456(+05)	9.600(+03)
45,000	1.962(+00)	2.977(+05)	1.232(+04)
50,000	1.630(+00)	3.607(+05)	1.472(+04)

refer to the dissociation of CO_2, followed by the convolution of the dissociation processes of N_2 and CO, and then appear the first ionization of the C, N, O components occurring in the same temperature range followed by the second, third and fourth ionization processes of the same components. A fair amount of confidence of the transport coefficients can be expected as can be deduced by the different comparisons made in Catalfamo et al. (2009); André et al. (2010). Note also that despite the initial small concentration of N_2 in the mixture this species can not be neglected in accurate calculations of the Mars atmosphere (Catalfamo et al. 2009). Tables 11.19–11.22 report numerical values of transport coefficients for different pressures, while Table 11.23 reports the Mars thermodynamics at $p = 1,000$ bar.

11.3.3 Jupiter

The thermodynamic model considered for Jupiter (x_{H_2}:x_{He}=89:11) contains He, He^+, He^{++}, H, H^+, H^-, H_2, H_2^+ , H_3^+ and electrons, all of them being considered in the calculations (Capitelli et al. 2011; Pagano et al. 2008). The transport cross section database in Bruno et al. (2010) has been validated against existing values in literature. Figure 11.2 reports the total thermal conductivity of the Jupiter atmosphere at different pressures. The different peaks refer, in the order, to the dissociation of hydrogen, to the ionization of atomic hydrogen followed by the first and second ionization reactions of

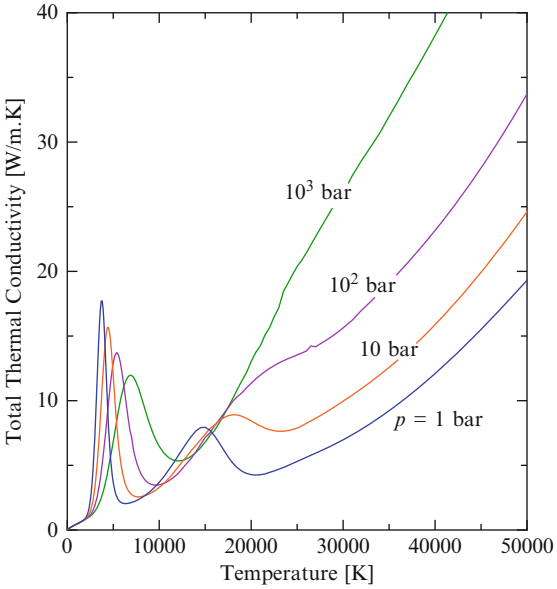

Fig. 11.2 Total thermal conductivity of Jupiter plasma as a function of temperature, at different pressures

Table 11.19 Transport coefficients for Mars atmosphere at $p = 1$ bar

T (K)	σ_e (S/m)	η (Kg/m.s)	λ_e (W/m.K)	λ_h (W/m.K)	λ_{int} (W/m.K)	λ_r (W/m.K)	λ_{tot} (W/m.K)
100	0.00(+00)	5.91(−06)	0.00(+00)	4.26(−03)	1.48(−03)	0.00(+00)	5.73(−03)
200	0.00(+00)	1.11(−05)	0.00(+00)	7.96(−03)	3.83(−03)	0.00(+00)	1.18(−02)
300	0.00(+00)	1.62(−05)	0.00(+00)	1.17(−02)	7.94(−03)	0.00(+00)	1.96(−02)
400	0.00(+00)	2.13(−05)	0.00(+00)	1.53(−02)	1.29(−02)	0.00(+00)	2.83(−02)
500	0.00(+00)	2.62(−05)	0.00(+00)	1.88(−02)	1.84(−02)	5.46(−11)	3.72(−02)
600	4.36(−39)	3.08(−05)	6.59(−44)	2.21(−02)	2.39(−02)	2.19(−09)	4.61(−02)
700	1.33(−32)	3.51(−05)	2.36(−37)	2.52(−02)	2.95(−02)	2.30(−08)	5.47(−02)
800	8.38(−28)	3.91(−05)	1.68(−32)	2.81(−02)	3.50(−02)	1.35(−07)	6.31(−02)
900	4.21(−24)	4.28(−05)	9.31(−29)	3.08(−02)	4.02(−02)	5.27(−07)	7.10(−02)
1,000	3.79(−21)	4.63(−05)	9.06(−26)	3.33(−02)	4.53(−02)	1.56(−06)	7.86(−02)
1,500	3.03(−12)	6.14(−05)	9.30(−17)	4.41(−02)	6.75(−02)	7.73(−04)	1.12(−01)
2,000	1.21(−07)	7.40(−05)	4.22(−12)	5.36(−02)	8.53(−02)	6.44(−02)	2.03(−01)
2,500	8.85(−05)	8.53(−05)	3.18(−09)	6.58(−02)	9.62(−02)	4.00(−01)	5.62(−01)
3,000	5.87(−03)	9.61(−05)	2.11(−07)	8.81(−02)	9.40(−02)	9.24(−01)	1.11(+00)
3,500	1.06(−01)	1.07(−04)	3.84(−06)	1.22(−01)	8.22(−02)	1.15(+00)	1.36(+00)
4,000	7.98(−01)	1.20(−04)	3.46(−05)	1.61(−01)	7.06(−02)	7.35(−01)	9.66(−01)
4,500	3.27(+00)	1.31(−04)	1.78(−04)	1.88(−01)	6.87(−02)	2.35(−01)	4.92(−01)
5,000	9.29(+00)	1.42(−04)	6.27(−04)	2.07(−01)	7.32(−02)	1.08(−01)	3.89(−01)
6,000	4.81(+01)	1.62(−04)	4.78(−03)	2.41(−01)	8.56(−02)	5.45(−01)	8.76(−01)
7,000	3.73(+02)	1.81(−04)	3.93(−02)	3.05(−01)	8.20(−02)	3.40(+00)	3.83(+00)
8,000	1.34(+03)	1.99(−04)	1.32(−01)	3.93(−01)	6.07(−02)	1.96(+00)	2.54(+00)
9,000	2.42(+03)	2.12(−04)	2.66(−01)	4.34(−01)	6.41(−02)	6.95(−01)	1.46(+00)

(continued)

Table 11.19 (continued)

T (K)	σ_e (S/m)	η (Kg/m.s)	λ_e (W/m.K)	λ_h (W/m.K)	λ_{int} (W/m.K)	λ_r (W/m.K)	λ_{tot} (W/m.K)
10,000	3.50(+03)	2.18(−04)	4.31(−01)	4.38(−01)	8.81(−02)	7.19(−01)	1.68(+00)
11,000	4.55(+03)	2.12(−04)	6.20(−01)	4.08(−01)	1.20(−01)	1.01(+00)	2.16(+00)
12,000	5.54(+03)	1.90(−04)	8.26(−01)	3.46(−01)	1.68(−01)	1.28(+00)	2.62(+00)
13,000	6.48(+03)	1.54(−04)	1.05(+00)	2.64(−01)	2.17(−01)	1.44(+00)	2.97(+00)
14,000	7.35(+03)	1.12(−04)	1.28(+00)	1.84(−01)	2.46(−01)	1.47(+00)	3.18(+00)
15,000	8.15(+03)	7.65(−05)	1.52(+00)	1.23(−01)	2.42(−01)	1.35(+00)	3.24(+00)
16,000	8.89(+03)	5.17(−05)	1.77(+00)	8.35(−02)	2.11(−01)	1.09(+00)	3.15(+00)
17,000	9.58(+03)	3.68(−05)	2.02(+00)	6.10(−02)	1.70(−01)	7.69(−01)	3.02(+00)
18,000	1.02(+04)	2.85(−05)	2.27(+00)	4.90(−02)	1.29(−01)	4.97(−01)	2.95(+00)
19,000	1.08(+04)	2.41(−05)	2.54(+00)	4.30(−02)	9.55(−02)	3.09(−01)	2.99(+00)
20,000	1.14(+04)	2.20(−05)	2.81(+00)	4.05(−02)	7.12(−02)	1.95(−01)	3.12(+00)
22,000	1.24(+04)	2.04(−05)	3.39(+00)	3.91(−02)	4.10(−02)	1.06(−01)	3.57(+00)
24,000	1.31(+04)	1.96(−05)	3.98(+00)	3.79(−02)	2.87(−02)	1.17(−01)	4.17(+00)
26,000	1.34(+04)	1.78(−05)	4.58(+00)	3.39(−02)	2.40(−02)	1.89(−01)	4.83(+00)
28,000	1.36(+04)	1.52(−05)	5.19(+00)	2.84(−02)	2.21(−02)	2.71(−01)	5.51(+00)
30,000	1.37(+04)	1.23(−05)	5.82(+00)	2.28(−02)	2.05(−02)	3.38(−01)	6.21(+00)
35,000	1.46(+04)	6.91(−06)	7.65(+00)	1.35(−02)	1.57(−02)	2.84(−01)	7.96(+00)
40,000	1.60(+04)	5.40(−06)	9.82(+00)	1.09(−02)	1.18(−02)	1.35(−01)	9.98(+00)
45,000	1.69(+04)	4.64(−06)	1.21(+01)	9.30(−03)	9.26(−03)	1.39(−01)	1.23(+01)
50,000	1.76(+04)	3.74(−06)	1.45(+01)	7.54(−03)	7.73(−03)	1.61(−01)	1.47(+01)

Table 11.20 Transport coefficients for Mars atmosphere at $p = 10\,\text{bar}$

T (K)	σ_e (S/m)	η (Kg/m.s)	λ_e (W/m.K)	λ_h (W/m.K)	λ_{int} (W/m.K)	λ_r (W/m.K)	λ_{tot} (W/m.K)
100	0.00(+00)	5.91(−06)	0.00(+00)	4.26(−03)	1.48(−03)	0.00(+00)	5.73(−03)
200	0.00(+00)	1.11(−05)	0.00(+00)	7.96(−03)	3.83(−03)	0.00(+00)	1.18(−02)
300	0.00(+00)	1.62(−05)	0.00(+00)	1.17(−02)	7.94(−03)	0.00(+00)	1.96(−02)
400	0.00(+00)	2.13(−05)	0.00(+00)	1.53(−02)	1.29(−02)	0.00(+00)	2.83(−02)
500	0.00(+00)	2.62(−05)	0.00(+00)	1.88(−02)	1.84(−02)	1.73(−10)	3.72(−02)
600	4.67(−40)	3.08(−05)	7.01(−45)	2.21(−02)	2.39(−02)	2.54(−09)	4.61(−02)
700	1.72(−33)	3.51(−05)	3.05(−38)	2.52(−02)	2.95(−02)	2.37(−08)	5.47(−02)
800	1.44(−28)	3.91(−05)	2.89(−33)	2.81(−02)	3.50(−02)	1.36(−07)	6.31(−02)
900	9.25(−25)	4.28(−05)	2.04(−29)	3.08(−02)	4.02(−02)	5.28(−07)	7.10(−02)
1,000	9.75(−22)	4.63(−05)	2.33(−26)	3.33(−02)	4.53(−02)	1.55(−06)	7.86(−02)
1,500	9.30(−13)	6.14(−05)	2.86(−17)	4.41(−02)	6.75(−02)	2.69(−04)	1.12(−01)
2,000	3.35(−08)	7.40(−05)	1.19(−12)	5.33(−02)	8.57(−02)	2.84(−02)	1.67(−01)
2,500	2.45(−05)	8.53(−05)	9.28(−10)	6.34(−02)	9.92(−02)	1.98(−01)	3.61(−01)
3,000	1.72(−03)	9.59(−05)	6.89(−08)	7.87(−02)	1.05(−01)	5.48(−01)	7.31(−01)
3,500	3.21(−02)	1.06(−04)	1.30(−06)	1.02(−01)	1.01(−01)	8.46(−01)	1.05(+00)
4,000	2.71(−01)	1.18(−04)	1.23(−05)	1.34(−01)	9.25(−02)	9.49(−01)	1.17(+00)
4,500	1.35(+00)	1.29(−04)	7.39(−05)	1.68(−01)	8.40(−02)	7.45(−01)	9.96(−01)
5,000	4.54(+00)	1.41(−04)	3.04(−04)	1.96(−01)	8.07(−02)	3.80(−01)	6.57(−01)
6,000	2.42(+01)	1.62(−04)	2.36(−03)	2.36(−01)	8.86(−02)	1.69(−01)	4.96(−01)
7,000	9.84(+01)	1.81(−04)	1.29(−02)	2.74(−01)	1.01(−01)	9.26(−01)	1.31(+00)
8,000	4.96(+02)	2.00(−04)	6.11(−02)	3.40(−01)	9.78(−02)	3.01(+00)	3.51(+00)
9,000	1.49(+03)	2.18(−04)	1.73(−01)	4.23(−01)	8.05(−02)	2.11(+00)	2.79(+00)

(continued)

Table 11.20 (continued)

T (K)	σ_e (S/m)	η (Kg/m.s)	λ_e (W/m.K)	λ_h (W/m.K)	λ_{int} (W/m.K)	λ_r (W/m.K)	λ_{tot} (W/m.K)
10,000	2.74(+03)	2.33(−04)	3.44(−01)	4.75(−01)	8.20(−02)	8.66(−01)	1.77(+00)
11,000	4.09(+03)	2.44(−04)	5.69(−01)	5.00(−01)	1.01(−01)	6.08(−01)	1.78(+00)
12,000	5.50(+03)	2.49(−04)	8.40(−01)	5.02(−01)	1.21(−01)	7.07(−01)	2.17(+00)
13,000	6.93(+03)	2.44(−04)	1.15(+00)	4.78(−01)	1.41(−01)	9.07(−01)	2.68(+00)
14,000	8.33(+03)	2.27(−04)	1.50(+00)	4.30(−01)	1.47(−01)	1.11(+00)	3.19(+00)
15,000	9.68(+03)	2.00(−04)	1.87(+00)	3.65(−01)	1.50(−01)	1.28(+00)	3.66(+00)
16,000	1.10(+04)	1.66(−04)	2.26(+00)	2.94(−01)	1.53(−01)	1.39(+00)	4.09(+00)
17,000	1.22(+04)	1.32(−04)	2.66(+00)	2.28(−01)	1.47(−01)	1.41(+00)	4.45(+00)
18,000	1.33(+04)	1.02(−04)	3.07(+00)	1.76(−01)	1.32(−01)	1.34(+00)	4.73(+00)
19,000	1.43(+04)	7.95(−05)	3.49(+00)	1.38(−01)	1.18(−01)	1.18(+00)	4.93(+00)
20,000	1.53(+04)	6.37(−05)	3.91(+00)	1.12(−01)	1.05(−01)	9.64(−01)	5.09(+00)
22,000	1.70(+04)	4.67(−05)	4.75(+00)	8.63(−02)	7.98(−02)	5.55(−01)	5.47(+00)
24,000	1.85(+04)	4.03(−05)	5.62(+00)	7.75(−02)	6.18(−02)	3.09(−01)	6.06(+00)
26,000	1.97(+04)	3.87(−05)	6.51(+00)	7.57(−02)	5.59(−02)	2.11(−01)	6.86(+00)
28,000	2.06(+04)	3.79(−05)	7.43(+00)	7.42(−02)	5.53(−02)	2.22(−01)	7.78(+00)
30,000	2.11(+04)	3.54(−05)	8.36(+00)	6.88(−02)	5.84(−02)	3.05(−01)	8.80(+00)
35,000	2.17(+04)	2.53(−05)	1.08(+01)	4.82(−02)	7.73(−02)	5.69(−01)	1.15(+01)
40,000	2.27(+04)	1.69(−05)	1.35(+01)	3.28(−02)	7.51(−02)	5.15(−01)	1.42(+01)
45,000	2.43(+04)	1.32(−05)	1.67(+01)	2.63(−02)	5.43(−02)	3.11(−01)	1.71(+01)
50,000	2.56(+04)	1.14(−05)	2.01(+01)	2.28(−02)	3.85(−02)	2.70(−01)	2.04(+01)

Table 11.21 Transport coefficients for Mars atmosphere at $p = 100$ bar

T (K)	σ_e (S/m)	η (Kg/m.s)	λ_e (W/m.K)	λ_h (W/m.K)	λ_{int} (W/m.K)	λ_r (W/m.K)	λ_{tot} (W/m.K)
100	0.00(+00)	5.91(−06)	0.00(+00)	4.26(−03)	1.48(−03)	0.00(+00)	5.73(−03)
200	0.00(+00)	1.11(−05)	0.00(+00)	7.96(−03)	3.83(−03)	0.00(+00)	1.18(−02)
300	0.00(+00)	1.62(−05)	0.00(+00)	1.17(−02)	7.94(−03)	0.00(+00)	1.96(−02)
400	0.00(+00)	2.13(−05)	0.00(+00)	1.53(−02)	1.29(−02)	0.00(+00)	2.83(−02)
500	0.00(+00)	2.62(−05)	0.00(+00)	1.88(−02)	1.84(−02)	5.46(−10)	3.72(−02)
600	4.70(−41)	3.08(−05)	1.40(−45)	2.21(−02)	2.39(−02)	3.63(−09)	4.61(−02)
700	1.78(−34)	3.51(−05)	3.16(−39)	2.52(−02)	2.95(−02)	2.60(−08)	5.47(−02)
800	1.60(−29)	3.91(−05)	3.21(−34)	2.81(−02)	3.50(−02)	1.40(−07)	6.31(−02)
900	1.18(−25)	4.28(−05)	2.60(−30)	3.08(−02)	4.02(−02)	5.34(−07)	7.10(−02)
1,000	1.47(−22)	4.63(−05)	3.51(−27)	3.33(−02)	4.53(−02)	1.55(−06)	7.86(−02)
1,500	2.39(−13)	6.14(−05)	7.34(−18)	4.41(−02)	6.75(−02)	1.09(−04)	1.12(−01)
2,000	8.58(−09)	7.40(−05)	3.07(−13)	5.32(−02)	8.58(−02)	1.15(−02)	1.50(−01)
2,500	5.85(−06)	8.54(−05)	2.30(−10)	6.23(−02)	1.01(−01)	9.51(−02)	2.58(−01)
3,000	4.33(−04)	9.59(−05)	1.86(−08)	7.37(−02)	1.11(−01)	2.92(−01)	4.76(−01)
3,500	8.28(−03)	1.06(−04)	3.79(−07)	9.00(−02)	1.14(−01)	5.33(−01)	7.37(−01)
4,000	7.24(−02)	1.16(−04)	3.57(−06)	1.12(−01)	1.12(−01)	6.94(−01)	9.18(−01)
4,500	3.85(−01)	1.27(−04)	2.19(−05)	1.38(−01)	1.08(−01)	7.60(−01)	1.01(+00)
5,000	1.47(+00)	1.38(−04)	1.00(−04)	1.68(−01)	1.03(−01)	7.17(−01)	9.87(−01)
6,000	1.07(+01)	1.60(−04)	1.04(−03)	2.22(−01)	9.87(−02)	3.55(−01)	6.76(−01)
7,000	4.09(+01)	1.81(−04)	5.51(−03)	2.62(−01)	1.08(−01)	2.59(−01)	6.34(−01)
8,000	1.31(+02)	2.00(−04)	2.15(−02)	3.01(−01)	1.22(−01)	8.98(−01)	1.34(+00)
9,000	4.75(+02)	2.19(−04)	7.20(−02)	3.59(−01)	1.28(−01)	2.34(+00)	2.89(+00)

(continued)

Table 11.21 (continued)

T (K)	σ_e (S/m)	η (Kg/m.s)	λ_e (W/m.K)	λ_h (W/m.K)	λ_{int} (W/m.K)	λ_r (W/m.K)	λ_{tot} (W/m.K)
10,000	1.32(+03)	2.37(−04)	1.86(−01)	4.36(−01)	1.17(−01)	2.39(+00)	3.13(+00)
11,000	2.56(+03)	2.53(−04)	3.77(−01)	5.01(−01)	1.10(−01)	1.38(+00)	2.36(+00)
12,000	4.04(+03)	2.67(−04)	6.44(−01)	5.45(−01)	1.12(−01)	7.75(−01)	2.08(+00)
13,000	5.71(+03)	2.79(−04)	9.89(−01)	5.73(−01)	1.18(−01)	6.10(−01)	2.29(+00)
14,000	7.53(+03)	2.87(−04)	1.41(+00)	5.87(−01)	1.34(−01)	6.43(−01)	2.77(+00)
15,000	9.45(+03)	2.89(−04)	1.90(+00)	5.86(−01)	1.51(−01)	7.53(−01)	3.39(+00)
16,000	1.14(+04)	2.85(−04)	2.47(+00)	5.69(−01)	1.44(−01)	8.93(−01)	4.07(+00)
17,000	1.34(+04)	2.73(−04)	3.08(+00)	5.37(−01)	1.41(−01)	1.03(+00)	4.79(+00)
18,000	1.54(+04)	2.55(−04)	3.74(+00)	4.92(−01)	1.44(−01)	1.15(+00)	5.53(+00)
19,000	1.73(+04)	2.32(−04)	4.44(+00)	4.41(−01)	1.42(−01)	1.24(+00)	6.26(+00)
20,000	1.91(+04)	2.06(−04)	5.16(+00)	3.88(−01)	1.37(−01)	1.28(+00)	6.97(+00)
22,000	2.25(+04)	1.59(−04)	6.65(+00)	2.96(−01)	1.21(−01)	1.22(+00)	8.29(+00)
24,000	2.54(+04)	1.24(−04)	8.15(+00)	2.34(−01)	1.04(−01)	1.01(+00)	9.50(+00)
26,000	2.78(+04)	1.04(−04)	9.63(+00)	1.99(−01)	9.15(−02)	7.58(−01)	1.07(+01)
28,000	3.00(+04)	9.29(−05)	1.11(+01)	1.81(−01)	8.46(−02)	5.58(−01)	1.19(+01)
30,000	3.18(+04)	8.74(−05)	1.26(+01)	1.72(−01)	8.32(−02)	4.48(−01)	1.33(+01)
35,000	3.47(+04)	7.89(−05)	1.65(+01)	1.56(−01)	9.95(−02)	5.62(−01)	1.73(+01)
40,000	3.59(+04)	6.44(−05)	2.04(+01)	1.25(−01)	1.16(−01)	9.74(−01)	2.16(+01)
45,000	3.70(+04)	4.79(−05)	2.47(+01)	9.31(−02)	1.11(−01)	1.14(+00)	2.60(+01)
50,000	3.86(+04)	3.71(−05)	2.94(+01)	7.32(−02)	9.39(−02)	9.34(−01)	3.05(+01)

Table 11.22 Transport coefficients for Mars atmosphere at $p = 1,000$ bar

T (K)	σ_e (S/m)	η (Kg/m.s)	λ_e (W/m.K)	λ_h (W/m.K)	λ_{int} (W/m.K)	λ_r (W/m.K)	λ_{tot} (W/m.K)
100	0.00(+00)	5.91(−06)	0.00(+00)	4.26(−03)	1.48(−03)	0.00(+00)	5.73(−03)
200	0.00(+00)	1.11(−05)	0.00(+00)	7.96(−03)	3.83(−03)	0.00(+00)	1.18(−02)
300	0.00(+00)	1.62(−05)	0.00(+00)	1.17(−02)	7.94(−03)	0.00(+00)	1.96(−02)
400	0.00(+00)	2.13(−05)	0.00(+00)	1.53(−02)	1.29(−02)	0.00(+00)	2.83(−02)
500	0.00(+00)	2.62(−05)	0.00(+00)	1.88(−02)	1.84(−02)	1.73(−09)	3.72(−02)
600	4.69(−42)	3.08(−05)	0.00(+00)	2.21(−02)	2.39(−02)	7.09(−09)	4.61(−02)
700	1.78(−35)	3.51(−05)	3.16(−40)	2.52(−02)	2.95(−02)	3.32(−08)	5.47(−02)
800	1.62(−30)	3.91(−05)	3.25(−35)	2.81(−02)	3.50(−02)	1.52(−07)	6.31(−02)
900	1.21(−26)	4.28(−05)	2.68(−31)	3.08(−02)	4.02(−02)	5.53(−07)	7.10(−02)
1,000	1.57(−23)	4.63(−05)	3.76(−28)	3.33(−02)	4.53(−02)	1.58(−06)	7.86(−02)
1,500	3.61(−14)	6.14(−05)	1.11(−18)	4.41(−02)	6.75(−02)	5.79(−05)	1.12(−01)
2,000	1.44(−09)	7.40(−05)	5.17(−14)	5.32(−02)	8.58(−02)	4.20(−03)	1.43(−01)
2,500	9.20(−07)	8.54(−05)	3.69(−11)	6.17(−02)	1.01(−01)	4.44(−02)	2.08(−01)
3,000	7.31(−05)	9.59(−05)	3.24(−09)	7.11(−02)	1.14(−01)	1.46(−01)	3.31(−01)
3,500	1.52(−03)	1.06(−04)	7.54(−08)	8.30(−02)	1.22(−01)	2.98(−01)	5.03(−01)
4,000	1.42(−02)	1.16(−04)	7.70(−07)	9.84(−02)	1.26(−01)	4.42(−01)	6.67(−01)
4,500	8.03(−02)	1.26(−04)	4.88(−06)	1.17(−01)	1.27(−01)	5.34(−01)	7.79(−01)
5,000	3.14(−01)	1.36(−04)	2.21(−05)	1.39(−01)	1.27(−01)	5.79(−01)	8.45(−01)
6,000	2.87(+00)	1.57(−04)	2.81(−04)	1.87(−01)	1.25(−01)	5.64(−01)	8.76(−01)
7,000	1.31(+01)	1.78(−04)	1.77(−03)	2.36(−01)	1.26(−01)	4.11(−01)	7.74(−01)
8,000	4.60(+01)	1.98(−04)	8.16(−03)	2.79(−01)	1.36(−01)	3.45(−01)	7.67(−01)
9,000	1.15(+02)	2.17(−04)	2.26(−02)	3.19(−01)	1.56(−01)	6.63(−01)	1.16(+00)

(continued)

Table 11.22 (continued)

T (K)	σ_e (S/m)	η (Kg/m.s)	λ_e (W/m.K)	λ_h (W/m.K)	λ_{int} (W/m.K)	λ_r (W/m.K)	λ_{tot} (W/m.K)
10,000	3.57(+02)	2.36(−04)	6.63(−02)	3.67(−01)	1.76(−01)	1.48(+00)	2.09(+00)
11,000	8.87(+02)	2.54(−04)	1.56(−01)	4.29(−01)	1.83(−01)	2.10(+00)	2.86(+00)
12,000	1.87(+03)	2.71(−04)	3.32(−01)	4.96(−01)	1.73(−01)	1.93(+00)	2.93(+00)
13,000	3.20(+03)	2.86(−04)	6.02(−01)	5.55(−01)	1.60(−01)	1.39(+00)	2.70(+00)
14,000	4.85(+03)	3.01(−04)	9.79(−01)	6.01(−01)	1.45(−01)	9.61(−01)	2.69(+00)
15,000	6.77(+03)	3.13(−04)	1.47(+00)	6.36(−01)	1.43(−01)	7.51(−01)	3.00(+00)
16,000	8.95(+03)	3.24(−04)	2.07(+00)	6.63(−01)	1.46(−01)	6.88(−01)	3.57(+00)
17,000	1.14(+04)	3.33(−04)	2.80(+00)	6.82(−01)	1.44(−01)	7.07(−01)	4.33(+00)
18,000	1.39(+04)	3.39(−04)	3.64(+00)	6.93(−01)	1.48(−01)	7.66(−01)	5.24(+00)
19,000	1.66(+04)	3.42(−04)	4.59(+00)	6.97(−01)	1.49(−01)	8.43(−01)	6.28(+00)
20,000	1.94(+04)	3.41(−04)	5.66(+00)	6.92(−01)	1.18(−01)	9.36(−01)	7.40(+00)
22,000	2.51(+04)	3.31(−04)	8.03(+00)	6.65(−01)	1.09(−01)	1.08(+00)	9.88(+00)
24,000	3.06(+04)	3.11(−04)	1.06(+01)	6.20(−01)	1.01(−01)	1.16(+00)	1.25(+01)
26,000	3.58(+04)	2.87(−04)	1.34(+01)	5.69(−01)	9.78(−02)	1.16(+00)	1.53(+01)
28,000	4.05(+04)	2.64(−04)	1.63(+01)	5.23(−01)	9.73(−02)	1.10(+00)	1.80(+01)
30,000	4.47(+04)	2.45(−04)	1.91(+01)	4.86(−01)	1.03(−01)	1.01(+00)	2.07(+01)
35,000	5.30(+04)	2.17(−04)	2.62(+01)	4.32(−01)	1.34(−01)	8.54(−01)	2.76(+01)
40,000	5.84(+04)	2.04(−04)	3.31(+01)	4.06(−01)	1.85(−01)	1.07(+00)	3.48(+01)
45,000	6.17(+04)	1.83(−04)	4.03(+01)	3.60(−01)	2.28(−01)	1.65(+00)	4.26(+01)
50,000	6.39(+04)	1.55(−04)	4.77(+01)	3.03(−01)	2.45(−01)	2.20(+00)	5.05(+01)

Table 11.23 Thermodynamic properties for Mars atmosphere at $p = 1,000$ bar

T (K)	ρ (kg/m^3)	h (kJ/kg)	c_p (J/kg.K)
100	5.295(+03)	−8.554(+03)	6.954(+02)
200	2.648(+03)	−8.484(+03)	7.908(+02)
300	1.765(+03)	−8.405(+03)	8.886(+02)
400	1.324(+03)	−8.316(+03)	9.684(+02)
500	1.059(+03)	−8.219(+03)	1.034(+03)
600	8.826(+02)	−8.116(+03)	1.088(+03)
700	7.565(+02)	−8.007(+03)	1.133(+03)
800	6.619(+02)	−7.894(+03)	1.170(+03)
900	5.884(+02)	−7.777(+03)	1.202(+03)
1,000	5.295(+02)	−7.657(+03)	1.228(+03)
1,500	3.530(+02)	−7.024(+03)	1.308(+03)
2,000	2.647(+02)	−6.358(+03)	1.392(+03)
2,500	2.106(+02)	−5.609(+03)	1.722(+03)
3,000	1.716(+02)	−4.630(+03)	2.371(+03)
3,500	1.400(+02)	−3.280(+03)	3.195(+03)
4,000	1.136(+02)	−1.538(+03)	3.853(+03)
4,500	9.263(+01)	4.591(+02)	4.128(+03)
5,000	7.657(+01)	2.527(+03)	4.096(+03)
6,000	5.525(+01)	6.491(+03)	3.693(+03)
7,000	4.284(+01)	9.905(+03)	2.976(+03)
8,000	3.538(+01)	1.268(+04)	2.661(+03)
9,000	3.016(+01)	1.560(+04)	3.622(+03)
10,000	2.555(+01)	2.008(+04)	6.328(+03)
11,000	2.118(+01)	2.692(+04)	8.305(+03)
12,000	1.761(+01)	3.476(+04)	7.218(+03)
13,000	1.510(+01)	4.161(+04)	5.698(+03)
14,000	1.337(+01)	4.697(+04)	4.399(+03)
15,000	1.210(+01)	5.145(+04)	3.975(+03)
16,000	1.108(+01)	5.567(+04)	4.262(+03)
17,000	1.021(+01)	5.996(+04)	4.553(+03)
18,000	9.438(+00)	6.462(+04)	4.986(+03)
19,000	8.742(+00)	6.973(+04)	5.250(+03)
20,000	8.102(+00)	7.507(+04)	6.048(+03)
22,000	6.969(+00)	8.784(+04)	6.706(+03)
24,000	6.008(+00)	1.024(+05)	7.895(+03)
26,000	5.199(+00)	1.185(+05)	7.913(+03)
28,000	4.534(+00)	1.352(+05)	7.824(+03)
30,000	3.996(+00)	1.519(+05)	8.089(+03)
35,000	3.061(+00)	1.918(+05)	7.795(+03)
40,000	2.475(+00)	2.328(+05)	9.255(+03)
45,000	2.031(+00)	2.848(+05)	1.206(+04)
50,000	1.680(+00)	3.500(+05)	1.436(+04)

helium. Tables 11.24–11.27 report numerical values of transport coefficients for different pressures, while Table 11.28 reports the Jupiter thermodynamics at $p = 1,000$ bar.

As already anticipated, the translational thermal conductivity and the viscosity contain the contribution of both heavy particles and electrons.

Table 11.24 Transport coefficients for Jupiter atmosphere at $p = 1\,\text{bar}$

T (K)	σ_e (S/m)	η (Kg/m.s)	λ_{tr} (W/m.K)	λ_{int} (W/m.K)	λ_r (W/m.K)	λ_{tot} (W/m.K)
100	0.00(+00)	4.69(−06)	6.48(−02)	4.46(−03)		6.92(−02)
200	0.00(+00)	7.51(−06)	1.04(−01)	2.66(−02)		1.31(−01)
300	0.00(+00)	9.90(−06)	1.37(−01)	4.42(−02)		1.82(−01)
400	0.00(+00)	1.21(−05)	1.68(−01)	5.67(−02)		2.24(−01)
500	1.37(−81)	1.41(−05)	1.96(−01)	6.73(−02)		2.63(−01)
600	1.21(−81)	1.60(−05)	2.22(−01)	7.75(−02)		3.00(−01)
700	1.09(−81)	1.78(−05)	2.48(−01)	8.80(−02)		3.36(−01)
800	2.90(−31)	1.96(−05)	2.73(−01)	9.91(−02)		3.72(−01)
900	2.70(−27)	2.13(−05)	2.97(−01)	1.11(−01)		4.08(−01)
1,000	4.05(−24)	2.29(−05)	3.20(−01)	1.25(−01)	2.79(−07)	4.45(−01)
1,500	1.35(−14)	3.07(−05)	4.29(−01)	2.07(−01)	1.43(−03)	6.37(−01)
2,000	7.72(−10)	3.80(−05)	5.31(−01)	3.02(−01)	9.98(−02)	9.33(−01)
2,500	5.22(−07)	4.50(−05)	6.42(−01)	3.97(−01)	1.23(+00)	2.27(+00)
3,000	3.38(−05)	5.28(−05)	8.25(−01)	4.62(−01)	6.02(+00)	7.30(+00)
3,500	6.80(−04)	5.99(−05)	1.11(+00)	4.31(−01)	1.44(+01)	1.59(+01)
4,000	1.07(−02)	5.99(−05)	1.30(+00)	2.66(−01)	1.43(+01)	1.59(+01)
4,500	1.08(−01)	5.82(−05)	1.40(+00)	1.11(−01)	6.28(+00)	7.80(+00)
5,000	6.95(−01)	6.02(−05)	1.52(+00)	4.27(−02)	2.09(+00)	3.65(+00)
6,000	1.16(+01)	6.88(−05)	1.77(+00)	8.64(−03)	3.04(−01)	2.08(+00)
7,000	8.52(+01)	7.87(−05)	2.03(+00)	2.70(−03)	9.47(−02)	2.13(+00)
8,000	3.54(+02)	8.86(−05)	2.32(+00)	2.16(−03)	1.27(−01)	2.45(+00)
9,000	9.69(+02)	9.77(−05)	2.63(+00)	9.48(−03)	3.28(−01)	2.97(+00)

10,000	1.95(+03)	1.03(−04)	2.88(+00)	3.88(−02)	7.81(−01)	3.70(+00)
11,000	3.15(+03)	1.02(−04)	2.91(+00)	1.10(−01)	1.59(+00)	4.61(+00)
12,000	4.42(+03)	9.18(−05)	2.68(+00)	2.23(−01)	2.75(+00)	5.66(+00)
13,000	5.66(+03)	7.72(−05)	2.38(+00)	2.83(−01)	4.10(+00)	6.76(+00)
14,000	6.81(+03)	6.45(−05)	2.19(+00)	2.90(−01)	5.19(+00)	7.67(+00)
15,000	7.85(+03)	5.63(−05)	2.16(+00)	3.09(−01)	5.47(+00)	7.94(+00)
16,000	8.75(+03)	5.27(−05)	2.25(+00)	2.38(−01)	4.81(+00)	7.30(+00)
17,000	9.53(+03)	5.24(−05)	2.43(+00)	2.13(−01)	3.56(+00)	6.20(+00)
18,000	1.02(+04)	5.35(−05)	2.66(+00)	2.28(−01)	2.29(+00)	5.18(+00)
19,000	1.09(+04)	5.42(−05)	2.91(+00)	2.04(−01)	1.43(+00)	4.55(+00)
20,000	1.15(+04)	5.27(−05)	3.18(+00)	1.95(−01)	9.13(−01)	4.28(+00)
22,000	1.27(+04)	3.98(−05)	3.71(+00)	2.40(−01)	5.02(−01)	4.46(+00)
24,000	1.39(+04)	2.34(−05)	4.31(+00)	2.15(−01)	4.62(−01)	4.98(+00)
26,000	1.51(+04)	1.47(−05)	5.00(+00)	1.96(−01)	4.32(−01)	5.63(+00)
28,000	1.63(+04)	1.15(−05)	5.78(+00)	1.39(−01)	3.41(−01)	6.26(+00)
30,000	1.75(+04)	1.10(−05)	6.65(+00)	1.08(−01)	2.18(−01)	6.97(+00)
35,000	2.07(+04)	1.29(−05)	9.12(+00)	3.66(−02)	6.23(−02)	9.22(+00)
40,000	2.39(+04)	1.62(−05)	1.20(+01)	1.20(−02)	4.67(−02)	1.21(+01)
45,000	2.70(+04)	1.96(−05)	1.54(+01)	1.01(−02)	1.25(−01)	1.55(+01)
50,000	2.98(+04)	2.23(−05)	1.90(+01)	1.65(−02)	2.54(−01)	1.93(+01)

Table 11.25 Transport coefficients for Jupiter atmosphere at $p = 10\,\text{bar}$

T (K)	σ_e (S/m)	η (Kg/m.s)	λ_{tr} (W/m.K)	λ_{int} (W/m.K)	λ_r (W/m.K)	λ_{tot} (W/m.K)
100	0.00(+00)	4.69(−06)	6.48(−02)	4.46(−03)		6.92(−02)
200	0.00(+00)	7.51(−06)	1.04(−01)	2.66(−02)		1.31(−01)
300	0.00(+00)	9.90(−06)	1.37(−01)	4.42(−02)		1.82(−01)
400	0.00(+00)	1.21(−05)	1.68(−01)	5.67(−02)		2.24(−01)
500	4.35(−82)	1.41(−05)	1.96(−01)	6.73(−02)		2.63(−01)
600	3.84(−82)	1.60(−05)	2.22(−01)	7.75(−02)		3.00(−01)
700	3.45(−82)	1.78(−05)	2.48(−01)	8.80(−02)		3.36(−01)
800	1.63(−31)	1.96(−05)	2.73(−01)	9.91(−02)		3.72(−01)
900	1.52(−27)	2.13(−05)	2.97(−01)	1.11(−01)		4.08(−01)
1,000	2.28(−24)	2.29(−05)	3.20(−01)	1.25(−01)	8.83(−08)	4.45(−01)
1,500	7.60(−15)	3.07(−05)	4.29(−01)	2.07(−01)	4.54(−04)	6.36(−01)
2,000	4.35(−10)	3.80(−05)	5.31(−01)	3.02(−01)	3.16(−02)	8.64(−01)
2,500	3.04(−07)	4.49(−05)	6.31(−01)	4.01(−01)	3.93(−01)	1.42(+00)
3,000	2.23(−05)	5.20(−05)	7.57(−01)	4.92(−01)	2.03(+00)	3.28(+00)
3,500	4.29(−04)	5.99(−05)	9.56(−01)	5.52(−01)	6.05(+00)	7.56(+00)
4,000	4.23(−03)	6.74(−05)	1.22(+00)	5.41(−01)	1.16(+01)	1.33(+01)
4,500	3.47(−02)	7.06(−05)	1.44(+00)	4.30(−01)	1.37(+01)	1.56(+01)
5,000	2.19(−01)	6.98(−05)	1.57(+00)	2.70(−01)	1.01(+01)	1.19(+01)
6,000	3.72(+00)	7.19(−05)	1.79(+00)	7.83(−02)	2.57(+00)	4.44(+00)
7,000	2.87(+01)	7.98(−05)	2.03(+00)	2.54(−02)	6.75(−01)	2.73(+00)
8,000	1.31(+02)	8.94(−05)	2.31(+00)	1.07(−02)	2.59(−01)	2.58(+00)
9,000	4.16(+02)	9.94(−05)	2.61(+00)	8.80(−03)	1.99(−01)	2.82(+00)

10,000	1.00(+03)	1.09(−04)	2.96(+00)	2.02(−02)	3.01(−01)	3.28(+00)
11,000	1.96(+03)	1.17(−04)	3.33(+00)	7.08(−02)	5.57(−01)	3.96(+00)
12,000	3.26(+03)	1.22(−04)	3.65(+00)	1.69(−01)	9.90(−01)	4.81(+00)
13,000	4.82(+03)	1.21(−04)	3.83(+00)	2.54(−01)	1.62(+00)	5.70(+00)
14,000	6.50(+03)	1.14(−04)	3.84(+00)	3.03(−01)	2.40(+00)	6.55(+00)
15,000	8.22(+03)	1.02(−04)	3.78(+00)	3.97(−01)	3.24(+00)	7.41(+00)
16,000	9.89(+03)	9.03(−05)	3.75(+00)	3.46(−01)	4.01(+00)	8.10(+00)
17,000	1.15(+04)	8.06(−05)	3.81(+00)	3.66(−01)	4.50(+00)	8.67(+00)
18,000	1.29(+04)	7.42(−05)	3.99(+00)	3.62(−01)	4.57(+00)	8.91(+00)
19,000	1.41(+04)	7.08(−05)	4.25(+00)	3.41(−01)	4.21(+00)	8.80(+00)
20,000	1.53(+04)	6.94(−05)	4.56(+00)	3.11(−01)	3.55(+00)	8.43(+00)
22,000	1.72(+04)	6.88(−05)	5.32(+00)	2.74(−01)	2.17(+00)	7.76(+00)
24,000	1.88(+04)	6.30(−05)	6.14(+00)	2.71(−01)	1.28(+00)	7.69(+00)
26,000	2.03(+04)	4.96(−05)	7.01(+00)	3.57(−01)	8.87(−01)	8.25(+00)
28,000	2.19(+04)	3.54(−05)	7.96(+00)	3.16(−01)	7.75(−01)	9.05(+00)
30,000	2.34(+04)	2.64(−05)	9.01(+00)	2.54(−01)	6.94(−01)	9.96(+00)
35,000	2.71(+04)	2.08(−05)	1.21(+01)	1.52(−01)	3.59(−01)	1.26(+01)
40,000	3.09(+04)	2.29(−05)	1.57(+01)	6.37(−02)	1.48(−01)	1.59(+01)
45,000	3.48(+04)	2.76(−05)	1.98(+01)	2.99(−02)	9.44(−02)	1.99(+01)
50,000	3.86(+04)	3.24(−05)	2.45(+01)	2.01(−02)	1.40(−01)	2.46(+01)

Table 11.26 Transport coefficients for Jupiter atmosphere at $p = 100$ bar

T (K)	σ_e (S/m)	η (Kg/m.s)	λ_{tr} (W/m.K)	λ_{int} (W/m.K)	λ_r (W/m.K)	λ_{tot} (W/m.K)
100	0.00(+00)	4.69(−06)	6.48(−02)	4.46(−03)		6.92(−02)
200	0.00(+00)	7.51(−06)	1.04(−01)	2.66(−02)		1.31(−01)
300	0.00(+00)	9.90(−06)	1.37(−01)	4.42(−02)		1.82(−01)
400	0.00(+00)	1.21(−05)	1.68(−01)	5.67(−02)		2.24(−01)
500	1.37(−82)	1.41(−05)	1.96(−01)	6.73(−02)		2.63(−01)
600	1.21(−82)	1.60(−05)	2.22(−01)	7.75(−02)		3.00(−01)
700	1.09(−82)	1.78(−05)	2.48(−01)	8.80(−02)		3.36(−01)
800	9.17(−32)	1.96(−05)	2.73(−01)	9.91(−02)		3.72(−01)
900	8.55(−28)	2.13(−05)	2.97(−01)	1.11(−01)		4.08(−01)
1,000	1.28(−24)	2.29(−05)	3.20(−01)	1.25(−01)	2.79(−08)	4.45(−01)
1,500	4.27(−15)	3.07(−05)	4.29(−01)	2.07(−01)	1.43(−04)	6.36(−01)
2,000	2.44(−10)	3.80(−05)	5.30(−01)	3.02(−01)	9.99(−03)	8.43(−01)
2,500	1.72(−07)	4.48(−05)	6.28(−01)	4.02(−01)	1.25(−01)	1.15(+00)
3,000	1.32(−05)	5.16(−05)	7.32(−01)	5.01(−01)	6.54(−01)	1.89(+00)
3,500	2.78(−04)	5.87(−05)	8.63(−01)	5.94(−01)	2.07(+00)	3.52(+00)
4,000	2.59(−03)	6.65(−05)	1.05(+00)	6.64(−01)	4.64(+00)	6.36(+00)
4,500	1.53(−02)	7.46(−05)	1.29(+00)	6.89(−01)	7.98(+00)	9.95(+00)
5,000	7.55(−02)	8.12(−05)	1.53(+00)	6.51(−01)	1.07(+01)	1.29(+01)
6,000	1.17(+00)	8.58(−05)	1.87(+00)	4.19(−01)	9.66(+00)	1.19(+01)
7,000	9.06(+00)	8.82(−05)	2.09(+00)	2.12(−01)	4.87(+00)	7.17(+00)
8,000	4.41(+01)	9.35(−05)	2.33(+00)	9.18(−02)	1.95(+00)	4.37(+00)
9,000	1.51(+02)	1.02(−04)	2.60(+00)	4.75(−02)	9.21(−01)	3.57(+00)

10,000	4.00(+02)	1.12(−04)	2.92(+00)	3.43(−02)	5.45(−01)	3.50(+00)
11,000	8.83(+02)	1.22(−04)	3.29(+00)	4.59(−02)	4.46(−01)	3.79(+00)
12,000	1.68(+03)	1.32(−04)	3.74(+00)	8.90(−02)	5.07(−01)	4.34(+00)
13,000	2.85(+03)	1.40(−04)	4.25(+00)	2.25(−01)	6.86(−01)	5.16(+00)
14,000	4.41(+03)	1.47(−04)	4.79(+00)	2.97(−01)	9.77(−01)	6.06(+00)
15,000	6.26(+03)	1.50(−04)	5.30(+00)	4.51(−01)	1.40(+00)	7.16(+00)
16,000	8.40(+03)	1.49(−04)	5.76(+00)	4.31(−01)	1.85(+00)	8.05(+00)
17,000	1.07(+04)	1.44(−04)	6.15(+00)	5.19(−01)	2.32(+00)	8.99(+00)
18,000	1.31(+04)	1.36(−04)	6.51(+00)	5.84(−01)	2.85(+00)	9.94(+00)
19,000	1.55(+04)	1.27(−04)	6.87(+00)	4.09(−01)	3.32(+00)	1.06(+01)
20,000	1.79(+04)	1.18(−04)	7.28(+00)	4.12(−01)	3.65(+00)	1.14(+01)
22,000	2.22(+04)	1.06(−04)	8.27(+00)	3.87(−01)	3.84(+00)	1.25(+01)
24,000	2.57(+04)	9.90(−05)	9.45(+00)	3.52(−01)	3.44(+00)	1.32(+01)
26,000	2.87(+04)	9.48(−05)	1.08(+01)	3.34(−01)	2.75(+00)	1.38(+01)
28,000	3.12(+04)	8.81(−05)	1.21(+01)	3.38(−01)	2.13(+00)	1.46(+01)
30,000	3.34(+04)	7.71(−05)	1.36(+01)	3.36(−01)	1.72(+00)	1.56(+01)
35,000	3.83(+04)	5.11(−05)	1.75(+01)	3.76(−01)	1.20(+00)	1.91(+01)
40,000	4.30(+04)	4.21(−05)	2.22(+01)	2.16(−01)	7.73(−01)	2.32(+01)
45,000	4.77(+04)	4.33(−05)	2.75(+01)	1.18(−01)	4.22(−01)	2.80(+01)
50,000	5.23(+04)	4.99(−05)	3.34(+01)	7.85(−02)	2.51(−01)	3.37(+01)

Table 11.27 Transport coefficients for Jupiter atmosphere at $p = 1,000$ bar

T (K)	σ_e (S/m)	η (Kg/m.s)	λ_{tr} (W/m.K)	λ_{int} (W/m.K)	λ_r (W/m.K)	λ_{tot} (W/m.K)
100	0.00(+00)	4.69(−06)	6.48(−02)	4.46(−03)		6.92(−02)
200	0.00(+00)	7.51(−06)	1.04(−01)	2.66(−02)		1.31(−01)
300	0.00(+00)	9.90(−06)	1.37(−01)	4.42(−02)		1.82(−01)
400	0.00(+00)	1.21(−05)	1.68(−01)	5.67(−02)		2.24(−01)
500	4.35(−83)	1.41(−05)	1.96(−01)	6.73(−02)		2.63(−01)
600	3.84(−83)	1.60(−05)	2.22(−01)	7.75(−02)		3.00(−01)
700	3.45(−83)	1.78(−05)	2.48(−01)	8.80(−02)		3.36(−01)
800	5.16(−32)	1.96(−05)	2.73(−01)	9.91(−02)		3.72(−01)
900	4.81(−28)	2.13(−05)	2.97(−01)	1.11(−01)		4.08(−01)
1,000	7.20(−25)	2.29(−05)	3.20(−01)	1.25(−01)	8.83(−09)	4.45(−01)
1,500	2.40(−15)	3.07(−05)	4.29(−01)	2.07(−01)	4.54(−05)	6.36(−01)
2,000	1.37(−10)	3.80(−05)	5.30(−01)	3.02(−01)	3.16(−03)	8.36(−01)
2,500	9.54(−08)	4.48(−05)	6.27(−01)	4.02(−01)	3.94(−02)	1.07(+00)
3,000	7.31(−06)	5.15(−05)	7.23(−01)	5.04(−01)	2.08(−01)	1.43(+00)
3,500	1.58(−04)	5.81(−05)	8.27(−01)	6.07(−01)	6.69(−01)	2.10(+00)
4,000	1.53(−03)	6.51(−05)	9.53(−01)	7.05(−01)	1.57(+00)	3.22(+00)
4,500	8.85(−03)	7.26(−05)	1.11(+00)	7.88(−01)	2.95(+00)	4.85(+00)
5,000	3.65(−02)	8.05(−05)	1.31(+00)	8.44(−01)	4.69(+00)	6.84(+00)
6,000	3.95(−01)	9.59(−05)	1.77(+00)	8.42(−01)	8.06(+00)	1.07(+01)
7,000	2.84(+00)	1.06(−04)	2.16(+00)	6.94(−01)	9.09(+00)	1.19(+01)
8,000	1.39(+01)	1.12(−04)	2.45(+00)	4.87(−01)	7.46(+00)	1.04(+01)
9,000	5.01(+01)	1.16(−04)	2.70(+00)	3.13(−01)	5.11(+00)	8.12(+00)

10,000	1.41(+02)	1.22(−04)	2.97(+00)	2.01(−01)	3.31(+00)	6.47(+00)
11,000	3.33(+02)	1.30(−04)	3.27(+00)	1.44(−01)	2.20(+00)	5.61(+00)
12,000	6.83(+02)	1.39(−04)	3.64(+00)	1.33(−01)	1.57(+00)	5.35(+00)
13,000	1.26(+03)	1.49(−04)	4.10(+00)	1.63(−01)	1.25(+00)	5.51(+00)
14,000	2.10(+03)	1.59(−04)	4.65(+00)	2.37(−01)	1.11(+00)	5.99(+00)
15,000	3.35(+03)	1.69(−04)	5.33(+00)	3.48(−01)	1.11(+00)	6.79(+00)
16,000	5.02(+03)	1.77(−04)	6.14(+00)	3.28(−01)	1.22(+00)	7.68(+00)
17,000	7.05(+03)	1.84(−04)	7.04(+00)	4.13(−01)	1.39(+00)	8.85(+00)
18,000	9.51(+03)	1.89(−04)	8.05(+00)	4.90(−01)	1.63(+00)	1.02(+01)
19,000	1.24(+04)	1.91(−04)	9.13(+00)	5.49(−01)	1.88(+00)	1.16(+01)
20,000	1.55(+04)	1.92(−04)	1.02(+01)	5.95(−01)	2.20(+00)	1.30(+01)
22,000	2.12(+04)	1.88(−04)	1.23(+01)	6.43(−01)	2.66(+00)	1.56(+01)
24,000	2.83(+04)	1.81(−04)	1.48(+01)	7.10(−01)	3.55(+00)	1.91(+01)
26,000	3.52(+04)	1.70(−04)	1.73(+01)	3.39(−01)	3.79(+00)	2.14(+01)
28,000	4.14(+04)	1.61(−04)	1.98(+01)	3.17(−01)	3.76(+00)	2.39(+01)
30,000	4.68(+04)	1.54(−04)	2.23(+01)	2.99(−01)	3.39(+00)	2.60(+01)
35,000	5.71(+04)	1.35(−04)	2.88(+01)	5.72(−01)	2.62(+00)	3.20(+01)
40,000	6.48(+04)	1.12(−04)	3.55(+01)	4.82(−01)	2.23(+00)	3.82(+01)
45,000	7.15(+04)	9.74(−05)	4.29(+01)	3.35(−01)	1.71(+00)	4.49(+01)
50,000	7.76(+04)	9.42(−05)	5.09(+01)	2.18(−01)	1.20(+00)	5.23(+01)

Table 11.28 Thermodynamic properties for Jupiter atmosphere at $p = 1,000$ bar

T (K)	ρ (kg/m^3)	h (kJ/kg)	c_p (J/kg.K)
100	2.670(+02)	1.376(+03)	1.230(+04)
200	1.335(+02)	2.490(+03)	1.237(+04)
300	8.901(+01)	3.724(+03)	1.263(+04)
400	6.676(+01)	4.992(+03)	1.272(+04)
500	5.341(+01)	6.267(+03)	1.275(+04)
600	4.451(+01)	7.544(+03)	1.280(+04)
700	3.815(+01)	8.825(+03)	1.286(+04)
800	3.338(+01)	1.011(+04)	1.295(+04)
900	2.967(+01)	1.141(+04)	1.307(+04)
1,000	2.670(+01)	1.271(+04)	1.322(+04)
1,500	1.780(+01)	1.949(+04)	1.413(+04)
2,000	1.335(+01)	2.669(+04)	1.500(+04)
2,500	1.068(+01)	3.432(+04)	1.613(+04)
3,000	8.881(+00)	4.258(+04)	1.830(+04)
3,500	7.565(+00)	5.200(+04)	2.220(+04)
4,000	6.525(+00)	6.338(+04)	2.797(+04)
4,500	5.650(+00)	7.756(+04)	3.517(+04)
5,000	4.887(+00)	9.517(+04)	4.285(+04)
6,000	3.625(+00)	1.410(+05)	5.429(+04)
7,000	2.713(+00)	1.958(+05)	5.346(+04)
8,000	2.122(+00)	2.483(+05)	4.346(+04)
9,000	1.752(+00)	2.912(+05)	3.377(+04)
10,000	1.510(+00)	3.249(+05)	2.806(+04)
11,000	1.338(+00)	3.531(+05)	2.586(+04)
12,000	1.208(+00)	3.790(+05)	2.613(+04)
13,000	1.102(+00)	4.050(+05)	2.826(+04)
14,000	1.014(+00)	4.322(+05)	3.191(+04)
15,000	9.370(−01)	4.632(+05)	3.687(+04)
16,000	8.692(−01)	4.970(+05)	4.183(+04)
17,000	8.081(−01)	5.364(+05)	4.826(+04)
18,000	7.523(−01)	5.818(+05)	5.512(+04)
19,000	7.007(−01)	6.342(+05)	6.207(+04)
20,000	6.531(−01)	6.924(+05)	6.876(+04)
22,000	5.688(−01)	8.170(+05)	7.994(+04)
24,000	4.967(−01)	9.681(+05)	8.712(+04)
26,000	4.319(−01)	1.125(+06)	9.030(+04)
28,000	3.783(−01)	1.305(+06)	9.018(+04)
30,000	3.339(−01)	1.489(+06)	8.728(+04)
35,000	2.572(−01)	1.938(+06)	7.314(+04)
40,000	2.091(−01)	2.292(+06)	6.052(+04)
45,000	1.768(−01)	2.596(+06)	5.100(+04)
50,000	1.543(−01)	2.851(+06)	4.547(+04)

References

Alagia M, Brunetti B, Candori P, Falcinelli S, Teixidor MM, Pirani F, Richter R, Stranges S, Vecchiocattivi F (2004) Low-lying electronic states of HBr^{2+}. J Chem Phys 120(15):6985–6991

André P, Aubreton J, Clain S, Dudeck M, Duffour E, Elchinger MF, Izrar B, Rochette D, Touzani R, Vacher D (2010) Transport coefficients in thermal plasma. Applications to Mars and Titan atmospheres. Eur Phys J D 57:227–234

Aubreton J, Elchinger M, Fauchais P, Rat V, André P (2004a) Thermodynamic and transport properties of a ternary Ar-H_2-He mixture out of equilibrium up to 30,000 K at atmospheric pressure. J Phys D: Appl Phys 37(16):2232–2246

Aubreton J, Elchinger M, Rat V, Fauchais P (2004b) Two-temperature transport coefficients in argon-helium thermal plasmas. J Phys D: Appl Phys 37(1):34–41

Biagi S (2012) http://consult.cern.ch/writeup/magboltz/ or http://rjd.web.cern.ch/rjd/cgi-bin/cross

Blaha M, Davis J (1975) Elastic scattering of electrons by oxygen and nitrogen at intermediate energies. Phys Rev A 12(6):2319–2324

Bray I, Konovalov D, McCarthy IE (1991) Coupled-channel optical calculation of electron-hydrogen scattering: Elastic scattering from 0.5 to 30 eV. Phys Rev A 43(11):5878–5885

Brunger MJ, Buckman SJ (2002) Electron-molecule scattering cross-sections. I. experimental techniques and data for diatomic molecules. Phys Rep 357(3–5):215–458

Bruno D, Catalfamo C, Laricchiuta A, Giordano D, Capitelli M (2006) Convergence of Chapman-Enskog calculation of transport coefficients of magnetized argon plasma. Phys Plasmas 13(7):072307

Bruno D, Catalfamo C, Capitelli M, Colonna G, De Pascale O, Diomede P, Gorse C, Laricchiuta A, Longo S, Giordano D, Pirani F (2010) Transport properties of high-temperature Jupiter atmosphere components. Phys Plasmas 17(11):112315

Bruno D, Capitelli M, Catalfamo C, Giordano D (2011) Transport properties of high-temperature air in a magnetic field. Phys Plasmas 18(1):012308

Capitelli M (1977) Transport coefficients of partially ionized gases. Journal de Physique Supplemént Colloque C3 (Paris) 38(8):C3 227–C3 237

Capitelli M, Gorse C, Fauchais P (1976) Transport coefficients of Ar-H_2 high temperature mixtures. Journal de Chimie Physique et de Physico-Chimie Biologique 73:755–759

Capitelli M, Colonna G, Gorse C, D'Angola A (2000a) Transport properties of high temperature air in local thermodynamic equilibrium. Eur Phys J D 11(2):279–289

Capitelli M, Gorse C, Longo S, Giordano D (2000b) Collision integrals of high-temperature air species. J Thermophys Heat Transf 14(2):259–268

Capitelli M, Colonna G, Giordano D, Marraffa L, Casavola A, Minelli P, Pagano D, Pietanza L, Taccogna F (2005) High-temperature thermodynamic properties of Mars-atmosphere components. J Spacecr Rockets 42(6):980–989

Capitelli M, Colonna G, D'Angola A (2011) Fundamental aspects of plasma chemical physics: Thermodynamics. Springer series on atomic, optical, and plasma physics, vol 66. Springer, New York

Catalfamo C, Bruno D, Colonna G, Laricchiuta A, Capitelli M (2009) High temperature Mars atmosphere. Part II: Transport properties. Eur Phys J D 54(3):613–621

Chandra N (1977) Low-energy electron scattering from CO. II. ab initio study using the frame transformation theory. Phys Rev A 16(1):80–108

Colonna G, D'Angola A, Laricchiuta A, Bruno D, Capitelli M (2013) Analytical expressions of thermodynamic and transport properties of the Martian atmosphere in a wide temperature and pressure range. Plasma Chem Plasma P 33(1):401–431

Dalgarno A, McDowell M (1956) Charge transfer and the mobility of H^- ions in atomic hydrogen. Proc Phys Soc (London) A69(8):615

D'Angola A, Colonna G, Gorse C, Capitelli M (2008) Thermodynamic and transport properties in equilibrium air plasmas in a wide pressure and temperature range. Eur Phys J D 46(1):129–150

D'Angola A, Colonna G, Bonomo A, Bruno D, Laricchiuta A, Capitelli M (2012) A phenomenological approach for the transport properties of air plasmas. Eur Phys J D 66(8):205

Das AK, Ray D, Mukherjee PK (1992) Static dipole polarizabilities of open-shell negative ions. Theor Chim Acta 82(3–4):223–227

Davidović D, Janev R (1969) Resonant charge exchange of the negative ions in slow collisions with atoms. Phys Rev 186(1):89–95

Devoto RS (1967) Simplified expressions for the transport properties of ionized monatomic gases. Phys Fluids 10(10):2105–2112

Ewig CS, Waldman M, Maple JR (2002) Ab initio atomic polarizability tensors for organic molecules. J Phys Chem A 106(2):326–334

Flannery MR, Cosby PC, Moran TF (1973) Molecular charge transfer: Experimental and theoretical investigation of the role of incident-ion vibrational states in N_2^+-N_2 and CO^+-CO collisions. J Chem Phys 59(10):5494–5510

Gavezzotti A (2003) Calculation of intermolecular interaction energies by direct numerical integration over electronic densities. An improved polarization model and the evaluation of dispersion and repulsion energies. J Phys Chem B 107(10):2344–2353

Gorfinkiel JD, Tennyson J (2004) Electron-H_3^+ collisions at intermediate energies. J Phys B At Mol Opt Phys 37(20):L343–L350

Gorse C, Capitelli M (2001) Collision integrals of high temperature hydrogen species. At Plasma Mater Interact Data Fusion (APID series) 9:75–82

Gote M, Ehrhardt H (1995) Rotational excitation of diatomic molecules at intermediate energies: absolute differential state-to-state transition cross sections for electron scattering from N_2, Cl_2, CO and HCl. J Phys B At Mol Phys 28(17):3957–3986

Gupta GP, Mathur KC (1980) Corrigendum differential cross sections for the elastic scattering of electrons by hydrogen atoms at intermediate energies. J Phys B: At Mol Phys 13:1719

Hati S, Datta D (1995) Electronegativity and static electric dipole polarizability of atomic species. a semiempirical relation. J Phys Chem 99(27):10742–10746

Hati S, Datta D (1996) At most, one electron can be added to a free atom in gas phase. J Phys Chem 100(12):4828–4830

Hayashi M (1989) Electron collision cross sections determined from beam and swarm data by Boltzmann analysis. NATO ASI Series B 220:333–340

Hirschfelder JO, Curtiss CF, Bird RB (1966) Molecular theory of gases and liquids. Wiley, New York

Huels M, Champion R, Doverspike L, Wang Y (1990) Charge transfer and electron detachment for collisions of H^- and D^- with H. Phys Rev A 41(9):4809–4815

Hurly JJ, Mehl JB (2007) ^{4}He thermophysical properties: new ab initio calculations. J Res Natl Inst Stand Technol 112(2):75–94

Itikawa Y (2002) Cross sections for electron collisions with carbon dioxide. J Phys Chem Ref Data 31(3):749–767

Itikawa Y (2006) Cross sections for electron collisions with nitrogen molecules. J Phys Chem Ref Data 35(1):31–53

Itikawa Y, Ichimura A, Onda K, Sakimoto K, Takayanagi K, Hatano Y, Hayashi M, Nishimura M, Tsurubuchi S (1989) Cross sections for collisions of electrons and photons with oxygen molecules. J Phys Chem Ref Data 18(1):23–42

Janev RK, Langer WD, Evans Jr K, Post Jr D (1987) Elementary processes in hydrogen-helium plasmas. Springer, Berlin

Kosarim AV, Smirnov BM (2005) Electron terms and resonant charge exchange involving oxygen atoms and ions. J Exp Theor Phys 101(4):611–627

Kosarim AV, Smirnov BM, Capitelli M, Celiberto R, Laricchiuta A (2006) Resonant charge exchange involving electronically excited states of nitrogen atoms and ions. Phys Rev A 74(6):062707

Krstiċ PS (2002) Inelastic processes from vibrationally excited states in slow H^+-H_2 and H-H_2^+ collisions: excitations and charge transfer. Phys Rev A 66(4):042717

Krstiċ PS, Schultz DR (1999) Elastic scattering and charge transfer in slow collisions: isotopes of H and H^+ colliding with isotopes of H and with He. J Phys B: At Mol Phys 32(14):3485–3509

Krstiċ PS, Schultz DR (2003) Elastic processes involving vibrationally excited molecules in cold hydrogen plasmas. J Phys B: At Mol Phys 36(2):385–398

Laricchiuta A, Bruno D, Capitelli M, Catalfamo C, Celiberto R, Colonna G, Diomede P, Giordano D, Gorse C, Longo S, Pagano D, Pirani F (2009) High temperature Mars atmosphere. Part I: Transport cross sections. Eur Phys J D 54(3):607–612

Li Y, Lin C (1999) Calculations of some weakly bound diatomic molecular negative ions. Phys Rev A 60(3):2009–2014

Magnasco V, Ottonelli M (1999) Dipole polarizability pseudospectra and C_6 dispersion coefficients for H_2^+-H_2^+. J Mol Struct (Theochem) 469:31–40

Meyer W, Frommhold L (1994) Long-range interactions in H-He: ab initio potential, hyperfine pressure shift and collision-induced absorption in the infrared. Theor Chim Acta 88(3):201–216

Miller T, Bederson B (1977) In: Bates, DR, Bederson, B (eds) Advances in atomic and molecular physics, vol 13. Academic, New York

Mojarrabi B, Gulley RJ, Middleton AG, Cartwright DC, Teubner PJO, Buckman SJ, Brunger MJ (1995) Electron collisions with NO: elastic scattering and rovibrational (0 to 1, 2, 3, 4) excitation cross sections. J Phys B: At Mol Phys 28(3):487–504

Moran TF, Flannery MR, Cosby PC (1974) Molecular charge transfer II. experimental and theoretical investigation of the role of incident-ion vibrational states in O_2^+-O_2 and NO^+-NO collisions. J Chem Phys 61(4):1261–1273

Nikitin EE, Smirnov BM (1978) Quasiresonant processes in slow collisions. Sov Phys Usp 21(2):95–116

Olney TN, Cann NM, Cooper G, Brion CE (1997) Absolute scale determination for photoabsorption spectra and the calculation of molecular properties using dipole sum-rules. Chem Phys 223(1):59–98

Olson R, Liu B (1980) Interactions of H and H^- with He and Ne. Phys Rev A 22(4):1389–1394

Pagano D, Casavola A, Pietanza L, Colonna G, Giordano D, Capitelli M (2008) Thermodynamic properties of high-temperature Jupiter-atmosphere components. J Thermophys Heat Transf 22(3):434–441

Phelps AV (2007) Collision data compilation. JILA, University of Colorado http://jilawwwcoloradoedu/~avp/collision_data/electronneutral/electrontxt

Rundel R, Nitz D, Smith K, Geis M, Stebbings R (1979) Resonant charge transfer in He^+-He collisions studied with the merging-beams technique. Phys Rev A 19(1):33–42

Sharp TE (1970) Potential-energy curves for molecular hydrogen and its ions. At Data Nucl Data Tables 2:119–169

Shyn TW, Sharp WE (1981) Angular distribution of electrons elastically scattered from H_2. Phys Rev A 24(4):1734–1740

Shyn TW, Sharp WE (1982) Angular distribution of electrons elastically scattered from O_2: 2.0–200 eV impact energy. Phys Rev A 26(3):1369–1372

Smirnov BM (2001) Atomic structure and the resonant charge exchange process. Phys Usp 44(3):221–253

Sourd B, Aubreton J, Elchinger MF, Labrot M, Michon U (2006) High temperature transport coefficients in e/C/H/N/O mixtures. J Phys D: Appl Phys 39(6):1105–1119

Stallcop JR, Levin E, Partridge H (1996) H-H_2 collision integrals and transport coefficients. Chem Phys Lett 254(1–2):25–31

Stallcop JR, Levin E, Partridge H (1998) Transport properties of hydrogen. J Thermophys Heat Transf 12(4):514–519

Sullivan JP, Gibson J, Gulley RJ, Buckman SJ (1995) Low-energy electron scattering from O_2. J Phys B: At Mol Phys 28(19):4319–4328

Sun W, Morrison MA, Isaacs WA, Trail WK, Alle DT, Gulley RJ, Brennan MJ, Buckman SJ (1995) Detailed theoretical and experimental analysis of low energy electron-N_2 scattering. Phys Rev A 52(2):1229–1256

Thomas LD, Nesbet RK (1975a) Addendum: Low-energy electron scattering by atomic oxygen. Phys Rev A 12(4):1729–1730

Thomas LD, Nesbet RK (1975b) Low-energy electron scattering by atomic carbon. Phys Rev A 12(6):2378–2382

Thomas LD, Nesbet RK (1975c) Low-energy electron scattering by atomic nitrogen. Phys Rev A 12(6):2369–2377

van Duijnen PT, Swart M (1998) Molecular and atomic polarizabilities: Thole's model revisited. J Phys Chem A 102(14):2399–2407

Williams JF (1975a) Electron scattering from atomic hydrogen. III. absolute differential cross sections for elastic scattering of electrons of energies from 20 to 680 eV. J Phys B: At Mol Phys 8:2191

Williams JF (1975b) Electron scattering from hydrogen atoms. II. elastic scattering at low energies from 0.5 to 8.7 eV. J Phys B: At Mol Phys 8:1683

Winstead C, McKoy V (1998) Electron collisions with nitrous oxide. Phys Rev A 57(5):3589–3597

Wright MJ, Bose D, Palmer GE, Levin E (2005) Recommended collision integrals for transport property computations part 1: air species. AIAA J 43(12):2558–2564

Yevseyev AV, Radtsig AA, Smirnov BM (1982) The asymptotic theory of resonance charge exchange between diatomics. J Phys B: At Mol Phys 15(23):4437–4452

Index

M. Capitelli et al., *Fundamental Aspects of Plasma Chemical Physics*,
Springer Series on Atomic, Optical, and Plasma Physics 74,
DOI 10.1007/978-1-4419-8172-1, © Springer Science+Business Media, LLC 2013